



Thèse

2018

Open Access

This version of the publication is provided by the author(s) and made available in accordance with the copyright holder(s).

Synthesis and applications of chiral polyether macrocycles

Homberg, Alexandre

How to cite

HOMBERG, Alexandre. Synthesis and applications of chiral polyether macrocycles. Doctoral Thesis, 2018. doi: 10.13097/archive-ouverte/unige:110497

This publication URL: <https://archive-ouverte.unige.ch/unige:110497>

Publication DOI: [10.13097/archive-ouverte/unige:110497](https://doi.org/10.13097/archive-ouverte/unige:110497)

Synthesis and Applications of Chiral Polyether Macrocycles

THÈSE

présentée à la Faculté des sciences de l'Université de Genève
pour obtenir le grade de Docteur ès sciences, mention chimie

par

Alexandre HOMBERG

de

Genève (Genève)

Thèse N° 5268

GENÈVE

Centre d'impression de l'Université de Genève, ReproMail, Unimail

2018



DOCTORAT ÈS SCIENCES, MENTION CHIMIE

Thèse de Monsieur Alexandre HOMBERG

intitulée :

«Synthesis and Applications of Chiral Polyether Macrocycles»

La Faculté des sciences, sur le préavis de Monsieur J. LACOUR, professeur ordinaire et directeur de thèse (Département de chimie organique), Monsieur N. WINSSINGER, professeur ordinaire (Département de chimie organique), Madame H. LEBEL, professeure (Département de chimie, Université de Montréal, Québec, Canada), Monsieur A. MARTINEZ, professeur (Institut des sciences moléculaires de Marseille, Université Aix-Marseille, Marseille France), autorise l'impression de la présente thèse, sans exprimer d'opinion sur les propositions qui y sont énoncées.

Genève, le 17 octobre 2018

Thèse - 5268 -

Le Dècanat

Much to learn, you still have.

Yoda

Résumé

La synthèse de macrocycles polyétherés insaturés par condensation catalysée au rhodium(II) de α -diao- β -cétoesters et d'éthers cycliques (par exemple 1,4-dioxane, THP ou THF) a été décrite par le groupe du Prof. Lacour.^A Plus récemment, en 2015, la transformation en une seule étape de synthèse de ces même structures en éthers couronnes chiraux a été mise en évidence par le développement d'une séquence d'amidation – transposition d'oléfines induite par le traitement des macrocycles avec des amines aromatiques en conditions basiques.

Bien que la transformation tolère dans la plupart des cas une large variété d'amines aromatiques, l'introduction d'amines aliphatiques, et en particulier celles portant des centres stéréogènes, restait inaccessible au début de cette thèse. Il était nécessaire de développer une approche alternative pour introduire ces amines. Pour se faire, une procédure séquentielle a été développée avec, en premier lieu, une préformation des amides à l'aide d'une activation par le TBD (1,5,7-triazabicyclo[4.4.0]déc-5-ène) suivie dans un deuxième temps de la transposition des oléfines en conditions basiques pour obtenir les éthers couronnes chiraux appropriés. Ces macrocycles ont été ensuite utilisés comme catalyseurs en catalyse asymétrique de transfert de phase pour la synthèse d'acides aminés α -substitués (jusqu'à 45% ee).

Dans une nouvelle optique, une famille de cryptands hétéroditopiques a été synthétisée en une ou deux étapes à partir des molécules transposées. La capacité de ces récepteurs à se lier à des cations métalliques, des anions classiques et surtout à la combinaison des deux a été étudiée en solution par RMN du proton et en phase solide par diffraction des rayons X. De manière générale, une préférence pour les cations monovalents (Na^+ et K^+) associés aux anions

^A (a) Zeghida, W.; Besnard, C.; Lacour, J., *Angew. Chem. Int. Ed.* **2010**, 49, 7253-7256. (b) Poggiali, D.; Homberg, A.; Lathion, T.; Piguet, C.; Lacour, J., *ACS Catal.* **2016**, 6, 4877-4881.

triatomiques linéaires (N_3^- , NCO^- , SCN^-) ou les oxyanions trigonaux (NO_3^-) a été démontrée. Les sels se lient coopérativement dans le cryptand en tant que paire d'ions de contact.^B

Une série de macrocycles polyéthérés substitués avec des groupements fluorescents a ensuite été synthétisée. Grâce à la conformation rigide de ces dérivés, les fluorophores sont proches spatialement les uns des autres et, en conséquence, émettent une fluorescence excimérique (EF) intense. Après séparation des énantiomères par CSP-HPLC, les propriétés chiroptiques ont été étudiées par dichroïsme circulaire (ECD) et luminescence circulairement polarisée (CPL). En CPL, des valeurs élevées de facteur dissymétrique associées à l'EF ont été mesurées (valeurs de g_{lum} jusqu'à $1.7 \cdot 10^{-2}$). L'addition de cations métalliques (Na^+ , Ba^{2+}) provoque un changement conformationnel des dérivés et peut être suivie par l'inversion de certains ou de la majorité des signaux en ECD et par une extinction du signal en CPL. Le signal original peut être récupéré par addition d'un agent chélatant pour le métal (18-Crown-6 commercial) faisant du système un exemple rare d'interrupteur moléculaire alliant à la fois une inversion (+/-) du signal ECD et une fonction on/off du signal CPL.^C

Finalement, le protocole d'amidation – transposition d'oléfines a été étendu aux précurseurs macrocycliques diazotés. La réaction semble être limitée à certaines amines aromatiques, mais les atomes d'azotes du macrocycle peuvent être fonctionnalisés par la suite par amination réductrice. L'étude des propriétés des composés formés devra être menée ultérieurement.

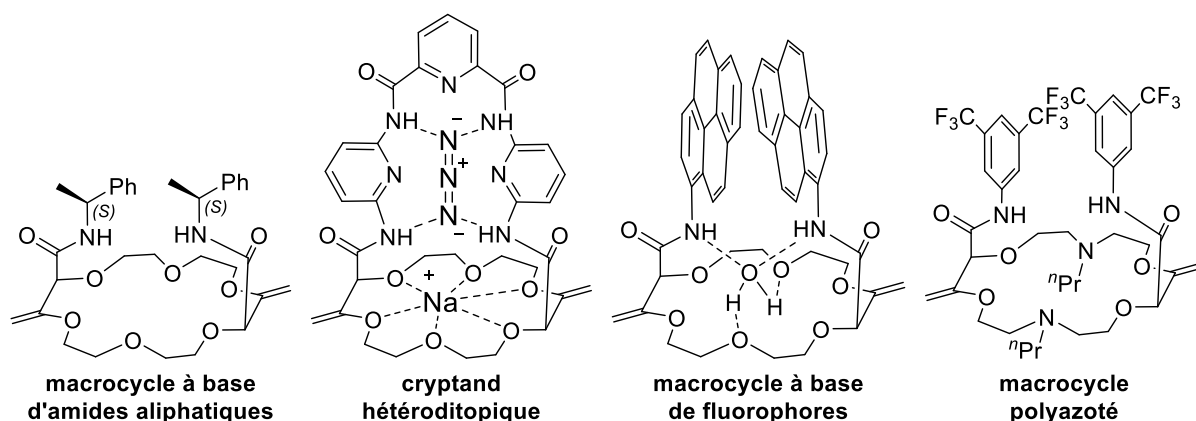


Figure 1 Macrocycles polyéthérés étudiés.

^B Ray, S. K.; Homberg, A.; Vishe, M.; Besnard, C.; Lacour, J., *Chem. Eur. J.* **2018**, 24, 2944-2951.

^C Homberg, A.; Brun, E.; Zinna, F.; Pascal, S.; Górecki, M.; Monnier, L.; Besnard, C.; Pescitelli, G.; Di Bari, L.; Lacour, J., *Chem. Sci.* **2018**, 9, 7043-7052.

Remerciements

Les résultats rapportés dans ce manuscrit ont été obtenus dans le cadre d'un travail de thèse réalisé au sein du laboratoire du Prof. Jérôme Lacour, dans le département de chimie organique de l'Université de Genève, du 1er septembre 2013 au 20 septembre 2018.

J'aimerais exprimer toute ma gratitude envers le Prof. Jérôme Lacour pour m'avoir accepté dans son groupe de recherche et m'avoir offert l'opportunité de réaliser ce travail de thèse. Je le remercie aussi pour tous ses conseils, son enseignement, sa confiance et toute l'autonomie accordée durant cette période.

Je voudrais remercier le Prof. Hélène Lebel (Université de Montréal, Canada), le Prof. Alexandre Martinez (Aix-Marseille Université, France) et le Prof. Nicolas Winssinger (Université de Genève, Suisse) pour avoir accepté de juger ce travail de thèse.

J'aimerais aussi remercier les personnes avec qui j'ai eu le plaisir de collaborer pendant cette thèse : le Prof. Claude Piguet et Timothée Lathion pour la partie chimie inorganique ; le Prof. Eric Vauthey et Oleksandr Yushchenko pour la partie spectroscopie ; le Prof. Eric Bakker et Zdeňka Jarolímová pour la partie chimie analytique ; Prof. Lorenzo Di Bari, Prof. Gennaro Pescitelli et Marcin Górecki pour la partie spectroscopie chiroptique. Je remercie également les équipes des services RMN (Dr. Damien Jeannerat et Marion Pupier), de spectrométrie de masse (Dr. Sophie Michalet, Eliane Sandmeier, Henry Théraulaz) et de cristallographie (Dr. Laure Guénée et Dr. Céline Besnard).

J'aimerais également remercier Dr. Elodie Brun, Dr. Johann Bosson et Dr. Romain Duwald pour leurs remarques et corrections constructives lors de la rédaction de cette thèse.

Je remercie tous les membres du groupe, collègues et amis, avec qui j'ai eu le plaisir de travailler : Alejandro, Alessandro, Alexandre, Alvina, Andjela, Antoine, Cecilia, Florian, Géraldine,

Irene, Jérôme, Joël, Johann, Júlia, Julie, Manon, Margaux, Marie-Louise, Maya, Nidal, Pau, Pavol, Kota, Rémi, Rebecca, Romain, Sandip, Sébastien, Simon, Shinya, Stéphane, et Thierry ; et plus particulièrement ceux de l'équipe macrocycle : Daniele, Elodie, Francesco, Mahesh, Radim et Sumit.

Enfin, j'aimerais remercier ma famille et mes proches qui m'ont toujours soutenu lors de toutes ces années.

Abbreviations

Ac: acetate	IR: infrared
Ar: aryl	Me: methyl
BAr _F : tetrakis[3,5-bis(trifluoromethyl)phenyl] borate	m.p.: melting point
Bn: benzyl	MS: mass spectrometry
Boc: <i>tert</i> -butoxycarbonyl	Ms: mesyl
c: concentration	NaOMe: sodium methoxide
c _H : concentration host	naphth: naphthyl
CE: crown ether	NMI: 1,8-naphthalene monoimide
Cbz: carboxybenzyl	ⁿ Oct: <i>n</i> -octyl
CPL: circularly polarized luminescence	ⁿ Pr: <i>n</i> -propyl
CSP: chiral stationary phase	PNP: <i>para</i> -nitro-phenyl
CuAAC: Copper-catalyzed azide alkyne cycloaddition	PTC: phase transfer catalysis
DBU: 1,8-Diazabicyclo[5.4.0]undec-7-ene	RCM: ring closure metathesis
<i>dr</i> : diastereomeric ratio	R _f : retardation factor
ECD: electronic circular dichroism	TBD: 1,5,7-triazabicyclo[4.4.0]dec-5-ene
<i>ee</i> : enantiomeric excess	TBS: <i>tert</i> -butyldimethylsilyl ether
EF: excimer fluorescence	<i>t</i> -BuOK: potassium <i>tert</i> -butoxide
El: electron ionization	THF: tetrahydrofuran
equiv: equivalent	THP: tetrahydropyran
ESI: electrospray ionization	TLC: thin layer chromatography
Et: ethyl	Trityl: triphenylmethyl
<i>g</i> _{abs} : dissymmetry factor in absorbance	Troc: 2,2,2-trichloroethoxycarbonyl
GC: gas chromatography	
<i>g</i> _{lum} : dissymmetry factor in luminescence	
HPLC: high pressure liquid chromatography	
<i>i</i> -Bu: <i>iso</i> -butyl	
ⁱ Pr: <i>iso</i> -propoyl	
ⁱ PrOH: <i>iso</i> propanol	

Symbols

δ : chemical shift (ppm)

λ : wavelength

J : coupling constant (Hz)

t_R : retention time

T : temperature (K)

ϵ : extinction coefficient

I : intensity

ϕ_f : fluorescence quantum yield

Units

$^{\circ}\text{C}$: degree Celsius

g: gram

L: liter

mol: mole

M: molarity (mol/L)

min: minute

h: hours

ppm: part per million

Hz: Hertz

\AA : Ångström

Table of contents

1	INTRODUCTION	1
1.1	PREAMBLE	1
1.2	MACROCYCLES	2
1.2.1	<i>Macrocyclization strategies</i>	<i>3</i>
1.2.2	<i>Macrocycles with supramolecular abilities</i>	<i>5</i>
1.3	POLYETHER MACROCYCLES	7
1.3.1	<i>Synthesis of crown ethers.....</i>	<i>8</i>
1.3.2	<i>Applications of crown ethers and related compounds.....</i>	<i>11</i>
1.4	CHIRAL CROWN ETHERS.....	14
1.4.1	<i>Structures of chiral crown ethers</i>	<i>14</i>
1.4.2	<i>Applications of chiral crown ethers</i>	<i>16</i>
1.5	MACROCYCLES SYNTHETIZED FROM DIAZO PRECURSORS	25
1.5.1	<i>Macrocyclization from simple cyclic ethers.....</i>	<i>26</i>
1.5.2	<i>Macrocyclization from oxetanes</i>	<i>30</i>
1.5.3	<i>Miscellaneous syntheses of macrocycles</i>	<i>31</i>
1.5.4	<i>Functionalization of polyether macrocycles.....</i>	<i>32</i>
1.6	CONCLUSION	36
2	SYNTHESIS OF CHIRAL CROWN ETHERS BEARING ALIPHATIC SUBSTITUENTS.....	39
2.1	INTRODUCTION	39
2.2	SYNTHESIS OF ALIPHATIC AMIDE MACROCYCLES.....	40
2.2.1	<i>Transformation of ester into amides (aminolysis)</i>	<i>42</i>
2.2.2	<i>Transposition of the olefins</i>	<i>46</i>
2.2.3	<i>Tandem aminolysis – transposition conditions</i>	<i>49</i>
2.2.4	<i>Crown ethers bearing α-branched aliphatic substituents</i>	<i>53</i>

2.2.5	<i>Hydrogenation of Aliphatic-18C6</i>	59
2.3	APPLICATIONS OF ALIPHATIC-18C6 CROWN ETHERS IN ASYMMETRIC PTC.....	60
2.3.1	<i>Synthesis of protected phenylalanine</i>	60
2.3.2	<i>Asymmetric addition by PTC</i>	65
2.3.3	<i>Asymmetric epoxide syntheses by PTC</i>	66
2.4	CONCLUSION	67
3	HETERODITOPIC CRYPTANDS: SYNTHESIS AND ION PAIR RECOGNITION.....	69
3.1	INTRODUCTION	69
3.1.1	<i>Heteroditopic receptors</i>	69
3.1.2	<i>Examples of crown ether-based heteroditopic receptors</i>	71
3.2	NOVEL HETERODITOPIC CRYPTANDS.....	75
3.2.1	<i>Synthesis of the diamino precursors</i>	76
3.2.2	<i>Ring closure reactions</i>	77
3.3	HETERODITOPIC BINDING ABILITIES.....	82
3.3.1	<i>Titration of pyr-cryptand</i>	83
3.3.2	<i>Solid state structure of coordinated pyr-cryptand</i>	85
3.3.3	<i>Solution studies of the cryptands with Na⁺ and N₃⁻</i>	87
3.3.4	<i>Binding mode of NaN₃ within the cryptands</i>	90
3.3.5	<i>Quantitative analysis</i>	90
3.4	CONCLUSION	91
4	FLUORESCENT MACROCYCLES AS CHIROPTICAL SWITCHES	93
4.1	INTRODUCTION	93
4.1.1	<i>Sensing of metal ions using excimer fluorescence</i>	93
4.1.2	<i>Chiroptical switches</i>	98
4.2	SYNTHESIS AND RESOLUTION OF THE MACROCYCLES	102
4.3	(CHIR)OPTICAL PROPERTIES OF THE MACROCYCLES	105
4.3.1	<i>Absorption properties</i>	105
4.3.2	<i>Emission properties</i>	112
4.3.3	<i>ECD and CPL reversibility</i>	118
4.4	CONCLUSION	121

5	AZA-CROWN ETHER SYNTHESIS.....	123
5.1	INTRODUCTION	123
5.2	SYNTHESIS OF AZA-CROWN ETHERS	124
5.2.1	<i>Synthesis of unsaturated ester building blocks</i>	<i>124</i>
5.2.2	<i>Amidation/transposition of aza macrocycles</i>	<i>126</i>
5.3	CONCLUSION	135
6	CONCLUSIONS AND PERSPECTIVES.....	137
6.1	CONCLUSION	137
6.2	PERSPECTIVES	138
7	EXPERIMENTAL PART.....	143
7.1	GENERAL INFORMATION AND MATERIALS.....	143
7.2	SYNTHESIS OF POLYETHER MACROCYCLES.....	144
7.2.1	<i>Synthesis of 16C4 macrocycle</i>	<i>144</i>
7.2.2	<i>Synthesis of 18C4 macrocycle</i>	<i>145</i>
7.2.3	<i>Synthesis of ester-18C6</i>	<i>146</i>
7.3	SYNTHESIS OF POLYETHER MACROCYCLES (AROMATIC AMINES)	150
7.3.1	<i>General procedure II.....</i>	<i>150</i>
7.3.2	<i>Synthesis of 2-naphth-18C6.....</i>	<i>150</i>
7.3.3	<i>Synthesis of 3,5-dibromo-18C6</i>	<i>151</i>
7.3.4	<i>Synthesis of 3,5-diiodo-18C6</i>	<i>152</i>
7.3.5	<i>Synthesis of o-CN-18C6</i>	<i>152</i>
7.3.6	<i>Synthesis of m-OMe-18C6</i>	<i>153</i>
7.3.7	<i>Synthesis of m-CN-18C6</i>	<i>154</i>
7.3.8	<i>Synthesis of m-I-18C6.....</i>	<i>154</i>
7.3.9	<i>Synthesis of p-NO₂-18C6.....</i>	<i>155</i>
7.3.10	<i>Synthesis of p-OMe-18C6</i>	<i>156</i>
7.3.11	<i>Synthesis of p-OH-18C6</i>	<i>156</i>
7.3.12	<i>Synthesis of p-CN-18C6</i>	<i>157</i>
7.3.13	<i>Synthesis of p-NC-18C6</i>	<i>158</i>
7.3.14	<i>Synthesis of p-Br-18C6.....</i>	<i>158</i>

7.3.15	Synthesis of <i>p</i> -I-18C6.....	159
7.3.16	Synthesis of <i>p</i> -I- <i>p</i> -Ph-18C6	160
7.3.17	Synthesis of 5-pyrimidine-18C6.....	160
7.3.18	Synthesis of <i>m</i> -NH ₂ -pyr-18C6.....	161
7.3.19	Synthesis of <i>m</i> -NH ₂ -18C6 ¹¹⁹	161
7.3.20	Synthesis of fluorene-18C6.....	162
7.3.21	Synthesis of fluorene-18C4.....	162
7.3.22	Synthesis of fluorene-16C4.....	163
7.3.23	Synthesis of NMI-18C6	164
7.3.24	Synthesis of perylene-18C6	165
7.3.25	Synthesis of perylene-18C4	166
7.3.26	Synthesis of perylene-16C4 ¹²³	167
7.3.27	CSP-HPLC separation of polyether macrocycles ⁸³	168
7.4	SYNTHESIS OF CROWN ETHERS (ALIPHATIC AMINES)	170
7.4.1	General procedure III (aliphatic-18C6).....	170
7.4.2	Reaction of aminolysis	171
7.4.3	Linear aliphatic amides macrocycle synthesis	174
7.4.4	α -Branched aliphatic amides macrocycle synthesis.....	179
7.4.5	Hydrogenation of aliphatic amides crown ethers	189
7.5	PHASE TRANSFER CATALYSIS.....	191
7.5.1	Synthesis of 2.20	191
7.5.2	Screening of the solvent for the synthesis of 2.20	193
7.6	SYNTHESIS OF CRYPTANDS	194
7.6.1	General procedure V (cryptands)	194
7.6.2	Synthesis of pyr-cryptand.....	194
7.6.3	Synthesis of Ph-cryptand.....	195
7.6.4	Synthesis of thio-cryptand.....	196
7.6.5	Synthesis of pyr-Ph-cryptand	196
7.6.6	Synthesis of 4[H]-pyr-cryptand.....	197
7.6.7	Synthesis of phos-cryptand	198
7.6.8	Synthesis of thiophos-cryptand.....	199
7.6.9	Synthesis of thiourea-cryptand	200

7.7	SYNTHESIS OF FLUORESCENT MONOMERS	202
7.7.1	<i>General procedure VI (monomers)</i>	202
7.7.2	<i>Synthesis of pyrene-monomer</i>	202
7.7.3	<i>Synthesis of perylene-monomer</i>	203
7.7.4	<i>Synthesis of fluorene-monomer</i>	203
7.7.5	<i>Synthesis of NMI-monomer</i>	204
7.8	SYNTHESIS OF AZA-CROWN ETHERS	206
7.8.1	<i>Synthesis of N18C6-Trityl</i>	206
7.8.2	<i>Synthesis of bisCF₃-N18C6-Ms</i>	207
7.8.3	<i>Synthesis of bisCF₃-N18C6-ⁿPr</i>	208
7.8.4	<i>Synthesis of 4[H]-bisCF₃-N18C6-Ms</i>	209
7.9	SYNTHESIS OF P-PYRENE-PH-18C6	210
7.10	SYNTHESIS OF 6.2	211
7.11	¹ H NMR TITRATIONS	212
7.11.1	<i>¹H NMR titration of Bn-18C6</i>	212
7.11.2	<i>¹H NMR titration of cryptands</i>	213
7.12	SPECTROSCOPIC DATA	219
7.12.1	<i>UV-Vis absorption and fluorescence spectroscopies</i>	219
7.12.2	<i>Procedure for ECD and CPL experiments</i>	223
7.12.3	<i>Reversibility experiments</i>	223
7.13	TDDFT CALCULATIONS	229
7.13.1	<i>General remarks</i>	229
7.13.2	<i>Calculation results</i>	230
7.14	CRYSTALLOGRAPHIC PART	233
7.14.1	<i>Crystallographic data of 2.1</i>	233
7.14.2	<i>Crystallographic data of [Na·Bn-18C6][BAr_F]</i>	235
7.14.3	<i>Crystallographic data of [Na·(S)-Me-1-naphth-(S)-18C6][BAr_F]</i>	236
7.14.4	<i>Crystallographic data of m-NH₂-pyr-18C6</i>	237
7.14.5	<i>Crystallographic data of pyr-cryptand</i>	238
7.14.6	<i>Crystallographic data of thiophos-cryptand</i>	239
7.14.7	<i>Crystallographic data of thiourea-cryptand</i>	240
7.14.8	<i>Crystallographic data of [pyr-cryptand·NaN₃]</i>	241

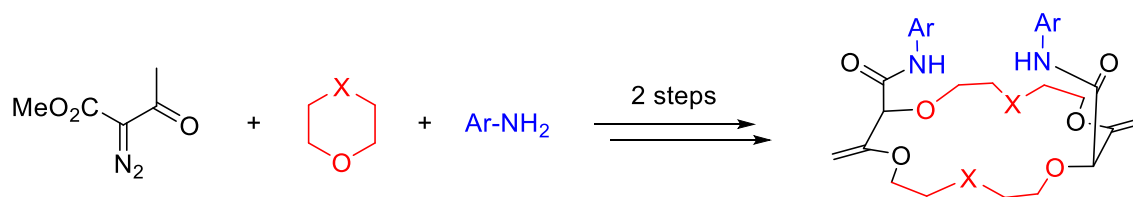
7.14.9	<i>Crystallographic data of [pyr-cryptand·NaNO₃]</i>	242
7.14.10	<i>Crystallographic data of [pyr-cryptand·KNCO]</i>	243
7.14.11	<i>Crystallographic data of [pyr-cryptand·NaSCN]</i>	244
7.14.12	<i>Crystallographic data of [pyr-cryptand·KSCN]</i>	245
7.14.13	<i>Crystallographic data of [Ph-cryptand·NaN₃]</i>	246
7.14.14	<i>Summary of the cryptand-salt distances</i>	247
8	APPENDIX	249

1 Introduction

1.1 Preamble

Since the first efficient synthesis by Charles J. Pedersen in the 1960's and his pioneer work on their complexation abilities, crown ethers (cyclic polyethers) have received a particular attention.¹ In that context, C. J. Pedersen jointly with D. J. Cram and J.-M. Lehn received the Nobel Prize in Chemistry in 1987 for their contributions on the synthesis and applications of crown ethers and for the development of supramolecular chemistry.²

Recently, the group of Prof. Jérôme Lacour reported the straightforward two-step synthesis of chiral crown ethers from simple cyclic ether building blocks (5,6,7-membered rings), α -diazo- β -ketoesters and aromatic amines (**Scheme 1.1**).³ The project of this PhD was to extend this chemistry to the larger possible range of macrocyclic structures, to different endo and exocyclic substituents, to develop strategies for the post-functionalization of the obtained macrocycles and to find potential applications for the various types of polyether derivatives generated.



Scheme 1.1 Two-steps synthesis of chiral crown ethers.

¹ Pedersen, C. J., *J. Am. Chem. Soc.* **1967**, 89, 7017-7036.

² (a) Pedersen, C. J., *Angew. Chem. Int. Ed.* **1988**, 27, 1021-1027. (b) Lehn, J. M., *Angew. Chem. Int. Ed.* **1988**, 27, 89-112. (c) Cram, D. J., *Angew. Chem. Int. Ed.* **1988**, 27, 1009-1020.

³ (a) Poggiali, D.; Homberg, A.; Lathion, T.; Piguet, C.; Lacour, J., *ACS Catal.* **2016**, 6, 4877-4881. (b) Vishe, M.; Hrdina, R.; Poblador-Bahamonde, A. I.; Besnard, C.; Guénée, L.; Bürgi, T.; Lacour, J., *Chem. Sci.* **2015**, 6, 4923-4928.

A brief introduction on the general synthesis of macrocycles will be presented first. Then, a presentation of crown ethers and derivatives will be given along with some applications with a particular focus on the chiral examples. The synthetic approach developed in Geneva will finally be described.

1.2 Macrocycles

Macrocyclic structures are a common feature in nature. About 20% of known natural products possess a cyclic structure with at least 11 atoms within the ring.⁴ Some common examples are Muscone, porphyrins, cyclic peptides or plasmids (**Figure 1.1**). This particular class of compounds display a variety of interesting biological⁵ or medicinal properties⁶ and were applied for many applications, including their use as fragrance (Muscone). Irrelevant of their synthetic nature, the natural macrocyclic structures can also be employed in drug discovery systems.⁷ It is postulated that the cyclic pattern allied with the (large) functionalization and stereochemical complexity induce a conformational preorganization of the structure and lead to high affinities and selectivities towards biological receptors. Macrocycles can also be used in chemical analysis for the sensing and quantification of various analytes (*vide infra*).⁸ Finally, some applications in nanotechnologies are possible with a use of the macrocycles as nanosized reactors (cages), switches or shuttles.⁹ Other macrocyclic structures formed through non-covalent bond such as organometallic, supramolecular assemblies or cages are also well documented but will not be discussed in this chapter.⁹

⁴ Frank, A. T.; Farina, N. S.; Sawwan, N.; Wauchope, O. R.; Qi, M.; Brzostowska, E. M.; Chan, W.; Grasso, F. W.; Haberfield, P.; Greer, A., *Mol. Divers.* **2007**, *11*, 115-118.

⁵ Kopp, F.; Marahiel, M. A., *Nat. Prod. Rep.* **2007**, *24*, 735-749.

⁶ Wessjohann, L. A.; Ruijter, E.; Garcia-Rivera, D.; Brandt, W., *Mol. Divers.* **2005**, *9*, 171-186.

⁷ (a) Yu, X.; Sun, D., *Molecules* **2013**, *18*. (b) Mallinson, J.; Collins, I., *Future Med. Chem.* **2012**, *4*, 1409-1438. (c) Driggers, E. M.; Hale, S. P.; Lee, J.; Terrett, N. K., *Nat. Rev. Drug Discov.* **2008**, *7*, 608. (d) Walsh Christopher, T., *ChemBioChem* **2002**, *3*, 124-134.

⁸ (a) Khopkar, S. M., *Analytical Chemistry of Macrocyclic and Supramolecular Compounds* Springer-Verlag: Berlin, **2002**. (b) Kolthoff, I. M., *Anal. Chem.* **1979**, *51*, 1-22.

⁹ Davis, F.; Higson, S., *Macrocycles: Construction, Chemistry and Nanotechnology Applications*. John Wiley & Son, Ltd.: Chichester, U.K., **2011**.

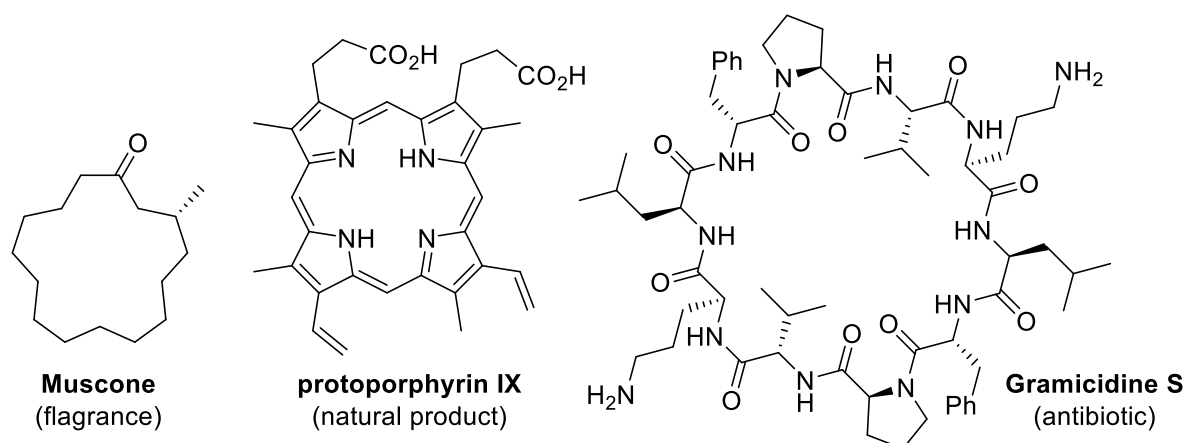


Figure 1.1 Examples of natural macrocycles.

1.2.1 Macrocyclization strategies

In view of the importance of this family of molecules, significant synthetic efforts have been devoted to the efficient preparation of macrocyclic structures. Diverse ring closure methodologies have been applied to obtain the macrocycles in good yields.¹⁰ In **Figure 1.2** are shown the main disconnection strategies for ring closure reactions (illustrated for selected examples) including nucleophilic substitutions,¹¹ lactonisations¹² or lactamizations,¹³ Wittig or Horner-Wadsworth-Emmons reactions,^{11,14} Diels-Alder processes,¹⁵ transition metal catalyzed

¹⁰ (a) Abdelraheem, E. M. M.; Shaabani, S.; Dömling, A., *Synlett* **2018**, 29, 1136-1151. (b) Martí-Centelles, V.; Pandey, M. D.; Burguete, M. I.; Luis, S. V., *Chem. Rev.* **2015**, 115, 8736-8834. (c) White, C. J.; Yudin, A. K., *Nat. Chem.* **2011**, 3, 509.

¹¹ Harrowven, D. C.; Kostiuk, S. L., *Nat. Prod. Rep.* **2012**, 29, 223-242.

¹² (a) Parenty, A.; Moreau, X.; Niel, G.; Campagne, J. M., *Chem. Rev.* **2013**, 113, PR1-PR40. (b) Parenty, A.; Moreau, X.; Campagne, J. M., *Chem. Rev.* **2006**, 106, 911-939.

¹³ Fitzgerald, M. E.; Mulrooney, C. A.; Duvall, J. R.; Wei, J.; Suh, B.-C.; Akella, L. B.; Vrcic, A.; Marcaurelle, L. A., *ACS Comb. Sci.* **2012**, 14, 89-96.

¹⁴ Lafontaine, J. A.; Provencal, D. P.; Gardelli, C.; Leahy, J. W., *J. Org. Chem.* **2003**, 68, 4215-4234.

¹⁵ Stocking, E. M.; Williams, R. M., *Angew. Chem. Int. Ed.* **2003**, 42, 3078-3115.

reactions (mostly ring closing metathesis (RCM)), cross coupling or copper-catalyzed azide-alkyne cycloadditions (CuAAC)^{11,16} and multicomponent macrocyclizations.¹⁷

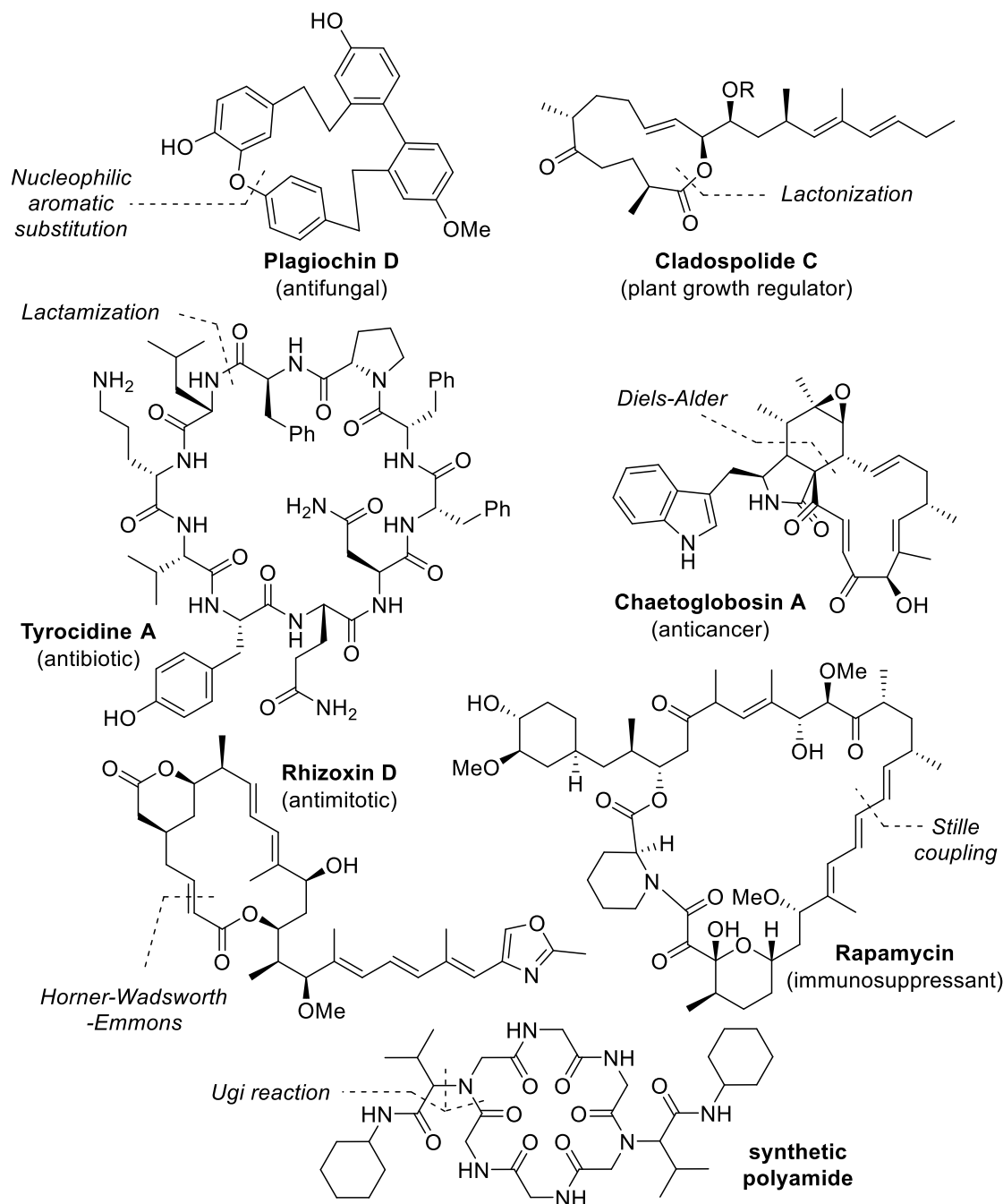


Figure 1.2 Disconnection strategies for the synthesis of macrocycles.

¹⁶ (a) Fürstner, A., *Acc. Chem. Res.* **2014**, *47*, 925-938. (b) Lonsdale, D. E.; Bell, C. A.; Monteiro, M. J., *Macromolecules* **2010**, *43*, 3331-3339. (c) Lonsdale, D. E.; Monteiro, M. J., *J. Polym. Sci. A* **2010**, *48*, 4496-4503. (d) Gradillas, A.; Pérez-Castells, J., *Angew. Chem. Int. Ed.* **2006**, *45*, 6086-6101. (e) Nicolaou, K. C.; Bulger Paul, G.; Sarlah, D., *Angew. Chem. Int. Ed.* **2005**, *44*, 4442-4489.

¹⁷ (a) Isidro-Llobet, A.; Murillo, T.; Bello, P.; Cilibrizzi, A.; Hodgkinson, J. T.; Galloway, W. R. J. D.; Bender, A.; Welch, M.; Spring, D. R., *Proc. Natl. Acad. Sci.* **2011**, *108*, 6793. (b) Terrett, N. K., *Drug Discov. Today Technol.* **2010**, *7*, e97-e104. (c) Kleiner, R. E.; Dumelin, C. E.; Tiu, G. C.; Sakurai, K.; Liu, D. R., *J. Am. Chem. Soc.* **2010**, *132*, 11779-11791. (d) Wessjohann, L. A.; Rivera, D. G.; Vercillo, O. E., *Chem. Rev.* **2009**, *109*, 796-814.

However, in order to achieve an efficient ring closure, the preorganization of the acyclic precursor is a key parameter as a suitable conformation is necessary to facilitate the encounter of the terminal sites. In the case where no favorable intrinsic preorganization is available, the use of an external template can induce a more adapted conformation, leading to the expected ring closure reaction.^{10b} As the key step for the cyclization is an intramolecular process, the concentration of the reagents can also be critical. Dilution needs to be kept at a concentration for which the intramolecular process remains kinetically favored over intermolecular pathways such as oligomerization or polymerization. Another important drawback originates from the molecular complexity of certain linear precursors. Indeed, to access them, long synthetic sequences may be required, comprising usually multiple protection and deprotection steps, influencing the overall yield.^{10b} For these reasons, efficient macrocyclization reactions remain challenging.

1.2.2 Macrocycles with supramolecular abilities

Particularly, an important family of macrocycles is the class of derivatives with supramolecular abilities usually containing multiple heteroatoms such as oxygen, nitrogen or sulfur with a recurrent motif (**Figure 1.3**). Within this class, crown ethers are the most famous ones, and will be presented in the next section. Three other types of structures can be mentioned with, first, the calix[*n*]arenes formed by condensation of phenols with formaldehyde – which can be further functionalized for diverse applications.¹⁸ Then, cyclodextrins which are natural cyclic oligosaccharide cages are synthesized by a 1,4-linkage of D-glucose units (typically 6 to 8 units).¹⁹ Their hydrophobic cavity is well adapted for the encapsulation of small organic molecules. Finally, another class of supramolecular cages are the cucurbit[*n*]urils.²⁰ They are readily prepared by condensation of glycoluril and formaldehyde. They present the advantage of having also an

¹⁸ (a) Gutsche, C. D., *Calixarenes: An Introduction*. The Royal Society of Chemistry: Cambridge, U.K., **2008**. (b) Kim, J. S.; Quang, D. T., *Chem. Rev.* **2007**, *107*, 3780-3799. (c) Böhmer, V., *Angew. Chem. Int. Ed.* **1995**, *34*, 713-745.

¹⁹ (a) Prochowicz, D.; Kornowicz, A.; Lewiński, J., *Chem. Rev.* **2017**, *117*, 13461-13501. (b) Crini, G., *Chem. Rev.* **2014**, *114*, 10940-10975. (c) Li, J.; Loh, X. J., *Adv. Drug Deliv. Rev.* **2008**, *60*, 1000-1017. (d) Del Valle, E. M. M., *Process Biochem.* **2004**, *39*, 1033-1046.

²⁰ (a) Assaf, K. I.; Nau, W. M., *Chem. Soc. Rev.* **2015**, *44*, 394-418. (b) Lagona, J.; Mukhopadhyay, P.; Chakrabarti, S.; Isaacs, L., *Angew. Chem. Int. Ed.* **2005**, *44*, 4844-4870. (c) Lee, J. W.; Samal, S.; Selvapalam, N.; Kim, H.-J.; Kim, K., *Acc. Chem. Res.* **2003**, *36*, 621-630.

internal hydrophobic cavity and polar rims designed for the binding of amphiphilic molecules. The simple and readily available starting materials required, allied with the single step synthesis, render this class of macrocycles easily accessible. Moreover, the repetition of the motif favor efficient encapsulation and complexation of guest molecules or atoms. The size of the ring can also be varied by adaptation of the concentration of the reagents. Therefore, the main applications of such receptors can be found in the field of chemical analysis as host-guest systems for chemical sensing, recognition or in catalysis.

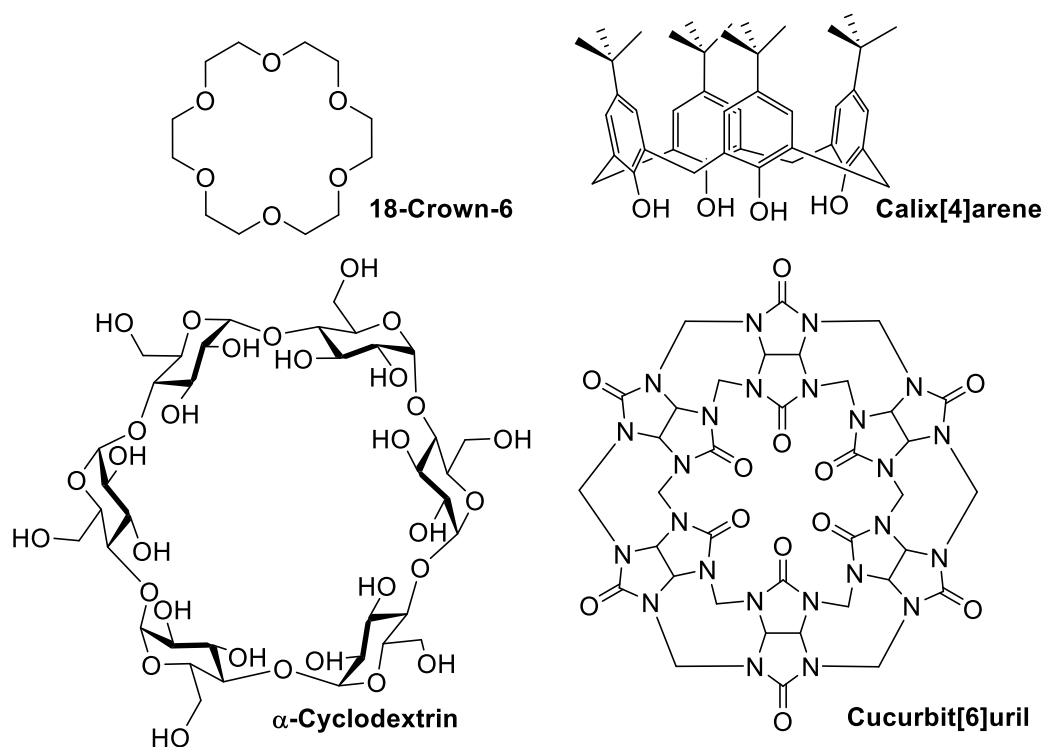


Figure 1.3 Typical macrocycles with supramolecular abilities.

1.3 Polyether macrocycles

Polyether macrocycles have always received a particular attention either from the synthetic point of view or from the binding properties, opening the way to the development of supramolecular chemistry.^{1,21} Various ring sizes (typically 9- to 24-membered ring) can be found with different substitutions or functionalizations (**Figure 1.4**).²² The crown ethers are a particular subgroup in the family of polyether macrocycles, defined as a cyclic succession of ethylene oxide moieties with possibly various functionalizations. Among them, the cryptands differ by their bridge bicyclic nature. For all the series, the oxygen atoms can be (partially) replaced by other heteroatoms such as nitrogen (aza crown ether) or sulfur atoms (thia crown ethers) and lead to complementary binding properties.

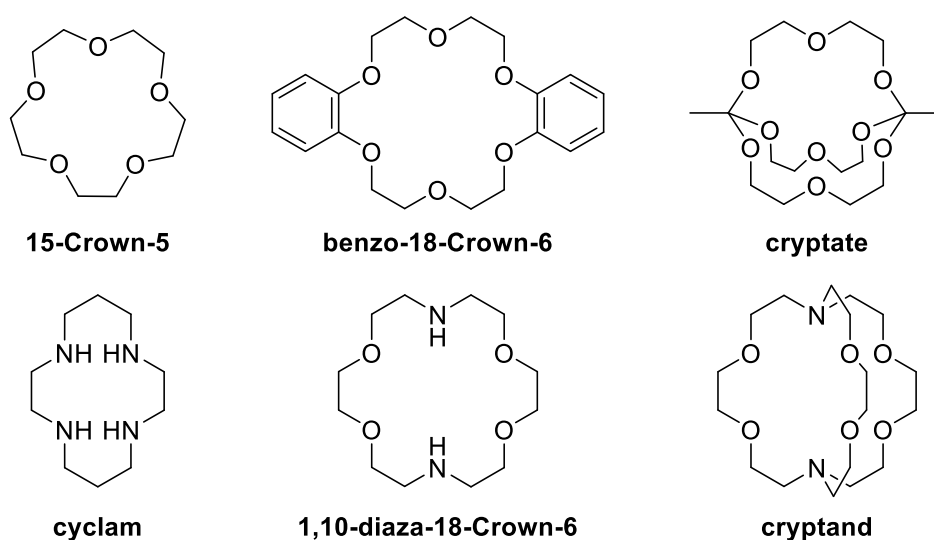


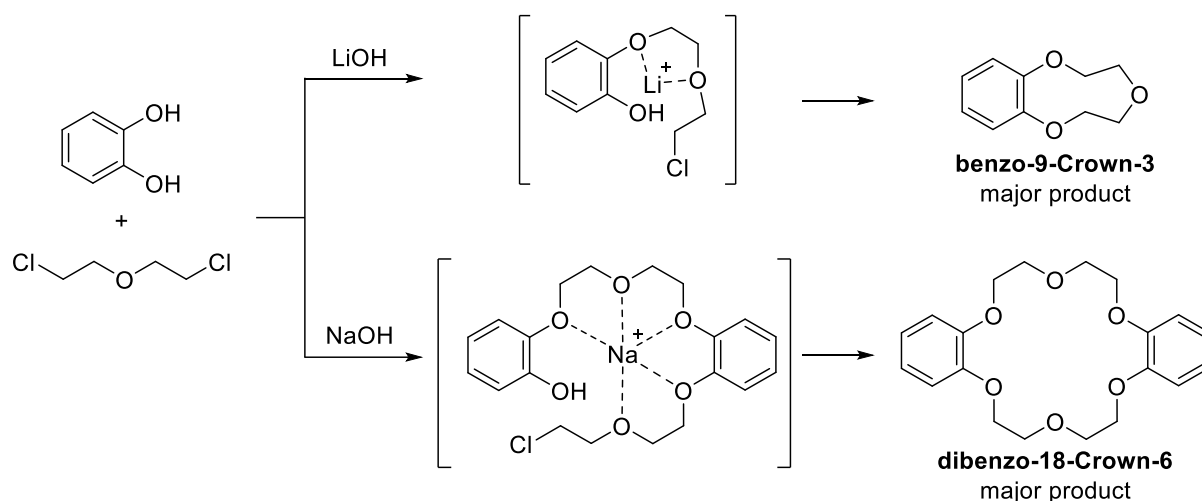
Figure 1.4 Examples (aza)-crown ethers and cryptands.

²¹ Pedersen, C. J., *J. Am. Chem. Soc.* **1967**, 89, 2495-2496.

²² (a) Bradshaw Jerald, S.; Krakowiak, K. E.; Izatt Reed, M., *Chemistry of Heterocyclic Compounds: Aza-Crown Macrocycles*. John Wiley & Son, Ltd.: New York, **2009**. (b) Gokel, G. W., *Crown Ethers and Cryptands*. Royal Society of Chemistry: Cambridge, U.K., **1991**. (c) Weber, E.; Patai, S.; Rappoport, Z., *Crown Ethers and Analogs*. Wiley: Chichester, U.K., **1989**.

1.3.1 Synthesis of crown ethers

Crown ethers are usually synthesized through nucleophilic substitution reactions.²³ Their preparation is a classical example of templated assisted synthesis – the ring size of the macrocyclic product being highly dependent of the cationic template used. The cation (metal ion or ammonium) allows by coordination the wrapping of the acyclic precursor to favor the ring closure step into the expected ring size. For instance, selective synthesis of **benzo-9-Crown-3** or **dibenzo-18-Crown-6** can be reached by mixing catechol and bis(2-chloroethyl) ether with lithium or sodium hydroxide respectively. (**Scheme 1.2**).²⁴



Scheme 1.2 Templated assisted synthesis of crown ethers.

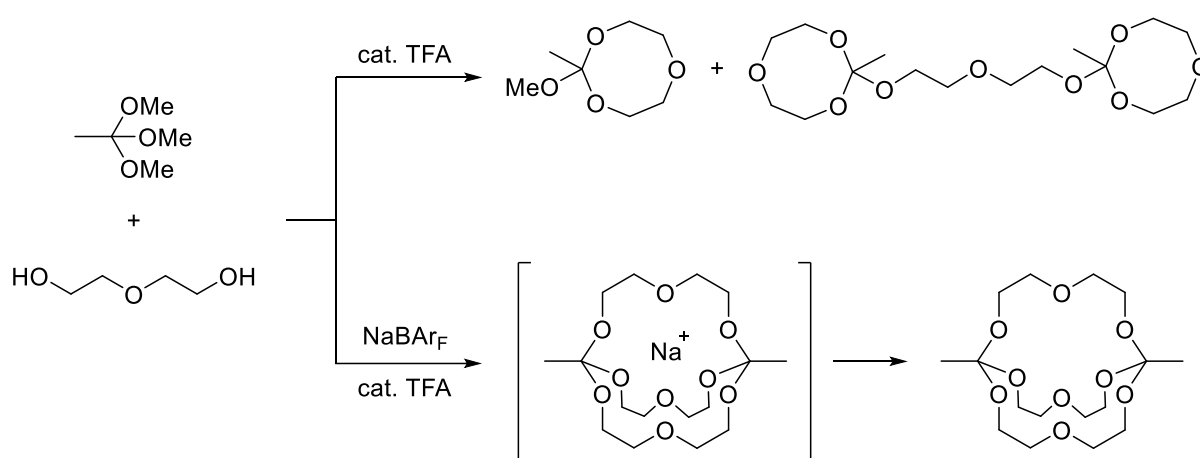
Most of these synthetic approaches are variations of the Williamson ether synthesis: diols are used as nucleophiles and the leaving group can vary from halogens (Cl, Br, I) to sulfonyl groups (Ms, Ts). The concentration of the diverse components of the reaction have a huge influence on the yield of the macrocycles and often high dilutions are required for an efficient synthesis. One way to prevent the high dilution issues is the slow addition of the reagents in order to keep a low effective concentration of the reactive species (addition slower than the rate of

²³ Christensen, J. J.; Eatough, D. J.; Izatt, R. M., *Chem. Rev.* **1974**, 74, 351-384.

²⁴ (a) Khazaei, A.; Saednia, S.; Borazjani, M. K.; Saien, J.; Kiani, M.; Afkhami, A., *Supramol. Sci.* **2014**, 26, 88-93. (b) Pedersen, C. J., *Org. Synth.* **1988**, Coll. Vol 6, 395-400. (c) Gokel, G. W.; Cram, D. J.; Liotta, C. L.; Harris, H. P.; Cook, F. L., *Org. Synth.* **1977**, Coll. Vol. 6, 301-303.

polymerization).^{24a} An alternative strategy uses phase transfer catalysis advantageously with this type of reaction condition. The substrate is contained in the organic phase at a relatively high concentration while the base stays in the polar phase. The reaction occurs thus at the interface maintaining the reactive activated species in low concentration all along the reaction.²⁵

Recently, a different methodology was proposed by Von Delius and coworkers to synthesize cryptate in one step using orthoesters exchange procedure.²⁶ The presence of a metal ion is crucial to the formation of the bicyclic structures, otherwise leading to medium sized rings (**Scheme 1.3**).



Scheme 1.3 Templated synthesis of cryptate.²⁶

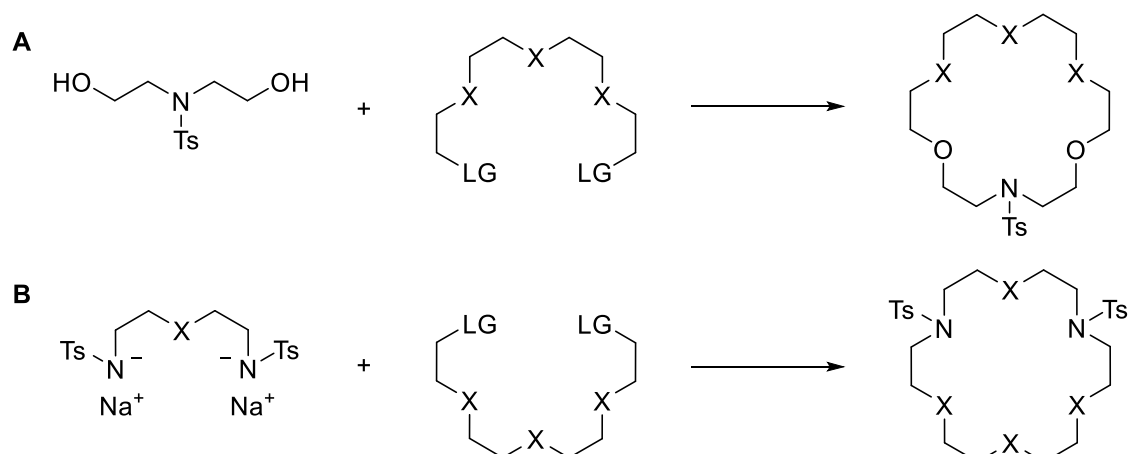
Aza containing macrocycles can be synthesized similarly to crown ethers using nucleophilic substitutions. Two approaches are possible starting from (i) diols already bearing protected nitrogen atom intramolecularly (**Scheme 1.4A**) or (ii) diamino precursors acting as nucleophile for the closures.²⁷ For the second strategy, tosyl protected nitrogens are usually selected for the Richman-Atkins procedure (**Scheme 1.4B**).²⁸

²⁵ Bogaschenko, T.; Basok, S.; Kulygina, C.; Lyapunov, A.; Lukyanenko, N., *Synthesis* **2002**, 2002, 2266-2270.

²⁶ (a) Low, H.; Mena-Osteritz, E.; von Delius, M., *Chem. Sci.* **2018**, 9, 4785-4793. (b) Shyshov, O.; Brachvogel, R. C.; Bachmann, T.; Srikantharajah, R.; Segets, D.; Hampel, F.; Puchta, R.; von Delius, M., *Angew. Chem. Int. Ed.* **2016**, 56, 776-781. (c) Brachvogel, R.-C.; Hampel, F.; von Delius, M., *Nat. Commun.* **2015**, 6, 7129.

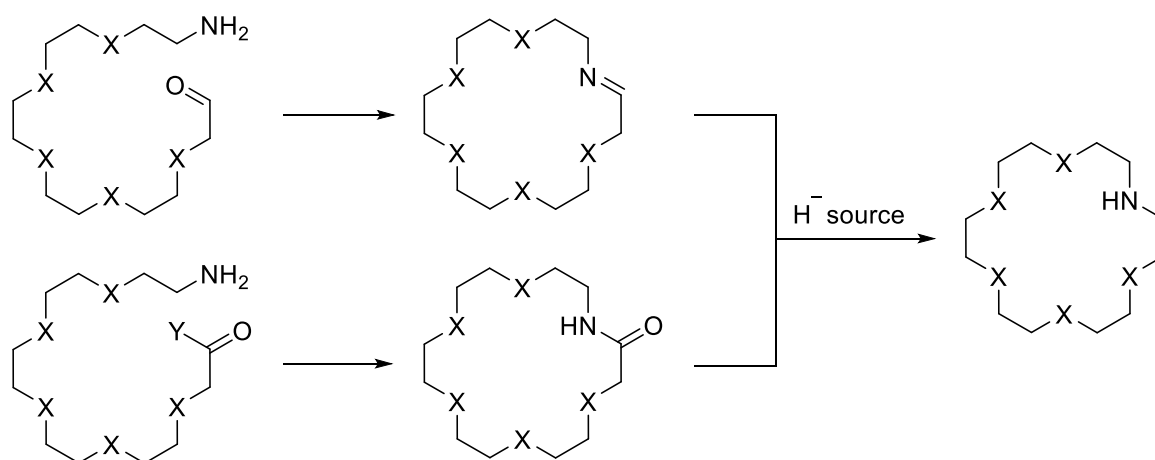
²⁷ (a) Krakowiak, K. E.; Bradshaw, J. S.; Zamecka-Krakowiak, D. J., *Chem. Rev.* **1989**, 89, 929-972. (b) Hancock, R. D.; Martell, A. E., *Chem. Rev.* **1989**, 89, 1875-1914.

²⁸ Atkins, T. J.; Richman, J. E.; Oettle, W. F. O., *Org. Synth.* **1988**, Coll. Vol. 6, 652-661.



Scheme 1.4 Synthesis of aza-crown ethers (LG = OTs, OMs, Cl, I; X = O, N, C).²⁸

Also, a large number of aza-macrocycles are synthesized in two consecutive steps by, first, intramolecular condensations of amines with aldehydes or carboxylic acid derivatives for the formation of cyclic imines or amides respectively. The products are then reduced with hydride reagents, for instance, to afford the corresponding aza-crown ether (**Scheme 1.5**).²⁷



Scheme 1.5 Strategies for the synthesis of aza-containing macrocycles (X = O, N, C).

Cryptands are usually synthesized by bridging strategies from the monocyclic diaza-macrocycles presented above. A different approach takes advantage of the functionalization of dibenzo-crown ethers to anchor the bridge chain. **Figure 1.5** presents two examples proposed by Smith and Huang of such an approach.²⁹

²⁹ (a) Zhu, K.; Wu, L.; Yan, X.; Zheng, B.; Zhang, M.; Huang, F., *Chem. Eur. J.* **2010**, *16*, 6088-6098. (b) Deetz, M. J.; Shang, M.; Smith, B. D., *J. Am. Chem. Soc.* **2000**, *122*, 6201-6207.

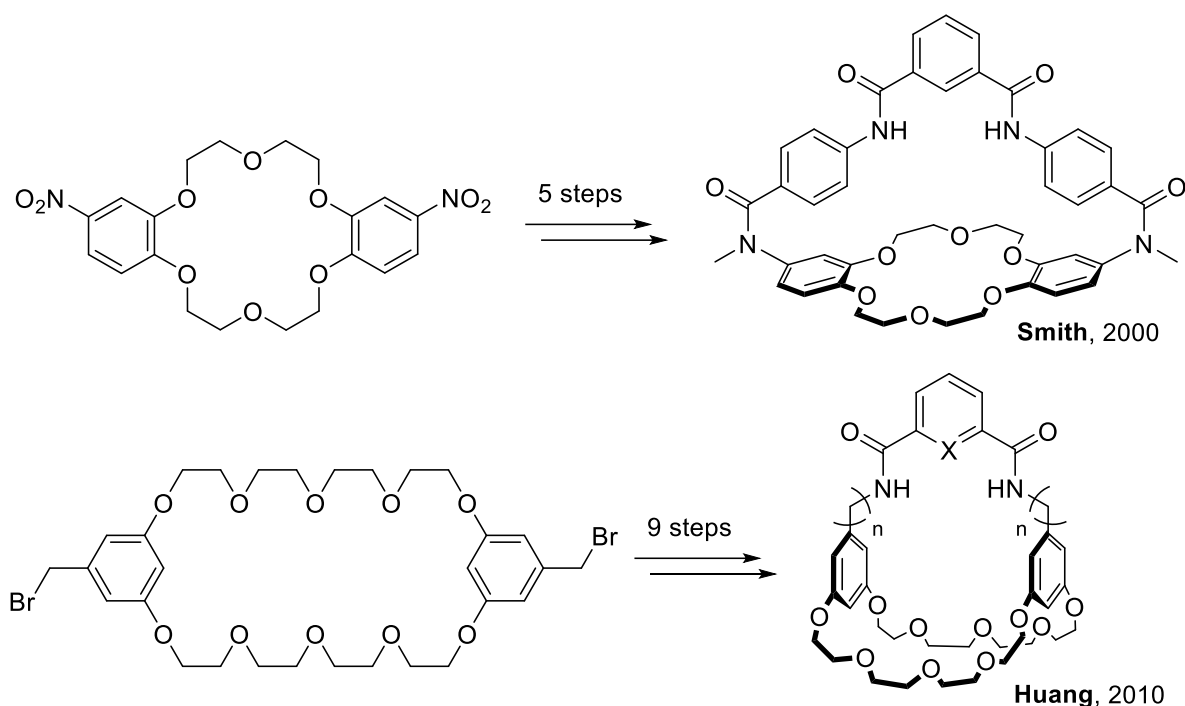


Figure 1.5 Examples of cryptands by Smith and Huang groups.²⁹

1.3.2 Applications of crown ethers and related compounds

The ability of crown ethers to efficiently bind cations has led to the development of many applications. **Figure 1.6** shows the binding constants ($\log K = 0.6$ to 3.6) of different mono- and divalent metal ions as well as ammonium ion with **dicyclohexyl-18-Crown-6** in water.²³ Therefore, crown ethers and their derivatives are mainly used as sensors for the quantification of such ions.^{8a,30} They can be applied as ion selective substrate for artificial transmembrane channels.^{2b, 30}

³⁰ Gokel, G. W.; Leevy, W. M.; Weber, M. E., *Chem. Rev.* **2004**, *104*, 2723-2750.

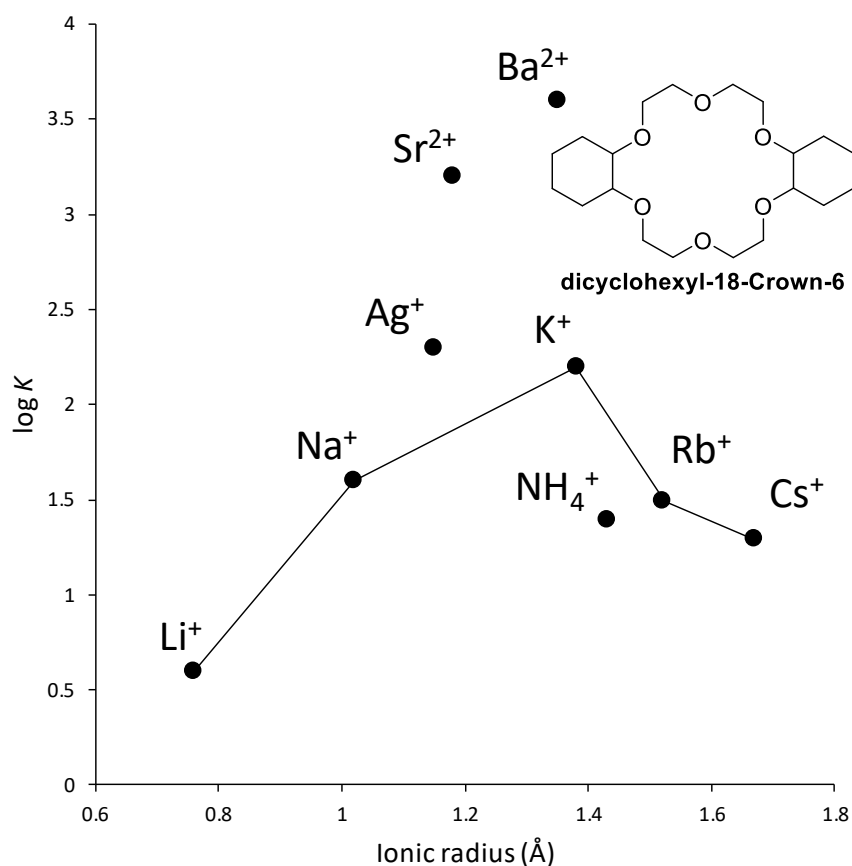


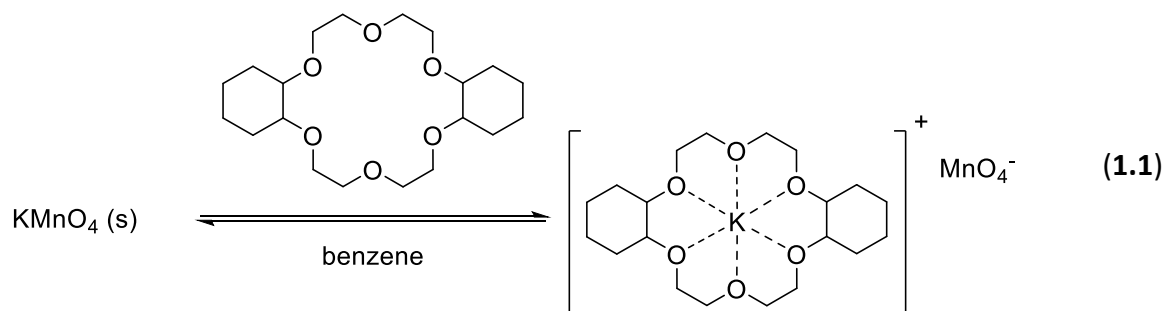
Figure 1.6 Binding constant as a function of ionic radii for dicyclohexyl-18-Crown-6 in water.²³

Phase transfer catalysis (PTC) is one possible application.³¹ Crown ethers usually allow the transfer of a salt to the organic phase in which reactions occur. The macrocycle helps solubilize salts that are usually not soluble in the reaction conditions (organic solvents) and thus reaction rates are drastically increased. Potassium salts such as KF or KOH in organic apolar solvents (toluene, CH₂Cl₂, etc.) are usually well adapted for such systems.³² The first example of such transfer properties was reported by Sam and Simmons in 1972 when they mixed KMnO₄ salt and **dicyclohexyl-18-Crown-6** in benzene. The normally insoluble salt became soluble in the presence of the crown ether as observed by the coloration of the solution (**equation 1.1**).³³

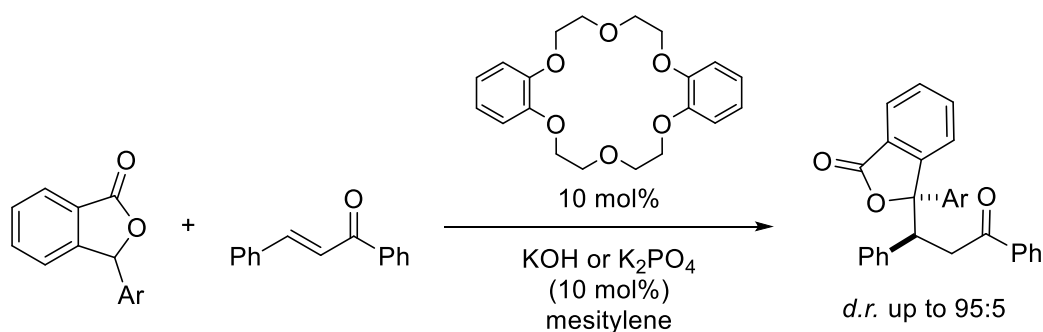
³¹ (a) Dehmlow, E. V.; Dehmlow, S. S., *Phase transfer catalysis*. VCH - Weinheim: New York, **1993**. (b) Starks, C. M.; Liotta, C. L., *Phase transfer catalysis: principles and techniques*. Academic Press ed.; **1978**. (c) Weber, W.; Gokel, G. W., *Phase Transfer Catalysis in Organic Synthesis*. Springer-Verlag Berlin: Heidelberg, **1977**.

³² Sam, D. J.; Simmons, H. E., *J. Am. Chem. Soc.* **1974**, *96*, 2252-2253.

³³ Sam, D. J.; Simmons, H. E., *J. Am. Chem. Soc.* **1972**, *94*, 4024-4025.



As an example, the diastereoselective Michael addition of 3-aryl-phthalides to chalcones catalyzed by **dibenzo-18-Crown-6** was proposed by Della Sala (**Scheme 1.6**).³⁴ Finally, larger crown ethers (*i.e.* 24- to 32-membered rings) are exploited as key structures in rotaxanes. This class of assemblies finds applications for instance as sensors, switches, encapsulation for target molecules and molecular motors.³⁵



Scheme 1.6 Diastereoselective Michael additions catalyzed by dibenzo-18-crown-6.³⁴

³⁴ Sicignano, M.; Dentoni Litta, A.; Schettini, R.; De Riccardis, F.; Pierri, G.; Tedesco, C.; Izzo, I.; Della Sala, G., *Org. Lett.* **2017**, *19*, 4383-4386.

³⁵ (a) Jamieson, E. M. G.; Modicom, F.; Goldup, S. M., *Chem. Soc. Rev.* **2018**, *47*, 5266-5311. (b) Pairault, N.; Barat, R.; Tranoy-Opalinski, I.; Renoux, B.; Thomas, M.; Papot, S., *C. R. Chim.* **2016**, *19*, 103-112. (c) Xue, M.; Yang, Y.; Chi, X.; Yan, X.; Huang, F., *Chem. Rev.* **2015**, *115*, 7398-7501. (d) Yang, W.; Li, Y.; Liu, H.; Chi, L.; Li, Y., *Small* **2012**, *8*, 504-516. (e) Ma, X.; Tian, H., *Chem. Soc. Rev.* **2010**, *39*, 70-80. (f) Harada, A.; Hashidzume, A.; Yamaguchi, H.; Takashima, Y., *Chem. Rev.* **2009**, *109*, 5974-6023.

1.4 Chiral crown ethers

Only achiral (or racemic) crown ethers were discussed until now. However, over the years, chiral (enantioenriched) crown ethers were specifically developed and their relevant syntheses and applications will be presented briefly in this section.

1.4.1 Structures of chiral crown ethers

Quite logically, most of chiral crown ethers are synthesized by Williamson procedures (nucleophilic substitution, see **Scheme 1.2**) and are structurally based on chiral diols. A classification in two classes or subgroups can be considered with (i) synthetic (non-natural) chiral diols on one side (**Figure 1.7**) and (ii) naturally occurring enantiopure diols precursors on the other (**Figure 1.8**). Cram proposed first a chiral crown ether **1.1** using (*S*)-BINOL as a chiral backbone,³⁶ many research groups proposed then variations on the resulting structure over the years.³⁷ Diols derived from functionalized natural products such as camphor or tartaric acid were also used as synthons (**1.2** and **1.3**).³⁸ Similarly to this strategy, Johnston and Jeminet independently introduced spirocyclic units in the structure (**1.4**).³⁹ Alternatively more simple diols can be used as for **1.5** and **1.6**.⁴⁰

³⁶ (a) Tarnowski, T. L.; Cram, D. J., *J. Chem. Soc. Chem. Comm.* **1976**, 661-663. (b) Helgeson, R. C.; Timko, J. M.; Moreau, P.; Peacock, S. C.; Mayer, J. M.; Cram, D. J., *J. Am. Chem. Soc.* **1974**, *96*, 6762-6763. (c) Kyba, E. B.; Koga, K.; Sousa, L. R.; Siegel, M. G.; Cram, D. J., *J. Am. Chem. Soc.* **1973**, *95*, 2692-2693.

³⁷ (a) Pham, T. S.; Czirok, J. B.; Balázs, L.; Pál, K.; Kubinyi, M.; Bitter, I.; Jászay, Z., *Tetrahedron: Asymmetry* **2011**, *22*, 480-486. (b) Tang, D.-H.; Chen, X.-M.; Fan, Q.-H., *J. Chem. Res.* **2004**, *2004*, 702-703. (c) Kiyooka, S.-i.; Tada, M.; Kan, S.; Fujio, M., *Bull. Chem. Soc. Jpn.* **1996**, *69*, 2595-2601. (d) Curtis, W. D.; King, R. M.; Stoddart, J. F.; Jones, G. H., *J. Chem. Soc. Chem. Comm.* **1976**, 284-285.

³⁸ (a) Irurre, J.; Riera, M.; Cintora, M., *Synthesis* **2001**, *2001*, 0647-0653. (b) Brisdon, B. J.; England, R.; Mahon, M. F.; Reza, K.; Sainsbury, M., *J. Chem. Soc. Perkin Trans. 2* **1995**, 1909-1914. (c) Brunet, E.; Poveda, A. M.; Rabasco, D.; Oreja, E.; Font, L. M.; Batra, M. S.; Rodriguez-Ubis, J. C., *Tetrahedron: Asymmetry* **1994**, *5*, 935-948.

³⁹ (a) Garcia, C.; Pointud, Y.; Jeminet, G.; Dugat, D.; Beltran, J. L., *Tetrahedron: Asymmetry* **1998**, *9*, 4253-4265. (b) A. Brimble, M.; D. Johnston, A., *J. Chem. Soc. Perkin Trans. 1* **1998**, 265-270.

⁴⁰ (a) Nakamura, M.; Taniguchi, T.; Ishida, N.; Hayashi, K.; Muraoka, M.; Nakatsuji, Y., *Tetrahedron* **2011**, *67*, 9298-9304. (b) Turgut, Y.; Aral, T.; Hosgoren, H., *Tetrahedron: Asymmetry* **2009**, *20*, 2293-2298. (c) Nakatsuji, Y.; Nakahara, Y.; Nagamiya, K.; Itoh, Y.; Uesugi, K.; Ishida, N.; Muraoka, M.; Kida, T.; Akashi, M., *Synthesis* **2007**, *2007*, 2973-2978. (d) Škarić, V.; Čaplar, V.; Škarić, Đ.; Žinić, M., *Helv. Chim. Acta* **2004**, *75*, 493-506. (e) Correa, H. W.; Scott, L. J.,

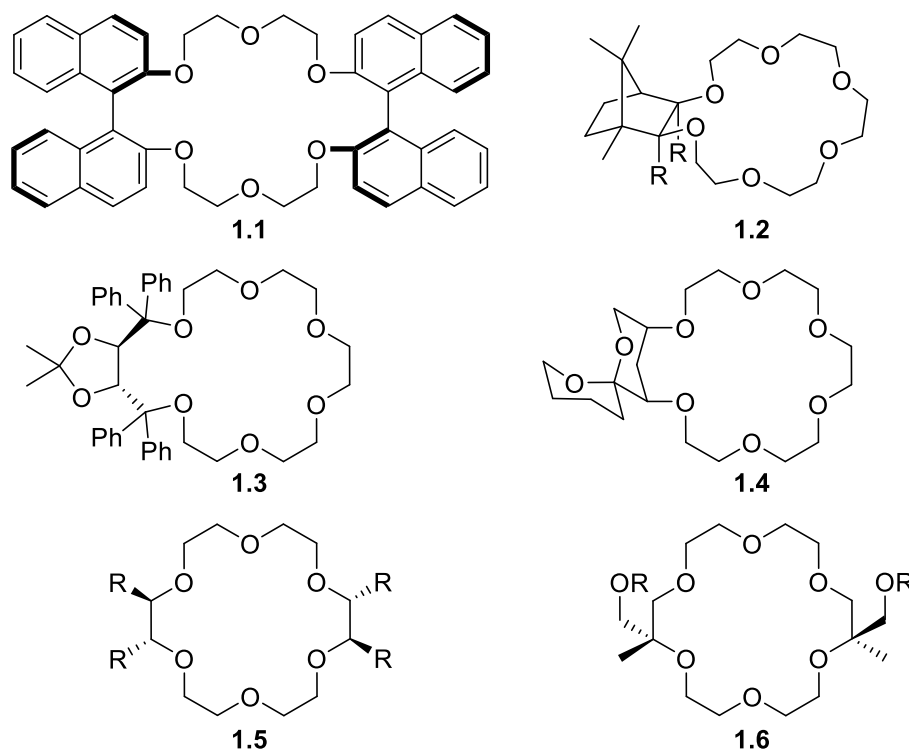


Figure 1.7 Chiral crown ethers based on synthetic diols (R = Bn, Ph, Ac, Me).

In the subgroup of natural diols, mainly L-tartrate or carbohydrates such as D-mannitol, D-glucose, D-xylose or lactose were used as building blocks (**1.7-1.12**).⁴¹ The building blocks are introduced either within the ring (**1.10**) or attached externally. The straightforward availability of these natural products as enantiopure building blocks and the well-documented protection strategies have rendered their use popular.⁴²

Molecules **2004**, *9*. (f) Hirose, K.; Fujiwara, A.; Matsunaga, K.; Aoki, N.; Tobe, Y., *Tetrahedron: Asymmetry* **2003**, *14*, 555-566. (g) Lee, C.-W.; Jung, E. J.; Lee, S. J.; Ahn, K. H.; Kim, K. S., *J. Org. Chem.* **2000**, *65*, 7225-7227. (h) Naemura, K.; Miyabe, H.; Shingai, Y.; Tobe, Y., *J. Chem. Soc. Perkin Trans. 1* **1993**, 1073-1077. (i) Huszthy, P.; Oue, M.; Bradshaw, J. S.; Zhu, C. Y.; Wang, T.; Dalley, N. K.; Curtis, J. C.; Izatt, R. M., *J. Org. Chem.* **1992**, *57*, 5383-5394.

⁴¹ Stoddart, J. F., *Chem. Soc. Rev.* **1979**, *8*, 85-142.

⁴² (a) Faltin, F.; Fehring, V.; Miethchen, R., *Synthesis* **2002**, 2002, 1851-1856. (b) Faltin, F.; Fehring, V.; Kadyrov, R.; Arrieta, A.; Schareina, T.; Selke, R.; Miethchen, R., *Synthesis* **2001**, 2001, 0638-0646. (c) Espínola, C. G.; Pérez, R.; Martín, J. D., *Org. Lett.* **2000**, *2*, 3161-3164. (d) Dumont-Hornebeck, B.; Joly, J.-P.; Coulon, J.; Chapleur, Y., *Carbohydr. Res.* **1999**, *320*, 147-160. (e) Dumont-Hornebeck, B.; Joly, J.-P.; Coulon, J.; Chapleur, Y., *Carbohydr. Res.* **1999**, *321*, 214-227. (f) Miethchen, R.; Fehring, V., *Synthesis* **1998**, 1998, 94-98. (g) Mani, N. S.; Kanakamma, P. P., *Tetrahedron Lett.* **1994**, *35*, 3629-3632. (h) Miethchen, R.; Gabriel, T., *Chem. Ber.* **1993**, *126*, 2309-2316. (i) Vicent, C.; Bosso, C.; Cano, F. H.; De Paz, J. L. G.; Foces-Foces, C.; Jimenez-Barbero, J.; Martín-Lomas, M.; Penades, S., *J. Org. Chem.* **1991**, *56*, 3614-3618. (j) A. Laidler, D.; Stoddart, J. F.; Wolstenholme, J. B., *Tetrahedron Lett.* **1979**, *20*, 465-468. (k) Curtis, W. D.; Laidler, D. A.; Stoddart, J. F.; Jones, G. H., *J. Chem. Soc. Chem. Comm.* **1975**, 833-835.

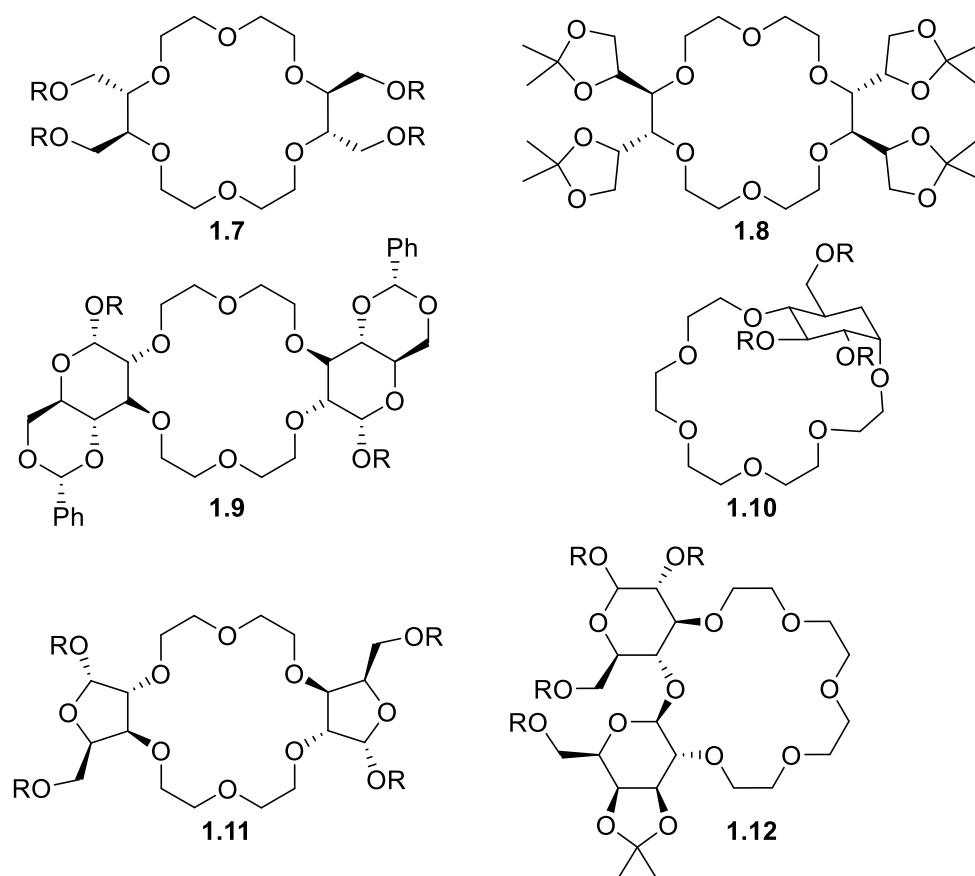


Figure 1.8 Chiral crown ethers based on natural diols (R = Bn, Ph, Ac, Me).

1.4.2 Applications of chiral crown ethers

1.4.2.1 Recognition and extraction of ammonium salts

Chiral crown ethers have found many applications in diverse fields taking advantage of the positive interactions of the polyether ring, with organic cations in particular. The most direct application is the stereoselective recognition of compounds such as chiral (racemic) amines or amino acids in their acidic form.⁴³ For instance, the occurrence of chiral discriminations have

⁴³ (a) Späth, A.; König, B., *Beilstein J. Org. Chem.* **2010**, 6, 32. (b) Zhang, X. X.; Bradshaw, J. S.; Izatt, R. M., *Chem. Rev.* **1997**, 97, 3313-3362.

been evidenced using methods like ^1H NMR spectroscopy,⁴⁴ electronic spectroscopic techniques (UV-Vis, ECD, or fluorescence),⁴⁵ potentiometry⁴⁶ or mass spectrometry.⁴⁷ In addition and importantly, these techniques can be used for the determination of the enantiopurity of chiral products.

As a consequence of this ability to interact differently with each enantiomer, chiral crown ethers were employed as complexing agent for the enantiomeric extraction of salts.⁴⁸ The racemic salts are generally solubilized in water and put in contact with an organic phase (*i.e.* chloroform) containing the macrocycle, the partition of each enantiomer between the two phases defining the efficiency of the extractor on a chiral selector.

⁴⁴ (a) Liu, L.-z.; He, C.-h.; Yang, L.; Huang, Y.; Wu, Q.; Duan, W.-g.; Wang, H.-s.; Pan, Y.-m., *Tetrahedron* **2014**, *70*, 9545-9553. (b) Nakatsuji, Y.; Nakahara, Y.; Muramatsu, A.; Kida, T.; Akashi, M., *Tetrahedron Lett.* **2005**, *46*, 4331-4335. (c) Wenzel, T. J.; Freeman, B. E.; Sek, D. C.; Zopf, J. J.; Nakamura, T.; Yongzhu, J.; Hirose, K.; Tobe, Y., *Anal. Bioanal. Chem.* **2004**, *378*, 1536-1547. (d) Wenzel, T. J.; Thurston, J. E.; Sek, D. C.; Joly, J.-P., *Tetrahedron: Asymmetry* **2001**, *12*, 1125-1130. (e) Weinstein, S. E.; Vining, M. S.; Wenzel, T. J., *Magn. Reson. Chem.* **1998**, *35*, 273-280.

⁴⁵ (a) Huszthy, P.; Farkas, V.; Tóth, T.; Székely, G.; Hollósi, M., *Tetrahedron* **2008**, *64*, 10107-10115. (b) Tsubaki, K.; Tanima, D.; Nuruzzaman, M.; Kusumoto, T.; Fuji, K.; Kawabata, T., *J. Org. Chem.* **2005**, *70*, 4609-4616. (c) Karakaplan, M.; Aral, T., *Tetrahedron: Asymmetry* **2005**, *16*, 2119-2124. (d) Turgut, Y.; Elif Sahin, I.; Hoşgören, H., *J. Chem. Res.* **2004**, *2004*, 605-607. (e) Turgut, Y.; Hoşgören, H., *Tetrahedron: Asymmetry* **2003**, *14*, 3815-3818. (f) Demirel, N.; Bulut, Y., *Tetrahedron: Asymmetry* **2003**, *14*, 2633-2637. (g) Samu, E.; Huszthy, P.; Somogyi, L.; Hollósi, M., *Tetrahedron: Asymmetry* **1999**, *10*, 2775-2795. (h) Somogyi, L.; Huszthy, P.; Bradshaw Jerald, S.; Izatt Reed, M.; Hollósi, M., *Chirality* **1998**, *9*, 545-549. (i) Naemura, K.; Ogasahara, K.; Hirose, K.; Tobe, Y., *Tetrahedron: Asymmetry* **1997**, *8*, 19-22. (j) Lehn, J.-M.; Sirlin, C., *J. Chem. Soc. Chem. Comm.* **1978**, 949-951.

⁴⁶ (a) Behr, J. P.; Lehn, J. M.; Vierling, P., *Helv. Chim. Acta* **2004**, *65*, 1853-1867. (b) Luk'yanenko, N. G.; Lobach, A. V.; Leus, O. N.; Titova, N. Y., *Russ. J. Org. Chem.* **2002**, *38*, 895-899.

⁴⁷ (a) Wollschlager, J. M.; Simon, K.; Gaedke, M.; Schalley, C. A., *Chem. Commun.* **2018**, *54*, 4967-4970. (b) Sharma, G. V. M.; Reddy, V. G.; Krishna, P. R., *Tetrahedron: Asymmetry* **1999**, *10*, 3777-3784. (c) Sawada, M.; Takai, Y.; Yamada, H.; Sawada, M.; Yamaoka, H.; Azuma, T.; Fujioka, T.; Kawai, Y.; Tanaka, T., *Chem. Commun.* **1998**, 1569-1570. (d) Sawada, M.; Takai, Y.; Yamada, H.; Nishida, J.; Kaneda, T.; Arakawa, R.; Okamoto, M.; Hirose, K.; Tanaka, T.; Naemura, K., *J. Chem. Soc. Perkin Trans. 2* **1998**, 701-710. (e) Dearden, D. V.; Dejsupa, C.; Liang, Y.; Bradshaw, J. S.; Izatt, R. M., *J. Am. Chem. Soc.* **1997**, *119*, 353-359. (f) Pócsfalvi, G.; Lipták, M.; Huszthy, P.; Bradshaw, J. S.; Izatt, R. M.; Vékey, K., *Anal. Chem.* **1996**, *68*, 792-795. (g) Sawada, M.; Takai, Y.; Yamada, H.; Hirayama, S.; Kaneda, T.; Tanaka, T.; Kamada, K.; Mizooku, T.; Takeuchi, S., *J. Am. Chem. Soc.* **1995**, *117*, 7726-7736. (h) Sawada, M.; Okumura, Y.; Shizuma, M.; Takai, Y.; Hidaka, Y.; Yamada, H.; Tanaka, T.; Kaneda, T.; Hirose, K., *J. Am. Chem. Soc.* **1993**, *115*, 7381-7388.

⁴⁸ (a) Rubio, O. H.; Taouil, R.; Muniz, F. M.; Monleon, L. M.; Simon, L.; Sanz, F.; Moran, J. R., *Org. Biomol. Chem.* **2017**, *15*, 477-485. (b) Pietraszkiewicz, M.; Koźbial, M.; Pietraszkiewicz, O., *J. Memb. Sci.* **1998**, *138*, 109-113. (c) Nazhaoui, M.; Joly, J.-P.; Kitane, S.; Berrada, M., *J. Chem. Soc. Perkin Trans. 1* **1998**, 3845-3850. (d) Pietraszkiewicz, M.; Kozbial, M., *J. Incl. Phenom. Moll. Recognit. Chem.* **1992**, *14*, 339-348. (e) Gehin, D.; Di Cesare, P.; Gross, B., *J. Org. Chem.* **1986**, *51*, 1906-1908. (f) Peacock, S. C.; Cram, D. J., *J. Chem. Soc. Chem. Comm.* **1976**, 282-284. (g) Curtis, W. D.; Laidler, D. A.; Stoddart, J. F.; Jones, G. H., *J. Chem. Soc. Chem. Comm.* **1975**, 835-837.

1.4.2.2 Chiral stationary phases in chromatography

Chiral crown ethers can be further functionalized with groups able to link the macrocycle to a coated surface. The whole entity can then be employed as chiral stationary phase (CSP) for chromatographic separations.⁴⁹ One possibility is to use BINOL-based crown ethers (**1.1**). Another version of chiral selectors is synthesized from a tetracarboxylic acid derivative (**1.5**, R = COOH) and is depicted in **Figure 1.9**. Chiral amines and amino acids can then be efficiently separated depending on their affinity with the CSP either in GC or in HPLC.⁵⁰

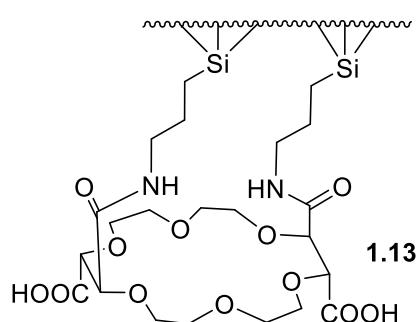


Figure 1.9 Chiral crown ether as CSP for chromatographic separation.

1.4.2.3 Chiral crown ethers as asymmetric catalysts

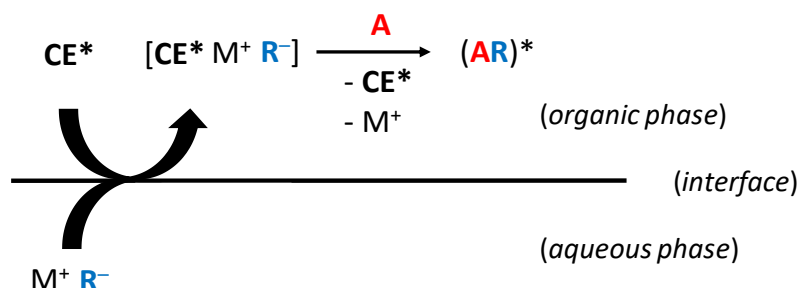
The ability of chiral crown ether to bind metal ions was also exploited in asymmetric phase transfer catalysis.⁵¹ With a neutral chiral crown ethers (**CE***), salts, made of achiral cation (**M⁺**, typically a small metallic ion) and a prochiral anion (**R⁻**), are solubilized in the organic layer by complexation with the **CE***. The resulting ion pair [**CE* M⁺ R⁻**] lies within the cavity formed by the chiral backbone of the crown ether (**Scheme 1.7**). Upon addition of a reagent able to interact

⁴⁹ (a) Mohammadzadeh Kakhki, R., *J. Incl. Phenom. Macrocycl. Chem.* **2013**, 75, 11-22. (b) Choi, H. J.; Hyun, M. H., *J. Liq. Chromatogr. Relat. Technol.* **2007**, 30, 853-875.

⁵⁰ (a) Paik, M.-J.; Kang, J. S.; Huang, B.-S.; Carey, J. R.; Lee, W., *J. Chromatogr. A* **2013**, 1274, 1-5. (b) Cho, Y. J.; Choi, H. J.; Hyun, M. H., *J. Chromatogr. A* **2008**, 1191, 193-198. (c) Hyun, M. H.; Tan, G.; Xue, J. Y., *J. Chromatogr. A* **2005**, 1097, 188-191. (d) Zhou, X.-C.; Yan, H.; Chen, Y.-Y.; Wu, C.-Y.; Lu, X.-R., *J. Chromatogr. A* **1996**, 753, 269-277. (e) Joly, J. P.; Moll, N., *J. Chromatogr. A* **1990**, 521, 134-140. (f) Joly, J.-P.; Gross, B., *Tetrahedron Lett.* **1989**, 30, 4231-4234. (g) Sousa, L. R.; Sogah, G. D. Y.; Hoffman, D. H.; Cram, D. J., *J. Am. Chem. Soc.* **1978**, 100, 4569-4576.

⁵¹ (a) Shirakawa, S.; Maruoka, K., *Angew. Chem. Int. Ed.* **2013**, 52, 4312-4348. (b) Ooi, T.; Maruoka, K., *Angew. Chem. Int. Ed.* **2007**, 46, 4222-4266.

with R^- , the chiral environment ought to induce a stereoselective reaction and hence the enantioinduction observed in the final product. A brief overview of the asymmetric PTC catalyzed by chiral crown ethers is presented herein.



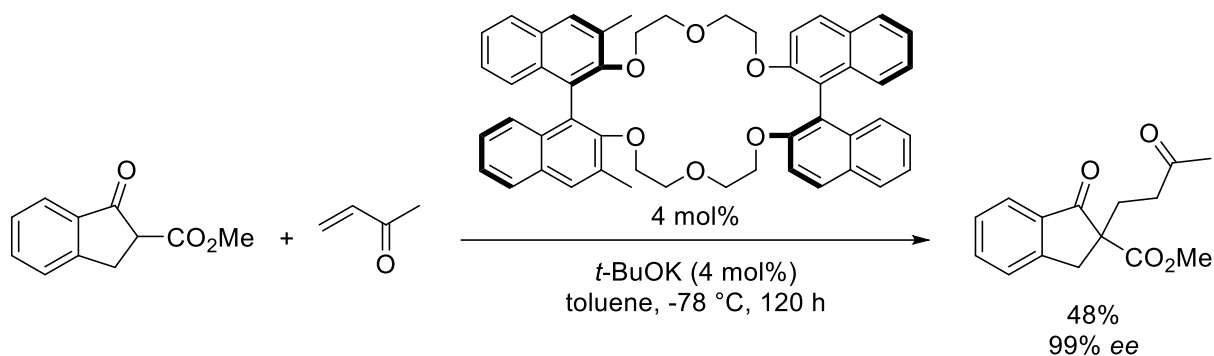
Scheme 1.7 Schematic asymmetric PTC model with chiral crown ethers (CE^*).

Accordingly, Cram and coworkers reported in 1981 the asymmetric Michael addition of cyclic ketoesters to methyl vinyl ketone catalyzed by a BINOL-based crown ether complexing *t*-BuOK. The reaction yields the addition products in medium yields but excellent enantioselectivity (**Scheme 1.8**).⁵² In the following years, Penadés, Koga, Pandit, Stoddart and Nair independently employed the same transformation using phenyl acetate derivatives and methyl acrylate to yield the addition product with generally medium to good enantiomeric excesses (*ee*) using mainly carbohydrate-based catalysts.⁵³ Similarly, Kobayashi proposed more recently a 1,4-addition of non-activated amides on α - β -unsaturated amides using a BINOL-based 32-Crown-10 catalyst in very high yield and *ee* (**Scheme 1.9**).⁵⁴ Notably, the preformation of the potassium – crown ether complex was necessary for a good enantioinduction.

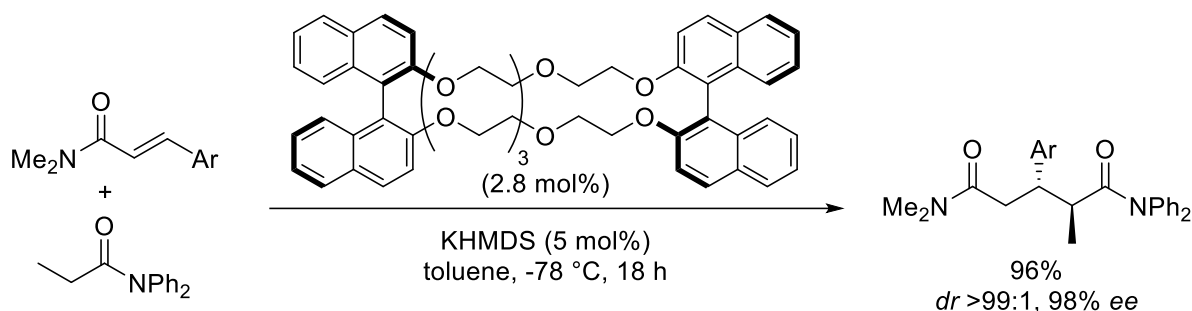
⁵² Cram, D. J.; Sogah, G. D. Y., *J. Chem. Soc. Chem. Comm.* **1981**, 625-628.

⁵³ (a) Kanakamma, P. P.; Mani, N. S.; Maitra, U.; Nair, V., *J. Chem. Soc. Perkin Trans. 1* **1995**, 2339-2344. (b) Crosby, J.; Stoddart, J. F.; Sun, X.; Venner, M. R. W., *Synthesis* **1993**, 1993, 141-145. (c) van Maarschalkerwaart, D. A. H.; Willard, N. P.; Pandit, U. K., *Tetrahedron* **1992**, *48*, 8825-8840. (d) Aoki, S.; Sasaki, S.; Koga, K., *Tetrahedron Lett.* **1989**, *30*, 7229-7230. (e) Alonso-Lopez, M.; Jimenez-Barbero, J.; Martin-Lomas, M.; Penades, S., *Tetrahedron* **1988**, *44*, 1535-1543. (f) Alonso-López, M.; Martin-Lomas, M.; Penadés, S., *Tetrahedron Lett.* **1986**, *27*, 3551-3554.

⁵⁴ (a) Yamashita, Y.; Kobayashi, S., *Chem. Eur. J.* **2017**, *24*, 10-17. (b) Yamashita, Y.; Sato, I.; Suzuki, H.; Kobayashi, S., *Chem. Asian J.* **2015**, *10*, 2143-2146. (c) Suzuki, H.; Sato, I.; Yamashita, Y.; Kobayashi, S., *J. Am. Chem. Soc.* **2015**, *137*, 4336-4339.



Scheme 1.8 Cram's enantioselective Michael addition catalyzed by a chiral crown ether.⁵²



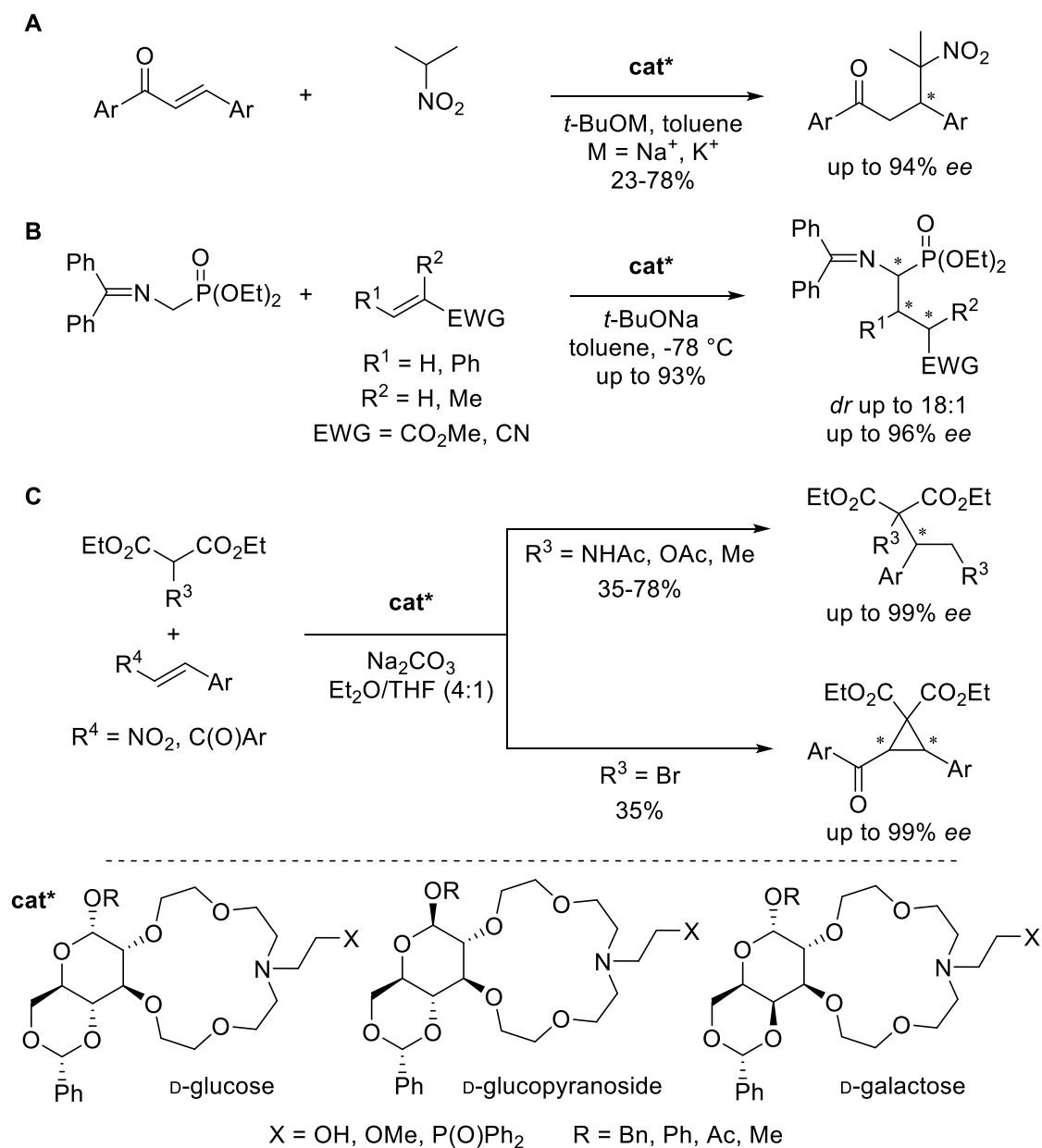
Scheme 1.9 Kobayashi's enantioselective 1,4-addition of amides catalyzed by a chiral crown ether.⁵⁴

The major contribution to the application of chiral crown ethers as catalysts was performed conjointly by the groups of Tőke, Bakó, Keglevich and Jászay. They developed reaction conditions with carbohydrate-based monoaza-15-Crown-5 as phase transfer catalysts. The first reaction studied was an asymmetric Michael addition in PTC conditions. Using D-glucose, D-glucopyranoside or D-galactose monoaza crown ethers catalysts, they proposed the enantioselective 1,4-addition of 2-nitropropane to chalcones with *ee* up to 94% (**Scheme 1.10A**).⁵⁵ Similarly, amino phosphonates were also added to methyl acrylates and acrylonitriles in high yields with high diastereoselectivities and enantioselectivities (**Scheme 1.10B**).⁵⁶ Substituted malonates were then reacted with enones and afforded the addition products in

⁵⁵ (a) Bakó, T.; Bakó, P.; Szöllősy, Á.; Czugler, M.; Keglevich, G.; Tőke, L., *Tetrahedron: Asymmetry* **2002**, *13*, 203-209. (b) Novák, T.; Bakó, P.; Keglevich, G.; Dobó, A.; Vékey, K.; Tőke, L., *J. Incl. Phenom. Macrocycl. Chem.* **2001**, *40*, 207-212. (c) Bakó, P.; Novák, T.; Ludányi, K.; Pete, B.; Tőke, L.; Keglevich, G., *Tetrahedron: Asymmetry* **1999**, *10*, 2373-2380. (d) Bakó, P.; Vizvárdi, K.; Bajor, Z.; Vizvárdi, K.; Tőke, L., *Chem. Commun.* **1998**, 1193-1194. (e) Bakó, P.; Kiss, T.; Tőke, L., *Tetrahedron Lett.* **1997**, *38*, 7259-7262.

⁵⁶ (a) Pham, S. T.; Rapi, Z.; Bakó, P.; Petnehazy, I.; Stirling, A.; Jaszay, Z., *New J. Chem.* **2017**, *41*, 14945-14953. (b) Jászay, Z.; Pham, T. S.; Németh, G.; Bakó, P.; Petneházy, I.; Tőke, L., *Synlett* **2009**, *2009*, 1429-1432.

moderate yields and high *ee* (**Scheme 1.10C**).⁵⁷ When bromo-substituted malonates were used, the corresponding cyclopropanes was obtained instead of the addition product also in moderate yields and excellent enantioselectivity.

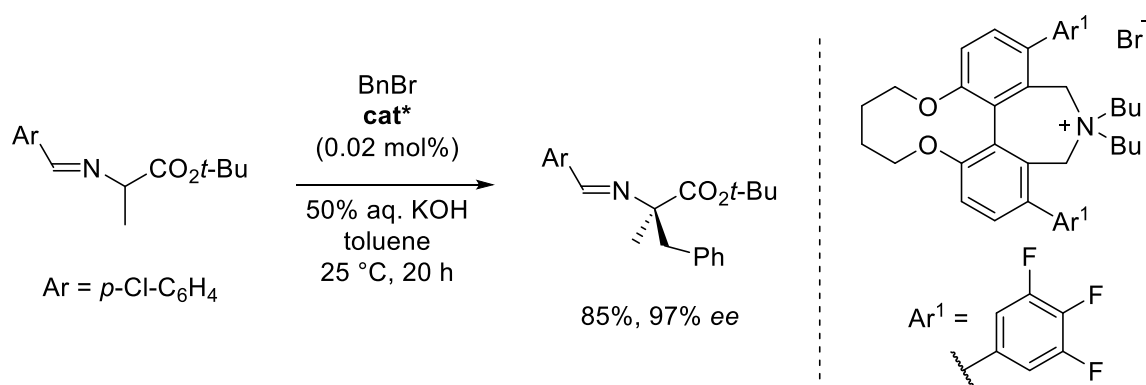


Scheme 1.10 Enantioselective Michael additions with carbohydrate-based aza-crown ethers.

⁵⁷ (a) Rapi, Z.; Grün, A.; Nemcsok, T.; Hessz, D.; Kállay, M.; Kubinyi, M.; Keglevich, G.; Bakó, P., *Tetrahedron: Asymmetry* **2016**, 27, 960-972. (b) Rapi, Z.; Grün, A.; Keglevich, G.; Stirling, A.; Bakó, P., *New J. Chem.* **2016**, 40, 7856-7865. (c) Bakó, P.; Rapi, Z.; Grün, A.; Nemcsok, T.; Hegedűs, L.; Keglevich, G., *Synlett* **2015**, 26, 1847-1851.

The common feature of these sugar-based catalysts are the presence of a lariat chain introduced on the nitrogen atom. This chain contains a terminal alcohol, methoxy or phosphono group and seems to influence the binding of the metal ion (Na^+ or K^+) and thus increases the enantioinduction of the reactions.^{55b, c}

One of the major drawbacks of the use of chiral crown ethers in asymmetric PTC appears in these latest studies. Indeed, relatively high amounts of catalyst are required for efficient enantioinduction, typically 7 to 10 mol% of crown ether. In comparison, chiral quaternary ammonium salt use 1 mol% in similar reactions.⁵¹ An example with catalyst loading down to 0.02 mol% was even proposed in 2012 by Maruoka using a bridged biphenyl ammonium salt to catalyzed alkylation of a protected alanine (**Scheme 1.11**).⁵⁸ Moreover, excellent enantioselectivity are often limited to a couple of specific substrates while most of the other substrates exhibit only moderate to low *ee*.



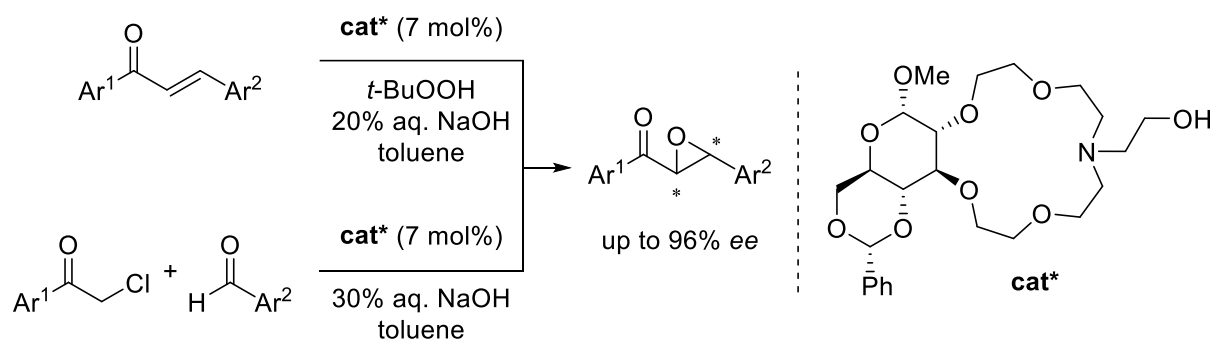
Scheme 1.11 Enantioselective alkylation of protected alanine.⁵⁸

Using the same D-glucose-based catalyst (7 mol%), the formation of α,β -epoxyketones was then investigated by the same groups (**Scheme 1.12**). Two approaches were considered – the first one by direct epoxidation of chalcones with *tert*-butyl hydroperoxide⁵⁹ and the second one

⁵⁸ Kubota, Y.; Shirakawa, S.; Inoue, T.; Maruoka, K., *Tetrahedron Lett.* **2012**, 53, 3739-3741.

⁵⁹ (a) Makó, A.; Rapi, Z.; Keglevich, G.; Szöllősy, Á.; Drahos, L.; Hegedűs, L.; Bakó, P., *Tetrahedron: Asymmetry* **2010**, 21, 919-925. (b) Bakó, T.; Bakó, P.; Keglevich, G.; Bombicz, P.; Kubinyi, M.; Pál, K.; Bodor, S.; Makó, A.; Tőke, L., *Tetrahedron: Asymmetry* **2004**, 15, 1589-1595.

by addition of chloroacetates to aldehydes (Darzens reaction).⁶⁰ Here again, the inconvenients observed in the Michael additions reactions (narrow scope) have become apparent.



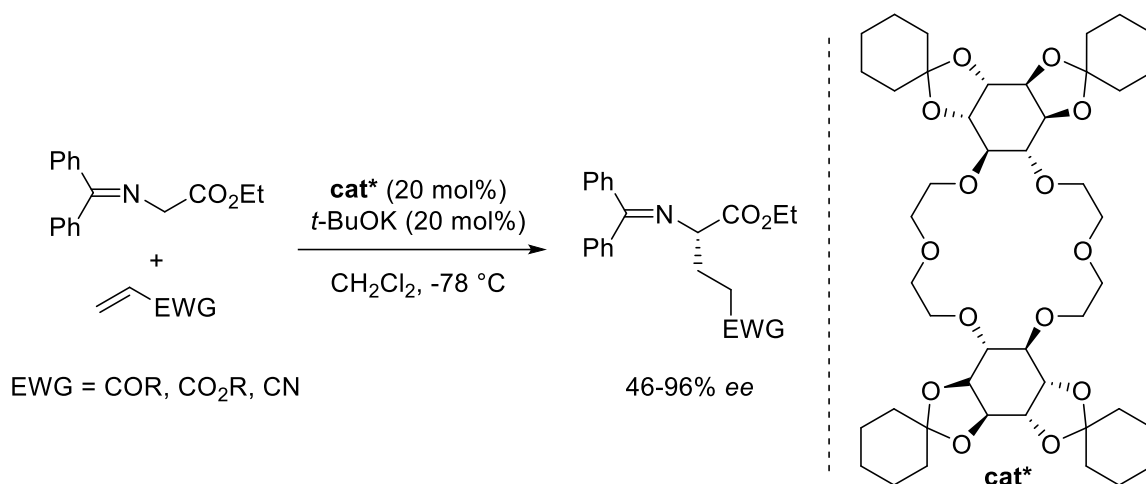
Scheme 1.12 Enantioselective synthesis of α,β -epoxyketones catalyzed by D-glucose-based azacrown ether.

In another unrelated development, the group of Akiyama designed a catalyst based on L-quebrachitol, a naturally occurring optically active cyclitol (**Scheme 1.13**).⁶¹ The researchers demonstrated its asymmetric PTC activity by performing the enantioselective 1,4-addition of protected glycines to acrylates derivatives in generally high *ee* but with relatively high catalyst loading (20 mol%). Finally, Brussee proposed an enantioselective α -hydroxylation of aromatic ketones with molecular oxygen catalyzed by a monoaza-crown ether in moderate enantioselectivities (**Scheme 1.14**).⁶²

⁶⁰ (a) Rapi, Z.; Bakó, P.; Keglevich, G.; Szöllősy, Á.; Drahos, L.; Botyánszki, A.; Holczbauer, T., *Tetrahedron: Asymmetry* **2012**, 23, 489-496. (b) Rapi, Z.; Szabó, T.; Keglevich, G.; Szöllősy, Á.; Drahos, L.; Bakó, P., *Tetrahedron: Asymmetry* **2011**, 22, 1189-1196. (c) Bakó, P.; Rapi, Z.; Keglevich, G.; Szabó, T.; Solti, P. L.; Vígh, T.; Grün, A.; Holczbauer, T., *Tetrahedron Lett.* **2011**, 52, 1473-1476.

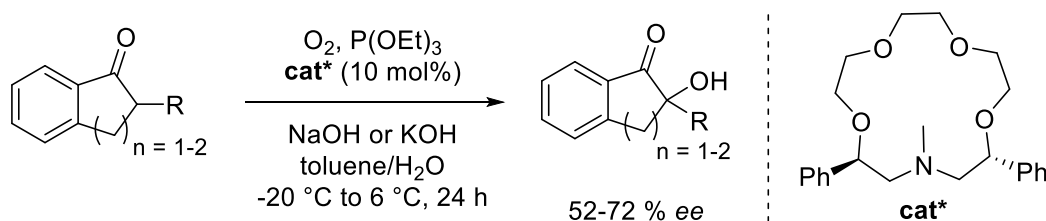
⁶¹ Akiyama, T.; Hara, M.; Fuchibe, K.; Sakamoto, S.; Yamaguchi, K., *Chem. Commun.* **2003**, 1734-1735.

⁶² de Vries, E. F. J.; Ploeg, L.; Colao, M.; Brussee, J.; van der Gen, A., *Tetrahedron: Asymmetry* **1995**, 6, 1123-1132.



Scheme 1.13 Enantioselective Michael addition of glycines on acrylates catalyzed by a chiral crown ether.⁶¹

The effective use of chiral crown ethers in asymmetric phase transfer catalysis has been validated by these studies. However, it was deemed at the beginning of this thesis that there has still place for improvement as efficient processes were achieved with a relative narrow pool of substrates with relatively high catalyst loadings (typically 5 to 20 mol%). The necessity to bring the four components (crown ether, cation, anionic reactive substrate and reagent) together as a complexed ion pair could be an issue in comparison with quaternary ammonium salts (three components: ammonium, anionic reactive substrate and reagent).



Scheme 1.14 Enantioselective α -hydroxylation of aromatic ketones catalyzed by a chiral crown ether.⁶²

1.5 Macrocycles synthesized from diazo precursors

The decomposition of diazo compounds by transition metal catalysis is an efficient way to form electrophilic metal carbenes.⁶³ These species can undergo various transformations including dimerizations, insertions, cyclopropanations, dipolar additions, ylide formations (and subsequent rearrangements). In that context, different strategies were utilized and applied to the synthesis of macrocycles using α -diazocarbonyls compounds as precursors. For instance, McKervy and Doyle proposed independently the use of copper-⁶⁴ or dirhodium-catalyzed⁶⁵ for the formation of macrocycles by intramolecular cross-coupling of diazo acetates (formal dimerization of carbenes) with moderate to good yields (**Figure 1.10**, left). McKervy also synthesized polyether macrocycles of different sizes in moderate yield applying an OH insertion strategies for the key ring closure step (**Figure 1.10**, right).⁶⁶

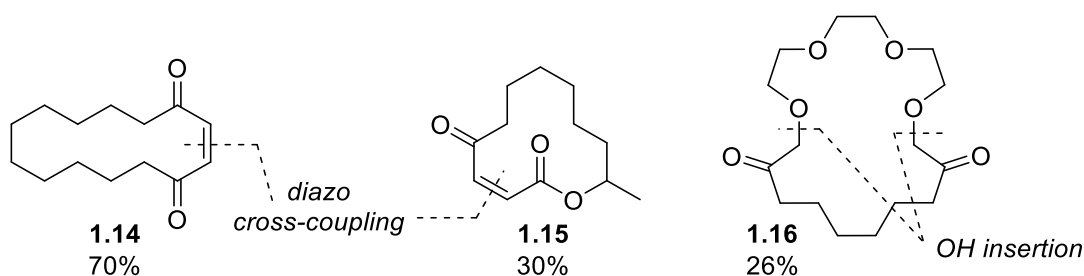


Figure 1.10 Examples of macrocycles formed by dimerization of carbenes or OH insertion.

Metal carbenes formed under dirhodium catalysis are known to undergo cyclopropanation reactions in the presence of double bonds (or cyclopropanation with alkyne). Doyle took advantage of this reactivity to form macrocyclic lactones by intramolecular reaction of α -diazoesters linked to remote alkenes under Rh(II) catalysis (**Scheme 1.15**).⁶⁷

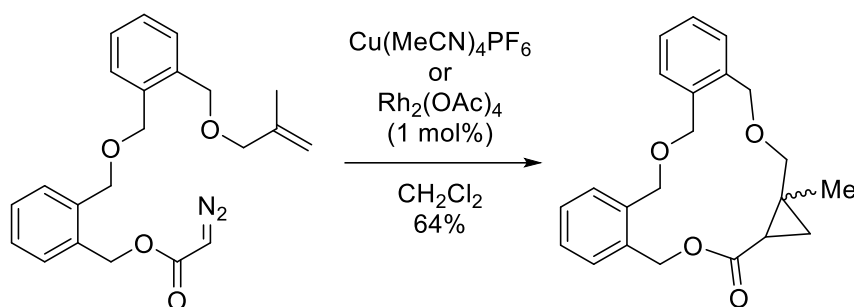
⁶³ Doyle, M. P.; McKervy, M. A., *Modern Catalytic Methods for Organic Synthesis with Diazo Compounds: From Cyclopropanes to Ylides*. John Wiley & Son, Ltd.: New York, **1998**.

⁶⁴ Doyle, M. P.; Hu, W.; Phillips, I. M.; Wee, A. G. H., *Org. Lett.* **2000**, 2, 1777-1779.

⁶⁵ Kulkowit, S.; McKervy, M. A., *J. Chem. Soc. Chem. Comm.* **1978**, 1069-1070.

⁶⁶ Kulkowit, S.; McKervy, M. A., *J. Chem. Soc. Chem. Comm.* **1981**, 616-617.

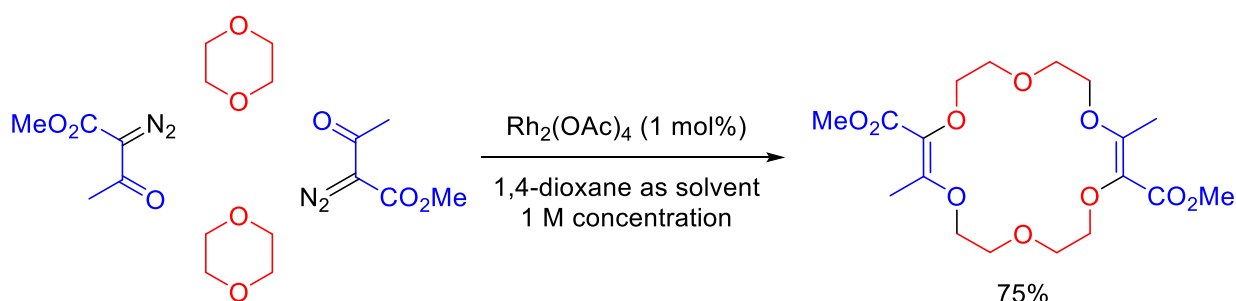
⁶⁷ (a) Doyle, M. P.; Hu, W.; Chapman, B.; Marnett, A. B.; Peterson, C. S.; Vitale, J. P.; Stanley, S. A., *J. Am. Chem. Soc.* **2000**, 122, 5718-5728. (b) Doyle, M. P.; Ene, D. G.; Peterson, C. S.; Lynch, V., *Angew. Chem. Int. Ed.* **1999**, 38, 700-702. (c) Doyle, M. P.; Chapman, B. J.; Hu, W.; Peterson, C. S.; McKervy, M. A.; Garcia, C. F., *Org. Lett.* **1999**, 1,



Scheme 1.15 Macrocycles synthesized by cyclopropanation.^{67a}

1.5.1 Macrocyclization from simple cyclic ethers

Ylides, and in particular oxonium ylides, can be generated by the reaction of metal carbenes and ether moieties.⁶⁸ In that context, our group reported in 2010 the one-pot rhodium(II)-catalyzed synthesis of 18-membered polyether macrocycles by [3+6+3+6] condensations of α -diazo- β -ketoesters and 1,4-dioxane (**Scheme 1.16**).⁶⁹ Products of condensation of THF and THP were reported as well but will be discussed later.



Scheme 1.16 Rh(II)-catalyzed [3+6+3+6] condensation of α -diazo- β -ketoesters and 1,4-dioxane.

1327-1329. (d) Doyle, M. P.; Peterson, C. S.; Protopopova, M. N.; Marnett, A. B.; Parker, D. L.; Ene, D. G.; Lynch, V., *J. Am. Chem. Soc.* **1997**, *119*, 8826-8837. (e) Doyle, M., P.; Peterson, C., S.; Parker, D., L., *Angew. Chem. Int. Ed.* **1996**, *35*, 1334-1336. (f) Doyle, M. P.; Protopopova, M. N.; Poulter, C. D.; Rogers, D. H., *J. Am. Chem. Soc.* **1995**, *117*, 7281-7282.

⁶⁸ (a) Egger, L.; Guénée, L.; Bürgi, T.; Lacour, J., *Adv. Synth. Catal.* **2017**, *359*, 2918-2923. (b) Achard, T.; Tortoreto, C.; Poblador-Bahamonde, A. I.; Guénée, L.; Bürgi, T.; Lacour, J., *Angew. Chem. Int. Ed.* **2014**, *53*, 6140-6144. (c) Tortoreto, C.; Achard, T.; Zeghida, W.; Austeri, M.; Guénée, L.; Lacour, J., *Angew. Chem. Int. Ed.* **2012**, *51*, 5847-5851. (d) Ballesteros-Garrido, R.; Rix, D.; Besnard, C.; Lacour, J., *Chem. Eur. J.* **2012**, *18*, 6626-6631. (e) Austeri, M.; Rix, D.; Zeghida, W.; Lacour, J., *Org. Lett.* **2011**, *13*, 1394-1397.

⁶⁹ Zeghida, W.; Besnard, C.; Lacour, J., *Angew. Chem. Int. Ed.* **2010**, *49*, 7253-7256.

On the contrary to conventional polyether macrocycle syntheses, this transformation occurs at relatively high concentration of diazo reagent (1 M) and under strictly non-templated conditions. This behavior can be explained using the proposed mechanism (**Figure 1.11**). The diazo compound **1.17** is decomposed by the dirhodium catalyst to form an electrophilic metal carbene **A**. Then a cyclic ether (here 1,4-dioxane) acts as a *Lewis* base and generates the metal bound oxonium ylide **B**. After release of the catalyst and formation of the metal free oxonium ylide **C**, this species dimerize to form the **18C6** macrocycle. In order to favor the dimerization, which is a second-order in rate determining step, high concentrations are specifically required. The effect of the concentration on the yield as well as the mechanistic investigations were studied by Daniele Poggiali during his PhD thesis.⁷⁰

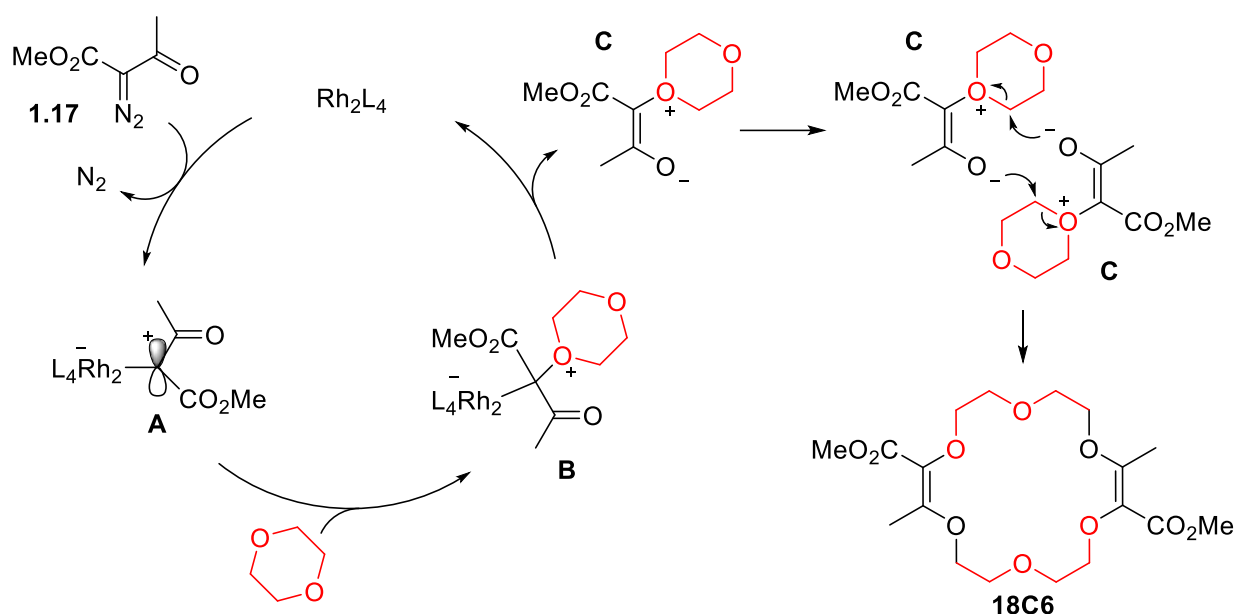


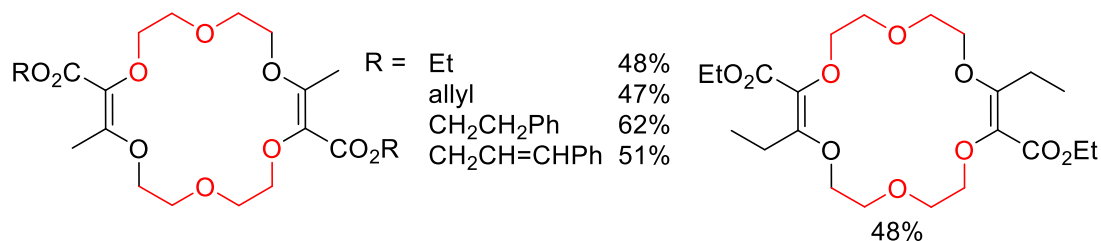
Figure 1.11 Proposed mechanism for the [3+6+3+6] macrocyclization.

The reaction scope is quite general and various diazo reagents can be used to afford the macrocycles in moderate to good yields. The 1,4-dioxane can also be replaced by other 5- and 6- or 7-membered ring ethers such as THF (tetrahydrofuran), THP (tetrahydropyran), or oxepane.

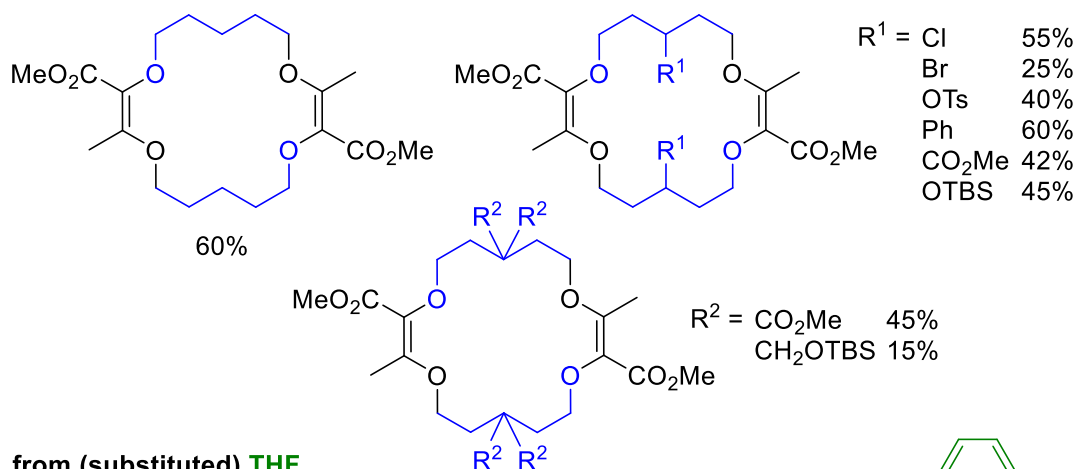
⁷⁰ Poggiali, D., *Mechanistic investigations and development of Rh(II)-catalyzed [3+6+3+6] macrocyclization reactions*, University of Geneva, PhD Thesis, **2016**.

With further functionalized analogs,⁷¹ densely functionalized 16- or 18-membered ring macrocycles can be obtained in moderate to good yields (**Figure 1.12**).⁷²⁻⁷³

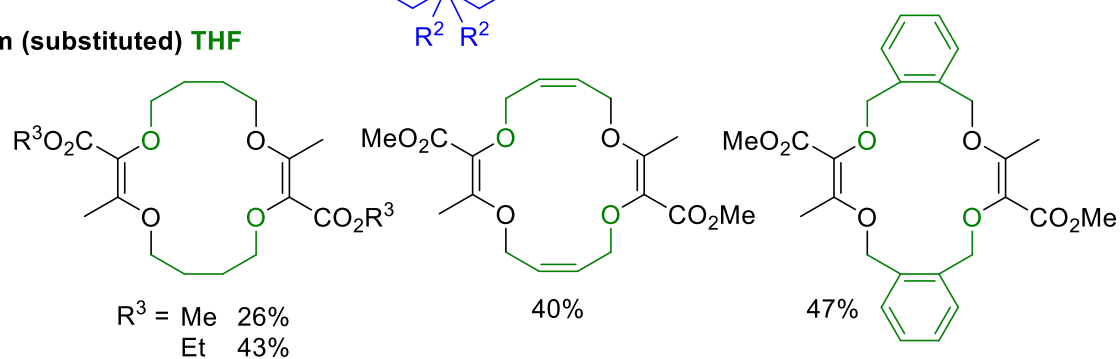
from **1,4-dioxane**



from (substituted) **THP**



from (substituted) **THF**



from **oxepane**

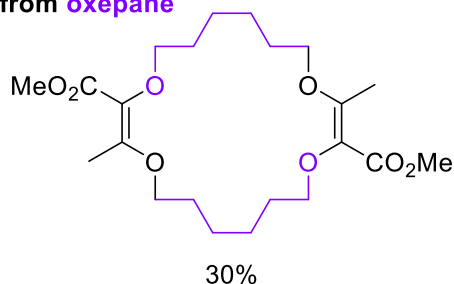


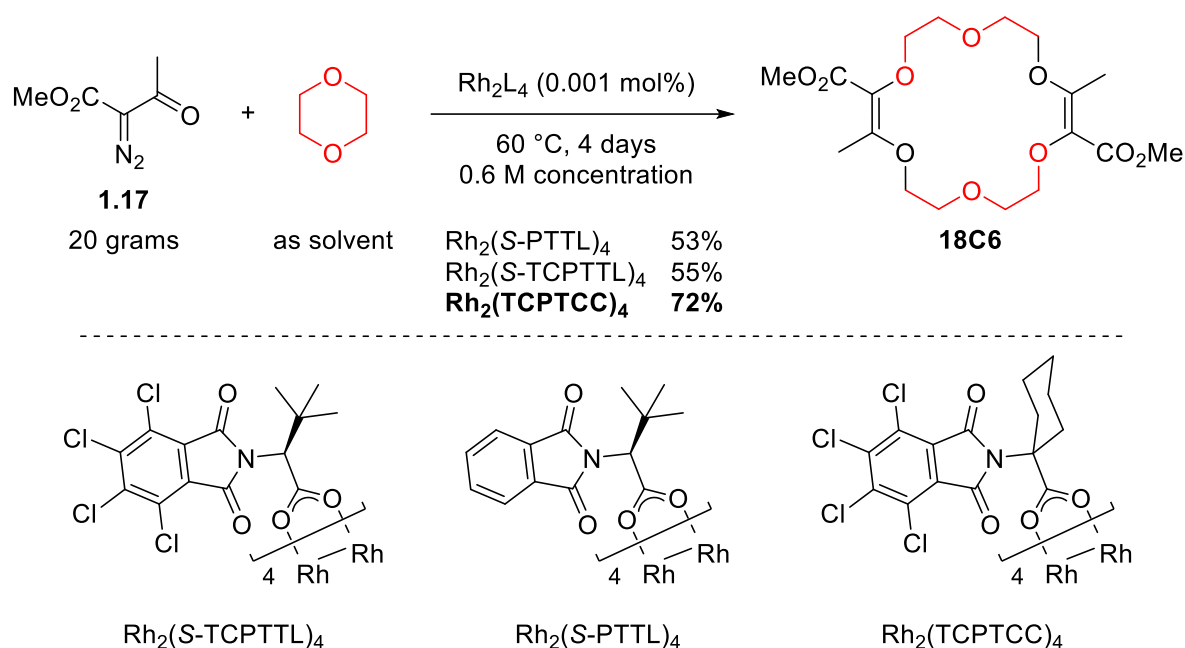
Figure 1.12 Scope of Rh(II)-catalyzed [3+X+3+X] macrocyclization.

⁷¹ Reaction conditions are adapted with 6 equivalents of cyclic ether and toluene as solvent for these substituted substrates.

⁷² In the case of mono-substituted THP, the macrocycle was obtained as a 1:1 mixture of diastereoisomers.

⁷³ Vishe, M.; Hrdina, R.; Guénée, L.; Besnard, C.; Lacour, J., *Adv. Synth. Catal.* **2013**, 355, 3161-3169.

The kinetics of the diazo decomposition of **1.17** was studied with different catalysts using *in situ* infrared (IR) monitoring.^{3a} The $\text{Rh}_2(\text{OAc})_4$ catalyst used originally has shown to induce the slowest reaction rates for the diazo decomposition (0.24 h^{-1}). Changing the catalytic complex to $\text{Rh}_2(\text{Oct})_4$ or $\text{Rh}_2(R\text{-DOSP})_4$ increased the reaction rate by a factor of two (0.54 h^{-1} and 0.55 h^{-1}). Finally, Hashimoto-Ikegami catalysts,⁷⁴ $\text{Rh}_2(\text{S-TCPTTL})_4$ or $\text{Rh}_2(\text{S-PTTL})_4$, showed the highest activity in the decomposition of diazo **1.17** with first-order kinetic constants of 2.63 h^{-1} and 3.39 h^{-1} respectively. Thanks in part to this higher reactivity, it was possible to decrease the amount of catalyst down to 10^{-3} mol\% and perform the macrocyclization on multigram scale. Additionally, using achiral phthalimido-based cyclohexyl-derived $\text{Rh}_2(\text{TCPTCC})_4$ (10^{-3} mol\%), the polyether macrocycle **18C6** was satisfactorily synthesized in 72% yield (**Scheme 1.17**). These optimizations lead to the routine synthesis of **18C6** on large scale, up to 20 grams per batch.

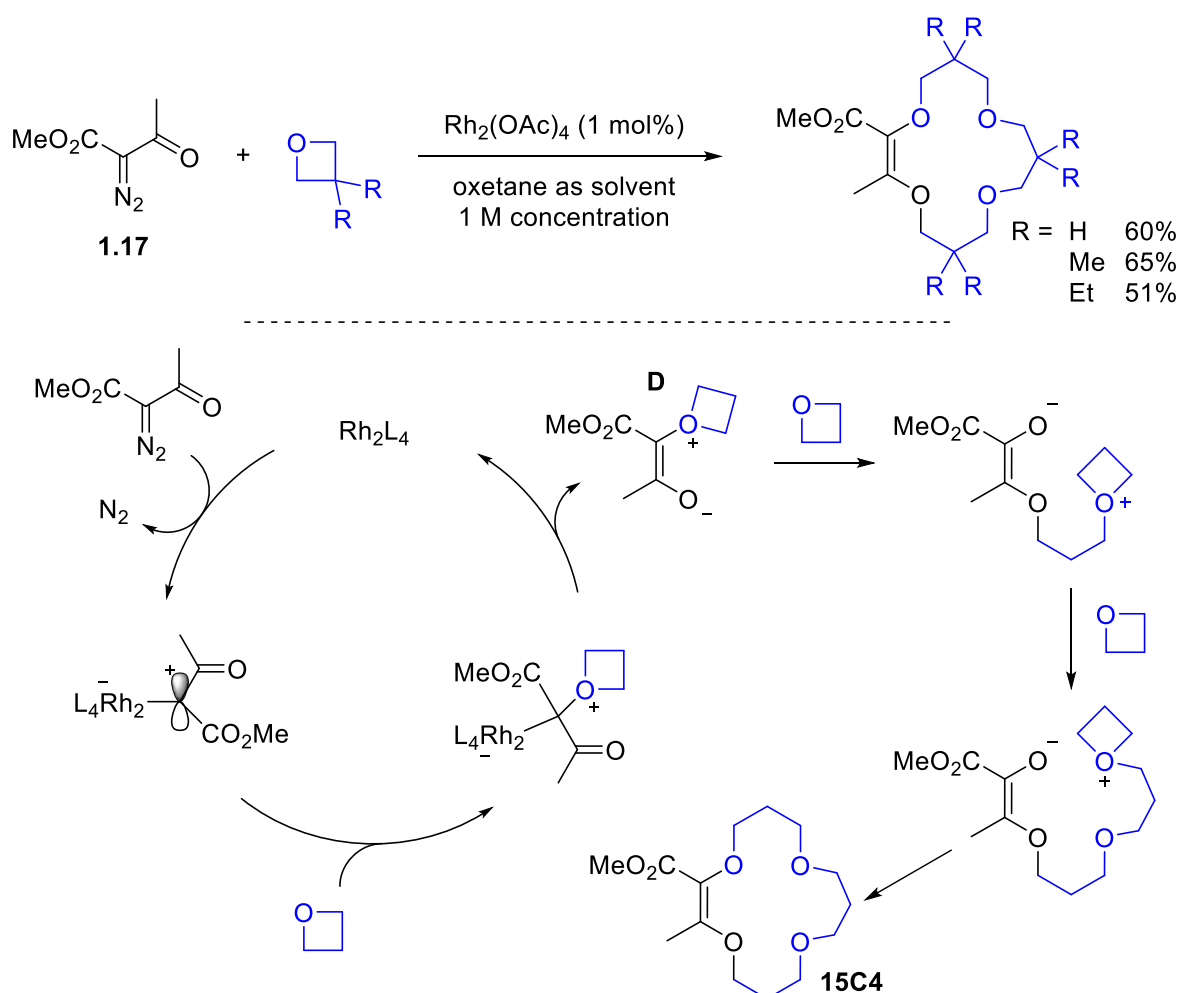


Scheme 1.17 [3+6+3+6] macrocyclization on multigram scale.

⁷⁴ Tsutsui, H.; Abe, T.; Nakamura, S.; Anada, M.; Hashimoto, S., *Chem. Pharm. Bull* **2005**, 53, 1366-1368.

1.5.2 Macrocyclization from oxetanes

When smaller and more reactive 4-membered ring cyclic ethers (oxetanes) are condensed with acceptor-acceptor diazo compounds under dirhodium catalysis, 15-membered ring macrocycles are afforded following a different mechanism (**Scheme 1.18**).⁷⁵ After decomposition of the diazo reagent and formation of ylide **D**, the dimerization of the oxonium ylide does not proceed. In fact, due to the ring-strain that renders the oxonium fragment quite more electrophilic, two successive additions of oxetanes, acting as nucleophile, happened. This type of intermolecular reaction is kinetically favored until a favored ring closure occurs to form the 15-membered ring through a formal [3+4+4+4] condensation.

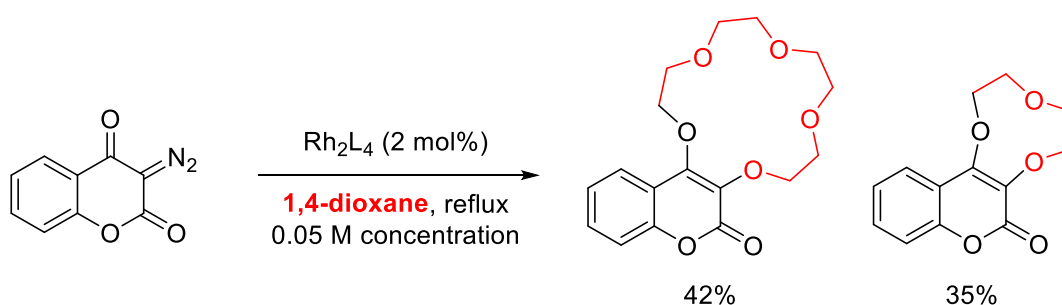


Scheme 1.18 Rh(II)-catalyzed [3+4+4+4] condensation of α -diazo- β -ketoesters and oxetanes.

⁷⁵ Rix, D.; Ballesteros-Garrido, R.; Zeghida, W.; Besnard, C.; Lacour, J., *Angew. Chem. Int. Ed.* **2011**, *50*, 7308-7311.

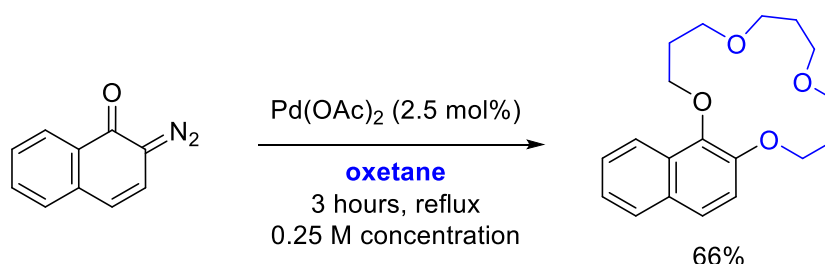
1.5.3 Miscellaneous syntheses of macrocycles

Other research groups proposed alternative approaches for the condensation of cyclic ether with diazo compounds. For instance, Tollari and coworkers reported a dirhodium-catalyzed decomposition of diazo coumarins in presence of 1,4-dioxane to form a 15-membered ring macrocycle (42%) along with a 9-membered ring (35%).⁷⁶ THP and THF cyclic ethers also afforded the corresponding 15-, 13-, 9-, and 8-membered ring macrocycle in the same conditions in moderate yields (31% - 43%, **Scheme 1.19**).



Scheme 1.19 Rh(II)-catalyzed decomposition of diazo coumarin for the synthesis of macrocycle.⁷⁶

Instead of rhodium(II), palladium catalysis can be used for the decomposition of diazo compounds. As example, this reaction was reported by the group of Kitamura who synthesized 15-membered ring macrocycles in good yields (66%) from oxetane and diazonaphthoquinone (**Scheme 1.20**).⁷⁷ Besides oxetane, THF and THP yield the corresponding macrocycle in moderate yields (36% and 15% respectively).

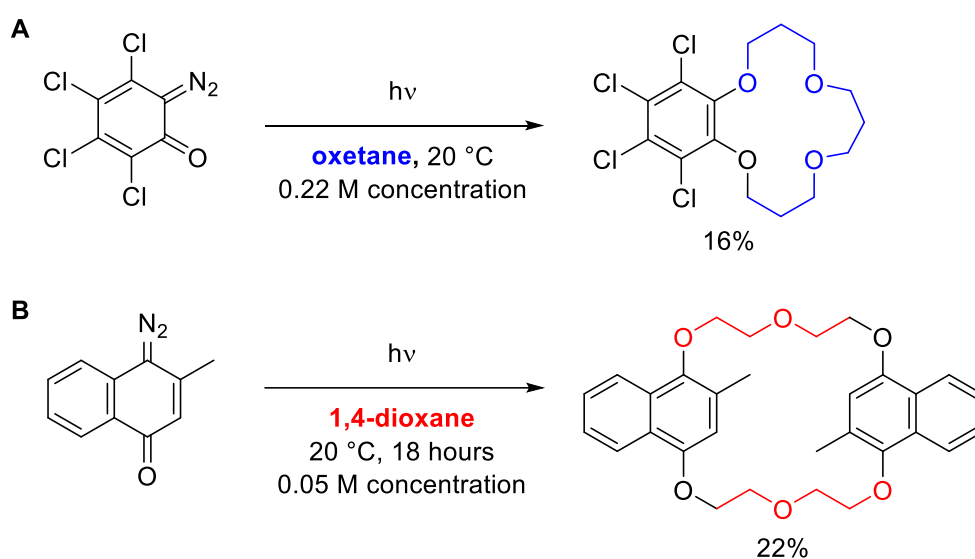


Scheme 1.20 Pd-catalyzed decomposition of diazonaphthoquinone for the synthesis of macrocycle.⁷⁷

⁷⁶ Cenini, S.; Cravotto, G.; Giovenzana, G. B.; Palmisano, G.; Tollari, S., *Tetrahedron* **1999**, 55, 6577-6584.

⁷⁷ Kitamura, M.; Kisanuki, M.; Kanemura, K.; Okauchi, T., *Org. Lett.* **2014**, 16, 1554-1557.

Finally, light activation is an interesting alternative procedure to decompose diazo compounds and generate carbene species (**Scheme 1.21**). Already in the 1990's, Kirmse and coworkers proposed a photochemical decomposition of orthoquinone diazo to form 15-membered ring macrocycles in presence of oxetanes (**Scheme 1.21A**).⁷⁸ The group of Liu also applied this strategy to form a 22-membered ring polyether macrocycle by photolysis of diazodihydronaphthalenone in presence of 1,4 dioxane (**Scheme 1.21B**).⁷⁹ However these two examples afforded the macrocycles in only low yields (16% and 22%) and this reactivity seems unfortunately to be limited to oxetane and 1,4-dioxane cyclic ethers respectively.



Scheme 1.21 Photodecomposition of diazo in presence of cyclic ether.⁷⁸⁻⁷⁹

1.5.4 Functionalization of polyether macrocycles

Despite the structural similarity of **18C6** with crown ethers, this polyether macrocycle does not present any binding properties toward cations. In fact, the lone pairs of the consecutive oxygen atoms are not appropriately oriented for a favorable binding of cations (**Figure 1.13**).^{69, 73} The rigidity of the macrocycle mainly imposed by the conjugate ester/double bond system avoid the structural rearrangement required for the reorientation of the oxygen's lone pair.

⁷⁸ Kirmse, W.; Lelgemann, R., *Chem. Ber.* **1991**, 124, 1865-1866.

⁷⁹ Zhang, W.; Shao, X.; Yang, L.; Liu, Z.-L.; Chow, Y. L., *J. Chem. Soc. Perkin Trans. 2* **2002**, 1029-1032.

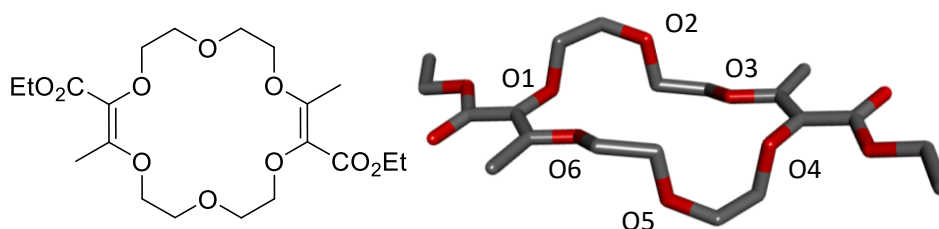
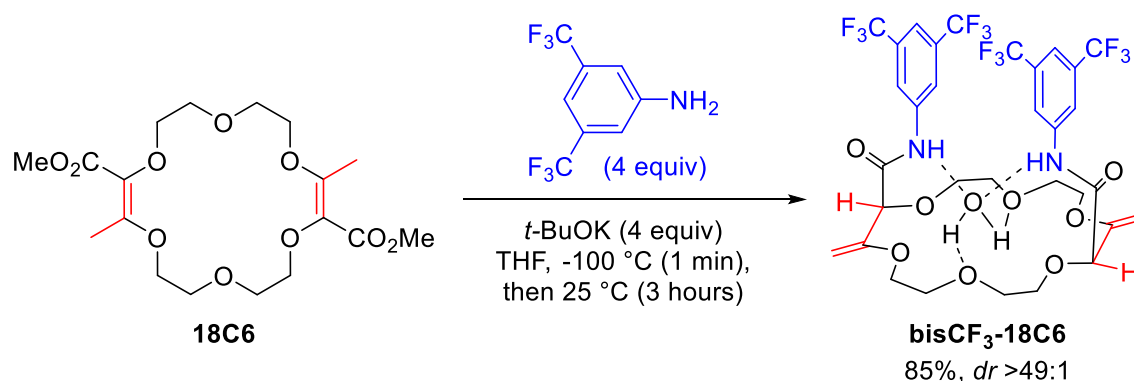


Figure 1.13 Stick view of the crystal structure of **18C6** (ethyl ester).⁶⁹

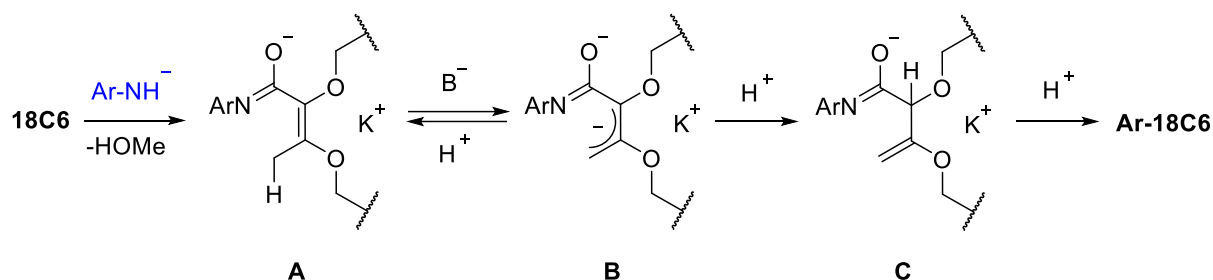
It was deemed that removing the strain imposed by the olefin should change the conformation of the ring and improve the binding abilities of such macrocycles. Fortunately, a transposition protocol was developed and **18C6** or other macrocycle of this type can be transformed in one pot into chiral polyether macrocycles in the presence of an excess of aromatic amines in strongly basic conditions (**Scheme 1.22**).^{3b,3b,80}



Scheme 1.22 Example of a one pot tandem amidation - transposition.

Two transformations occur in this process (**Scheme 1.23**) with (i) an amidation of the ester functions (**18C6** to **A**) and (ii) the transposition of the olefins (**A** to **Ar-18C6**). The reaction is highly diastereoselective ($dr > 49:1$) as only the chiral (racemic) diastereoisomer is generally formed; the achiral (*meso*) diastereoisomer not being observed. The induction is thought to originate from a template effect of the potassium ion which remotely direct the two stereocenters through coordination to the amide and ethers function at the key irreversible reprotonation step (**B** to **C**). This transformation is also a rare example of deconjugation of α,β -unsaturated esters.

⁸⁰ Kim, B. R.; Lee, H.-G.; Kang, S.-B.; Sung, G. H.; Kim, J.-J.; Park, J. K.; Lee, S.-G.; Yoon, Y.-J., *Synthesis* **2012**, 44, 42-50.



Scheme 1.23 Proposed pathway for the formation of **Ar-18C6**.

The structure of the product can explain this favorable transposition. Indeed, the system, formed by the olefin and the C-H group of the stereogenic center of **Ar-18C6**, create an allylic 1,3-strain forcing the two amides substituents to be orthogonally oriented to the plane of the crown ether skeleton (example with **bisCF₃-18C6** in **Figure 1.14**). This conformation renders the reversibility of the isomerization of double bond inoperative in the reaction conditions. As a consequence, the two aromatic moieties are favorably and closely located facing each other. A water molecule is also complexed inside the crown ether linked by hydrogen bonding with the N-H amide and the oxygen atoms of the ring.

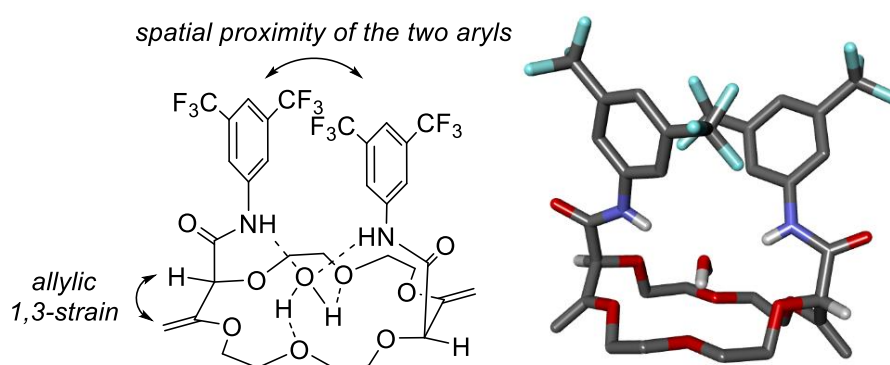


Figure 1.14 Conformation and stick view of the crystal structure of **bisCF₃-18C6**.

The transformation is also possible starting from other macrocycles obtained by similar methodologies namely the **15C4**, **16C4** and **18C4** polyether macrocycles. The amidation - transposition process with bis-3,5-trifluoromethyl aniline yields the chiral crown ethers **bisCF₃-15C4**, **bisCF₃-16C4** and **bisCF₃-18C4** in high yields (**Figure 1.15**).⁸¹ In these three cases, no water molecule is complexed in the final product. However, the conformation of the macrocycles is

⁸¹ **bisCF₃-16C4** and **bisCF₃-18C4** are obtained as single distereoisomers (*dr* > 49:1).

comparable to the one presented for **bisCF₃-18C6** with the constrain imposed by the allylic 1,3-strain.

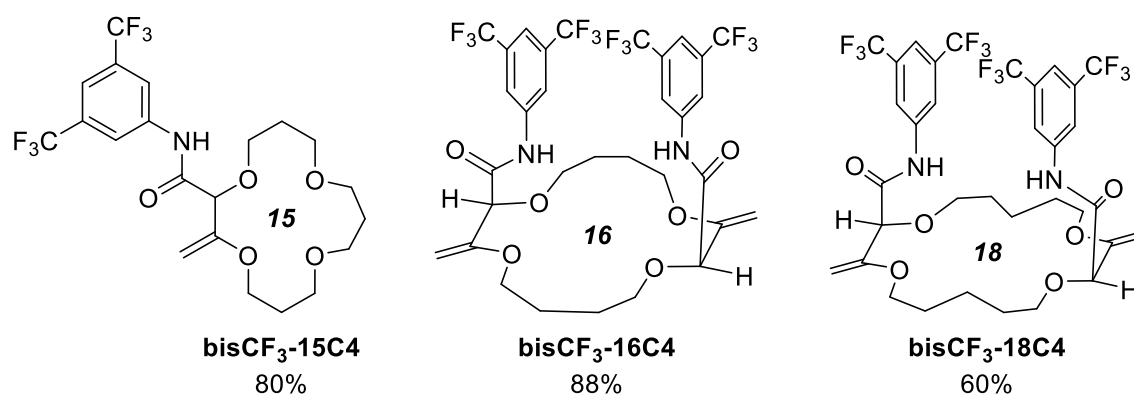
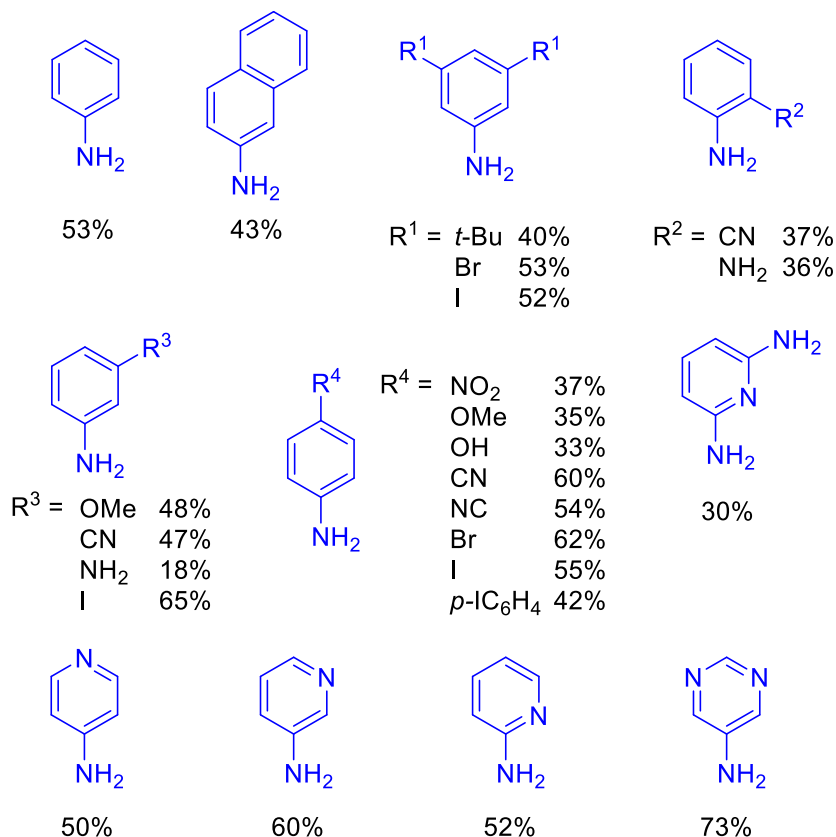
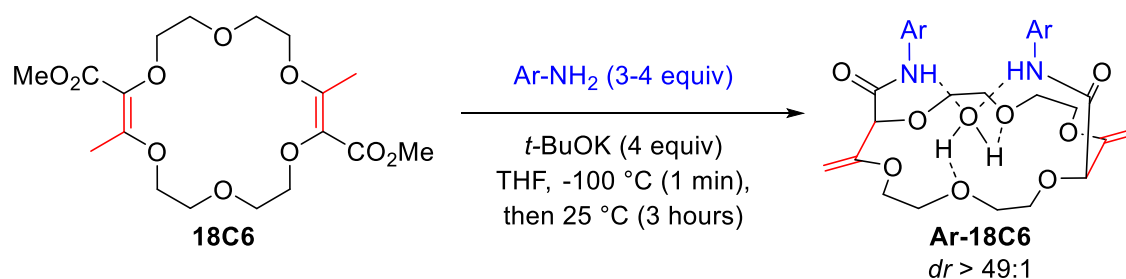


Figure 1.15 Examples of 15-, 16- and 18-membered ring chiral polyether macrocycles.

Finally, the reaction was extended to various anilines and aromatic amines (**Scheme 1.24**). All chiral macrocycles were obtained in moderate to good yields as single diastereoisomers (*dr* > 49:1). Electron-rich or electron-poor anilines are tolerated as well as extended aromatic compounds such as 2-naphthalene. Diamino phenyl or nitrogen containing heteroaromatics complete the scope. However, this transformation is, for now, only limited to aromatic amines and anilines. The use of aliphatic amines in the one-pot process leading to extensive decomposition of the substrate and a complete lack of isolable products.



Scheme 1.24 Scope of the aromatic amines for the synthesis of chiral crown ethers.

1.6 Conclusion

The synthesis of chiral crown ethers often requires several synthetic steps and uses generally high dilution conditions for the key ring closure step. The strategy applied by our group circumvents these drawbacks by using (i) very simple and commercially available reagents and (ii) high concentration conditions for the macrocyclization. The formation of the polyether

macrocycles on large scales (up to 20 grams/batch) is then possible with a minimum of material and time. Then, an unprecedented tandem amidation – olefin transposition process was developed giving access in one step to chiral and highly substituted polyether macrocycles.

One project of this PhD (Chapter 2) was to overcome the limitation of the use of aromatic amines and find ways to introduce aliphatic amines. Instead a new stepwise synthetic strategy was developed to introduce such N-containing moieties with first the aminolysis of the ester function followed by a subsequent transposition in basic medium. The newly synthesized macrocycles were tested in asymmetric PTC and proved to be effective catalysts for the alkylation of protected glycine with however moderate enantioselectivity levels (45% *ee*).

In the 3rd Chapter, the late-stage functionalization of amino substituted crown ethers led to the synthesis of a series of heteroditopic cryptands in one step. The key ring closure step proceeded well with aromatic dicarbonyl dichloride or (thio)phosgene reagents affording seven different cryptands. Using ¹H NMR spectroscopy and solid state analyses, the ditopic character of the new receptors was demonstrated in presence of monovalent cations and linear triatomic anions in particular. The salts are cooperatively complexed as close contact ion pairs within the cryptand. Unfortunately, no reliable binding constant could be extracted from the titration experiments principally due to the high concentration of the analytes required and the relatively small variations in ¹H-NMR chemical shifts upon the binding of the ions.⁸²

The application of chiral polyether macrocycles as sensors was then considered. Using fluorescent polyaromatic amides as substituents (pyrene, perylene, NMI or fluorene), these derivatives exhibit strong excimer fluorescence (EF) in a large emission range depending on the chromophore (λ_{em} 300 nm to 650 nm). Efficient separation of the enantiomers was achieved using CSP-HPLC. Thus, the chiroptical properties of the enantiopure material was studied by ECD and CPL spectroscopies. Upon complexation – decomplexation of metal ions within the polyether macrocycles (Na⁺ or Ba²⁺), the chiroptical signals were reversibly inverted (ECD) or quenched (CPL) proving these systems as remarkable +/- ECD and on/off CPL switches. The reversibility was achieved using regular (commercial) 18-Crown-6 as cation scavenger (Chapter 4).⁸³

⁸² Ray, S. K.; Homberg, A.; Vishe, M.; Besnard, C.; Lacour, J., *Chem. Eur. J.* **2018**, *24*, 2944-2951.

⁸³ Homberg, A.; Brun, E.; Zinna, F.; Pascal, S.; Górecki, M.; Monnier, L.; Besnard, C.; Pescitelli, G.; Di Bari, L.; Lacour, J., *Chem. Sci.* **2018**, *9*, 7043-7052.

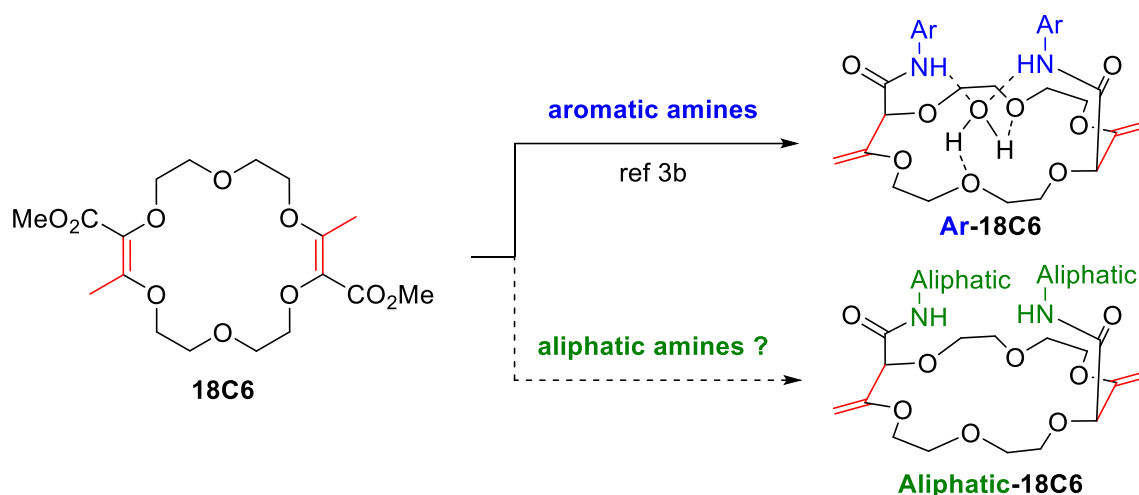
Finally, the amidation – transposition protocol developed for the synthesis of chiral crown ether was extended to new nitrogen-containing polyether building blocks with aromatic and aliphatic amines. The influence of different substituents on the nitrogen atoms of the macrocycle was also studied (Chapter 5).

2 Synthesis of chiral crown ethers bearing aliphatic substituents

2.1 Introduction

Our group previously reported the straightforward synthesis of unsaturated macrocycles.^{3a, 69,}
⁷³ Then, in a single step, these ester polyether precursors (**18C6**, **18C4** and **16C4**) were transformed into bis-amides, this functional groups transformation occurring together with a transposition of the double bonds that move from endo to exocyclic positions concomitantly (**Scheme 2.1**, top).^{3b} A high diastereoselectivity ($dr > 49:1$) was obtained. The process tolerated a large variety of electron-rich or electron-poor aromatic amines and heteroaromatic or extended aromatic amines. It was deemed interesting to study the introduction of aliphatic amides on the crown ethers instead of aromatic variants as it would open the way to new functionalities and potentially new applications. Such a development was considered during this PhD (**Scheme 2.1**, bottom). It was envisaged that the incorporation of chiral enantiopure amines would add a second set of stereogenic elements interesting, for instance, in asymmetric phase transfer catalysis (PTC) reactions.

However, at the start of this thesis, the addition of aliphatic amines remained elusive. In fact, using the reported conditions, when **18C6** was mixed with an excess of aliphatic amine (benzylamine) and *t*-BuOK, only degradation of the starting polyether macrocycle was observed. Thus, there was a need for different conditions to introduce aliphatic amines as substituents which required a two-step approach. This chapter will focus on the development of such a transformation, and on the applications of the corresponding products in asymmetric PTC in particular.



Scheme 2.1 Synthesis of chiral crown ethers.

2.2 Synthesis of aliphatic amide macrocycles

The synthesis of amides is a well-documented topic.⁸⁴ Amides can be synthesized from carboxylic acids and amines with the help of coupling agents (**Scheme 2.2**, top).⁸⁵ The use of carboxylic acid derivatives, such as acyl chlorides, anhydrides or activated esters, provides an alternative pathway (**Scheme 2.2**, middle).⁸⁶ However, employing non-activated esters as precursors is less common and usually requires the assistance of an external reagent or a catalyst (**Scheme 2.2**, bottom).⁸⁷ Accordingly, acetic acid⁸⁸ or Lewis acids such as AlMe₃, La(OTf)₃, MnBr(CO)₅, CaI₂, InI₃, BF₃·OEt₂, group (IV) metals, Sb(OEt)₃ or Zn dust⁸⁹ can be utilized to enforced

⁸⁴ (a) Bode, J. W., *Reinventing Amide Bond Formation*. In *Inventing Reactions*, Gooßen, L. J., Ed. Springer Berlin Heidelberg: Berlin, Heidelberg, 2013; pp 13-33. (b) Pattabiraman, V. R.; Bode, J. W., *Nature* **2011**, *480*, 471. (c) Montalbetti, C. A. G. N.; Falque, V., *Tetrahedron* **2005**, *61*, 10827-10852.

⁸⁵ (a) El-Faham, A.; Albericio, F., *Chem. Rev.* **2011**, *111*, 6557-6602. (b) Valeur, E.; Bradley, M., *Chem. Soc. Rev.* **2009**, *38*, 606-631. (c) Sperry, J. B.; Minter, C. J.; Tao, J.; Johnson, R.; Duzguner, R.; Hawksworth, M.; Oke, S.; Richardson, P. F.; Barnhart, R.; Bill, D. R.; Giusto, R. A.; Weaver, J. D., *Org. Process Res. Dev.* **2018**.

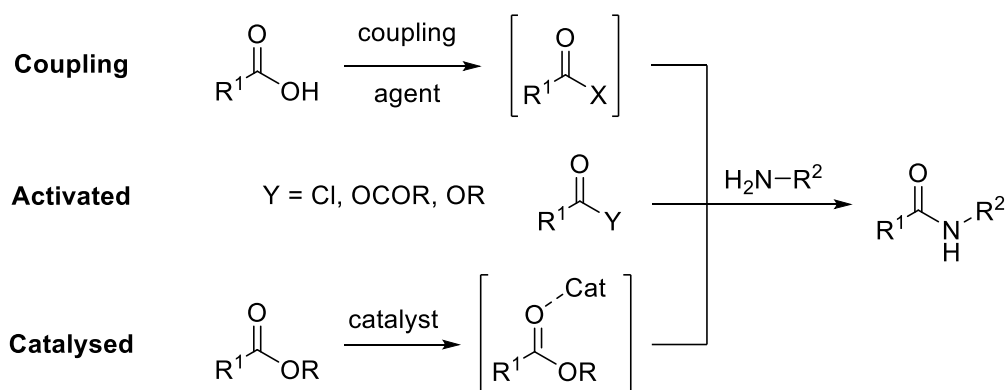
⁸⁶ de Figueiredo, R. M.; Suppo, J.-S.; Campagne, J.-M., *Chem. Rev.* **2016**, *116*, 12029-12122.

⁸⁷ For examples of aminolysis of ester without the help of external reagent or catalyst see: (a) Furukawa, S.; Fukuyama, T.; Matsui, A.; Kuratsu, M.; Nakaya, R.; Ineyama, T.; Ueda, H.; Ryu, I., *Chem. Eur. J.* **2015**, *21*, 11980-11983. (b) Karis, N. D.; Loughlin, W. A.; Jenkins, I. D., *Tetrahedron* **2007**, *63*, 12303-12309. (c) Zradni, F.-Z.; Hamelin, J.; Derdour, A., *Synth. Comm.* **2002**, *32*, 3525-3531.

⁸⁸ Sanz Sharley, D. D.; Williams, J. M. J., *Chem. Commun.* **2017**, *53*, 2020-2023.

⁸⁹ (a) Mondal, A.; Subaramanian, M.; Nandakumar, A.; Balaraman, E., *Org. Lett.* **2018**, *20*, 3381-3384. (b) Nguyen, D. T.; Lenstra, D. C.; Mecinovic, J., *RCS Adv.* **2015**, *5*, 77658-77661. (c) Morimoto, H.; Fujiwara, R.; Shimizu, Y.;

the coupling. Base-assisted aminolysis was also reported using K_3PO_4 , phosphazine bases or NaOMe.⁹⁰ Finally, transition-metal catalysis (Ru),⁹¹ organocatalysis (TBD, DBU, NHCs, triazoles)⁹² or enzyme catalysis (lipase)⁹³ can also afford amides from ester precursors.



Scheme 2.2 Synthesis of amides.

Morisaki, K.; Ohshima, T., *Org. Lett.* **2014**, *16*, 2018-2021. (d) Allen, C. L.; Williams, J. M. J., *Chem. Soc. Rev.* **2011**, *40*, 3405-3415. (e) de Oliveira, V. M.; Silva de Jesus, R.; Gomes, A. F.; Gozzo, F. C.; Umpierre, A. P.; Suarez, P. A. Z.; Rubim, J. C.; Neto, B. A. D., *ChemCatChem* **2011**, *3*, 1911-1920. (f) Novak, A.; Humphreys, L. D.; Walker, M. D.; Woodward, S., *Tetrahedron Lett.* **2006**, *47*, 5767-5769. (g) Arora, R.; Paul, S.; Gupta, R., *Can. J. Chem.* **2005**, *83*, 1137-1140. (h) Han, C.; Lee, J. P.; Lobkovsky, E.; Porco, J. A., *J. Am. Chem. Soc.* **2005**, *127*, 10039-10044. (i) Ranu, B. C.; Dutta, P., *Synth. Comm.* **2003**, *33*, 297-301. (j) Ishihara, K.; Kuroki, Y.; Hanaki, N.; Ohara, S.; Yamamoto, H., *J. Am. Chem. Soc.* **1996**, *118*, 1569-1570.

⁹⁰ (a) Caldwell, N.; Jamieson, C.; Simpson, I.; Watson, A. J. B., *Chem. Commun.* **2015**, *51*, 9495-9498. (b) Caldwell, N.; Campbell, P. S.; Jamieson, C.; Potjewyd, F.; Simpson, I.; Watson, A. J. B., *J. Org. Chem.* **2014**, *79*, 9347-9354. (c) Caldwell, N.; Jamieson, C.; Simpson, I.; Watson, A. J. B., *ACS Sustain. Chem. Eng.* **2013**, *1*, 1339-1344. (d) Ohshima, T.; Hayashi, Y.; Agura, K.; Fujii, Y.; Yoshiyama, A.; Mashima, K., *Chem. Commun.* **2012**, *48*, 5434-5436. (e) Chintareddy, V. R.; Ho, H.-A.; Sadow, A. D.; Verkade, J. G., *Tetrahedron Lett.* **2011**, *52*, 6523-6529.

⁹¹ Gnanaprakasam, B.; Milstein, D., *J. Am. Chem. Soc.* **2011**, *133*, 1682-1685.

⁹² (a) Guo, H.; Wang, Y.; Du, G.-F.; Dai, B.; He, L., *Tetrahedron* **2015**, *71*, 3472-3477. (b) Weiberth, F. J.; Yu, Y.; Subotkowski, W.; Pemberton, C., *Org. Process Res. Dev.* **2012**, *16*, 1967-1969. (c) Yang, X.; Birman, V. B., *Org. Lett.* **2009**, *11*, 1499-1502. (d) Price, K. E.; Larrivée-Aboussafy, C.; Lillie, B. M.; McLaughlin, R. W.; Mustakis, J.; Hettenbach, K. W.; Hawkins, J. M.; Vaidyanathan, R., *Org. Lett.* **2009**, *11*, 2003-2006. (e) Sabot, C.; Kumar, K. A.; Meunier, S.; Mioskowski, C., *Tetrahedron Lett.* **2007**, *48*, 3863-3866. (f) Movassaghi, M.; Schmidt, M. A., *Org. Lett.* **2005**, *7*, 2453-2456.

⁹³ (a) Dhake, K. P.; Qureshi, Z. S.; Singhal, R. S.; Bhanage, B. M., *Tetrahedron Lett.* **2009**, *50*, 2811-2814. (b) Couturier, L.; Taupin, D.; Yvergnaux, F., *J. Mol. Catal. B: Enzym.* **2009**, *56*, 29-33. (c) Aoyagi, N.; Kawauchi, S.; Izumi, T., *Tetrahedron Lett.* **2003**, *44*, 5609-5612.

2.2.1 Transformation of ester into amides (aminolysis)

2.2.1.1 Optimization of the aminolysis reaction

First, to test the feasibility of the aminolysis, **18C6** and benzyl amine were selected as model substrates and reagents. (**Table 2.1**). Without any external reagent or catalyst, full recovery of the starting **18C6** macrocycle was observed after heating at 60 °C in THF (entry 1). Under previously reported conditions for the aromatic amines (excess of *t*-BuOK), only degradation products were observed on the other hand (entry 2). Using *n*BuLi as base (4 equiv), the formation of the expected product was observed by ESI-MS monitoring but with a poor conversion. The isolation of the bis-amide product was attempted but failed (entry 3). The use of catalytic or stoichiometric amounts of *Lewis* acids, Yb(OTf)₃ or BF₃·OEt₂,⁹⁴ to activate the ester function was also not conclusive (entries 4-7). Next, we turned our attention to organocatalysis.

In 2007, Mioskowski proposed the use of a cyclic guanidine base, 1,5,7-triazabicyclo[4.4.0]dec-5-ene (TBD), as catalyst for the transformation of esters to amides.^{92e} This organocatalyst is usually applied in transesterification or ester polymerization reactions.⁹⁵ With **18C6** macrocycle, Mioskowski's conditions (20 mol% of TBD) did not show any aminolysis (entry 8) but when the cyclic guanidine was used in stoichiometric amount (2 equiv), macrocycle **2.1** was obtained in a satisfactory yield (47%) after 4 hours and a simple filtration (entry 9). Increasing reaction time to 15 hours afforded the product in a good yield (75%, entry 10). Changing the solvent to CH₂Cl₂ prevented the formation of **2.1** for reasons undetermined (entry 11). Alternatively, combination of NHCs (*N*-heterocyclic carbenes) and *t*-BuOK are also known to catalyze aminolysis or transesterification reactions.^{92a, f, 96} However, IMes or SIMes did not catalyze or induced the formation of **2.1** (entries 12-14). Conditions presented in entry 10 were thus selected for the rest of the study.

⁹⁴ Dharma Rao, G. B.; Kaushik, M. P., *Tetrahedron Lett.* **2011**, 52, 5104-5106.

⁹⁵ Kiesewetter, M. K.; Scholten, M. D.; Kirn, N.; Weber, R. L.; Hedrick, J. L.; Waymouth, R. M., *J. Org. Chem.* **2009**, 74, 9490-9496.

⁹⁶ (a) Grasa, G. A.; Kissling, R. M.; Nolan, S. P., *Org. Lett.* **2002**, 4, 3583-3586. (b) Nyce, G. W.; Lamboy, J. A.; Connor, E. F.; Waymouth, R. M.; Hedrick, J. L., *Org. Lett.* **2002**, 4, 3587-3590.

Table 2.1 Optimization of aminolysis conditions.

<div style="display: flex; justify-content: space-around; align-items: center;"> <div style="text-align: center;"> TBD </div> <div style="text-align: center;"> IMes·HCl </div> <div style="text-align: center;"> SIMes·HCl </div> </div>					
Entry	Base	equiv	Time (h)	Temperature (°C)	Yield
1	—	—	15	60	no conversion
2	<i>t</i> -BuOK	4	3	-100 then 25	degradation
3	<i>n</i> BuLi	4	3	-100 then 25	< 30% conv.
4	Yb(OTf) ₃	10 mol%	15	60	no conversion
5	Yb(OTf) ₃	2	15	60	no conversion
6	BF ₃ ·OEt ₂	20 mol%	15	60	no conversion
7	BF ₃ ·OEt ₂	2	15	60	no conversion
8	TBD	20 mol%	15	60	no conversion
9	TBD	2	4	60	47%
10	TBD	2	15	60	75%
11 ^[a]	TBD	2	15	60	no conversion
12	IMes·HCl/ <i>t</i> -BuOK	5 mol%	15	60	no conversion
13	IMes·HCl/ <i>t</i> -BuOK	2	15	60	degradation
14	SIMes·HCl/ <i>t</i> -BuOK	2	15	60	degradation

[a] CH₂Cl₂ instead of THF

2.2.1.2 Solid state structure of 2.1

Satisfactorily, with **2.1** in hand, structural information of the derivative was required. Recrystallization of **2.1** from acetonitrile gave single crystals suitable for X-ray analysis (**Figure**

2.1A).⁹⁷ The solid state structure is very similar to that of the ester homologue described by our group in 2013 (section 1.5.4): the amide function and the double bond are coplanar, confirming the conjugation from the nitrogen atom to oxygen O6.^{69, 73} This latter oxygen is sp^2 -hybridized as confirmed by the bond distance between C3 and O6 (1.364 Å) and the C3-O6-C5 angle of 119.3°. On the other hand, oxygen O1 is sp^3 -hybridized and its substituents are orthogonally oriented to the plane of the neighboring conjugation. The bond angle C1-O1-C2 is also only of 111.9° closer to the angle expected for a tetrahedral conformation (**Figure 2.1B**).

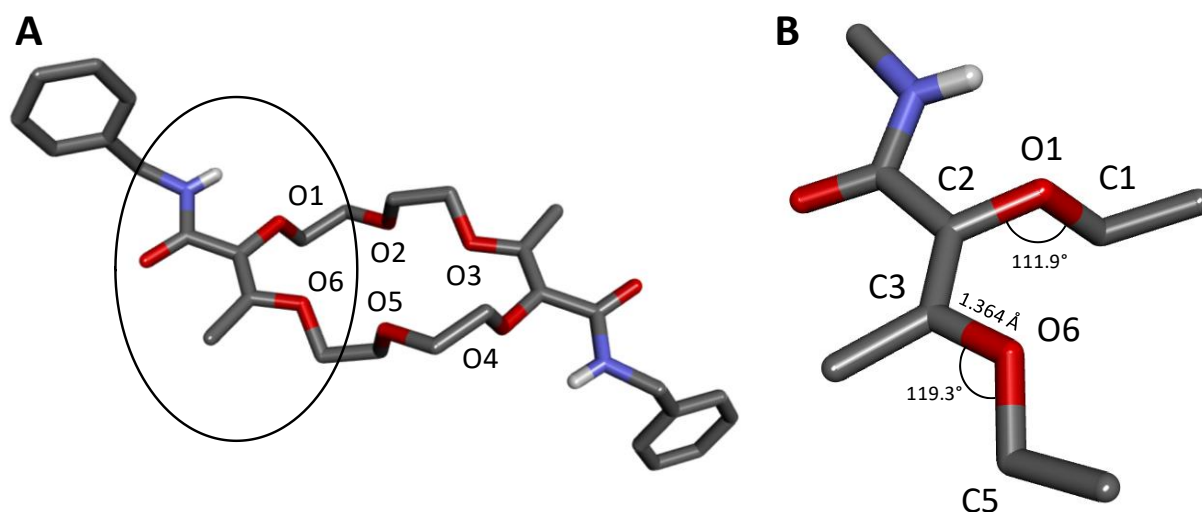


Figure 2.1 Stick view of the crystal structure of **2.1** (A) and dioxo amide segment (B, circled).

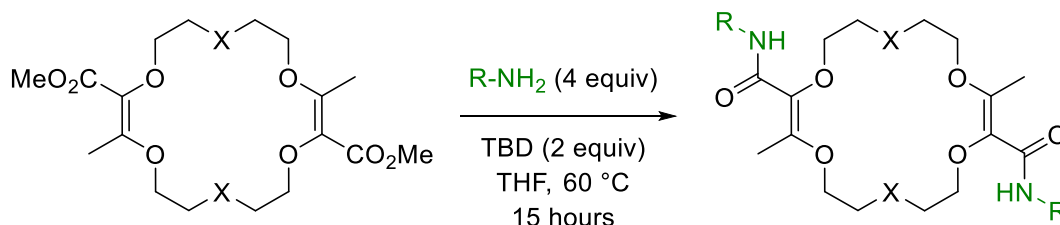
2.2.1.3 Scope of the aminolysis

With the TBD conditions in hand, the aminolysis was tested with different linear amines (**Table 2.2**). Using benzylamine, methylamine, *n*-propylamine, *n*-octylamine, 2-aminoethanol or 3-aminopropanol, macrocycles **2.1** to **2.6** precipitated out the reaction mixture and were obtained in moderate to good yields (entries 1-6, 53 to 75%) by single filtration. Terminal alcohol were selected to take advantage of the potential lariat effect or the possibility to use them to link the macrocycle to surfaces.^{55c} Using hydrazine, macrocycle **2.7** was successively formed in 97% yield

⁹⁷ Slow cooling of the acetonitrile reaction was required to isolate crystals suitable for X-ray analysis.

(entry 7). The reaction with benzylamine is also possible starting from the **18C4** macrocycle to afford **2.8** in 37% yield (entry 8).

Table 2.2 Scope of the aminolysis.



Entry	R	X	product	Yield (%)
1	Bn	O	2.1	75
2	Me	O	2.2	53
3	<i>n</i> Pr	O	2.3	59
4	<i>n</i> Oct	O	2.4	65
5	(CH ₂) ₂ OH	O	2.5	78
6	(CH ₂) ₃ OH	O	2.6	65
7	NH ₂	O	2.7	97
8	Bn	CH ₂	2.8	37

However, some amines did not lead to the formation of amide macrocycles (**Figure 2.2**). The use of ammonia, either from THF or MeOH solutions, or ethylene diamine induced the degradation of the **18C6** starting material. *Tert*-butyl amine is probably too hindered and also led to degradation products. No conversion was observed for *p*-nitro-benzylamine, protected glycine or 3,5-bis(trifluoromethyl) aniline. Similarly, trifluoroacetamide and benzylcarbamate led also to an absence of conversion of the ester macrocycle **18C6**.

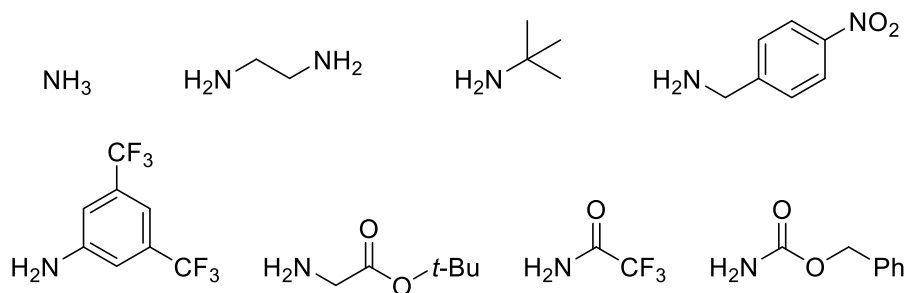


Figure 2.2 Amines that did not lead to aminolysis.

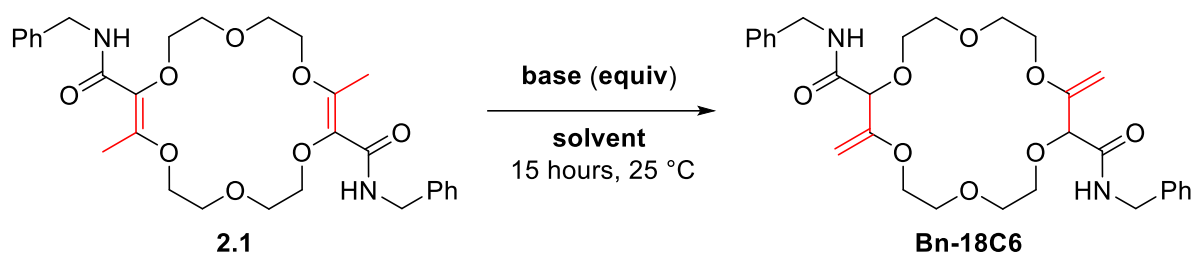
2.2.2 Transposition of the olefins

2.2.2.1 Optimization of the olefin transposition reaction

With the bis-amides in hand, the olefin transposition was considered next. Base-induced conditions were selected, as they had proven to be efficient with aromatic compounds (section 1.5.4). The results of the screening of bases and solvents on model substrate **2.1** are gathered in **Table 2.3**. The optimization was started with *t*-BuOK as base, in THF. The transposed product **Bn-18C6** was satisfactorily obtained in 63% yield, also as a single diastereoisomer (*dr* > 49:1, ¹H NMR monitoring, entry 1). The use of 1,4-dioxane instead of THF slightly increased the yield to 65% (entry 2). However, *t*-BuOMe or Et₂O as solvents led to partial or no conversion of **2.1** respectively (entries 3-4). In these two cases, the lack of solubility of **2.1** seems to be the reason for the poor conversion. In theory, this transformation could be catalytic in base. The use of 0.2 equivalent of *t*-BuOK led only to a partially-induced isomerization (entry 5). This indicates that the amide functions are too acidic and are deprotonated quantitatively by *t*-BuOK after the rearrangement. Finally, bases such as NaOMe, DBU or TBD were not able to transpose the olefin (entries 6-8).

2.2.2.2 Solid state structure of [Na·Bn-18C6][BAR_F]

Unfortunately, crystals of **Bn-18C6** suitable for X-ray analysis could not be obtained. The addition of a cationic template (Na⁺) to organize the structure and facilitate the crystallization was envisaged. Solubilizing **Bn-18C6** macrocycle and NaBAR_F salt (1:1 ratio) in a CH₂Cl₂/heptane bilayer system followed by a slow evaporation of the solvent furnished single crystals of the [Na·**Bn-18C6**][BAR_F] complex suitable for X-ray analysis (**Figure 2.3**).

Table 2.3 Optimization of the olefin transposition conditions.

Entry	Base	equiv	Solvent	Yield (%)
1	<i>t</i> -BuOK	2	THF	63
2	<i>t</i>-BuOK	2	1,4-dioxane	65
3	<i>t</i> -BuOK	2	Et ₂ O	low conversion
4	<i>t</i> -BuOK	2	<i>t</i> -BuOMe	no conversion
5	<i>t</i> -BuOK	0.2	1,4-dioxane	low conversion
6	NaOMe	2	1,4-dioxane	no conversion
7	DBU	2	1,4-dioxane	no conversion
8	TBD	2	1,4-dioxane	no conversion

This solid state structure confirmed that only the chiral (racemic) diastereoisomer is formed during the reaction, the achiral (*meso*) diastereoisomer not being detected either in solution or solid states. The sodium cation is coordinated to the six oxygen atoms of the crown ether ring and with one of the two carbonyls of the amides. In comparison with the bis-anilide derivatives (section 1.5.4), one amide function rotates to allow the C=O bond to point inwards while the N-H bond turns outwards. A hydrogen bonding interaction can be observed between the inwards N-H and oxygen O1 (2.173 Å). However, the ¹H and ¹³C NMR spectroscopic analysis of **Bn-18C6** at 298 K showed only a single set of signals which is consistent with a symmetrical conformation for the macrocycle. This indicates either a fast positional interchange or a C₂-symmetrical conformation in solution. Similarly to the **Ar-18C6** series, the allylic 1,3-strain between the exocyclic olefins and the C-H bond of the stereogenic centers is also present.

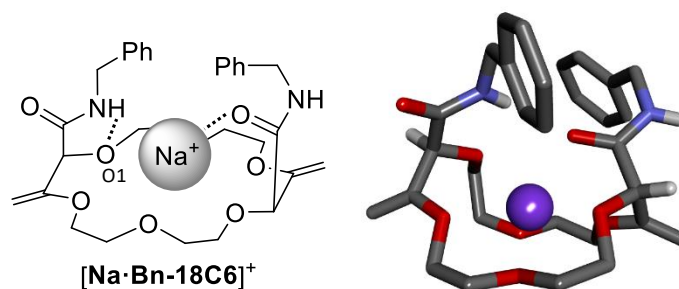


Figure 2.3 Stick view of the crystal structure of $[\text{Na}\cdot\text{Bn-18C6}][\text{BARF}]$ (BARF^- anion hidden for clarity).

2.2.2.3 Coordination of water in Bn-18C6

Compounds of the **Ar-18C6** series possess a water molecule complexed inside the cavity of the crown ether by hydrogen bonding interactions both in the solid state and in solution. This adduct was studied in solution by M. Vishe, during his PhD,⁹⁸ using ^1H NMR spectroscopy: a titration with different concentrations of **bisCF₃-18C6** in CDCl_3 showed the shift of the water proton signal from 2.68 ppm (9 mM) to 4.21 ppm (125 mM). The same NMR experiment was performed with **Bn-18C6** with six different concentrations of the crown ether in CDCl_3 (8 mM to 116 mM, **Figure 2.4**). In comparison with **bisCF₃-18C6** the shift is less marked – only a 0.9 ppm variation (vs 1.53 ppm). Moreover, the signal for the protons are also more shielded. These two observations seem to indicate that, in this case, water molecules are not naturally included inside the crown ether. This assumption was also corroborated by the fact that the intensity of the proton signal of H_2O remains constant upon incremental addition of macrocycle – this water originating from the solvent used for the NMR solution experiments.⁹⁹

⁹⁸ Vishe, M., *Straightforward synthesis of densely functionalized crown ethers and their applications*. University of Geneva, *PhD Thesis*, **2015**.

⁹⁹ See section 7.11.1 for more precisions.

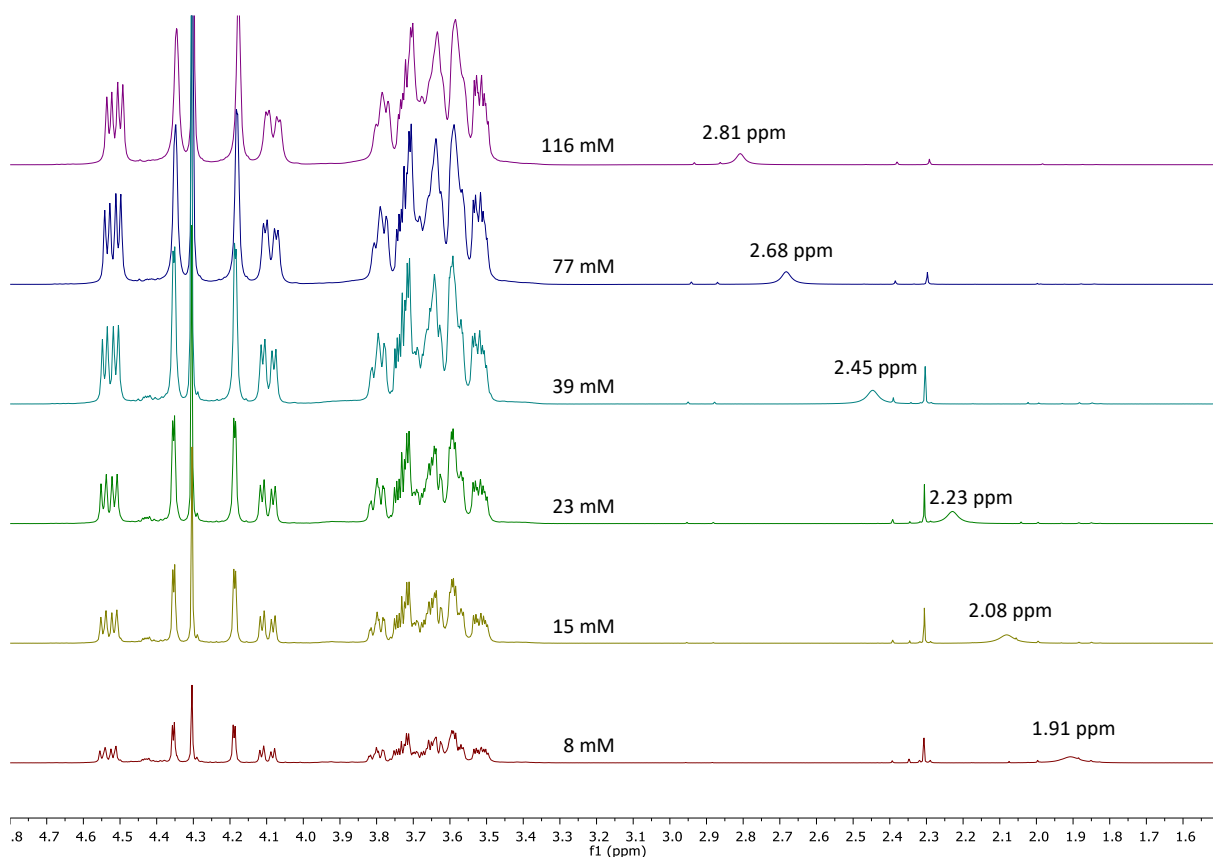


Figure 2.4 Bn-18C6 concentration effect by ^1H NMR (400 MHz, δ 4.8-1.5 ppm, CDCl_3 , 298K).

2.2.3 Tandem aminolysis – transposition conditions

The extension of the aminolysis with different amines was considered next. Unfortunately, the removal of the TBD reagent remained sometimes difficult during the purification step (precipitation or flash column chromatography). In other cases, the purity of the compounds was quite low. Henceforth, it was envisaged to engage directly the resulting product in the olefin transposition step without further purification in a successive process instead of a sequential process. For consistency and simplicity, the yields are, for now on, reported for the overall process.

At that stage, it was found that the stability of the bis-aliphatic amide macrocycles was, in general, quite low. The compounds are particularly sensitive to silica gel either after the aminolysis or after the transposition; the purification of the material causing a fast degradation of the products. This is why the purification of the transposition step was performed using neutral

alumina only – an additional precipitation step being required to remove the last impurities, causing some product loss at this stage as well.¹⁰⁰ Yet, the global instability of the products was still worrisome. As most derivatives were not susceptible to be isolated by simple precipitation/filtration protocols, a “single step” tandem aminolysis – transposition procedure was followed.

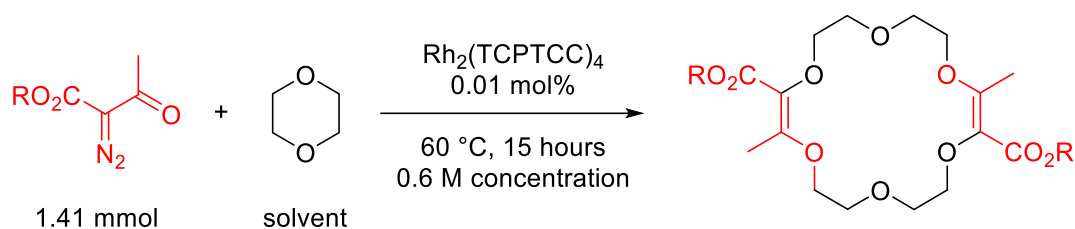
2.2.3.1 Influence of the ester nature on the aminolysis reaction

As the nature of ester substituents can have a huge influence on the reactivity of the aminolysis, a series of ester precursors was prepared applying the [3+6+3+6] macrocyclization protocol under Rh(II)-catalysis at low catalyst loading (**Table 2.4**).^{3a} All macrocycles (**2.9** to **2.15**) were obtained in moderate to good yields on gram scale (7.0 mmol of diazo compound) except for **2.14** which has a sensitive *p*-chlorophenol ester substituent. In comparison with the original conditions (Rh₂OAc₄ 1 mol%),⁶⁹ reported ethyl ester **2.9**, homobenzylic ester **2.12** and allylic ester macrocycles **2.13** were obtained in significantly higher yields (64% vs 48%, 78% vs 62% and 63% vs 47% respectively). For macrocycles **2.10** and **2.12** no trace of products of intramolecular C-H insertion (γ -lactone) of the derived metal-carbene were observed.¹⁰¹ In the case of allylic ester **2.13**, a competition between macrocyclization and intramolecular cyclopropanation reactions occurred, the formation of the macrocycle being favored over the corresponding cyclopropane (4:1 ratio) in agreement with reference 69.¹⁰²

¹⁰⁰ For the NMR analysis, freshly neutralized CDCl₃ (filtration over basic alumina) was used.

¹⁰¹ Doyle, M. P.; Westrum, L. J.; Wolthuis, W. N. E.; See, M. M.; Boone, W. P.; Bagheri, V.; Pearson, M. M., *J. Am. Chem. Soc.* **1993**, *115*, 958-964.

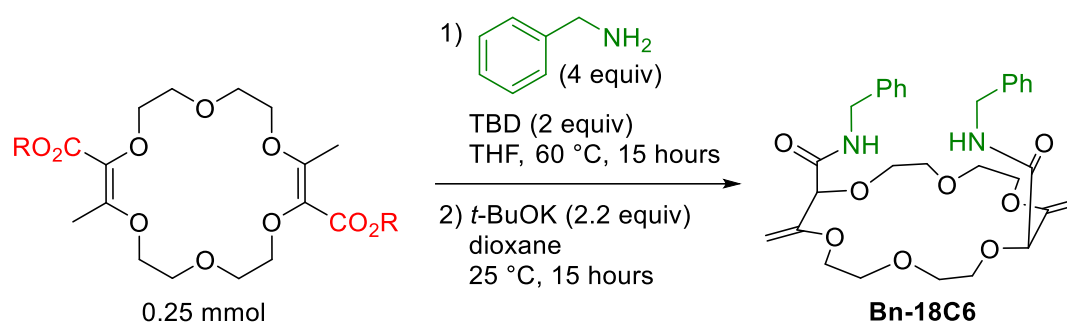
¹⁰² Welbes, L. L.; Lyons, T. W.; Cychosz, K. A.; Sanford, M. S., *J. Am. Chem. Soc.* **2007**, *129*, 5836-5837.

Table 2.4 Syntheses of substituted ester macrocycles under low catalyst loading.

Entry	R	macrocycle	Yield (%)
1 ^[a]	Me	18C6	72
2	Et	2.9	64
3	<i>i</i> Bu	2.10	40
4	Bn	2.11	55
5	Ph(CH ₂) ₂	2.12	78
6	allyl	2.13	63
7	<i>p</i> -ClC ₆ H ₄	2.14	15
8	CH ₂ CCl ₃	2.15	39

[a] 0.001 mol% of catalyst loading, 4 days

The influence of the ester substituents on the aminolysis was then tested under the optimized conditions using benzyl amine as reagent. **Table 2.5** summarizes the results for the two successive processes – the aminolysis followed directly by the olefin transposition. The superiority of the methyl ester precursor is noticeable, **Bn-18C6** product being obtained in 59% yield after two steps (entry 1), while ethyl, isobutyl, benzylic, homobenzylic and allylic esters gave slightly lower yields after two steps (45-55%, entries 2-6). However, either *p*-chlorophenyl ester or trichloroethyl ester gave poor yields (14% and 39% respectively, entries 7-8). For the first case (activated ester), TBD is probably not necessary and induces a decomposition of the starting material. This will be put in evidence later in this chapter.

Table 2.5 Screening of the ester precursors for the synthesis of **Bn-18C6**.


Entry	R	Yield (%) ^[a]
1	Me (18C6)	59
2	Et (2.9)	55
3	<i>i</i> Bu (2.10)	47
4	Bn (2.11)	45
5	Ph(CH ₂) ₂ (2.12)	47
6	allyl (2.13)	50
7	<i>p</i> -ClC ₆ H ₄ (2.14)	14
8	CH ₂ CCl ₃ (2.15)	39

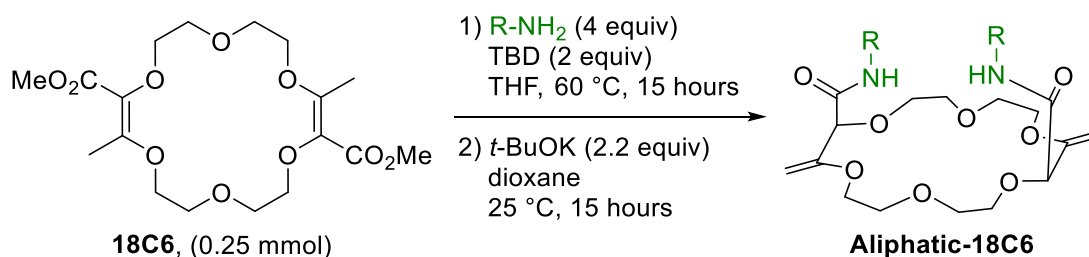
[a] overall yield for the two successive steps.

2.2.3.2 Scope of with linear amines

Next, with **18C6** as substrate, the scope of the tandem aminolysis – transposition was studied with various aliphatic amines. The scope of linear amines is presented in **Table 2.6**. In general, moderate to good yields were obtained for the combined process - the linear chain seems to have only a moderate influence on the final yields. In contrast, the transposition step did not work (no conversion) in the case of macrocycles with chains bearing acidic groups (alcohol or hydrazide **2.5** to **2.7**, section 2.2.1.3), even increasing the amount of base to four equivalents. The formation of four anions by full deprotonation of the acid functional groups and the amides in the highly basic conditions probably disfavors the transposition reaction. Thus, chains with protected alcohols (TBSO- or MeO-) were used instead and afforded in medium yields crown ethers **TBSO-ethyl-18C6** (35%), **MeO-ethyl-18C6** (54%) and **MeO-propyl-18C6** (54%, entries 6-8) respectively. The lower yield observed for the silyl protected alcohol (entry 6) could be attributed

to the instability of such protecting group under the highly basic conditions used for the transposition. Finally, the conversion of **18C4**-based macrocycle **2.8** did not occur because of solubility issues.

Table 2.6 Scope aliphatic amines.



Entry	R	Aliphatic-18C6	Yield (%) ^[a]
1	Bn	Bn-18C6	59
2	Me	Me-18C6	46
3	ⁿ Pr	ⁿPr-18C6	42
4	ⁿ Oct	ⁿOct-18C6	55
5	allyl	allyl-18C6	44
6	(CH ₂) ₂ OTBS	TBSO-ethyl-18C6	35
7	(CH ₂) ₂ OMe	MeO-ethyl-18C6	54
8	(CH ₂) ₃ OMe	MeO-propyl-18C6	54

[a] overall yield for two successive steps.

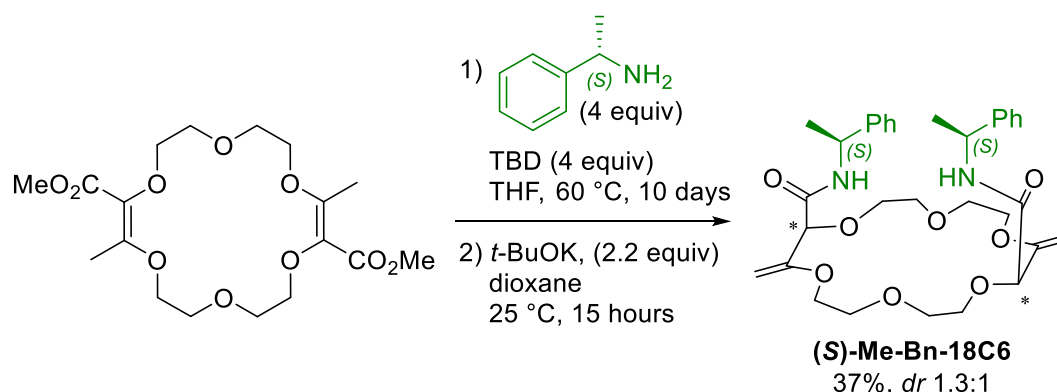
2.2.4 Crown ethers bearing α -branched aliphatic substituents

2.2.4.1 Adaptation of the reactions conditions

At this stage, only primary linear amines had been considered and, for potential applications, the introduction of α -branched substituents was considered as a necessity. However, the previously-developed aminolysis conditions were found to be inefficient (poor conversion) in the case of α -substituted aliphatic amine (*S*)- α -methyl-benzylamine. Such amines are much less reactive than the linear ones in the reaction conditions, probably because of a higher steric

hindrance. Conditions needed thus to be adapted by increasing both the amount of TBD and the reaction time.

So using (*S*)- α -methyl-benzylamine as model substrate with four equivalents of TBD and a ten days reaction time, the aminolysis proceeded to full conversion. The transposition step was then performed under the same basic conditions to afford (*S*)-Me-Bn-18C6 in 37% yield (**Scheme 2.3**). This time, a mixture of two out of three diastereoisomers was obtained (*dr* 1.3:1, ^1H NMR monitoring), which could not be separated during the purification. In fact, considering that the configuration of the added chiral amines remains intact under the reaction conditions,^{92e} three diastereoisomers are theoretically possible, namely derivatives (*S,S,S,S*) and (*S,R,R,S*) and (*S,S,R,S*). The two letters at the extremities indicates the configuration of the chiral amines and the two internal letters the configurations of the newly created stereocenters on the macrocycle. The (*S,S,R,S*) diastereoisomer can be discarded as both products presenting evidences of a local C_2 -symmetry in NMR spectroscopy. The result fits also what is known of the transposition reaction as the relative configuration of the newly created centers remains homochiral (*S,S* or *R,R*). However, only a low induction was observed as the added enantiopure chains exercised little control over the new centers. Clearly, during the irreversible protonation α to the amide functional group (section 1.5.4), the α -methyl-benzyl moieties does not allow a strong enough discrimination of the diastereotopic faces of the dienolate intermediates and hence the 1.3:1 *dr* value. The absolute configuration of the major diastereoisomer will be discussed in details in section 2.2.4.3.

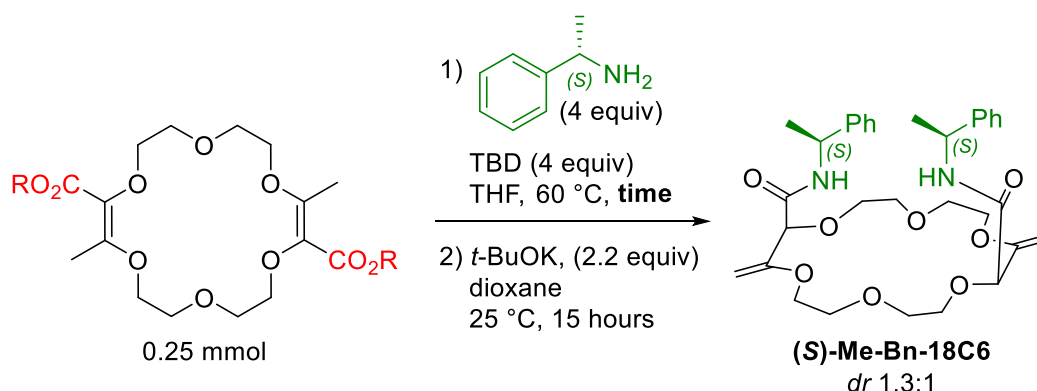


Scheme 2.3 Synthesis of chiral crown ether (*S*)-Me-Bn-18C6.

Macrocyclic precursors with different ester substituents (**2.9** - **2.15**) were also tested with α -branched aliphatic amines (**Table 2.7**). The superiority of methyl ester macrocycles was again

proved – the overall yields strongly decreasing with larger ester groups. Additionally, taking advantage of the higher reactivity of *p*-chlorophenyl and trichloroethyl ester towards aminolysis (activated esters), the reaction was reproduced using only catalytic amounts of TBD (entry 8 and 10). Unfortunately, similar yields were obtained for the *p*-chlorophenyl substituent after two steps, and no conversion was observed with the trichloroethyl ester macrocycle. In all cases, the macrocycles were afforded with the same diastereomeric ratio (*dr* 1.3:1, **Scheme 1.22**).

Table 2.7 Screening of the ester substituents for the synthesis of **(S)-Me-Bn-18C6**.



Entry	R	Time	Yield (%) ^[a]
1	Me (18C6)	10 days	37
2	Et (2.9)	10 days	17
3	<i>i</i> Bu (2.10)	10 days	15
4	Bn (2.11)	10 days	23
5	Ph(CH ₂) ₂ (2.12)	10 days	8
6	allyl (2.13)	10 days	16
7	<i>p</i> -ClC ₆ H ₄ (2.14)	15 hours	12
8 ^[b]	<i>p</i> -ClC ₆ H ₄ (2.14)	2 days	10
9	CH ₂ CCl ₃ (2.15)	15 hours	<5
10 ^[b]	CH ₂ CCl ₃ (2.15)	2 days	no conversion ^[c]

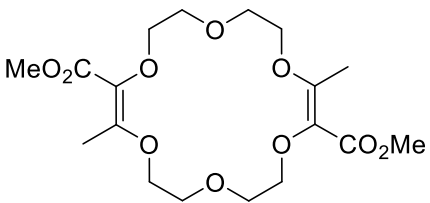
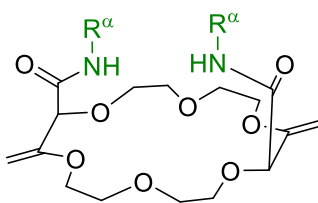
[a] overall yield for two successive steps; [b] with 10 mol% of TBD; [c] for the aminolysis step.

2.2.4.2 Scope with α -branched amines

The scope of the reaction was then studied using various achiral or enantiopure α -branched amines and TBD (4 equiv)/10 days reaction protocol (**Table 2.8**). Unfortunately, when **18C6** was treated with isopropylamine or cyclohexylamine, only moderate yields (29% and 18%) were obtained after the two successive steps (entries 1 and 2). Moderate to low yields were also observed using enantiopure α -substituted benzylamines or naphthylamine as substrate (4% - 35%, entries 3 - 12). The critical step was not the transposition step but the aminolysis. Indeed, slow but still competitive degradation of the starting **18C6** macrocycle occurs under the reaction conditions, lowering the yield of the bis-amide intermediate over time.¹⁰³ In general, as for **(S)-Me-Bn-18C6**, low diastereoselectivities (1:1 to 1.4:1) were again attained with these enantiopure amines. The two diastereoisomers could not be separated by flash column chromatography (neutral alumina). Increasing the length of the α -branched chain from methyl to ethyl and propyl has a small detrimental effect on the diastereoselectivity. However, changing the phenyl for a naphthyl group had a slightly positive effect and a diastereomeric ratio of 1.4:1 was obtained. It is worth mentioning that replacing the phenyl by a *tert*-butyl group prevented the formation of the desired macrocycle (entry 13). Besides, based on similarities in the ¹H NMR spectra, the major diastereoisomers (if any) have always the same relative configuration.

¹⁰³ Full conversion of the starting material was always reached. The degradation products could unfortunately neither be isolated nor identified.

Table 2.8 Scope of α -branched aliphatic amines.

<div style="display: flex; align-items: center; justify-content: space-around;"> <div style="text-align: center;">  <p>18C6, (0.25 mmol)</p> </div> <div style="text-align: center;"> <p>1) R^α-NH₂ (4 equiv) TBD (4 equiv) THF, 60 °C, 10 days</p> <p>2) <i>t</i>-BuOK, (2.2 equiv) dioxane 25 °C, 15 hours</p> </div> <div style="text-align: center;">  <p>Aliphatic-18C6</p> </div> </div>				
Entry	R^α	Aliphatic-18C6	<i>dr</i>	Yield (%) ^[a]
1	<i>i</i> Pr	<i>i</i> Pr-18C6	–	29
2	Cy	Cy-18C6	–	18
3	(<i>S</i>)- α -Me-Bn	(<i>S</i>)-Me-Bn-18C6	1.3:1	25
4	(<i>R</i>)- α -Me-Bn	(<i>R</i>)-Me-Bn-18C6	1.3:1	25
5	(<i>S</i>)- α -Et-Bn	(<i>S</i>)-Et-Bn-18C6	1.1:1	15
6	(<i>R</i>)- α -Et-Bn	(<i>R</i>)-Et-Bn-18C6	1.1:1	15
7	(<i>S</i>)- α -Pr-Bn	(<i>S</i>)-Pr-Bn-18C6	1:1	4
8	(<i>R</i>)- α -Me- <i>p</i> F-Bn	(<i>R</i>)-Me- <i>p</i> F-Bn-18C6	1.2:1	26
9	(<i>S</i>)- α -Me- <i>p</i> OMe-Bn	(<i>S</i>)-Me- <i>p</i> OMe-Bn-18C6	1.2:1	35
10	(<i>S</i>)- α -Me-1-naphth	(<i>S</i>)-Me-1-naphth-18C6	1.4:1	20
11	(<i>R</i>)- α -Me-1-naphth	(<i>R</i>)-Me-1-naphth-18C6	1.4:1	20
12	(<i>R</i>)- α -Me-2-naphth	(<i>S</i>)-Me-2-naphth-18C6	1.4:1	15
13	(<i>S</i>)- α -Me- <i>t</i> -Bu	(<i>S</i>)-Me- <i>t</i> -Bu-18C6	n.d.[b]	–

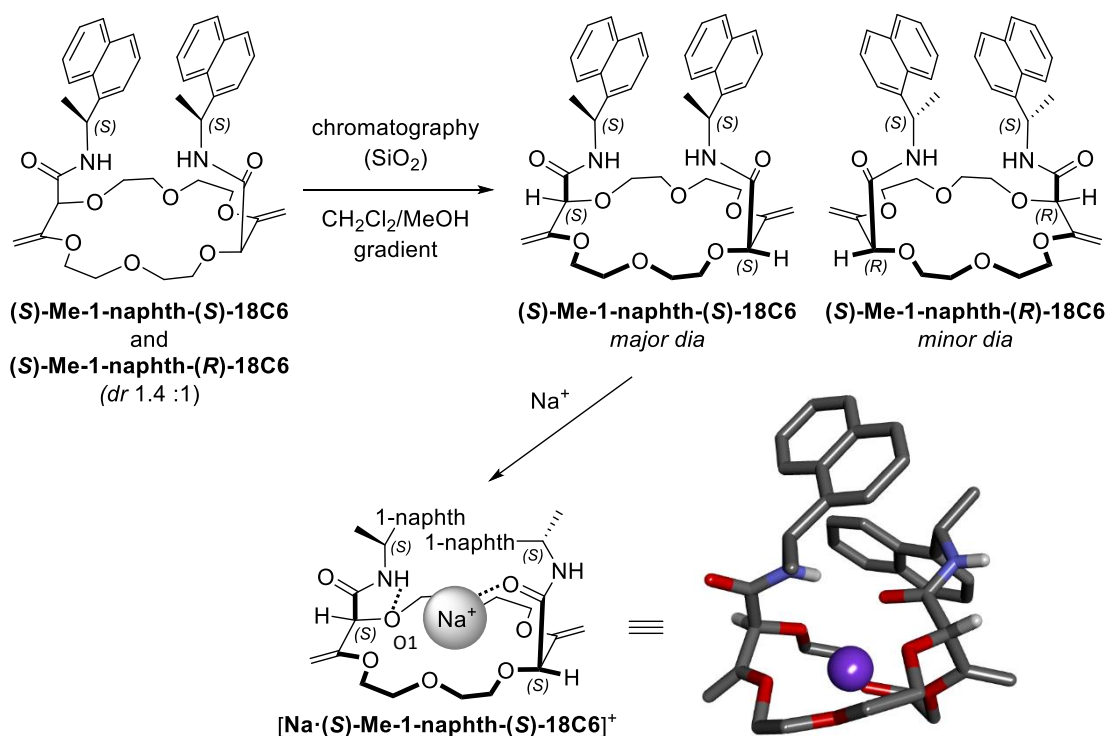
[a] overall yield for two successive steps; [b] not determined.

2.2.4.3 Configuration of (*S*)-Me-1-naphth-18C6

As mentioned, the purification of crown ether derivatives bearing α -branched enantiopure amines (**Table 2.8**) over neutral alumina did not allow a separation of the two diastereoisomers. However, in the specific case of (*S*)-Me-1-naphth-18C6 (*dr* 1.4:1), combining chromatography over silica gel and subsequent precipitation, a separation of the 1.4:1 mixture of diastereoisomers afforded the major and minor derivatives in 58% and 16% yields respectively – the major diastereoisomer being more polar and isolated as the second eluted fraction (**Scheme**

2.4).¹⁰⁴ A loss of material occurs during this purification sequence. The minor diastereoisomer is less stable than the major one, and it explains the lower isolated yield.

Then, using the major isolated fraction, suitable single crystals of the $[\text{Na}\cdot(\text{S})\text{-Me-1-naphth-18C6}][\text{BAR}_\text{F}]$ complex were obtained using the same procedure than for **Bn-18C6** (section 2.2.2.2, **Scheme 2.4**).¹⁰⁵ The solid state structural indicated that the absolute configuration of the major diastereoisomer was (S,S,S,S). Similarly to $[\text{Na}\cdot\text{Bn-18C6}][\text{BAR}_\text{F}]$, the sodium ion is coordinated through the six oxygen atoms of the crown ether ring and one of the two carbonyls of the amides. In addition, a similar hydrogen bonding interaction is observed between the inwards N-H and oxygen O1 (2.209 Å).



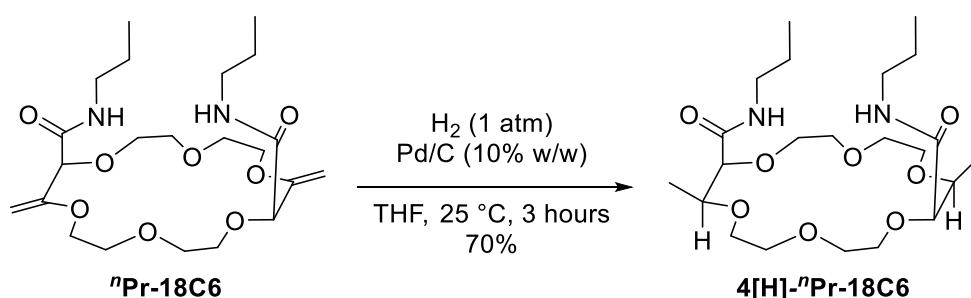
Scheme 2.4 Separation of the two diastereoisomers of (S)-Me-1-naphth-18C6 and stick view of the crystal structure of $[\text{Na}\cdot(\text{S})\text{-Me-1-naphth-(S)-18C6}][\text{BAR}_\text{F}]$ (BAR_F anion hidden for clarity).

¹⁰⁴ Slow gradient of MeOH (1% to 10%) in CH₂Cl₂, starting from a 1.4:1 mixture of diastereoisomers.

¹⁰⁵ No crystals of (S)-Me-1-naphth-(S)-18C6 suitable for X-ray analysis were obtained without the sodium salt.

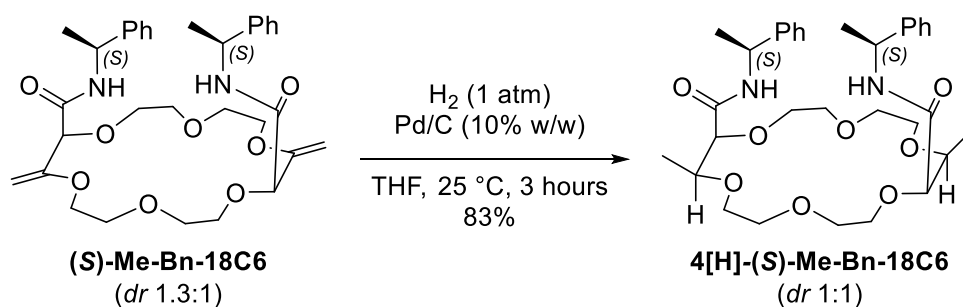
2.2.5 Hydrogenation of Aliphatic-18C6

In prevision of possible future applications, the hydrogenation of the exocyclic double bonds was considered. The viability of the transformation was first tested on ***n*Pr-18C6** (**Scheme 2.5**). Mild heterogeneous conditions (10% w/w Pd/C (10% Pd, unreduced), H₂ (1 atm)) afforded the crude hydrogenated crown ether **4[H]-*n*Pr-18C6** in a diastereomeric ratio of 96:4. After filtration and selective precipitation, the **4[H]-*n*Pr-18C6** was afforded in 70% yield as a single diastereoisomer. Assuming a (*S,S*) configuration of ***n*Pr-18C6**, the hydrogenation is thought to occurs from the *re* face of both olefin for steric reasons (respectively *si* face in case of (*R,R*) crown ether). In fine, the methyl and amide groups are positioned on the same face of the macrocycle after hydrogenation and hence an all-*cis* configuration for the products.



Scheme 2.5 Hydrogenation of **4[H]-*n*Pr-18C6**.

The same procedure was applied on (*S*)-Me-Bn-18C6 macrocycle (**Scheme 2.6**). Starting from a 1.3:1 mixture of diastereoisomers, the crude **4[H]-(*S*)-Me-Bn-18C6** was obtained as a diastereomeric mixture of four compounds in a 48:42:6:4 ratio. After filtration and selective precipitation, the macrocycle was afforded in 83% yield as 1:1 mixture of all-*cis* diastereoisomers. The loss of the minor diastereoisomers occurred during the purification by precipitation – the minor diastereoisomers being more soluble than the major ones.



Scheme 2.6 Hydrogenation of **4[H]-(*S*)-Me-Bn-18C6**.

2.3 Applications of Aliphatic-18C6 crown ethers in asymmetric PTC

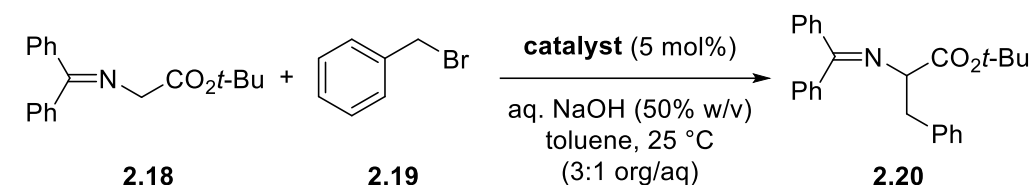
With these chiral crown ethers in hand and in particular the α -branched ones, their applications as asymmetric phase transfer catalysts were studied, in liquid-liquid biphasic systems in particular. The use of chiral crown ethers in asymmetric PTC is well established and was already presented in section 1.4.2.3.

2.3.1 Synthesis of protected phenylalanine

The alkylation of *N*-(diphenylmethylene)glycine ester **2.18** is a benchmark reaction to study the efficiency of catalysts in asymmetric PTC.^{51, 106} The use of the *tert*-butyl ester and the diphenylmethylene protection on the nitrogen atom ensures the stability of the compounds towards saponification and avoids the deprotonation of the α -alkylated products and hence a lack of racemization or double addition.

The alkylation of **2.18** with benzyl bromide **2.19** was first considered to test the ability of the new crown ethers to act as phase transfer catalyst (**Table 2.9**). Blank reactions were also conducted to ensure that the background reaction was negligible (entries 1-4). Using **Bn-18C6** as catalyst, protected phenylalanine **2.20** was satisfactorily obtained in 82% and 93% yield depending on the solvent (toluene or CH₂Cl₂ respectively, entries 5-6). According to previous work from the group of Bakó, the use of a lariat chain can improve the efficiency of the catalyst towards PTC,^{55c, d} however the use of crown ethers **MeO-ethyl-18C6** or **MeO-propyl-18C6** did not affect the yield or the reaction time of **2.20** significantly (entries 7-8). Nevertheless, this new type of **Aliphatic-18C6** crown ethers presents phase transfer abilities.

¹⁰⁶ Patel, N.; Sood, R.; Bharatam, P. V., *Chem. Rev.* **2018**, DOI: 10.1021/acs.chemrev.8b00169.

Table 2.9 Alkylation of protected glycine **2.18** using crown ethers as phase transfer catalyst.

Entry	Catalyst	Time	Conversion (%) ^[a]	Yield (%)
1	—	1 day	2	n.d. ^[b]
2	—	2.5 days	10	n.d.
3	—	6 days	35	n.d.
4 ^[c]	—	15 hours	<1	n.d.
5	Bn-18C6	2.5 days	>99	82
6 ^[c]	Bn-18C6	15 hours	>99	93
7	MeO-ethyl-18C6	2.5 days	>99	82
8	MeO-propyl-18C6	2.5 days	>99	79

[a] ¹H NMR monitoring [b] n.d. = not determined; [c] CH₂Cl₂ instead of toluene.

With these encouraging results with catalysts bearing achiral linear side chains, the use of catalysts bearing enantiopure arms was considered next. Assuming that the metal ion coordinates within the crown ether core as shown in the solid state structures (**Scheme 2.4**), it was expected that the chiral induction would come from both the amide substituents and the crown ether skeleton. Reactions should thus be performed on diastereomerically pure derivatives. Yet, as a first measure and to test the global reactivity, the alkylation was tested with 1.3:1 mixture of (**S**)-**Me-Bn-18C6** as catalyst (**Table 2.10**). Phenylalanine **2.20** was satisfactory obtained in 84% yield and in 17% *ee* (CSP-HPLC, entry 1).¹⁰⁷ Using (**R**)-**Me-Bn-18C6**, **2.20** was yielded with an inverted *ee* (-17%, entry 2). According to reported literature,¹⁰⁸ the first eluted enantiomer (*t_R* = 11.9 min) of **2.20** was assigned to the (*R*) configuration while the second eluted (*t_R* = 16.0 min) is of (*S*) configuration.

Substrate concentration was also found to influence the enantioselectivity. A 3:1 ratio between the organic phase (CH₂Cl₂) and the aqueous phase gave an enantiomeric excess of 17%

¹⁰⁷ **CSP HPLC:** Chiralcel® OD-H column, hexanes/*i*-PrOH (99:1), 0.5 mL/min, 23 °C, 2 μL/inj., λ = 254 nm.

¹⁰⁸ Shi, Q.; Lee, Y.-J.; Kim, M.-J.; Park, M.-K.; Lee, K.; Song, H.; Cheng, M.; Jeong, B.-S.; Park, H.-g.; Jew, S.-s., *Tetrahedron Lett.* **2008**, 49, 1380-1383.

using **(S)-Me-Bn-18C6** (Table 2.10, entries 1-2) while a 5:1 ratio gave 11% *ee* (entry 3). An analogue result was obtained with **(R)-Me-Bn-18C6** (entry 4). The use of toluene as solvent increased the reaction time and gave a lower *ee* but, interestingly, in favor of the other enantiomer of phenylalanine **2.20** (entry 5). CH₂Cl₂ was then kept as solvent for the rest of the study.¹⁰⁹ These initial results although poor in term of enantioselectivity led us to performed the reaction with other aqueous bases and non-racemic chiral crown ethers.

Table 2.10 Alkylation of protected glycine using asymmetric PTC and chiral crown ethers.

2.18	2.19			2.20	
Entry	Catalyst* ^[a]	Time	Yield (%)	<i>ee</i> (%)	Preferred configuration
1	(S)-Me-Bn-18C6	15 hours	84	17	<i>R</i>
2	(R)-Me-Bn-18C6	15 hours	84	-17	<i>S</i>
3^[b]	(S)-Me-Bn-18C6	15 hours	84	11	<i>R</i>
4^[b]	(R)-Me-Bn-18C6	15 hours	84	-11	<i>S</i>
5^[c]	(S)-Me-Bn-18C6	4 days	84	-12	<i>S</i>

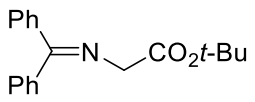
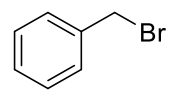
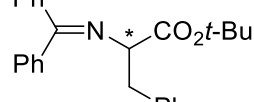
[a] *dr* 1.3:1; [b] ratio 5:1 (instead of 3:1) between organic and aqueous phases; [c] toluene instead of CH₂Cl₂.

The screening of bases was thus performed (Table 2.11).¹¹⁰ Sodium hydroxide turned out to be better than the potassium and cesium analogues that gave lower reactivity and enantioinductions (entries 1-4). Decreasing the concentration of the base to 1 M, provoked a lack of conversion of **2.18** to **2.20** (entry 5). Only an increase of catalyst loading to 10 mol% improved slightly the enantiomeric excess to 21% (entry 6).

¹⁰⁹ Various solvents were also tested but none of them showed a better enantioinduction than CH₂Cl₂. See section 7.5.2 for details.

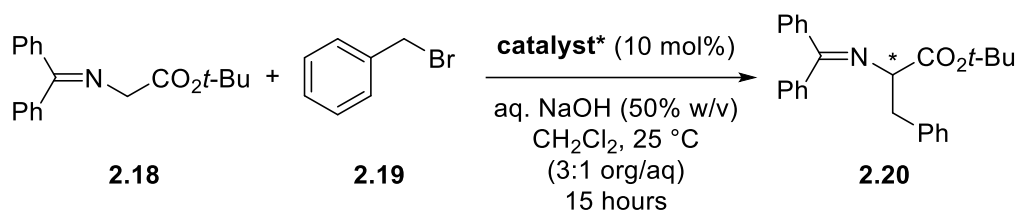
¹¹⁰ For now on, the conversion of the transformation is monitored by TLC analysis.

Table 2.11 Screening of the conditions for asymmetric PTC.

<div style="display: flex; align-items: center; justify-content: space-around;"> <div style="text-align: center;">  <p>2.18</p> </div> <div style="text-align: center;">  <p>2.19</p> </div> <div style="text-align: center;"> <p>(S)-Me-Bn-18C6 (cat.) (<i>dr</i> 1.3:1)</p> <p>aq. MOH (50% w/v) CH₂Cl₂, 25 °C (3:1 org/aq)</p> </div> <div style="text-align: center;">  <p>2.20</p> </div> </div>					
Entry	Cat. loading	MOH	Time	Conversion (%)	<i>ee</i> (%)
1	5 mol%	NaOH	15 hours	>99	17
2	5 mol%	KOH	4 days	75%	4
3	10 mol%	KOH	4 days	>99%	5
4	5 mol%	CsOH	4 days	10%	3
5 ^[a]	5 mol%	NaOH	4 days	<1	n.d. ^[b]
6	10 mol%	NaOH	15 hours	>99	21

[a] 1 M NaOH instead of 50% (w/v); [b] n.d. = not determined.

The different non-racemic crown ether catalysts were also tested as diastereomeric mixtures (**Table 2.12**). The use of hydrogenated catalyst **4[H]-(S)-Me-Bn-18C6**, was detrimental to the enantioselectivity of the transformation (3% vs 21% *ee*, entries 1-2). However, adding bulk by elongating the methyl branch for ethyl or propyl gave two different results: **(S)-Et-Bn-18C6** improved the *ee* to 27% while **(S)-Pr-Bn-18C6** decreased it to 11% (entries 3-4). The modulation of the electronic properties of the phenyl ring was also tested with *p*-fluoro or *p*-methoxy group leading to 18% and 26% *ee* respectively (entries 5-6). Unfortunately, neither the steric or the electronic parameters seemed to influence the enantioinduction in a systematic manner. We next considered the replacement of the phenyl with a more sterically demanding naphthyl groups. With 2-naphthyl, **2.20** is afforded in 22% *ee* similarly to **(S)-Me-Bn-18C6** (entry 7) but the highest *ee* was obtained with **(S)-Me-1-naphth-18C6** (*dr* 1.4:1, 32%, entry 8).

Table 2.12 Screening of the catalysts for asymmetric PTC.


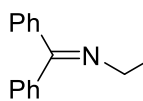
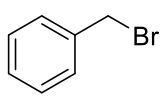
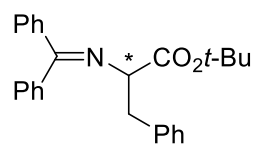
Entry	Catalyst*	<i>dr</i> (cat.)	<i>ee</i> (%)
1	(<i>S</i>)-Me-Bn-18C6	1.3:1	21
2	4[H]-(<i>S</i>)-Me-Bn-18C6	1:1	3
3	(<i>S</i>)-Et-Bn-18C6	1.1:1	27
4	(<i>S</i>)-Pr-Bn-18C6	1:1	11
5	(<i>R</i>)-Me- <i>p</i> F-Bn-18C6	1.2:1	-18
6	(<i>S</i>)-Me- <i>p</i> OMe-Bn-18C6	1.2:1	26
7	(<i>S</i>)-Me-2-naphth-18C6	1.4:1	22
8	(<i>S</i>)-Me-1-naphth-18C6	1.4:1	32

As (*S*)-Me-1-naphth-(*S*)-18C6 proved to be the better catalyst of the series, other parameters were investigated (temperature and catalyst loading, **Table 2.13**). The temperature was modulated first (entries 1-3) and had a positive effect on the enantioselectivity with 40% *ee* at 10 °C and 43% *ee* at 0 °C (catalyst *dr* 1.4:1).

Finally, and as it was conceived initially, diastereomerically pure catalysts were investigated. With the (*S,S,S,S*) major diastereoisomer of (*S*)-Me-1-naphth-(*S*)-18C6 (entries 4-6), the induction improved slightly to 39%, 45% and 44% *ee* at 25, 10 and 0 °C respectively. However, at 10 °C, using the minor (*S,R,R,S*) diastereoisomer, the reaction time increased drastically to two days and only a low enantioselectivity was obtained in favor the other enantiomer of **2.20** (-13% *ee*, entry 11). There is a clear matched and mismatched situation in the reaction with (*S,S,S,S*) and (*S,R,R,S*)-diastereoisomer respectively.

Finally, attempts to increase the catalyst loading to 20 or 30 mol% (major diastereoisomer, entries 8-9) did not improve further the enantioselectivity (both 45% *ee*, at 10 °C). A maximum induction of 45% *ee* was thus obtained for this transformation at 10 °C and 10 mol% catalyst loading.

Table 2.13 Screening of the catalysts for asymmetric PTC.

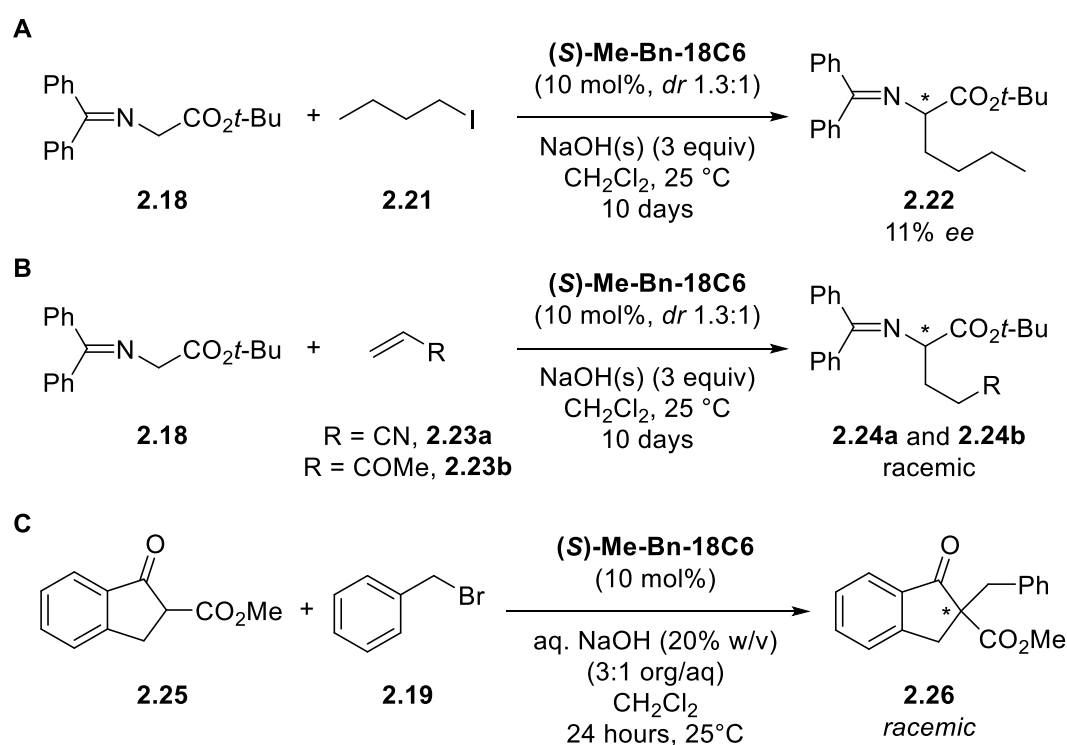
<div style="display: flex; align-items: center; justify-content: center;"> <div style="text-align: center;">  <p>2.18</p> </div> <div style="margin: 0 10px;">+</div> <div style="text-align: center;">  <p>2.19</p> </div> <div style="margin-left: 20px;"> <p>(S)-Me-1-naphth-18C6 (cat. loading)</p> <p>aq. NaOH (50% w/v) CH₂Cl₂, temperature (3:1 org/aq) time</p> </div> <div style="text-align: center;">  <p>2.20</p> </div> </div>					
Entry	<i>dr</i> (cat.)	Cat. loading (mol%)	Temperature (°C)	Time (h)	<i>ee</i> (%)
1	1.4:1	10	25	15	32
2	1.4:1	10	10	24	40
3	1.4:1	10	0	24	43
4	major	10	25	15	39
5	major	10	10	24	45
6	major	10	0	24	44
7	minor	10	10	48	-13
8	major	20	10	24	45
9	major	30	10	24	45

The use of the new crown ethers as effective asymmetric phase transfer catalysts was demonstrated with a maximum of 45% *ee* afforded for the enantioselective alkylation of a protected glycine. Despite the moderate enantioselectivity, the study proved that the substituents on the crown ether, together with the chiral crown ether geometry, can be used to build robust catalysts in asymmetric PTC. It was shown that the major (*S,S,S,S*) diastereoisomer reacted faster than the minor (*S,R,R,S*) one but the reason for this difference still remains unclear.

2.3.2 Asymmetric addition by PTC

In view of the moderate enantiomeric excesses obtained in the last section, different modulations were considered (**Scheme 2.7**). First changing the electrophile and using solid-liquid extraction conditions, the addition of **2.18** to iodobutane **2.21** yielded the protect amino acid

2.22 only in 11% *ee* after 10 days (**Scheme 2.7A**). Then, the Michael addition on acrylonitrile **2.23a** or methyl vinyl ketone **2.23b** yielded unfortunately **2.24a** and **2.24b** respectively in racemic form after 10 days (**Scheme 2.7B**). These three examples suffer from the lower reactivity of the substrate in comparison with the precedent transformation. Yet, changing the nucleophile for cyclic ketoester **2.25** under liquid-liquid extraction also led to a racemic mixture of **2.26** after one day when reacted with benzyl bromide **2.19** (**Scheme 2.7C**). These four examples indicate a limitation both in substrate and scope presented by the chiral crown ethers-catalyzed reaction (section 1.4.2.3).

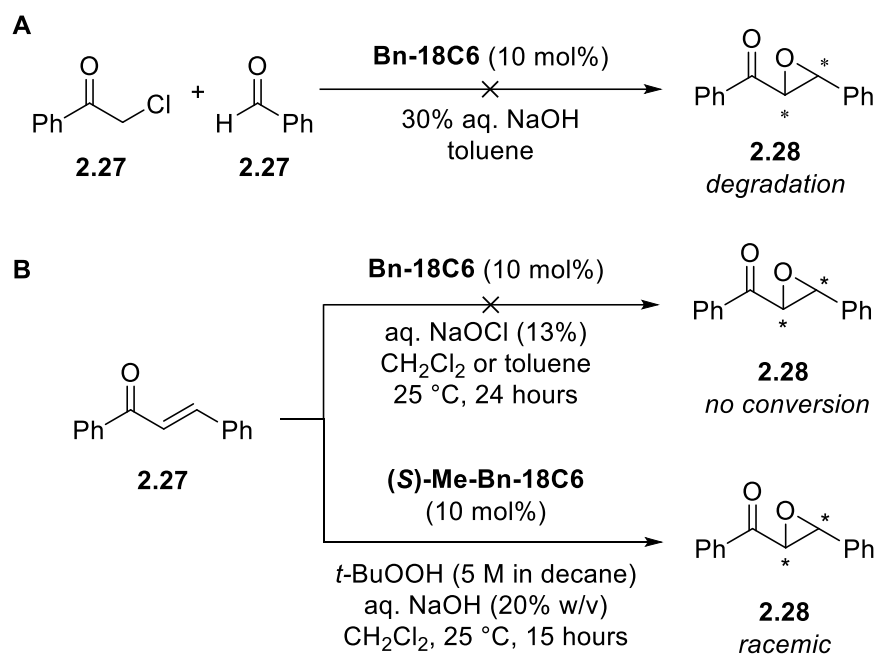


Scheme 2.7 Alkylations by asymmetric PTC.

2.3.3 Asymmetric epoxide syntheses by PTC

Facing the disappointing results of the alkylation and Michael addition reactions, the crown ether-catalyzed formation of epoxides was investigated next. As presented in section 1.4.2.3, two approaches are possible to synthesize α,β -epoxyketones: (i) an oxidation of olefins or with a direct Darzens reaction.⁵⁹⁻⁶⁰ Sadly, the Darzens condensation catalyzed by **Bn-18C6** led only to

degradation or absence of conversion of the chloroacetates and aldehydes (**Scheme 2.8A**). On one hand, the **Bn-18C6**-catalyzed epoxidation of **2.27** with sodium hypochlorite did not proceed either (**Scheme 2.8B**, top).¹¹¹ On the other hand, the oxidation with *t*-BuOOH proposed by Bakó could be catalyzed by (**S**)-**Me-Bn-18C6** but only racemic compound **2.28** was obtained (**Scheme 2.8B**, bottom).^{59b}



Scheme 2.8 Epoxidation by asymmetric PTC.

2.4 Conclusion

The access to bis-amide chiral crown ethers carrying aliphatic nitrogen substituents was presented in this chapter. Using linear amines, the crown ethers were obtained in moderate yields using a two-steps process – an aminolysis induced by an organoreagent (TBD) followed by a transposition under strongly basic conditions (*t*-BuOK). The chiral crown ethers were obtained as single diastereoisomers (*dr* > 49:1). On the contrary to the aromatic series, water molecules

¹¹¹ Ooi, T.; Ohara, D.; Tamura, M.; Maruoka, K., *J. Am. Chem. Soc.* **2004**, 126, 6844-6845.

are not naturally included inside the crown ether. This sequence was found to be very specific to the **18C6** backbone as product could not be formed starting from **18C4** macrocycle. Also harsher conditions were necessary to introduce α -branched amines during the aminolysis reaction and the corresponding crown ethers were obtained in low to moderate yields. When enantiopure amines were utilized, the macrocycles were obtained as mixtures of diastereoisomers (1:1 to 1.4:1).

These new crown ethers (bearing enantiopure substituents) were tested as catalysts in asymmetric PTC for the synthesis of protected phenylalanine from protected glycine with enantioselectivities up to 45% *ee*. A few other examples of asymmetric PTC (alkylation, Michael addition, Darzen reaction and oxidation of olefin) were also tested but afforded low enantioinduction or racemic products.

As presented in the introduction (section 1.4.2.3), the use of chiral crown ethers as efficient asymmetric catalysts is challenging and limited to specific substrates and catalysts, the results presented in this chapter corroborating this statement. It was shown that the a matched – mismatched situation is present with both diastereomerically pure **(S)-Me-1-naphth-18C6**. Finally, other asymmetric transformations could be tested in order to find one which would lead to high enantioselectivities.

3 Heteroditopic cryptands: synthesis and ion pair recognition

3.1 Introduction

3.1.1 Heteroditopic receptors

Anions and cations play a significant and indispensable role in biological and environmental systems. If cation binding is a well-established field of research, anion binding developed more slowly.¹¹² Nevertheless, the design and synthesis of receptors for the recognition of anions have recently received an increasing attention.¹¹³ Anion recognition is challenging due to the high free solvation energies and the various shapes and sizes of these entities. In spite of this issues, several host structures, such as protonated polyamines,¹¹⁴ quaternary ammonium-derived,¹¹⁵ Lewis

¹¹² (a) Beer, P. D.; Gale, P. A., *Angew. Chem. Int. Ed.* **2001**, *40*, 486-516. (b) Sessler, J. L.; Sansom, P. I.; Andrievsky, A.; Král, V., Application Aspects involving the Supramolecular Chemistry of Anions. In *The Supramolecular Chemistry of Anions*, Bianchi, A.; Bowman-James, K.; García-España, E., Eds. John Wiley & Son, Ltd.: Weinheim 1997; Vol. 4, pp 355-419.

¹¹³ (a) Davis, A. P.; Perry, J. J.; Williams, R. P., *J. Am. Chem. Soc.* **1997**, *119*, 1793-1794. (b) Berger, M.; Schmidtchen, F. P., *J. Am. Chem. Soc.* **1996**, *118*, 8947-8948. (c) Gale, P. A.; Sessler, J. L.; Král, V.; Lynch, V., *J. Am. Chem. Soc.* **1996**, *118*, 5140-5141. (d) Král, V.; Furuta, H.; Shreder, K.; Lynch, V.; Sessler, J. L., *J. Am. Chem. Soc.* **1996**, *118*, 1595-1607. (e) Izatt, R. M.; Pawlak, K.; Bradshaw, J. S.; Bruening, R. L., *Chem. Rev.* **1995**, *95*, 2529-2586. (f) Dietrich, B., *Pure Appl. Chem.* **1993**, *65*, 1457-1464.

¹¹⁴ Kimura, E.; Sakonaka, A.; Yatsunami, T.; Kodama, M., *J. Am. Chem. Soc.* **1981**, *103*, 3041-3045.

¹¹⁵ Langton, M. J.; Serpell, C. J.; Beer, P. D., *Angew. Chem. Int. Ed.* **2016**, *55*, 1974-1987.

acid,¹¹⁶ amides,¹¹⁷ ureas¹¹⁸ or thioureas¹¹⁹ among others, have been successfully applied for anion recognition over the last few decades.¹²⁰

Monotopic receptors are competent for binding only single ions. However, the binding of an individual cation or anion usually requires an important energetic cost to separate it from its counterion. To overcome these issues, and taking advantage of ion pairing effects, the design of heteroditopic receptors containing recognition sites for both cation and anion has emerged as a new area of research.¹²¹ In that sense, thanks to the predisposition of oppositely charged ions to form ion pairs,¹¹⁴⁻¹¹⁸ heteroditopic receptors containing distinct recognition sites for both cations¹²² and anions¹²⁰ in single molecular frameworks are particularly attractive for salt recognition. These (neutral) synthetic moieties offer many advantages in terms of affinity and/or selectivity by favoring electrostatic and allosteric contributions in the ion pair binding.¹²³ Elegant studies have been reported by Barboiu,¹²⁴ Beer,¹²⁵ Flood,¹²⁶ Nam,¹²⁷ Piątek,¹²⁸ Reinhoudt,¹²⁹

¹¹⁶ Reetz, M. T.; Niemeyer, C. M.; Harms, K., *Angew. Chem. Int. Ed.* **1991**, *30*, 1472-1474.

¹¹⁷ Gale, P. A., *Chem. Commun.* **2005**, 3761-3772.

¹¹⁸ Carroll, C. N.; Coombs, B. A.; McClintock, S. P.; Johnson II, C. A.; Berryman, O. B.; Johnson, D. W.; Haley, M. M., *Chem. Commun.* **2011**, *47*, 5539-5541.

¹¹⁹ Krishnamurthi, J.; Ono, T.; Amemori, S.; Komatsu, H.; Shinkai, S.; Sada, K., *Chem. Commun.* **2011**, *47*, 1571-1573.

¹²⁰ (a) Gale, P. A.; Busschaert, N.; Haynes, C. J. E.; Karagiannidis, L. E.; Kirby, I. L., *Chem. Soc. Rev.* **2014**, *43*, 205-241. (b) Wenzel, M.; Hiscock, J. R.; Gale, P. A., *Chem. Soc. Rev.* **2012**, *41*, 480-520. (c) Gale, P. A., *Chem. Soc. Rev.* **2010**, *39*, 3746-3771.

¹²¹ Kim, S. K.; Sessler, J. L., *Acc. Chem. Res.* **2014**, *47*, 2525-2536.

¹²² (a) Steed, J. W.; Atwood, J. L., *Supramolecular Chemistry*. John Wiley & Son, Ltd.: Chichester, U.K., 2009. (b) Lehn, J.-M., *Supramolecular Chemistry*. Wiley: Weinheim, 1995; Vol. 1.

¹²³ Smith, B. D., Ion-Pair Recognition by Ditopic Macrocyclic Receptors. In *Macrocyclic Chemistry: Current Trends and Future Perspectives*, Gloe, K., Ed. Springer Netherlands: Dordrecht, 2005; pp 137-151.

¹²⁴ Barboiu, M.; Vaughan, G.; van der Lee, A., *Org. Lett.* **2003**, *5*, 3073-3076.

¹²⁵ (a) McConnell, A. J.; Beer, P. D., *Angew. Chem. Int. Ed.* **2012**, *51*, 5052-5061. (b) Picot, S. C.; Mullaney, B. R.; Beer, P. D., *Chem. Eur. J.* **2012**, *18*, 6230-6237.

¹²⁶ Qiao, B.; Sengupta, A.; Liu, Y.; McDonald, K. P.; Pink, M.; Anderson, J. R.; Raghavachari, K.; Flood, A. H., *J. Am. Chem. Soc.* **2015**, *137*, 9746-9757.

¹²⁷ Jeon, N.-J.; Yeo, H.-M.; Nam, K.-C., *Bull. Korean Chem. Soc.* **2008**, *29*, 663-665.

¹²⁸ Załubiniak, D.; Kos, J.; Piątek, P., *Tetrahedron* **2017**, *73*, 7190-7194.

¹²⁹ (a) Rudkevich, D. M.; Mercer-Chalmers, J. D.; Verboom, W.; Ungaro, R.; de Jong, F.; Reinhoudt, D. N., *J. Am. Chem. Soc.* **1995**, *117*, 6124-6125. (b) Rudkevich, D. M.; Verboom, W.; Reinhoudt, D. N., *J. Org. Chem.* **1994**, *59*, 3683-3686.

Schubert,¹³⁰ Sessler,¹³¹ Smith¹³² and Thordarson¹³³ among others. Applications in various fields such as salt solubilization, extraction, membrane transports, catalysis and sensing have been developed.¹³⁴

3.1.2 Examples of crown ether-based heteroditopic receptors

Amid such derivatives, a common motif for the binding of cations is the crown ether functionality. In this section, the heteroditopic receptors using a crown ether motif will be presented briefly. As an example, Rissanen and co-workers synthesized heteroditopic receptors based on (di)benzo-crown ethers and ureas for the binding of cations and anions respectively (**Figure 3.1**).¹³⁵ The receptors demonstrated positive cooperativity towards halides or oxyanions (acetate, carbonate and sulfate) and alkali metals or ammonium. The binding studies were conducted in solution (¹H NMR), solid state (X-ray diffraction) and gas phase (ESI-MS). Different binding modes as contact or separated ion pairs were demonstrated, depending on the size of the cation guest or the crown ethers host. Additionally, the stoichiometry between the receptor and the salts also varied from 1:1 to 2:1 or 1:2.

¹³⁰ Tepper, R.; Schulze, B.; Bellstedt, P.; Heidler, J.; Gorls, H.; Jäger, M.; Schubert, U. S., *Chem. Commun.* **2017**, 53, 2260-2263.

¹³¹ (a) He, Q.; Peters, G. M.; Lynch, V. M.; Sessler, J. L., *Angew. Chem. Int. Ed.* **2017**, 56, 13396-13400. (b) Sessler, J. L.; Brucker, E. A., *Tetrahedron Lett.* **1995**, 36, 1175-1176.

¹³² Shukla, R.; Kida, T.; Smith, B. D., *Org. Lett.* **2000**, 2, 3099-3102.

¹³³ Howe, E. N. W.; Bhadbhade, M.; Thordarson, P., *J. Am. Chem. Soc.* **2014**, 136, 7505-7516.

¹³⁴ (a) Kim, S. K.; Sessler, J. L., *Chem. Soc. Rev.* **2010**, 39, 3784-3809. (b) Caltagirone, C.; Gale, P. A., *Chem. Soc. Rev.* **2009**, 38, 520-563. (c) Mahoney, J. M.; Nawaratna, G. U.; Beatty, A. M.; Duggan, P. J.; Smith, B. D., *Inorg. Chem.* **2004**, 43, 5902-5907. (d) Smith, B. D.; Mahoney, J. M., In *Encyclopedia of Supramolecular Chemistry*, Atwood, J. L.; Steed, J. W., Eds. Pergamon: New York, 2004; Vol. 2, pp 1291-1294. (e) Kirkovits, G. J.; Shriver, J. A.; Gale, P. A.; Sessler, J. L., *J. Incl. Phenom. Macrocycl. Chem.* **2001**, 41, 69-75. (f) Antonisse, M. G.; Reinhoudt, D. N., *Chem. Commun.* **1998**, 443-448.

¹³⁵ (a) Mäkelä, T.; Rissanen, K., *Dalton Trans.* **2016**, 45, 6481-6490. (b) Mäkelä, T.; Kiesilä, A.; Kalenius, E.; Rissanen, K., *Chem. Eur. J.* **2016**, 22, 14264-14272. (c) Mäkelä, T.; Kalenius, E.; Rissanen, K., *Inorg. Chem.* **2015**, 54, 9154-9165.

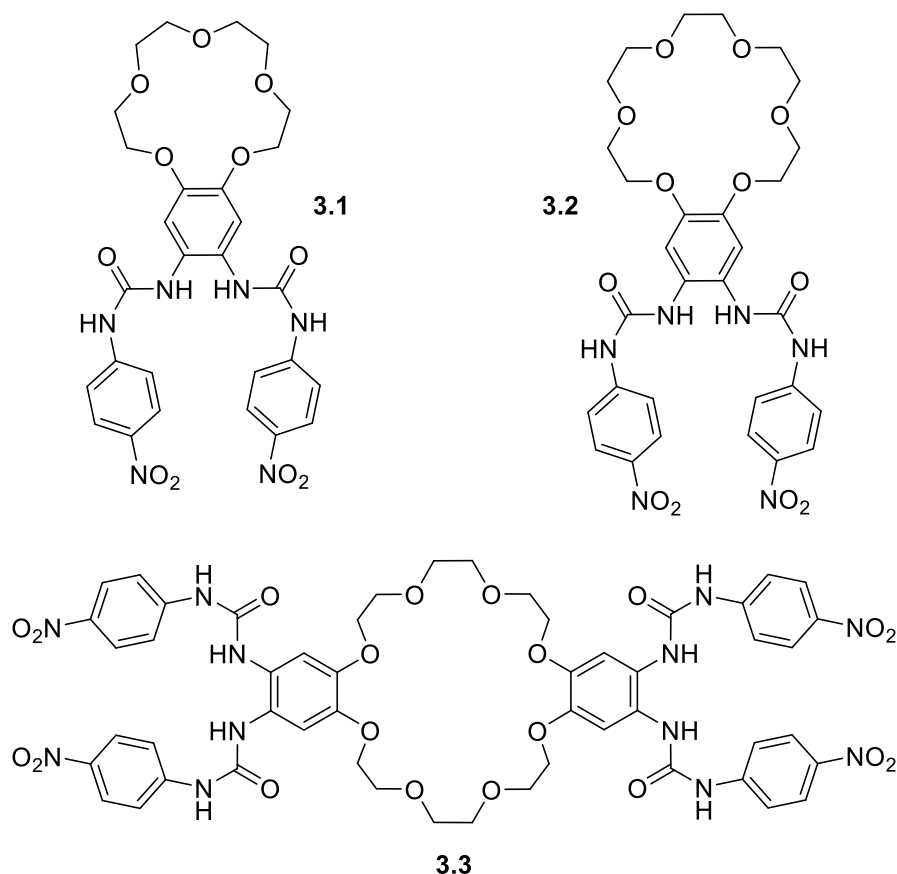


Figure 3.1 Heteroditopic receptors synthesized by Rissanen and co-workers.¹³⁵

In the same manner, the group of Romański also proposed ditopic receptors based on **monoaza-18-Crown-6** and L-ornithine (**Figure 3.2**, receptors **3.4** to **3.6**). The crown ether domain coordinates the cation while the (thio)urea or the squaramide unit binds the anion. The R chains was selected to enable the use of different analytical techniques (¹H NMR spectroscopy, spectrophotometry and electrochemistry) to confirm the ditopic character of these derivatives. Receptor **3.6** could also be functionalized with polyethylene glycol spacers and be incorporated into polymeric resins. These ligands were able to bind cooperatively alkali metals (Na⁺, K⁺) or ammonium with halides (Cl[−], Br[−]), acetate, nitrate or nitrite.¹³⁶ In addition, they investigated the possibility to extract efficiently and selectively nitrite anion (as sodium salt) out of aqueous or

¹³⁶ (a) Ziach, K.; Karbarz, M.; Romański, J., *Dalton Trans.* **2016**, 45, 11639-11643. (b) Zdanowski, S.; Piątek, P.; Romański, J., *New J. Chem.* **2016**, 40, 7190-7196. (c) Karbarz, M.; Romański, J., *Inorg. Chem.* **2016**, 55, 3616-3623. (d) Piątek, P.; Zdanowski, S.; Romański, J., *New J. Chem.* **2015**, 39, 2090-2095. (e) Piątek, P.; Karbarz, M.; Romański, J., *Dalton Trans.* **2014**, 43, 8515-8522. (f) Romański, J.; Trzaskowski, B.; Piątek, P., *Dalton Trans.* **2013**, 42, 15271-15274. (g) Romański, J.; Piątek, P., *Chem. Commun.* **2012**, 48, 11346-11348.

organic solutions over other naturally occurring anions. In that context, the macrotricyclic cryptand **3.7** exhibited an enhanced affinity for ammonium nitrate and nitrite over other combinations of cations (alkali metals) or anions (acetate or dihydrogenphosphate) for instance.¹³⁷

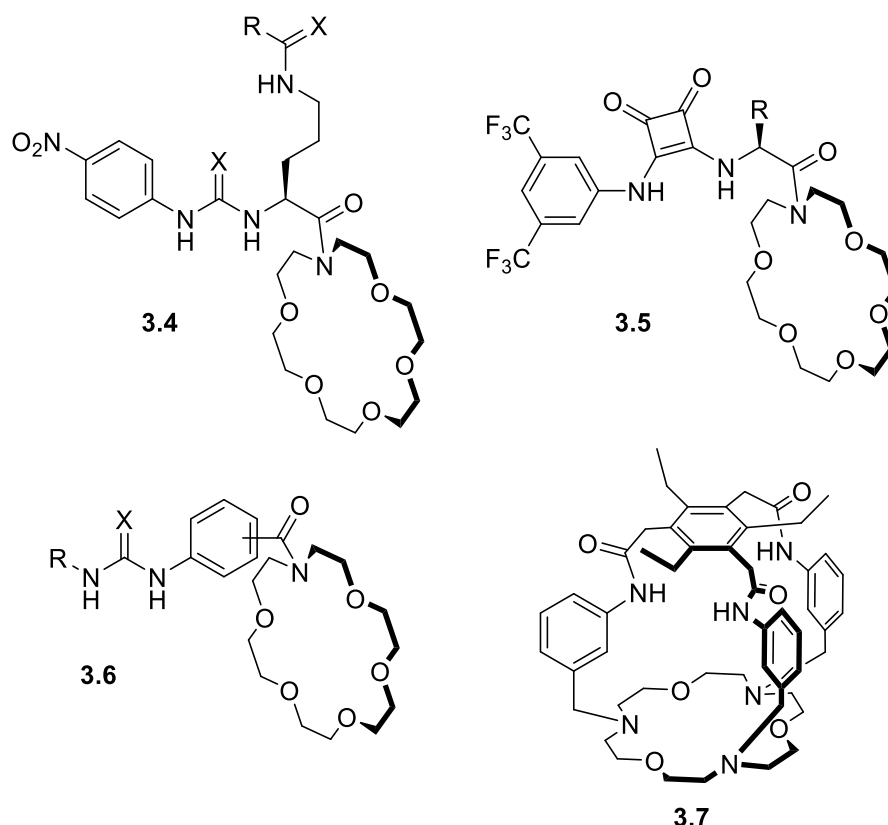


Figure 3.2 Heteroditopic receptors synthesized by Romański and co-workers (X = O, S; R = anthraquinone, *p*-nitro phenyl, PEG).¹³⁶⁻¹³⁷

Following a different approach for the ion pairing interaction, Smith and co-workers have prepared cryptands **3.8** and **3.9** starting from **dibenzo-18-Crown-6** and **diaza-18-Crown-6** macrocycles respectively (**Figure 3.3**, section 1.3.1).^{29b, 138} Using ¹H NMR spectroscopy and single-crystal X-ray diffraction, they demonstrated that cryptands **3.8** are able to bind cooperatively alkali halides as solvent-separated ion pairs. The cation is complexed by the crown ether while the halide is bonded through hydrogen bonding interactions with the N-H bonds of the amides.

¹³⁷ Romański, J.; Piątek, P., *J. Org. Chem.* **2013**, 78, 4341-4347.

¹³⁸ (a) Mahoney, J. M.; Stucker, K. A.; Jiang, H.; Carmichael, I.; Brinkmann, N. R.; Beatty, A. M.; Noll, B. C.; Smith, B. D., *J. Am. Chem. Soc.* **2005**, 127, 2922-2928. (b) Mahoney, J. M.; Davis, J. P.; Beatty, A. M.; Smith, B. D., *J. Org. Chem.* **2003**, 68, 9819-9820. (c) Mahoney, J. M.; Beatty, A. M.; Smith, B. D., *J. Am. Chem. Soc.* **2001**, 123, 5847-5848.

Similarly, **3.9** also binds salts but as contact ion pairs. In this case, not only alkali halides but also ammonium halides or alkali trigonal oxyanions such as nitrate, nitrite and acetate are recognized.

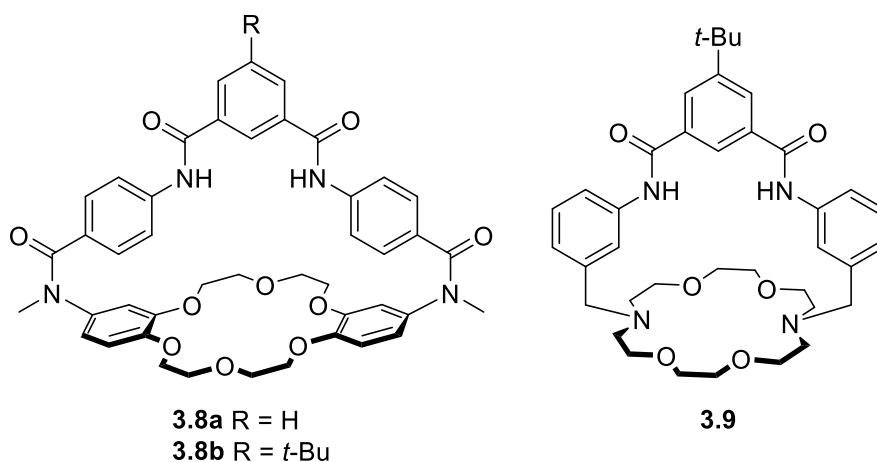


Figure 3.3 Cryptands synthesized by Smith and co-workers.^{29b, 138}

Finally, the group of Huang proposed receptor **3.10** which is structurally similar to **3.3** (Figure 3.4).¹³⁹ Instead of alkali metals, they studied the binding of paraquat cations (bipyridinium cations) with different counterions. Different species were observed depending on the anion used. With the trifluoroacetate anion, a pseudorotaxane is observed on the solid state (paraquat through the crown ether) while complexes, with the paraquat sandwiched between the two phenylene rings, are formed with chloride or hexafluorophosphate anions. In continuation of their work, cryptand **3.11** was synthesized (section 1.3.1) and the host-guest interaction with paraquat chloride was analyzed in solution (¹H NMR, spectrophotometry), solid state (X-ray diffraction) and gas phase (EI-MS) showing that the salt is cooperatively complexed as contact ion pair within the cryptand.^{29a}

¹³⁹ Zhu, K.; Li, S.; Wang, F.; Huang, F., *J. Org. Chem.* **2009**, 74, 1322-1328.

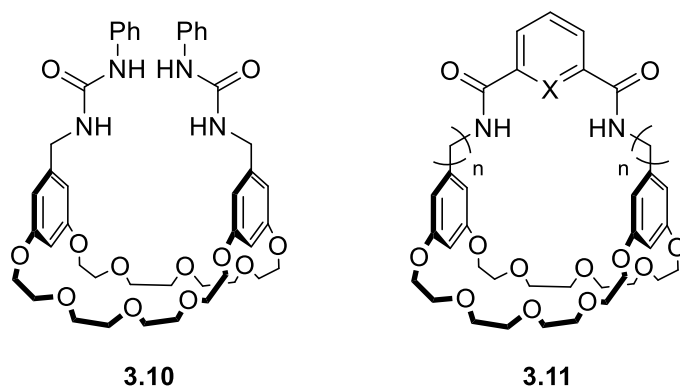
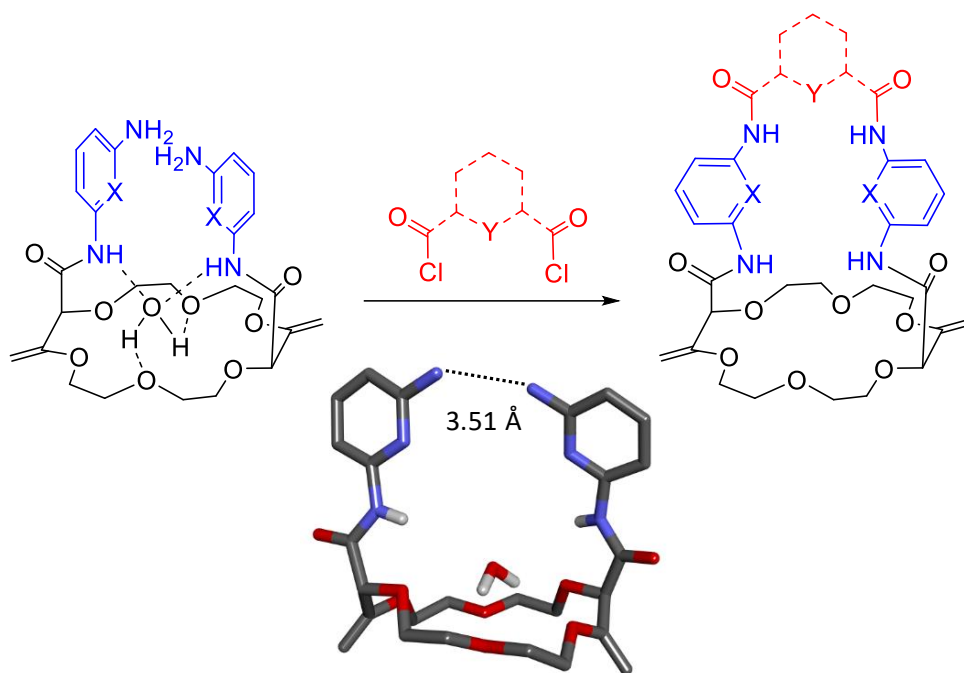


Figure 3.4 Heteroditopic receptors synthesized by Huang and co-workers.^{29a, 139}

3.2 Novel heteroditopic cryptands

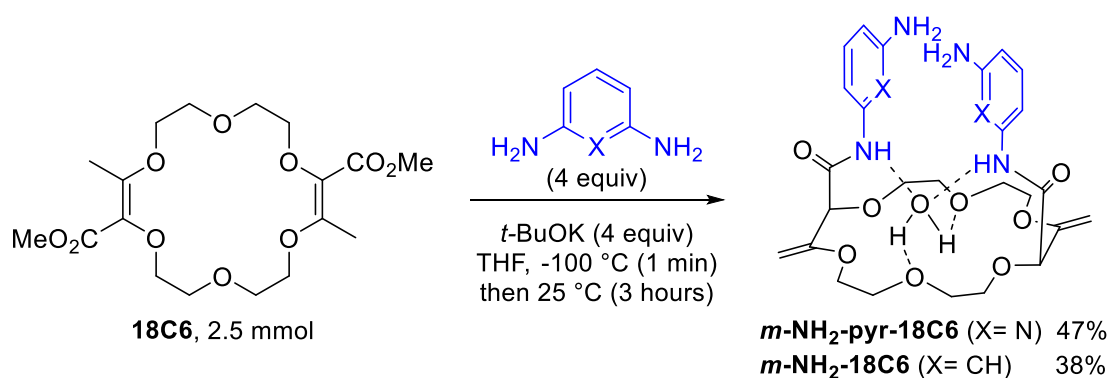
Despite these various examples, the preparation of ditopic receptors is still challenging and it suffers from the drawback of synthesizing efficiently (highly) functionalized crown ether derivatives (section 1.3.1). In that sense and inspired by the work of Rissanen, Romański, Smith and Huang, we envisaged to take advantage of the straightforward access to ***m*-NH₂-pyr-18C6** or ***m*-NH₂-18C6** crown ethers to transform them into cryptands (**Scheme 3.1**). Synthetically, this strategy could afford cryptands in three steps only from simple 1,4-dioxane substrate. Analysis of the solid state structure of ***m*-NH₂-pyr-18C6** revealed that the two nitrogen atoms of the amino groups are separated by a rather short distance (3.51 Å) ideal for ring closure reactions with dicarbonyl dichloride reagents. The obtained cryptands could then benefit from the H-donor abilities of the N-H bonds for anion binding and, coupled with the cation binding abilities of the crown ether domain, act as ditopic receptors. The work presented in this chapter will focus on the synthesis of such derivatives and on the investigation of their binding properties towards salts made of monovalent cations and linear triatomic anions in particular. Both solution and solid state analysis, using ¹H NMR spectroscopy and single-crystal X-ray diffraction respectively, were utilized. This work was performed in collaboration with Dr. Sumit Kumar Ray and was reported in the literature during this PhD.⁸²



Scheme 3.1 Synthesis of novel heteroditopic cryptands and stick view of the crystal structure of *m*-NH₂-pyr-18C6.

3.2.1 Synthesis of the diamino precursors

The synthesis of *m*-NH₂-pyr-18C6 and *m*-NH₂-18C6 was previously reported on a 0.25 mmol scale and the purification involved a silica gel preparative TLC.^{3b} A more convenient procedure was thus required to access these two diamino precursors efficiently on a larger scale. We thus attempted the synthesis of the derivatives on a gram scale (2.5 mmol, **Scheme 3.2**) but unfortunately the purification procedure by direct precipitation from the crude mixture failed. However standard purification by column chromatography followed by a selective precipitation afforded the desired crown ethers in 47% and 38% yield respectively improving the yield previously reported on smaller scales (30% and 18%).



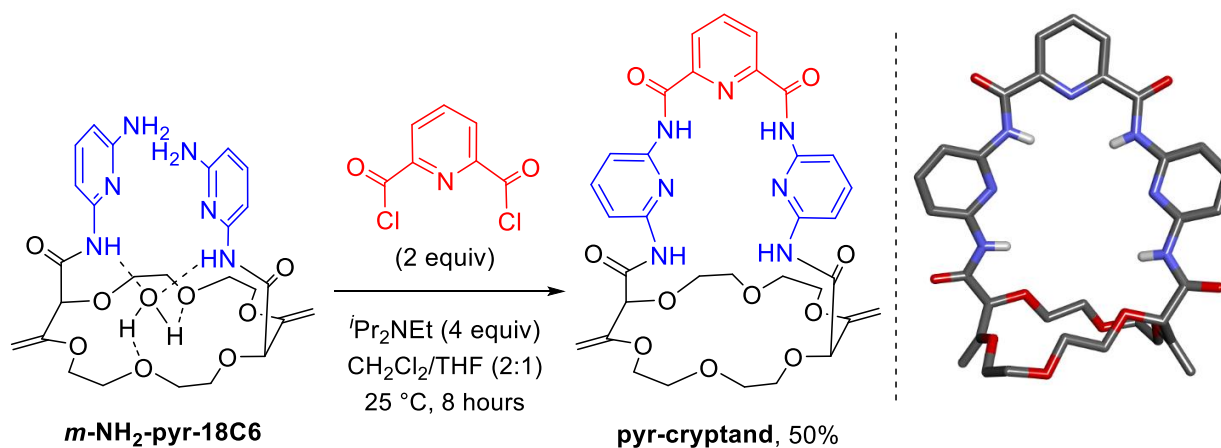
Scheme 3.2 Gram-scale synthesis of ***m*-NH₂-pyr-18C6** and ***m*-NH₂-18C6**.

3.2.2 Ring closure reactions

Having the precursors in hand, the ring closure was considered next. Dicarbonyl dichloride reagents were selected as valuable and readily available linkers. The ring closure was performed by treatment of ***m*-NH₂-pyr-18C6** or ***m*-NH₂-18C6** with these reagents in presence of a base (Hünig's base) and the scope is presented in the following section.

3.2.2.1 Ring closure with aromatic dichlorides

Satisfactorily, slow addition of 2,6-pyridine dicarbonyl dichloride (2 equiv) to a solution of ***m*-NH₂-pyr-18C6** in presence of Hünig's base (4 equiv) at relatively high concentration (10^{-2} M) yielded **pyr-cryptand** (50%) after double condensation (**Scheme 3.3**). The solution NMR spectroscopic analysis revealed a C_2 -symmetry of the cryptand. Crystallization of **pyr-cryptand** by slow evaporation of a $\text{CH}_2\text{Cl}_2/\text{MeOH}$ mixture furnished crystals suitable for X-ray analysis. The obtained structure is presented in **Scheme 3.3** and is compatible with the solution conformations observed in NMR spectroscopy. In this geometry, all four donor N-H bonds point gratifyingly inwards the cavity with the carbonyls function oriented outwards as expected for favorable anion binding (**Scheme 3.3**, right).



Scheme 3.3 Synthesis and stick view of the crystal structure of **pyr-cryptand**.

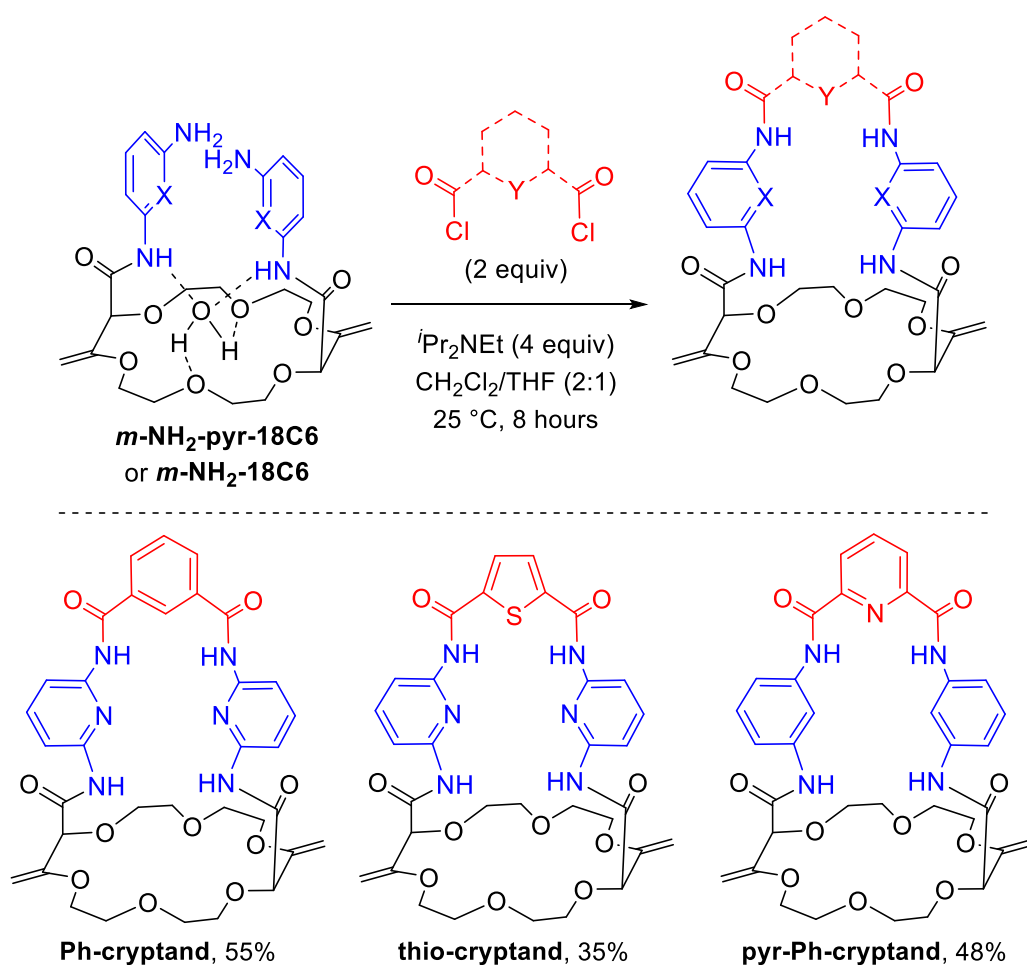
Using the same reaction conditions, the condensation with *m*-phenylenedicarbonyl dichloride and the corresponding thiophene-based reagent led to the efficient synthesis of **Ph-cryptand** and **thio-cryptand** in 55% and 35% respectively (**Scheme 3.4**). The lower yield for **thio-cryptand** can be explained by a disfavored ring closure induced by the larger bond angle (carbonyl – sulfur/nitrogen – carbonyl) of the five-membered thiophene ring (212.39°), compared to the six-membered pyridine ring (175.73°).¹⁴⁰ The condensation of 2,6-pyridine dicarbonyl dichloride was then tested with ***m*-NH₂-18C6** and **pyr-Ph-cryptand** was isolated in 48% yield. For these three cryptands, the solution studies (NMR spectroscopy) also revealed a C₂-symmetry similarly to **pyr-cryptand**.

3.2.2.2 Hydrogenation of *pyr-cryptand*

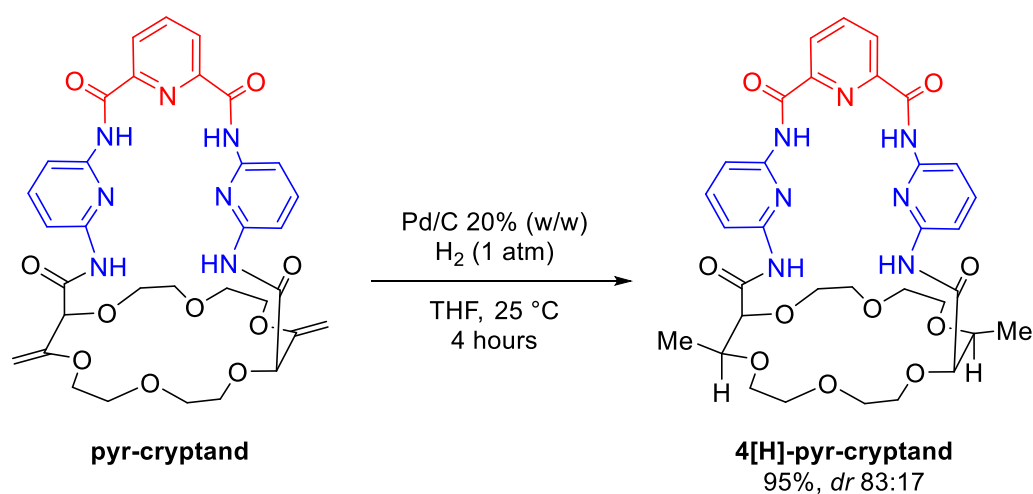
It was then possible to hydrogenate the exocyclic double bonds of **pyr-cryptand** (**Scheme 3.5**). Mild heterogeneous hydrogenation conditions (20% w/w, Pd/C (10% Pd, unreduced), 1 atm H₂, 25 °C) were sufficient to afford the corresponding derivative **4[H]-pyr-cryptand** in 95% yield. Surprisingly, the reaction proceeded with a moderate diastereoselectivity (*dr* 83:17) which could be improved (*dr* 93:7) by selective precipitation of the diastereomeric mixture in a CH₂Cl₂/hexanes mixture. The configuration of the major diastereoisomer could not be

¹⁴⁰ (a) Corrêa, C. C.; Scaldini, F. M.; Machado, F. C.; Pinheiro, C. B., *J. Struct. Chem.* **2016**, 57, 1235-1242. (b) Carranza Téllez, V.; Sánchez Gaytán, B.; Bernès, S.; González Vergara, E., *Acta Cryst. C* **2002**, 58, o228-o230.

determined unambiguously, but accordingly to section 2.2.5 the all-*cis* configuration is thought to be more favored for steric reasons.



Scheme 3.4 Synthesis of **Ph-cryptand**, **thio-cryptand** and **pyr-Ph-cryptand**.

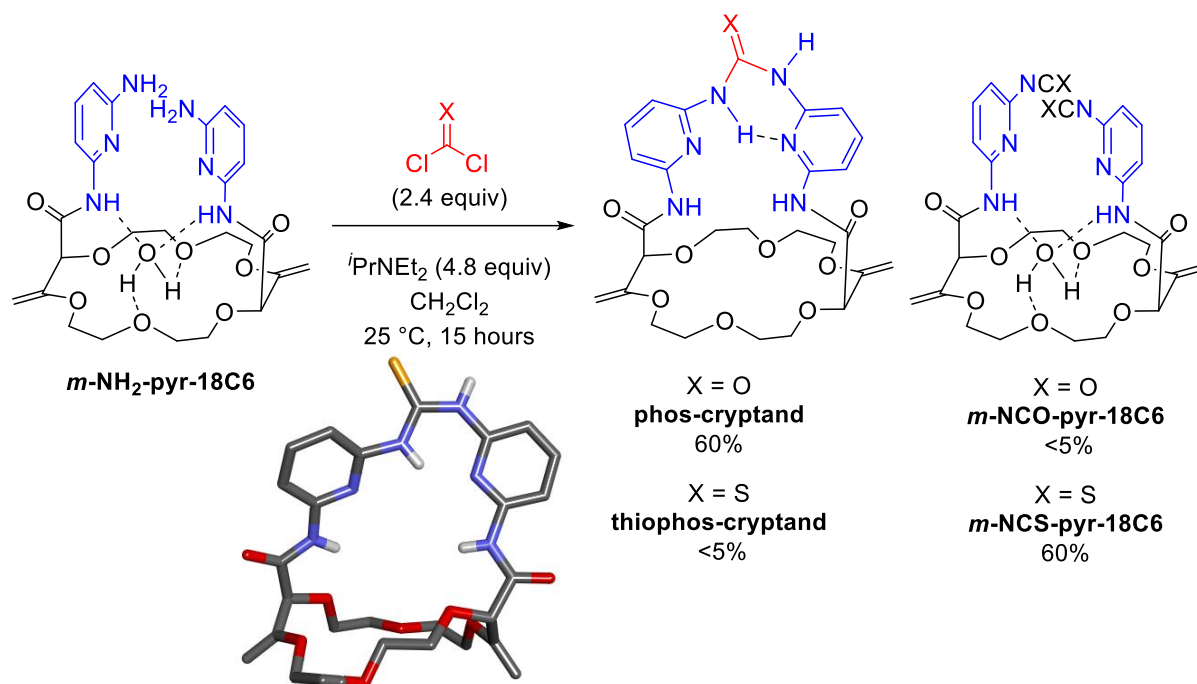


Scheme 3.5 Synthesis of **4[H]-pyr-cryptand**.

3.2.2.3 Condensation with (thio)phosgene

Next, ***m*-NH₂-pyr-18C6** was treated with phosgene and thiophosgene under the previously considered conditions for ring closure (**Scheme 3.6**, top). In presence of an excess of COCl₂ (2.4 equiv), cryptand **phos-cryptand** was obtained in 60% yield. However, when treated with a twofold excess of thiophosgene, **thiophos-cryptand** was only obtained in trace amount (<5% yield). In fact, the major product originated from the double addition of thiophosgene to form bis-isothiocyanate crown ether ***m*-NCS-pyr-18C6** in 60% yield (**Scheme 3.6**, bottom). In spite of the low yield, a sample of **thiophos-cryptand** could be isolated and analyzed. Interestingly, the ¹H NMR spectroscopic analysis of **phos-cryptand** and **thiophos-cryptand** revealed an anisotropy of all hydrogen atoms and hence the occurrence of unsymmetrical conformations in solution. Most probably, the urea/thiourea functional groups adopt *s-cis* and *s-trans* conformations for the consecutive amide bonds (**Scheme 3.6**).¹⁴¹ This geometry facilitates intramolecular H-bonds between inwards N-H (*s-trans* amide) and neighboring pyridine rings. In fact, in the ¹H NMR spectra of **thiophos-cryptand**, one of the two hydrogen atoms is strongly deshielded compared to the other (**thiophos-cryptand**: δ 13.07 vs. 9.09 ppm). Recrystallization of **thiophos-cryptand** by slow evaporation in a CH₂Cl₂/heptane mixture furnished crystals suitable for X-ray analysis. This solution behavior was confirmed by the structural analysis of **thiophos-cryptand**.

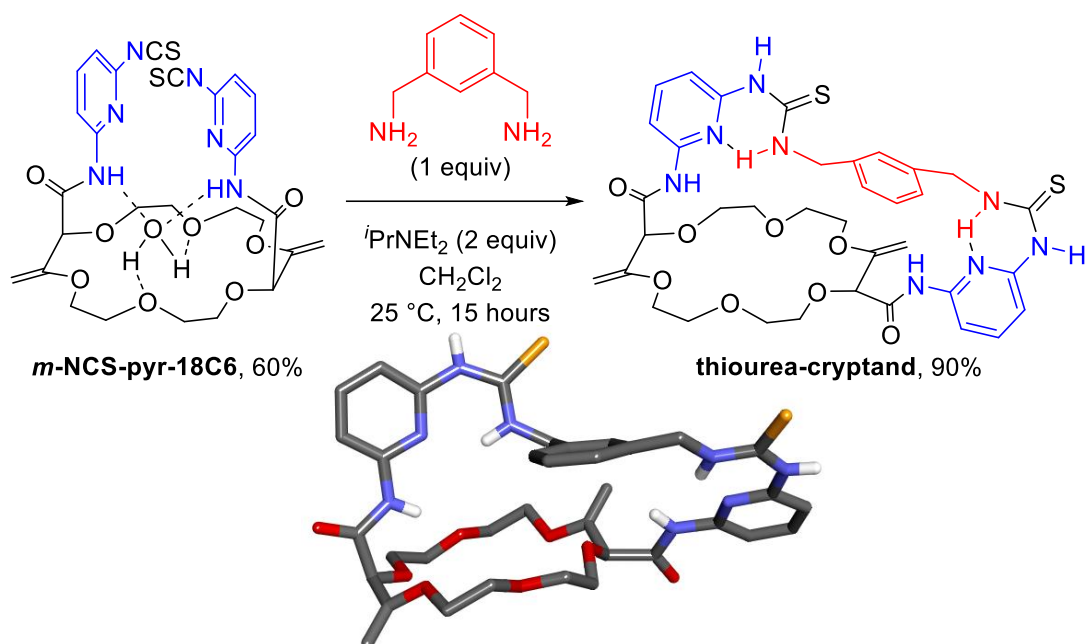
¹⁴¹ (a) Paisner, K.; Zakharov, L. N.; Doxsee, K. M., *Cryst. Growth Des.* **2010**, *10*, 3757-3762. (b) Custelcean, R.; Gorbunova, M. G.; Bonnesen, P. V., *Chem. Eur. J.* **2005**, *11*, 1459-1466.



Scheme 3.6 Condensation using (thio)phosgene and stick view of the crystal structure of **thiophos-cryptand**.

Finally, slow addition of *m*-xylylenediamine to a solution of the crown ether ***m*-NCS-pyr-18C6** and Hünig's base afforded **thiourea-cryptand** in 90% yield (**Scheme 3.7**). Recrystallization by slow evaporation of **thiourea-cryptand** in a CH_2Cl_2 /heptane mixture furnished crystals suitable for X-ray analysis. In this case, the structural analysis revealed a distorted geometry in the solid state (**Scheme 3.7**, bottom). In contrast with previously determined structures, the amide bonds that originates from the polyether macrocycle adopt both perpendicular and parallel orientations to the mean plane of the crown ether domain. This is clearly induced by the longer tether that pushes the aromatic rings apart and distorts the classical organization. Each of the thiourea moieties present also *s-cis* and *s-trans* conformations. However, in solution (NMR), no evidence of such a non-symmetric conformation can be found. In fact, the ^1H and ^{13}C NMR spectra indicate that given functional groups are magnetically equivalent. This signifies either a fast positional interchanges on the NMR time scale¹⁴² or the adoption of a different, C_2 -symmetrical, conformation in solution. Of the two, the first hypothesis is judged more likely.

¹⁴² The lack of solubility of **thiourea-cryptand** in solvents amenable to low temperature VT-NMR did not allow us to probe the dynamics of conformational exchange at $T < 298\text{ K}$.



Scheme 3.7 Synthesis and stick view of the crystal structure of thiourea-cryptand.

3.3 Heteroditopic binding abilities

With this novel series of cryptands in hand, their ability to bind (i) alkali metal cations, (ii) small anions or (iii) salts as ion pairs was examined in solution (¹H NMR spectroscopy) and solid state. For the solution studies, mixtures of CDCl₃ and DMSO-*d*₆ (4:1) were used as solvent. The large proportion of DMSO was necessary to ensure a good solubility of all engaged species. For the experiments targeting alkali cations (Na⁺ and K⁺), tetrphenylborate (BPh₄⁻) counterion was selected. For the anion binding studies, tetrabutylammonium (TBA⁺) salts of N₃⁻, Cl⁻, Br⁻, I⁻, NCO⁻, SCN⁻, NO₃⁻ and H₂PO₄⁻ were utilized. The large counterions TBA⁺ and BPh₄⁻ were chosen for the solubility of their salts in CDCl₃/DMSO-*d*₆ mixtures and their lack of interactions with organic receptors.^{135c}

3.3.1 Titration of pyr-cryptand

The binding abilities of **pyr-cryptand** in solution were considered first. When treated with NaBPh_4 or TBAN_3 salts, no interaction could be evidenced by ^1H NMR spectroscopy. Neither the sodium nor the azide ion seemed to coordinate to the host molecule (**Figure 3.5**, spectra **a-c**). However, when **pyr-cryptand** was treated with NaN_3 salt (1.0 equiv), enlargements of most signals of the cryptand and variations of chemical shifts were noticed (**Figure 3.5d**). Importantly, an identical behavior was observed upon consecutive additions of NaBPh_4 and TBAN_3 (1.0 equiv each, **Figure 3.5e**). These results indicate a clear ditopic character for **pyr-cryptand** in the presence of Na^+ and N_3^- ions.

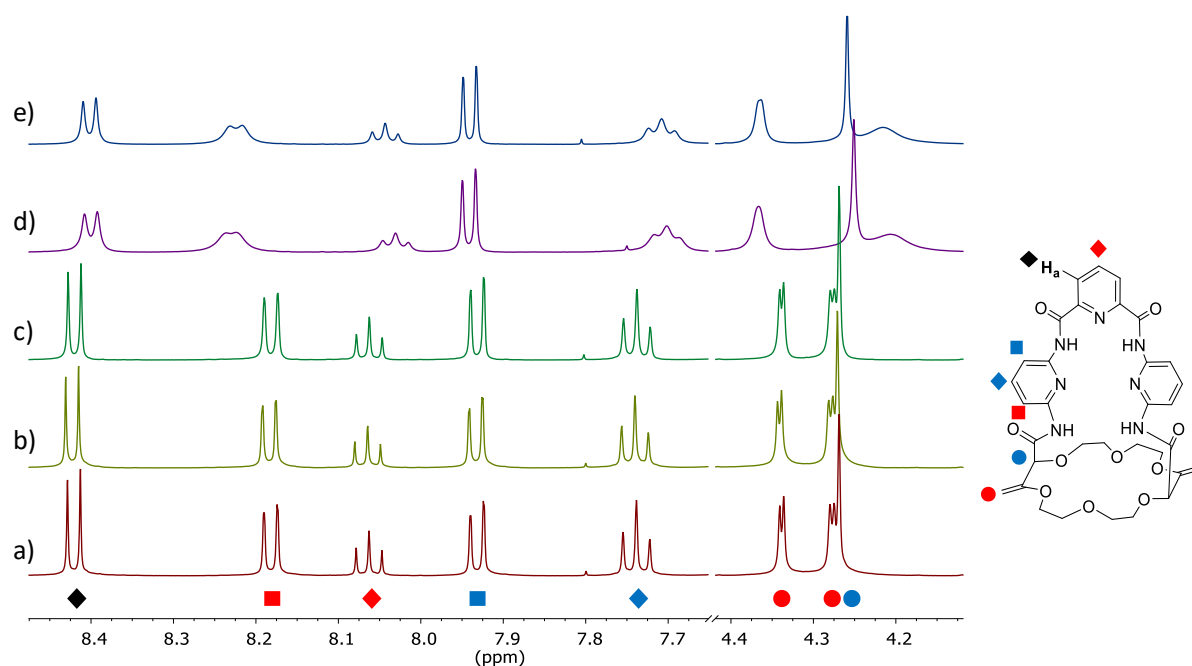


Figure 3.5 ^1H -NMR spectra, selected region (λ 8.5–4.1 ppm), 4:1 $\text{CDCl}_3/\text{DMSO}-d_6$, 298 K, c_H 2.5 mM. a) **pyr-cryptand**; b) **pyr-cryptand** + NaBPh_4 (1:1 ratio); c) **pyr-cryptand** + TBAN_3 (1:1 ratio); d) **pyr-cryptand** + NaN_3 (1:1 ratio); e) **pyr-cryptand** + NaBPh_4 + TBAN_3 (1:1:1 ratio).

The same series of experiments was then performed with KBPh_4 and TBAN_3 . Evidences of interactions were observed for KBPh_4 (0.2 to 1.0 equiv) with **pyr-cryptand**. For instance, in the presence of 1.0 equivalents of KBPh_4 , a +0.07 ppm downfield shift of proton H_a (**Figure 3.6**, δ_0 8.42 ppm, black diamond) was noticed; the titration experiment is displayed on **Figure 3.6** (bottom). Then, subsequent additions of TBAN_3 were performed (0.2 to 10 equiv, **Figure 3.6**, top). In the ^1H NMR spectra, an upfield shift (up to -0.13 ppm) was measured for the same proton H_a

upon addition of the anion. A recognition of the combination of $\text{KBPh}_4/\text{TBAN}_3$ is thus afforded by **pyr-cryptand**.

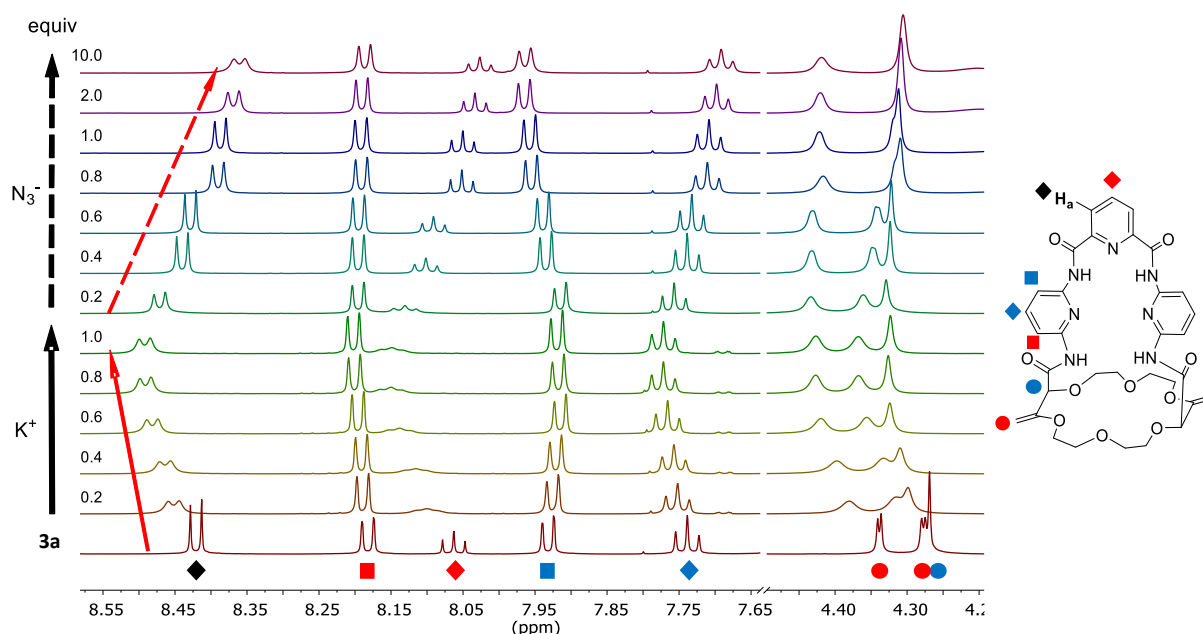


Figure 3.6 ^1H -NMR spectra, selected region (δ 8.6–4.2 ppm), 4:1 $\text{CDCl}_3/\text{DMSO}-d_6$, 298 K, c_H 2.5 mM, of **pyr-cryptand** upon addition of KBPh_4 (0.2, 0.4, 0.6, 0.8, 1.0 equiv, solid arrow) followed by TBAN_3 (0.2, 0.4, 0.6, 0.8, 1.0, 2.0, 10.0 equiv, dashed arrow).

Next, the affinity of Cl^- , Br^- , I^- , NCO^- , SCN^- , NO_3^- and H_2PO_4^- towards **pyr-cryptand** was examined. As earlier with TBAN_3 , none of these tetrabutylammonium salts (1.0 and 5.0 equiv) showed any observable interactions (^1H NMR) with the host when utilized alone. However, when added together with one equivalent of NaBPh_4 , downfield shifts were observed for certain anions. In fact, with NCO^- and SCN^- or NO_3^- , the signal of proton H_a experienced chemical shift variations in the same manner as with the NaBPh_4 and TBAN_3 couple (see experimental part, **Figures 7.3–7.5**). However, such changes did not occur with the three classical halogen anions (Cl^- , Br^- , I^-) or the tetrahedral H_2PO_4^- anion. It is possible that the cavity of the cryptand is too small to include this (large) anions or that the energy cost to rearrange the macrocycle for an appropriate binding is too high. In the presence of Na^+ , the ditopic affinity of **pyr-cryptand** is thus restricted to linear anions (N_3^- , NCO^- , SCN^-) and trigonal oxyanion NO_3^- . NMR addition experiments were also performed with mixtures of KBPh_4 and TBASCN . Overall, a behavior similar to that of the combination of KBPh_4 and TBAN_3 was noticed (**Figure 7.6**).

3.3.2 Solid state structure of coordinated pyr-cryptand

The precedent experiments highlighted the interaction of the cryptand with alkali metals and linear anions in solution. To get more insight on the binding mode, solid state analysis was considered. Solubilizing **pyr-cryptand** with an excess of NaN_3 salt in a CH_2Cl_2 /hexanes bilayer system followed by slow evaporation of the solvents furnished single crystals of [**pyr-cryptand**· NaN_3] complex suitable for X-ray analysis (**Figure 3.7**). The solid state structure confirmed the encapsulation of NaN_3 by the cryptand as a contact ion pair within the cavity. As expected, the sodium ion is coordinated inside the crown ether moiety. Each terminal ends of the azide molecule interacts with two N-H bonds, thus locking effectively the anion inside the cryptand.

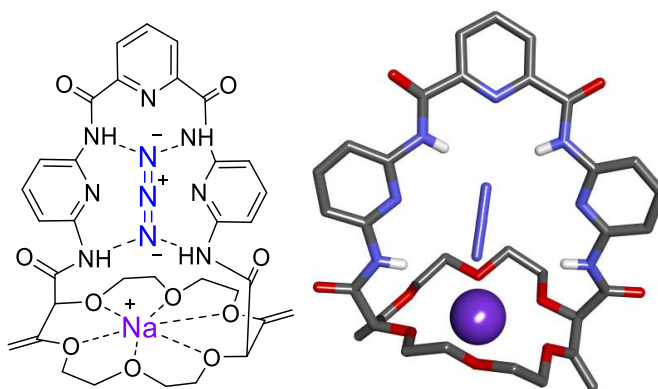


Figure 3.7 Stick view of the crystal structure of [**pyr-cryptand**· NaN_3].

Applying the same strategy, single crystals suitable for X-ray analysis of **pyr-cryptand** with NaSCN , KSCN , NaNO_3 and KNCO were also obtained and compared with [**pyr-cryptand**· NaN_3] (**Figure 3.8**, and experimental section **Table 7.6**). Four of them (with NaN_3 , NaSCN , NaNO_3 and KNCO) are very similar with a coordination of 8 around the alkali cation and the anion coordinated to the N-H bonds of the four amides. For the cations, hexagonal bipyramid coordination polyhedra are formed with the six oxygen atoms of the macrocycle being almost planar and forming the base of the bipyramid. The alkali cation lies within this plane and the M-O distances ranges from 2.52 to 2.99 Å for $M = \text{Na}$ and 2.65 to 2.87 Å for $M = \text{K}$ (**Table 7.6**). One of the summits of the pyramid is formed by the coordinating atom of the anion. The second

summit is either an oxygen atom of the second loop of a neighboring cryptand (NaN_3 , NaNO_3 and KNCO) or an extra water molecule (NaSCN).

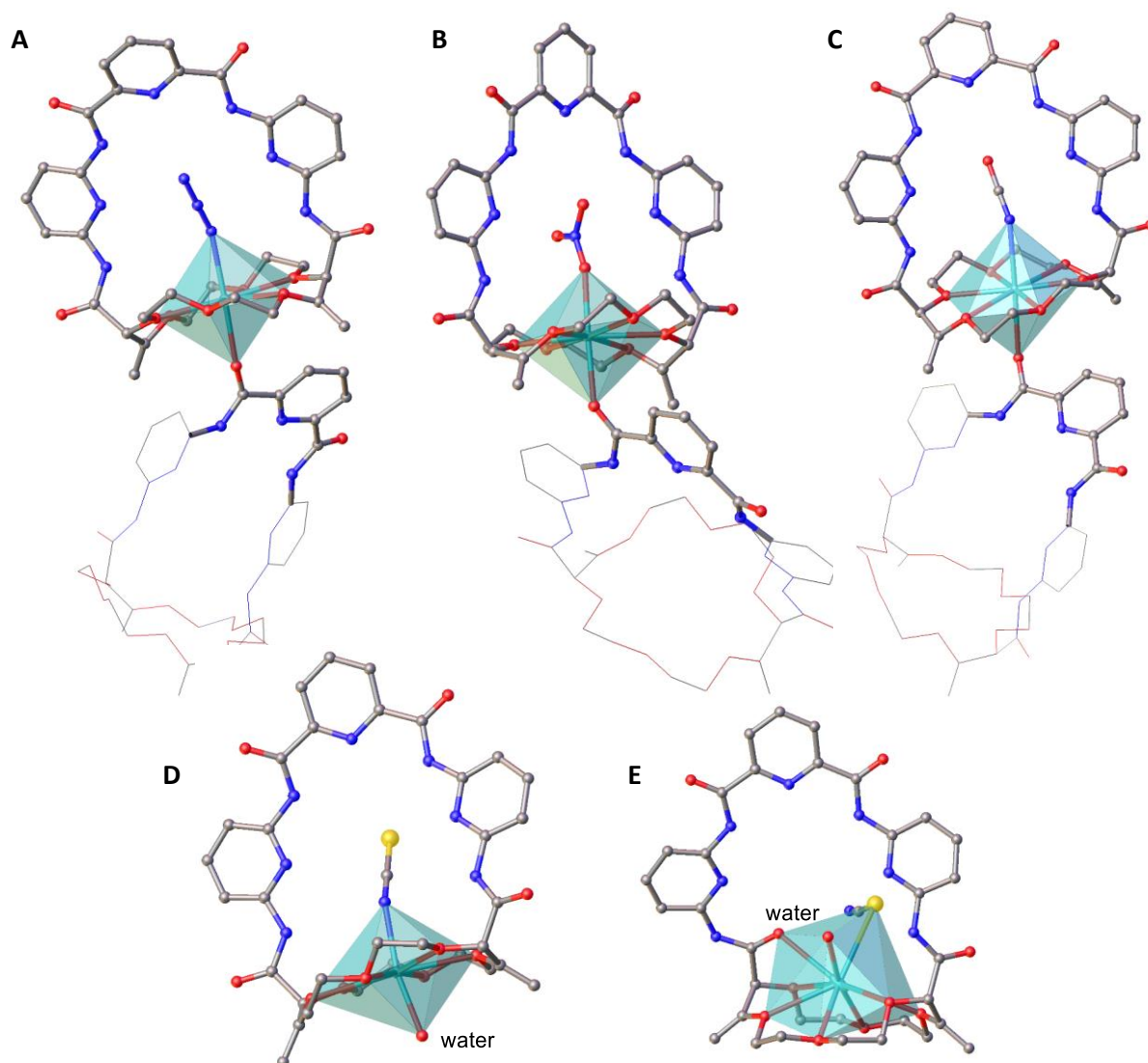


Figure 3.8 Stick view of the crystal structure of **[pyr-cryptand·NaN₃]** (A), **[pyr-cryptand·NaNO₃]** (B), **[pyr-cryptand·KNCO]** (C), **[pyr-cryptand·NaSCN·H₂O]** (D) and **[pyr-cryptand·KSCN·H₂O]** (E) and coordination polyhedra of the alkali cation.

However, for KSCN, the coordination is totally different. A 9-coordination of the potassium ion is found with larger K-O distances (from 2.78 to 3.15 Å). The six atoms of the macrocycle are still coordinated to the metal but they are not any longer planar. The coordination polyhedra is completed by the sulfur of the thiocyanate anion, a water molecule and a carbonyl bond. Also, while the three anions N_3^- , NO_3^- , NCO^- occupy the center of the cavity within **pyr-cryptand**, the larger thiocyanate anions do not seem to fit the cavity with the same efficiency. In **[pyr-cryptand·NaSCN]** complex, the sulfur atom lies already slightly outside of the cavity with the N-

atom coordinated to the alkali cation. With the larger potassium ion, an inclusion of the thiocyanate is not observed, a smaller water molecule occupying the central place of the cavity while the sulfur atom coordinates to the cation.

In [**pyr-cryptand**·KSCN] complex, the amide bonds present two different orientations. In one instance, one N-H bond points inwards while, for the other amide bond, the carbonyl C=O bond faces the inserted potassium cation. This dissymmetrical arrangement creates a distortion of the internal cavity and forces a 9-coordination of the cation. Consequently, the anion is forced to adopt a different (perpendicular) binding mode while keeping the contact ion pair nature of the association. However, the solution studies of the complex indicate a C_2 -symmetry for the inclusion adduct (**Figure 7.6**, see experiemtal part). Either a fast positional interchanges on the NMR time scale or the adoption of a C_2 -symmetrical conformation in solution can explain this behavior.

3.3.3 Solution studies of the cryptands with Na^+ and N_3^-

Next, the propensity of cryptands **Ph-cryptand**, **thio-cryptand**, **pyr-Ph-cryptand**, **4[H]-pyr-cryptand**, **phos-cryptand** and **thiourea-cryptand** to behave as ditopic receptors was tested (section 7.11.2 for additional details, **Figures 7.7-7.12**). The affinity of these cryptands towards NaBPh_4 was monitored first in solution by ^1H -NMR spectroscopy. Interestingly, to the exception of **Ph-cryptand**, variations in chemical shifts were noticed in presence of Na^+ ion, proving an interaction with the cation. Amide protons and protons from the crown ether skeleton were particularly sensitive to the inclusion of Na^+ ion indicating a binding of the cation within the crown ether domain.

Titration with TBAN_3 demonstrated, on the other hand, a general lack of interactions with N_3^- . Only cryptand **pyr-Ph-cryptand** and **4[H]-pyr-cryptand** seemed to be sensitive to the presence of the azide anion (**Figures 7.9-7.10**). In compound **pyr-Ph-cryptand**, the formal replacement of two pyridine $\text{N}(\text{sp}^2)$ atoms by CH bonds removes the possibility of electrostatic repulsions between N_3^- and the nitrogen lone pairs and hence enhances a certain sensitivity. **4[H]-pyr-cryptand**, with the same upper ring as **pyr-cryptand** but with a modified platform

(hydrogenated olefins), displays NH signals for both the bound and free macrocycle. It is the single case for which a slow exchange on the NMR time scale is observed.

After these control experiments, titrations of **Ph-cryptand**, **thio-cryptand**, **pyr-Ph-cryptand**, **4[H]-pyr-cryptand**, **phos-cryptand** and **thiourea-cryptand** were performed directly with combinations of NaBPh₄ and TBAN₃ salts. Interestingly, all systems displayed noticeable variations of the NMR chemical shifts in the presence of the two salts and indicated an interaction with both the Na⁺ cation and the N₃⁻ anion. Qualitatively, for **Ph-cryptand**, **thio-cryptand** and **4[H]-pyr-cryptand**, the solution analysis exhibit similar chemical shift variation patterns for the amide and crown ether protons (**Figures 7.7, 7.8 and 7.10**) compared to **pyr-cryptand**. Neither the bridging functionality (phenyl, thiophene, pyridine) nor the platform (hydrogenated olefins) seemed to drastically influence the ion pairing properties of this four derivatives

As a non-typical example, the ion pair recognition by cryptand **pyr-Ph-cryptand** is depicted in **Figure 3.9**. In fact, this compound is one of the two hosts that displays interactions with the azide anion in the absence of sodium salt. In fact, the addition of TBAN₃ (**Figure 3.9c**) leads to stronger perturbations in solution than that of NaBPh₄ (**Figure 3.9b**). The absence of the two N(sp²) atoms compared to **pyr-cryptand** seems to be crucial for a more effective binding of the anion even in absence sodium ion. The simultaneous addition of NaBPh₄ and TBAN₃ leads to further modifications confirming the ion pairing effect (**Figure 3.9d**).

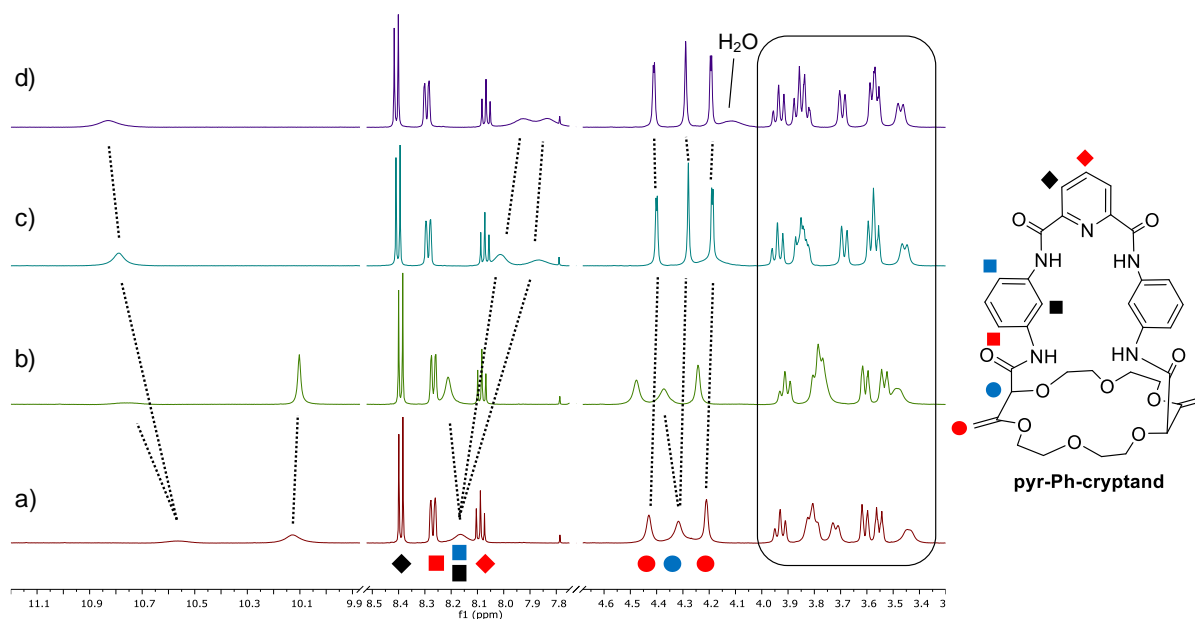


Figure 3.9 ¹H-NMR spectra, selected region (δ 11.2–3.3 ppm), 4:1 CDCl₃/DMSO-*d*₆, 298 K, *c*_H 2.5 mM. a) **pyr-Ph-cryptand**; b) **pyr-Ph-cryptand** + NaBPh₄ (1:1 ratio); c) **pyr-Ph-cryptand** + TBAN₃ (1:1 ratio); d) **pyr-Ph-cryptand** NaBPh₄ +TBAN₃ (1:1:1 ratio). Crown-ether protons are all contained in the frame.

Compared to the other derivatives, phosgene-derived **phos-cryptand** showed less pronounced variations in chemical shifts in the presence of NaBPh_4 and TBAN_3 , independently or together (**Figure 7.11**). Furthermore, in the presence of these salts, the anisotropy of all hydrogen remains intact. This indicates that Na^+ or N_3^- ions do not change the intramolecular H-bond situation (see the X-ray structure of related **thiophos-cryptand**, **Scheme 3.6**) and that the smaller cavity disfavors the binding of the anion within the cavity. However, the formation of an ion pair is still possible with the azide ion lying slightly outside the cavity as (contact) ion pair in a similar manner to **[pyr-cryptand·KSCN]** (**Figure 3.8E**).

Lastly, **thiourea-cryptand**, despite its lower symmetry, display variations of chemical shifts as strong as that of hosts **pyr-cryptand**, **Ph-cryptand** or **pyr-Ph-cryptand** (**Figure 3.10**). The changes are less pronounced for the crown ether protons than for the amide or the benzylic hydrogen atoms. The larger and more flexible cavity can explain this behavior. Possibly, the crown ether domain is already less restrained and may require less reorganization to incorporate the cation, reducing the variations in this region (δ 3.9–3.3 ppm).

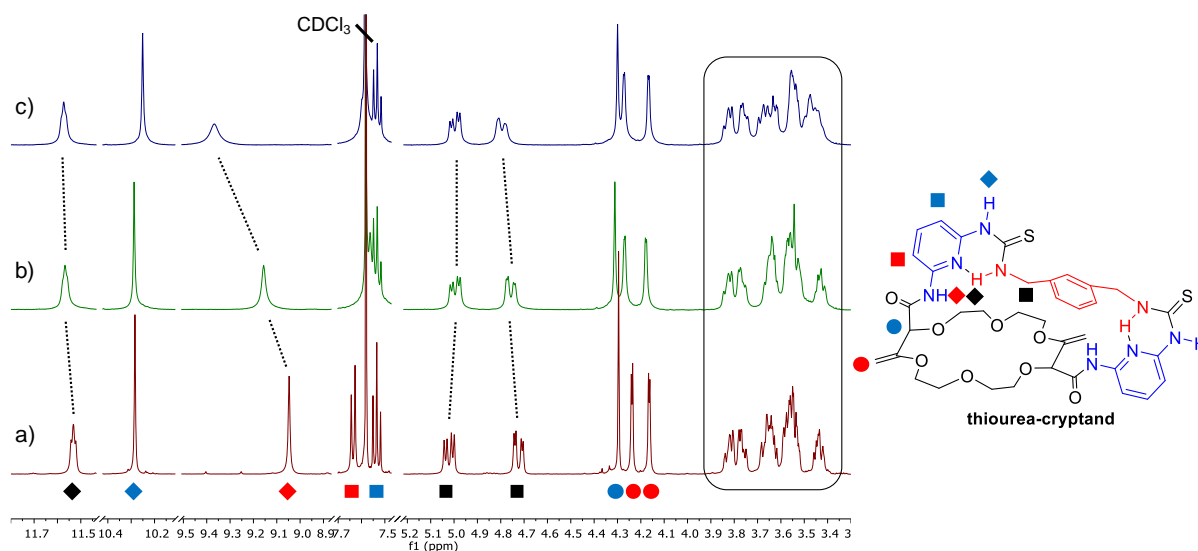


Figure 3.10 ^1H -NMR spectra, selected region (δ 11.8–3.3 ppm), 4:1 $\text{CDCl}_3/\text{DMSO}-d_6$, 298 K, c_H 2.5 mM. a) **thiourea-cryptand**; b) **thiourea-cryptand** + NaBPh_4 (1:1 ratio); c) **thiourea-cryptand** + NaBPh_4 + TBAN_3 (1:1:1 ratio). Crown-ether protons are all contained in the frame.

3.3.4 Binding mode of NaN_3 within the cryptands

The solutions studies evidenced the existence of ion pairing interactions and the ditopic character of the cryptands towards NaBPh_4 and TBAN_3 salts. The binding mode of the ion pair (NaN_3) was considered next.

The inclusion as contact ion pair within the internal cavity of sodium azide is confirmed for the complex [**Ph-cryptand**· NaN_3] by the X-ray structure analysis (**Figure 3.11**). In comparison with [**pyr-cryptand**· NaN_3], the same binding mode occurs with the sodium coordinated in the crown ether and the azide anion encapsulated within the cavity. For the other complexes, no crystal structures were obtained to confirm the inclusion of the salt in a similar manner. Yet, according to the solution analysis and by analogy (structural resemblance), the cations are always coordinated within the crown ether as demonstrated by the variation of the associated NMR signals. Most likely, the anion lies within the cavity through N-H bonding interactions, to the exception of **phos-cryptand** having most probably the anion lying slightly outside.

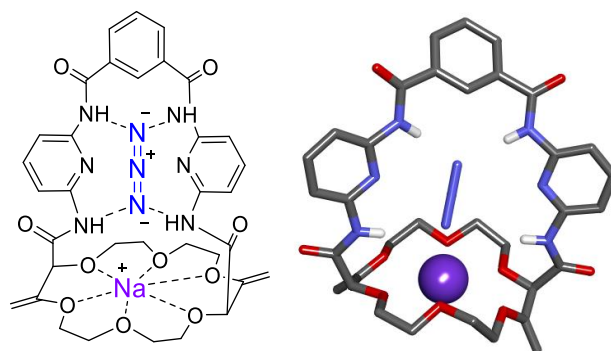


Figure 3.11 Stick view of the crystal structure of [**Ph-cryptand**· NaN_3].

3.3.5 Quantitative analysis

After considering the qualitative analysis of the heteroditopic cryptands, the determination of binding constants ($\log K$) was envisaged. We attempted to extract binding constants from the

titration data using HypNMR2008 software,¹⁴³ least square methods or tools provided on www.supramolecular.org web site. Unfortunately, no meaningful data could be extracted from these methods.

The choice of analytical method (¹H NMR spectroscopy) was not adapted for quantitative measurement of binding constant. In fact, four issues appeared: (i) the fairly high concentration of host (2.5 mM) required for an adapted detection of the signal, (ii) the relatively small variations in ¹H NMR chemical shifts upon binding of the various ions, (iii) the fact that mixtures of lipophilic salts were required for the assays (*i.e.* NaBPh₄ + TBAN₃ instead of NaN₃) and (iv) the strong activity γ of ions in organic solvents like CHCl₃.¹⁴³⁻¹⁴⁴ Instead of NMR spectroscopy, different methods could be envisaged such as spectrophotometry or electrochemistry which would overcome some of the issues highlighted (concentrations and signal intensity variations). With reliable values of binding constants, more thermodynamic information could be extracted, such as the electrostatic and allosteric cooperativity of the ion pairing.¹²⁶

3.4 Conclusion

Following a late-stage functionalization strategy, a series of heteroditopic cryptand receptors were prepared – in one or two steps only from ***m*-NH₂-pyr-18C6** or ***m*-NH₂-18C6** crown ethers. As evidenced by ¹H NMR spectroscopic and solid state analyses, these polyamide-crown ether conjugates present a general ion pair binding capacity towards salts of monovalent cations and linear triatomic anions. In particular, small cations (Na⁺, K⁺) and linear triatomic anions (N₃⁻, NCO⁻, SCN⁻) or trigonal oxyanion (NO₃⁻) interact cooperatively within the heteroditopic receptors. The salts are coordinated within the cryptand as contact ion pairs.

¹⁴³ Frassinetti, C.; Ghelli, S.; Gans, P.; Sabatini, A.; Moruzzi, M. S.; Vacca, A., *Anal. Biochem.* **1995**, *231*, 374-382.

¹⁴⁴ (a) Babel, L.; Guénée, L.; Besnard, C.; Eliseeva, S. V.; Petoud, S.; Piguet, C., *Chem. Sci.* **2018**, *9*, 325-335. (b) Baudet, K.; Guerra, S.; Piguet, C., *Chem. Eur. J.* **2017**, *23*, 16787-16798. (c) von Krbek, L. K. S.; Schalley, C. A.; Thordarson, P., *Chem. Soc. Rev.* **2017**, *46*, 2622-2637. (d) Brynn Hibbert, D.; Thordarson, P., *Chem. Commun.* **2016**, 52, 12792-12805. (e) Thordarson, P., *Chem. Soc. Rev.* **2011**, *40*, 1305-1323.

Interestingly, in contrast with the crown-ether receptors made by Huang,^{29a, 139} Rissanen,¹³⁵ Romanski and Piątek,^{128,136d} and Smith,¹³⁸ the cryptands do not interact with (salts of) halogen Cl^- , Br^- , I^- anions making this class of derivatives apart from previously reported structures.

Unfortunately, in solution, the NMR spectroscopy employed for qualitative analyses presented some issues (concentration, signal intensity) which prevented the determination of meaningful binding constants. Thus different analytical methods (spectrophotometry, electrochemistry) could be considered next to obtain such information.

Nitrite salts were not tested in this study, but effective binding of sodium nitrate was demonstrated. Thus, it seems reasonable to envision that NaNO_2 should exhibit similar properties. The ability of the presented cryptands to bind cooperatively salts could also be exploited in the future to engineer systems for the selective extraction of salts.

4 Fluorescent macrocycles as chiroptical switches

4.1 Introduction

4.1.1 Sensing of metal ions using excimer fluorescence

Detection and sensing of metal ions is essential to the analysis of biological, chemical and environmental processes. In the previous chapter, the interaction of macrocycles with alkali cations was monitored using NMR spectroscopy and solid state structure analysis. An alternative method is to use absorbance and fluorescence techniques¹⁴⁵ which present the advantage of being highly sensitive (nanomolar detection).¹⁴⁶ These methods require the presence of an efficient reporting unit (chromophore). One popular fluorophore is the pyrene moiety, which exhibits a characteristic emission band at *ca.* 380-400 nm. In case of spatial proximity between two (or more) pyrene units, a tell-tale excimer fluorescence centered at 500 nm is observed. The intensity of this transition strongly depends on the distance and the orientation between the two aromatic moieties.¹⁴⁷

¹⁴⁵ (a) Yin, J.; Hu, Y.; Yoon, J., *Chem. Soc. Rev.* **2015**, *44*, 4619-4644. (b) Callan, J. F.; de Silva, A. P.; Magri, D. C., *Tetrahedron* **2005**, *61*, 8551-8588. (c) Prodi, L.; Bolletta, F.; Montalti, M.; Zaccheroni, N., *Coord. Chem. Rev.* **2000**, *205*, 59-83. (d) Keefe, M. H.; Benkstein, K. D.; Hupp, J. T., *Coord. Chem. Rev.* **2000**, *205*, 201-228. (e) Valeur, B.; Leray, I., *Coord. Chem. Rev.* **2000**, *205*, 3-40. (f) Bargossi, C.; Fiorini, M. C.; Montalti, M.; Prodi, L.; Zaccheroni, N., *Coord. Chem. Rev.* **2000**, *208*, 17-32. (g) Bryan, A. J.; de Silva, A. P.; De Silva, S. A.; Rupasinghe, R. A. D. D.; Sandanayake, K. R. A. S., *Biosensors* **1989**, *4*, 169-179.

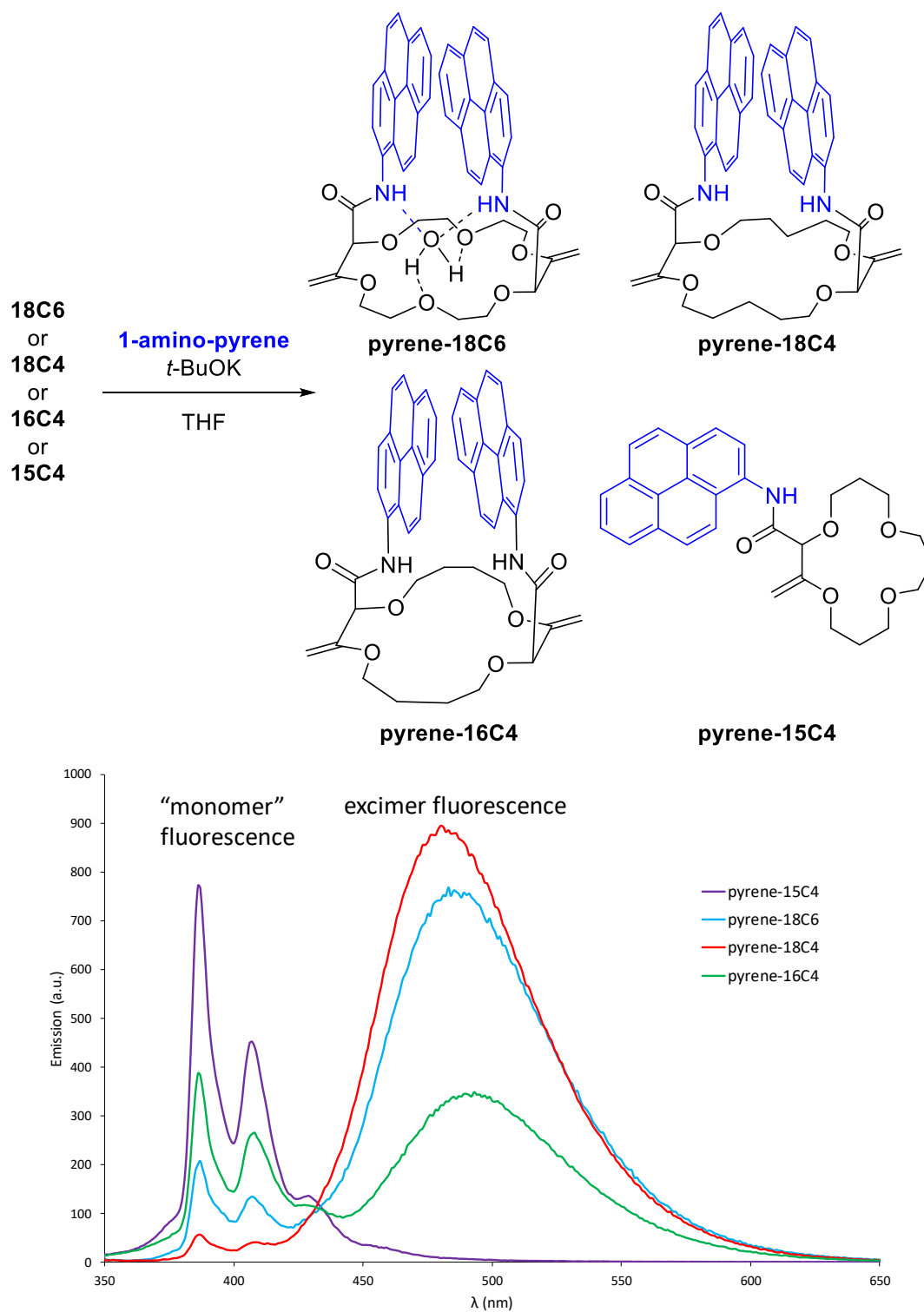
¹⁴⁶ (a) *Chemosensors: Principles, Strategies, and Applications*. John Wiley & Sons: 2011. (b) *Introduction to Fluorescence Sensing*. Springer Netherlands: 2009.

¹⁴⁷ Winnik, F. M., *Chem. Rev.* **1993**, *93*, 587-614.

The straightforward synthesis of chiral polyether macrocycles presented in this thesis is applicable to a large variety of aromatic amines including extended aromatic amines (section 1.5.4). For instance, during his PhD, Mahesh Vishe treated **18C6**, **18C4**, **16C4** or **15C4** building blocks with 1-amino-pyrene and *t*-BuOK (excess), under the previously reported conditions, leading to the formation of **pyrene-18C6**, **pyrene-18C4**, **pyrene-16C4** and **pyrene-15C4** macrocycles respectively (**Scheme 4.1**, top).^{3b, 98, 148} He recorded then the fluorescence spectra of the four derivatives in CH₂Cl₂ (**Scheme 4.1**, bottom). **Pyrene-18C6**, **pyrene-18C4** and **pyrene-16C4** derivatives exhibit a strong excimer fluorescence (EF). In fact, this EF originate from the somewhat constrained geometry of the macrocycles – the two pyrene units facing closely each other. However, with **pyrene-15C4** only the characteristic monomer emission is recorded because, in dilute solution, the distance between two pyrene units (*i.e.* intermolecular interactions) are too large to create an EF.

Similarly to the cryptands, cations should be able to complex the macrocyclic core but inducing this time important conformational changes. In the previous chapter, it has been shown that the amide C=O bonds can turn inwards in presence of potassium ion to enhance the complexation.⁸² Consequently, in similar conditions with pyrene derivatives, the environment of the aromatic units should be modified with the two chromophores parting from each other and elongating the distance between them. Hence, the excimer fluorescence ought to be (partially) quenched and only the characteristic emission of (monomeric) pyrene should be observed (**Figure 4.1**).

¹⁴⁸ Jarolímová, Z.; Vishe, M.; Lacour, J.; Bakker, E., *Chem. Sci.* **2016**, 7, 525-533.



Scheme 4.1 Synthesis of pyrene polyether macrocycles (top) and fluorescence spectra (CH_2Cl_2 , $c\ 10^{-6}$ M) of the pyrene derivatives (bottom).

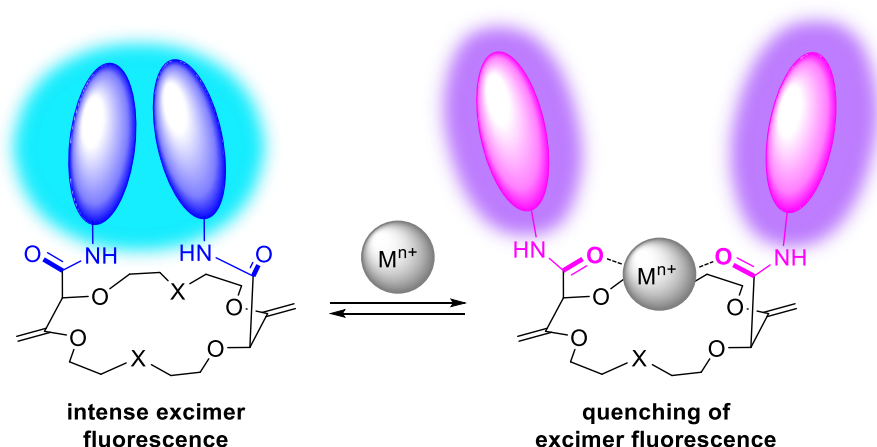


Figure 4.1 Proposed conformational change upon cation binding.

To demonstrate this hypothesis, two studies were performed in collaboration with groups from Geneva. One of the studies was performed in collaboration with the groups of Prof. Claude Piguet (University of Geneva, department of inorganic and analytical chemistry) and Prof. Eric Vauthey (University of Geneva, department of physical chemistry). Using the different pyrene derivatives in acetonitrile (**Scheme 4.1**), a systematic analysis of the binding properties of a large range of mono-, di- and trivalent cations (alkaline, alkaline earth, *p*-, *d*-, and *f*-block metals) was performed by means of UV-Vis spectrophotometric titrations, cyclic voltammetry, excimer fluorescence quenching and transient absorption spectroscopy experiments.¹⁴⁹ **Pyrene-18C6** was able to recognize several cations. The binding efficiency of the cations was followed in fluorescence by monitoring the percentage of quenching of excimer fluorescence. The highest stability constants and better quenching of EF were obtained with divalent cations, Ca^{2+} and Ba^{2+} specifically (**Figure 4.3**).¹⁵⁰ It was also shown that **pyrene-18C4** and **pyrene-16C4** derivatives does not bind cations with induced conformational changes in acetonitrile.

¹⁴⁹ Vishe, M.; Lathion, T.; Pascal, S.; Yushchenko, O.; Homberg, A.; Brun, E.; Vauthey, E.; Piguet, C.; Lacour, J., *Helv. Chim. Acta* **2018**, *101*, e1700265.

¹⁵⁰ For Cu^{2+} , Hg^{2+} and Pb^{2+} , the efficient quenching mechanism was not associated to conformational changes but to redox or heavy atom quenching processes.

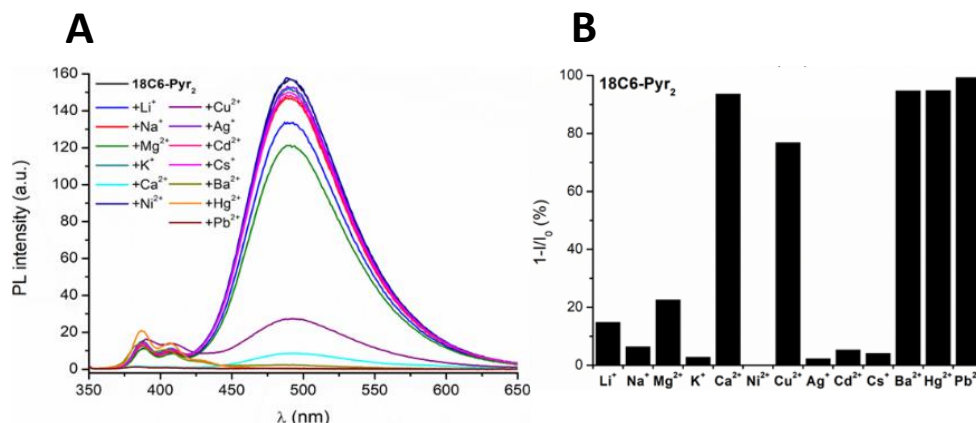


Figure 4.3 Photoluminescence spectra in presence of various cations (A) and percentage of fluorescence quenched (B) of $[M(\text{pyrene-18C6})]^{n+}$ complexes (CH_3CN , 293 K, c 10^{-6} M).¹⁴⁹

Another study was performed in collaboration with the group of Prof. Eric Bakker (University of Geneva, department of inorganic and analytical chemistry). There, the excimer fluorescence quenching properties were used for the direct sensing of cations. Reverse micelles composed of bis(2-ethylhexyl)sebacate (DOS), PEG, NaBAR_F and the pyrene derivatives (**pyrene-18C6**, **pyrene-18C4** or **pyrene-16C4**) were designed (Figure 4.2A). Using excimer fluorescence quenching, these pH independent nanosensors allowed the sensing of potassium ions after exchange with the sodium contained within the micelle. A selectivity for the potassium ion over other metal ions was demonstrated with **pyrene-18C6** macrocycle in particular (Figure 4.2B).

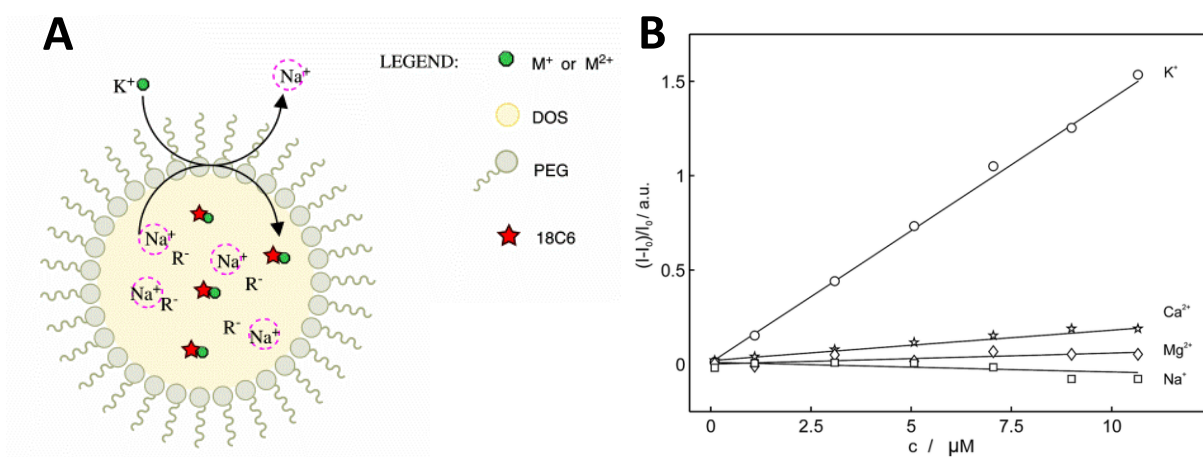


Figure 4.2 Ion-selective reversed micelles (A), normalized fluorescence (406 nm) as a function of concentration of different cations for **pyrene-18C6** (B).¹⁴⁸

Yet, the two studies presented above were performed using racemic compounds only. To better appreciate the conformational changes induced by the presence of cations, it was deemed

interesting to investigate the chiroptical properties of the derivatives in enantiopure form by means of electronic circular dichroism (ECD) and circularly polarized luminescence (CPL) spectroscopies and their modulation upon complexation with metallic cations.

4.1.2 Chiroptical switches

The ability to tune the chiroptical properties of molecules or supramolecular assemblies is a key feature to develop interesting applications in material science.¹⁵¹ For instance, switchable memories¹⁵² and molecular machines,¹⁵³ polarized light emitting devices,¹⁵⁴ chiral transistors^{154a, 155} or chiral spin filters¹⁵⁶ have been proposed in the last two decades. In that context, molecules able to reversibly switch their optical properties in response to external stimuli are particularly interesting.¹⁵⁷ From their interaction with circularly polarized light, either in absorption or in emission, important information can then be extracted about the conformations or the configurations of the targeted species.¹⁵⁸

In absorption, several reversible switches monitored by electronic circular dichroism (ECD) spectroscopy have already been reported. These systems are usually based on metallated

¹⁵¹ Brandt, J. R.; Salerno, F.; Fuchter, M. J., *Nat. Rev. Chem.* **2017**, *1*, 0045.

¹⁵² Wang, C.; Fei, H.; Qiu, Y.; Yang, Y.; Wei, Z.; Tian, Y.; Chen, Y.; Zhao, Y., *Appl. Phys. Lett.* **1999**, *74*, 19-21.

¹⁵³ Feringa, B. L., *Acc. Chem. Res.* **2001**, *34*, 504-513.

¹⁵⁴ (a) Lee, D. M.; Song, J. W.; Lee, Y. J.; Yu, C. J.; Kim, J. H., *Adv. Mater.* **2017**, *29*, 1700907. (b) Zinna, F.; Pasini, M.; Galeotti, F.; Botta, C.; Di Bari, L.; Giovanella, U., *Adv. Funct. Mater.* **2017**, *27*, 1603719. (c) Brandt, J. R.; Wang, X.; Yang, Y.; Campbell, A. J.; Fuchter, M. J., *J. Am. Chem. Soc.* **2016**, *138*, 9743-9746. (d) Zinna, F.; Giovanella, U.; Di Bari, L., *Adv. Mater.* **2015**, *27*, 1791-1795. (e) Yang, Y.; Correa da Costa, R.; Smilgies, D. M.; Campbell, A. J.; Fuchter, M. J., *Adv. Mater.* **2013**, *25*, 2624-2628.

¹⁵⁵ Yang, Y.; Correa da Costa, R.; Fuchter, M. J.; Campbell, A. J., *Nature Photon.* **2013**, *7*, 634-638.

¹⁵⁶ (a) Kiran, V.; Mathew, S. P.; Cohen, S. R.; Hernández Delgado, I.; Lacour, J.; Naaman, R., *Adv. Mater.* **2016**, *28*, 1957-1962. (b) Mondal, P. C.; Kantor-Uriel, N.; Mathew, S. P.; Tassinari, F.; Fontanesi, C.; Naaman, R., *Adv. Mater.* **2015**, *27*, 1924-1927. (c) Göhler, B.; Hamelbeck, V.; Markus, T.; Kettner, M.; Hanne, G.; Vager, Z.; Naaman, R.; Zacharias, H., *Science* **2011**, *331*, 894-897.

¹⁵⁷ (a) Isla, H.; Crassous, J., *C. R. Chim.* **2016**, *19*, 39-49. (b) Dai, Z.; Lee, J.; Zhang, W., *Molecules* **2012**, *17*, 1247-1277.

¹⁵⁸ (a) Pescitelli, G.; Di Bari, L.; Berova, N., *Chem. Soc. Rev.* **2014**, *43*, 5211-5233. (b) Berova, N.; Di Bari, L.; Pescitelli, G., *Chem. Soc. Rev.* **2007**, *36*, 914-931.

helicenes,^{157a, 159} gels,¹⁶⁰ polymers,¹⁶¹ lanthanide complexes¹⁶² or supramolecular assemblies¹⁶³. The switching can be triggered with various parameters such as light,^{153, 164} electrochemical processes,¹⁶⁵ thermal or mechanic stress,¹⁶⁶ pH variations,¹⁶⁷ ions coordination¹⁶⁸ or concentration.¹⁶⁹

In emission, circular polarization of emitted light can be exploited as a selective read-out. However, circularly polarized luminescence (CPL) switches remain rare and most of them take advantage of the presence of metals or are polymers.^{157a, 159a, 167, 168c, 170}. In fact, only a few examples of purely organic derivatives acting as reversible CPL switches were reported in the

¹⁵⁹ (a) Saleh, N.; Moore II, B.; Srebro, M.; Vanthuyne, N.; Toupet, L.; Williams, J. A. G.; Roussel, C.; Deol, K. K.; Muller, G.; Autschbach, J.; Crassous, J., *Chem. Eur. J.* **2015**, *21*, 1673-1681. (b) Srebro, M.; Anger, E.; Moore II, B.; Vanthuyne, N.; Roussel, C.; Réau, R.; Autschbach, J.; Crassous, J., *Chem. Eur. J.* **2015**, *21*, 17100-17115. (c) Anger, E.; Srebro, M.; Vanthuyne, N.; Roussel, C.; Toupet, L.; Autschbach, J.; Réau, R.; Crassous, J., *Chem. Commun.* **2014**, *50*, 2854-2856. (d) Anger, E.; Srebro, M.; Vanthuyne, N.; Toupet, L.; Rigaut, S.; Roussel, C.; Autschbach, J.; Crassous, J.; Réau, R., *J. Am. Chem. Soc.* **2012**, *134*, 15628-15631.

¹⁶⁰ (a) Miao, W.; Wang, S.; Liu, M., *Adv. Funct. Mater.* **2017**, *27*, 1701368. (b) Miao, W.; Qin, L.; Yang, D.; Jin, X.; Liu, M., *Chem. Eur. J.* **2015**, *21*, 1064-1072. (c) Zhao, W.; Wang, D.; Lu, H.; Wang, Y.; Sun, X.; Dong, S.; Hao, J., *Langmuir* **2015**, *31*, 2288-2296. (d) Miao, W.; Zhang, L.; Wang, X.; Cao, H.; Jin, Q.; Liu, M., *Chem. Eur. J.* **2013**, *19*, 3029-3036.

¹⁶¹ Kim, M.-J.; Yoo, S.-J.; Kim, D.-Y., *Adv. Funct. Mater.* **2006**, *16*, 2089-2094.

¹⁶² (a) Shuvaev, S.; Fox, M. A.; Parker, D., *Angew. Chem. Int. Ed.* **2018**, *57*, 7488-7492. (b) Zinna, F.; Di Bari, L., *Chirality* **2015**, *27*, 1-13. (c) Carr, R.; Evans, N. H.; Parker, D., *Chem. Soc. Rev.* **2012**, *41*, 7673-7686. (d) Muller, G., *Dalton Trans.* **2009**, 9692-9707.

¹⁶³ (a) Liu, C.; Yang, D.; Jin, Q.; Zhang, L.; Liu, M., *Adv. Mater.* **2016**, *28*, 1644-1649. (b) Qiu, Y.; Chen, P.; Guo, P.; Li, Y.; Liu, M., *Adv. Mater.* **2008**, *20*, 2908-2913. (c) Bottari, G.; Leigh, D. A.; Pérez, E. M., *J. Am. Chem. Soc.* **2003**, *125*, 13360-13361.

¹⁶⁴ (a) Hu, F.-L.; Wang, H.-F.; Guo, D.; Zhang, H.; Lang, J.-P.; Beves, J. E., *Chem. Commun.* **2016**, *52*, 7990-7993. (b) Liu, W.; Cao, D.; Peng, J.; Zhang, H.; Meier, H., *Chem. Asian J.* **2010**, *5*, 1896-1901.

¹⁶⁵ (a) Brandt, J. R.; Pospíšil, L.; Bednářová, L.; da Costa, R. C.; White, A. J. P.; Mori, T.; Teplý, F.; Fuchter, M. J., *Chem. Commun.* **2017**, *53*, 9059-9062. (b) Cortijo, M.; Viala, C.; Reynaldo, T.; Favereau, L.; Fabing, I.; Srebro-Hooper, M.; Autschbach, J.; Ratel-Ramond, N.; Crassous, J.; Bonvoisin, J., *Inorg. Chem.* **2017**, *56*, 4555-4567. (c) Li, D.; Wang, Z. Y.; Ma, D., *Chem. Commun.* **2009**, *12*, 1529-1531. (d) Canary, J. W., *Chem. Soc. Rev.* **2009**, *38*, 747-756. (e) Canary, J. W.; Zahn, S., *Trends Biotechnol.* **2001**, *19*, 251-255.

¹⁶⁶ (a) Zhang, X.-P.; Mei, J.-F.; Lai, J.-C.; Li, C.-H.; You, X.-Z., *J. Mater. Chem. C* **2015**, *3*, 2350-2357. (b) Fujiki, M., *J. Am. Chem. Soc.* **2000**, *122*, 3336-3343.

¹⁶⁷ Pascal, S.; Besnard, C.; Zinna, F.; Di Bari, L.; Le Guennic, B.; Jacquemin, D.; Lacour, J., *Org. Biomol. Chem.* **2016**, *14*, 4590-4594.

¹⁶⁸ (a) Gon, M.; Morisaki, Y.; Chujo, Y., *Chem. Commun.* **2017**, *53*, 8304-8307. (b) Morcillo, S. P.; Miguel, D.; de Cienfuegos, L. Á.; Justicia, J.; Abbate, S.; Castiglioni, E.; Bour, C.; Ribagorda, M.; Cárdenas, D. J.; Paredes, J. M.; Crovetto, L.; Choquesillo-Lazarte, D.; Mota, A. J.; Carmen, C. M.; Longhi, G.; Cuerva, J. M., *Chem. Sci.* **2016**, *7*, 5663-5670. (c) Maeda, H.; Bando, Y.; Shimomura, K.; Yamada, I.; Naito, M.; Nobusawa, K.; Tsumatori, H.; Kawai, T., *J. Am. Chem. Soc.* **2011**, *133*, 9266-9269.

¹⁶⁹ Ito, S.; Ikeda, K.; Nakanishi, S.; Imai, Y.; Asami, M., *Chem. Commun.* **2017**, *53*, 6323-6326.

¹⁷⁰ (a) Isla, H.; Srebro-Hooper, M.; Jean, M.; Vanthuyne, N.; Roisnel, T.; Lunkley, J. L.; Muller, G.; Williams, J. A. G.; Autschbach, J.; Crassous, J., *Chem. Commun.* **2016**, *52*, 5932-5935. (b) Maeda, H.; Bando, Y., *Pure Appl. Chem.* **2013**, *85*, 1967-1978. (c) Maeda, H.; Shirai, T.; Bando, Y.; Takaishi, K.; Uchiyama, M.; Muranaka, A.; Kawai, T.; Naito, M., *Org. Lett.* **2013**, *15*, 6006-6009. (d) Haketa, Y.; Bando, Y.; Takaishi, K.; Uchiyama, M.; Muranaka, A.; Naito, M.; Shibaguchi, H.; Kawai, T.; Maeda, H., *Angew. Chem. Int. Ed.* **2012**, *51*, 7967-7971. (e) Hayasaka, H.; Miyashita, T.; Tamura, K.; Akagi, K., *Adv. Funct. Mater.* **2010**, *20*, 1243-1250.

literature. For instance, the groups of Longhi and Cuerva designed a macrocyclic *o*-oligo(phenylene)ethynylene that exhibit a strong CPL signal ($g_{\text{lum}} = 1.1 \cdot 10^{-2}$) associated with the helical conformation of the derivative (**Figure 4.4**). Upon addition of AgBF_4 , the helical conformation is lost and a complete quench of the CPL signal is observed. The CPL signal can be recovered by addition of acetonitrile – making the system an effective reversible on/off CPL switch.^{168b}

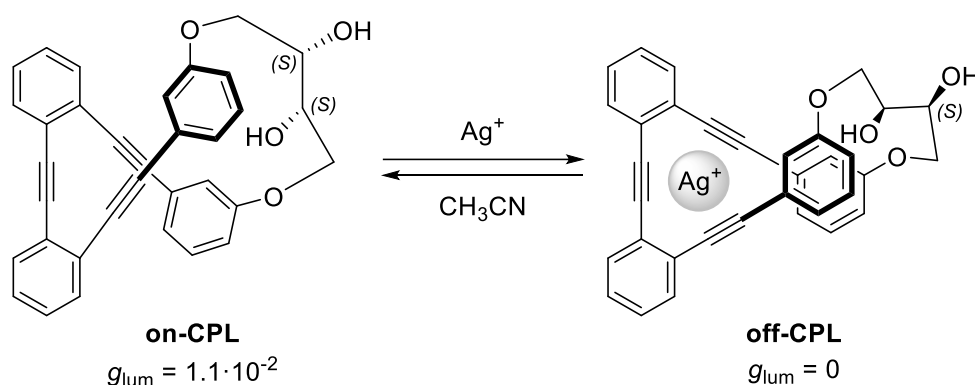


Figure 4.4 Macrocyclic *o*-oligo(phenylene)ethynylene as on/off CPL switch.^{168b}

Nakashima, Kawai and coworkers, inspired by the work of Akagi with chirally aggregated conjugated polymers made of photoresponsive dithienylethenes,^{170e} synthesized a bis-pyrene-bearing helical tetrathiazole scaffold (**Figure 4.5**). The two pyrene units are located close enough to observed an excimer fluorescence and a CPL signal associated with it ($g_{\text{lum}} \sim 10^{-2}$). In this case, the photoisomerization of the tetrathiazole (at 365 nm) led to a large structural change which almost completely quench the excimer fluorescence and consequently the CPL signal. The system can be switch back by irradiation with visible light (> 400 nm).¹⁷¹

¹⁷¹ Hashimoto, Y.; Nakashima, T.; Shimizu, D.; Kawai, T., *Chem. Commun.* **2016**, 52, 5171-5174.

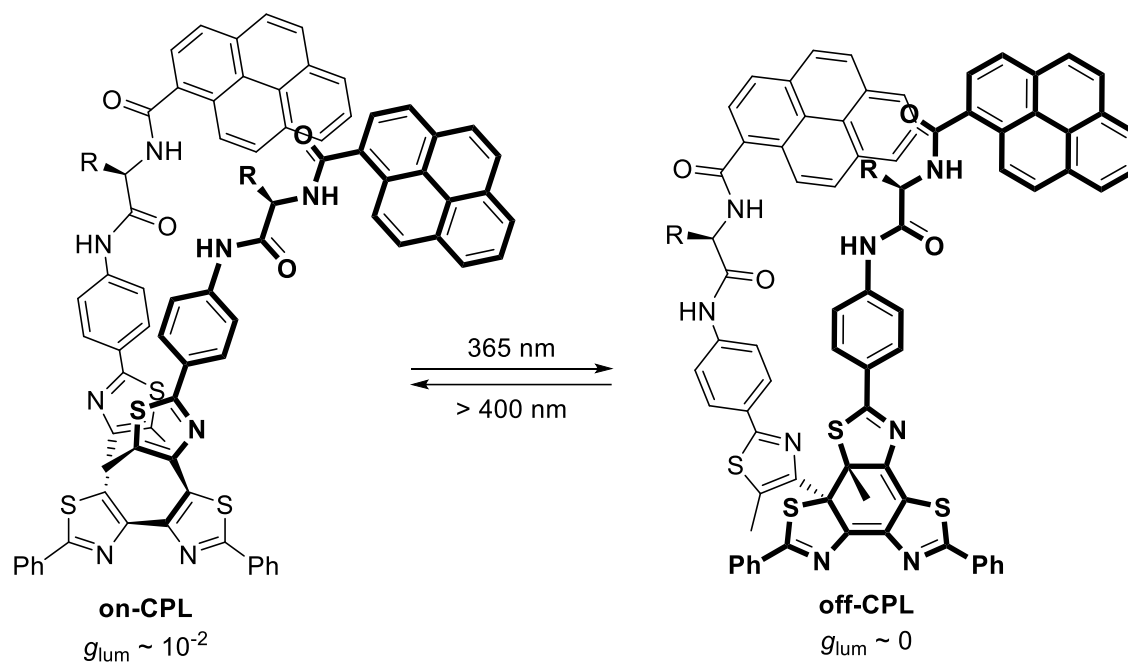


Figure 4.5 Bis-pyrene-bearing helical tetrathiazole as on/off CPL switch.¹⁷¹

The excimer fluorescence of pyrene was also used by Ito, Imai, Asami and co-workers (**Figure 4.6**). They proposed a bis-pyrene-dibenzofuran scaffold as a concentration-dependent CPL switch. The CPL signal associated with the excimer fluorescence was quenched upon dilution while the monomer intensity increased. Despite the relatively low dissymmetry factors measured ($g_{\text{lum}} 10^{-4} - 10^{-3}$), the system had the advantage to allow the detection of CPL signal associated with the monomer emission of the pyrene.¹⁶⁹

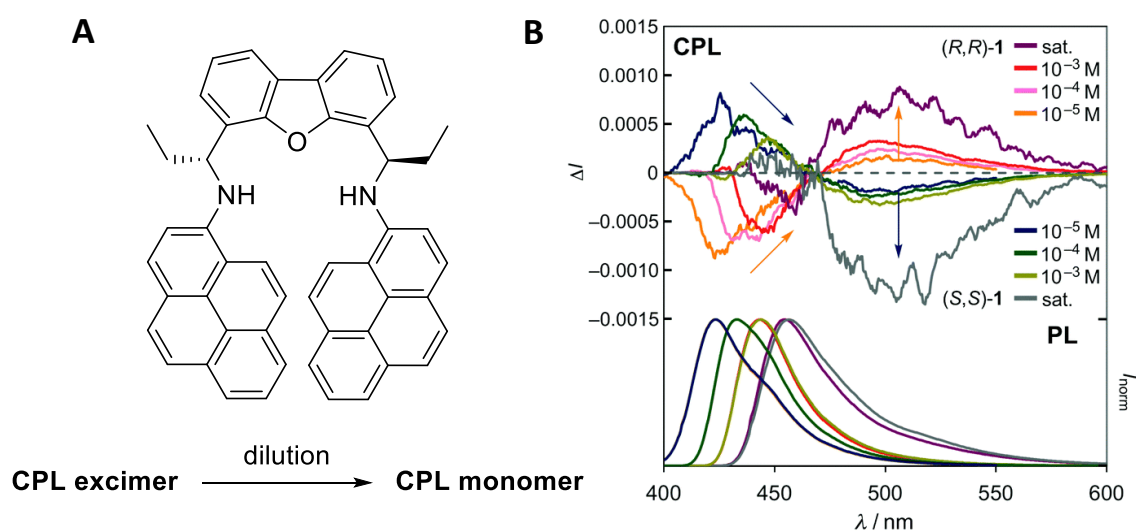


Figure 4.6 Bis-pyrene-dibenzofuran derivative as reversal CPL switch (**A**) and CPL spectra (**B**).¹⁶⁹

Finally, Takaishi and Ema developed a macrocyclic binaphthyl-bipyridyl dyad as on/off CPL switch (**Figure 4.7**). An acid/base (TFA/NEt₃) couple triggered the reversible quenching of the CPL signal ($g_{\text{lum}} = 1.6 \cdot 10^{-3}$ to 0). However, in that case, as the photoluminescence was not associated with the conformation of the molecule, no quenching of the fluorescence was measured.¹⁷²

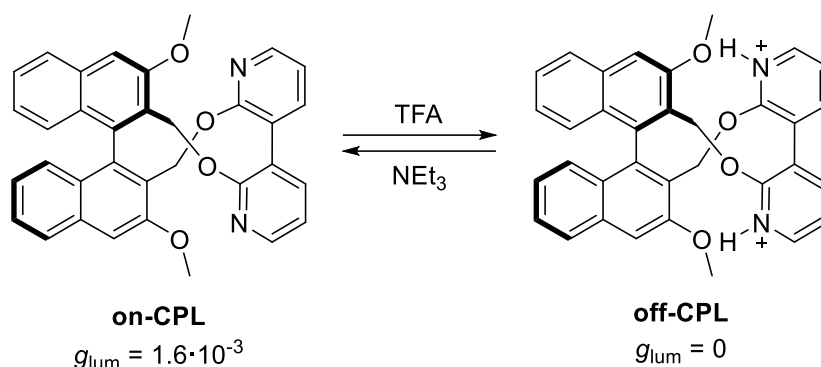


Figure 4.7 Binaphthyl-bipyridyl dyad as on/off CPL switch.¹⁷²

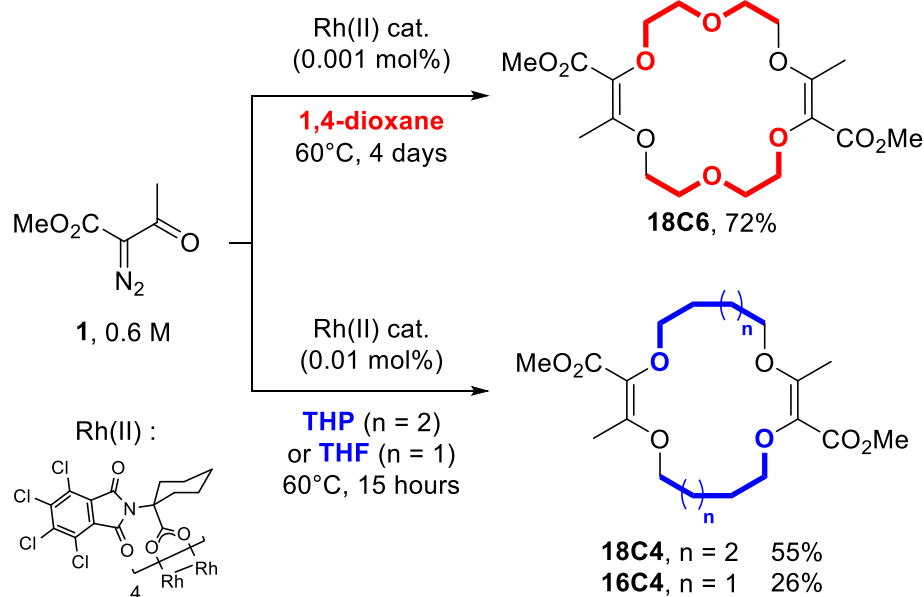
Based on the previously reported optical properties of our macrocycles and inspired by these latest studies, it was envisaged to (i) expand the scope to various fluorophores exhibiting excimer fluorescence, (ii) resolve these platforms by chiral stationary phase HPLC (CSP-HPLC) in order to (iii) investigate their optical and chiroptical properties through ECD and CPL (associated with the excimer band), and their modulation upon interaction with alkaline or alkaline earth cations. This work was performed in collaboration with Dr. Elodie Brun and Dr. Francesco Zinna and was reported in the literature during this PhD.⁸³

4.2 Synthesis and resolution of the macrocycles

The unsaturated macrocycles **18C6**, **18C4** and **16C4** (**Scheme 4.2**) previously considered were selected as valuable building blocks for the present study.¹⁴⁸ The synthesis of **18C6** from 1,4-dioxane was achieved as presented on section 1.5.1 on a multigram scale using the low catalyst loading procedure (0.001 mol%, **Scheme 4.2**, top).^{3a} Precursors **18C4** and **16C4** were synthesized

¹⁷² Takaishi, K.; Yasui, M.; Ema, T., *J. Am. Chem. Soc.* **2018**, *140*, 5334-5338.

from THP or THF cyclic ethers using a larger amount of catalyst (0.01 mol%) in 55% and 26% yield respectively (see section 2.2.3.1, **Scheme 4.2**, bottom).



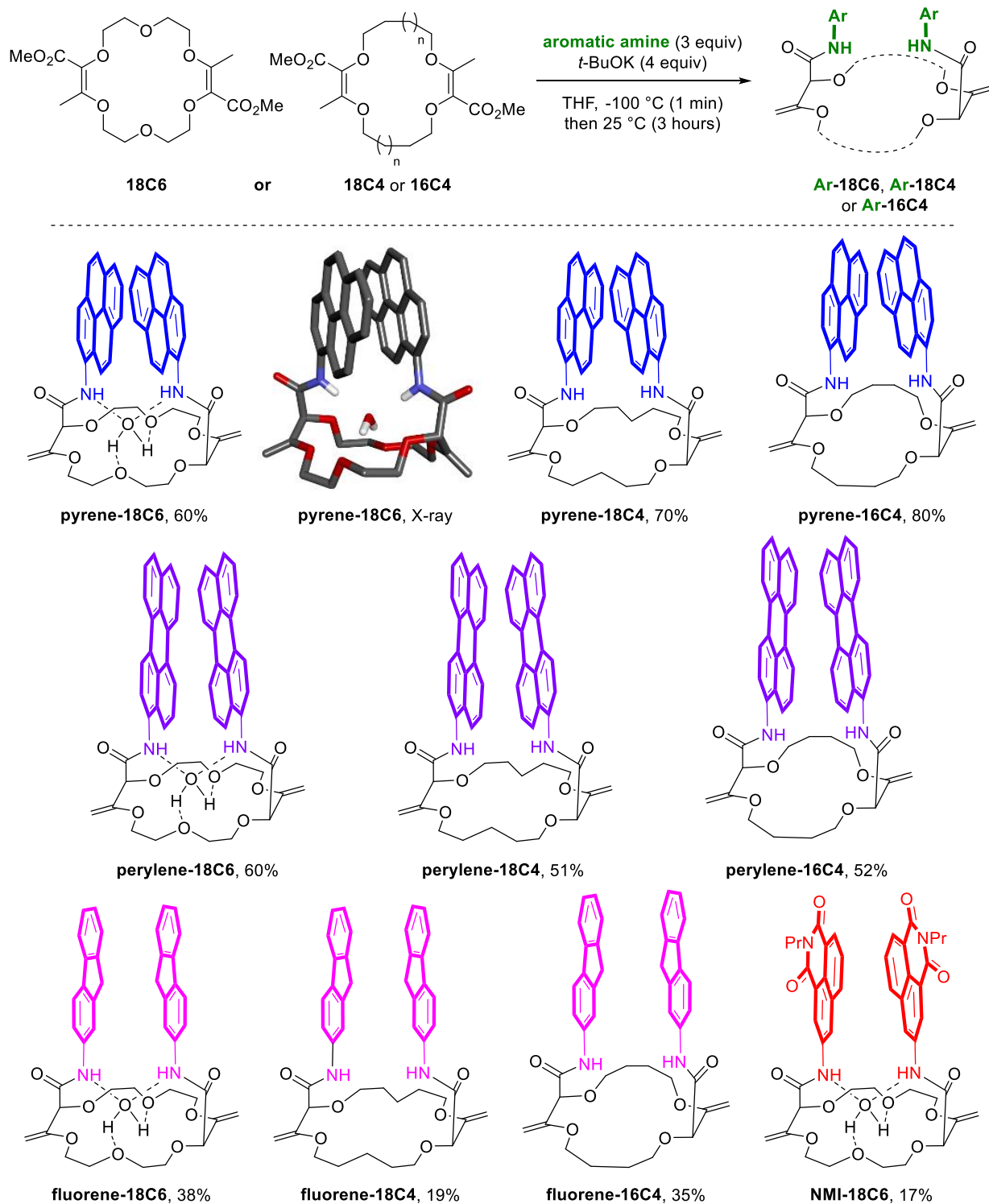
Scheme 4.2 Synthesis of unsaturated macrocycles **18C6**, **18C4** and **16C4**.^{3a}

In addition to the 1-amino-pyrene, different fluorophores were considered, namely 1-amino-perylenene, 2-amino-fluorene and 3-amino-NMI (NMI: *N*-propyl-1,8-naphthalene monoimide). The corresponding macrocycles were synthesized by treatment of the building block precursors with the appropriate aromatic amine (3.0 equiv) under strongly basic conditions (*t*-BuOK, 4.0 equiv).^{3b} It should be mentioned that the amount of amine was reduced to three equivalents for the tandem amidation – olefin transposition process to simplify the purification procedures. All chiral (racemic) polyether macrocycles were afforded in moderate to good yields (17-80%, **Scheme 4.3**) as single diastereoisomers (*dr* > 49:1). For the fluorene derivatives, it has been noticed that the use of degassed THF increased substantially the yield due to the possible competitive oxidation of fluorene by oxygen under basic conditions.¹⁷³

With the ten fluorescent compounds in hand, the resolution of the derivatives was performed by CSP-HPLC. A general and practical protocol was developed using eluents in which the macrocyclic derivatives are soluble to render the semi-preparative separation operational. Using CHIRALPAK® IG as CSP and a mixture of CH₂Cl₂ (+ 0.1% Et₂NH) and CH₃CN (+ 0.1% Et₂NH) as mobile

¹⁷³ Zhang, X.; Ji, X.; Jiang, S.; Liu, L.; Weeks, B. L.; Zhang, Z., *Green Chem.* **2011**, *13*, 1891-1896.

phase, pure samples of each enantiomer were obtained. The separation data (retention times and selectivity factors α) are summarized in **Table 7.1** (see experimental part, section 7.3.27) and the specific optical rotations of each enantiomer are collected in **Table 7.2**.



Scheme 4.3 Synthesis of the different fluorophores.

4.3 (Chir)optical properties of the macrocycles

4.3.1 Absorption properties

4.3.1.1 Conditions of analysis

In the presence of monovalent or divalent cations, very different spectroscopic results were observed depending on the nature of the macrocyclic cores used. Experimentally, it was necessary to find a solvent in which both the macrocycle and the salt are soluble and in which the salt induce a sufficient conformational change required for the modulation of the optical properties. Within the *18C6*-series, studies were conducted in acetonitrile with $\text{Ba}(\text{ClO}_4)_2$ as metal ion source as this set of conditions proved to be effective in the previous studies.¹⁴⁹ However, in presence of Ba^{2+} cation in acetonitrile, no conformational changes were observed with the *18C4*- and *16C4*-based macrocycles. It was found that a less competitive solvent is necessary (CH_2Cl_2) to compensate (possibly) for the loss of two oxygen atoms in comparison with *18C6* derivatives. The barium salt was changed for a NaBAr_F salt, soluble in CH_2Cl_2 , to achieve an efficient modulation of the optical properties in the *18C4* and *16C4* series.

4.3.1.2 ECD properties

The ECD spectra were recorded for each enantiomer of the ten different derivatives (**Figures 4.8-4.11**). Compounds of the perylene and fluorene series (**Figures 4.9 and 4.10**) displayed strong exciton couplets (bisignate ECD features) in correspondence with their most red-shifted absorption band, which is broad and intense in both cases. The exciton couplets are symmetric (the two component bands have similar integrals) and show clear vibrational substructures.

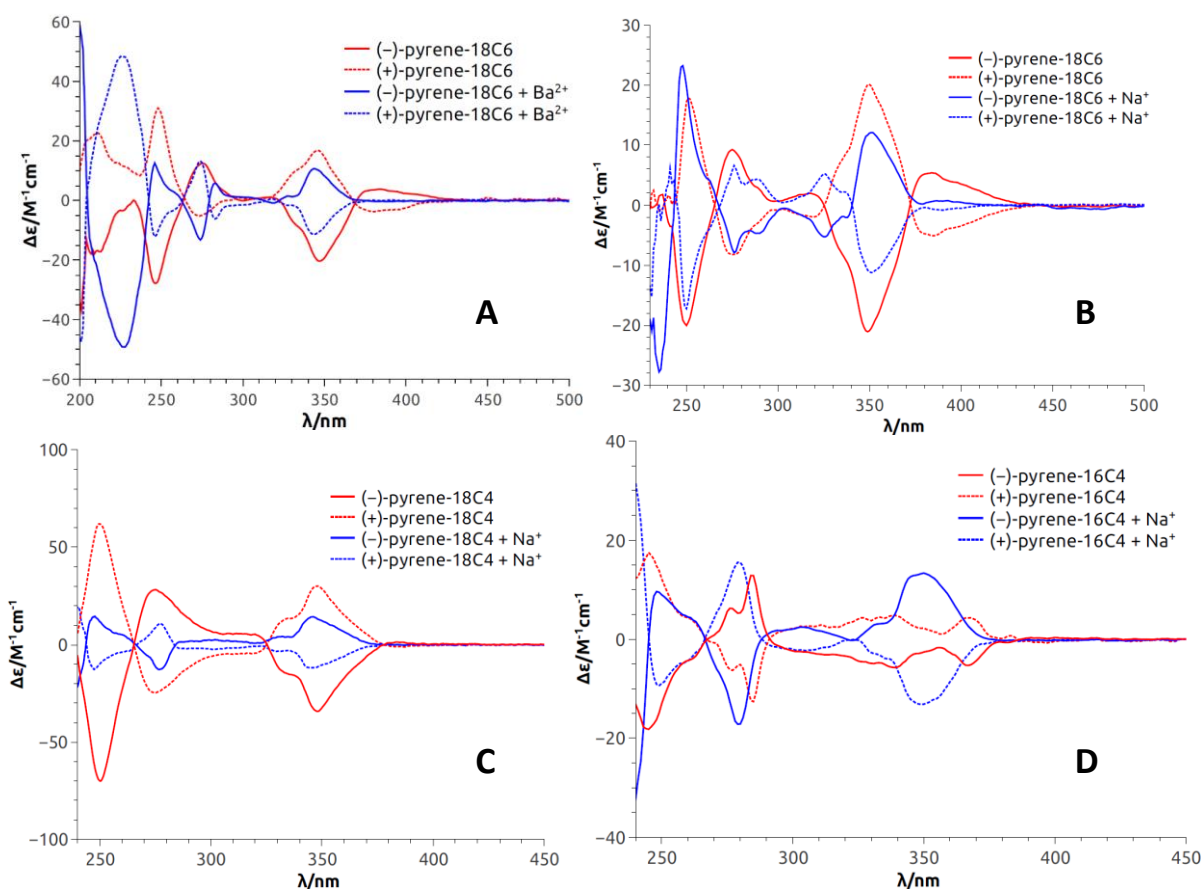


Figure 4.8 ECD spectra of both enantiomers of **pyrene-18C6** (A, CH₃CN and B, CH₂Cl₂), **pyrene-18C4** (C, CH₂Cl₂) and **pyrene-16C4** (D, CH₂Cl₂) without (red) and with (blue) Ba(ClO₄)₂ or NaBAR_F.

Surprisingly, the ECD spectra of pyrene derivatives displayed only a monosignate signal for the first absorption band (**Figure 4.8**). In fact, in the case of **pyrene-18C6** in particular, an exciton coupling was expected for this transition in view of its crystallographic geometry (**Scheme 4.3**) that indicates a spatial proximity and a skewed arrangement of the two aromatic moieties. For these pyrene derivatives, some difference between solution and solid state structures is likely to occur, including the possibility of a dynamic reorientation of the aromatic rings (*vide infra*). Finally, **NMI-18C6** displayed intense exciton couplets in the region between 230 and 300 nm (**Figure 4.11**), where strong absorptions occur, and very weak ECD bands on the right edge of the spectrum, in correspondence with weaker absorption bands.

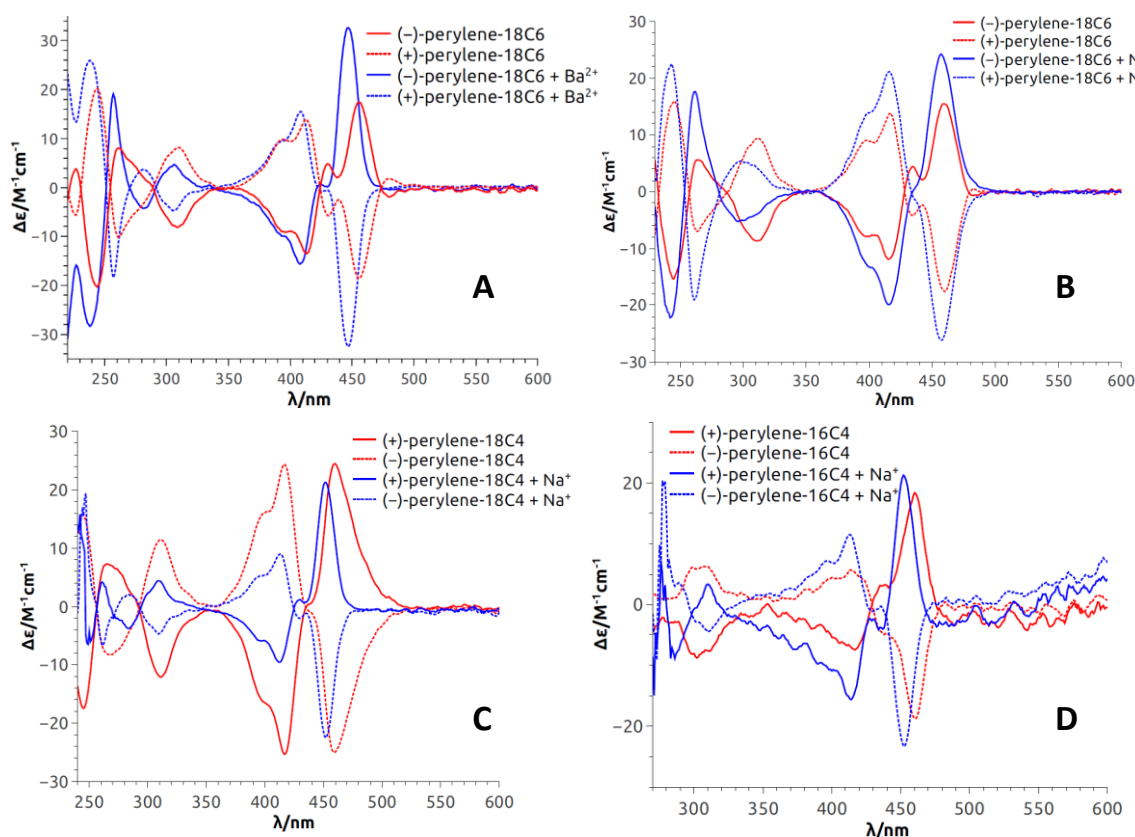


Figure 4.9 ECD spectra of both enantiomers of **perylene-18C6** (A, CH₃CN and B, CH₂Cl₂), **perylene-18C4** (C, CH₂Cl₂) and **perylene-16C4** (D, CH₂Cl₂) without (red) and with (blue) Ba(ClO₄)₂ or NaBAR_F.

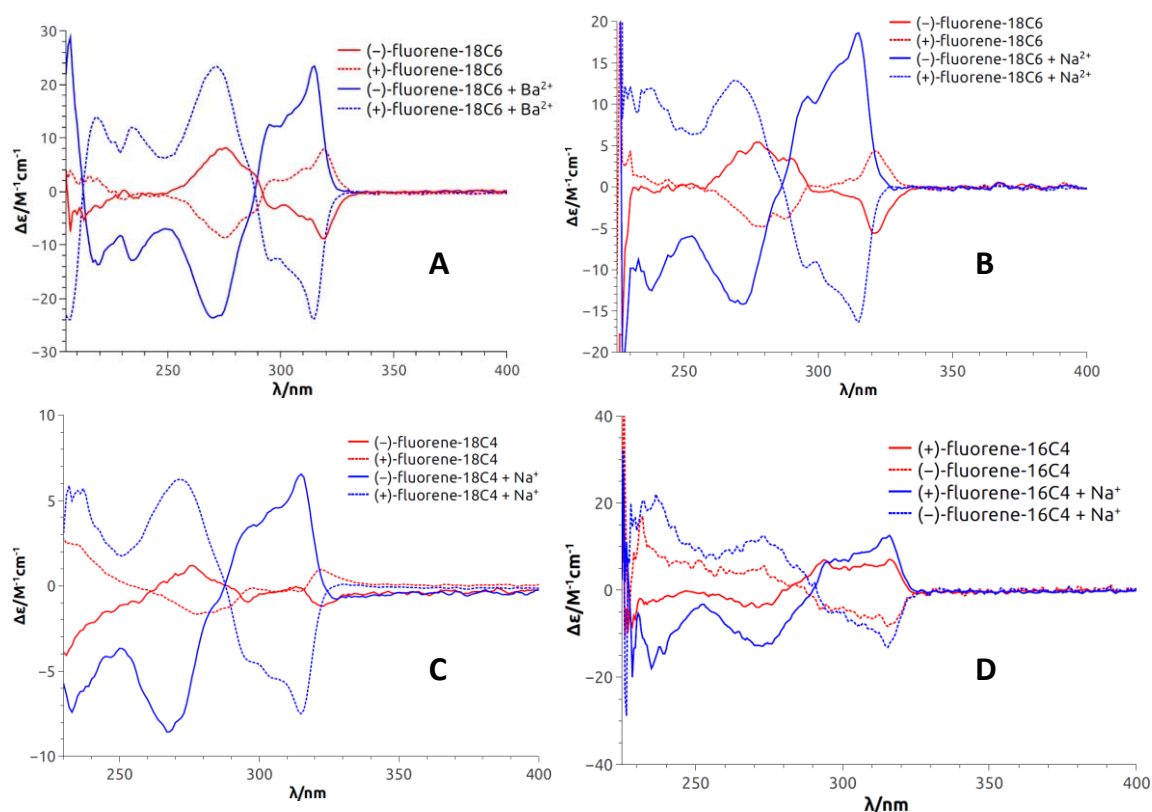


Figure 4.10 ECD spectra of both enantiomers of **fluorene-18C6** (A, CH₃CN and B, CH₂Cl₂), **fluorene-18C4** (C, CH₂Cl₂) and **fluorene-16C4** (D, CH₂Cl₂) without (red) and with (blue) Ba(ClO₄)₂ or NaBAR_F.

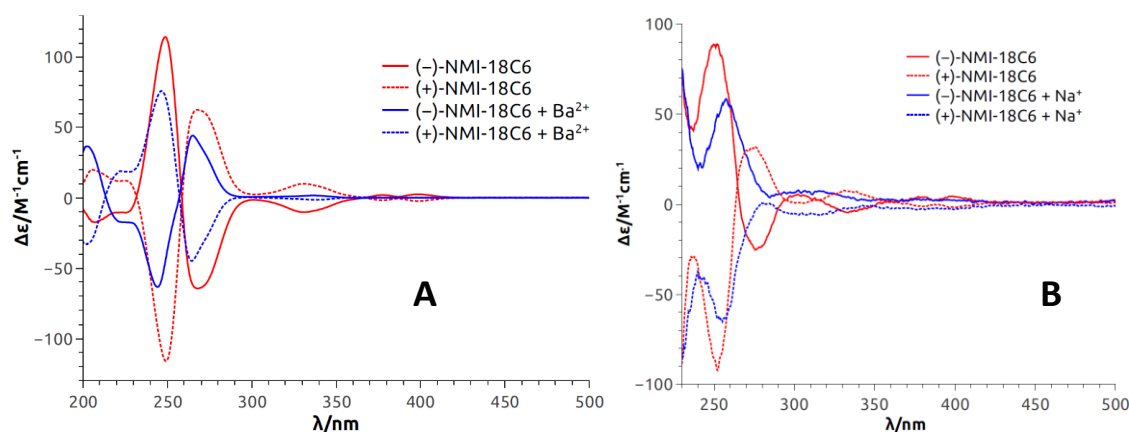


Figure 4.11 ECD spectra of both enantiomers of **NMI-18C6** in CH_3CN (**A**) and in CH_2Cl_2 (**B**) without (red) and with (blue) $\text{Ba}(\text{ClO}_4)_2$ or NaBAR_F .

4.3.1.3 TDDFT calculations

Dr. Gennaro Pescitelli (Università di Pisa, dipartimento di chimica e chimica industriale) proceeded to calculations with the aim of interpreting the observed chiroptical properties and possibly establishing the absolute configuration of the macrocycles with respect to the elution order. In that sense, ECD spectra of the **18C6** series were simulated by means of time-dependent density functional theory (TDDFT) calculations¹⁷⁴. Input geometries were generated starting from the available X-ray structure of **pyrene-18C6** with (*S,S*) configuration (bound to one water molecule), and optimized with DFT using the M06-2X functional with D3 dispersion correction,¹⁷⁵ to properly describe intramolecular π -stacking. TDDFT calculations were run with different combinations of functionals, basis sets and environment description (see section 7.13). From the start, the attempt for accurate simulation of the ECD spectra of the functionalized **18C6**-based macrocycles was a challenging task because of (a) the molecular size, associated with the complexity of the involved chromophores, and (b) the conformational ambiguity. In fact, even assuming a strong preference for π -stacked structures in solution, the two *N*-aryl amide moieties can assume several reciprocal arrangements, by varying the orientation of the macrocycle–C(=O) and *N*-aryl bonds (**Figure 4.12**), which are likely to produce very different ECD spectra. This is

¹⁷⁴ Srebro-Hooper, M.; Autschbach, J., *Annu. Rev. Phys. Chem.* **2017**, 68, 399-420.

¹⁷⁵ (a) Grimme, S.; Antony, J.; Ehrlich, S.; Krieg, H., *J. Chem. Phys.* **2010**, 132, 154104. (b) Zhao, Y.; Truhlar, D. G., *Theor. Chem. Acc.* **2008**, 120, 215-241.

illustrated in **Figure 7.23** (see experimental part) for **fluorene-18C6**. The most immediate result was that, for any given input structure, a strong exciton-coupled ECD spectrum was calculated in each case. This is easily appreciable in the DFT-optimized geometries for **fluorene-18C6** in which the aromatic rings are partially stacked over each other defining a negative or positive exciton chirality, depending on the reciprocal arrangement of the fluorene rings, associated with strong negative and positive ECD couplet, respectively (**Figure 7.23**).

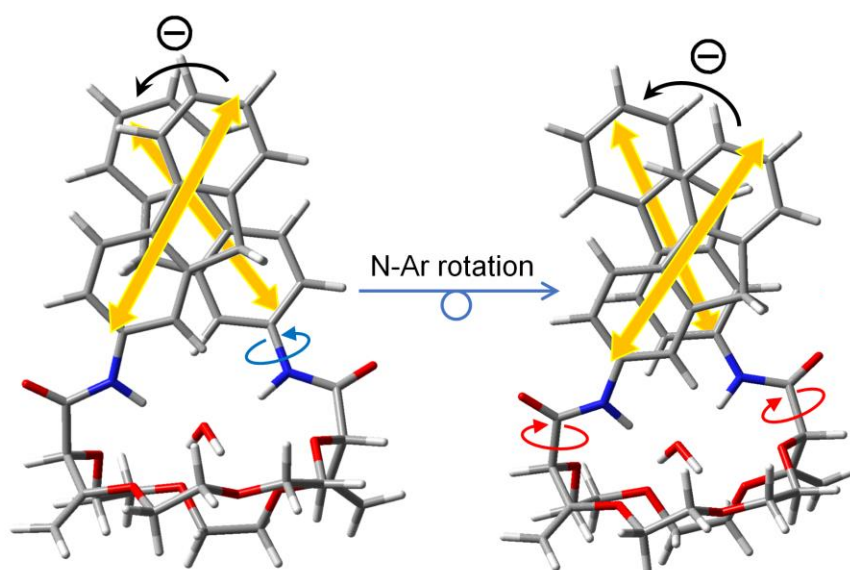


Figure 4.12 Example of rotation of the N-aryl moieties.

If the relative energies from DFT optimizations are entirely trusted, the Boltzmann-weighted calculated ECD spectrum for **(S,S)-fluorene-18C6** consists into a negative exciton couplet at long wavelength, as found experimentally for the 1st eluted enantiomer (**Figure 4.10A**). When a clear-cut couplet is not apparent from experimental spectra, like for the red-shifted bands of **pyrene-18C6** or **NMI-18C6** (**Figure 4.7A** and **4.8A**), the reason must be sought in the coexistence of multiple conformations with different arrangements of the aromatic rings which yield ECD spectra canceling each other in the red-shifted portion of the spectrum, as illustrated in **Figure 7.24**. The calculated ECD profiles suggest that for **pyrene-**, **perylene-** and **NMI-18C6**, the 2nd eluted enantiomers have (S,S) configuration.

4.3.1.4 ECD switching properties

After analyzing the ECD properties of the chromophores, the switching properties were then considered. It should be mentioned that when sodium or barium salts were added to the macrocycles only little effects were observed in UV-Vis absorption spectra (**Figures 7.13-7.16**, experimental part). However, in the case of ECD, strong variations of the signals were observed upon complexation of cations (**Figures 4.8-4.11**) – this chiroptical spectroscopy being particularly sensitive to conformational changes.^{158b} All changes were quantified using **equation 4.1**, in which $\Delta\epsilon_{(\text{cation})}$ and $\Delta\epsilon_{(\text{without})}$ represent the normalized ECD intensity (in $\Delta\epsilon$) of the compound in presence or absence of tested metal ions, respectively. The $\delta\Delta\epsilon$ values are summarized in **Table 1**.

$$\delta\Delta\epsilon = |\Delta\epsilon_{(\text{cation})} - \Delta\epsilon_{(\text{without})}| \quad (4.1)$$

The results with the **18C6** series are first discussed. In the case of **pyrene-18C6**, the spectra undergo a remarkable ECD sign reversal for almost all transitions between 200 nm and 500 nm (**Figure 4.8A**). With **perylene-18C6**, the ECD switch is less impressive. Above 446 nm, no reversal of the sign of the signal is observed, but below this value the inversion remains present (**Figure 4.9A**). It might be due to the bulkier nature of the perylene moiety, which does not allow for the necessary conformational freedom to attain a complete rearrangement upon addition of the Ba^{2+} . However, the **fluorene-18C6** derivative presents not only the sign reversal in the exciton couplet region but also a strong increase of the intensity (**Figure 4.10A**). For **NMI-18C6**, sign inversion is observed at a higher energy (around 260 nm) for the exciton coupling-like feature (**Figure 4.11A**). The ECD behavior of these compounds was also monitored with the other set of conditions (NaBAR_f in CH_2Cl_2). Variations are also observed upon addition of Na^+ and similar results were obtained (**Figures 4.8B-4.11B**).

With the **18C4** (**Figures 4.8C-4.10C**) and **16C4** (**Figures 4.8D-4.10D**) series ($\text{Na}^+/\text{CH}_2\text{Cl}_2$ conditions), the trends are comparable to the one observed in the **18C6** series to the exception of **fluorene-16C4**. Interestingly, this macrocycle displayed a small difference with a couplet of different sign compared to **fluorene-18C6** and **fluorene-18C4**. The intensity of the couplet increases but no change in sign appeared upon Na^+ addition. In general, for each compound (apart from **fluorene-16C4**), transition(s) can always be found for which the sign of the Cotton

effect switches from positive to negative or vice-versa making these macrocycles effective +/- ECD switches.

Table 4.1 Chiroptical properties (g_{abs} , $\delta\Delta\epsilon$ and g_{lum}), without and with cations ^{[a], [b]}

Compound	Enantiomer	λ_{abs} (nm)	$g_{\text{abs}} (10^{-4})$		$\delta\Delta\epsilon$ ($\text{M}^{-1} \text{cm}^{-1}$) ^[c]	λ_{em} (nm)	$g_{\text{lum}} (10^{-2})$	
			without $\text{M}^{\text{n+}}$	with $\text{M}^{\text{n+}}$			without $\text{M}^{\text{n+}}$	with $\text{M}^{\text{n+}}$ ^[d]
pyrene-18C6	(-) ^[e]	345	-3.9	+1.6	30	490	+0.9	n.d.
	(+) ^[f]		+3.9	-1.6			-0.88	n.d.
pyrene-18C4	(-) ^[e]	348	-10	+5.2	45	481	-1.0	n.d.
	(+) ^[f]		+9.2	-5.4			+0.99	n.d.
pyrene-16C4	(-) ^[e]	342	-0.83	+4.6	11	491	+1.7	n.d.
	(+) ^[f]		+0.6	-4.6			-1.8	n.d.
perylene-18C6	(-) ^[e]	446	+1.2	+5.5	21	543 ^[g]	+0.3	+0.05
	(+) ^[f]		-1.3	-5.5			-0.3	-0.05
perylene-18C4	(+) ^[e]	446	+5.2	+23	12	536 ^[g]	+0.6	+0.04
	(-) ^[f]		-5.4	-24			-0.6	-0.04
perylene-16C4	(+) ^[e]	446	+1.6	+3.3	8	544 ^[g]	-0.4	+0.02
	(-) ^[f]		-1.8	-3.6			+0.4	-0.02
fluorene-18C6	(-) ^[e]	314	-3.6	+5.6	23	337	-	-
	(+) ^[f]		+3.5	-5.6			-	-
fluorene-18C4	(-) ^[e]	315	<0.1	+6.3	6	338	-	-
	(+) ^[f]		<0.1	-6.7			-	-
fluorene-16C4	(+) ^[e]	316	+3.3	+6.3	6	336	-	-
	(-) ^[f]		-3.5	-6.5			-	-
NMI-18C6	(-) ^[e]	398	+2.6	+0.2	3	485	+0.82	n.d.
	(+) ^[f]		-2.5	-0.2			-0.86	n.d.

[a] $\text{Ba}(\text{ClO}_4)_2/\text{CH}_3\text{CN}$ system used for 18C6 derivatives, $\text{NaBAR}_F/\text{CH}_2\text{Cl}_2$ system used for 18C4 and 16C4 derivative, g_{abs} and g_{lum} are calculated on reported λ_{abs} and λ_{em} respectively (unless otherwise stated);

[b] n.d. = not detected; [c] As defined by **equation 4.1**; [d] Determined on the monomer emission band;

[e] First eluted; [f] second eluted; [g] λ associated with excimer emission.

4.3.2 Emission properties

4.3.2.1 Fluorescence properties

With these results in hands, we turned next our attention to the emission properties. For this study, the “monomer” emission of each fluorophore was compared with a reference made of the fluorophore of interest linked to a simple neopentylcarboxamide function (**Figure 4.13**).

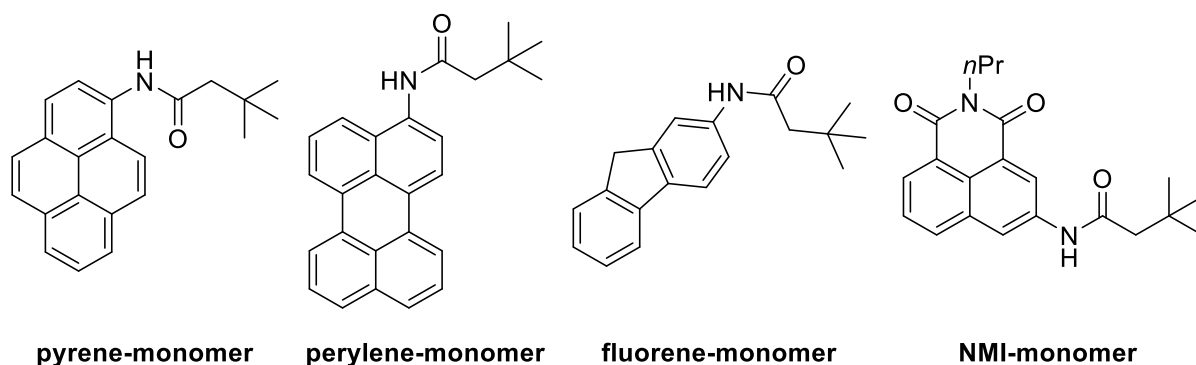


Figure 4.13 Monomers used as reference for the fluorescence properties analysis.

As already reported for the pyrene derivatives, the functionalized macrocycles display excimer fluorescence, which is red shifted compared to the monomer emission (**Figures 4.14** and **7.13-7.16**).¹⁴⁸⁻¹⁴⁹ Delightfully, all new functionalized derivatives also displayed excimer fluorescence (EF). Depending on the aromatic substituent, a large spectral window, spanning from UV to green-yellow (*ca.* 300 nm to *ca.* 650 nm), can be accessed. Thanks to the close proximity between the two aromatic moieties, the excimer band is particularly intense. The spectra of the **18C6** series are reported in **Figure 4.14** as representative examples (see experimental section for the other derivatives, section 7.12.1.3).

In the pyrene series, the excimer band is particularly intense at 490 nm (λ_{max}) and, for the **18C4** moiety specifically, the interaction is so strong that the emission band of the monomer is no longer observable. With compounds carrying perylene moieties, a weaker and broad EF is observed around 540 nm. Fluorene derivatives present very strong EF (337 nm) in comparison to the almost non-detectable monomer band. Finally, **NMI-18C6** presents similar characteristics to **perylene-18C6** although with a more intense excimer band (485 nm) in respect to the monomer.

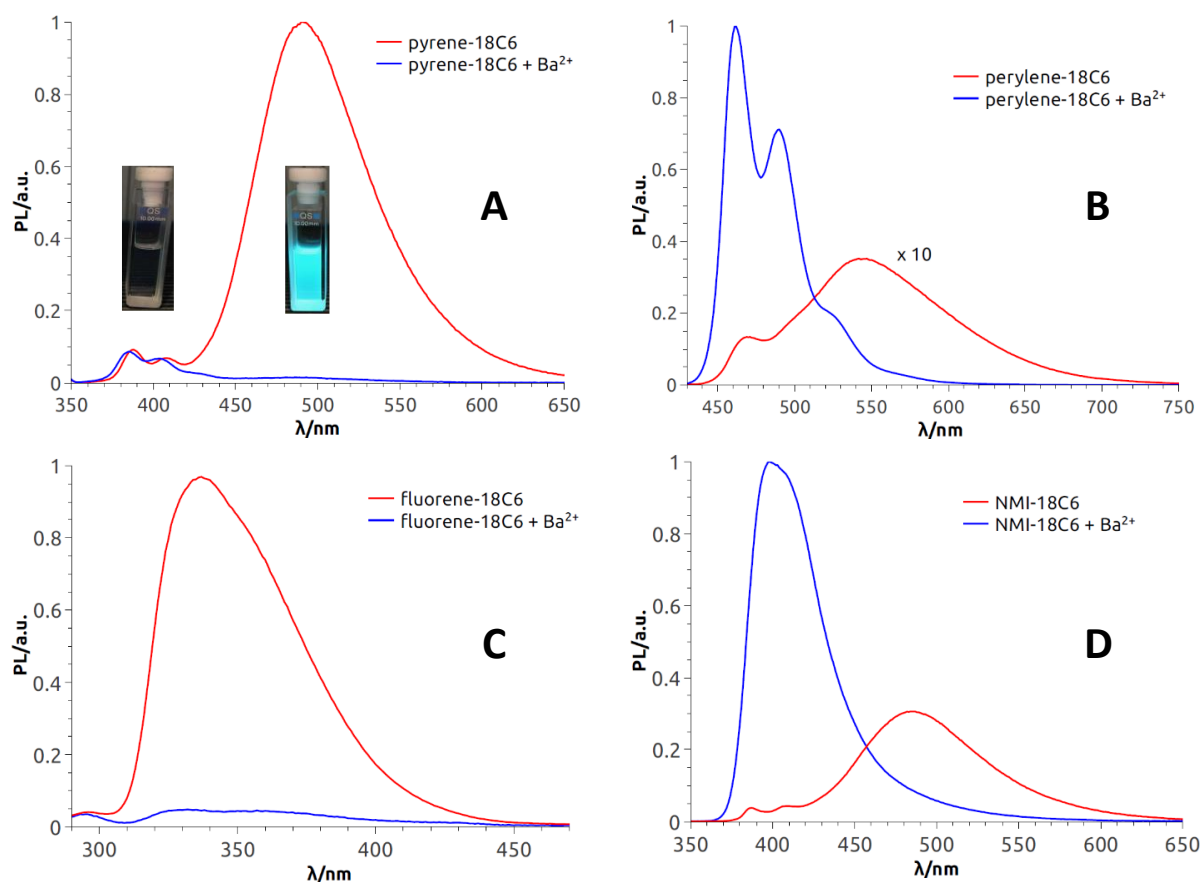


Figure 4.14 Fluorescence spectra (CH_3CN) of **pyrene-18C6** (A), **perylene-18C6** (B), **fluorene-18C6** (C) and **NMI-18C6** (D) without (red) and with (blue) $\text{Ba}(\text{ClO}_4)_2$. In panel A: picture of **pyrene-18C6** without (left) and with (right) Ba^{2+} under UV irradiation (366 nm).

Also, while 18C6 and 18C4 derivatives display strong EF contribution with respect to the monomer fluorescence, the effect is less pronounced with 16C4 analogues. In fact, for the smaller ring size compounds such as **pyrene-16C4**, solid-state analysis indicates a non-parallel arrangement of the aromatic moieties (**Figure 4.15**) and hence the possible reduction in EF efficiency.

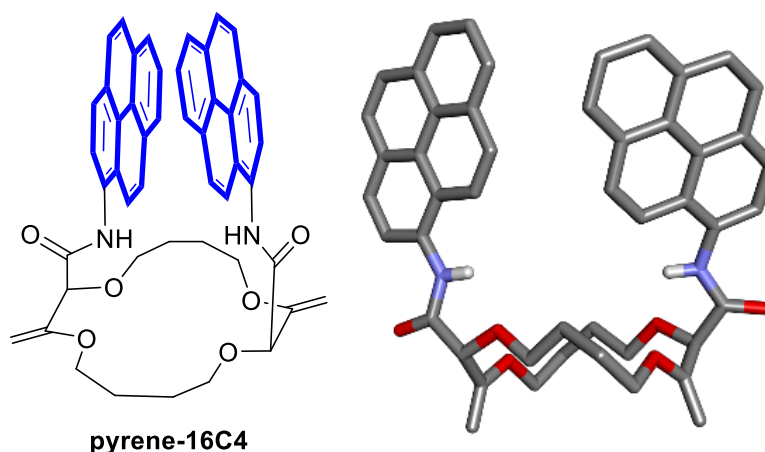


Figure 4.15 Stick view of the crystal structure of **pyrene-16C4**.

4.3.2.2 Quenching of fluorescence

Upon addition of cations, the excimer fluorescence is completely quenched and only the sharper monomer emission remains visible. This is the case with all the fluorophores independently of the size of the polyether macrocycle. This observation is in agreement with the proposed conformational change upon cation complexation (**Figure 4.1**). Emission maxima (λ_{max}) and fluorescence quantum yields (ϕ) of all compounds are reported in **Table 7.4**.

4.3.2.3 CPL properties

Some pyrene-based compounds are known to exhibit a CPL signal associated with the excimer fluorescence.¹⁷⁶ This property has been used by several groups in the last four years to design CPL active pyrene-based platforms.^{169, 171, 177} As a consequence of the strong excimer

¹⁷⁶ For the initial description of pyrene-based compounds exhibiting excimer associated CPL emission, see: (a) Brittain, H.; Ambrozich, D. L.; Saburi, M.; Fendler, J. H., *J. Am. Chem. Soc.* **1980**, *102*, 6372-6374. (b) Kano, K.; Matsumoto, H.; Hashimoto, S.; Sisido, M.; Imanishi, Y., *J. Am. Chem. Soc.* **1985**, *107*, 6117-6118. (c) Inai, Y.; Sisido, M.; Imanishi, Y., *J. Phys. Chem.* **1990**, *94*, 2734-2735.

¹⁷⁷ For other recent examples of CPL active pyrene-based platforms, see: (a) Takaishi, K.; Takehana, R.; Ema, T., *Chem. Commun.* **2018**, *54*, 1449-1452. (b) Mimura, Y.; Nishikawa, T.; Fuchino, R.; Nakai, S.; Tajima, N.; Kitamatsu,

fluorescence observed for our new compounds, we thought that they might show an interesting circularly polarized luminescence as well.

As expected, pyrene, perylene and NMI derivatives presented strong CPL signals associated with the excimer fluorescence (**Figures 4.16-4.18**). A weak contribution from the monomer circularly polarized emission was observed only in the perylene series (**Figures 4.17**). However, in the fluorene series, due to the technical limitations of the CPL apparatus in the UV region, CPL spectra could not be measured. Yet, by analogy, if the apparatus could measure such signals, a strong CPL signal associated with the allied EF would be expected with the fluorene derivatives.

To quantify the circular polarization degree of the emission, the luminescence dissymmetry factor g_{lum} was used as defined by **equation 4.2** – where I_L and I_R correspond to left and right circularly polarized component of the emission respectively. The g_{lum} factors for all tested compounds are reported in **Table 4.1**.

$$g_{\text{lum}} = 2 \cdot \frac{I_L - I_R}{I_L + I_R} \quad (4.2)$$

For most compounds, the luminescence dissymmetry factors calculated on the CPL/fluorescence maxima are around 10^{-2} (**Table 4.1**). These g_{lum} values are in the upper range recorded for single (non-aggregated) organic molecules,¹⁷⁸ and in line with the values reported

M.; Fujiki, M.; Imai, Y., *Org. Biomol. Chem.* **2017**, *15*, 4548-4553. (c) Li, J.; Yang, C.; Huang, C.; Wan, Y.; Lai, W.-Y., *Tetrahedron Lett.* **2016**, *57*, 1256-1260. (d) Nakanishi, S.; Nakabayashi, K.; Mizusawa, T.; Suzuki, N.; Guo, S.; Fujiki, M.; Imai, Y., *RSC Advances* **2016**, *6*, 99172-99176. (e) Nakamura, M.; Suzuki, J.; Ota, F.; Takada, T.; Akagi, K.; Yamana, K., *Chem. Eur. J.* **2016**, *22*, 9121-9124. (f) Nishikawa, T.; Kitamura, S.; Kitamatsu, M.; Fujiki, M.; Imai, Y., *ChemistrySelect* **2016**, *4*, 831-835. (g) Nishikawa, T.; Tajima, N.; Kitamatsu, M.; Fujiki, M.; Imai, Y., *Org. Biomol. Chem.* **2015**, *13*, 11426-11431. (h) Amako, T.; Nakabayashi, K.; Suzuki, N.; Guo, S.; Rahim, N. A. A.; Harada, T.; Fujiki, M.; Imai, Y., *Chem. Commun.* **2015**, *51*, 8237-8240. (i) Nakabayashi, K.; Amako, T.; Tajima, N.; Fujiki, M.; Imai, Y., *Chem. Commun.* **2014**, *50*, 13228-13230. (j) Inouye, M.; Hayashi, K.; Yonenaga, Y.; Itou, T.; Fujimoto, K.; Uchida, T. a.; Iwamura, M.; Nozaki, K., *Angew. Chem. Int. Ed.* **2014**, *53*, 14392-14396.

¹⁷⁸ Sánchez-Carnerero, E. M.; Agarrabeitia, A. R.; Moreno, F.; Maroto, B. L.; Muller, G.; Ortiz, M. J.; de la Moya, S., *Chem. Eur. J.* **2015**, *21*, 13488-13500.

with pyrenes,^{169, 171, 179} naphthalimides¹⁸⁰ and naphthalene diimides¹⁸¹ or perylene bisimides.¹⁸² In the perylene series, g_{lum} values not higher than 10^{-3} were obtained. The decrease of the observed dissymmetry factor is possibly due to the contribution of the weakly polarized perylene monomer emission.¹⁸³

Since, in these systems, CPL stems from the excimer, a photophysical state formed only in the excited state, the g_{lum} factor does not need to be related to the ECD dissymmetry factor ($g_{\text{abs}} = \Delta\epsilon/\epsilon$) measured on the first Cotton effect, as it would be expected if the same electronic states were involved both in absorption and emission.¹⁸⁴ Indeed, in the present case, g_{abs} values are in the 10^{-3} – 10^{-4} range while g_{lum} factors, calculated on the CPL/fluorescence maxima, are higher by at least one order of magnitude (10^{-2}).

¹⁷⁹ (a) Takaishi, K.; Takehana, R.; Ema, T., *Chem. Commun.* **2018**, 54, 1449-1452. (b) Mimura, Y.; Nishikawa, T.; Fuchino, R.; Nakai, S.; Tajima, N.; Kitamatsu, M.; Fujiki, M.; Imai, Y., *Org. Biomol. Chem.* **2017**, 15, 4548-4553. (c) Li, J.; Yang, C.; Huang, C.; Wan, Y.; Lai, W.-Y., *Tetrahedron Lett.* **2016**, 57, 1256-1260. (d) Nakanishi, S.; Nakabayashi, K.; Mizusawa, T.; Suzuki, N.; Guo, S.; Fujiki, M.; Imai, Y., *RCS Adv.* **2016**, 6, 99172-99176. (e) Nakamura, M.; Suzuki, J.; Ota, F.; Takada, T.; Akagi, K.; Yamana, K., *Chem. Eur. J.* **2016**, 22, 9121-9124. (f) Nishikawa, T.; Kitamura, S.; Kitamatsu, M.; Fujiki, M.; Imai, Y., *ChemistrySelect* **2016**, 4, 831-835. (g) Nishikawa, T.; Tajima, N.; Kitamatsu, M.; Fujiki, M.; Imai, Y., *Org. Biomol. Chem.* **2015**, 13, 11426-11431. (h) Amako, T.; Nakabayashi, K.; Suzuki, N.; Guo, S.; Rahim, N. A. A.; Harada, T.; Fujiki, M.; Imai, Y., *Chem. Commun.* **2015**, 51, 8237-8240. (i) Nakabayashi, K.; Amako, T.; Tajima, N.; Fujiki, M.; Imai, Y., *Chem. Commun.* **2014**, 50, 13228-13230. (j) Inouye, M.; Hayashi, K.; Yonenaga, Y.; Itou, T.; Fujimoto, K.; Uchida, T. a.; Iwamura, M.; Nozaki, K., *Angew. Chem. Int. Ed.* **2014**, 53, 14392-14396. (k) Inai, Y.; Sisido, M.; Imanishi, Y., *J. Phys. Chem.* **1990**, 94, 2734-2735. (l) Kano, K.; Matsumoto, H.; Hashimoto, S.; Sisido, M.; Imanishi, Y., *J. Am. Chem. Soc.* **1985**, 107, 6117-6118. (m) Brittain, H.; Ambrozich, D. L.; Saburi, M.; Fendler, J. H., *J. Am. Chem. Soc.* **1980**, 102, 6372-6374.

¹⁸⁰ Sheng, Y.; Ma, J.; Liu, S.; Wang, Y.; Zhu, C.; Cheng, Y., *Chem. Eur. J.* **2016**, 22, 9519-9522.

¹⁸¹ Salerno, F.; Berrocal, J. A.; Haedler, A. T.; Zinna, F.; Meijer, E. W.; Di Bari, L., *J. Mater. Chem. C* **2017**, 5, 3609-3615.

¹⁸² (a) Kumar, J.; Nakashima, T.; Tsumatori, H.; Kawai, T., *J. Phys. Chem. Lett.* **2014**, 5, 316-321. (b) Kumar, J.; Nakashima, T.; Tsumatori, H.; Mori, M.; Naito, M.; Kawai, T., *Chem. Eur. J.* **2013**, 19, 14090-14097. (c) Tsumatori, H.; Nakashima, T.; Kawai, T., *Org. Lett.* **2010**, 12, 2362-2365.

¹⁸³ A g_{lum} in the order of 10^{-4} is observed for the CPL signal associated with the monomer emission.

¹⁸⁴ Tanaka, H.; Inoue, Y.; Mori, T., *ChemPhotoChem* **2018**, 2, 386-402.

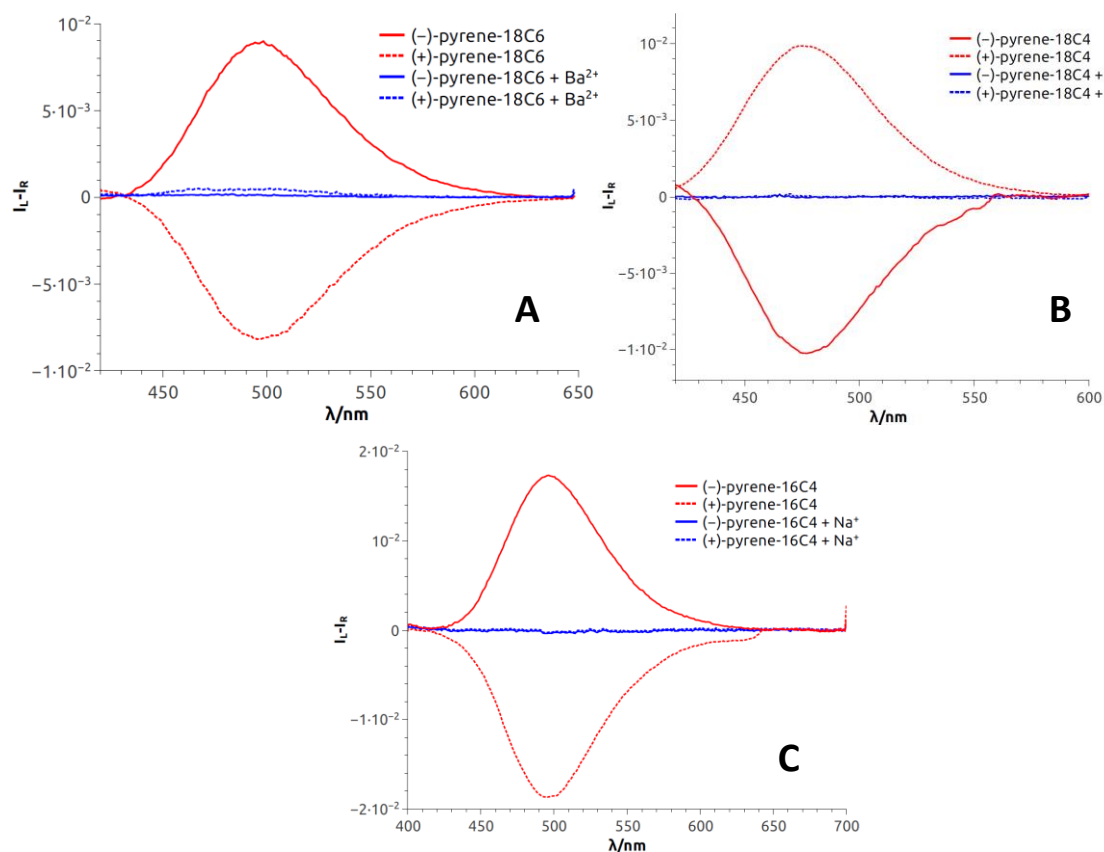


Figure 4.16 CPL spectra of both enantiomers of **pyrene-18C6** (A, CH_3CN), **pyrene-18C4** (B, CH_2Cl_2) and **pyrene-16C4** (C, CH_2Cl_2) without (red) and with (blue) $\text{Ba}(\text{ClO}_4)_2$ or NaBAR_F .

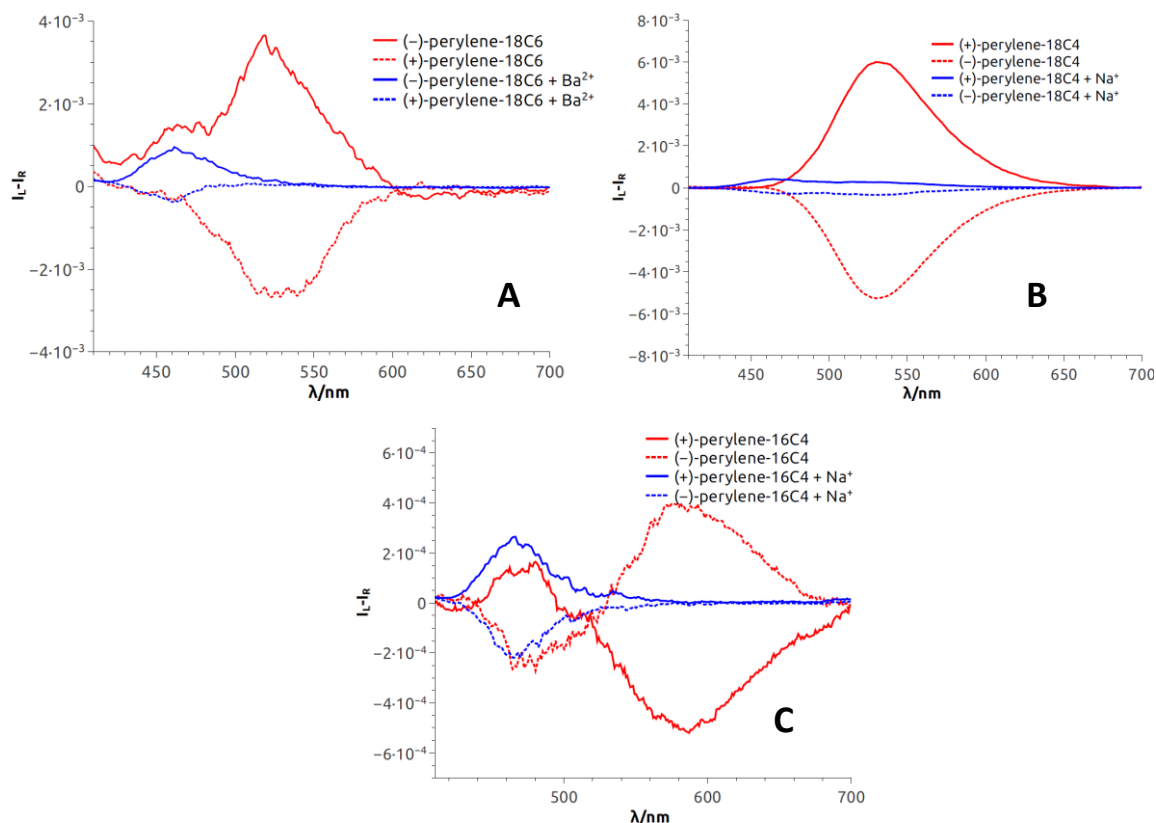


Figure 4.17 CPL spectra of both enantiomers of **perylene-18C6** (A, CH_3CN), **perylene-18C4** (B, CH_2Cl_2) and **perylene-16C4** (C, CH_2Cl_2) without (red) and with (blue) $\text{Ba}(\text{ClO}_4)_2$ or NaBAR_F .

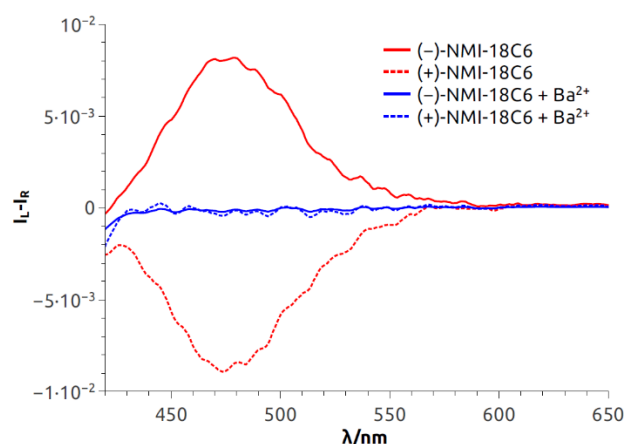


Figure 4.18 CPL spectra of both enantiomers of **NMI-18C6** (CH_3CN) without (red) and with (blue) $\text{Ba}(\text{ClO}_4)_2$.

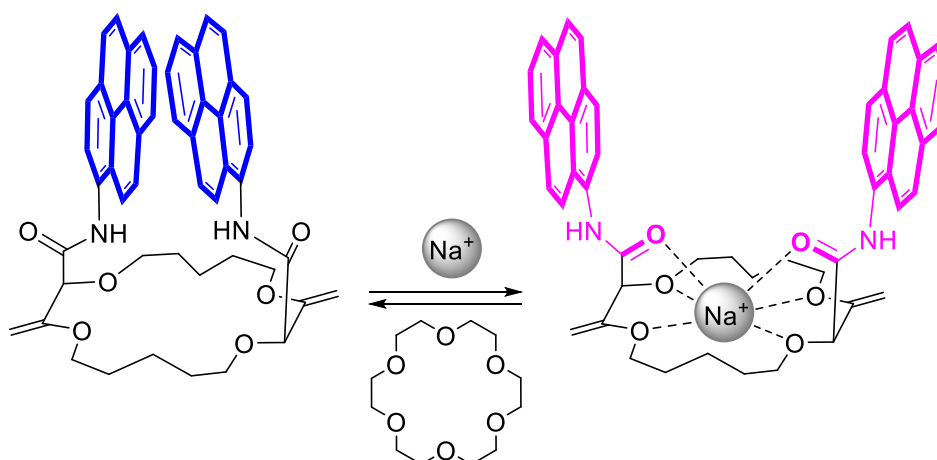
4.3.2.4 Quenching of CPL

Then, similarly to the excimer fluorescence experiments, complete quenching of CPL signals was achieved with pyrene and NMI macrocycles upon addition of cations (Na^+ or Ba^{2+} , **Figures 4.16** and **4.18**). In these cases, the CPL signals associated with the monomer bands were too weak to be detected. However, with perylene compounds (**Figure 4.17**), it was possible to measure a weak CPL signal allied with the stronger monomer emission (g_{lum} up to 5×10^{-4}), in the expected g_{lum} range for (weakly) chirally-perturbed fluorophores.

4.3.3 ECD and CPL reversibility

As the polyether macrocycles exhibited effective chiroptical switching properties, both in ECD and CPL, the reversibility of the metal complexation was then considered. Because of the strong binding of barium cations to 18C6 derivatives in acetonitrile, the reversibility was studied using a monovalent cation as complexing agent instead (NaBAR_F in CH_2Cl_2).¹⁴⁹ In order to switch back the system, it was envisaged to use regular 18-Crown-6 as a cation scavenger (**Scheme 4.4**). This

system already proved to be efficient with this type of macrocycles in ratiometric luminescent switches for the decomplexation of potassium ions.¹⁸⁵



Scheme 4.4 Model for reversible switching.

Equimolar amounts of NaBAr_F and 18-Crown-6 solutions were thus successively added to dichloromethane solutions of the pyrene, perylene, fluorene and NMI fluorophores. After each addition, ECD, then fluorescence and finally CPL spectra were recorded. Data for the **pyrene-18C4** derivative, selected as a representative example, is displayed in **Figure 4.19**. Remaining data are reported in the experimental part (**Figures 7.17-7.22**).

As desired, upon addition of 18-Crown-6 to the [macrocycle·Na]⁺ adduct, it was possible to completely switch back the system and recover the ECD signals of the uncomplexed material (**Figure 4.19A**). The switching experiment could be repeated over several cycles without significant signal loss or modification (**Figure 4.19B** at 348 nm). In fluorescence, using the same system, almost complete reversible switching – from excimer to monomer – was monitored (**Figure 4.19C-D**). Finally, in CPL, these conditions led also to a good recovery of the signal, over several cycles (**Figure 4.19E-F**). **Pyrene-18C4** may therefore be considered as a completely reversible +/- ECD and on/off CPL switch.

¹⁸⁵ Sinn, S.; Biedermann, F.; Vishe, M.; Aliprandi, A.; Besnard, C.; Lacour, J.; De Cola, L., *ChemPhysChem* **2016**, *17*, 1829-1834.

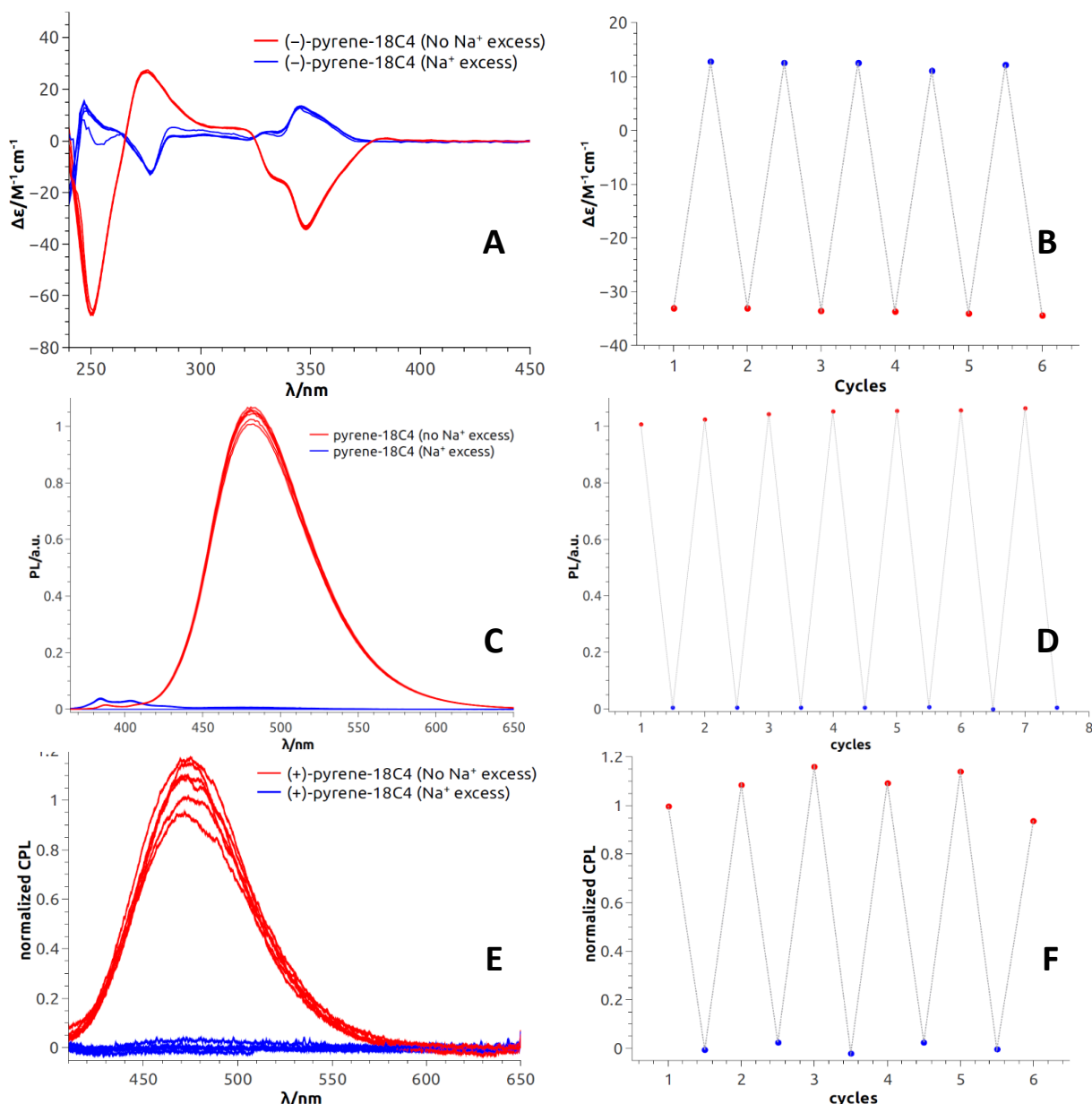


Figure 4.19 Pyrene-18C4 (NaBARF, CH₂Cl₂). Reversible ECD (A, first eluted (-)-enantiomer) and intensities at 348 nm (B); reversible fluorescence (C) and normalized intensities at 480 nm (D) and reversible CPL (E, second eluted (+)-enantiomer) and normalized intensities at 480 nm (F).

Favorably, using the same reagent combination, all pyrene and fluorene macrocycles behave as fully reversible ECD switches over several cycles (**Figures 7.17** and **7.19**). In CPL, **pyrene-18C6** demonstrated reversibility in spite of an attenuation of the excimer luminescence intensity over the cycles (**Figures 4.20A-B**). This trend is even more acute with analogous **pyrene-16C4** that showed reversibility over only two cycles – presumably due to the strong photobleaching occurring under the CPL measurement conditions for this compound (**Figures 4.20C-D**). Unfortunately, in ECD, with perylene and NMI derivatives, signal recovery to the expected intensity and shape could not be achieved over successive additions of NaBARF and 18-Crown-6

(Figures 7.19 and 7.20). Consequently, the reversibility of the CPL signal was not studied for these cases.

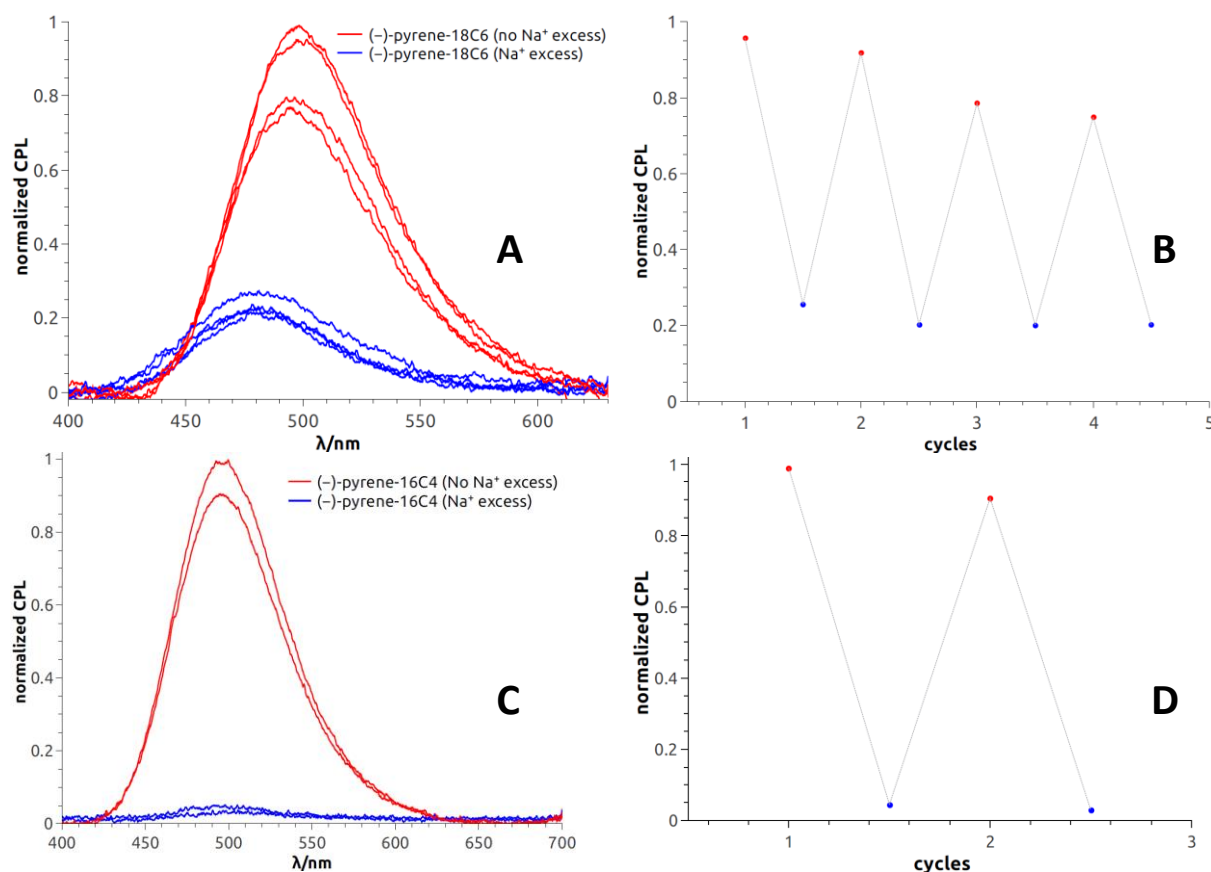


Figure 4.20 CPL reversibility of **pyrene-18C6** (A, first eluted (–)-enantiomer) with normalized intensities at 480 nm (B) and **pyrene-16C4** (C, first eluted (–)-enantiomer) with normalized intensities at 480 nm (D).

4.4 Conclusion

In summary, we presented a series of readily prepared functionalized macrocycles with 1-amino-pyrene, 1 amino-perylene, 2-amino-fluorene and 3-amino-NMI. All derivatives showed efficient excimer luminescence in different spectral regions (λ_{em} 300 to 650 nm) due to the spatial proximity of fluorophores held in place by the constrained macrocyclic structures. Upon addition

of monovalent or divalent cation (Na^+ or Ba^{2+}), important conformational changes occurred, elongating the distance between the fluorophores and, consequently, a quenching of the EF was observed.

Using enantiopure materials, obtained through CSP-HPLC resolution, the chiroptical properties of the macrocycles were studied. A sign inversion of certain of most ECD signal(s) was demonstrated in all cases upon addition of cations like Na^+ or Ba^{2+} supporting the conformational change proposed. In addition, these molecules displayed a highly circularly polarized luminescence associated with the excimer fluorescence with g_{lum} values up to $1.7 \cdot 10^{-2}$, which can be quenched upon cation binding. For several systems, a complete recovery of ECD/CPL signals over several cycles was observed after reversible complexation of the sodium cation with commercial 18-Crown-6 scavenger. These two chiroptical behaviors gave rise to rare examples of allied $+/-$ ECD and on/off CPL switches.

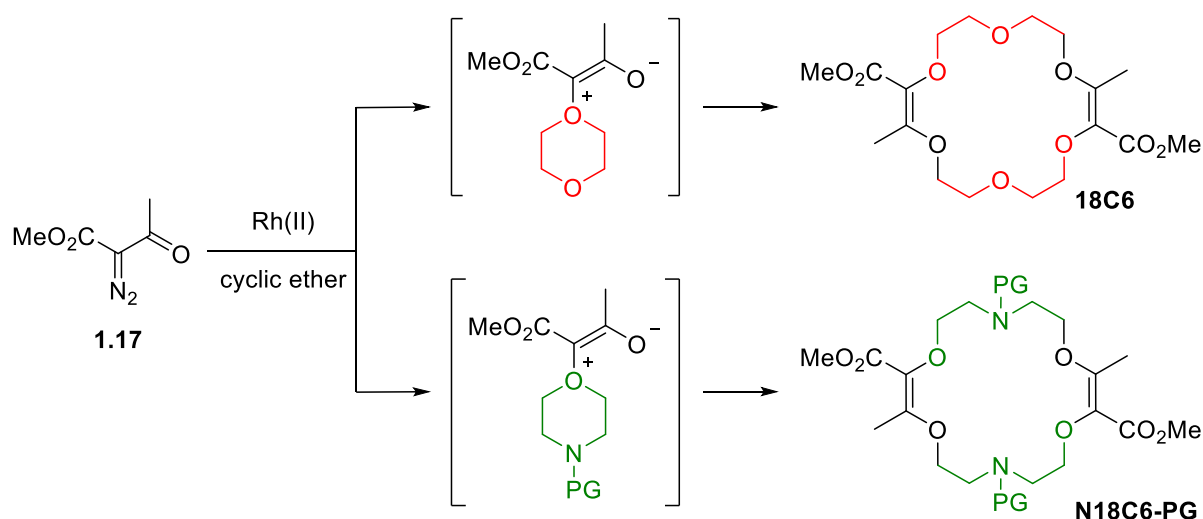
5 Aza-crown ether synthesis

5.1 Introduction

The synthesis of unsaturated polyether macrocycles (**18C6**, **18C4** and **16C4**) by condensation of diazo **1.17** with simple cyclic ethers under rhodium(II) catalysis was presented in section 1.5.1.^{3a, 69, 73} Further derivatization into chiral polyether macrocycles by treatment with various aliphatic and aromatic amines were presented in the previous chapters.^{3b, 83, 148} One important manner to modulate the binding properties of crown ethers is to substitute some of the oxygen atoms within the macrocycles by nitrogen atoms; their highest *Lewis* character inducing stronger binding with many metal ions.^{27b, 186} With this goal in mind, Daniele Poggiali demonstrated during his PhD that protected morpholines can also be used as efficient cyclic precursors for the Rh(II)-catalyzed formation of oxonium ylides by condensation with diazo **1.17**. Then a subsequent dimerization of two ylides led to aza-polyether macrocycles **N18C6-PG** after a formal [3+6+3+6] macrocyclization (**Scheme 5.1**).⁷⁰

These new derivatives were seen as valuable building blocks and their transformation into chiral diaza-crown ethers was envisaged, applying the amidation – transposition strategies presented in the previous chapters. The investigation of such reactions will be presented in this chapter.

¹⁸⁶ (a) Hancock, R. D., *J. Chem. Educ.* **1992**, 69, 615. (b) An, H.; Bradshaw, J. S.; Izatt, R. M., *Chem. Rev.* **1992**, 92, 543-572.



Scheme 5.1 Synthesis of unsaturated ester macrocycles through dimerization of oxonium ylide (PG = Ms, carbamate, COCF₃, trityl).

5.2 Synthesis of aza-crown ethers

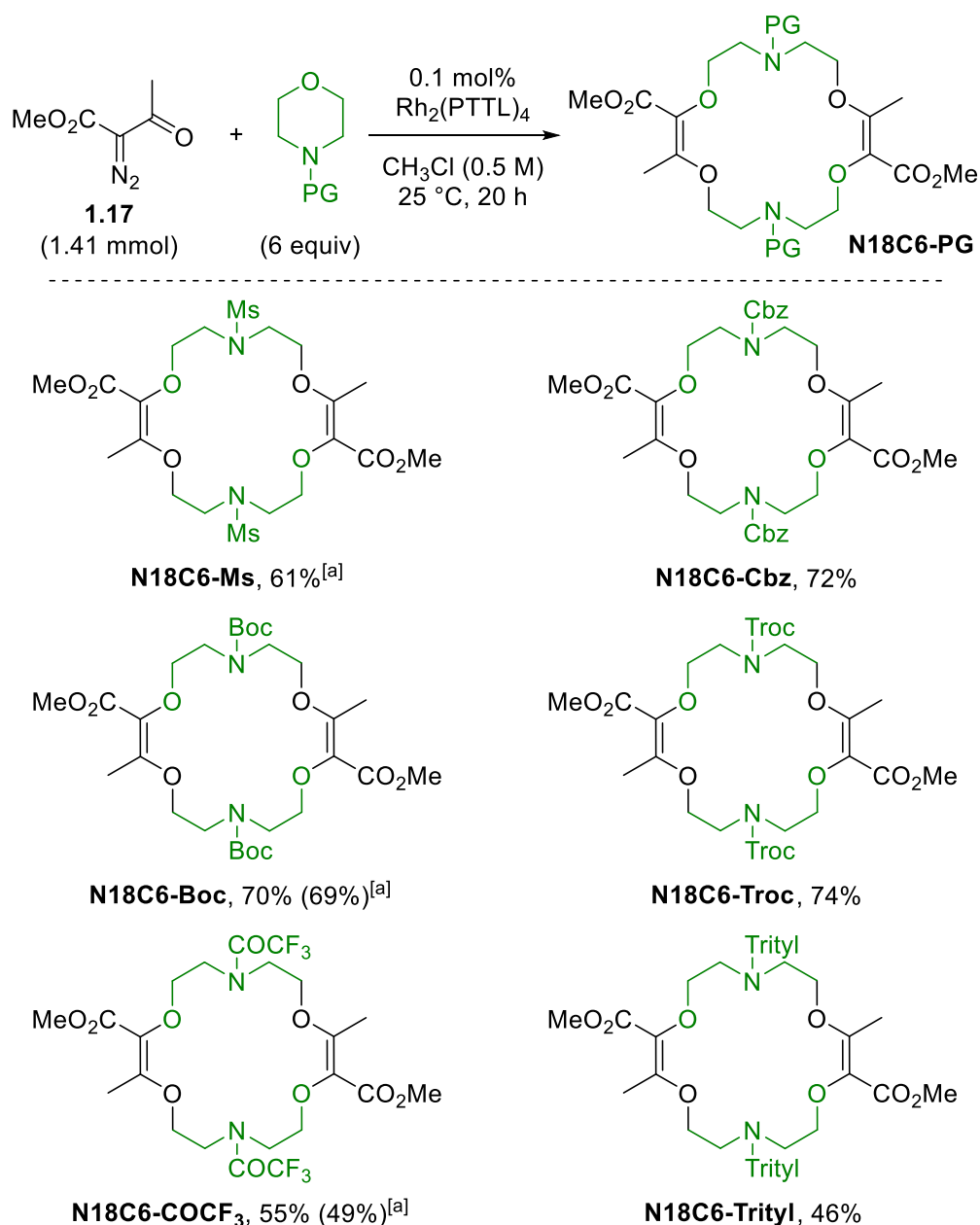
5.2.1 Synthesis of unsaturated ester building blocks¹⁸⁷

As first mentioned, the synthesis of unsaturated aza-macrocycles by [3+6+3+6] condensation of morpholine units and α -diazo- β -ketoesters **1.17** under rhodium(II) catalysis was considered. In the case of N-containing cyclic ethers, due to the higher nucleophilicity of the nitrogen atom, a competition between the formation of oxonium ylides and nitrogen ylides occurs – generally in favor of the later.¹⁸⁸ To overcome this synthetic problem, the introduction of protecting groups on the nitrogen atoms was considered. However, it was shown that the introduction of electrowithdrawing or sterically hindered moieties has a global influence on the nucleophilicity of the oxygen atom. Such morpholines do not react with metal carbenes with the same rate than 1,4-dioxane, THP or THF. A competitive Wolf rearrangement of the metal carbene occurs instead

¹⁸⁷ This work was performed by Daniele Poggiali during his PhD. See reference 70.

¹⁸⁸ (a) Yun Sang, H.; Xia, L.; Kim Sung, H.; Lee Yong, R., *Asian J. Org. Chem.* **2016**, 5, 1142-1147. (b) Vanecko, J. A.; West, F. G., *Org. Lett.* **2005**, 7, 2949-2952. (c) Zhou, C.-Y.; Yu, W.-Y.; Chan, P. W. H.; Che, C.-M., *J. Org. Chem.* **2004**, 69, 7072-7082. (d) Molchanov, A. P.; Stepanov, A. V.; Kopf, J.; Zenkevich, I. G.; Kostikov, R. R., *Russ. Chem. Bull.* **2001**, 50, 2144-2148. (e) Padwa, A.; Dean, D. C.; Osterhout, M. H.; Precado, L.; Semones, M. A., *J. Org. Chem.* **1994**, 59, 5347-5357.

that is detrimental to the macrocycle synthesis. Daniele Poggiali found that a lower catalyst loading (0.1 mol%) favors the O-ylide formation and hence, following the same dimerization mechanism, diaza-macrocycles of type **N18C6-PG** were satisfactorily afforded in moderate to good yields (**Scheme 5.2**).

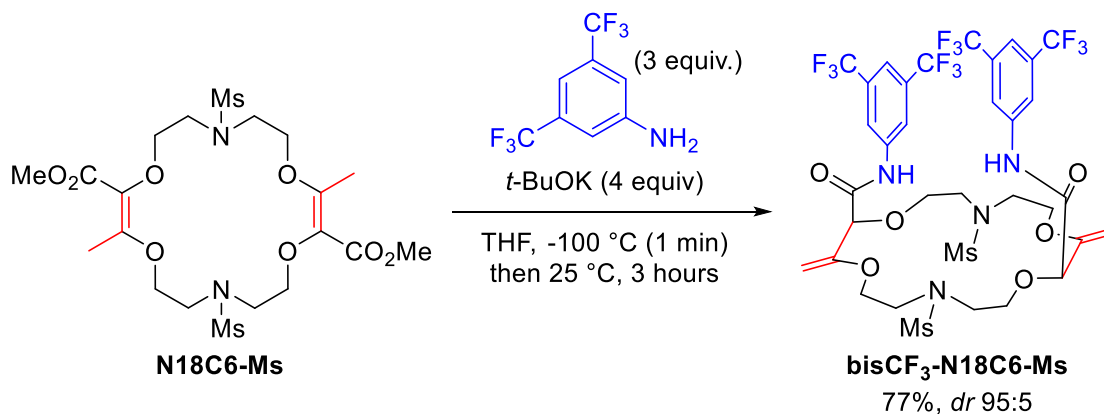


Scheme 5.2 Synthesis of aza-macrocycles ([a] 7 mmol scale, 1.0 g of α -diazo- β -ketoester **1.17**).

5.2.2 Amidation/transposition of aza macrocycles

5.2.2.1 Transformation with N18C6-Ms macrocycle

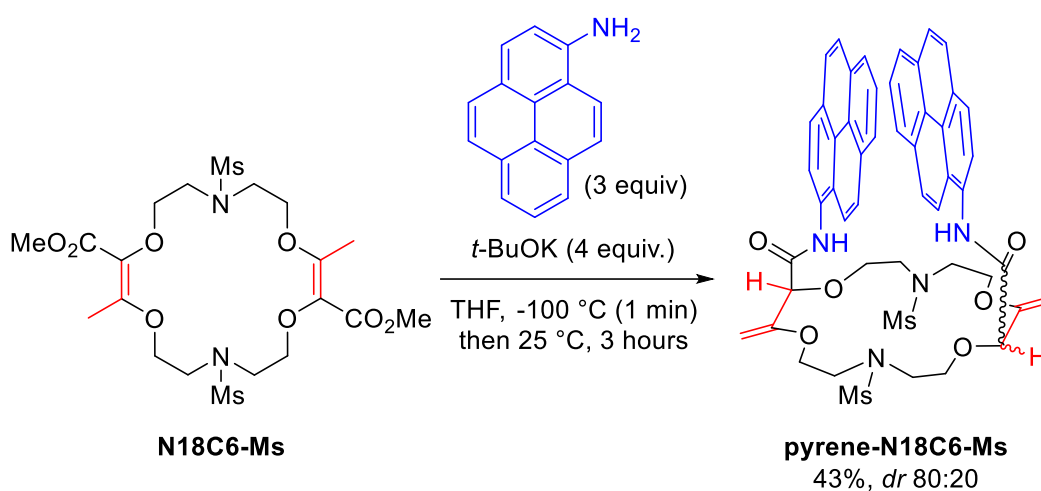
The study of the amidation – transposition process was started with **N18C6-Ms** macrocycle and 3,5-bis(trifluoromethyl) aniline as model reagent. The ester building block was thus treated with three equivalents of anilines and four equivalents of *t*-BuOK in THF and, to our satisfaction, **bisCF₃-N18C6-Ms** crown ether was obtained in 77% yield (**Scheme 5.3**). The high diastereoselectivity (*dr* > 49:1) usually observed in the case of fully oxygenated macrocycles (section 1.5.4) could not be confirmed in this example. Indeed, the ¹H NMR spectroscopic analysis revealed the presence of a second minor product in a 95:5 ratio, attributed possibly to the *meso* diastereoisomer. Reliable information could not be extracted from the ¹H and ¹³C NMR spectra to demonstrate the presence of a second diastereoisomer; the signals being too weak to be analyzed properly. The exact nature of the minor product was thus not ascertained and it was impossible to separate by chromatography this impurity from the major component.



Scheme 5.3 Synthesis of **bisCF₃-N18C6-Ms** macrocycle.

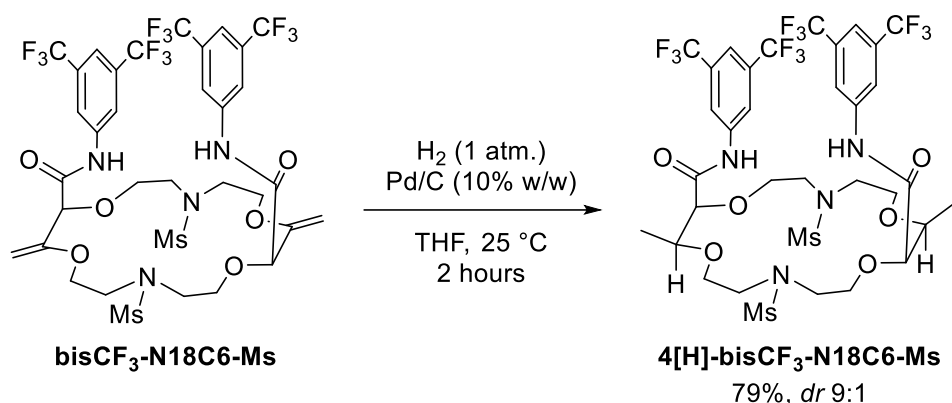
After this first result, the use of the other aromatic amines was considered next. Treatment of **N18C6-Ms** with 1-aminopyrene under the standard amidation conditions yielded **pyrene-N18C6-Ms** macrocycle in moderate yield (43%, **Scheme 5.4**). In this case, however, the presence of a second product was clear, in both ¹H and ¹³C NMR spectroscopies. Specifically, in the later case, all signals were split (*dr* 80:20) and could be attributed to the *meso* diastereoisomer. The presence of nitrogen atoms seems to have a strong influence on the diastereoselectivity of the

transformation. The proposed remote induction by the potassium ion template may not occur efficiently in these cases (see section 1.5.4). The nitrogen atoms probably changed enough the conformation of the ring to disfavor the long range stereochemical interaction required for a totally efficient remote diastereoselective transformation. The reaction was also tested with two other aromatic amines namely 3,5-dimethyl aniline or *para*-iodo-aniline. However, in these two cases, despite the full conversion of **N18C6-Ms** substrate, no corresponding products could be isolated after the reaction. It seems that the transformation is limited to a small number of aromatic amines.



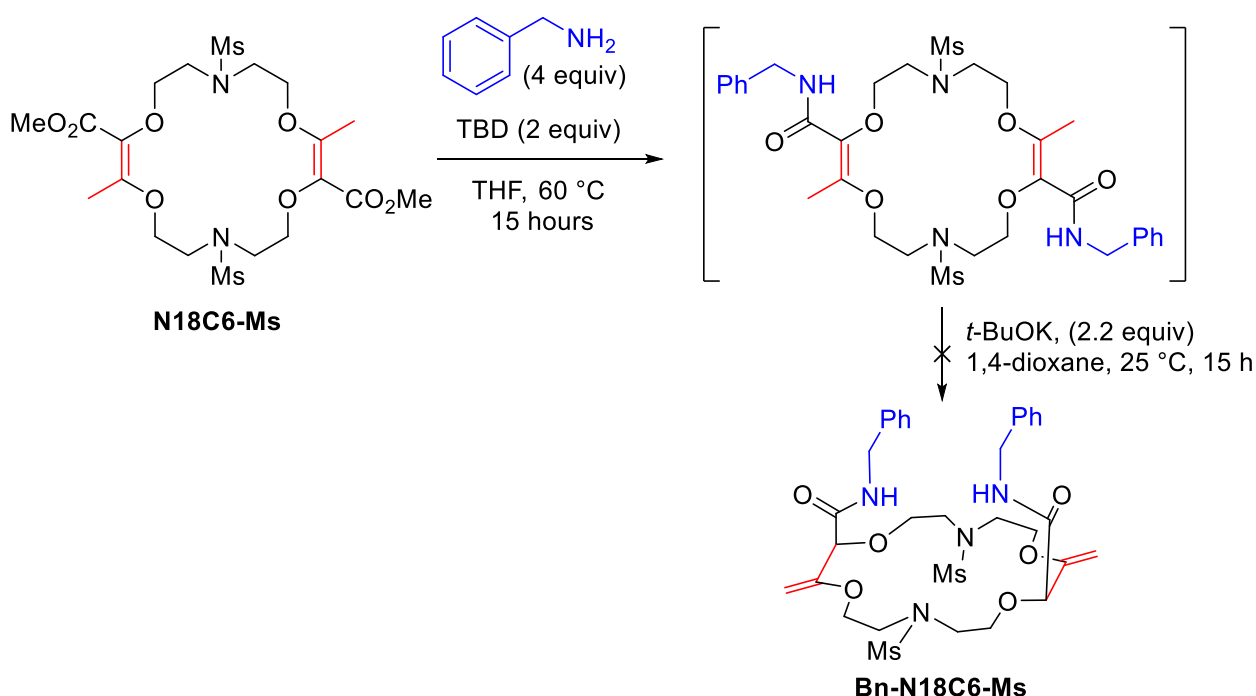
Scheme 5.4 Synthesis of **pyrene-N18C6-Ms** macrocycle.

The hydrogenation of **bisCF₃-N18C6-Ms** macrocycle was then attempted (**Scheme 5.6**): mild heterogeneous hydrogenation conditions (10% w/w, Pd/C (10% Pd, unreduced), 1 atm H₂, 25 °C) were sufficient to afford the corresponding crown ether **4[H]-bisCF₃-N18C6-Ms** in 79% yield as a 9:1 diastereomeric ratio after filtration and precipitation. The configuration of the major diastereoisomer could not be attributed unambiguously but the all-*cis* product is assumed to be the major diastereoisomer; the hydrogenation occurring most probably on the least hindered face, the one not occupied by aromatic amides.



Scheme 5.6 Synthesis of **4[H]-bisCF₃-N18C6-Ms** by hydrogenation.

We also investigated the introduction of aliphatic amines. Using **N18C6-Ms** and benzyl amine as model substrate and reagent, the aminolysis mediated by TBD was tested using conditions developed in section 2.2.1.1 (**Scheme 5.5**). The corresponding unsaturated bis-amide product was obtained after precipitation from the crude reaction mixture. Unfortunately, any attempts to transpose the olefins in basic medium failed and no conversion of the intermediate product could be observed. The insolubility of the bis-conjugated amide intermediate is thought to be the reason of the lack of reactivity.

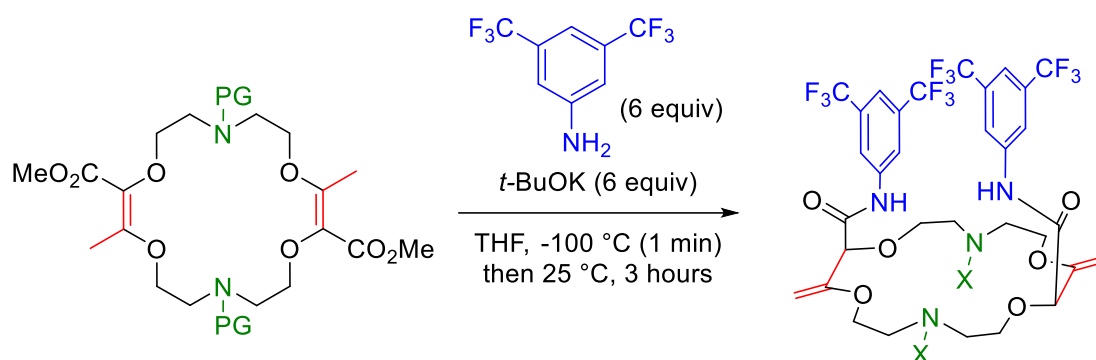


Scheme 5.5 Synthesis of **Bn-N18C6-Ms** from **N18C6-Ms**.

5.2.2.2 Transformation with other N18C6-PG macrocycles

The transformation was then envisaged with other unsaturated macrocycle building blocks. **N18C6-Boc** and **N18C6-Cbz** macrocycles were treated with 3,5-bistrifluoromethyl aniline (3 equiv) and *t*-BuOK (4 equiv) but, unfortunately, only very low conversions of the starting materials were observed and the formation of **bisCF₃-N18C6-Boc** or **bisCF₃-N18C6-Cbz** was not observed (**Table 5.1**, entries 1-2). The same result was obtained when the amounts of aniline and base were increased to six equivalents each. In fact, by mass spectrometry (ESI-MS), an intense signal corresponding to the potassium adduct of the starting macrocycles [**N18C6-Boc**] and [**N18C6-Cbz**] was detected. It is possible that the Boc and Cbz carbamate units enhance the affinity of such macrocycles for potassium ions preventing the aminolysis by quenching the overall reactivity.

Table 5.1 Synthesis of **bisCF₃-N18C6** macrocycles.

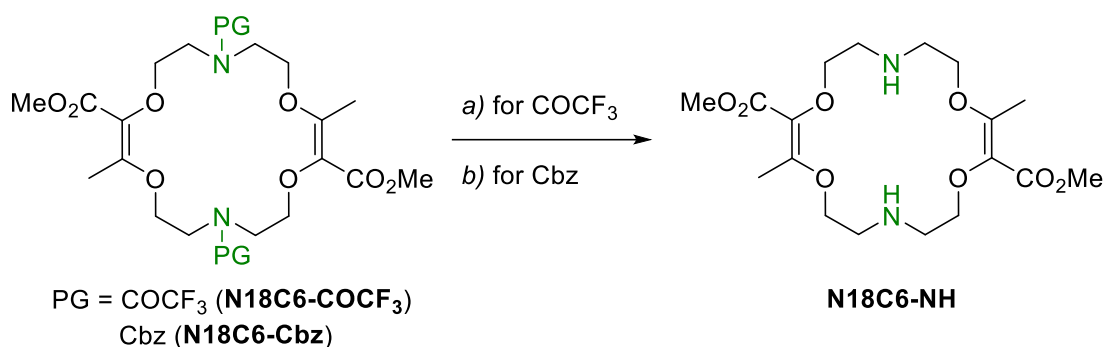


Entry	PG	S.M.	X	product	result
1	Boc	N18C6-Boc	Boc	bisCF₃-N18C6-Boc	no conversion
2	Cbz	N18C6-Cbz	Cbz	bisCF₃-N18C6-Cbz	no conversion
3	COCF ₃	N18C6-COCF₃	NH	bisCF₃-N18C6-NH	full conversion

Interestingly, for the same transformation, starting from **N18C6-COCF₃** substrate, full conversion of the macrocycle was observed instead.¹⁸⁹ Mass spectrometry however revealed the formation of **bisCF₃-N18C6-NH** crown ether with two free N-H amines in the final product. In fact,

¹⁸⁹ In this case, 6 equivalents of aniline and base were necessary to ensure a complete conversion.

in addition to the tandem amidation – transposition process, a concomitant deprotection of the trifluoroacetamide groups occurs due to the strongly basic conditions (**Table 5.1**, entry 3). Isolation was nevertheless an issue as the high polarity of the product rendered any attempts of purification by chromatography over silica gel complicated. At that stage, it was decided to further modify the structure of the starting macrocycles and introduce N-alkyl on the nitrogen atom instead of carbamate or amide groups. The synthesis of N-H containing conjugated esters **N18C6-NH**, already developed by Daniele Poggiali during his PhD, was used.⁷⁰ In fact, trifluoroacetamide deprotection of **N18C6-COCF₃** is achieved by addition of an excess of NaBH₄ leading to **N18C6-NH** in 92% yield. Similarly, the benzyl carbamate group of **N18C6-Cbz** is removed by hydrogenolysis in 94% yield without reduction of the double bonds present within the structure (**Scheme 5.7**).

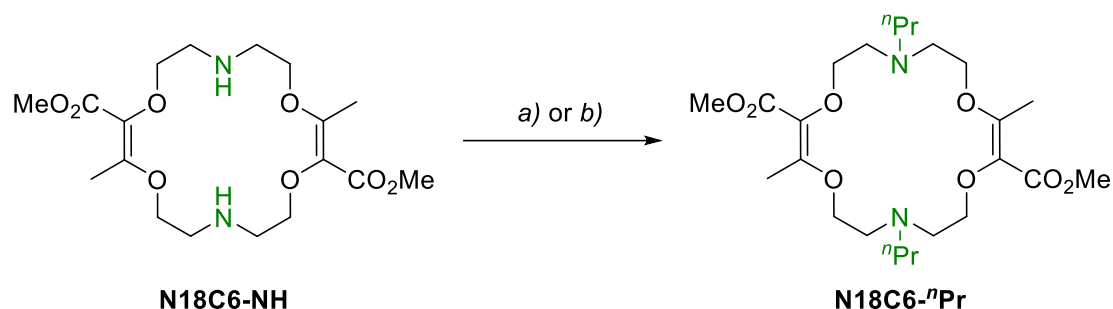


Scheme 5.7 Removal of N-protecting groups by reduction or hydrogenolysis. Conditions: a) NaBH₄ (5 equiv), CH₂Cl₂/MeOH (1:1), 25 °C, 1 hour, 92%; b) H₂ (1 atm.), 10% w/w Pd/C (10%, unreduced), CH₂Cl₂/MeOH (1:1), 25 °C, 2 hours, 94%.

Two approaches were considered to access **N18C6-ⁿPr** from **N18C6-NH** by either direct alkylation with propyl halide or by reductive amination with propanal as reagent (**Scheme 5.8**).¹⁹⁰ Treating **N18C6-NH** with *n*-propyl bromide (3 equiv) and potassium carbonate (10 equiv) for 15 hours in acetonitrile at 80 °C afforded the desired unsaturated macrocycle **N18C6-ⁿPr** in 70% yield. Unsurprisingly, the analysis of the crude mixture by mass spectrometry (ESI-MS) revealed in addition the presence of by-products originating from the mono- and tris-alkylation of *n*-propyl bromide on the macrocyclic nitrogen. The reductive amination was then considered. The premixing of **N18C6-NH** with propanal followed by *in-situ* reduction with sodium triacetoxyborohydride afforded the corresponding macrocycle in 74% yield after two hours. To

¹⁹⁰ Abdel-Magid, A. F.; Mehrman, S. J., *Org. Process Res. Dev.* **2006**, *10*, 971-1031.

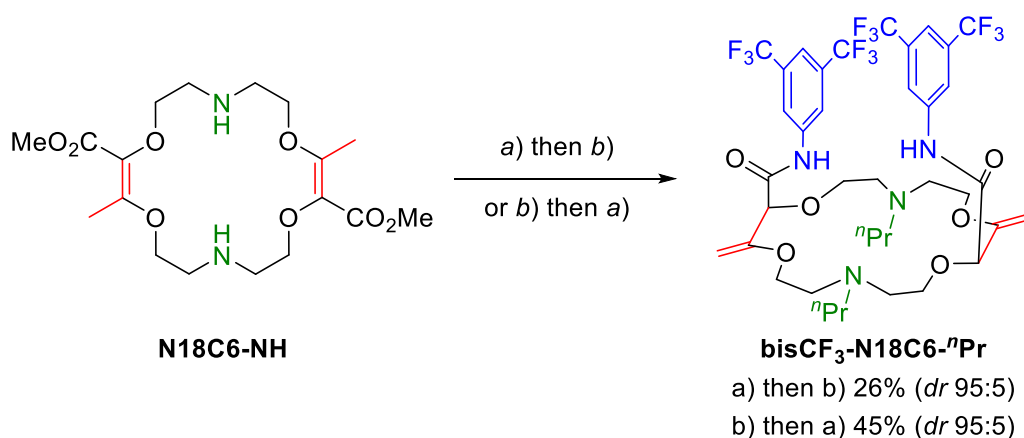
our satisfaction, this time, no traces of mono- or tri-addition by-products were observed in the crude mixture (ESI-MS).



Scheme 5.8 Synthesis of **N18C6-ⁿPr**. Conditions: *a*) propyl bromide (3 equiv), K₂CO₃ (10 equiv), CH₃CN, 80 °C, 15 hours, 70%; *b*) propanal (4 equiv), NaBH(OAc)₃ (6 equiv), 1,2-dichloroethane, 25 °C, 2 hours, 74%.

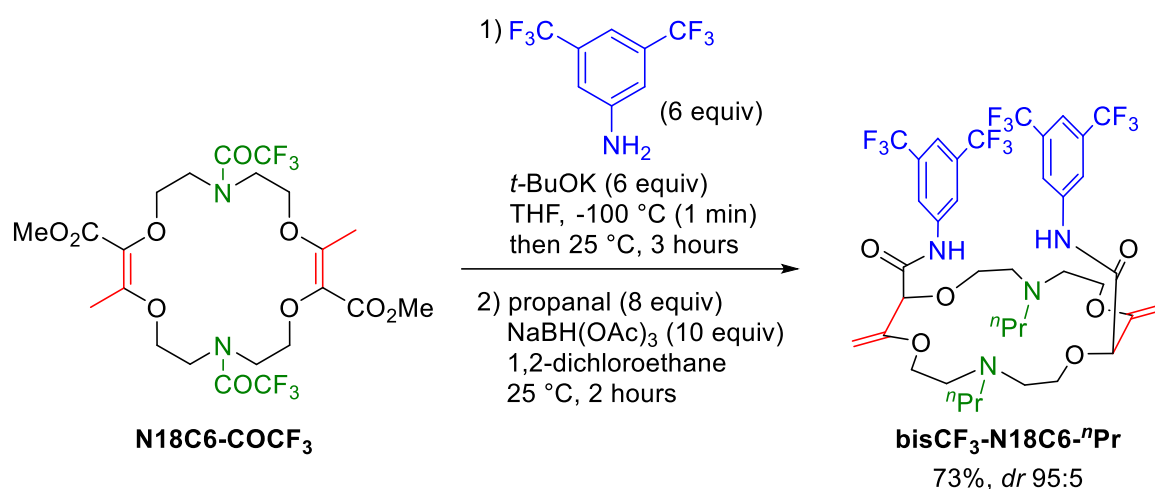
With **N18C6-ⁿPr** unsaturated macrocycle in hand, the amidation – transposition process was tested next. Using standard conditions (aniline, 3 equivalents and *t*-BuOK, 4 equivalents) **bisCF₃-N18C6-ⁿPr** crown ether was afforded in 35% yield (26% yield over two steps, **Scheme 5.9**). As for **bisCF₃-N18C6-Ms**, a minor product was obtained. Based on the previous results, it is assumed that the second product is always the *meso* compound (*dr* 95:5). This example shows again the influence of the nitrogen atoms on the conformation of the molecule and on the diastereoselectivity of the reaction.

Alternatively, it was decided to use **N18C6-NH** as substrate directly and, after the double aniline addition, submit the crude product to the reductive amidation protocol. Following this strategy, **bisCF₃-N18C6-ⁿPr** was afforded after two steps in 45% yield (*dr* 95:5, **Scheme 5.9**).



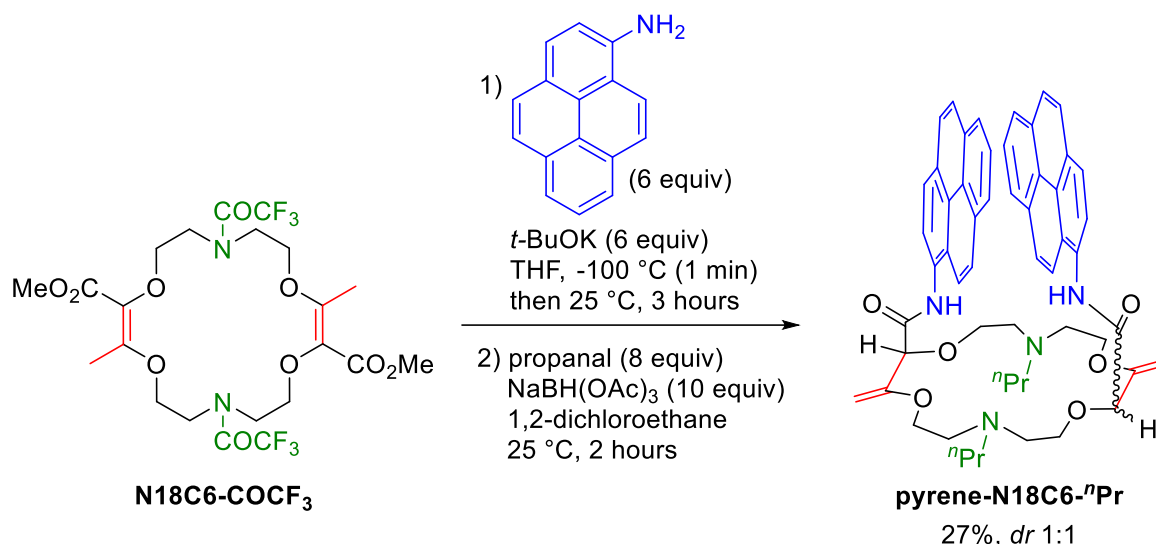
Scheme 5.9 Synthesis of **bisCF₃-N18C6-ⁿPr** from **N18C6-NH**. Conditions: *a*) propanal (4 equiv), NaBH(OAc)₃ (6 equiv), 1,2-dichloroethane, 25 °C, 2 hours; *b*) 3,5-bis(trifluoromethyl) aniline (3 equiv) and *t*-BuOK (4 equiv), THF, -100 °C (1 min) then 25 °C, 3 hours.

A third synthetic strategy was possible. It had been shown that the strongly basic conditions of the crown ether synthesis led to the deprotection of trifluoroacetamide groups. Thus the formation of **bisCF₃-N18C6-ⁿPr** could be attempted directly from the **N18C6-COCF₃** precursor by a consecutive tandem amidation – transposition – deprotection – reductive amination protocol. To our satisfaction, **bisCF₃-N18C6-ⁿPr** crown ether was obtained in 73% (*dr* 95:5) yield after the four transformations (**Scheme 5.10**). From the three approaches considered for the formation of **bisCF₃-N18C6-ⁿPr**, all of them yielded the compound with the same diastereomeric ratio (*dr* 95:5) but the best yield was afforded with the latest conditions.



Scheme 5.10 Synthesis of **bisCF₃-N18C6-ⁿPr** from **N18C6-COCF₃**.

With these conditions in hand, the use of another aromatic amine was then considered. Unfortunately, changing 3,5-bis(trifluoromethyl) aniline for 1-aminopyrene led to the formation of **pyrene-N18C6-ⁿPr** in only low yield (27%) as a 1:1 mixture of diastereoisomers (**Scheme 5.11**). The limitations in substrate scope observed with the mesyl substituted macrocycle appears also in this case and other anilines were thus not tested.



Scheme 5.11 Synthesis of **pyrene-N18C6-ⁿPr** from **N18C6-COCF₃**.

We also investigated the introduction of different functional groups on the nitrogen atoms. It was envisaged that the addition of methylpyridine or methylquinoline units would be interesting as their introduction would add additional binding sites for interaction with metal ions in particular. In fact, such nitrogen containing aromatic units can be found in aza-macrocyclic ligand used for the formation of lanthanide(III) complexes (**Figure 5.1**). Such assemblies can form chiral complexes and find application as probe in circularly polarized luminescence.^{162c, 191}

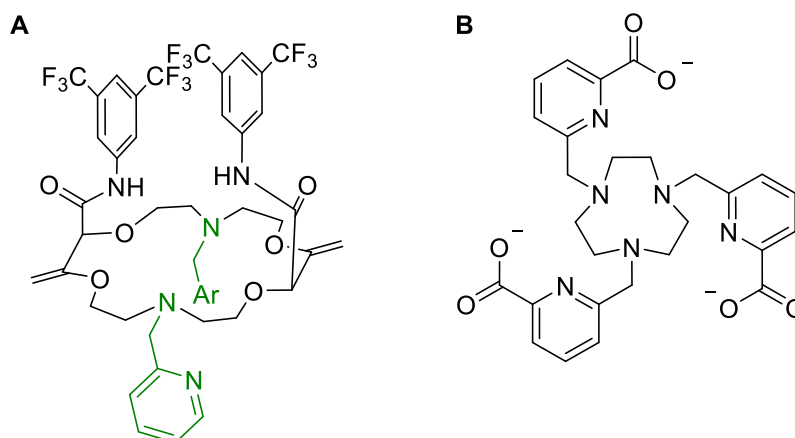
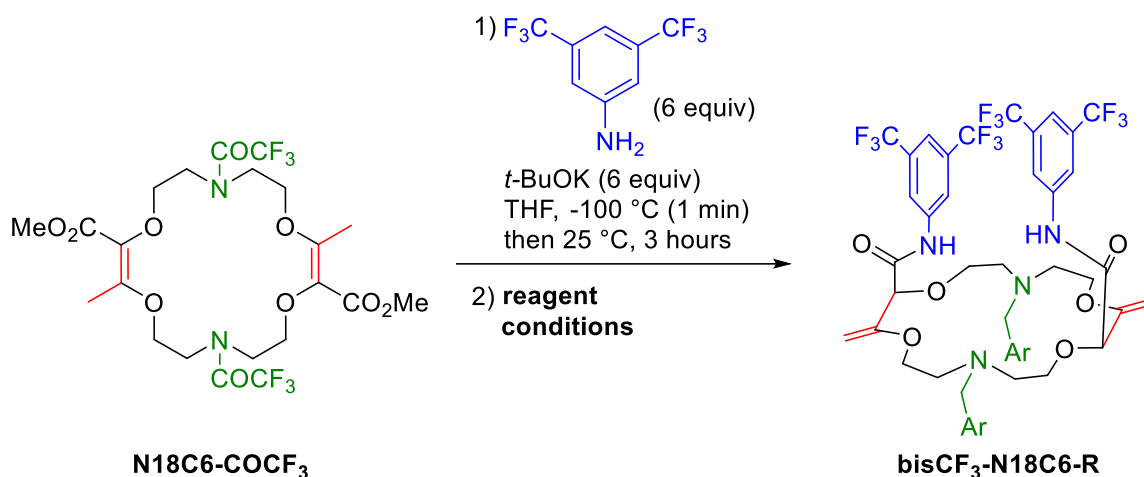
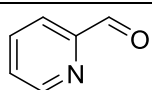
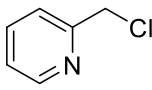
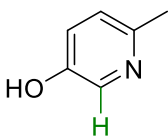
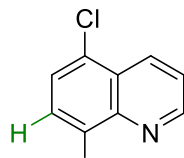


Figure 5.1 Targeted crown ethers (**A**) and representative structure of a macrocyclic ligand for lanthanide(III) complexes (**B**).

¹⁹¹ Zinna, F.; Di Bari, L., *Chirality* **2014**, 27, 1-13.

Table 5.2 Synthesis of **bisCF₃-N18C6-R** macrocycles.

Entry	Reagent	Conditions ^[a]	Result
1		A	<35% ^[b]
2		B	observed by ESI-MS
3	 + formaldehyde	C	observed by ESI-MS
4	 + paraformaldehyde	D	observed by ESI-MS

[a] Conditions A: aldehyde (10 equiv), NaBH(OAc)₃ (15 equiv), 1,2-dichloroethane, 25 °C, 15 hours; B: chloride (3.5 equiv), Na₂CO₃ (10 equiv), CH₃CN, 80 °C, 15 hours; C: pyridine (10 equiv), formaldehyde (37%, 10 equiv), EtOH, 80 °C 15 hours; D: quinoline (10 equiv), paraformaldehyde (10 equiv), toluene, 80 °C, 15 hours; [b] degradation of the product during purification.

Keeping the procedure for the synthesis of **bisCF₃-N18C6-NH** intermediate from **N18C6-COCF₃**, different conditions of functionalization of the nitrogen atoms were considered. First, reductive amination with 2-pyridinecarboxaldehyde was attempted (**Table 5.2**, entry 1). The formation of the expected product was observed by ESI-MS monitoring but, unfortunately, degradation of the product occurred during the purification by chromatography over silica gel or

alumina. An alkylation protocol was selected next with 2-(chloromethyl)pyridine (entry 2).¹⁹² Similarly, the expected product was observed by ESI-MS monitoring but the purification of the product failed again. The formation of the targeted derivatives was also attempted using a Mannich reaction with (para)formaldehyde and phenols (entries 3-4).¹⁹²⁻¹⁹³ However, despite the observation of the expected products by ESI-MS monitoring, degradation of the product during the purification phase occurred again. These results demonstrate that the introduction of nitrogen containing aromatic units on this particular crown ether scaffold is a challenging task. More investigations should be conducted to effectively introduce valuable substituents for further applications.

5.3 Conclusion

The transformation of unsaturated diaza-polyether macrocycles into chiral diaza-crown ethers was presented in this chapter. Applying the tandem amidation – transposition protocol developed in the group, some of the diaza building blocks were successfully transformed into chiral structures. Unfortunately, the amidation step was limited to 3,5-bistrifluoromethyl aniline reagent – other aromatic amines leading to disappointing results or no result at all.

Various protecting groups can be used on the N-atoms. It was found that trifluoroacetamide groups are cleaved during the reaction and that the free N-H group could be further functionalized by reductive amination in particular.

The aminolysis protocol in presence of benzyl amine was also demonstrated, but the olefin transposition step remains unachieved yet. More investigations on that transformation should be conducted in the future to possibly access new structures and hence applications. Despite the limitation revealed in this chapter, these preliminary results indicate that the access to chiral diaza-crown ethers is possible using the methodologies developed in Geneva.

¹⁹² Song, H.-C.; Bradshaw, J. S.; Chen, Y.-W.; Xue, G.-P.; Li, W.-M.; Krakowiak, K. E.; Savage, P. B.; Xu, Z.-L.; Izatt, R. M., *Supramol. Sci.* **2002**, *14*, 263-269.

¹⁹³ Jia, X.; Zhu, W.; Zhang, Y.; Yan, X., *J. Mol. Struct.* **2002**, *604*, 159-164.

6 Conclusions and Perspectives

6.1 Conclusion

In 2010, a [3+X+3+X] rhodium(II)-catalyzed condensation of α -diazo- β -ketoesters with cyclic ethers (1,4-dioxane, THP, THF) was developed to afford unsaturated polyether macrocycles in a single step.⁶⁹ Later, a tandem amidation – olefin transposition protocol allowed the transformation of such building blocks into chiral crown ethers by treatment with aromatic amines under strongly basic conditions – in a single step again.^{3b} The aim of this PhD was to extend these transformations to a larger variety of substrates and substituents in order to access multiple and novel applications.

Despite the large variety of amines tolerated, aliphatic amines remained elusive at the start of this PhD including chiral amines with side chains possessing stereogenic centers. To achieve this goal, an approach was developed by preformation of the amides mediated by TBD (1,5,7-triazabicyclo[4.4.0]dec-5-ene). A subsequent transposition of the olefins in basic conditions affords then the expected chiral crown ether with aliphatic chains on the nitrogen atoms. Such macrocycles made from enantiopure chiral amines were applied efficiently in asymmetric phase transfer catalysis for the synthesis of protected amino acids (up to 45% *ee*). A matched – mismatched situation was evidenced using the two isolated diastereomerically pure **(S)-Me-1-naphth-18C6** derivatives. The next step will be to design more elaborated catalysts to extend the scope of possible transformations.

Following a late-stage functionalization strategy of the chiral crown ethers, a series of heteroditopic cryptand receptors were also synthesized in a few steps only. Their binding properties towards cations, various anions and combinations of both were studied in solution and solid state by means of ¹H NMR spectroscopy and X-ray diffraction analysis respectively. The cryptands presented a general ion pair binding capacity towards salts of monovalent cations (Na⁺,

K⁺) and linear triatomic anions (N₃⁻, NCO⁻, SCN⁻) or trigonal oxyanion (NO₃⁻) in particular. The salts cooperatively bind within the polyamide-crown ether conjugates as contact ion pairs.⁸²

A series of polyether macrocycles substituted with fluorescent units were synthesized. It was our purpose to take advantage of the constrained structure of the derivatives to bring the two fluorophores in spatial proximity. In this conformation, those systems exhibit intense excimer fluorescence in different spectral regions depending on the chromophore (λ_{em} 300 to 650 nm). The enantiomers of the derivatives were separated by CSP-HPLC and studied by ECD and CPL spectroscopies. In CPL, high g_{lum} values (up to 10⁻²) associated with the excimer fluorescence were measured. Upon addition of monovalent sodium or divalent barium ions, important conformational changes of the macrocycles occurred and induced sign inversions of ECD and a quench of the CPL signals. The original signals can be reversibly recovered by addition of a cation scavenger (regular 18-Crown-6) giving rise to a rare example of allied +/- ECD and on/off CPL switches.⁸³

Finally, the extension of the amidation – transposition protocol to nitrogen-containing macrocycles was presented. Using 3,5-bistrifluoromethyl aniline, chiral diaza-crown ethers can be obtained in moderate to good yield with various substituents on the nitrogen atoms. However, the transformation seemed to be limited in term of possible aromatic amines.

6.2 Perspectives

During this PhD, it was shown that the rearranged chiral crown ethers could be versatile platforms for the development of applications in a rather large variety of domains. Further development can be foreseen. For instance, the stereoselective recognition and extraction (solid/liquid or liquid/liquid) of chiral ammonium salts could be explored. Chiral amines or amino acids in their acidic or zwitterionic form could be recognized by the macrocycles and studied using methods such as ¹H NMR or ECD spectroscopy under certain conditions.^{37d, 38b, 40f, 44-45, 45g, h, 50a} The use of crown ethers bearing enantiopure aliphatic substituents such as **(S)-Me-Bn-18C6** are potentially good candidates. Strong conformational changes are expected upon recognition: the response of such host towards chiral ammonium could be very different as function of the enantiomers and could be monitored by ECD spectroscopy. Some preliminary results were

already attempted by ^1H NMR spectroscopy. Crown ether **(S)-Me-Bn-18C6** (*dr* 1.3:1) was mixed with various amounts of ammonium chloride salt **6.1** in CDCl_3 . The methyl proton signals of the host and guest were monitored (**Figure 6.1**). The signals of the methyl protons of **(S)-Me-Bn-18C6** diastereoisomer was modified from an apparent triplet (partially overlapped doublets) to two separated yet close doublets ($\Delta\delta = 0.014$ ppm, upon addition of 1.0 equivalents of **6.1**) indicating the existence of diastereomeric interactions between the components.

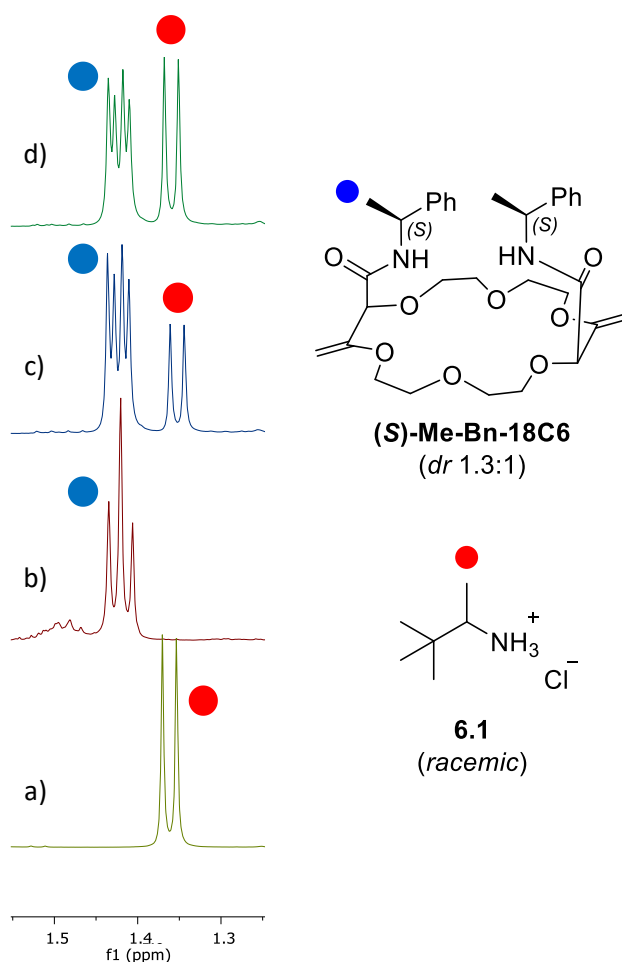


Figure 6.1 ^1H NMR spectra (400 MHz), selected window (δ 1.55–1.35 ppm), CDCl_3 , 298 K, c_H 12 mM: a) ammonium **6.1**; b) **(S)-Me-Bn-18C6**; c) **(S)-Me-Bn-18C6** + **6.1** (0.5 equiv); d) **(S)-Me-Bn-18C6** + **6.1** (1 equiv).

In the case of the heteroditopic cryptands, only sodium and potassium salts were tested. It could be interesting to perform experiments with other cations as the study conducted in the chapter 4 indicated that divalent cations (Ba^{2+} notably) exhibit very good affinity towards the macrocycles. The cryptands showed preferences for linear (N_3^- , NCO^- , SCN^-) and planar (NO_3^-) anions as the four N-H bonds of the amide functions are well oriented for the efficient binding of

such guest (**Figure 6.2A**). The nitrite anion was already mentioned as a valuable anion that could be studied. However, the binding of neutral linear or bent triatomic gases has not been considered so far. In fact, by analogy with the azide anion, carbon dioxide (linear), nitrogen dioxide or sulfur dioxide (bent) could be complexed in a similar manner inside the cavity of the receptor (**Figure 6.2B**). Such toxic gases could benefit from an efficient recognition and be extracted with potential environmental applications.

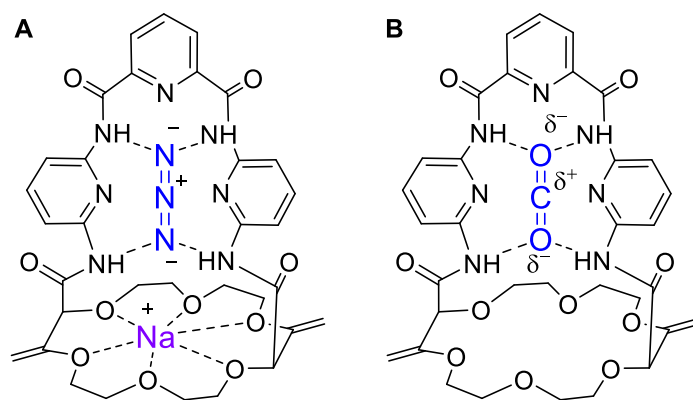
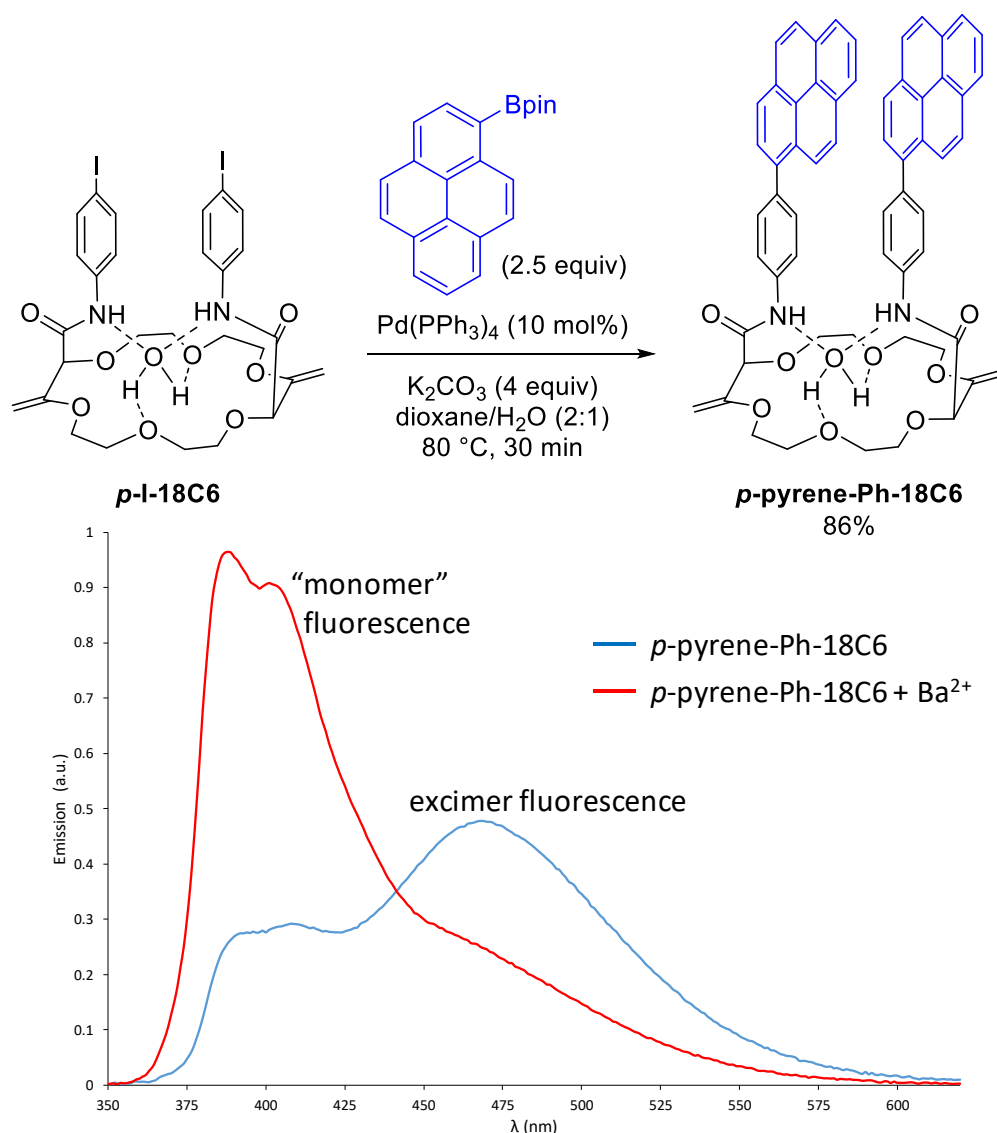


Figure 6.2 [pyr-cryptand·NaN₃] complex (**A**) and possible binding mode of CO₂ within the cryptands (**B**).

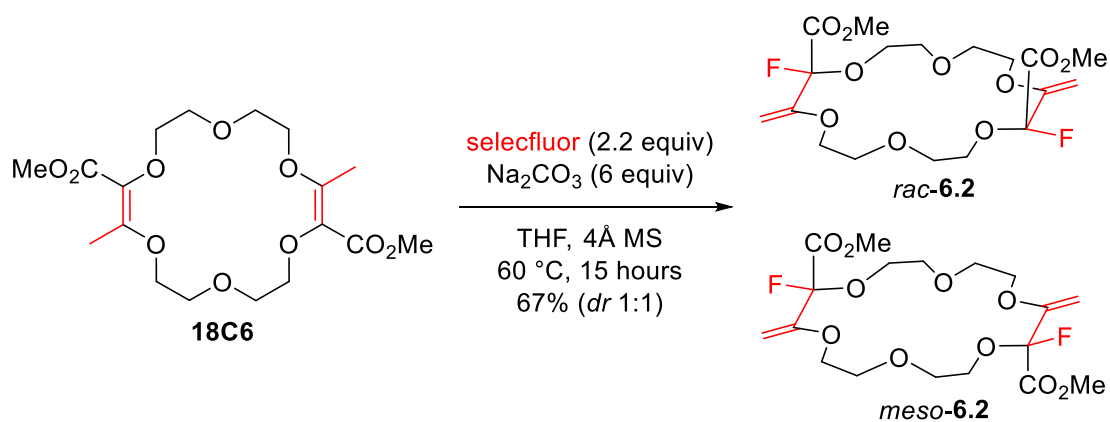
In the study of the chiroptical properties of fluorescent macrocycles, the important CPL signal (g_{lum} up to 10^{-2}) was associated with the presence of an intense excimer fluorescence. One should take advantage of the favorable conformation of the chiral macrocycles to study more precisely the possibility of excimer fluorescence of various fluorophores. One possibility is to introduce new chromophore units to extend the spectral regions accessible in absorption and fluorescence. But the need to access the chromophores as amino substituted derivatives is a synthetic limitation. A strategy that would utilize general building blocks easily functionalized by cross-coupling chemistry would be favorable. For instance, the synthesis of ***p*-pyrene-Ph-18C6** by Pd-catalyzed Suzuki-Miyaura cross-coupling of 1-pyrene boronic ester with ***p*-I-18C6** was achieved in high yield (86%, **Scheme 6.1**, top). Satisfactorily, the macrocycle exhibits an excimer fluorescence with a maximum centered at 468 nm which is almost completely quenched upon addition of barium ion (**Scheme 6.1**, bottom). This preliminary result indicates the possibility to use this and other iodoaryl substituted macrocycles for cross coupling reactions and thus extend the variety of fluorophores accessible as boronic acids or esters. Other reactions could also be envisaged such as Sonogashira, Heck or Buchwald-Hartwig couplings to yield functionalized alkynes, alkenes or amines respectively.



Scheme 6.1 Synthesis by Pd-catalyzed Suzuki-Miyaura cross coupling of *p*-pyrene-Ph-18C6 (top) and normalized fluorescence spectra of *p*-pyrene-Ph-18C6 (CH₃CN, *c* 10⁻⁵ M) without (blue) and with (red) Ba(ClO₄)₂ (bottom).

Finally, with most unsaturated macrocyclic precursors, the subsequent tandem amidation – transposition process occurs with a very high diastereoselectivity (*dr* > 49:1) in favor of the chiral (racemic) diastereoisomer. While this stereoselectivity is generally seen as an advantage, the geometry associated with the achiral (*meso*) derivatives could be beneficial for other type of applications. In that regard, it was found that, a treatment of **18C6** with an electrophilic source of fluorine (selectfluor®) leads to a tandem electrophilic fluorination – olefin transposition to afford derivative **6.2** in good yield (67%) and as a 1:1 (*rac/meso*) mixture of diastereoisomers. These compounds could be further separated by column chromatography (**Scheme 6.2**). The next

step will be to study aminolysis protocols to afford analogues of the polyethers presented in this thesis and to measure the difference in reactivity and behavior of the diastereoisomers.



Scheme 6.2 Synthesis of *rac*-6.2 and *meso*-6.2 (1:1) by a tandem fluorination – transposition protocol.

7 Experimental Part

7.1 General information and Materials

All reactions involving air sensitive compounds were carried out under N₂ or argon by means of an inert gas/vacuum double manifold line and standard Schlenk techniques using dry solvents. Reactions involving oxygen sensitive reagents were performed using degassed solvents. Unless otherwise stated, all reagents were purchased from commercial sources and used without further purification. Dioxane, THF and THP were dried by distillation over Na/benzophenone. Dry CH₂Cl₂, THF, NEt₃ and toluene were obtained by filtration through appropriate activated-alumina drying columns. *t*-BuOK was sublimed prior to use. Propoanal and 2-pyridinecarboxaldehyde were distilled prior to use.

Analytical thin-layer chromatographies (TLC) were performed with Silicagel 60 F₂₅₄ aluminium sheets from Merck. Flash column chromatographies were performed with Silica SiliaFlash P60, 40-63 µm (230-400 mesh) and Aluminium oxide (neutral, Brockmann I, 50-200 µm, 60 Å).

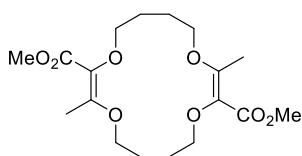
NMR spectra were recorded on a Bruker AVANCE I 300 MHz spectrometer, equipped with a 5 mm QNP D133 probe, a Bruker AVANCE III HD-*NanoBay* 300 MHz spectrometer, equipped with a 5 mm BB(F)-H-D probe, on a Bruker AVANCE III HD-*NanoBay* 400 MHz spectrometer, equipped with a 5 mm CryoProbe Prodigy, or on a Bruker II 500 MHz spectrometer, equipped with a 5 mm Cryogenic DCH (¹H/¹³C) probe. ¹H NMR chemical shifts are given in ppm relative to Me₄Si using solvent resonances as internal standards (CDCl₃ δ = 7.26 ppm, DMSO-*d*₆ δ = 2.50 ppm, CD₂Cl₂ δ = 5.32 ppm). Data were reported as follows: chemical shift (δ) in ppm, multiplicity (s = singlet, d = doublet, t = triplet, dd = doublet of doublet, ddd = doublet of doublet of doublet, td = triplet of doublet, q = quartet, hept = heptuplet and m = multiplet), coupling constant (Hz) and integration. ¹³C-NMR chemicals shifts are given in ppm relative to Me₄Si with solvent resonances used as internal standards (CDCl₃ δ = 77.16 ppm, DMSO-*d*₆ δ = 39.52 ppm, CD₂Cl₂ δ = 53.84 ppm). ¹⁹F-

NMR chemicals shifts are given in ppm. IR spectra were recorded with a Perkin-Elmer 100 FT-IR spectrometer using a diamond ATR Golden Gate sampling and are reported in wave numbers (cm^{-1}). Melting points (m.p.) were measured in open capillary tubes with a Büchi B-550 melting point apparatus and were uncorrected. Low resolution electrospray mass spectra (LR-ESI-MS) were obtained on an API 150EX (AB/MDS Sciex) spectrometer. High resolution mass spectra (HR-MS) were recorded on a QSTAR Pulsar (AB/MDS Sciex) spectrometer by the Department of Mass Spectroscopy at the University of Geneva. Optical rotations were measured in a thermostated ($20\text{ }^{\circ}\text{C}$) 10 cm long microcell at 589 nm (Na lamp). CSP-HPLC analyses were performed on a Agilent 1100 apparatus (binary pump, autosampler, column thermostat and diode array detector).

7.2 Synthesis of polyether macrocycles

18C6 was synthesized according to reported procedure.^{3a}

7.2.1 Synthesis of 16C4 macrocycle



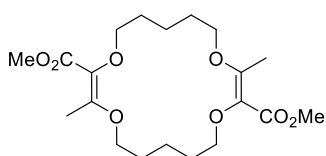
In a 5 mg vial, 1.42 mg (0.0007 mmol, 0.0001 equiv) of $\text{Rh}_2(\text{TCPTCC})_4$ was dissolved in 1.0 mL of dry THF. In a flame dried Schlenk, adapted with a condenser, under nitrogen atmosphere, was introduced the rhodium solution and the vial was washed with 0.7 mL of dry THF. Then, 10.0 mL of THF (for a total of 11.7 mL) were added, followed by α -diazo- β -keto-methyl-ester **1.17**¹⁹⁴ (1.00 g, 7 mmol, 1 equiv, $c = 0.6\text{ M}$). The solution was heated at $60\text{ }^{\circ}\text{C}$ for 15 hours. The completion of the reaction was followed by TLC analysis and infrared spectroscopy (2146 cm^{-1}). The solvent was removed under reduced pressure. The mixture was filtered through a pad of neutral alumina (solid deposit, EtOAc/ CH_2Cl_2 1:1) and the solvent was evaporated. The residual solid was dissolved in 4 mL of CH_2Cl_2 and 100 mL of pentane was added to precipitate the macrocycle. The macrocycle was

¹⁹⁴ Davies, H. M. L.; Cantrell, W. R. J.; Romines, K. R.; Baum, J. S., *Org. Synth.* **1992**, 70, 93.

filtered on a filtration funnel and washed with 100 mL of Et₂O/pentane (1:9) to yield 338 mg (0.91 mmol, 372.41 g/mol, 26%) of **16C4** as a white solid.

R_f = 0.8 (SiO₂, CH₂Cl₂/methanol 90:10); **m.p.**: 129 °C - 132 °C; **¹H-NMR** (500 MHz, CDCl₃): δ/ppm = 1.78 - 1.84 (m, 4H, -CH₂-), 1.89 - 1.95 (m, 4H, -CH₂-), 2.38 (s, 6H, -CH₃), 3.73 (t, 4H, *J* = 7.2 Hz, -CH₂-), 3.75 (s, 6H, -CH₃), 4.00 (t, 4H, *J* = 5.8 Hz, -CH₂-); **¹³C-NMR** (126 MHz, CDCl₃): δ/ppm = 14.4 (2 -CH₃), 26.2 (2 -CH₂-), 26.8 (2 -CH₂-), 51.5 (2 CH₃), 67.7 (2 -CH₂-), 73.6 (2 -CH₂-), 130.1 (2 =C), 158.7 (2 =C), 166.9 (2 C=O); **IR** (neat): $\tilde{\nu}$ /cm⁻¹ 2944, 2886, 1689, 1604, 1439, 1379, 1304, 1266, 1207, 1190, 1157, 1083, 1034, 1013, 972, 776, 631; **HR MS (ESI)** [M+H]⁺ *m/z* calculated for C₁₈H₂₉O₈ 373.1857, observed 373.1856 (-0.2 ppm).

7.2.2 Synthesis of 18C4 macrocycle



In a 3 mL vial, 1.42 mg (0.0007 mmol, 0.0001 equiv) of Rh₂(TCPTCC)₄ was dissolved in 1.0 mL of dry tetrahydropyran (THP). In a flame dried Schlenk, adapted with a condenser, under nitrogen atmosphere, was introduced the rhodium solution and the vial was washed with 0.7 mL of dry THP. Then, 10.0 mL of THP (for a total of 11.7 mL) were added, followed by α-diazo-β-keto-methyl-ester **1.17** (1.00 g, 7 mmol, 1 equiv, *c* = 0.6 M). The solution was heated at 60 °C for 15 hours. The completion of the reaction was followed by TLC analysis and infrared spectroscopy (2146 cm⁻¹). The solvent was removed under reduced pressure. The residual solid was dissolved in 3 mL of CH₂Cl₂ and 100 mL of pentane were added to precipitate the macrocycle. The macrocycle was filtered and washed with 100 mL of Et₂O/pentane (1:9) to yield 771 mg (1.93 mmol, 400.47 g/mol, 55%) of **18C4** as a white solid.

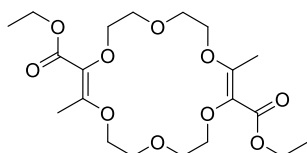
R_f = 0.8 (SiO₂, CH₂Cl₂/methanol 90:10); **m.p.**: 95 °C - 96 °C; **¹H-NMR** (500 MHz, CDCl₃): δ/ppm = 1.65 - 1.76 (m, 12H, -CH₂-), 2.36 (s, 6H, -CH₃), 3.68 - 3.71 (m, 4H, -CH₂-), 3.74 (s, 6H, -CH₃), 3.99 - 4.01 (m, 4H, -CH₂-); **¹³C-NMR** (126 MHz, CDCl₃): δ/ppm = 14.4 (2 CH₃), 23.4 (2 -CH₂-), 29.8 (2 -CH₂-), 30.1 (2 -CH₂-), 51.5 (2 -CH₃), 67.9 (2 -CH₂-), 72.8 (2 -CH₂-), 129.8 (2 =C), 158.7 (2 =C), 167.0 (2 C=O); **IR** (neat): $\tilde{\nu}$ /cm⁻¹ 2939, 1700, 1607, 1461, 1435, 1403, 1374, 1285, 1248, 1191, 1162, 1124, 1082, 1020, 1003, 971, 932, 885, 774, 732, 688, 620, 558; **HR MS (ESI)** [M+H]⁺ *m/z* calculated for C₂₀H₃₃O₈ 401.2170, observed 401.2176 (1.5 ppm).

7.2.3 Synthesis of ester-18C6

7.2.3.1 General procedure I (ester-18C6)

In a 5 mL vial, 1.42 mg (0.0007 mmol, 0.0001 equiv) of $\text{Rh}_2(\text{TCPTCC})_4$ is dissolved into 1.0 mL of dry dioxane. In a flame dried Schlenk, adapted with a condenser, under nitrogen atmosphere, is added the rhodium solution and the vial is washed with 0.7 mL of dry dioxane. Then, 10.0 mL of dry dioxane (for a total of 11.7 mL) are added, followed by the α -diazo- β -ketoester (7 mmol).¹⁹⁴⁻¹⁹⁵ The solution is heated at 60 °C for 15 hours. The completion of the reaction is followed by TLC analysis (EtOAc/pentane 2:8) and infrared spectroscopy (*ca.* 2150 cm^{-1}). The solvent is removed under reduced pressure and purified using an appropriate method. **Method A:** the residual solid is dissolved in a minimum of CH_2Cl_2 and 100 mL of pentane is added to precipitate the macrocycle. The macrocycle is filtered on a filtration funnel and washed with 100 mL of Et_2O /pentane (1:9) to yield the pure **ester-18C6**. **Method B:** the mixture is filtered on a pad of neutral alumina (solid deposit, EtOAc/ CH_2Cl_2 1:1) and the solvent is evaporated. The residual solid is dissolved in a minimum of CH_2Cl_2 and 100 mL of pentane is added to precipitate the macrocycle. The macrocycle is filtered on a filtration funnel and washed with 100 mL of Et_2O /pentane (1:9) to yield the pure **ester-18C6**. **Method C:** The product is purified by chromatographic column (neutral alumina, solid deposit, EtOAc/pentane (1:9, 3:7, 1:1), then EtOAc/ CH_2Cl_2 (1:1)) to yield the pure **ester-18C6**.

7.2.3.2 Synthesis of 2.9

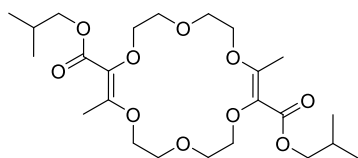


According to general procedure I with 1.09 g (7 mmol, 1 equiv, 0.6 M) of α -diazo- β -keto-ethyl-ester to yield 969 mg (2.24 mmol, 432.47 g/mol, 64%) of **2.9** as a white solid. **Purification:** method A.

Spectral and physical data are in agreement with previously reported literature.⁶⁹

¹⁹⁵ Hyatt, J. A.; Feldman, P. L.; Clemens, R. J., *J. Org. Chem.* **1984**, 49, 5105-5108.

7.2.3.3 Synthesis of 2.10

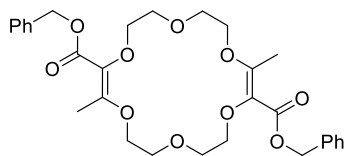


According to general procedure I with 1.29 g (7 mmol, 1 equiv, 0.6 M) of α -diazo- β -keto-isobutyl-ester to yield 684 mg (1.40 mmol, 488.57 g/mol, 40%) of **2.10** as a white solid. **Purification:** method

B.

R_f = 0.6 (SiO₂, CH₂Cl₂/MeOH (10%)); **m.p.:** 86 °C - 89 °C; **¹H-NMR** (500 MHz, CDCl₃): δ /ppm = 0.96 (d, 12H, J = 6.7 Hz, -CH₃), 1.98 (hept, 2H, J = 6.7 Hz, -CH-), 2.34 (s, 6H, -CH₃), 3.79 - 3.81 (m, 4H, -CH₂-), 3.83 - 3.85 (m, 4H, -CH₂-), 3.91 - 3.93 (m, 8H, -CH₂-), 4.19 - 4.21 (m, 4H, -CH₂-); **¹³C-NMR** (126 MHz, CDCl₃): δ /ppm = 15.4 (2 -CH₃), 19.4 (4 -CH₃), 28.0 (2 -CH-), 68.9 (2 -CH₂-), 70.2 (2 -CH₂-), 70.6 (2 -CH₂-), 70.7 (2 -CH₂-), 72.3 (2 -CH₂-), 130.1 (2 =C), 158.35 (2 =C), 166.2 (2 C=O); **IR** (neat): $\tilde{\nu}$ /cm⁻¹ 2952, 2894, 1701, 1615, 1462, 1378, 1309, 1269, 1237, 1162, 1129, 1085, 1030, 983, 929, 896, 870, 833, 813, 776, 690, 632, 577; **HR MS (ESI)** [M+NH₄]⁺ m/z calculated for C₂₄H₄₄O₁₀N 506.2960, observed 506.2945 (-2.8 ppm).

7.2.3.4 Synthesis of 2.11

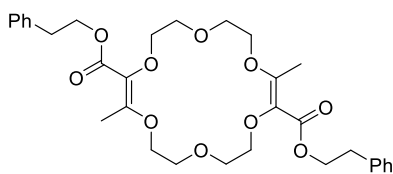


According to general procedure I with 1.53 g (7 mmol, 1 equiv, 0.6 M) of α -diazo- β -keto-benzyl-ester to yield 1071 mg (1.93 mmol, 556.61 g/mol, 55%) of **2.11** as a white solid. **Purification:** method

B.

R_f = 0.6 (SiO₂, CH₂Cl₂/MeOH (10%)); **m.p.:** 100 °C - 101 °C; **¹H-NMR** (500 MHz, CDCl₃): δ /ppm = 2.34 (s, 6H, -CH₃), 3.75 - 3.77 (m, 4H, -CH₂-), 3.80 - 3.81 (m, 4H, -CH₂-), 3.89 - 3.91 (m, 4H, -CH₂-), 4.18 - 4.20 (m, 4H, -CH₂-), 5.20 (s, 4H, benzylic protons), 7.28 - 7.38 (m, 10H, aromatic protons); **¹³C-NMR** (126 MHz, CDCl₃): δ /ppm = 15.5 (2 -CH₃), 66.0 (2 -CH₂-), 68.6 (2 -CH₂-), 70.1 (2 -CH₂-), 70.7 (2 -CH₂-), 72.3 (2 -CH₂-), 128.0 (2 CH aromatic), 128.1 (2 CH aromatic), 128.6 (2 CH aromatic), 129.8 (2 =C), 136.6 (2 C aromatic), 158.9 (2 =C), 165.9 (2 C=O); **IR** (neat): $\tilde{\nu}$ /cm⁻¹ 3060, 2941, 2882, 1692, 1614, 1500, 1453, 1436, 1268, 1233, 1162, 1099, 1030, 981, 934, 903, 871, 814, 773, 728, 694, 630, 575; **HR MS (ESI)** [M+Na]⁺ m/z calculated for C₃₀H₃₆O₁₀Na 579.2201, observed 579.2189 (-1.9 ppm).

7.2.3.5 Synthesis of 2.12

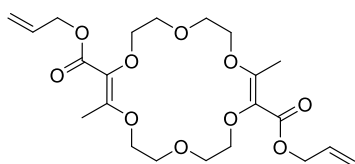


According to general procedure I with 1.63 g (7 mmol, 1 equiv, 0.6 M) of α -diazo- β -keto-homobenzyl-ester to yield 1596 mg (2.73 mmol, 584.66 g/mol, 78%) of **2.12** as a white solid.

Purification: method A.

Spectral and physical data are in agreement with previously reported literature.⁶⁹

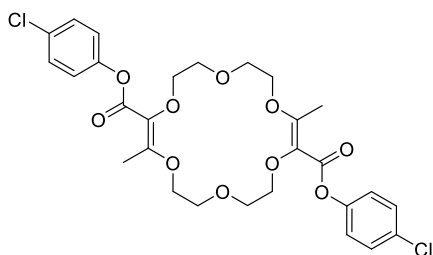
7.2.3.6 Synthesis of 2.13



According to general procedure I with 1.18 g (7 mmol, 1 equiv, 0.6 M) of α -diazo- β -keto-allyl-ester to yield 1006 mg (2.21 mmol, 456.20 g/mol, 63%) of **2.13** as a white solid. **Purification:** method C.

Spectral and physical data are in agreement with previously reported literature.⁶⁹

7.2.3.7 Synthesis of 2.14



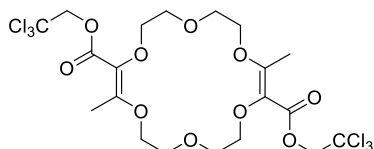
According to general procedure I with 1.67 g (7 mmol, 1 equiv, 0.6 M) of α -diazo- β -keto-*para*-chloro-phenyl-ester to yield 314 mg (0.53 mmol, 597.44 g/mol, 15 %) of **2.14** as a white solid. **Purification:** method C.

R_f = 0.7 (SiO₂, CH₂Cl₂/MeOH (10%)); **m.p.:** 149 °C - 150 °C;

¹H-NMR (500 MHz, CDCl₃): δ /ppm = 2.41 (s, 6H, -CH₃), 3.87 - 3.91 (m, 8H, -CH₂-), 4.04 - 4.06 (m, 4H, -CH₂-), 4.27 - 4.28 (m, 4H, -CH₂-), 7.04 (m, 4H, aromatic), 4.33 - 7.36, 4H, aromatic); **¹³C-NMR** (126 MHz, CDCl₃): δ /ppm = 15.3 (2 -CH₃), 68.7 (2 -CH₂-), 70.0 (2 -CH₂-), 70.8 (2 -CH₂-), 72.6 (2 -CH₂-), 123.5 (2 -CH- aromatic), 128.8 (2 =C), 129.5 (2 -CH- aromatic), 131.1 (2 C-Cl aromatic), 149.5 (2 C aromatic), 161.2 (2 =C), 164.7 (2 C=O); **IR** (neat): $\tilde{\nu}$ /cm⁻¹ 2941, 2886, 1718, 1610, 1489, 1434, 1380, 1271, 1236, 1201, 1154, 1127, 1094, 1059, 1034, 1013, 982, 936, 892, 856, 812, 792,

763, 617; **HR MS (ESI)** $[M+Na]^+$ m/z calculated for $C_{28}H_{30}Cl_2O_{10}Na$ 619.1108, observed 619.1103 (-0.9 ppm).

7.2.3.8 Synthesis of 2.15



According to general procedure I with 1.80 g (7 mmol, 1 equiv, 0.6 M) of α -diazo- β -keto-trichloroethyl-ester to yield 872 mg (1.37 mmol, 639.12 g/mol, 39%) of **2.15** as a white solid.

Purification: method C.

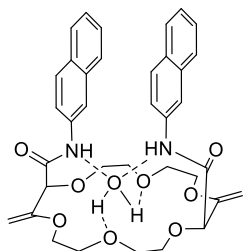
R_f = 0.7 (SiO_2 , $CH_2Cl_2/MeOH$ (10%)); **m.p.:** 91 °C - 93 °C; **1H -NMR** (500 MHz, $CDCl_3$): δ/ppm = 2.40 (s, 6H, - CH_3), 3.82 3.84 (m, 4H, - CH_2 -), 3.86 - 3.88 (m, 4H, - CH_2 -), 3.98 - 4.00 (m, 4H, - CH_2 -), 4.24 - 4.25 (m, 4H, - CH_2 -), 4.81 (s, 4H, - CH_2 -); **^{13}C -NMR** (126 MHz, $CDCl_3$): δ/ppm = 15.4 (2 - CH_3), 68.8 (2 - CH_2 -), 70.0 (2 - CH_2 -), 70.7 (2 - CH_2 -), 72.7 (2 - CH_2 -), 74.0 (2 - CH_2 -), 95.5 (2 CCl_3), 128.5 (2 =C), 161.2 (2 =C), 164.4 (2 C=O); **IR** (neat): $\tilde{\nu}/cm^{-1}$ 2941, 1758, 1714, 1614, 1438, 1380, 1366, 1267, 1240, 1157, 1091, 1059, 975, 940, 862, 822, 783, 766, 710, 629, 570; **HR MS (ESI)** $[M+Na]^+$ m/z calculated for $C_{20}H_{26}Cl_6O_{10}Na$ 658.9549, observed 658.9552 (0.4 ppm).

7.3 Synthesis of polyether macrocycles (aromatic amines)

7.3.1 General procedure II

In a one neck flask under nitrogen atmosphere, dry tetrahydrofuran was added to 1 equivalent of polyether macrocycle (**18C6**, **18C4** or **16C4**) and 3 equivalents of aromatic amine. The mixture was cooled down to -100 °C (EtOH/liquid nitrogen bath). Then 4 equivalents of freshly sublimed *t*-BuOK were added in one portion. After stirring for *ca.* 2 minutes at -100 °C (EtOH/liquid nitrogen bath), the cooling bath was removed and the reaction was allowed to reach 25 °C on its own and stirred for an additional 3 hours. The conversion was followed by TLC analysis and LR-ESI-MS (soft positive mode, CH₂Cl₂). Upon completion, the reaction was quenched by adding a few drops of methanol and directly purified by column chromatography (SiO₂) without further treatment. A second column chromatography (Al₂O₃, neutral) could be required. Finally, the resulting oil or solid was purified by selective precipitation (dissolution in a minimal amount of CH₂Cl₂ or EtOAc required for solubility, followed by addition of a large excess of pentane, 15 hours) affording the desired chiral polyether macrocycle.

7.3.2 Synthesis of 2-naphth-18C6

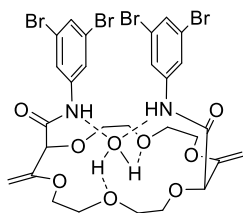


According to general procedure II, 101 mg (0.25 mmol) of **18C6**, 107 (0.75 mmol) of 2-naphthyl-amine, 2.5 mL of THF and 112 mg (1.00 mmol) of *t*-BuOK yield 69 mg (0.11 mmol, 644.72 g/mol, 43%) of **2-naphth-18C6** as a white solid. **Purification:** column 1 (SiO₂) EtOAc for the remaining aniline, then CH₂Cl₂/MeOH gradient (5%, 10%); column 2 (Al₂O₃, neutral) CH₂Cl₂ for

the packing of the column, then CH₂Cl₂/MeOH gradient (1%, 3%, 5%). **Precipitation:** CH₂Cl₂ then pentane.

$R_f = 0.5$ (SiO₂, CH₂Cl₂/MeOH (10%)); **m.p.**: 88 °C - 91 °C; **¹H-NMR** (500 MHz, DMSO d₆): δ /ppm = 3.62 - 3.76 (m, 12H, -CH₂-), 3.81 - 3.85 (m, 2H, -CH₂-), 3.87 - 3.91 (m, 2H, -CH₂-), 4.33 (d, 2H, $J = 2.2$ Hz, =CH₂), 4.40 (d, 2H, $J = 2.2$ Hz, =CH₂), 4.56 (s, 2H, -CH-), 7.37 (ddd, 2H, $J = 8.0$ Hz, 6.8 Hz, 1.3 Hz, aromatic), 7.43 (ddd, 2H, $J = 8.0$ Hz, 6.8 Hz, 1.3 Hz, aromatic), 7.66 (dd, 2H, $J = 8.8$ Hz, 2.1 Hz, aromatic), 7.73 - 7.78 (m, 6H, aromatic), 8.29 (d, 2H, $J = 2.1$ Hz, aromatic), 9.63 (s, 2H, NH); **¹³C-NMR** (126 MHz, DMSO d₆): δ /ppm = 67.3 (2 -CH₂-), 68.3 (2 -CH₂-), 68.5 (2 -CH₂-), 69.5 (2 -CH₂-), 81.3 (2 -CH-), 87.5 (2 =CH₂), 115.9 (2 CH aromatics), 120.4 (2 CH aromatics), 124.8 (2 CH aromatics), 126.4 (2 CH aromatics), 127.3 (2 CH aromatics), 127.4 (2 CH aromatics), 128.3 (2 CH aromatics), 130.0 (2 C aromatics), 133.2 (2 C aromatics), 135.7 (2 C aromatics), 157.4 (2 =C), 164.5 (2 C=O); **IR** (neat): $\tilde{\nu}$ /cm⁻¹ 3270, 3055, 2903, 1682, 1631, 1604, 1585, 1544, 1503, 1433, 1392, 1358, 1287, 1095, 1075, 993, 930, 888, 857, 814, 746, 662; **HR MS (ESI)** [M+H]⁺ m/z calculated for C₃₆H₃₉N₂O₈ 627.2701, observed 627.2695 (-0.9 ppm).

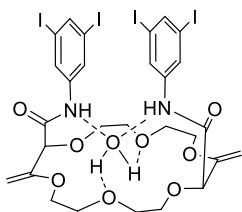
7.3.3 Synthesis of 3,5-dibromo-18C6



According to general procedure II, 303 mg (0.75 mmol) of **18C6**, 565 mg (2.25 mmol) of 3,5-dibromo-aniline, 7.5 mL of THF and 336 mg (3.00 mmol) of *t*-BuOK yield 342 mg (0.40 mmol, 860.19 g/mol, 53%) of **3,5-dibromo-18C6** as an off-white solid. **Purification**: column (SiO₂) EtOAc (pure) for the remaining aniline, followed by CH₂Cl₂/MeOH gradient (1%, 3%, 5%, 10%). **Precipitation**: CH₂Cl₂ then pentane and evaporation

$R_f = 0.6$ (SiO₂, CH₂Cl₂/MeOH (10%)); **m.p.**: 164 °C - 166 °C; **¹H-NMR** (500 MHz, CDCl₃): δ /ppm = 3.53 - 3.56 (m, 2H, -CH₂-), 3.60 - 3.64 (m, 2H, -CH₂-), 3.67 - 3.70 (m, 2H, -CH₂-), 3.78 - 3.89 (m, 8H, -CH₂-), 3.95 - 4.00 (m, 2H, -CH₂-), 4.31 (d, 2H, $J = 2.9$ Hz, =CH₂), 4.34 (s, 2H, -CH-), 4.46 (d, 2H, $J = 2.9$ Hz, =CH₂), 4.31 (t, 2H, $J = 1.7$ Hz, aromatics), 7.78 (d, 4H, $J = 1.7$ Hz, aromatics), 9.85 (s, 2H, NH); **¹³C-NMR** (126 MHz, CDCl₃): δ /ppm = 66.6 (2 -CH₂-), 68.2 (2 -CH₂-), 69.3 (2 -CH₂-), 70.6 (2 -CH₂-), 83.6 (2 -CH-), 89.0 (2 =CH₂), 121.4 (4 CH aromatics), 123.0 (4 CBr aromatics), 129.5 (2 CH aromatics), 140.4 (2 C aromatics), 155.8 (2 =C), 167.7 (2 C=O); **IR** (neat): $\tilde{\nu}$ /cm⁻¹ 3238, 2906, 1692, 1630, 1581, 1523, 1439, 1402, 1296, 1277, 1244, 1130, 1097, 1070, 999, 940, 915, 827, 739, 668; **HR MS (ESI)** [M+H]⁺ m/z calculated for C₂₈H₃₁Br₄N₂O₈ 838.8808, observed 838.8810 (0.2 ppm).

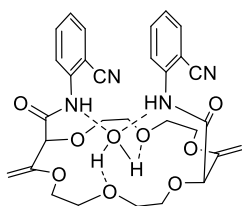
7.3.4 Synthesis of 3,5-diiodo-18C6



According to general procedure II, 303 mg (0.75 mmol) of **18C6**, 776 mg (2.25 mmol) of 3,5-diiodo-aniline,¹⁹⁶ 7.5 mL of THF and 336 mg (3.00 mmol) of *t*-BuOK yield 409 mg (0.39 mmol, 1048.19 g/mol, 52%) of **3,5-diiodo-18C6** as an off-white solid. **Purification:** column (SiO₂) EtOAc (pure) for the remaining aniline, followed by CH₂Cl₂/MeOH gradient (1%, 3%, 5%, 10%). **Precipitation:** CH₂Cl₂ then pentane and evaporation.

R_f = 0.7 (SiO₂, CH₂Cl₂/MeOH (10%)); **m.p.:** 183 °C - 184 °C; **¹H-NMR** (500 MHz, CDCl₃): δ/ppm = 3.56 - 3.60 (m, 2H, -CH₂-), 3.65 - 3.76 (m, 6H, -CH₂-), 3.85 - 3.90 (m, 4H, -CH₂-), 3.92 - 3.96 (m, 2H, -CH₂-), 3.99 - 4.03 (m, 2H, -CH₂-), 4.34 (d, 2H, *J* = 2.9 Hz, =CH₂), 4.35 (s, 2H, -CH-), 4.50 (d, 2H, *J* = 2.9 Hz, =CH₂), 7.69 (t, 2H, *J* = 1.5 Hz, aromatics), 7.93 (d, 4H, *J* = 1.5 Hz, aromatics), 9.17 (s, 2H, NH); **¹³C-NMR** (126 MHz, CDCl₃): δ/ppm = 66.6 (2 -CH₂-), 68.7 (2 -CH₂-), 68.9 (2 -CH₂-), 70.1 (2 -CH₂-), 82.7 (2 -CH-), 88.7 (2 =CH₂), 94.7 (4 Cl aromatic), 127.4 (4 CH aromatic), 139.8 (2 C aromatic), 140.6 (2 CH aromatic), 156.4 (2 =C), 167.6 (2 C=O); **IR** (neat): $\tilde{\nu}$ /cm⁻¹ 3319, 2900, 1689, 1635, 1563, 1510, 1428, 1397, 1394, 1260, 1208, 1134, 1093, 1072, 989, 906, 886, 834, 707, 672, 598. **HR MS (ESI)** [M+H]⁺ *m/z* calculated for C₂₈H₃₁I₄N₂O₈ 1030.8254, observed 1030.8249 (-0.5 ppm).

7.3.5 Synthesis of *o*-CN-18C6



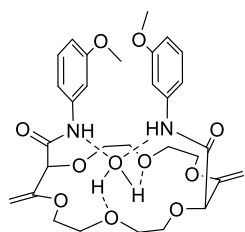
According to general procedure II, 303 mg (0.75 mmol) of **18C6**, 266 mg (2.25 mmol) of 2-aminobenzonitrile, 7.5 mL of THF and 336 mg (3.00 mmol) of *t*-BuOK yield 165 mg (0.28 mmol, 594.62 g/mol, 37%) of ***o*-CN-18C6** as an off-white solid. **Purification:** column 1 (SiO₂) EtOAc/pentane 1:1 then

EtOAc (pure) for the remaining aniline, followed by CH₂Cl₂/MeOH gradient (5%, 10%, 20%); column 2 (Al₂O₃, neutral) EtOAc for the packing of the column, then CH₂Cl₂/MeOH gradient (1%, 3%, 5%). **Precipitation:** CH₂Cl₂ then pentane.

¹⁹⁶ Höger, S.; Bonrad, K.; Mourran, A.; Beginn, U.; Möller, M., *J. Am. Chem. Soc.* **2001**, 123, 5651-5659.

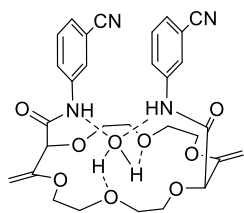
R_f = 0.6 (SiO₂, CH₂Cl₂/MeOH (10%)); **m.p.**: 156 °C - 160 °C; **¹H-NMR** (500 MHz, DMSO-d₆): δ/ppm = 3.65 - 3.87 (m, 16H, -CH₂-), 4.30 (d, 2H, *J* = 2.3 Hz, =CH₂), 4.36 (d, 2H, *J* = 2.3 Hz, =CH₂), 4.57 (s, 2H, -CH-), 7.35 (td, 2H, *J* = 7.6 Hz, 1.2 Hz, aromatics), 7.68 (ddd, 2H, *J* = 8.3 Hz, 7.4 Hz, 1.6 Hz, aromatics), 7.75 (dd, 2H, *J* = 8.3 Hz, 1.2 Hz, aromatics), 7.80 (dd, 2H, *J* = 7.8 Hz, 1.5 Hz, aromatics), 9.74 (s, 2H, NH); **¹³C-NMR** (126 MHz, DMSO-d₆): δ/ppm = 67.7 (2 -CH₂-), 68.3 (2 -CH₂-), 68.6 (2 -CH₂-), 69.8 (2 -CH₂-), 81.1 (2 -CH-), 87.7 (2 =CH₂), 106.7 (2 C aromatics), 116.5 (2 -CN), 124.5 (2 CH aromatics), 125.8 (2 CH aromatics), 133.0 (2 CH aromatics), 133.9 (2 CH aromatics), 139.4 (2 C aromatics), 156.9 (2 =C), 167.7 (2 C=O); **IR** (neat): $\tilde{\nu}$ /cm⁻¹ 3339, 2936, 2881, 2226, 1701, 1639, 1580, 1517, 1448, 1288, 1215, 1138, 1106, 1083, 1040, 985, 924, 877, 834, 756, 687, 631, 571; **HR MS (ESI)** [M+NH₄]⁺ *m/z* calculated for C₃₀H₃₆N₅O₈ 594.2558, observed 594.2569 (1.8 ppm).

7.3.6 Synthesis of *m*-OMe-18C6



According to general procedure II, 303 mg (0.75 mmol) of **18C6**, 251 μ L (2.25 mmol) of ***m*-anisidine**, 7.5 mL of **THF** and 336 mg (3.00 mmol) of ***t*-BuOK** yield 217 mg (0.36 mmol, 604.65 g/mol, 48%) of ***m*-OMe-18C6** as a white solid. **Purification**: column 1 (SiO₂) EtOAc for the remaining aniline, then CH₂Cl₂/MeOH gradient (5%, 10%, 20%); column 2 (Al₂O₃, neutral) EtOAc for the packing of the column, then CH₂Cl₂/MeOH gradient (1%, 3%, 5%). **Precipitation**: CH₂Cl₂ then pentane.

R_f = 0.9 (SiO₂, CH₂Cl₂/MeOH (10%)); **m.p.**: 47 °C - 49 °C; **¹H-NMR** (500 MHz, CDCl₃): δ/ppm = 3.62 - 3.66 (m, 4H, -CH₂-), 3.71 - 3.74 (m, 10H, -CH₂-, -CH₃), 3.75 - 3.89 (m, 7H, -CH₂-), 3.96 - 4.00 (m, 2H, -CH₂-), 4.28 (d, 2H, *J* = 2.8 Hz, =CH₂), 4.36 (s, 2H, -CH-), 4.44 (d, 2H, *J* = 2.8 Hz, =CH₂), 6.59 - 6.62 (m, 2H, aromatics), 7.08 - 7.14 (m, 4H, aromatics), 7.49 (t, 2H, *J* = 2.1 Hz, aromatics), 9.46 (s, 2H, NH); **¹³C-NMR** (126 MHz, CDCl₃): δ/ppm = 55.2 (2 -CH₃), 66.8 (2 -CH₂-), 68.4 (2 -CH₂-), 69.1 (2 -CH₂-), 70.3 (2 -CH₂-), 83.3 (2 -CH-), 88.1 (2 =CH₂), 105.2 (2 CH aromatics), 110.4 (2 CH aromatics), 112.2 (2 CH aromatics), 129.4 (2 CH aromatics), 139.3 (2 C aromatics), 156.5 (2 C=), 160.0 (2 C aromatics), 167.4 (2 C=O); **IR** (neat): $\tilde{\nu}$ /cm⁻¹ 3518, 2915, 1685, 1599, 1542, 1493, 1455, 1425, 1284, 1155, 1091, 1075, 1045, 994, 934, 829, 776, 745, 689, 569; **HR MS (ESI)** [M+H]⁺ *m/z* calculated for C₃₀H₃₉N₂O₁₀ 587.2599, observed 587.2587 (-2.1 ppm).

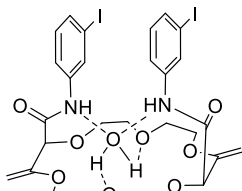
7.3.7 Synthesis of *m*-CN-18C6

According to general procedure II, 303 mg (0.75 mmol) of **18C6**, 266 mg (2.25 mmol) of 3-aminobenzonitrile, 7.5 mL of THF and 336 mg (3.00 mmol) of *t*-BuOK yield 210 mg (0.35 mmol, 594.62 g/mol, 47%) of ***m*-CN-18C6** as a white solid. **Purification:** column 1 (SiO₂): EtOAc/pentane 1:1 then EtOAc

(pure) for the remaining aniline, followed by CH₂Cl₂/MeOH gradient (5%, 10%, 20%); column 2 (Al₂O₃, neutral) EtOAc for the packing of the column, then CH₂Cl₂/MeOH gradient (1%, 3%, 5%).

Precipitation: CH₂Cl₂ then pentane.

R_f = 0.6 (SiO₂, CH₂Cl₂/MeOH (10%)); **m.p.:** 154 °C - 156 °C; **¹H-NMR** (500 MHz, DMSO-*d*₆): δ/ppm = 3.58 - 3.73 (m, 12H, -CH₂-), 3.78 - 3.82 (m, 2H, -CH₂-), 3.86 - 3.90 (m, 2H, -CH₂-), 4.32 (d, 2H, *J* = 2.3 Hz, =CH₂), 4.36 (d, 2H, *J* = 2.3 Hz, =CH₂), 4.51 (s, 2H, -CH-), 7.45 - 7.51 (m, 4H, aromatics), 7.85 - 7.87 (m, 2H, aromatics), 8.09 - 8.09 (m, 2H, aromatics), 9.76 (s, 2H, NH); **¹³C-NMR** (126 MHz, DMSO-*d*₆): δ/ppm = 67.2 (2 -CH₂-), 68.2 (2 -CH₂-), 68.7 (2 -CH₂-), 69.3 (2 -CH₂-), 81.3 (2 -CH-), 87.9 (2 =CH₂), 111.4 (2 C aromatics), 118.6 (2 -CN), 122.4 (2 CH aromatics), 124.4 (2 CH aromatics), 127.3 (2 CH aromatics), 130.1 (2 CH aromatics), 138.8 (2 C aromatics), 157.0 (2 =C), 167.9 (2 C=O); **IR** (neat): $\tilde{\nu}$ /cm⁻¹ 3326, 2937, 2861, 2228, 1691, 1632, 1587, 1530, 1478, 1428, 1318, 1286, 1223, 1132, 1106, 1094, 1069, 988, 895, 817, 789, 684, 653, 614; **HR MS (ESI)** [M+H]⁺ *m/z* calculated for C₃₀H₃₃N₄O₈ 577.2293, observed 577.2301 (1.3 ppm).

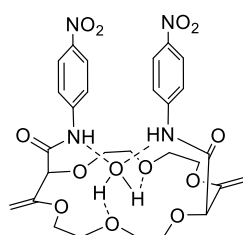
7.3.8 Synthesis of *m*-I-18C6

According to general procedure II, 303 mg (0.75 mmol) of **18C6**, 493 mg (2.25 mmol) of *m*-iodo-aniline, 7.5 mL of THF and 336 mg (3.00 mmol) of *t*-BuOK yield 388 mg (0.49 mmol, 796.39 g/mol, 65%) of ***m*-I-18C6** as an off-white solid. **Purification:** column (SiO₂): EtOAc (pure) for the remaining aniline,

followed by CH₂Cl₂/MeOH gradient (1%, 3%, 5%, 10%). **Precipitation:** CH₂Cl₂ then pentane and evaporation.

R_f = 0.6 (SiO₂, CH₂Cl₂/MeOH (10%)); **m.p.**: 130 °C - 132 °C; **¹H-NMR** (500 MHz, CDCl₃): δ/ppm = 3.56 - 3.65 (m, 4H, -CH₂-), 3.68 - 3.90 (m, 10H, -CH₂-), 3.95 - 4.00 (m, 2H, -CH₂-), 4.29 (d, 2H, *J* = 2.7 Hz, =CH₂), 4.35 (s, 2H, -CH-), 4.45 (d, 2H, *J* = 2.7 Hz, =CH₂), 6.91 (t, 2H, *J* = 8.0 Hz, aromatics), 7.37 (d, 2H, *J* = 8.0 Hz, aromatics), 7.57 (d, 2H, *J* = 8.0 Hz, aromatics), 8.12 (s, 2H, aromatics), 9.67 (s, 2H, NH); **¹³C-NMR** (126 MHz, CDCl₃): δ/ppm = 66.7 (2 -CH₂-), 68.3 (2 -CH₂-), 69.3 (2 -CH₂-), 70.5 (2 -CH₂-), 83.5 (2 -CH-), 88.6 (2 =CH₂), 94.3 (2 Cl aromatics), 119.2 (2 CH aromatics), 128.7 (2 CH aromatics), 130.4 (2 CH aromatics), 133.2 (2 CH aromatics), 139.5 (2 C aromatics), 156.2 (2 =C), 167.6 (2 C=O); **IR** (neat): $\tilde{\nu}$ /cm⁻¹ 3494, 3305, 3067, 2922, 1685, 1639, 1582, 1527, 1473, 1416, 1287, 1243, 1093, 1073, 993, 932, 830, 776, 681, 585; **HR MS (ESI)** [M+H]⁺ *m/z* calculated for C₂₈H₃₃I₂N₂O₈ 779.0321, observed 779.0321 (0.0 ppm).

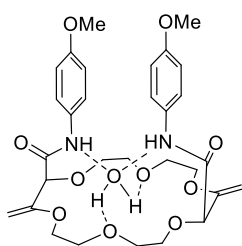
7.3.9 Synthesis of *p*-NO₂-18C6



According to general procedure II, 303 mg (0.75 mmol) of **18C6**, 311 mg (2.25 mmol) of *p*-nitro-aniline, 7.5 mL of THF and 336 mg (3.00 mmol) of *t*-BuOK yield 176 mg (0.28 mmol, 634.60 g/mol, 37%) of ***p*-NO₂-18C6** as a yellow solid. **Purification:** column (SiO₂) EtOAc (pure) for the remaining aniline, followed by CH₂Cl₂/MeOH gradient (1%, 5%, 10%). **Precipitation:**

CH₂Cl₂ then pentane and evaporation.

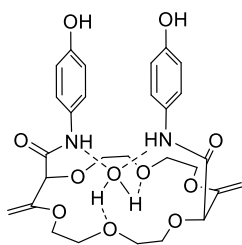
R_f = 0.6 (SiO₂, CH₂Cl₂/MeOH (10%)); **m.p.**: 157 °C - 163 °C; **¹H-NMR** (500 MHz, CDCl₃): δ/ppm = 3.57 - 3.64 (m, 4H, -CH₂-), 3.71 - 3.90 (m, 10H, -CH₂-), 3.98 - 4.02 (m, 2H, -CH₂-), 4.34 (d, 2H, *J* = 2.9 Hz, =CH₂), 4.39 (s, 2H, -CH-), 4.48 (d, 2H, *J* = 2.9 Hz, =CH₂), 7.82 - 7.84 (m, 4H, aromatics), 8.05 - 8.08 (m, 4H, aromatics), 10.17 (s, 2H, NH); **¹³C-NMR** (126 MHz, CDCl₃): δ/ppm = 66.6 (2 -CH₂-), 68.3 (2 -CH₂-), 69.4 (2 -CH₂-), 70.4 (2 -CH₂-), 83.8 (2 -CH-), 89.4 (2 =CH₂), 119.4 (4 CH aromatics), 125.0 (4 CH aromatics), 143.6 (2 C aromatics), 144.1 (2 C aromatics), 155.7 (2 =C), 168.1 (2 C=O); **IR** (neat): $\tilde{\nu}$ /cm⁻¹ 3341, 2928, 1693, 1642, 1597, 1538, 1502, 1407, 1329, 1285, 1252, 1175, 1138, 1091, 1025, 907, 840, 800, 750, 687, 613; **HR MS (ESI)** [M+H]⁺ *m/z* calculated for C₂₈H₃₃N₄O₁₂ 617.2090, observed 617.2087 (-0.4 ppm).

7.3.10 Synthesis of *p*-OMe-18C6

According to general procedure II, 303 mg (0.75 mmol) of **18C6**, 277 mg (2.25 mmol) of *p*-anisidine, 7.5 mL of THF and 336 mg (3.00 mmol) of *t*-BuOK yield 159 mg (0.26 mmol, 604.65 g/mol, 35%) of ***p*-OMe-18C6** as an off-white solid. **Purification:** column 1 (SiO₂) EtOAc for the remaining aniline, then CH₂Cl₂/MeOH gradient (5%, 10%, 20%); column 2 (Al₂O₃, neutral)

EtOAc for the packing of the column, then CH₂Cl₂/MeOH gradient (1%, 3%, 5%). **Precipitation:** CH₂Cl₂ then pentane.

R_f = 0.6 (SiO₂, CH₂Cl₂/MeOH (10%)); **m.p.:** 140 °C - 142 °C; **¹H-NMR** (500 MHz, CDCl₃): δ/ppm = 3.57 - 3.65 (m, 4H, -CH₂-), 3.72 - 3.74 (m, 9H, -CH₂- and -CH₃), 3.77 - 3.90 (m, 7H, -CH₂-), 3.95 - 3.99 (m, 2H, -CH₂-), 4.27 (d, 2H, *J* = 2.7 Hz, =CH₂), 4.35 (s, 2H, -CH-), 4.43 (d, 2H, *J* = 2.7 Hz, =CH₂), 6.74 - 6.77 (m, 4H, aromatics), 7.55 - 7.58 (m, 4H, aromatics), 9.38 (s, 2H, NH); **¹³C-NMR** (126 MHz, CDCl₃): δ/ppm = 55.5 (2 -CH₃), 66.9 (2 -CH₂-), 68.5 (2 -CH₂-), 69.3 (2 -CH₂-), 70.5 (2 -CH₂-), 83.3 (2 -CH-), 88.3 (2 =CH₂), 114.1 (4 CH aromatics), 121.6 (4 CH aromatics), 131.5 (2 C aromatics), 156.3 (2 C aromatics), 156.8 (2 =C), 167.1 (2 C=O); **IR** (neat): $\tilde{\nu}$ /cm⁻¹ 3324, 2912, 1677, 1600, 1535, 1511, 1465, 1414, 1291, 1236, 1178, 1130, 1076, 1029, 994, 932, 901, 829, 804, 752, 701, 587; **HR MS (ESI)** [M+H]⁺ *m/z* calculated for C₃₀H₃₉N₂O₁₀ 587.2599, observed 587.2610 (1.8 ppm).

7.3.11 Synthesis of *p*-OH-18C6

According to general procedure II, 101 mg (0.25 mmol) of **18C6**, 167.5 mg (0.75 mmol) of *p*-OTBDMS-aniline,^{197,198} 2.5 mL of THF and 112 mg (1.00 mmol) of *t*-BuOK yield 48 mg (0.08 mmol, 576.60 g/mol, 33%) of ***p*-OH-18C6** as a brown solid. **Purification:** column 1 (SiO₂) EtOAc for the remaining aniline, then CH₂Cl₂/MeOH gradient (5%, 10%, 20%); column 2 (Al₂O₃, neutral)

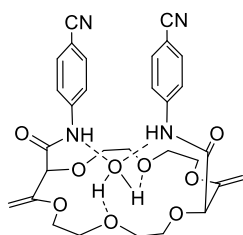
no column on neutral alumina is required. **Precipitation:** CH₂Cl₂ then pentane.

¹⁹⁷ The OTBDMS group is cleaved during the reaction.

¹⁹⁸ Sawamura, Y.; Nakatsuji, H.; Sakakura, A.; Ishihara, K., *Chem. Sci.* **2013**, 4, 4181-4186.

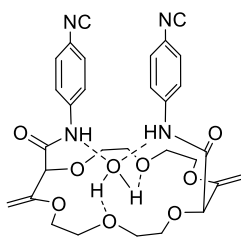
R_f = 0.6 (SiO₂, CH₂Cl₂/MeOH (10%)); **m.p.**: 237 °C - 239 °C; **¹H-NMR** (500 MHz, DMSO-d₆): δ/ppm = 3.57 - 3.69 (m, 12H, -CH₂-), 3.75 - 3.84 (m, 4H, -CH₂-), 4.25 (d, 2H, *J* = 2.2 Hz, =CH₂), 4.31 (d, 2H, *J* = 2.2 Hz, =CH₂), 4.42 (s, 2H, -CH-), 6.66 - 6.69 (m, 4H, aromatics), 7.37 - 7.40 (m, 4H, aromatics), 9.22 (s, 2H, OH), 9.24 (s, 2H, NH); **¹³C-NMR** (126 MHz, DMSO-d₆): δ/ppm = 67.3 (2 -CH₂), 68.3 (2 -CH₂), 68.4 (2 -CH₂), 69.6 (2 -CH₂), 81.2 (2 -CH-), 86.8 (2 =CH₂), 115.0 (4 CH aromatics), 121.6 (4 CH aromatics), 129.7 (2 C aromatics), 153.6 (2 C aromatics), 157.6 (2 =C), 166.5 (2 C=O); **IR** (neat): $\tilde{\nu}$ /cm⁻¹ 3248, 3147, 3081, 2933, 1674, 1643, 1611, 1554, 1513, 1436, 1356, 1286, 1244, 1131, 1089, 1077, 993, 946, 835, 816, 708, 638; **HR MS (ESI)** [M+H]⁺ *m/z* calculated for C₂₈H₃₅N₂O₁₀ 559.2286, observed 559.2276 (-1.9 ppm).

7.3.12 Synthesis of *p*-CN-18C6



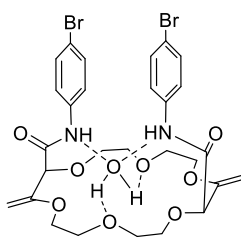
According to general procedure II, 303 mg (0.75 mmol) of **18C6**, 266 mg (2.25 mmol) of 4-aminobenzonitrile, 7.5 mL of THF and 336 mg (3.00 mmol) of *t*-BuOK yield 267 mg (0.45 mmol, 594.62 g/mol, 60%) of ***p*-CN-18C6** as an off-white solid. **Purification**: column 1 (SiO₂) EtOAc/pentane 1:1 then EtOAc (pure) for the remaining aniline, followed by CH₂Cl₂/MeOH gradient (5%, 10%, 20%); column 2 (Al₂O₃, neutral) EtOAc for the packing of the column, then CH₂Cl₂/MeOH gradient (1%, 3%). **Precipitation**: CH₂Cl₂ then pentane.

R_f = 0.7 (SiO₂, CH₂Cl₂/MeOH (10%)); **m.p.**: 143 °C - 146 °C; **¹H-NMR** (500 MHz, DMSO-d₆): δ/ppm = 3.57 - 3.72 (m, 12H, -CH₂-), 3.77 - 3.80 (m, 2H, -CH₂-), 3.85 - 3.89 (m, 2H, -CH₂-), 4.32 (d, 2H, *J* = 2.3 Hz, =CH₂), 4.36 (d, 2H, *J* = 2.3 Hz, =CH₂), 4.52 (s, 2H, -CH-), 7.68 - 7.71 (m, 4H, aromatics), 7.80 - 7.83 (m, 4H, aromatics), 9.82 (s, 1H, NH); **¹³C-NMR** (126 MHz, DMSO-d₆): δ/ppm = 67.2 (2 -CH₂-), 68.3 (2 -CH₂-), 68.7 (2 -CH₂-), 69.3 (2 -CH₂-), 81.3 (2 -CH-), 88.0 (2 =CH₂), 105.6 (2 C aromatics), 118.9 (2 -CN), 119.7 (4 CH aromatics), 133.1 (4 CH aromatics), 142.1 (2 C aromatics), 157.0 (2 =C), 168.1 (2 C=O); **IR** (neat): $\tilde{\nu}$ /cm⁻¹ 3315, 2926, 2878, 2224, 1696, 1639, 1589, 1516, 1463, 1409, 1316, 1290, 1249, 1176, 1091, 1073, 992, 929, 903, 834, 719, 697, 657, 587; **HR MS (ESI)** [M+H]⁺ *m/z* calculated for C₃₀H₃₃N₄O₈ 577.2293, observed 577.2285 (-1.4 ppm).

7.3.13 Synthesis of *p*-NC-18C6

According to general procedure II, 303 mg (0.75 mmol) of **18C6**, 266 mg (2.25 mmol) of *p*-isonitrile-aniline,¹⁹⁹ 7.5 mL of THF and 336 mg (3.00 mmol) of *t*-BuOK yield 241 mg (0.41 mmol, 594.62 g/mol, 54%) of ***p*-NC-18C6** as a yellow solid. **Purification:** column (SiO₂) EtOAc (pure) for the remaining aniline, followed by CH₂Cl₂/MeOH gradient (1%, 5%, 10%). **Precipitation:** CH₂Cl₂ then pentane and evaporation.

R_f = 0.5 (SiO₂, CH₂Cl₂/MeOH (10%)); **m.p.:** 90 °C - 96 °C; **¹H-NMR** (500 MHz, CDCl₃): δ/ppm = 3.56 - 3.65 (m, 4H, -CH₂-), 3.71 - 3.78 (m, 4H, -CH₂-), 3.82 - 3.89 (m, 6H, -CH₂-), 3.97 - 4.02 (m, 6H, -CH₂-), 4.32 (d, 2H, *J* = 2.9 Hz, =CH₂), 4.35 (s, 2H, -CH-), 4.47 (d, 2H, *J* = 2.9 Hz, =CH₂), 7.19 - 7.21 (m, 4H, aromatics), 7.65 - 7.68 (m, 4H, aromatics), 9.77 (s, 2H, NH); **¹³C-NMR** (126 MHz, CDCl₃): δ/ppm = 66.6 (2 -CH₂-), 68.5 (2 -CH₂-), 69.2 (2 -CH₂-), 70.2 (2 -CH₂-), 83.5 (2 -CH-), 89.1 (2 =CH₂), 120.2 (4 CH aromatics), 127.1 (4 CH aromatics), 139.1 (2 C aromatics), 156.1 (2 C aromatics), 163.7 (2 =C), 167.8 (2 C=O), C from NC not detected; **IR** (neat): $\tilde{\nu}$ /cm⁻¹ 3482, 3281, 2923, 2123, 1690, 1638, 1599, 1527, 1508, 1414, 1288, 1247, 1193, 1096, 1074, 995, 930, 836; **HR MS (ESI)** [M+H]⁺ *m/z* calculated for C₃₀H₃₃N₄O₈ 577.2293, observed 577.2283 (-1.8 ppm).

7.3.14 Synthesis of *p*-Br-18C6

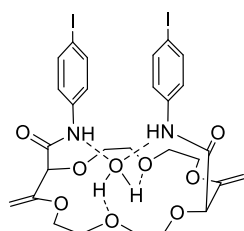
According to general procedure II, 303 mg (0.75 mmol) of **18C6**, 383 mg (2.25 mmol) of *p*-bromo-aniline, 7.5 mL of THF and 336 mg (3.00 mmol) of *t*-BuOK yield 327 mg (0.47 mmol, 702.39 g/mol, 62%) of ***p*-Br-18C6** as an off-white solid. **Purification:** column (SiO₂) EtOAc (pure) for the remaining aniline, followed by CH₂Cl₂/MeOH gradient (1%, 5%, 10%). **Precipitation:**

CH₂Cl₂ then pentane and evaporation.

¹⁹⁹ Heinze, K.; Jacob, V., *Eur. J. Inorg. Chem.* **2003**, 2003, 3918-3923.

$R_f = 0.6$ (SiO₂, CH₂Cl₂/MeOH (10%)); **m.p.**: 90 °C - 107 °C; **¹H-NMR** (500 MHz, CDCl₃): δ /ppm = 3.57 - 3.89 (m, 14H, -CH₂-), 3.96 - 4.01 (m, 2H, -CH₂-), 4.30 (d, 2H, $J = 2.9$ Hz, =CH₂), 4.34 (s, 2H, -CH-), 4.45 (d, 2H, $J = 2.9$ Hz, =CH₂), 7.29 - 7.32 (m, 4H, aromatics), 7.52 - 7.55 (m, 4H, aromatics), 9.48 (s, 2H, NH); **¹³C-NMR** (126 MHz, CDCl₃): δ /ppm = 66.8 (2 -CH₂-), 68.6 (2 -CH₂-), 69.2 (2 -CH₂-), 70.2 (2 -CH₂-), 83.3 (2 -CH-), 88.7 (2 =CH₂), 116.9 (2 CBr aromatics), 121.5 (4 CH aromatics), 131.9 (4 CH aromatics), 137.2 (2 C aromatics), 156.4 (2 =C), 167.5 (2 C=O); **IR** (neat): $\tilde{\nu}$ /cm⁻¹ 3476, 3248, 3184, 3114, 3056, 2918, 1687, 1634, 1590, 1534, 1489, 1395, 1286, 1243, 1099, 1072, 999, 931, 824, 694, 591; **HR MS (ESI)** [M+H]⁺ m/z calculated for C₂₈H₃₃Br₂N₂O₈ 683.0598, observed 683.0618 (2.9 ppm).

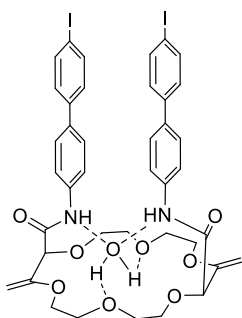
7.3.15 Synthesis of *p*-I-18C6



According to general procedure II, 303 mg (0.75 mmol) of **18C6**, 493 mg (2.25 mmol) of *p*-iodo-aniline, 7.5 mL of THF and 336 mg (3.00 mmol) of *t*-BuOK yield 329 mg (0.41 mmol, 796.39 g/mol, 55%) of ***p*-I-18C6** as an off-white solid. **Purification**: column (SiO₂) EtOAc (pure) for the remaining aniline, followed by CH₂Cl₂/MeOH gradient (1%, 3%, 5%, 10%).

Precipitation: CH₂Cl₂ then pentane and evaporation.

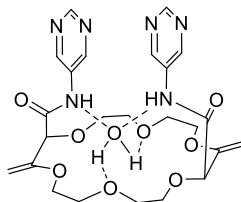
$R_f = 0.7$ (SiO₂, CH₂Cl₂/MeOH (10%)); **m.p.**: 111 °C - 118 °C; **¹H-NMR** (500 MHz, CDCl₃): δ /ppm = 3.54 - 3.61 (m, 4H, -CH₂-), 3.70 - 3.84 (m, 8H, -CH₂-), 3.86 (m, 2H, -CH₂-), 3.95 - 3.99 (m, 2H, -CH₂-), 4.28 (d, 2H, $J = 2.8$ Hz, =CH₂), 4.32 (s, 2H, -CH-), 4.43 (d, 2H, $J = 2.8$ Hz, =CH₂), 7.44 - 7.46 (m, 4H, aromatics), 7.49 - 7.52 (m, 4H, aromatics), 9.81 (s, 2H, NH); **¹³C-NMR** (126 MHz, CDCl₃): δ /ppm = 66.5 (2 -CH₂-), 68.3 (2 -CH₂-), 69.4 (2 -CH₂-), 70.4 (2 -CH₂-), 83.8 (2 -CH-), 87.5 (2 Cl aromatics), 88.9 (2 =CH₂), 122.0 (4 CH aromatics), 137.9 (4 CH aromatics), 138.0 (2 C aromatics), 156.1 (2 =C), 167.6 (2 C=O); **IR** (neat): $\tilde{\nu}$ /cm⁻¹ 3494, 3250, 3174, 3100, 3048, 2913, 1689, 1633, 1598, 1585, 1530, 1487, 1393, 1358, 1318, 1284, 1241, 1101, 1276, 1001, 929, 902, 821, 783, 703, 691, 586; **HR MS (ESI)** [M+H]⁺ m/z calculated for C₂₈H₃₃I₂N₂O₈ 779.0321, observed 779.0328 (0.9 ppm).

7.3.16 Synthesis of *p*-I-*p*-Ph-18C6

According to general procedure II, 303 mg (0.75 mmol) of **18C6**, 664 mg (2.25 mmol) of *p*-I-*p*-Ph-aniline,²⁰⁰ 7.5 mL of THF and 336 mg (3.00 mmol) of *t*-BuOK yield 299 mg (0.32 mmol, 948.59 g/mol, 42%) of ***p*-I-*p*-Ph-18C6** as an off-white solid. **Purification:** column (SiO₂) EtOAc (pure) for the remaining aniline, followed by CH₂Cl₂/MeOH gradient (1%, 3%, 5%, 10%). **Precipitation:** CH₂Cl₂ then pentane and evaporation.

R_f = 0.7 (SiO₂, CH₂Cl₂/MeOH (10%)); **m.p.:** 226 °C - 227 °C; **¹H-NMR** (500 MHz, CDCl₃): δ/ppm = 3.60 - 3.68 (m, 4H, -CH₂-), 3.71 - 3.82 (m, 4H, -CH₂-), 3.83 - 3.89 (m, 4H, -CH₂-), 3.91 - 3.95 (m, 2H, -CH₂-), 4.00 - 4.04 (m, 2H, -CH₂-), 4.32 (d, 2H, *J* = 2.7 Hz, =CH₂), 4.37 (s, 2H, -CH-), 4.47 (d, 2H, *J* = 2.7 Hz, =CH₂), 7.11 - 7.14 (m, 4H, aromatics), 7.32 - 7.35 (m, 4H, aromatics), 7.63 - 7.66 (m, 4H, aromatics), 7.71 - 7.73 (m, 4H, aromatics), 9.66 (s, 2H, NH); **¹³C-NMR** (126 MHz, CDCl₃): δ/ppm = 66.8 (2 -CH₂-), 68.5 (2 -CH₂-), 69.2 (2 -CH₂-), 70.2 (2 -CH₂-), 83.5 (2 -CH-), 88.8 (2 =CH₂), 92.8 (2 C aromatics), 120.4 (4 CH aromatics), 127.2 (4 CH aromatics), 128.6 (4 CH aromatics), 135.4 (2 C aromatics), 137.86 (2 C aromatics), 137.94 (4 CH aromatics), 140.0 (2 C aromatics), 155.7 (2 =C), 168.1 (2 C=O); **IR** (neat): $\tilde{\nu}$ /cm⁻¹ 3352, 3041, 2923, 1686, 1641, 1603, 1522, 1503, 1478, 1413, 1386, 1317, 1289, 1247, 1091, 1075, 996, 960, 895, 807, 728, 681, 647, 574; **HR MS (ESI)** [M+H]⁺ *m/z* calculated for C₄₀H₄₁N₂O₈ 931.0947, observed 931.0933 (-1.5 ppm).

7.3.17 Synthesis of 5-pyrimidine-18C6

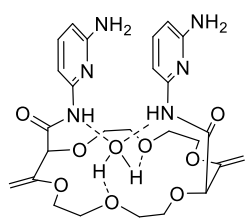


According to general procedure II, 303 mg (0.75 mmol) of **18C6**, 214 mg (2.25 mmol) of pyrimidine-5-amine, 7.5 mL of THF and 336 mg (3.00 mmol) of *t*-BuOK yield 300 mg (0.55 mmol, 548.55 g/mol, 73%) of **5-pyrimidine-18C6** as a yellow solid. **Purification:** column (SiO₂) EtOAc/MeOH (1:0, 9:1) for the remaining aniline, followed by CH₂Cl₂/MeOH gradient (5%, 10%, 20%).

²⁰⁰ Hammerich, M.; Rusch, T.; Krekieleh, N. R.; Bloedorn, A.; Magnussen, O. M.; Herges, R., *ChemPhysChem* **2016**, *17*, 1870-1874.

$R_f = 0.4$ (SiO_2 , $\text{CH}_2\text{Cl}_2/\text{MeOH}$ (10%)); **m.p.**: 141 °C - 145 °C; $^1\text{H-NMR}$ (500 MHz, CDCl_3): $\delta/\text{ppm} = 3.56 - 3.71$ (m, 6H, $-\text{CH}_2-$), 3.74 - 3.88 (m, 8H, $-\text{CH}_2-$), 3.97 - 4.01 (m, 2H, $-\text{CH}_2-$), 4.33 (d, 2H, $J = 2.9$ Hz, $=\text{CH}_2$), 4.39 (s, 2H, $-\text{CH}-$), 4.47 (d, 2H, $J = 2.9$ Hz, $=\text{CH}_2$), 8.94 (s, 2H, aromatics), 9.17 (s, 4H, aromatics), 9.99 (s, 2H, NH); $^{13}\text{C-NMR}$ (126 MHz, CDCl_3): $\delta/\text{ppm} = 66.9$ (2 $-\text{CH}_2-$), 68.2 (2 $-\text{CH}_2-$), 69.6 (2 $-\text{CH}_2-$), 70.5 (2 $-\text{CH}_2-$), 83.5 (2 $-\text{CH}-$), 89.4 (2 $=\text{CH}_2$), 133.8 (2 C aromatics), 148.0 (4 CH aromatics), 145.2 (2 CH aromatics), 155.7 (2 $=\text{C}$), 168.3 (2 $\text{C}=\text{O}$); **IR** (neat): $\tilde{\nu}/\text{cm}^{-1}$ 3306, 2857, 1692, 1645, 1575, 1520, 1464, 1430, 1416, 1335, 1288, 1271, 1240, 1189, 1135, 1111, 1088, 975, 952, 933, 906, 872, 855, 838, 904, 720, 685, 668, 623; **HR MS (ESI)** $[\text{M}+\text{H}]^+$ m/z calculated for $\text{C}_{24}\text{H}_{31}\text{N}_6\text{O}_8$ 531.2198, observed 531.2192 (-1.1 ppm).

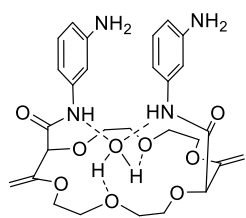
7.3.18 Synthesis of *m*-NH₂-pyr-18C6²⁰¹



According to general procedure II, 1000 mg (2.47 mmol) of **18C6**, 1100 mg (10 mmol) of 2,6-diaminopyridine, 60 mL of THF and 1100 mg (10 mmol) of *t*-BuOK yield 610 mg (1.06 mmol, 576.61 g/mol, 47%) of ***m*-NH₂-pyr-18C6** as a brown-pale yellow solid. **Purification**: column (SiO_2) EtOAc/MeOH (1:0, 9:1) for the remaining aniline, followed by $\text{CH}_2\text{Cl}_2/\text{MeOH}$ (10%). **Precipitation**: CH_2Cl_2 then pentane.

Spectral and physical data are in agreement with previously reported literature.^{3b}

7.3.19 Synthesis of *m*-NH₂-18C6¹¹⁹

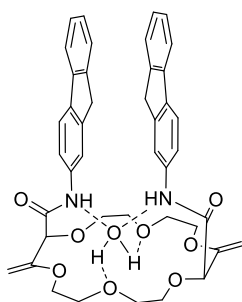


According to general procedure II, 1000 mg (2.47 mmol) of **18C6**, 1100 mg (10 mmol) of *m*-phenylenediamine, 60 mL of THF and 1100 mg (10 mmol) of *t*-BuOK yield 491 mg (0.86 mmol, 574.63 g/mol, 38%) of ***m*-NH₂-18C6** as a brown solid. **Purification**: column (SiO_2) EtOAc/MeOH (1:0, 9:1) for the remaining aniline, followed by $\text{CH}_2\text{Cl}_2/\text{MeOH}$ (10%). **Precipitation**: CH_2Cl_2 then pentane.

Spectral and physical data are in agreement with previously reported literature.^{3b}

²⁰¹ Crown ether synthesized by Dr. Sumit Kumar Ray.

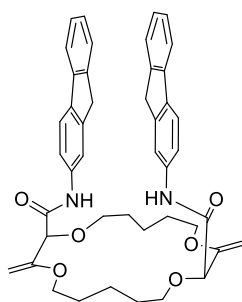
7.3.20 Synthesis of fluorene-18C6



According to general procedure II, 101 mg (0.25 mmol) of **18C6**, 136 mg (0.75 mmol, 3 equiv) of 2-fluorene-amine, 2.5 mL of dry and degassed THF and 112 mg (1.00 mmol, 4 equiv) of *t*-BuOK yield 77 mg (0.11 mmol, 720.82 g/mol, 38%) of **fluorene-18C6** as a yellow solid. **Purification:** column 1 (SiO₂) EtOAc for the remaining aniline, then CH₂Cl₂/MeOH gradient (5%, 10%, 20%); column 2 (Al₂O₃, neutral) EtOAc for the packing of the column, then CH₂Cl₂/MeOH gradient (1%, 3%, 5%). **Precipitation:** EtOAc then pentane.

R_f = 0.5 (SiO₂, CH₂Cl₂/MeOH (10%)); **m.p.:** 104 °C - 109 °C, **¹H-NMR** (500 MHz, CDCl₃): δ/ppm = 3.58 - 3.66 (m, 5H, -CH₂-), 3.67 - 3.76 (m, 5H, -CH₂-), 3.79 - 3.83 (m, 2H, -CH₂-), 3.87 - 3.96 (m, 6H, -CH₂-), 4.02 - 4.07 (m, 2H, -CH₂-), 4.33 (d, 2H, *J* = 2.7 Hz, =CH₂), 4.39 (s, 2H, -CH-), 4.49 (d, 2H, *J* = 2.7 Hz, =CH₂), 7.15 - 7.22 (m, 4H, aromatics), 7.34 - 7.36 (m, 2H, aromatics), 7.44 - 7.46 (m, 4H, aromatics), 7.50 - 7.52 (m, 2H, aromatics), 7.94 (s, 2H, aromatics), 9.52 (s, 2H, NH); **¹³C-NMR** (126 MHz, CDCl₃): δ/ppm = 37.1 (2 -CH₂-), 66.9 (2 -CH₂-), 68.7 (2 -CH₂-), 69.2 (2 -CH₂-), 70.2 (2 -CH₂-), 83.4 (2 -CH-), 88.7 (2 =CH₂), 116.6 (2 CH aromatics), 118.6 (2 CH aromatics), 119.5 (2 CH aromatics), 120.1 (2 CH aromatics), 124.9 (2 CH aromatics), 126.1 (2 CH aromatics), 126.7 (2 CH aromatics), 137.0 (2 C aromatics), 137.9 (2 C aromatics), 141.4 (2 C aromatics), 143.3 (2 C aromatics), 144.2 (2 C aromatics), 156.7 (2 =C), 167.3 (2 C=O); **IR** (neat): $\tilde{\nu}$ /cm⁻¹ 3316, 2921, 1681, 1593, 1534, 1492, 1457, 1424, 1352, 1290, 1094, 1074, 993, 948, 827, 766, 732, 702, 573; **HR MS (ESI)** [M+H]⁺ *m/z* calculated for C₄₂H₄₃N₂O₈ 703.3014, observed 703.3029 (2.1 ppm).

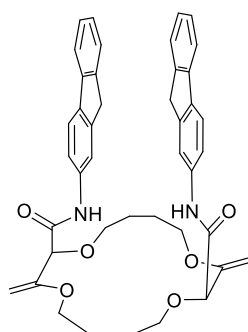
7.3.21 Synthesis of fluorene-18C4



According to the general procedure II, 100 mg (0.25 mmol) of **18C4**, 136 mg (0.75 mmol) of 2-amino-fluorene, 2.5 mL of dry and degassed THF and 112 mg (1.00 mmol) of *t*-BuOK yielded 33 mg (0.05 mmol, 698.86 g/mol, 19%) of **fluorene-18C4** as a yellow solid. **Purification:** column (SiO₂) EtOAc (remaining aniline co-eluted with **fluorene-18C4**). **Precipitation:** EtOAc then pentane (this step was repeated twice).

R_f = 0.7 (SiO₂, EtOAc); **m.p.**: 176 °C - 177 °C; **¹H-NMR** (500 MHz, CDCl₃): δ /ppm = 1.66 - 1.84 (m, 12H, -CH₂-), 3.52 - 3.78 (m, 10H, -CH₂-), 3.88 - 3.92 (m, 2H, -CH₂-), 4.27 (s, 2H, -CH-), 4.33 (d, 2H, J = 2.4 Hz, =CH₂), 4.36 (d, 2H, J = 2.4 Hz, =CH₂), 7.21 - 7.26 (m, 4H, aromatics), 7.32 - 7.34 (m, 2H, aromatics), 7.40 - 7.42 (m, 2H, aromatics), 7.48 - 7.46 (m, 2H, aromatics), 7.51 - 7.53 (m, 2H, aromatics), 7.90 (s, 2H, aromatics), 8.53 (s, 2H, NH); **¹³C-NMR** (126 MHz, CDCl₃): δ /ppm = 24.4 (2 -CH₂-), 28.8 (2 -CH₂-), 30.0 (2 -CH₂-), 37.1 (2 -CH₂-), 68.2 (2 -CH₂-), 69.7 (2 -CH₂-), 82.9 (2 -CH-), 88.5 (2 -CH₂-), 116.7 (2 CH aromatics), 118.5 (2 CH aromatics), 119.7 (2 CH aromatics), 120.3 (2 CH aromatics), 125.0 (2 CH aromatics), 126.4 (2 CH aromatics), 126.8 (2 CH aromatics), 136.3 (2 C aromatics), 138.2 (2 C aromatics), 141.3 (2 C aromatics), 143.3 (2 C aromatics), 144.5 (2 C aromatics), 156.9 (2 =C), 167.3 (2 C=O); **IR** (neat): $\tilde{\nu}$ /cm⁻¹ 3386, 2921, 2870, 1693, 1637, 1590, 1524, 1492, 1459, 1424, 1298, 1217, 1089, 998, 1217, 1089, 998, 947, 823, 766, 733, 566; **HR MS (ESI)** [M+H]⁺ m/z calculated for C₄₄H₄₇N₂O₆ 699.3429, observed 699.3439 (1.4 ppm).

7.3.22 Synthesis of fluorene-16C4

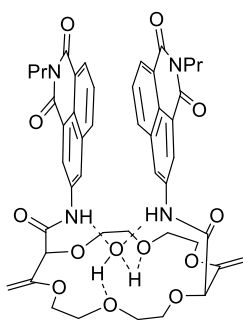


According to the general procedure II, 93 mg (0.25 mmol) of **16C4**, 136 mg (0.75 mmol) of 2-amino-fluorene, 2.5 mL of dry and degassed THF and 112 mg (1.00 mmol) of *t*-BuOK yielded 59 mg (0.09 mmol, 670.81 g/mol, 35%) of **fluorene-16C4** as a yellow solid. **Purification**: column eluent (SiO₂): EtOAc (remaining aniline co-eluted with **fluorene-16C4**). **Precipitation**: EtOAc then pentane (this step was repeated twice).

R_f = 0.6 (SiO₂, EtOAc); **m.p.**: 159 °C - 161 °C; **¹H-NMR** (500 MHz, CDCl₃): δ /ppm = 1.69 - 1.75 (m, 4H, -CH₂-), 1.94 - 2.01 (m, 4H, -CH₂-), 3.53 - 3.66 (m, 6H, -CH₂-), 3.80 - 3.89 (m, 6H, -CH₂-), 4.30 (s, 2H, -CH-), 4.35 (d, 2H, J = 2.4 Hz, =CH₂), 4.39 (d, 2H, J = 2.4 Hz, =CH₂), 7.26 - 7.29 (m, 2H, aromatics), 7.34 - 7.37 (m, 2H, aromatics), 7.47 - 7.53 (m, 4H, aromatics), 7.71 - 7.73 (m, 4H, aromatics), 7.98 (s, 2H, aromatics), 8.59 (s, 2H, NH); **¹³C-NMR** (126 MHz, CDCl₃): δ /ppm = 24.2 (2 -CH₂-), 25.5 (2 -CH₂-), 37.2 (2 -CH₂-), 66.4 (2 -CH₂-), 67.6 (2 -CH₂-), 82.3 (2 -CH-), 89.3 (2 =CH₂), 116.7 (2 CH aromatics), 118.6 (2 CH aromatics), 119.7 (2 CH aromatics), 120.2 (2 CH aromatics), 125.1 (2 CH aromatics), 126.5 (2 CH aromatics), 126.9 (2 CH aromatics), 136.4 (2 C aromatics), 138.3 (2 C aromatics), 141.5 (2 C aromatics), 143.3 (2 C aromatics), 144.5 (2 C aromatics), 156.6 (2 =C), 166.9 (2 C=O); **IR** (neat): $\tilde{\nu}$ /cm⁻¹ 3362, 3048, 2888, 1685, 1620, 1591, 1529, 1492, 1458,

1425, 1351, 1290, 1211, 1093, 1037, 951, 815, 762, 724, 570; **HR MS (ESI)** $[M+H]^+$ m/z calculated for $C_{42}H_{43}N_2O_6$ 671.3116, observed 671.3116 (0.1 ppm).

7.3.23 Synthesis of NMI-18C6

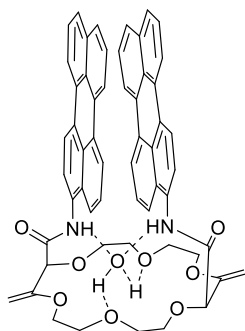


According to the general procedure II, 101 mg (0.25 mmol) of **18C6**, 191 mg (0.75 mmol) of 3-amino-NMI,²⁰² 2.5 mL of dry THF and 112 mg (1.00 mmol) of *t*-BuOK yielded 37 mg (0.043 mmol, 866.92 g/mol, 17%) of **NMI-18C6** as a yellow solid. **Purification:** column 1 (SiO_2) CH_2Cl_2 , then CH_2Cl_2 /methanol gradient (2%, 5%, 10%); column 2 (Al_2O_3 , neutral) CH_2Cl_2 for the packing of the column, then CH_2Cl_2 /methanol gradient (1%, 2%,

3%); preparative TLC (SiO_2): CH_2Cl_2 /methanol (5%).

R_f = 0.5 (SiO_2 , CH_2Cl_2 /methanol 9:1); **m.p.:** 213 °C - 218 °C; **¹H-NMR** (500 MHz, $CDCl_3$): δ /ppm = 0.92 (t, 6H, J = 7.4 Hz, -CH₃), 1.54 - 1.62 (m, 4H, -CH₂-), 3.64 - 3.69 (m, 4H, -CH₂-), 3.73 - 3.77 (m, 2H, -CH₂-), 3.82 - 3.98 (m, 8H, -CH₂-), 4.04 - 4.07 (m, 2H, -CH₂-), 4.13 - 4.23 (m, 4H, -CH₂-), 4.40 (d, 2H, J = 2.8 Hz, =CH₂), 4.41 (s, 2H, -CH-), 4.51 (d, 2H, J = 2.8 Hz, =CH₂), 7.48 (dd, 2H, J = 8.3 Hz, 7.2 Hz, aromatics), 7.79 (dd, 2H, J = 8.3 Hz, 1.1 Hz, aromatics), 8.13 (d, 2H, J = 2.1 Hz, aromatics), 8.16 (dd, 2H, J = 7.2 Hz, 1.1 Hz, aromatics), 8.67 (d, 2H, J = 2.1 Hz, aromatics), 9.85 (s, 2H, NH); **¹³C-NMR** (126 MHz, $CDCl_3$): δ /ppm = 11.5 (2 -CH₃), 21.2 (2 -CH₂-), 41.8 (2 -CH₂-), 65.7 (2 -CH₂-), 68.7 (2 -CH₂-), 69.0 (2 -CH₂-), 69.1 (2 -CH₂-), 83.1 (2 -CH-), 88.9 (2 =CH₂), 121.4 (2 CH aromatics), 121.8 (2 C aromatics), 122.7 (2 C aromatics), 123.8 (2 CH aromatics), 124.4 (2 C aromatics), 126.9 (2 CH aromatics), 129.4 (2 CH aromatics), 131.9 (2 C aromatics), 133.2 (2 CH aromatics), 136.5 (2 C aromatics), 156.5 (2 C=), 163.0 (2 C=O), 163.6 (2 C=O), 168.0 (2 C=O); **IR** (neat): $\tilde{\nu}/cm^{-1}$ 3315, 2926, 1691, 1658, 1592, 1537, 1463, 1427, 1377, 1336, 1293, 1233, 1130, 1090, 1073, 991, 926, 885, 930, 778, 737, 666; **HR MS (ESI)** $[M+H]^+$ m/z calculated for $C_{46}H_{49}N_4O_{12}$ 849.3342, observed 849.3340 (-0.2 ppm).

²⁰² Khosravi, A.; Moradian, S.; Gharanjig, K.; Afshar Taromi, F., *Dyes Pigment.* **2006**, 69, 79-92.

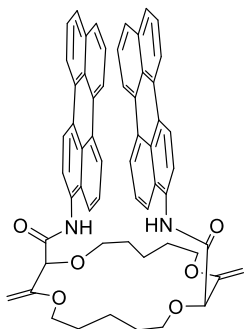
7.3.24 Synthesis of perylene-18C6²⁰³

According to the general procedure **II**, 101 mg (0.25 mmol) of **18C6**, 200 mg (0.75 mmol) of 3-amino-perylene,²⁰⁴ 2 mL of dry THF and 112 mg (1.0 mmol) of *t*-BuOK yielded 130 mg (0.15 mmol, 874.99 g/mol, 60%) of **perylen-18C6** as a yellow-orange solid. **Purification conditions:** column (SiO₂) CH₂Cl₂, then CH₂Cl₂/methanol gradient (2%, 5%, 10%). **Precipitation:** CH₂Cl₂ then pentane.

R_f = 0.3 (SiO₂, CH₂Cl₂/methanol (5%)); **m.p.:** 235 °C - 240 °C; **¹H-NMR** (500 MHz, CDCl₃): δ/ppm = 3.72 (m, 2H, -CH₂-), 3.80 (m, 2H, -CH₂-), 3.87 (m, 2H, -CH₂-), 3.95-4.13 (m, 10H, -CH₂-), 4.41 (d, 2H, *J* = 2.6 Hz, =CH₂), 4.47 (s, 2H, -CH-), 4.52 (d, 2H, *J* = 2.6 Hz, =CH₂), 7.04 - 7.11 (m, 6H, aromatics), 7.27 (d, 2H, *J* = 8.0 Hz, aromatics), 7.30 (d, 2H, *J* = 8.0 Hz, aromatics), 7.47 (d, 2H, *J* = 8.3 Hz, aromatics), 7.49 (d, 2H, *J* = 7.5 Hz, aromatics), 7.55 (d, 2H, *J* = 7.4 Hz, aromatics), 7.61 (d, 2H, *J* = 7.4 Hz, aromatics), 7.72 (d, 2H, *J* = 8.2 Hz, aromatics), 7.87 (d, 2H, *J* = 8.2 Hz, aromatics), 9.17 (s, 2H, NH); **¹³C-NMR** (126 MHz, CDCl₃): δ/ppm = 67.3 (2 -CH₂-), 68.7 (2 -CH₂-), 68.8 (2 -CH₂-), 70.3 (2 -CH₂-), 83.4 (2 -CH-), 89.7 (2 =CH₂), 119.5 (4 -CH- aromatics), 119.6 (2 -CH- aromatics), 119.7 (2 -CH- aromatics), 119.9 (2 -CH- aromatics), 120.2 (2 -CH- aromatics), 126.0 (2 -CH- aromatics), 126.1 (2 -CH- aromatics), 126.3 (2 -CH- aromatics), 127.0 (2 -CH- aromatics), 127.1 (2 C aromatics), 127.5 (2 -CH- aromatics), 127.8 (2 C aromatics), 128.3 (2 C aromatics), 128.5 (2 C aromatics), 130.6 (4 C aromatics), 131.0 (2 C aromatics), 131.4 (2 C aromatics), 134.2 (2 C aromatics), 156.3 (2 =C), 167.2 (2 C=O). **IR** (neat): $\tilde{\nu}/\text{cm}^{-1}$ 3366, 2924, 2874, 1693, 1542, 1509, 1389, 1324, 1288, 1099, 996, 919, 807, 765, 731. **HR MS (ESI)** [M+H]⁺ *m/z* calculated for C₅₆H₄₇N₂O₈ 875.3327, observed 875.3341 (1.6 ppm).

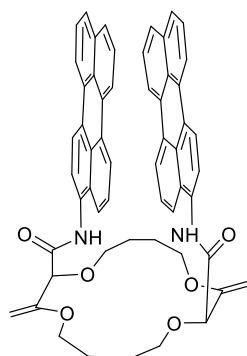
²⁰³ Crown ether synthesized by Dr. Francesco Zinna.

²⁰⁴ (a) Almonasy, N.; Nepraš, M.; Hyková, Š.; Lyčka, A.; Čermák, J.; Dvořák, M.; Michl, M., *Dyes Pigm.* **2009**, *82*, 164-170. (b) Looker, J. J., *J. Org. Chem.* **1972**, *37*, 3379-3381.

7.3.25 Synthesis of perylene-18C4²⁰⁵

According to the general procedure II, 50 mg (0.125 mmol) of **18C4**, 100 mg (0.375 mmol) of 3-amino-perylene, 1.5 mL of dry THF and 56 mg (0.5 mmol) of *t*-BuOK yielded 56 mg (0.064 mmol, 871.03 g/mol, 51%) of **peryene-18C4** as a yellow-brown solid. **Purification:** Column 1 (SiO₂) CH₂Cl₂, then CH₂Cl₂/methanol gradient (1%, 2%, 4%); column 2 (SiO₂) CH₂Cl₂, then CH₂Cl₂/methanol gradient (0.5%, 1%, 2%). **Precipitation:** CH₂Cl₂ then pentane.

R_f = 0.4 (SiO₂, CH₂Cl₂/methanol 98:2); **m.p.:** 246 °C - 248 °C; **¹H-NMR** (500 MHz, CDCl₃): δ/ppm = 1.54 (m, 2H, -CH₂-), 1.76 (m, 2H, -CH₂-), 1.84 (m, 2H, -CH₂-), 1.97-2.07 (m, 4H, -CH₂-), 2.40 (m, 2H, -CH₂-), 3.62 - 3.74 (m, 6H, -CH₂-), 4.02 (dt, *J* = 8.4, 3.8 Hz, 2H, -CH₂-), 4.37 (d, *J* = 2.4 Hz, 2H, =CH₂), 4.41 - 4.43 (m, 4H, -CH- and =CH₂), 6.98 (d, *J* = 7.7 Hz, 2H, aromatics), 7.18 (d, *J* = 7.4 Hz, 2H, aromatics), 7.23 (m, 2H, aromatics), 7.30 - 7.33 (m, 4H, aromatics), 7.36 (d, *J* = 8.1 Hz, 2H, aromatics), 7.40 (d, *J* = 8.1 Hz, 2H, aromatics), 7.43 - 7.47 (m, 4H, aromatics), 7.64 (d, *J* = 7.3 Hz, 2H, aromatics), 7.81 (d, *J* = 7.4 Hz, 2H, aromatics), 8.37 (s, 2H, NH); **¹³C-NMR** (126 MHz, CDCl₃): δ/ppm = 25.2 (2 -CH₂-), 29.8 (2 -CH₂-), 31.2 (2 -CH₂-), 68.5 (2 -CH₂-), 68.6 (2 -CH₂-), 83.3 (2 -CH-), 89.4 (2 -CH₂-), 119.5 (2 -CH- aromatics), 119.7 (4 -CH- aromatics), 120.0 (2 -CH- aromatics), 120.2 (2 -CH- aromatics), 122.3 (2 -CH- aromatics), 126.0 (2 -CH- aromatics), 126.1 (2 -CH- aromatics), 126.2 (2 -CH- aromatics), 127.1 (2 -CH- aromatics), 127.75 (2 -CH- aromatics), 127.82 (2 C aromatics), 128.5 (2 C aromatics), 128.6 (2 C aromatics), 128.9 (2 C aromatics), 130.2 (2 C aromatics), 130.7 (2 C aromatics), 130.8 (2 C aromatics), 131.4 (2 C aromatics), 134.2 (2 C aromatics), 156.3 (2 =C), 167.5 (2 C=O); **IR** (neat): $\tilde{\nu}$ /cm⁻¹ 3404, 2922, 2866, 1698, 1621, 1533, 1504, 1473, 1428, 1389, 1324, 1282, 1095, 1079, 1060, 994, 821, 806, 763; **HR MS (ESI)** [M+H]⁺ *m/z* calculated for C₅₈H₅₁N₂O₆ 871.3742, observed 871.3758 (1.8 ppm).

7.3.26 Synthesis of perylene-16C4¹²³

According to the general procedure II, 47 mg (0.125 mmol) of **16C4**, 100 mg (0.375 mmol) of 3-amino-perylene, 1.5 mL of dry THF and 56 mg (0.5 mmol) of *t*-BuOK yielded 55 mg (0.065 mmol, 842.99 g/mol, 52%) of **perylen-16C4** as a greenish-brown solid. **Purification:** column 1 (SiO₂) CH₂Cl₂, then CH₂Cl₂/methanol gradient (2%, 5%, 10%); column 2 (SiO₂) CH₂Cl₂, then CH₂Cl₂/EtOAc gradient (2%, 4%, 6%, 8%). **Precipitation:** CH₂Cl₂ then pentane.

R_f = 0.4 (SiO₂, CH₂Cl₂/methanol 98:2); **m.p.:** 249 °C - 250 °C; **¹H-NMR** (500 MHz, CDCl₃): δ/ppm = 1.79 - 1.90 (m, 4H, -CH₂-), 2.06 - 2.17 (m, 4H, -CH₂-), 3.64 (m, 2H, -CH₂-), 3.70 - 3.74 (m, 4H, -CH₂-), 3.93 (m, 2H, -CH₂-), 4.42 (d, *J* = 2.4 Hz, 2H, =CH₂), 4.46 (s, 2H, -CH-), 4.48 (d, *J* = 2.4 Hz, 2H, =CH₂), 7.37 - 7.44 (m, 6H, aromatics), 7.60 - 7.67 (m, 6H, aromatics), 8.02 - 8.10 (m, 6H, aromatics), 8.15 (s, 4H, aromatics), 9.06 (s, 2H, NH); **¹³C-NMR** (126 MHz, CDCl₃): δ/ppm = 24.5 (2 -CH₂-), 25.8 (2 -CH₂-), 66.5 (2 -CH₂-), 67.2 (2 -CH₂-), 82.7 (2 -CH-), 89.7 (2 -CH₂-), 119.8 (2 -CH- aromatics), 120.1 (2 -CH- aromatics), 120.2 (2 -CH- aromatics), 120.5 (4 -CH- aromatics), 120.6 (2 -CH- aromatics), 126.6 (2 -CH- aromatics), 126.8 (2 -CH- aromatics), 126.9 (2 -CH- aromatics), 127.6 (2 -CH- aromatics), 128.2 (2 -CH- + 2 C aromatics), 128.5 (2 C aromatics), 128.6 (2 C aromatics), 129.3 (2 C aromatics), 131.0 (2 C aromatics), 131.1 (2 C aromatics), 131.6 (2 C aromatics), 132.1 (2 C aromatics), 134.7 (2 C aromatics), 156.5 (2 =C), 167.2 (2 C=O); **IR** (neat): $\tilde{\nu}/\text{cm}^{-1}$ 3401, 3377, 3052, 2914, 2873, 1689, 1627, 1591, 1535, 1501, 1387, 1293, 1095, 1030, 952, 829, 808, 767, 728, 690; **HR MS (ESI)** [M+H]⁺ *m/z* calculated for C₅₆H₄₇N₂O₆ 843.3429, observed 843.3423 (-0.6 ppm).

7.3.27 CSP-HPLC separation of polyether macrocycles⁸³

Compounds were resolved by chiral stationary phase HPLC using a semi-preparative CHIRALPAK® IG column. It is worth mentioning that it is necessary to remove traces of Et₂NH.HCl present in the separated compounds. The residue was thus dissolved in CH₂Cl₂, the organic phase was washed three times with H₂O, dried over anhydrous Na₂SO₄, filtered and concentrated under vacuum to afford the pure products. The separation data are summarized in **Table 7.1** and the optical rotation of the enantiopure fractions are collected in **Table 7.2**.

Table 7.1 Enantiomer separations by CSP HPLC: mobile phase, retention times and α

Entry	Compound	Mobile phase ^[a]	retention time (min)		α
			1 st eluted	2 nd eluted	
1	pyrene-18C6	7:3	13.57	21.84	1.81
2	pyrene-18C4	7:3	12.06	26.18	2.53
3	pyrene-16C4	8:2 ^[b]	9.40	34.93	6.22
4	perylene-18C6	9:1 ^[b]	13.36	51.37	5.32
5	perylene-18C4	8:2 ^[b]	6.07	12.95	3.41
6	perylene-16C4	8:2 ^[b]	9.97	55.46	7.71
7	fluorene-18C6	7:3	11.12	24.17	2.69
8	fluorene-18C4	7:3 ^[b]	7.55	16.07	3.80
9	fluorene-16C4	7:3 ^[b]	8.92	26.56	4.99
10	NMI-18C6	9:1	8.64	14.12	2.05

[a] CH₂Cl₂+0.1% Et₂NH/CH₃CN+0.1% Et₂NH, flow = 2 mL/min, 20 °C; [b] flow = 3 mL/min.

Selectivity factor (α) is calculated using the following formula: $\alpha = \frac{t_{r2}-t_0}{t_{r1}-t_0}$, where t_{r1}/t_{r2} are the retention time of the first and the second eluted enantiomer and t_0 is the dead time.

Table 7.2 Optical rotation of enantiopure compounds

Entry	Compound	First eluted enantiomer		Second eluted enantiomer	
		concentration (g/mL)	$[\alpha]_{\text{D}}^{20}$	concentration (g/mL)	$[\alpha]_{\text{D}}^{20}$
1	pyrene-18C6 ^[a]	$8.74 \cdot 10^{-6}$	-400	$6.03 \cdot 10^{-6}$	+365
2	pyrene-18C4 ^[b]	$1.6 \cdot 10^{-4}$	-275	$1.2 \cdot 10^{-4}$	+223
3	pyrene-16C4 ^[b]	$1.0 \cdot 10^{-4}$	-144	$1.3 \cdot 10^{-4}$	+112
4	perylene-18C6 ^[b]	$2.5 \cdot 10^{-4}$	-184	$2.0 \cdot 10^{-4}$	+163
5	perylene-18C4 ^[c]	$4.50 \cdot 10^{-5}$	+133	$3.47 \cdot 10^{-5}$	-98
6	perylene-16C4 ^[c]	$4.06 \cdot 10^{-6}$	+271	$6.63 \cdot 10^{-6}$	-316
7	fluorene-18C6 ^[b]	$7.0 \cdot 10^{-5}$	-37	$7.0 \cdot 10^{-5}$	+31
8	fluorene-18C4 ^[b]	$3.5 \cdot 10^{-4}$	-23	$2.5 \cdot 10^{-4}$	+20
9	fluorene-16C4 ^[b]	$1.2 \cdot 10^{-4}$	+17	$1.3 \cdot 10^{-4}$	-15
10	NMI-18C6 ^a	$1.40 \cdot 10^{-4}$	-64	$1.02 \cdot 10^{-4}$	+43

[a] in acetonitrile; [b] in CHCl₃; [c] in CH₂Cl₂.

7.4 Synthesis of crown ethers (aliphatic amines)

7.4.1 General procedure III (aliphatic-18C6)²⁰⁶

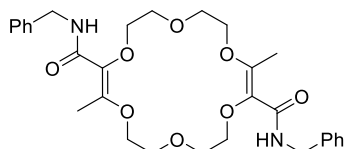
First step (aminolysis): In a 4 mL vial, 2 mL of dry THF are added to 101 mg (0.25 mmol, 1 equiv) of **18C6** and TBD (1,5,7-triazabicyclo[4.4.0]dec-5-ene, 2 or 4 equiv). The amine (1.00 mmol, 4 equiv) is added in one portion to the suspension and the mixture is stirred at 60 °C for 15 hours. The conversion is followed by TLC analysis (SiO₂, CH₂Cl₂/MeOH (10%)) and LR-ESI-MS (soft positive mode, CH₂Cl₂). The reaction is cooling down to 25 °C and purified. **Method D:** the product is purified by filtration on filtration funnel and washed with 3 mL of Et₂O. **Method E:** a drop of MeOH is added and directly purified by column chromatography (silica, EtOAc then CH₂Cl₂/MeOH gradient (5%, 10%)). The resulting oil is purified by selective precipitation (a minimum of EtOAc for solubility, followed by a large excess of pentane, 15 hours). The non-isomerized amide-18C6 compound is used without further purification in the second step.

Second step (transposition): Considering the non-isomerized amide-18C6 as pure, *t*-BuOK (2.2 equiv) is added in one portion to a suspension (or solution) of non-isomerized amide-18C6 in dry 1,4-dioxane (*c* = 0.1 M). The mixture is stirred at 25 °C for 15 hours. The conversion is followed by TLC analysis (SiO₂, CH₂Cl₂/MeOH, (10%), CMAS stain). The reaction is quenched with a drop of MeOH and directly purified by column chromatography (neutral Al₂O₃, EtOAc then CH₂Cl₂/MeOH gradient (1%, 3%, 5%)). Finally, the resulting oil is purified by selective precipitation (a minimum of EtOAc for solubility, followed by a large excess of pentane, 15 hours) affording the desired **aliphatic-18C6** as a white solid.

²⁰⁶ The use of freshly neutralized CDCl₃ (filtration over basic alumina) was necessary for this series of compounds to avoid degradation of the crown ethers in the NMR tube during the analysis.

7.4.2 Reaction of aminolysis

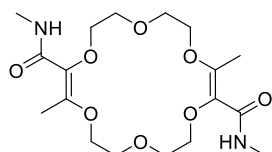
7.4.2.1 Synthesis of 2.1



According to general procedure **III** (first step only), with 101 mg (0.25 mmol) of **18C6**, 109 μ L (107 mg, 1.00 mmol, 4 equiv) of benzylamine and 69 mg (0.50 mmol, 2 equiv) of TBD to yield 104 mg (0.19 mmol, 554.64 g/mol, 75%) of **2.1** as a white solid. **Purification:** method D

m.p.: 173 °C – 174 °C; **$^1\text{H-NMR}$** (500 MHz, CDCl_3): δ/ppm = 2.47 (s, 6H, $-\text{CH}_3$), 3.74 - 3.77 (m, 8H, $-\text{CH}_2-$), 3.95 - 3.97 (m, 4H, $-\text{CH}_2-$), 4.05 - 4.07 (m, 4H, $-\text{CH}_2-$), 4.48 (s, 4H, $-\text{CH}_2-$), 6.99 - 7.01 (m, 2H, NH), 7.25 - 7.29 (m, 6H, aromatics), 7.31 - 7.34 (m, 4H, aromatics); **$^{13}\text{C-NMR}$** (126 MHz, CDCl_3): δ/ppm = 13.9 (2 $-\text{CH}_3$), 43.0 (2 $-\text{CH}_2-$), 67.3 (2 $-\text{CH}_2-$), 70.0 (2 $-\text{CH}_2-$), 70.5 (2 $-\text{CH}_2-$), 71.6 (2 $-\text{CH}_2-$), 127.4 (2 CH aromatic), 127.6 (4 CH aromatic), 128.8 (4 CH aromatic), 131.9 (2 =C), 138.9 (2 C aromatic), 153.7 (2 =C), 166.3 (2 C=O); **IR** (neat): $\tilde{\nu}/\text{cm}^{-1}$ 3347, 2934, 1646, 1607, 1503, 1453, 1421, 1371, 1303, 1259, 1205, 1161, 1129, 1098, 1058, 1031, 975, 929, 883, 847, 812, 768, 742, 698, 663, 608, 569; **HR MS (ESI)** $[\text{M}+\text{H}]^+$ m/z calculated for $\text{C}_{30}\text{H}_{39}\text{N}_2\text{O}_8$ 555.2701, observed 555.2710 (1.7 ppm).

7.4.2.2 Synthesis of 2.2

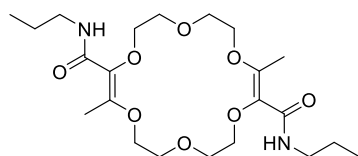


According to general procedure **III** (first step only), with 101 mg (0.25 mmol) of **18C6**, 500 μ L (2 M solution in THF, 0.99 mmol, 4 equiv) of methylamine, 69 mg (0.50 mmol, 2 equiv) of TBD and 1.5 mL of THF (total of 2 mL) to yield 53 mg (0.13 mmol, 402.44 g/mol, 53%) of **2.2** as a white solid. **Purification:** method D

R_f = 0.3 (SiO_2 , $\text{CH}_2\text{Cl}_2/\text{MeOH}$ (10%)); **m.p.:** 166 °C - 167 °C; **$^1\text{H-NMR}$** (500 MHz, CDCl_3): δ/ppm = 2.46 (s, 6H, $-\text{CH}_3$), 2.84 (d, 6H, J = 4.9 Hz, $-\text{CH}_3$), 3.79 - 3.81 (m, 8H, $-\text{CH}_2-$), 3.95 - 3.97 (m, 4H, $-\text{CH}_2-$), 4.08 - 4.10 (m, 4H, $-\text{CH}_2-$), 6.65 - 6.65 (m, 2H, NH); **$^{13}\text{C-NMR}$** (126 MHz, CDCl_3): δ/ppm = 13.8 (2 $-\text{CH}_3$), 26.0 (2 $-\text{CH}_3$), 67.3 (2 $-\text{CH}_2-$), 70.1 (2 $-\text{CH}_2-$), 70.6 (2 $-\text{CH}_2-$), 71.6 (2 $-\text{CH}_2-$), 132.2 (2 =C), 153.1

(2 =C), 166.1 (2 C=O); **IR** (neat): $\tilde{\nu}/\text{cm}^{-1}$ 3371, 2944, 2923, 2882, 1654, 1612, 1513, 1450, 1374, 1308, 1256, 1232, 1168, 1131, 1101, 1057, 1033, 978, 931, 891, 855, 810, 793, 775, 696, 665, 615, 575; **HR MS (ESI)** $[M+H]^+$ m/z calculated for $\text{C}_{18}\text{H}_{31}\text{N}_2\text{O}_8$ 403.2075, observed 403.2072 (-0.8 ppm).

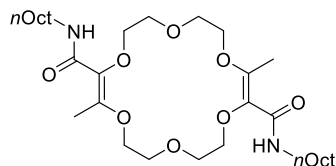
7.4.2.3 Synthesis of 2.3



According to general procedure III (first step only), with 101 mg (0.25 mmol) of **18C6**, 81 μL (59 mg, 1.00 mmol, 4 equiv) of *n*-propylamine and 69 mg (0.50 mmol, 2 equiv) of TBD to yield 68 mg (0.15 mmol, 458.55 g/mol, 59%) of **2.3** as a white solid. **Purification**: method E

R_f = 0.4 (SiO_2 , $\text{CH}_2\text{Cl}_2/\text{MeOH}$ (10%)); **m.p.**: 130 °C – 131 °C; **$^1\text{H-NMR}$** (500 MHz, CDCl_3): δ/ppm = 0.93 (t, 6H, J = 7.4 Hz, -CH₃), 1.54 (dq, 4H, J = 14.6, 7.4 Hz, -CH₂-), 2.46 (s, 6H, -CH₃), 3.22 - 3.26 (m, 4H, -CH₂-), 3.80 - 3.82 (m, 8H, -CH₂-), 3.96 (t, 4H, J = 5.3 Hz, -CH₂-), 4.08 - 4.10 (m, 4H, -CH₂-), 6.96 - 6.72 (m, 2H, NH); **$^{13}\text{C-NMR}$** (126 MHz, CDCl_3): δ/ppm = 11.6 (2 -CH₃), 13.9 (2 -CH₃), 23.2 (2 -CH₂-), 40.7 (-CH₂-), 40.8 (-CH₂-), 67.3 (2 -CH₂-), 70.1 (2 -CH₂-), 70.6 (2 -CH₂-), 71.6 (2 -CH₂-), 132.3 (2 =C), 153.2 (2 =C), 165.4 (2 C=O); **IR** (neat): $\tilde{\nu}/\text{cm}^{-1}$ 3345, 2927, 2870, 1650, 1612, 1506, 1460, 1372, 1305, 1259, 1235, 1166, 1127, 1063, 1036, 978, 935, 915, 884, 812, 790, 773, 708, 674, 621, 573, 547; **HR MS (ESI)** $[M+H]^+$ m/z calculated for $\text{C}_{22}\text{H}_{39}\text{N}_2\text{O}_8$ 459.2701, observed 459.2698 (-0.7 ppm).

7.4.2.4 Synthesis of 2.4

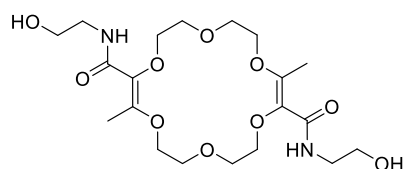


According to general procedure III (first step only), with 101 mg (0.25 mmol) of **18C6**, 164 μL (128 mg, 1.00 mmol, 4 equiv) of *n*-octylamine and 69 mg (0.50 mmol, 2 equiv) of TBD to yield 97 mg (0.16 mmol, 598.82 g/mol, 65%) of **2.4** as a white solid. **Purification**: method E

R_f = 0.6 (SiO_2 , $\text{CH}_2\text{Cl}_2/\text{MeOH}$ (10%)); **m.p.**: 129 °C – 131 °C; **$^1\text{H-NMR}$** (500 MHz, CDCl_3): δ/ppm = 0.87 (t, 6H, J = 6.9 Hz, -CH₃), 1.24 - 1.32 (m, 20H, -CH₂-), 1.49 - 1.52 (m, 4H, -CH₂-), 2.45 (s, 6H, -

CH₃), 3.24 - 3.28 (m, 4H, -CH₂-), 3.79 - 3.82 (m, 8H, -CH₂-), 3.95 (t, 4H, *J* = 5.3 Hz, -CH₂-), 4.08 - 4.10 (m, 4H, -CH₂-), 6.67 - 6.69 (m, 2H, NH); ¹³C-NMR (126 MHz, CDCl₃): δ/ppm = 13.9 (2 -CH₃), 14.3 (2 -CH₃), 22.8 (2 -CH₂-), 27.2 (2 -CH₂-), 29.4 (2 -CH₂-), 29.4 (2 -CH₂-), 29.9 (2 -CH₂-), 31.9 (2 -CH₂-), 39.2 (2 -CH₂-), 67.3 (2 -CH₂-), 70.1 (2 -CH₂-), 70.6 (2 -CH₂-), 71.6 (2 -CH₂-), 132.3 (2 =C), 153.1 (2 =C), 165.3 (2 C=O); IR (neat): $\tilde{\nu}$ /cm⁻¹ 3342, 2921, 2851, 1650, 1613, 1508, 1464, 1425, 1372, 1305, 1260, 1237, 1166, 1128, 1096, 1066, 1037, 978, 947, 934, 897, 877, 811, 773, 716, 675, 622, 576, 547, 521; HR MS (ESI) [M+H]⁺ *m/z* calculated for C₃₂H₅₉N₂O₈ 599.4266, observed 599.4291 (4.3 ppm).

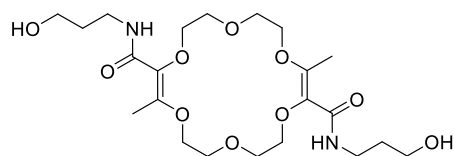
7.4.2.5 Synthesis of 2.5



According to general procedure III (first step only), with 101 mg (0.25 mmol) of **18C6**, 60 μ L (60 mg, 1.00 mmol, 4 equiv) of ethanolamine and 69 mg (0.50 mmol, 2 equiv) of TBD to yield 88 mg (0.20 mmol, 452.50 g/mol, 78%) of **2.3** as a white solid. **Purification:** method D

m.p.: 137 °C – 139 °C; ¹H-NMR (500 MHz, CDCl₃): δ/ppm = 2.44 (s, 6H, -CH₃), 3.43 - 3.45 (m, 4H, -CH₂-), 3.70 - 3.72 (m, 4H, -CH₂-), 3.79 - 3.83 (m, 8H, -CH₂-), 3.96 - 3.98 (m, 4H, -CH₂-), 4.10 - 4.11 (m, 4H, -CH₂-) (N-H not seen); ¹³C-NMR (126 MHz, CDCl₃): δ/ppm = 13.9 (2 -CH₃), 42.3 (2 -CH₂-), 63.0 (2 -CH₂-), 67.4 (2 -CH₂-), 70.1 (2 -CH₂-), 70.6 (2 -CH₂-), 71.6 (2 -CH₂-), 131.9 (2 =C), 153.9 (2 =C), 166.8 (2 C=O); IR (neat): $\tilde{\nu}$ /cm⁻¹ 3349, 2950, 2881, 1662, 1605, 1506, 1456, 1431, 1378, 1361, 1306, 1264, 1234, 1165, 1128, 1057, 1030, 980, 934, 891, 810, 769, 689, 628, 558; HR MS (ESI) [M+H]⁺ *m/z* calculated for C₂₀H₃₅N₂O₁₀ 463.2286, observed 463.2295 (1.8 ppm).

7.4.2.6 Synthesis of 2.6

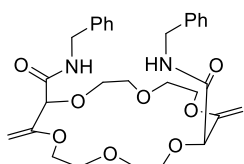


According to general procedure III (first step only), with 101 mg (0.25 mmol) of **18C6**, 76 μ L (74 mg, 1.00 mmol, 4 equiv) of propanolamine and 69 mg (0.50 mmol, 2 equiv) of TBD to yield 80 mg (0.16 mmol, 490.55 g/mol, 65%) of **2.3** as a white solid. **Purification:** method D

m.p.: 123 °C – 124 °C; **¹H-NMR** (500 MHz, CDCl₃): δ/ppm = 1.67 (p, 4H, *J* = 5.8 Hz, -CH₂-), 2.45 (s, 6H, -CH₃), 3.43 - 3.46 (m, 4H, -CH₂-), 3.57 - 3.60 (m, 4H, -CH₂-), 3.79 - 3.82 (m, 8H, -CH₂-), 3.95 (t, 4H, *J* = 5.3 Hz, -CH₂-), 4.09 - 4.11 (m, 4H, -CH₂-) (N-H not seen); **¹³C-NMR** (126 MHz, CDCl₃): δ/ppm = 13.9 (2 -CH₃), 32.8 (2 -CH₂-), 35.3 (2 -CH₂-), 58.9 (2 -CH₂-), 67.3 (2 -CH₂-), 70.1 (2 -CH₂-), 70.6 (2 -CH₂-), 71.6 (2 -CH₂-), 131.6 (2 =C), 154.0 (2 =C), 166.6 (2 C=O); **IR** (neat): $\tilde{\nu}/\text{cm}^{-1}$ 3481, 3427, 2948, 2882, 1656, 1611, 1509, 1457, 1376, 1305, 1265, 1234, 1163, 1129, 1069, 1049, 1029, 978, 938, 906, 810, 790, 685, 623; **HR MS (ESI)** [M+H]⁺ *m/z* calculated for C₂₂H₃₉N₂O₈ 491.2599, observed 491.2603 (0.8 ppm).

7.4.3 Linear aliphatic amides macrocycle synthesis

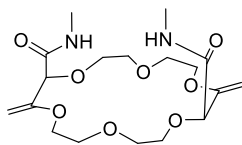
7.4.3.1 Synthesis of *Bn-18C6*



According to general procedure III, with 101 mg (0.25 mmol) of **18C6**, 109 μL (107 mg, 1.00 mmol, 4 equiv) of benzylamine and 69 mg (0.50 mmol, 2 equiv) of TBD to yield 75 mg (0.14 mmol, 554.64 g/mol, 59%) of **Bn-18C6** as a white solid. **Purification:** method D.

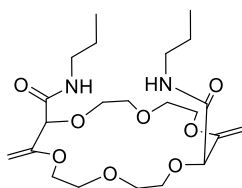
R_f = 0.5 (SiO₂, CH₂Cl₂/MeOH (10%)); **m.p.:** 122 °C – 123 °C; **¹H-NMR** (500 MHz, CDCl₃): δ/ppm = 3.49 - 3.53 (m, 2H, -CH₂-), 3.56 - 3.60 (m, 4H, -CH₂-), 3.62 - 3.75 (m, 8H, -CH₂-), 3.78 - 3.82 (m, 2H, -CH₂-), 4.10 (dd, 2H, *J* = 15.0, 5.3 Hz, benzylic), 4.19 (d, 2H, 2.7 Hz, =CH₂), 4.30 (s, 2H, -CH-), 4.35 (d, 2H, 2.7 Hz, =CH₂), 4.53 (dd, 2H, *J* = 15, 6.9 Hz, benzylic), 7.20 - 7.23 (m, 6H, aromatics), 7.26 - 7.29 (m, 4H, aromatics), 7.50 (m, 2H, NH); **¹³C-NMR** (126 MHz, CDCl₃): δ/ppm = 42.8 8 (2 -CH₂-), 67.5 (2 -CH₂-), 68.2 (2 -CH₂-), 68.9 (2 -CH₂-), 70.7 (2 -CH₂-), 82.1 (2 -CH-), 87.8 (2 =CH₂), 127.2 (2 CH aromatic), 127.7 (4 CH aromatic), 128.8 (4 CH aromatic), 138.8 (2 C aromatic), 157.1 (2 =CH), 169.1 (2 C=O); **IR** (neat): $\tilde{\nu}/\text{cm}^{-1}$ 3333, 3262, 3031, 2921, 2882, 1658, 1525, 1454, 1430, 1348, 1294, 1259, 1240, 1116, 1089, 1071, 1024, 993, 961, 937, 887, 827, 778, 734, 696, 621; **HR MS (ESI)** [M+H]⁺ *m/z* calculated for C₃₀H₃₉N₂O₈ 555.2701, observed 555.2686 (-2.6 ppm).

7.4.3.2 Synthesis of Me-18C6



According to general procedure III, with 100 mg (0.25 mmol) of **18C6**, 500 μ L (2 M solution in THF, 0.99 mmol, 4 equiv) of methylamine, 69 mg (0.50 mmol, 2 equiv) of TBD and 1.5 mL of THF (total of 2 mL) to yield 46 mg (0.12 mmol, 402.44 g/mol, 46%) of **Me-18C6** as a white solid. **Purification:** method D.

R_f = 0.3 (SiO₂, CH₂Cl₂/MeOH (10%)); **m.p.**: 141 °C - 142 °C; **¹H-NMR** (500 MHz, CDCl₃): δ /ppm = 2.81 (d, 6H, J = 4.9 Hz, -CH₃), 3.53 - 3.57 (m, 2H, -CH₂-), 3.68 - 3.72 (m, 6H, -CH₂-), 3.76 - 3.80 (m, 4H, -CH₂-), 3.84 - 3.93 (m, 4H, -CH₂-), 4.22 (d, 2H, J = 2.8 Hz, =CH₂), 4.29 (s, 2H, CH), 4.37 (d, 2H, J = 2.7 Hz, =CH₂), 7.34 - 7.36 (m, 2H, NH); **¹³C-NMR** (126 MHz, CDCl₃): δ /ppm = 26.0 (2 -CH₃), 67.6 (2 -CH₂-), 68.6 (2 -CH₂-), 69.0 (2 -CH₂-), 70.5 (2 -CH₂-), 82.3 (2 -CH-), 87.6 (2 =CH₂), 157.3 (2 =C), 169.7 (2 C=O); **IR** (neat): $\tilde{\nu}$ /cm⁻¹ 3518, 3276, 3097, 2911, 2881, 1661, 1639, 1545, 1454, 1405, 1362, 1280, 1241, 1130, 1097, 1071, 1005, 944, 842, 783, 753, 677, 622, 572; **HR MS (ESI)** [M+H]⁺ m/z calculated for C₁₈H₃₁N₂O₈ 403.2075, observed 403.2073 (-0.5 ppm).

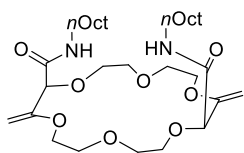
7.4.3.3 Synthesis of ⁿPr-18C6

According to general procedure III, with 101 mg (0.25 mmol) of **18C6**, 81 μ L (59 mg, 1.00 mmol, 4 equiv) of *n*-propylamine and 69 mg (0.50 mmol, 2 equiv) of TBD to yield 48 mg (0.11 mmol, 458.55 g/mol, 42%) of **ⁿPr-18C6** as a white solid. **Purification:** method E.

R_f = 0.4 (SiO₂, CH₂Cl₂/MeOH (10%)); **m.p.**: 134 °C - 136 °C; **¹H-NMR** (500 MHz, CDCl₃): δ /ppm = 0.93 (t, 6H, J = 7.4 Hz, -CH₃), 1.55 (hd, 4H, J = 7.3, 1.5 Hz, -CH₂-), 3.20 (dq, 2H, J = 13.1, 6.9 Hz, -CH₂-), 3.29 (dq, 2H, J = 13.4, 7.0 Hz, -CH₂-), 3.51 - 3.61 (m, 2H, -CH₂-), 3.64 - 3.83 (m, 12H, -CH₂-), 3.87 - 3.91 (m, 2H, -CH₂-), 4.21 (d, 2H, J = 2.7 Hz, =CH₂), 4.27 (s, 2H, -CH-), 4.36 (d, 2H, J = 2.7 Hz, =CH₂), 7.37 (t, 2H, J = 5.7 Hz, NH); **¹³C-NMR** (126 MHz, CDCl₃): δ /ppm = 11.6 (2 -CH₃), 22.9 (2 -CH₂-), 41.0 (2 -CH₂-), 67.4 (2 -CH₂-), 68.4 (2 -CH₂-), 69.1 (2 -CH₂-), 70.7 (2 -CH₂-), 82.4 (2 =CH₂), 87.5 (2 -CH-), 157.3 (2 =C), 169.0 (2 C=O); **IR** (neat): $\tilde{\nu}$ /cm⁻¹ 3304, 2961, 2933, 2874, 1678, 1656, 1636, 1527, 1460, 1347, 1292, 1263, 1218, 1135, 1115, 1093, 1058, 1019, 988, 856, 826, 810, 783, 732,

672, 621, 566; **HR MS (ESI)** $[M+H]^+$ m/z calculated for $C_{22}H_{39}N_2O_8$ 459.2701, observed 459.2699 (-0.5 ppm).

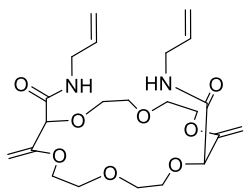
7.4.3.4 Synthesis of *n*Oct-18C6



According to general procedure III, with 101 mg (0.25 mmol) of **18C6**, 164 μ L (128 mg, 1.00 mmol, 4 equiv) of *n*-octylamine and 69 mg (0.50 mmol, 2 equiv) of TBD to yield 82 mg (0.14 mmol, 598.82 g/mol, 55%) of ***n*Oct-18C6** as a white solid. **Purification:** method E.

R_f = 0.5 (SiO₂, CH₂Cl₂/MeOH (10%)); **m.p.:** 115 °C - 116 °C; **¹H-NMR** (500 MHz, CDCl₃): δ /ppm = 0.88 (t, 6H, J = 6.8 Hz, -CH₃), 1.21 - 1.36 (m, 20H, -CH₂-), 1.51 (q, 4H, J = 7.1 Hz, -CH₂-), 3.19 - 3.33 (m, 4H, -CH₂-), 3.55 - 3.59 (m, 2H, -CH₂-), 3.84 - 3.65 (m, 12H, -CH₂-), 3.87 - 3.91 (m, 2H, -CH₂-), 4.20 (d, 2H, J = 2.7 Hz, =CH₂), 4.28 (s, 2H, -CH-), 4.35 (d, 2H, J = 2.7 Hz, =CH₂), H₂O and NH signals not detected; **¹³C-NMR** (126 MHz, CDCl₃): δ /ppm = 14.3 (2 -CH₃), 22.8 (2 -CH₂-), 27.1 (2 -CH₂-), 29.4 (2 -CH₂-), 29.5 (2 -CH₂-), 29.7 (2 -CH₂-), 32.0 (2 -CH₂-), 39.3 (2 -CH₂-), 67.5 (2 -CH₂-), 68.4 (2 -CH₂-), 69.1 (2 -CH₂-), 70.7 (2 -CH₂-), 82.2 (2 =CH₂), 87.3 (2 -CH-), 157.5 (2 =C), 168.9 (2 C=O); **IR** (neat): $\tilde{\nu}$ /cm⁻¹ 3315, 2921, 2853, 1679, 1657, 1635, 1528, 1464, 1432, 1374, 1348, 1298, 1258, 1222, 1153, 1135, 1117, 1089, 1057, 1021, 988, 938, 922, 858, 826, 804, 722, 669, 621, 572; **HR MS (ESI)** $[M+H]^+$ m/z calculated for $C_{32}H_{58}N_2O_8$ 599.4266, observed 599.4272 (1.0 ppm).

7.4.3.5 Synthesis of allyl-18C6

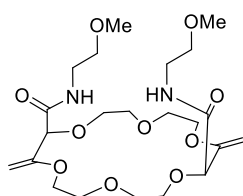


According to general procedure III, with 101 mg (0.25 mmol) of **18C6**, 74 μ L (57 mg, 1.00 mmol, 4 equiv) of allyl-amine and 69 mg (0.50 mmol, 2 equiv) of TBD to yield 50 mg (0.11 mmol, 454.52 g/mol, 44%) of **allyl-18C6** as a white solid. **Purification:** method E.

R_f = 0.5 (SiO₂, CH₂Cl₂/MeOH (10%)); **m.p.:** 126 °C - 128 °C; **¹H-NMR** (500 MHz, CDCl₃): δ /ppm = 3.54 - 3.58 (m, 2H, -CH₂-), 3.64 - 3.91 (m, 16H, -CH₂-), 3.94 - 4.00 (m, 2H, -CH₂-), 4.22 (d, 2H, J = 2.7 Hz, =CH₂), 4.30 (s, 2H, -CH-), 4.36 (d, 2H, J = 2.7 Hz, =CH₂), 5.10 (dq, 2H, J = 10.3, 1.4 Hz, =CH₂),

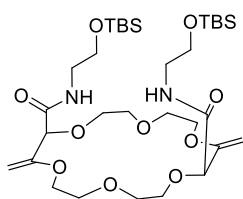
5.24 (dq, 2H, $J = 17.2, 1.6$ Hz, =CH₂), 5.85 (ddt, 2H, $J = 17.1, 10.5, 5.3$, =CH-), 7.41 - 7.43 (m, 2H, NH); **¹³C-NMR** (126 MHz, CDCl₃): δ /ppm = 41.6 (2 -CH₂-), 67.4 (2 -CH₂-), 68.3 (2 -CH₂-), 69.0 (2 -CH₂-), 70.7 (2 -CH₂-), 82.3 (2 -CH-), 87.8 (2 =CH₂), 115.9 (2 =CH₂), 134.5 (2 =CH-), 157.1 (2 =C), 169.0 (2 C=O); **IR** (neat): $\tilde{\nu}$ /cm⁻¹ 3300, 1917, 2878, 1680, 1657, 1639, 1520, 1463, 1418, 1345, 1292, 1266, 1221, 1135, 1114, 1097, 1056, 1021, 988. 959, 922, 854, 825, 800, 781, 742, 674, 653, 617, 558; **HR MS (ESI)** [M+H]⁺ m/z calculated for C₂₂H₃₅N₂O₈ 455.2388, observed 455.2390 (0.4 ppm).

7.4.3.6 Synthesis of MeO-ethyl-18C6



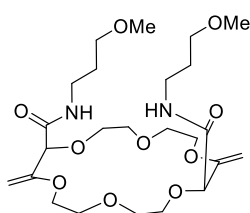
According to general procedure **III**, with 101 mg (0.25 mmol) of **18C6**, 87 μ L (75 mg, 1.00 mmol, 4 equiv) of 2-methoxyethylamine and 69 mg (0.50 mmol, 2 equiv) of TBD to yield 66 mg (0.14 mmol, 490.25 g/mol, 54%) of **MeO-ethyl-18C6** as a white solid. **Purification**: method E.

R_f = 0.4 (SiO₂, CH₂Cl₂/MeOH (10%)); **m.p.**: 109 °C - 110 °C; **¹H-NMR** (500 MHz, CDCl₃): δ /ppm = 3.34 (s, 6H, -CH₃), 3.43 - 3.53 (m, 8H, -CH₂-), 3.54 - 3.58 (m, 2H, -CH₂-), 3.67 - 3.80 (m, 10H, -CH₂-), 3.83 - 3.91 (m, 2H, -CH₂-), 4.23 (d, 2H, $J = 2.6$ Hz, =CH₂), 4.27 (s, 2H, -CH-), 4.34 (d, 2H, $J = 2.6$ Hz, =CH₂), 7.44 (s, 2H, NH); **¹³C-NMR** (126 MHz, CDCl₃): δ /ppm = 39.0 (2 -CH₂-), 58.8 (2 -CH₃), 67.9 (2 -CH₂-), 68.3 (2 -CH₂-), 69.1 (2 -CH₂-), 70.7 (2 -CH₂-), 71.2 (2 -CH₂-), 82.2 (2 =CH₂), 87.8 (2 -CH-), 157.2 (2 =C), 169.3 (2 C=O); **IR** (neat): $\tilde{\nu}$ /cm⁻¹ 3308, 2936, 2882, 2820, 1658, 1635, 1528, 1457, 1347, 1320, 1296, 1264, 1221, 1132, 1117, 1089, 1057, 1021, 988, 961, 945, 924, 882, 858, 826, 805, 738, 673, 622, 568; **HR MS (ESI)** [M+H]⁺ m/z calculated for C₂₂H₃₉N₂O₁₀ 491.2599, observed 491.2612 (2.6 ppm).

7.4.3.7 *Synthesis of TBSO-ethyl-18C6*

According to general procedure III, with 101 mg (0.25 mmol) of **18C6**, 175 mg (1.00 mmol, 4 equiv) of *tert*-butyl dimethylsilane ethanolamine²⁰⁷ and 69 mg (0.50 mmol, 2 equiv) of TBD to yield 60 mg (0.09 mmol, 691.02 g/mol, 35%) of **TBSO-ethyl-18C6** as a white solid. **Purification:** method E.

R_f = 0.54 (SiO₂, CH₂Cl₂/MeOH (10%)); **m.p.**: 100 °C - 101 °C; **¹H-NMR** (500 MHz, CDCl₃): δ/ppm = 0.06 (s, 12H, -CH₃), 0.89 (s, 18H, -CH₃), 3.28 - 3.34 (m, 2H, -CH₂-), 3.47 - 3.53 (m, 2H, -CH₂-), 3.57 - 3.61 (m, 2H, -CH₂-), 3.68 - 3.79 (m, 14H, -CH₂-), 3.83 - 3.90 (m, 4H, -CH₂-), 4.22 (d, 2H, *J* = 2.7 Hz, =CH₂), 4.28 (s, 2H, -CH-), 4.32 (d, 2H, *J* = 2.7 Hz, =CH₂), 7.33 (t, 2H, *J* = 5.7 Hz, NH); **¹³C-NMR** (126 MHz, CDCl₃): δ/ppm = -5.2 (2 -CH₃), -5.2 (2 -CH₃), 18.4 (2 C), 26.0 (6 -CH₃), 41.5 (2 -CH₂-), 61.9 (2 -CH₂-), 67.7 (2 -CH₂-), 68.6 (2 -CH₂-), 69.1 (2 -CH₂-), 70.6 (2 -CH₂-), 82.1 (2 -CH-), 87.4 (2 =CH₂), 157.6 (2 =C), 169.1 (2 C=O); **IR** (neat): $\tilde{\nu}$ /cm⁻¹ 3306, 2936, 2860, 1678, 2657, 1638, 1526, 1467, 1298, 1253, 1223, 1133, 1097, 1057, 1021, 940, 834, 775, 665, 622; **HR MS (ESI)** [M+H]⁺ *m/z* calculated for C₃₂H₆₃N₂O₁₀Si₂ 691.4016, observed 691.4016 (0.0 ppm).

7.4.3.8 *Synthesis of MeO-propyl-18C6*

According to general procedure III, with 101 mg (0.25 mmol) of **18C6**, 102 μ L (89 mg, 1.00 mmol, 4 equiv) of 3-methoxypropylamine and 69 mg (0.50 mmol, 2 equiv) of TBD to yield 70 mg (0.14 mmol, 518.60 g/mol, 54%) of **MeO-propyl-18C6** as a white solid. **Purification:** method E.

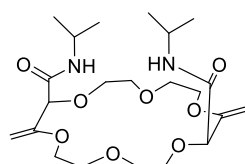
R_f = 0.4 (SiO₂, CH₂Cl₂/MeOH (10%)); **m.p.**: 99 °C - 100 °C; **¹H-NMR** (500 MHz, CDCl₃): δ/ppm = 1.81 (p, 4H, *J* = 6.5 Hz, -CH₂-), 3.32 (s, 6H, -CH₃), 3.33 - 3.41 (m, 4H, -CH₂-), 3.44 (t, 4H, *J* = 6.3 Hz, -CH₂-), 3.53 - 3.57 (m, 2H, -CH₂-), 3.66 - 3.84 (m, 12H, -CH₂-), 3.87 - 3.91 (m, 2H, -CH₂-), 4.21 (d, 2H, *J* = 2.6 Hz, =CH₂), 4.25 (s, 2H, -CH-), 4.34 (d, 2H, *J* = 2.6 Hz, =CH₂), 7.55 - 7.57 (m, 2H, NH); **¹³C-NMR** (126 MHz, CDCl₃): δ/ppm = 29.5 (2 -CH₂-), 36.9 (2 -CH₂-), 58.8 (2 -CH₃), 67.5 (2 -CH₂-), 68.4 (2 -CH₂-), 69.1 (2 -CH₂-), 70.7 (2 -CH₂-), 70.9 (2 -CH₂-), 82.4 (2 -CH-), 87.7 (2 =CH₂), 157.3 (2 =C), 169.1

²⁰⁷ Inman, M.; Moody, C. J., *Eur. J. Org. Chem.* **2013**, 2013, 2179-2187.

(2 C=O); **IR** (neat): $\tilde{\nu}/\text{cm}^{-1}$ 3296, 2932, 2874, 1678, 1656, 1639, 1518, 1454, 1397, 1370, 1349, 1298, 1258, 1222, 1194, 1114, 1085, 1057, 1021, 991, 942, 856, 824, 790, 739, 683, 621, 574; **HR MS (ESI)** $[M+H]^+$ m/z calculated for $\text{C}_{24}\text{H}_{43}\text{N}_2\text{O}_{10}$ 519.2912, observed 519.2927 (2.8 ppm).

7.4.4 α -Branched aliphatic amides macrocycle synthesis

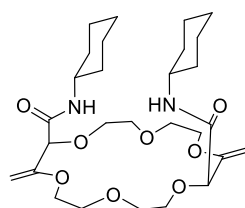
7.4.4.1 Synthesis of *i*Pr-18C6



According to general procedure III, with 101 mg (0.25 mmol) of **18C6**, 86 μL (59 mg, 1.00 mmol, 4 equiv) of isopropylamine and 138 mg (1.00 mmol, 4 equiv) of TBD to yield 34 mg (0.07 mmol, 458.55 g/mol, 29%) of *i*Pr-**18C6** as a white solid. **Purification:** method D.

R_f = 0.3 (SiO_2 , $\text{CH}_2\text{Cl}_2/\text{MeOH}$ (10%)); **m.p.:** 101 °C - 107 °C; **$^1\text{H-NMR}$** (500 MHz, CDCl_3): δ/ppm = 1.17 (d, 6H, J = 4.0 Hz, -CH₃), 1.18 (d, 6H, J = 4.0 Hz, -CH₃), 3.54 - 3.58 (m, 2H, -CH₂-), 3.64 - 3.81 (m, 12H, -CH₂-), 3.88 - 3.92 (m, 2H, -CH₂-), 4.10 - 4.17 (m, 2H, -CH-), 4.20 (d, 2H, J = 2.7 Hz, =CH₂), 4.21 (s, 2H, -CH-), 4.35 (d, 2H, J = 2.7 Hz, =CH₂), 7.20 - 7.22 (m, 2H, NH); **$^{13}\text{C-NMR}$** (126 MHz, CDCl_3): δ/ppm = 22.7 (2 -CH₃), 22.8 (2 -CH₃), 41.1 (2 -CH-), 67.3 (2 -CH₂-), 68.3 (2 -CH₂-), 69.2 (2 -CH₂-), 70.7 (2 -CH₂-), 82.3 (2 -CH-), 87.6 (2 =CH₂), 157.4 (2 =C), 168.1 (2 C=O); **IR** (neat): $\tilde{\nu}/\text{cm}^{-1}$ 3399, 3361, 2973, 2928, 2886, 1665, 1528, 1463, 1297, 1261, 1248, 1213, 1135, 1076, 1031, 994, 955, 887, 833, 811, 790, 679, 627, 584; **HR MS (ESI)** $[M+H]^+$ m/z calculated for $\text{C}_{22}\text{H}_{39}\text{N}_2\text{O}_8$ 459.2701, observed 459.2708 (1.5 ppm).

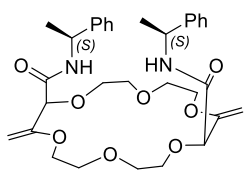
7.4.4.2 Synthesis of Cy-18C6



According to general procedure III, with 101 mg (0.25 mmol) of **18C6**, 115 μL (99 mg, 1.00 mmol, 4 equiv) of cyclohexylamine and 138 mg (1.00 mmol, 4 equiv) of TBD to yield 24 mg (0.05 mmol, 538.68 g/mol, 18 %) of **Cy-18C6** as a white solid. **Purification:** method D.

R_f = 0.3 (SiO₂, CH₂Cl₂/MeOH (10%)); **m.p.**: 131 °C - 133 °C; **¹H-NMR** (500 MHz, CDCl₃): δ /ppm = 1.10 - 1.27 (m, 6H, -CH₂-), 1.31 - 1.41 (m, 4H, -CH₂-), 1.61 - 1.65 (m, 2H, -CH₂-), 1.69 - 1.74 (m, 4H, -CH₂-), 1.88 - 1.92 (m, 4H, -CH₂-), 3.55 - 3.59 (m, 2H, -CH₂-), 3.64 - 3.91 (m, 16H, -CH₂-, -CH-), 4.19 (d, 2H, J = 2.7 Hz, =CH₂), 4.23 (s, 2H, -CH-), 4.34 (d, 2H, J = 2.7 Hz, =CH₂), 7.23 - 7.25 (m, 2H, NH); **¹³C-NMR** (126 MHz, CDCl₃): δ /ppm = 25.2 (4 -CH₂-), 25.7 (2 -CH₂-), 33.2 (4 -CH₂-), 48.1 (2 -CH-), 67.4 (2 -CH₂-), 68.3 (2 -CH₂-), 69.3 (2 -CH₂-), 70.8 (2 -CH₂-), 82.4 (2 -CH-), 87.3 (2 =CH₂), 157.5 (2 =C), 168.1 (2 C=O); **IR** (neat): $\tilde{\nu}$ /cm⁻¹ 3391, 3350, 3275, 2981, 2926, 2861, 1676, 1645, 1524, 1451, 1296, 1250, 1129, 1101, 1089, 1073, 1058, 1033, 990, 949, 860, 831, 808, 781, 748, 681, 623, 577; **HR MS (ESI)** [M+H]⁺ m/z calculated for C₂₈H₄₇N₂O₈ 539.3327, observed 539.3326 (-0.2 ppm).

7.4.4.3 Synthesis of (S)-Me-Bn-18C6



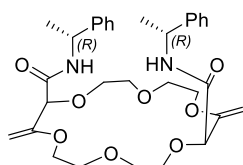
According to general procedure III, with 101 mg (0.25 mmol) of **18C6**, 129 μ L (121 mg, 1.00 mmol, 4 equiv) of (S)- α -methyl-benzylamine and 138 mg (1.00 mmol, 4 equiv) of TBD to yield 36 mg (0.06 mmol, 582.69 g/mol, 25%) of **(S)-Me-Bn-18C6** as a white solid and as an inseparable mixture of diastereoisomers (*dr* 1.3:1).

Purification: method E.

R_f = 0.46 and 0.43 (SiO₂, CH₂Cl₂/MeOH (10%)); **m.p.**: 116 °C - 117 °C; **¹H-NMR** (500 MHz, CDCl₃, inseparable mixture of diastereoisomers (*dr* 1.3:1)): δ /ppm = [1.41 (*minor*) and 1.43 (*major*) (d, 6H, J = 7.1 Hz, -CH₃)], 3.49 - 3.91 (m, 16H, -CH₂-), [4.15 (*minor*) and 4.20 (*major*) (d, 2H, 2.6 Hz, =CH₂)], [4.24 (*minor*) and 4.25 (*major*) (s, 2H, -CH-)], [4.31 (*minor*) and 4.36 (*major*) (d, 2H, 2.6 Hz, =CH₂)], 5.18 (p, 2H, J = 7.1 Hz, -CH-), 7.18 - 7.37 (m, 10H, aromatics), [7.78 (*major*) and 7.92 (*minor*) (d, 2H, J = 8.4 Hz, NH)]; **¹³C-NMR** (126 MHz, CDCl₃, inseparable mixture of diastereoisomers (*dr* 1.3:1)): δ /ppm = [22.0 (*major*) and 22.1 (*minor*) (2 -CH₃)], [48.2 (*minor*) and 48.4 (*major*) (2 -CH-)], [66.9 (*major*) and 67.0 (*minor*) (2 -CH₂-)], [68.2 (*minor*) and 68.4 (*major*) (2 -CH₂-)], [70.6 (*major*) and 70.6 (*minor*) (2 =CH₂)], [82.4 (*major*) and 83.0 (*minor*) (2 -CH-)], [87.4 (*major*) and 87.9 (*minor*) (2 =CH₂)], [126.5 (*minor*) and 126.6 (*major*) (4 CH aromatic)], [127.0 (*minor*) and 127.2 (*major*) (2 CH aromatic)], [128.4 (*minor*) and 128.5 (*major*) (4 CH aromatic)], [143.6 (*major*) and 144.0 (*minor*) (2 C aromatic)], [156.8 (*minor*) and 157.3 (*major*) (2 =C)], [168.1 (*minor*) and 168.3 (*major*) (2 C=O)]; **IR** (neat): $\tilde{\nu}$ /cm⁻¹ 3279, 3060, 3027, 2969, 2930, 2878, 1678, 1654, 1524,

1469, 1453, 1347, 1294, 1253, 1232, 1215, 1132, 1118, 1097, 1062, 1031, 988, 940, 824, 798, 760, 740, 696, 622, 560; **HR MS (ESI)** $[M+H]^+$ m/z calculated for $C_{32}H_{43}N_2O_8$ 583.3014, observed 583.3026 (2.0 ppm).

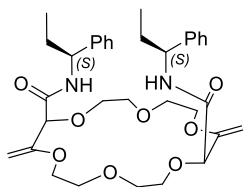
7.4.4.4 Synthesis of (R)-Me-Bn-18C6



According to general procedure **III**, with 101 mg (0.25 mmol) of **18C6**, 129 μ L (121 mg, 1.00 mmol, 4 equiv) of (R)- α -methyl-benzylamine and 138 mg (1.00 mmol, 4 equiv) of TBD to yield 36 mg (0.06 mmol, 582.69 g/mol, 25%) of **(R)-Me-Bn-18C6** as a white solid and as inseparable diastereoisomers (*dr*

1.3:1). **Purification:** method E.

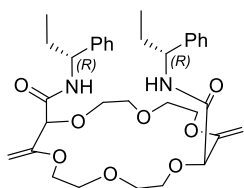
R_f = 0.46 and 0.43 (SiO_2 , $CH_2Cl_2/MeOH$ (10%)); **m.p.:** 118 °C - 119 °C; **1H -NMR** (500 MHz, $CDCl_3$, inseparable mixture of diastereoisomers (*dr* 1.3:1)): δ/ppm = [1.41 (*minor*) and 1.43 (*major*) (d, 6H, J = 7.1 Hz, $-CH_3$)], 3.50 - 3.91 (m, 16H, $-CH_2-$), [4.15 (*minor*) and 4.20 (*major*) (d, 2H, 2.7 Hz, $=CH_2$)], [4.24 (*minor*) and 4.26 (*major*) (s, 2H, $-CH-$)], [4.31 (*minor*) and 4.37 (*major*) (d, 2H, 2.7 Hz, $=CH_2$)], 5.18 (p, 2H, J = 7.1 Hz, $-CH-$), 7.18 - 7.37 (m, 10H, aromatics), [7.71 (*major*) and 7.84 (*minor*) (d, 2H, J = 8.5 Hz, NH)]; **^{13}C -NMR** (126 MHz, $CDCl_3$, inseparable mixture of diastereoisomers (*dr* 1.3:1)): δ/ppm = [22.0 (*major*) and 22.1 (*minor*) (2 $-CH_3$)], [48.2 (*minor*) and 48.4 (*major*) (2 $-CH-$)], [67.0 (*major*) and 67.0 (*minor*) (2 CH_2-)], [68.2 (*minor*) and 68.4 (*major*) (2 CH_2-)], [69.1 (*major*) and 70.6 (*minor*) (2 $=CH_2-$)], [82.3 (*major*) and 82.9 (*minor*) (2 $-CH-$)], [87.4 (*major*) and 87.9 (*minor*) (2 $=CH_2$)], [126.4 (*minor*) and 126.6 (*major*) (4 CH aromatic)], [127.0 (*minor*) and 127.2 (*major*) (2 CH aromatic)], [128.5 (*minor*) and 128.6 (*major*) (4 CH aromatic)], [143.5 (*major*) and 144.0 (*minor*) (2 C aromatic)], [156.9 (*minor*) and 157.4 (*major*) (2 =C)], [168.1 (*minor*) and 168.3 (*major*) (2 C=O)]; **IR** (neat): $\tilde{\nu}/cm^{-1}$ 3277, 3060, 3031, 2965, 2929, 2874, 1676, 1653, 1523, 1496, 1451, 1350, 1294, 1254, 1232, 1214, 1132, 1118, 1099, 1062, 1031, 987, 942, 827, 798, 760, 742, 696, 624, 561; **HR MS (ESI)** $[M+H]^+$ m/z calculated for $C_{32}H_{43}N_2O_8$ 583.3014, observed 583.3026 (1.6 ppm).

7.4.4.5 *Synthesis of (S)-Et-Bn-18C6*

According to general procedure III, with 101 mg (0.25 mmol) of **18C6**, 144 μL (135 mg, 1.00 mmol, 4 equiv) of (*S*)- α -ethyl-benzylamine and 138 mg (1.00 mmol, 4 equiv) of TBD to yield 23 mg (0.04 mmol, 610.75 g/mol, 15%) of **(S)-Et-Bn-18C6** as a white solid and as inseparable diastereoisomers (*dr*

1:1.1). **Purification:** method E.

R_f = 0.49 and 0.46 (SiO_2 , $\text{CH}_2\text{Cl}_2/\text{MeOH}$ (10%)); **m.p.:** 123 °C - 124 °C; **¹H-NMR** (500 MHz, CDCl_3 , inseparable mixture of diastereoisomers (*dr* 1:1.1)): δ/ppm = [0.90 (*major*) and 0.92 (*minor*) (t, 6H, J = 7.4 Hz, $-\text{CH}_3$)], 1.75 - 1.83 (m, 4H, $-\text{CH}_2$), 3.48 - 3.93 (m, 16H, $-\text{CH}_2-$), [4.12 (*major*) and 4.21 (*minor*) (d, 2H, 2.6 Hz, $=\text{CH}_2$)], [4.26 (*minor*) and 4.26 (*major*) (s, 2H, $-\text{CH}-$)], [4.29 (*major*) and 4.37 (*minor*) (d, 2H, 2.6 Hz, $=\text{CH}_2$)], 4.89 - 4.97 (m, 2H, $-\text{CH}-$), 7.18 - 7.37 (m, 10H, aromatics), [7.73 (*minor*) and 7.95 (*major*) (m, 2H, NH)]; **¹³C-NMR** (126 MHz, CDCl_3 , inseparable mixture of diastereoisomers (*dr* 1:1.1)): δ/ppm = [11.1 (*minor*) and 11.2 (*major*) (2 $-\text{CH}_3$)], [29.4 (*minor*) and 29.7 (*major*) (2 $-\text{CH}_2-$)], 54.6 (2 $-\text{CH}-$), [66.7 (*major*) and 66.9 (*minor*) (2 CH_2-)], [68.4 (*major*) and 68.5 (*minor*) (2 CH_2-)], 69.1 (2 CH_2-), [70.5 (*major*) and 70.6 (*minor*) (2 $=\text{CH}_2$)], [82.6 (*minor*) and 83.1 (*major*) (2 $-\text{CH}-$)], [87.3 (*minor*) and 87.7 (*major*) (2 $=\text{CH}_2$)], 126.9 (4 CH aromatic), [127.0 (*minor*) and 127.1 (*major*) (2 CH aromatic)], [128.4 (*minor*) and 128.5 (*major*) (4 CH aromatic)], [142.8 (*minor*) and 143.1 (*major*) (2 C aromatic)], [156.9 (*major*) and 157.3 (*minor*) (2 $=\text{C}$)], 168.5 (2 $\text{C}=\text{O}$); **IR** (neat): $\tilde{\nu}/\text{cm}^{-1}$ 3258, 2940, 2874, 1672, 1649, 1521, 1464, 1346, 1286, 1241, 1136, 1113, 1069, 1019, 987, 939, 822, 760, 700, 635, 567; **HR MS (ESI)** $[\text{M}+\text{H}]^+$ m/z calculated for $\text{C}_{34}\text{H}_{47}\text{N}_2\text{O}_8$ 611.3327, observed 611.3333 (0.9 ppm).

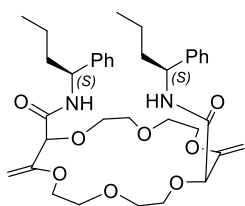
7.4.4.6 *Synthesis of (R)-Et-Bn-18C6*

According to general procedure III, with 101 mg (0.25 mmol) of **18C6**, 144 μL (135 mg, 1.00 mmol, 4 equiv) of (*R*)- α -ethyl-benzylamine and 138 mg (1.00 mmol, 4 equiv) of TBD to yield 23 mg (0.04 mmol, 610.75 g/mol, 15%) of **(R)-Et-Bn-18C6** as a white solid and as inseparable diastereoisomers (*dr* 1:1.1).

Purification: method E.

R_f = 0.49 and 0.46 (SiO_2 , $\text{CH}_2\text{Cl}_2/\text{MeOH}$ (10%)); **m.p.**: 124 °C - 125 °C; **$^1\text{H-NMR}$** (500 MHz, CDCl_3 , inseparable mixture of diastereoisomers (*dr* 1:1.1)): δ/ppm = [0.91 (*major*) and 0.93 (*minor*) (t, 6H, J = 7.4 Hz, $-\text{CH}_3$)], 1.75 - 1.86 (m, 4H, $-\text{CH}_2$), 3.45 - 3.96 (m, 16H, $-\text{CH}_2$ -), [4.12 (*major*) and 4.21 (*minor*) (d, 2H, 2.6 Hz, $=\text{CH}_2$)], 4.23 (s, 2H, $-\text{CH}$ -), [4.29 (*major*) and 4.37 (*minor*) (d, 2H, 2.6 Hz, $=\text{CH}_2$)], 4.89 - 4.97 (m, 2H, $-\text{CH}$ -), 7.17 - 7.40 (m, 10H, aromatics), [7.98 (*minor*) and 8.22 (*major*) (m, 2H, NH)]; **$^{13}\text{C-NMR}$** (126 MHz, CDCl_3 , inseparable mixture of diastereoisomers (*dr* 1:1.1)): δ/ppm = [11.2 (*minor*) and 11.2 (*major*) (2 $-\text{CH}_3$)], [29.5 (*minor*) and 29.8 (*major*) (2 $-\text{CH}_2$ -)], [54.7 (*major*) and 54.7 (*minor*) (2 $-\text{CH}$ -)], [66.4 (*major*) and 66.7 (*minor*) (2 $-\text{CH}_2$ -)], [68.3 (*major*) and 68.4 (*minor*) (2 $-\text{CH}_2$ -)], [69.2 (*major*) and 69.3 (*minor*) (2 $-\text{CH}_2$ -)], [70.5 (*major*) and 70.5 (*minor*) (2 $-\text{CH}_2$ -)], [83.0 (*minor*) and 83.5 (*major*) (2 $-\text{CH}$ -)], [87.6 (*minor*) and 87.8 (*major*) (2 $=\text{CH}_2$)], 126.9 (1 CH aromatic), [126.9 (*minor*) and 127.1 (*major*) (5 CH aromatic)], [128.3 (*major*) and 128.5 (*minor*) (4 CH aromatic)], [142.9 (*minor*) and 143.3 (*major*) (2 C aromatic)], [156.7 (*major*), and 157.1 (*minor*) (2 $=\text{C}$)], [168.5 (*major*) and 168.5 (*minor*) (2 $\text{C}=\text{O}$)]; **IR** (neat): $\tilde{\nu}/\text{cm}^{-1}$ 3553, 3285, 2965, 2924, 2878, 1668, 1639, 1535, 1496, 1457, 1376, 1294, 1244, 1207, 1095, 1079, 1054, 989, 928, 899, 834, 766, 705; **HR MS (ESI)** $[\text{M}+\text{H}]^+$ m/z calculated for $\text{C}_{34}\text{H}_{47}\text{N}_2\text{O}_8$ 611.3327, observed 611.3307 (-3.2 ppm).

7.4.4.7 Synthesis of (*S*)-Pr-Bn-18C6



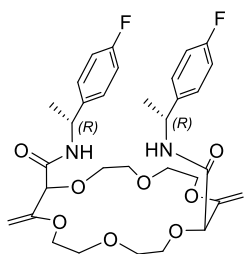
According to general procedure III, with 101 mg (0.25 mmol) of **18C6**, 161 μL (149 mg, 1.00 mmol, 4 equiv) of (*S*)- α -propyl-benzylamine and 138 mg (1.00 mmol, 4 equiv) of TBD to yield 6 mg (0.01 mmol, 638.80 g/mol, 4%) of **(S)-Pr-Bn-18C6** as a white solid and as inseparable diastereoisomers (*dr* 1:1).

Purification: method E.

R_f = 0.50 and 0.45 (SiO_2 , $\text{CH}_2\text{Cl}_2/\text{MeOH}$ (10%)); **m.p.**: 106 °C - 108 °C; **$^1\text{H-NMR}$** (500 MHz, CDCl_3 , inseparable mixture of diastereoisomers (*dr* 1:1)): δ/ppm [0.85 and 0.90 (t, 6H, J = 7.0 Hz, $-\text{CH}_3$)], 1.26 - 1.42 (m, 4H, $-\text{CH}_2$ -), 1.69 - 1.83 (m, 4H, $-\text{CH}_2$ -), 3.46 - 3.92 (m, 16H, $-\text{CH}_2$ -), [4.13 and 4.22 (d, 2H, 2.6 Hz, $=\text{CH}_2$)], 4.26 (s, 2H, $-\text{CH}$ -), [4.29 and 4.37 (d, 2H, 2.6 Hz, $=\text{CH}_2$)], 4.99 - 5.06 (m, 2H, $-\text{CH}$ -), 7.19 - 7.31 (m, 8H, aromatics), 7.35 - 7.38 (m, 2H, aromatics), [7.72 - 7.74 and 7.88 - 7.90 (m, 2H, NH)]; **$^{13}\text{C-NMR}$** (126 MHz, CDCl_3 , inseparable mixture of diastereoisomers (*dr* 1:1)): δ/ppm

= [13.9 and 14.1 (2 -CH₃)], [19.7 and 19.8 (2 -CH₂-)], [38.6 and 38.8 (2 -CH₂-)], 52.8 (2 -CH-), [66.8 and 67.1 (2 -CH₂-)], [68.3 and 68.4 (2 -CH₂-)], 69.2 (2 -CH₂-), [70.5 and 70.7 (2 -CH₂-)], [82.6 and 83.0 (2 -CH-)], [87.4 and 87.7 (2 =CH₂)], [126.9 and 127.0 (5 CH aromatic)], 127.1 (1 CH aromatic), [128.4 and 128.5 (4 CH aromatics)], [143.0 and 143.3 (2 C aromatics)], [157.0 and 157.3 (2 =C)], 168.4 (2 C=O); **IR** (neat): $\tilde{\nu}/\text{cm}^{-1}$ 3562, 3272, 2957, 2926, 2878, 1670, 1641, 15433, 1496, 1467, 1358, 1288, 1247, 1130, 1093, 1077, 995, 930, 838, 749, 700; **HR MS (ESI)** [M+H]⁺ *m/z* calculated for C₃₆H₅₁N₂O₈ 639.3640, observed 639.3639 (-0.1 ppm).

7.4.4.8 Synthesis of (R)-Me-pF-Bn-18C6

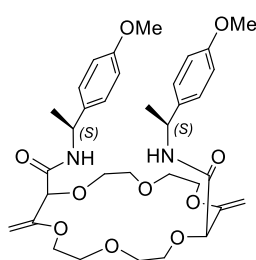


According to general procedure III, with 101 mg (0.25 mmol) of **18C6**, 133 μL (139 mg, 1.00 mmol, 4 equiv) of (*R*)- α -methyl-*p*-fluoro-benzylamine and 138 mg (1.00 mmol, 4 equiv) of TBD to yield 40 mg (0.07 mmol, 618.67 g/mol, 26%) of (*R*)-Me-pF-Bn-18C6 as a white solid and as inseparable diastereoisomers (*dr* 1.2:1). **Purification:** method E.

R_f = 0.49 and 0.46 (SiO₂, CH₂Cl₂/MeOH (10%)); **m.p.**: 128 °C - 1294 °C; **¹H-NMR** (500 MHz, CDCl₃, inseparable mixture of diastereoisomers (*dr* 1.2:1)): δ/ppm = 1.40 (d, 6H, *J* = 7.0 Hz, -CH₃), 3.51 - 3.92 (m, 16H, -CH₂-), [4.16 (*minor*) and 4.21 (*major*) (d, 2H, 2.7 Hz, =CH₂)], [4.23 (*minor*) and 4.25 (*major*) (s, 2H, -CH-)], [4.32 (*minor*) and 4.37 (*major*) (d, 2H, 2.7 Hz, =CH₂)], 5.15 (h, 2H, *J* = 7.0 Hz, -CH-), 6.90 - 6.97 (m, 4H, aromatics), 7.27 - 7.28 (m, 2H, aromatics), 7.33 - 7.35 (m, 2H, aromatics), [7.92 (*major*) and 8.01 (*minor*) (d, 2H, *J* = 8.5 Hz, NH)]; **¹³C-NMR** (126 MHz, CDCl₃, inseparable mixture of diastereoisomers (*dr* 1.2:1)): δ/ppm = [22.1 (*major*) and 22.2 (*minor*) (2 -CH₃)], [47.7 (*minor*) and 47.7 (*major*) (2 -CH-)], [66.7 (*minor*) and 66.7 (*major*) (2 -CH₂-)], [68.1 (*minor*) and 68.3 (*major*) (2 -CH₂-)], [69.2 (*minor*) and 69.2 (*major*) (2 -CH₂-)], [70.6 (*major*) and 70.6 (*minor*) (2 -CH₂-)], [82.6 (*major*) and 83.0 (*minor*) (2 -CH-)], [87.6 (*major*) and 88.1 (*minor*) (2 =CH₂)], [115.1 (*minor*) and 115.2 (*major*) (d, *J* = 21.2 Hz, 4 CH aromatic)], 128.1 (d, *J* = 8.0 Hz, 4 CH aromatic), [139.5 (*major*) and 139.9 (*minor*) (d, *J* = 3.2 Hz, 2 C aromatic)], [156.7 (2 =C, *minor*), 157.1 (2 =C, *major*)], [161.9 (*minor*) and 161.9 (*major*) (d, *J* = 244.0 Hz, 2 C-F aromatic)], [168.1 (*minor*) and 168.3 (*major*) (2 C=O)]; **¹⁹F-NMR** (282 MHz, CDCl₃, inseparable mixture of diastereoisomers (*dr* 1.3:1)) δ/ppm = [-115.6 (*minor*) and -115.3 (*major*)]; **IR** (neat): $\tilde{\nu}/\text{cm}^{-1}$ 3279, 2973, 2933, 2878,

1678, 1653, 1608, 1510, 1457, 1349, 1294, 1256, 1224, 1155, 1132, 1118, 1097, 1062, 1033, 1017, 987, 941, 856, 828, 794, 748, 721, 674, 623, 578; **HR MS (ESI)** $[M+H]^+$ m/z calculated for $C_{32}H_{41}F_2N_2O_8$ 619.2826, observed 619.2805 (-3.3 ppm).

7.4.4.9 Synthesis of (*S*)-Me-pMeO-Bn-18C6



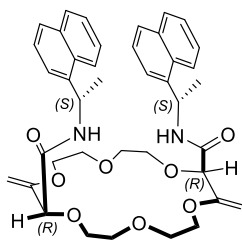
According to general procedure **III**, with 101 mg (0.25 mmol) of **18C6**, 151.21 μ L (151.21 mg, 1.00 mmol, 4 equiv) of (*S*)- α -methyl-*p*-methoxybenzylamine and 138 mg (1.00 mmol, 4 equiv) of TBD to yield 56 mg (0.09 mmol, 642.75 g/mol, 35%) of **(*S*)-Me-pMeO-Bn-18C6** as a white solid and as inseparable diastereoisomers (*dr* 1.2:1). **Purification:** method E.

R_f = 0.42 and 0.39 (SiO_2 , $CH_2Cl_2/MeOH$ (10%)); **m.p.:** 77 °C - 78 °C; **¹H-NMR** (500 MHz, $CDCl_3$, inseparable mixture of diastereoisomers (*dr* 1.3:1)): δ/ppm = 1.42 (d, 6H, J = 6.9 Hz, $-CH_3$), 3.49 - 3.82 (m, 20 H, $-CH_2-$ and $-OCH_3$), 3.87-3.91 (m, 2H, $-CH_2-$), [4.14 (*minor*) and 4.20 (*major*) (d, 2H, J = 2.7 Hz, $=CH_2$)], [4.22 (*minor*) and 4.23 (*major*) (s, 2H, $-CH-$)], [4.30 (*minor*) and 4.36 (*major*) (d, 2H, J = 2.7 Hz, $=CH_2$)], 5.10 - 5.16 (m, 2H, $-CH-$), 6.78 - 6.82 (m, 4H, aromatics), 7.23 - 7.30 (m, 4H, aromatics), [7.74 (*major*) and 7.87 (*minor*) (d, 2H, J = 8.6 Hz, NH)]; **¹³C-NMR** (126 MHz, $CDCl_3$, inseparable mixture of diastereoisomers (*dr* 1.3:1)): δ/ppm = [22.1 (*major*) and 22.1 (*minor*) (2 - CH_3)], [47.7 (*minor*) and 47.9 (*major*) (2 - $CH-$)], [55.4 (*major*) and 55.4 (*minor*) (2 - OCH_3)], 67.0 (2 - CH_2-), [68.2 (*minor*) and 68.4 (*major*) (2 - CH_2-)], [69.2 (*minor*) and 69.2 (*major*) (2 - CH_2-)], [70.6 (*major*) and 70.6 (*minor*) (2 - CH_2-)], [82.5 (*major*) and 83.0 (*minor*) (2 - $CH-$)], [87.5 (*major*) and 87.9 (*minor*) (2 $=CH_2$)], [113.9 (*minor*) and 113.9 (*major*) (4 CH aromatics)], [127.6 (*minor*) and 127.7 (*major*) (4 CH aromatics)], [135.8 (*major*) and 136.3 (*minor*) (2 C aromatics)], [156.9 (*minor*) and 157.3 (*major*) (2 $=C$)], [158.6 (*minor*) and 158.7 (*major*) (2 C-OMe aromatics)], [168.0 (*minor*) and 168.2 (*major*) (2 C=O)]; **IR** (neat): $\tilde{\nu}/cm^{-1}$ 3280, 2927, 1660, 1613, 1512, 1455, 1375, 1287, 1242, 1179, 1126, 1082, 1031, 994, 935, 829; **HR MS (ESI)** $[M+Na]^+$ m/z calculated for $C_{34}H_{47}N_2O_{10}Na$ 665.3045, observed 665.3019 (-3.9 ppm).

7.4.4.10 Synthesis of (S)-Me-1-naphth-18C6

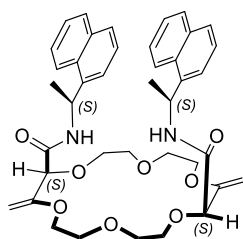
According to general procedure III, with 101 mg (0.25 mmol) of **18C6**, 160 μ L (171 mg, 1.00 mmol, 4 equiv) of (S)- α -methyl-1-naphthylamine and 138 mg (1.00 mmol, 4 equiv) of TBD to yield 34 mg (0.05 mmol, 682.81 g/mol, 20%) of **(S)-Me-1-naphth-18C6** as a white solid and as diastereoisomers (*dr* 1.4:1). **Purification:** method E.

Separation of the two diastereoisomers: On a 50 mg scale, the two diastereoisomers are separated by column chromatography (silica, CH₂Cl₂/MeOH gradient (1%, 2%, 3%, 4%, 5%, 6%, 7%, 8%, 9%, 10% and 20%)) followed by a column of each fractions (neutral Al₂O₃, EtOAc then CH₂Cl₂/MeOH gradient (1%, 3%)) and by a precipitation (a minimum of EtOAc for solubility, followed by a large excess of pentane, 15 hours).

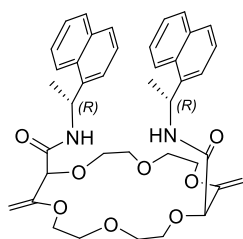
1st eluted diastereoisomer (minor diastereoisomer) (S)-Me-1-naphth-(R,R)-18C6

R_f (first eluted) = 0.49 (SiO₂, CH₂Cl₂/MeOH (10%)); **m.p.:** 117 °C - 118 °C; **¹H-NMR** (500 MHz, CDCl₃): δ /ppm = 1.62 (d, 6H, *J* = 6.9 Hz, -CH₃), 2.76 - 2.81 (m, 2H, -CH₂-), 3.18 - 3.22 (m, 2H, -CH₂-), 3.26 - 3.30 (m, 2H, -CH₂-), 3.32 - 3.39 (m, 6H, -CH₂-), 3.54 - 3.63 (m, 4H, -CH₂-), 4.05 (d, 2H, *J* = 2.7 Hz, =CH₂), 4.17 (s, 2H, -CH-), 4.25 (d, 2H, *J* = 2.7 Hz, =CH₂), 5.96 - 6.02 (m, 2H, -CH-),

7.34 - 7.37 (m, 2H, aromatics), 7.43 - 7.49 (m, 4H, aromatics), 7.55 - 7.57 (m, 2H, aromatics), 7.71 - 7.73 (m, 2H, aromatics), 7.81 - 7.83 (m, 2H, aromatics), 7.90 (d, 2H, *J* = 8.9 Hz, NH), 8.13 - 8.15 (m, 2H, aromatics); **¹³C-NMR** (126 MHz, CDCl₃): δ /ppm = 21.2 (2 -CH₃), 44.0 (2 -CH-), 66.9 (2 -CH₂-), 68.0 (2 -CH₂-), 68.6 (2 -CH₂-), 70.2 (2 -CH₂-), 82.9 (2 -CH-), 87.6 (2 =CH₂), 122.8 (2 CH aromatics), 124.1 (2 CH aromatics), 125.4 (2 CH aromatics), 125.7 (2 CH aromatics), 126.3 (2 CH aromatics), 128.0 (2 CH aromatics), 128.7 (2 CH aromatics), 131.4 (2 C aromatics), 134.0 (2 C aromatics), 139.1 (2 C aromatics), 156.6 (2 =C), 167.8 (2 C=O); **IR** (neat): $\tilde{\nu}$ /cm⁻¹ 3267, 2908, 1665, 1522, 1455, 1289, 1244, 1126, 1093, 1077, 994, 800, 779; **HR MS (ESI)** [M+H]⁺ *m/z* calculated for C₄₀H₄₇N₂O₈ 683.3327, observed 683.3314 (-1.9 ppm); $[\alpha]^{20}_D$ = -0.07 (c 0.07, CH₂Cl₂).

2nd eluted diastereoisomer (major diastereoisomer) (S)-Me-1-naphth-(S,S)-18C6

R_f (second eluted) = 0.43 (SiO₂, CH₂Cl₂/MeOH (10%)); **m.p.**: 154 °C - 155 °C; **¹H-NMR** (500 MHz, CDCl₃): δ/ppm = 1.57 (d, 6H, *J* = 6.8 Hz, -CH₃), 3.10 - 3.14 (m, 2H, -CH₂-), 3.20 - 3.24 (m, 2H, -CH₂-), 3.29 - 3.41 (m, 6H, -CH₂-), 3.45 - 3.52 (m, 4H, -CH₂-), 3.63 - 3.67 (m, 2H, -CH₂-), 4.16 (d, 2H *J* = 2.6 Hz, =CH₂), 4.26 (s, 2H, -CH-), 4.42 (d, 2H, *J* = 2.6 Hz, =CH₂), 5.95 - 6.01 (m, 2H, -CH-), 7.25 - 7.28 (m, 2H, aromatics), 7.41 - 7.48 (m, 8H, aromatics, NH), 7.68 - 7.69 (m, 2H, aromatics), 7.78 - 7.80 (m, 2H, aromatics), 8.07 - 8.09 (m, 2H, aromatics); **¹³C-NMR** (126 MHz, CDCl₃): δ/ppm = 20.9 (2 -CH₃), 44.1 (2 -CH-), 66.9 (2 -CH₂-), 68.1 (2 -CH₂-), 68.3 (2 -CH₂-), 70.2 (2 -CH₂-), 81.7 (2 -CH-), 86.49 (2 =CH₂), 123.1 (2 CH aromatics), 124.0 (2 CH aromatics), 125.3 (2 CH aromatics), 125.8 (2 CH aromatics), 126.4 (2 CH aromatics), 128.1 (2 CH aromatics), 128.7 (2 CH aromatics), 131.5 (2 C aromatics), 133.9 (2 C aromatics), 138.6 (2 C aromatics), 158.0 (2 =C), 168.2 (2 C=O); **IR** (neat): $\tilde{\nu}$ /cm⁻¹ 3328, 3039, 2936, 2883, 2845, 1665, 1645, 1537, 1522, 1455, 1288, 1250, 1209, 1150, 1124, 1082, 1000, 795, 773, 674, 662, 606; **HR MS (ESI)** [M+H]⁺ *m/z* calculated for C₄₀H₄₇N₂O₈ 683.3327, observed 683.3312 (-2.2 ppm); [α]_D²⁰ = -0.19 (c 0.07, CH₂Cl₂).

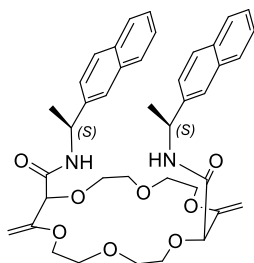
7.4.4.11 Synthesis of (R)-Me-1-naphth-18C6

According to general procedure **III**, with 101 mg (0.25 mmol) of **18C6**, 160 μL (171 mg, 1.00 mmol, 4 equiv) of (*R*)-α-methyl-1-naphthylamine and 138 mg (1.00 mmol, 4 equiv) of TBD to yield 34 mg (0.05 mmol, 682.81 g/mol, 20%) of **(R)-Me-1-naphth-18C6** as a white solid and as inseparable diastereoisomers (*dr* 1.4:1). **Purification**: method E.

R_f = 0.49 and 0.43 (SiO₂, CH₂Cl₂/MeOH (10%)); **m.p.**: 84 °C - 89 °C; **¹H-NMR** (500 MHz, CDCl₃, inseparable mixture of diastereoisomers (*dr* 1.4:1)): δ/ppm = 1.57 - 1.60 (t, 6H, -CH₃), [2.86 - 2.93 (minor) and 3.11 - 3.16 (*major*) (m, 2H, -CH₂-)], 3.22 - 3.69 (m, 15H, -CH₂-), [4.04 (*major*) and 4.17 (minor) (d, 2H, *J* = 2.7 Hz, =CH₂)], [4.18 (*major*) and 4.26 (minor) (s, 2H, -CH-)], [4.25 (*major*) and 4.42 (minor) (d, 2H, *J* = 2.7 Hz, =CH₂)], 5.95 - 6.01 (m, 2H, -CH-), [7.22 - 7.27 (*major*) and 7.30 - 7.34 (minor) (m, 2H, aromatics)], 7.41 - 7.49 (m, 8H, aromatics, NH), 7.67 - 7.71 (m, 2H, aromatics), 7.78 - 7.82 (m, 2H, aromatics), [8.08 (*major*) and 8.13 (minor) (d, 2H, *J* = 8.3 Hz,

aromatics)]; **¹³C-NMR** (126 MHz, CDCl₃, inseparable mixture of diastereoisomers (*dr* 1.4:1)): δ /ppm = [20.9 (*major*) and 21.1 (*minor*) (2 -CH₃)], [44.0 (*minor*) and 44.1 (*major*) (2 -CH-)], [66.8 (*major*) and 67.1 (*minor*) (2 -CH₂-)], [68.1 (*minor*) and 68.2 (*major*) (2 -CH₂-)], [68.3 (*major*) and 68.6 (*minor*) (2 -CH₂-)], 70.2 (2 -CH₂-), [81.8 (*major*) and 82.6 (*minor*) (2 -CH-)], [86.6 (*major*) and 87.5 (*minor*) (2 -CH-)], [122.7 (*minor*) and 123.1 (*major*) (2 CH aromatics)], [123.9 (*major*) and 124.1 (*minor*) (2 CH aromatics)], [125.3 (*major*) and 125.4 (*minor*) (2 CH aromatics)], 125.7 (2 CH aromatics), [126.3 (*minor*) and 126.4 (*major*) (2 CH aromatics)], 128.1 (2 CH aromatics), [128.7 (*major*) and 128.7 (*minor*) (2 CH aromatics)], [131.4 (*minor*) and 131.5 (*major*) (2 C aromatics)], [133.9 (*major*) and 140.0 (*minor*) (2 C aromatics)], [138.6 (*major*) and 139.0 (*minor*) (2 C aromatics)], [156.8 (*minor*) and 157.9 (*major*) (2 =C)], [167.8 (*minor*) and 168.1 (*major*) (2 C=O)]; **IR** (neat): $\tilde{\nu}$ /cm⁻¹ 3288, 2907, 1665, 1521, 1452, 1289, 1124, 1093, 1081, 994, 800, 779; **HR MS** (**ESI**) [M+H]⁺ *m/z* calculated for C₄₀H₄₇N₂O₈ 683.3327, observed 683.3320 (-1.0 ppm).

7.4.4.12 Synthesis of (*S*)-Me-2-naphth-18C6



According to general procedure **III**, with 101 mg (0.25 mmol) of **18C6**, 171 mg (1.00 mmol, 4 equiv) of (*S*)- α -methyl-2-naphthylamine and 138 mg (1.00 mmol, 4 equiv) of TBD to yield 25 mg (0.04 mmol, 682.81 g/mol, 15%) of **(*S*)-Me-2-naphth-18C6** as a white solid and as inseparable diastereoisomers (*dr* 1.4:1). **Purification**: method E.

R_f = 0.48 and 0.38 (SiO₂, CH₂Cl₂/MeOH (10%)); **m.p.**: 60 °C - 63 °C; **¹H-NMR** (500 MHz, CDCl₃, inseparable mixture of diastereoisomers (*dr* 1.4:1)): δ /ppm = 1.47 - 1.50 (m, 6H, -CH₃), 3.36 - 3.45 (m, 1H, -CH₂-), 3.50 - 3.80 (m, 14H, -CH₂-), 3.87 - 3.91 (m, 1H, -CH₂-), [4.11 (*minor*) and 4.20 (*major*) (d, 2H, *J* = 2.7 Hz, =CH₂)], [4.25 (*minor*) and 4.28 (*major*) (s, 2H, -CH-)], [4.30 (*minor*) and 4.38 (*major*) (d, 2H, *J* = 2.7 Hz, =CH₂)], 5.30 - 5.36 (m, 2H, -CH-), 7.40 - 7.47 (m, 6H, aromatics), 4.68 - 7.81 (m, 8H, aromatics), [7.92 - 7.94 (*major*) and 8.17 - 8.19 (*minor*) (m, 2H, NH)]; **¹³C-NMR** (126 MHz, CDCl₃, inseparable mixture of diastereoisomers (*dr* 1.4:1)): δ /ppm = [21.7 (*major*) and 22.1 (*minor*) (2 -CH₃)], [48.2 (*major*) and 48.5 (*minor*) (2 -CH-)], [66.8 (*minor*) and 66.8 (*major*) (2 -CH₂-)], [68.2 (*minor*) and 68.4 (*major*) (2 -CH₂-)], [69.1 (*minor*) and 69.2 (*major*) (2 -CH₂-)], 70.5 (2 -CH₂-), [82.5 (*major*) and 83.1 (*minor*) (2 -CH-)], [87.4 (*major*) and 87.8 (*minor*) (2 =CH₂)], 124.8

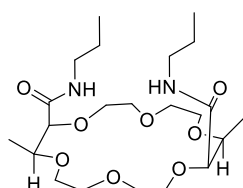
(2 CH aromatics), [125.3 (*major*) and 125.4 (*minor*) (2 CH aromatics)], [125.7 (*minor*) and 125.8 (*major*) (2 CH aromatics)], [126.1 (*minor*) and 126.1 (*major*) (2 CH aromatics)], [127.6 (*minor*) and 127.7 (*major*) (2 CH aromatics)], [128.0 (*major*) and 128.1 (*minor*) (2 CH aromatics)], [128.1 (*minor*) and 128.2 (*major*) (2 CH aromatics)], 132.7 (2 C aromatics), [133.4 (*major*) and 133.5 (*minor*) (2 C aromatics)], [141.0 (*major*) and 141.5 (*minor*) (2 C aromatics)], [156.8 (*minor*) and 157.4 (*major*) (2 =C)], [168.2 (*minor*) and 168.4 (*major*) (2 C=O)]; **IR** (neat): $\tilde{\nu}/\text{cm}^{-1}$ 3503, 3276, 3056, 2973, 2925, 2878, 1664, 1529, 1453, 1378, 1289, 1244, 1181, 1130, 1096, 1077, 993, 949, 895, 858, 821, 750; **HR MS (ESI)** $[\text{M}+\text{H}]^+$ m/z calculated for $\text{C}_{40}\text{H}_{47}\text{N}_2\text{O}_8$ 683.3327, observed 683.3327 (0.1 ppm).

7.4.5 Hydrogenation of aliphatic amides crown ethers

7.4.5.1 General procedure IV (4[H]-aliphatic-18C6)

In a 10 mL flask, to a stirred solution of the desired **aliphatic-18C6** (1 equiv) in dry THF was added 10% (w/w) of Pd/C (10% Pd, unreduced). The flask is flushed with H_2 and stirred under H_2 atmosphere (balloon, 1 atm.) for 3 hours. The conversion is followed by LR-ESI-MS (soft positive mode, CH_2Cl_2). The crude mixture is then filtrated (syringe filter) and the solvent is evaporated. The resulting oil is purified by selective precipitation (a minimum of Et_2O for solubility, followed by a large excess of pentane, 15 hours) affording the desired **4[H]-aliphatic-18C6** as a white solid.

7.4.5.2 Synthesis of 4[H]-ⁿPr-18C6

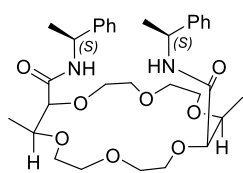


According to the general hydrogenation **IV**, procedure with 45.6 mg (0.1 mmol) of **ⁿPr-18C6** and 4.6 mg (10% w/w) of Pd/C (10% Pd, unreduced) yield 32 mg (0.07 mmol, 462.58 g/mol, 70%) of **4[H]-ⁿPr-18C6** as white needles.

R_f = 0.3 (SiO_2 , $\text{CH}_2\text{Cl}_2/\text{MeOH}$ (10%), magic stain (very weak spot)); **m.p.**: 83 °C - 84 °C; **¹H-NMR** (500 MHz, CDCl_3): δ/ppm = 0.92 (t, 6H, J = 7.4 Hz, $-\text{CH}_3$), 1.14 (d, 6H, J = 6.5 Hz, $-\text{CH}_3$), 1.53 (h, 4H, J = 7.4 Hz, $-\text{CH}_2-$), 3.16 - 3.29 (m, 4H, $-\text{CH}_2-$), 3.59 - 3.72 (m, 12H, $-\text{CH}_2-$), 3.77 - 3.81 (m, 2H, $-\text{CH}_2-$).

), 3.84 - 3.91 (m, 4H, -CH₂- and -CH-), 4.06 (d, J = 2.2 Hz, -CH-), 3.98 - 7.00 (m, 2H, NH); ¹³C-NMR (126 MHz, CDCl₃): δ /ppm = 11.6 (2 -CH₃), 14.8 (2 -CH₃), 23.0 (2 -CH₂-), 40.8 (2 -CH₂-), 69.1 (2 -CH₂-), 70.6 (2 -CH₂-), 70.7 (2 -CH₂-), 70.9 (2 -CH₂-), 77.5 (2 -CH-), 82.7 (2 -CH-), 170.3 (2 C=O); IR (neat): $\tilde{\nu}$ /cm⁻¹ 3289, 2968, 2935, 2911, 2874, 1648, 1527, 1481, 1463, 1442, 1381, 1346, 1302, 1279, 1233, 1141, 1112, 1090, 1075, 993, 977, 956, 942, 895, 839, 761, 734, 681, 632, 556; HR MS (ESI) [M+H]⁺ m/z calculated for C₂₂H₄₃N₂O₈ 463.3014, observed 463.3013 (-0.2 ppm).

7.4.5.3 Synthesis of 4[H]-(S)-Me-Bn-18C6

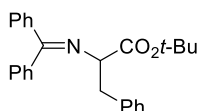


According to general hydrogenation procedure IV, 39.4 mg (0.067 mmol) of **(S)-Me-Bn-18C6** (*dr* 1.3:1) and 3.9 mg (10% w/w) of Pd/C (10% Pd, unreduced) yield 33 mg (0.056 mmol, 586.73 g/mol, 83%) of **4[H]-(S)-Me-Bn-18C6** as a white solid and as inseparable diastereoisomers (*dr* 1:1).

R_f = 0.4 (SiO₂, CH₂Cl₂/MeOH (10%), magic stain (very weak spot)); **m.p.**: 99 °C - 101 °C; ¹H-NMR (500 MHz, CDCl₃, inseparable mixture of diastereoisomers (*dr* 1:1)): δ /ppm = [1.04 and 1.14 (d, 3H, J = 6.5 Hz, -CH₃)], [1.47 and 1.48 (d, 3H, J = 4.4 Hz, -CH₃)], 3.43 - 3.46 (m, 1H, -CH₂), 3.52 - 3.70 (m, 11H, -CH₂-), 3.75 - 3.91 (m, 6H, -CH- and -CH₂), [4.10 and 4.11 (d, 2H, J = 2.2 Hz, -CH-)], 5.09 - 5.16 (m, 2H, -CH-), 7.21 - 7.37 (m, 12 H, aromatics and NH); ¹³C-NMR (126 MHz, CDCl₃, inseparable mixture of diastereoisomers (*dr* 1:1)): δ /ppm = 14.7 (2 -CH₃), [22.1 and 22.2 (2 -CH₃)], [48.2 and 48.3 (2 -CH-)], [68.9 and 69.1 (2 -CH₂-)], [70.7 and 70.9 (2 -CH₂-)], 70.8 (2 -CH₂-), [70.9 and 70.9 (2 -CH₂-)], [77.5 and 77.7 (2 -CH-)], [82.4 and 82.6 (2 -CH-)], [126.3 and 126.4 (4 CH aromatics)], [127.2 and 127.4 (2 CH aromatics)], [128.6 and 128.7 (4 CH aromatics)], [143.5 and 144.5 (2 C aromatics)], [169.5 and 169.6 (2 C=O)]; IR (neat): $\tilde{\nu}$ /cm⁻¹ 3310, 2986, 2912, 2868, 1643, 1521, 1455, 1380, 1340, 1305, 1248, 1203, 1113, 1091, 1071, 1038, 1008, 932, 871, 851, 792, 758, 724, 697, 659; HR MS (ESI) [M+H]⁺ m/z calculated for C₃₂H₄₇N₂O₈ 587.3327, observed 587.3320 (-1.1 ppm).

7.5 Phase transfer catalysis

7.5.1 Synthesis of **2.20**



Representative procedure: In a 1 mL vial, 3.4 mg (0.005 mmol, 10 mol%) of **(S)-Me-1-(S)-naphth-18C6** and 14.8 mg (0.05 mmol, 1 equiv.) of N-(diphenylmethylene)glycine *t*-butylester **2.18** are dissolved in 0.25 mL of CH₂Cl₂.

7.2 μ L (10.3 mg, 0.06 mmol, 1.2 equiv.) of benzylbromide **2.19** and 75 μ L of a freshly prepared solution of NaOH (aq. 50% w/v) are added consecutively. The solution is stirred for 15 hours at 10 °C at 1500 rpm. The consumption of **2.1** is monitored by TLC analysis. After completion of the reaction, the crude mixture is directly purified by column chromatography (SiO₂, pentane/Et₂O 9 :1) to yield 17 mg (0.043 mmol, 385.51 g/mol, 86%) of N-(diphenylmethylene)phenylalanine *t*-butylester **2.20** (enriched in **(R)-2.20**) as a colorless oil.

Spectral and physical data are in agreement with previously reported literature.²⁰⁸ **¹H NMR** (500 MHz, CDCl₃): δ /ppm = 1.44 (s, 9H, CH₃-), 3.14 - 3.25 (m, 2H, -CH₂-), 4.10 (dd, *J* = 9.3, 4.2 Hz, 1H, -CH₂-), 6.59 - 6.61 (m, 2H, aromatics), 7.04 - 7.06 (m, 2H, aromatics), 7.15 - 7.20 (m, 3H, aromatics), 7.26 - 7.38 (m, 6H, aromatics), 7.26 - 7.58 (m, 2H, aromatic); **¹³C NMR** (126 MHz, CDCl₃): δ /ppm = 28.2 (3 -CH₃), 39.7 (1 -CH₂-), 68.1 (1 -CH-), 81.3 (1 -CH-), 126.3 (1 CH aromatic), 127.8 (2 CH aromatic), 128.1 (2 CH aromatic), 128.19 (2 CH aromatic), 128.22 (2 CH aromatic), 128.3 (1 CH aromatic), 128.9 (2 CH aromatic), 130.0 (2 CH aromatic), 130.2 (1 CH aromatic), 136.5 (1 C aromatic), 138.5 (1 C aromatic), 139.7 (1 C aromatic), 170.5 (1 C=O), 171.0 (1 C=N); **CSP HPLC** (Chiralcel® OD-H column, hexanes/*i*-PrOH (99:1), 0.5 mL/min, 23 °C, 2 μ L/inj., λ = 254 nm): retention time, t_{R1} = (*R*) 12.2 min and t_{R2} = (*S*) 16.9 min.

²⁰⁸ Shi, Q.; Lee, Y.-J.; Kim, M.-J.; Park, M.-K.; Lee, K.; Song, H.; Cheng, M.; Jeong, B.-S.; Park, H.-g.; Jew, S.-s., *Tetrahedron Lett.* **2008**, 49, 1380-1383.

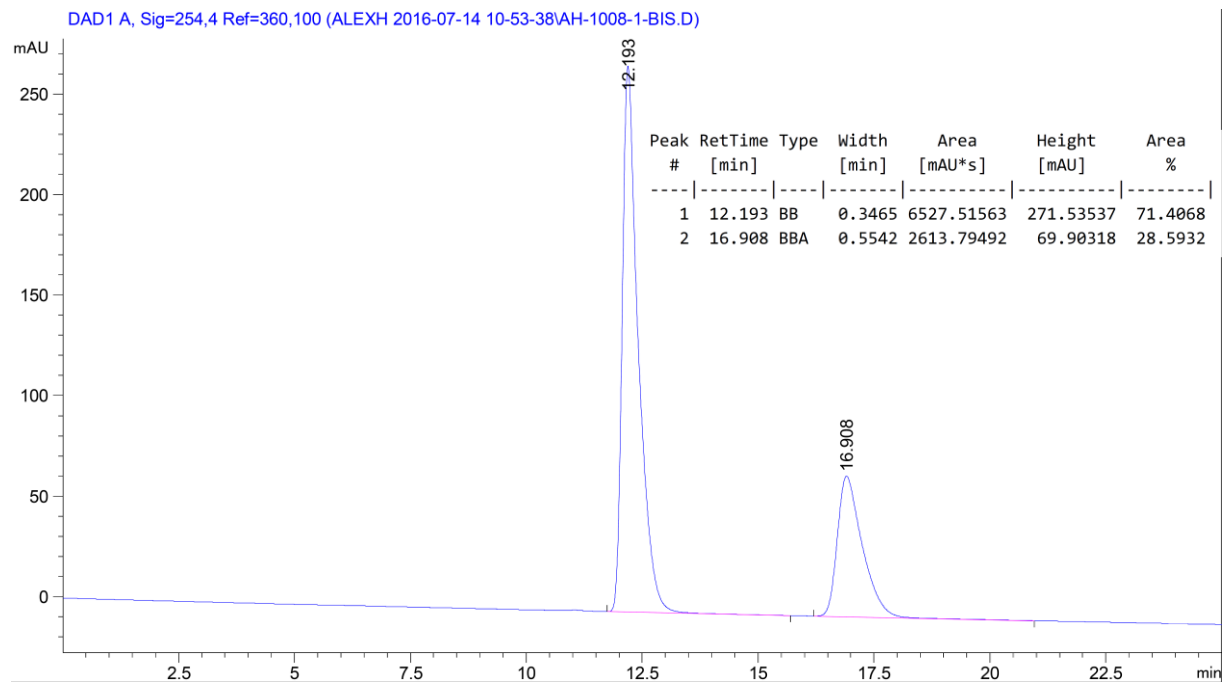


Figure 7.1 CSP HPLC of **2.20**: Chiralcel® OD-H column, hexanes/*i*-PrOH (99:1), 0.5 mL/min, 23 °C, 2 µL/inj., λ = 254 nm.

7.5.2 Screening of the solvent for the synthesis of 2.20

Table 7.3 Screening of the solvent for asymmetric PTC.

$ \begin{array}{c} \text{Ph} \\ \diagup \\ \text{C}=\text{N}-\text{CH}_2-\text{CO}_2t\text{-Bu} \\ \diagdown \\ \text{Ph} \end{array} + \begin{array}{c} \text{Br} \\ \\ \text{C}_6\text{H}_5-\text{CH}_2 \end{array} \xrightarrow[\text{solvent, } 10^\circ\text{C}]{\begin{array}{c} \text{(S)-Me-1-naphth-18C6} \\ (10 \text{ mol\%, } dr \text{ 1.4.1}) \\ \text{aq. NaOH (50\% w/v)} \\ (3:1 \text{ org/aq}) \end{array}} \begin{array}{c} \text{Ph} \\ \diagup \\ \text{C}=\text{N}-\text{C}^*-\text{CO}_2t\text{-Bu} \\ \diagdown \quad \\ \text{Ph} \quad \text{CH}_2-\text{Ph} \end{array} $				
	2.18	2.19		2.20
Entry	Solvent	Time	Conversion (%)	ee (%)
1	Chlorobenzene	36 hours	>99	31
2	Ethylacetate	1 month	86	n.d. ^[a]
3	CH ₃ CN	36 hours	>99	racemic
4	Hexanes	1 month	80	n.d.
5	1,1-Dichloroethane	2 days	>99	40
6	1,2-Dichloroethane	2 days	>99	33
7	Perchlorobuta-1,3-diene	15 hours	degradation	n.d.
8	1,1,2,2-Tetrachloroethane	15 hours	<1	n.d.
9	1,1,2,2-Tetrachloroethene	7 days	80	n.d.
10	1,1,1-Trichloroethane	2 days	>99	40
11	1,1,1-Trichlorotoluene	2 days	>99	31
12	Diiodomethane	7 days	>99	31
13	Perfluorohexane	7 days	<1	n.d.

[a] n.d. = not determined.

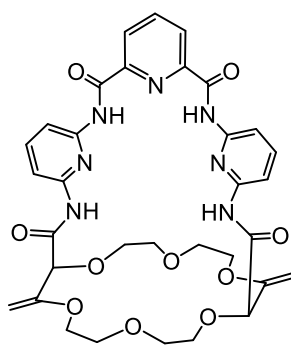
7.6 Synthesis of cryptands

All the cryptands from this section were synthesized by Dr. Sumit Kumar Ray.

7.6.1 General procedure V (cryptands)

In a 50 mL one neck flask, dry CH_2Cl_2 (20 mL) is added to 0.2 mmol (1 equiv) of ***m*-NH₂-pyr-18C6** or ***m*-NH₂-18C6** and 140 μL (103 mg, 0.8 mmol, 4 equiv) of *i*-Pr₂NEt. A solution of 0.4 mmol (2 equiv) of dichloride in 10 mL of dry THF is added through syringe pump over 5 hours under stirring. The reaction mixture is stirred for additional 3 hours. The conversion is followed by TLC analysis (EtOAc/MeOH (10%)). Upon completion, the reaction mixture is concentrated in vacuum and purified by column chromatography (solid deposit, EtOAc/MeOH (10%)). Finally, the resulting solid is purified by selective precipitation (dissolution in a minimal amount of CH_2Cl_2 (ca. 1 mL) required for solubility, followed by addition of a large excess of pentane, 15 hours) affording the desired cryptand.

7.6.2 Synthesis of pyr-cryptand

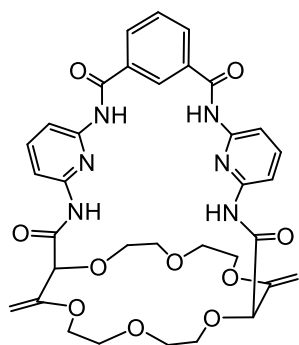


According to the general procedure **V**, 112 mg (0.2 mmol) of ***m*-NH₂-pyr-18C6** in 20 mL of dry THF, 140 μL (103 mg, 0.8 mmol, 4 equiv) of *i*-Pr₂NEt, 82 mg (0.4 mmol, 2 equiv) of 2,6-pyridinedicarbonyl dichloride in 10 mL of dry THF yielded **pyr-cryptand** (50%) as a white solid.

R_f = 0.5 (SiO₂, EtOAc/MeOH (10%)); **m.p.** 250 °C - 252 °C (crystallized from CH_2Cl_2 /MeOH); **¹H NMR** (500 MHz, CDCl_3): δ /ppm = 3.62 - 3.67 (m, 2H, -CH₂-), 3.72 - 3.92 (m, 12H, -CH₂-), 3.99 - 4.03 (m, 2H, -CH₂-), 4.32 (s, 2H, -CH-), 4.33 (d, *J* = 2.7 Hz, 2H, =CH₂), 4.43 (d, *J* = 2.7 Hz, 2H, =CH₂), 7.83 (t, *J* = 8.1 Hz, 2H, aromatics), 8.15 - 8.19 (m, 3H, aromatics), 8.33 (d, *J* = 8.1 Hz, 2H, aromatics), 8.58 (d, *J* = 7.8 Hz, 2H, aromatics), 9.09 (s, 2H, NH), 10.25 (s, 2H, NH); **¹³C NMR** (126 MHz, CDCl_3): δ /ppm = 68.5 (2 -CH₂-), 68.5 (2 -CH₂-), 69.1 (2 -CH₂-)

), 69.4 (2 -CH₂-), 83.5 (2 -CH-), 89.4 (2 =CH₂), 110.8 (2 CH aromatic), 111.2 (2 CH aromatic), 126.6 (2 CH aromatic), 139.5 (1 CH aromatic), 140.9 (2 CH aromatic), 148.9 (2 C aromatic), 149.5 (2 C aromatic), 149.6 (2 C aromatic), 155.9 (2 =C), 162.2 (2 C=O), 168.1 (2 C=O); **IR** (neat): $\tilde{\nu}/\text{cm}^{-1}$ = 3269, 2923, 2877, 1690, 1584, 1507, 1443, 1294, 1242, 1136, 1083, 992, 798, 680; **HR MS (ESI)** $[\text{M}+\text{H}]^+$ m/z calculated for C₃₃H₃₆N₇O₁₀ 690.2518, found 690.2521 (0.4 ppm). **X-ray** crystallized from CH₂Cl₂/MeOH.

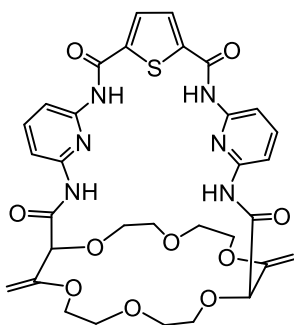
7.6.3 Synthesis of Ph-cryptand



According to the general procedure **V**, 112 mg (0.2 mmol) of *m*-NH₂-pyr-**18C6** in 20 mL of dry THF, 140 μL (103 mg, 0.8 mmol, 4 equiv) of *i*-Pr₂NEt, 81 mg (0.4 mmol, 2 equiv) of isophthaloyl dichloride in 10 mL of dry THF yielded **Ph-cryptand** (55%) as a white solid.

R_f = 0.6 (SiO₂, EtOAc/MeOH (10%)); **m.p.** 210 °C - 212 °C (crystallized from CH₂Cl₂/hexanes); **¹H NMR** (400 MHz, CDCl₃): δ/ppm = 3.64 - 3.78 (m, 12H, -CH₂-), 3.96 - 4.07 (m, 4H, -CH₂-), 4.28 (d, J = 2.7 Hz, 2H, =CH₂), 4.34 (s, 2H, -CH-), 4.44 (d, J = 2.7 Hz, 2H, =CH₂), 7.72 (t, J = 7.8 Hz, 1H, aromatics), 7.81 (t, J = 8.1 Hz, 2H, aromatics), 8.08 (d, J = 8.1 Hz, 2H, aromatics), 8.26 (d, J = 8.1 Hz, 2H, aromatics), 8.38 (dd, J = 7.8, 1.6 Hz, 2H, aromatics), 8.62 (s, 1H, aromatics), 9.20 (s, 2H, NH), 9.24 (s, 2H, NH). **¹³C NMR** (101 MHz, CDCl₃): δ/ppm = 66.5 (2 -CH₂-), 68.6 (2 -CH₂-), 69.2 (2 -CH₂-), 69.2 (2 -CH₂-), 84.0 (2 -CH-), 88.8 (2 =CH₂), 110.2 (2 CH aromatic), 110.3 (2 CH aromatic), 123.0 (1 CH aromatic), 130.3 (1 CH aromatic), 133.1 (2 CH aromatic), 133.9 (2 CH aromatic), 141.1 (2 CH aromatic), 149.5 (2 C aromatic), 150.2 (2 C aromatic), 156.0 (2 =C), 164.2 (2 C=O), 168.1 (2 C=O); **IR** (neat): $\tilde{\nu}/\text{cm}^{-1}$ = 3526, 3378, 2922, 2880, 1686, 1584, 1514, 1445, 1302, 1242, 1093, 986, 700, 709; **HR MS (ESI)** $[\text{M}+\text{H}]^+$ m/z calculated for C₃₄H₃₇N₆O₁₀ 689.2566, found 689.2566 (0.1 ppm).

7.6.4 Synthesis of thio-cryptand

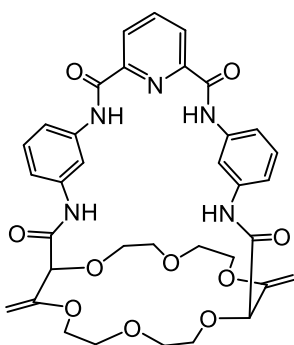


According to the general procedure **V**, 112 mg (0.2 mmol) of **m-NH₂-pyr-18C6** in 20 mL of dry THF, 140 μ L (103 mg, 0.8 mmol, 4 equiv) of *i*-Pr₂NEt, 84 mg (0.4 mmol, 2 equiv) of 2,5-thiophenedicarbonyl dichloride in 10 mL of dry THF yielded **thio-cryptand** (35%) as a white solid.

R_f = 0.5 (SiO₂, EtOAc/MeOH (10%)); **m.p.** 164 °C - 166 °C (crystallized from CH₂Cl₂/hexanes); **¹H NMR** (400 MHz, CDCl₃): δ /ppm = 3.58 - 3.63

(m, 2H, -CH₂-), 3.72 - 3.80 (m, 4H, -CH₂-), 3.84 - 3.98 (m, 10H, -CH₂-), 4.31 (d, *J* = 2.7 Hz, 2H, =CH₂), 4.39 (s, 2H, -CH-), 4.44 (d, *J* = 2.7 Hz, 2H, =CH₂), 7.75 - 7.82 (m, 4H, aromatics), 7.87 - 7.91 (m, 4H, aromatics), 8.36 (s, 2H, NH), 8.93 (s, 2H, NH); **¹³C NMR** (101 MHz, CDCl₃): δ /ppm = 67.5 (2 -CH₂-), 68.2 (2 -CH₂-), 69.5 (2 -CH₂-), 70.5 (2 -CH₂-), 82.5 (2 -CH-), 89.5 (2 -CH₂-), 108.6 (2 CH aromatic), 110.1 (2 CH aromatic), 133.2 (2 CH aromatic), 138.9 (2 C aromatic), 141.5 (2 CH aromatic), 148.9 (2 C aromatic), 149.2 (2 C aromatic), 155.9 (2 =C), 157.8 (2 C=O), 167.3 (2 C=O); **IR** (neat): $\tilde{\nu}$ /cm⁻¹ = 3376, 2933, 1694, 1581, 1515, 1447, 1303, 1234, 1073, 983, 799, 731; **HR MS (ESI)** [M+H]⁺ *m/z* calculated for C₃₂H₃₅N₆O₁₀S 695.2130, found 695.2148 (2.6 ppm).

7.6.5 Synthesis of pyr-Ph-cryptand



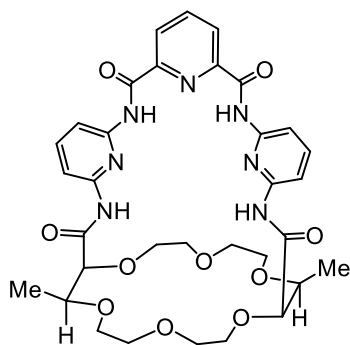
According to the general procedure **V**, 115 mg (0.2 mmol) of **m-NH₂-18C6** in 20 mL of dry THF, 140 μ L (103 mg, 0.8 mmol, 4 equiv) of *i*-Pr₂NEt, 82 mg (0.4 mmol, 2 equiv) of 2,6-pyridinedicarbonyl dichloride in 10 mL of dry THF yielded **pyr-Ph-cryptand** (48%) as a white solid.

R_f = 0.5 (SiO₂, EtOAc/MeOH (10%)); **m.p.** 195 °C - 197 °C (crystallized from CH₂Cl₂/pentane); **¹H NMR** (500 MHz, CDCl₃): δ /ppm = 3.48 - 3.51

(m, 2H, -CH₂-), 3.67 - 3.81 (m, 6H, -CH₂-), 3.91 - 4.09 (m, 6H, -CH₂-), 4.31 (d, *J* = 2.7 Hz, 2H, =CH₂), 4.34 (s, 2H, -CH-), 4.50 - 4.53 (m, 4H, =CH₂), 7.40 (t, *J* = 8.2 Hz, 2H, aromatics), 8.13 - 8.16 (m, 3H, aromatics), 8.35 (d, *J* = 6.4 Hz, 2H, aromatics), 8.44 (d, *J* = 7.6 Hz, 2H, aromatics), 8.56 (d, *J* = 7.6 Hz, 2H, aromatics), 9.78 (s, 2H, NH), 9.95 (s, 2H, NH); **¹³C NMR** (126 MHz, CDCl₃): δ /ppm = 67.3 (2

-CH₂-), 69.3 (2 -CH₂-), 69.4 (2 -CH₂-), 70.2 (2 -CH₂-), 84.0 (2 -CH-), 88.8 (2 -CH₂-), 111.4 (2 CH aromatic), 115.9 (2 CH aromatic), 116.0 (2 CH aromatic), 125.9 (2 CH aromatic), 129.9 (2 CH aromatic), 137.9 (2 C aromatic), 139.3 (2 C aromatic), 139.5 (1 CH aromatic), 149.1 (2 C aromatic), 155.4 (2 =C), 161.1 (2 C=O), 167.4 (2 C=O); **IR** (neat): $\tilde{\nu}/\text{cm}^{-1}$ = 3257, 2886, 1678, 1610, 1540, 1487, 1451, 1322, 1291, 1085, 996, 743, 684; **HR MS (ESI)** [M+NH₄]⁺ m/z calculated for C₃₅H₄₁N₆O₁₀ 705.2879, found 705.2902 (3.2 ppm).

7.6.6 Synthesis of 4[H]-pyr-cryptand

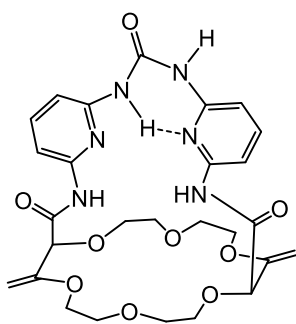


In 50 mL one neck flask, 142 mg (0.2 mmol) of ***m*-NH₂-pyr-18C6** is dissolved in 20 mL of dry THF and 28 mg of Pd/C (20% w/w, 10% Pd, unreduced) is added. The flask is flushed with H₂ and stirred under H₂ atmosphere (balloon, 1 atm.) for 2 hours. The suspension is filtered (syringe filter) and the solvent evaporated under vacuum. The resulting compound (*dr* 83:17) is purified by selective precipitation (solubilize in CH₂Cl₂ (ca. 1 mL) and precipitate in a large

excess of hexanes) affording **4[H]-pyr-cryptand** (95%) as a white solid (*dr* 93:7).

R_f = 0.2 (SiO₂, EtOAc/MeOH (10%)); **m.p.** 227 °C - 229 °C (crystallized from CH₂Cl₂/pentane); **¹H NMR** (500 MHz, CDCl₃, major diastereoisomer): δ/ppm = 1.31 (d, J = 6.5 Hz, 6H, -CH₃), 3.51 - 3.95 (m, 18H, -CH₂-, -CH-), 4.01 - 4.05 (m, 2H, -CH₂-), 7.82 (t, J = 8.1 Hz, 2H, aromatics), 8.12 - 8.17 (m, 3H, aromatics), 8.35 (d, J = 8.1, 2H, aromatics), 8.53 (d, J = 7.8 Hz, 2H, aromatics), 9.70 (s, 2H, NH), 11.20 (s, 2H, NH); **¹³C NMR** (125 MHz, CDCl₃, major diastereoisomer): δ/ppm = 15.6 (2 -CH₃), 65.7 (2 -CH₂-), 68.6 (2 -CH₂-), 70.1 (2 -CH₂-), 70.6 (2 -CH₂-), 75.6 (2 -CH-), 86.7 (2 -CH-), 110.8 (2 CH aromatic), 111.0 (2 CH aromatic), 126.1 (2 CH aromatic), 139.3 (2 CH aromatic), 140.8 (1 CH aromatic), 148.9 (2 C aromatic), 149.8 (2 C aromatic), 150.1 (2 C aromatic), 162.7 (2 C=O), 169.7 (2 C=O); **IR** (neat): $\tilde{\nu}/\text{cm}^{-1}$ = 3376, 2879, 1694, 1581, 1515, 1447, 1451, 1303, 1233, 1152, 833, 799, 731; **HR MS (ESI)** [M+H]⁺ m/z calculated for C₃₃H₄₀N₇O₁₀ 694.2831, found 694.2829 (-0.3 ppm).

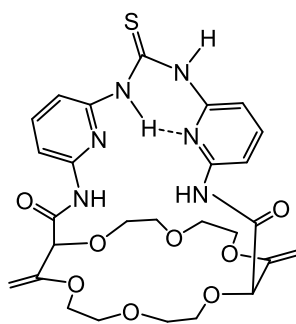
7.6.7 Synthesis of phos-cryptand



According to the general procedure **V**, 115 mg (0.2 mmol) of ***m*-NH₂-pyr-18C6** in 20 mL of dry THF, 280 μ L (206 mg, 1.6 mmol, 8 equiv) of *i*-Pr₂NEt, 30 mg (0.3 mmol, 1.5 equiv) of phosgene (20% solution in toluene) in 10 mL of dry CH₂Cl₂ (instead of THF) yielded **phos-cryptand** (60%) as a white solid. **Purification:** column (SiO₂) CH₂Cl₂/EtOAc/MeOH (47.5/47.5/5).

R_f = 0.3 (SiO₂, EtOAc/MeOH (10%)); **m.p.** 245 °C - 247 °C (crystallized from CH₂Cl₂/MeOH); **¹H NMR** (400 MHz, CDCl₃): δ /ppm = 3.49 - 3.57 (m, 2H, -CH₂-), 3.63 - 3.72 (m, 4H, -CH₂-), 3.75 - 4.03 (m, 9H, -CH₂-), 4.13 - 4.19 (m, 1H, -CH₂-), 4.28 (s, 1H, -CH-), 4.31 (d, *J* = 2.7 Hz, 1H, =CH₂), 4.35 (s, 1H, -CH-), 4.38 (d, *J* = 2.7 Hz, 1H, =CH₂), 4.41 (d, *J* = 2.7 Hz, 1H, =CH₂), 4.44 (d, *J* = 2.7 Hz, 1H, =CH₂), 6.53 (d, *J* = 7.9 Hz, 1H, aromatics), 7.68 (t, *J* = 8.1 Hz, 1H, aromatics), 7.75 (t, *J* = 8.1 Hz, 1H, aromatics), 7.86 (s, 1H, NH), 7.96 (d, *J* = 8.1 Hz, 1H, aromatics), 8.03 (dd, *J* = 8.1, 2.2 Hz, 2H, aromatics), 9.09 (s, 1H, NH), 9.32 (s, 1H, NH), 11.49 (s, 1H, NH); **¹³C NMR** (101 MHz, CDCl₃): δ /ppm = 67.3 (1 -CH₂-), 67.9 (1 -CH₂-), 68.9 (1 -CH₂-), 69.0 (1 -CH₂-), 69.3 (1 -CH₂-), 69.9 (1 -CH₂-), 70.2 (1 -CH₂-), 70.4 (1 -CH₂-), 82.7 (1 -CH-), 83.0 (1 -CH-), 89.2 (1 -CH-), 90.1 (1 -CH-), 107.5 (1 CH aromatic), 107.9 (1 CH aromatic), 108.8 (1 CH aromatic), 110.5 (1 CH aromatic), 140.8 (1 CH aromatic), 141.2 (1 CH aromatic), 148.6 (1 C aromatic), 149.3 (1 C aromatic), 150.5 (1 aromatic), 150.9 (1 aromatic), 152.7 (1 =C), 155.8 (1 =C), 155.9 (1 C=O), 167.7 (1 C=O), 167.8 (1 C=O); **IR** (neat): $\tilde{\nu}$ /cm⁻¹ = 3377, 3307, 2928, 2873, 1687, 1608, 1584, 1511, 1439, 1291, 1240, 1157, 1080, 988, 797, 796, 666; **HR MS (ESI)** [M+H]⁺ *m/z* calculated for C₂₇H₃₃N₆O₉ 585.2304, found 585.2301 (-0.5 ppm).

7.6.8 Synthesis of thiophos-cryptand

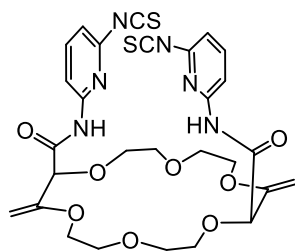


According to the general procedure **V**, 115 mg (0.2 mmol) of ***m*-NH₂-pyr-18C6** in 20 mL of dry THF, 280 μ L (206 mg, 1.6 mmol, 8 equiv) of *i*-Pr₂NEt, 18 μ L (28 mg, 0.24 mmol, 1.2 equiv) of thiophosgene in 2 mL of dry CH₂Cl₂ (instead of THF) yielded **thiophos-cryptand** (<5%) as a yellow solid. **Purification:** crude mixture is concentrated in vacuum and purified by preparative TLC (CH₂Cl₂/EtOAc/MeOH 47.5/47.5/5).

R_f = 0.3 (SiO₂, CH₂Cl₂/MeOH (5%)); **m.p.** 173 °C - 175 °C (crystallized from CH₂Cl₂/heptane); **¹H NMR** (400 MHz, CDCl₃): δ /ppm = 3.47 - 3.68 (m, 6H, -CH₂-), 3.72 - 4.01 (m, 9H, -CH₂-), 4.03 - 4.09 (m, 1H-CH₂-), 4.29 (s, 1H, -CH-), 4.33 (d, *J* = 2.7 Hz, 1H, =CH₂), 4.34 (s, 1H, -CH-), 4.39 (d, *J* = 2.7 Hz, 1H, =CH₂), 4.41 (d, *J* = 2.6 Hz, 1H, =CH₂), 4.43 (d, *J* = 2.7 Hz, 1H, =CH₂), 6.56 (d, *J* = 8.0 Hz, 1H, aromatics), 7.70 (t, *J* = 8.1 Hz, 1H, aromatics), 7.80 (t, *J* = 8.1 Hz, 1H, aromatics), 8.11 (d, *J* = 8.2 Hz, 1H, aromatics), 8.18 (d, *J* = 8.0 Hz, 1H, aromatics), 8.66 - 8.68 (m, 2H, aromatics), 9.09 (s, 1H, NH), 9.15 (s, 1H, NH), 13.07 (s, 1H, NH); **¹³C NMR** (101 MHz, CDCl₃): δ /ppm = 66.9 (1 -CH₂-), 68.2 (1 -CH₂-), 68.7 (1 -CH₂-), 68.9 (1 -CH₂-), 69.3 (2 -CH₂-), 70.1 (2 -CH₂-), 70.1 (2 -CH₂-), 82.5 (1 -CH-), 82.7 (1 -CH-), 89.5 (1 =CH₂), 90.3 (1 =CH₂), 108.1 (1 CH aromatic), 108.6 (1 CH aromatic), 110.6 (1 CH aromatic), 113.1 (1 CH aromatic), 140.1 (1 CH aromatic), 141.5 (1 CH aromatic), 148.3 (1 C aromatic), 149.5 (1 C aromatic), 150.5 (1 aromatic), 150.8 (1 aromatic), 155.8 (1 =C), 155.8 (1 =C), 167.7 (1 C=O), 167.8 (1 C=O), 177.1 (1 C=S); **IR** (neat): $\tilde{\nu}$ /cm⁻¹ = 3388, 2914, 2886, 1691, 1607, 1582, 1519, 1436, 1293, 1236, 1146, 1084, 989, 835, 796, 634, 542; **HR MS (ESI)** [M+H]⁺ *m/z* calculated for C₂₇H₃₃N₆O₈S 601.2075, found 601.2082 (0.6 ppm); **X-ray** crystallized from CH₂Cl₂/heptane.

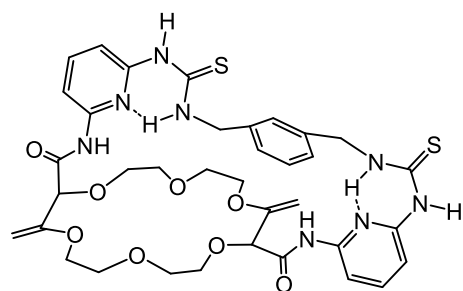
7.6.9 Synthesis of thiourea-cryptand

Thiourea-cryptand is synthesized in two steps from ***m*-NH₂-pyr-18C6**.



According to the general procedure **V**, 112 mg (0.2 mmol) of ***m*-NH₂-pyr-18C6** in 20 mL of dry THF, 168 μ L (124 mg, 0.96 mmol, 4.8 equiv) of *i*-Pr₂NEt, 37 μ L (55 mg, 0.48 mmol, 2.4 equiv) of thiophosgene in 10 mL of dry THF yielded ***m*-NCS-pyr-18C6** (60%) as a yellow solid.

R_f = 0.5 (SiO₂, EtOAc/MeOH (10%)); **m.p.** 142 °C - 145 °C (crystallized from CH₂Cl₂/hexanes); **¹H NMR** (400 MHz, CDCl₃): δ /ppm = 3.64 - 3.78 (m, 8H, -CH₂-), 3.83 - 3.97 (m, 6H, -CH₂-), 4.05 - 4.10 (m, 2H, -CH₂-), 4.34 (d, J = 2.7 Hz, 2H, =CH₂), 4.44 (d, J = 2.7 Hz, 2H, =CH₂), 4.50 (s, 2H, -CH-), 6.81 (dd, J = 7.7, 0.8 Hz, 2H, aromatics), 7.69 (t, J = 8.0 Hz, 2H, aromatics), 8.19 (dd, J = 8.4, 0.8 Hz, 2H, aromatics), 9.36 (s, 2H, NH); **¹³C NMR** (100 MHz, CDCl₃): δ /ppm = 67.9 (2 -CH₂-), 68.9 (2 -CH₂-), 69.0 (2 -CH₂-), 70.7 (2 -CH₂-), 81.7 (2 -CH-), 87.4 (2 =CH), 112.9 (2 CH aromatic), 115.4 (2 CH aromatic), 140.2 (2 C aromatic), 140.8 (2 CH aromatic), 144.0 (2 C aromatic), 151.1 (2 C aromatic), 157.1 (2 =C), 168.7 (2 C=O); **IR** (neat): $\tilde{\nu}$ /cm⁻¹ = 3360, 2904, 2061, 1707, 1695, 1572, 1524, 1441, 1396, 1286, 1118, 1087, 987, 800; **HR MS (ESI)** [M+H]⁺ m/z calculated for C₂₈H₃₁N₆O₈S₂ 643.1639, found 643.1633 (-1.0 ppm).



According to the general procedure **V**, 129 mg (0.2 mmol, 1 equiv) of ***m*-NCS-pyr-18C6** in 20 mL of dry THF, 70 μ L (51 mg, 0.4 mmol, 2 equiv) of *i*-Pr₂NEt, 53 μ L (54 mg, 0.4 mmol, 2 equiv) of *m*-xylylenediamine dichloride in 10 mL of dry CH₂Cl₂ (instead of THF) yielded **thiourea-cryptand** (90%) as a white solid.

R_f = 0.6 (SiO₂, EtOAc/MeOH (10%)); **m.p.** 214 °C - 216 °C (crystallized from CH₂Cl₂/hexanes); **¹H NMR** (500 MHz, DMSO-*d*₆): δ /ppm = 3.45 - 3.55 (m, 12H, -CH₂-), 3.70 - 3.80 (m, 4H, -CH₂-), 4.25 (s, 4H, =CH₂), 4.42 (s, 2H, -CH-), 4.91 (dd, J = 15.7, 5.7 Hz, 2H, -CH₂-), 5.04 (dd, J = 15.7, 6.5 Hz, 2H, -CH₂-), 6.90 (d, J = 8.1 Hz, 2H, aromatics), 7.13 - 7.16 (m, 3H, aromatics), 7.32 (t, J = 7.5 Hz, 1H,

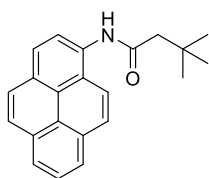
aromatics), 7.40 (d, $J = 8.0$ Hz, 2H, aromatics), 7.75 (t, $J = 8.1$ Hz, 2H, aromatics), 9.95 (s, 2H, NH), 10.65 (s, 2H, NH), 11.79 (s, 2H, NH); **^{13}C NMR** (126 MHz, DMSO- d_6): $\delta/\text{ppm} = 47.7$ (2 $-\text{CH}_2-$), 67.6 (2 $-\text{CH}_2-$), 68.3 (2 $-\text{CH}_2-$), 69.1 (2 $-\text{CH}_2-$), 69.5 (2 $-\text{CH}_2-$), 81.8 (2 $-\text{CH}-$), 88.0 (2 $=\text{CH}_2$), 106.7 (2 CH aromatic), 107.5 (2 CH aromatic), 124.3 (1 CH aromatic), 124.4 (2 CH aromatic), 128.6 (1 CH aromatic), 138.6 (2 C aromatic), 140.6 (2 CH aromatic), 147.9 (2 C aromatic), 151.8 (2 aromatic C), 156.6 (2 $=\text{C}$), 167.5 (2 $\text{C}=\text{O}$), 179.9 (2 $\text{C}=\text{S}$); **IR** (neat): $\tilde{\nu}/\text{cm}^{-1} = 3395, 3346, 2918, 1696, 1605, 1538, 1444, 1280, 1238, 1091, 989, 787, 686$; **HR MS (ESI)** $[\text{M}+\text{H}]^+$ m/z calculated for $\text{C}_{36}\text{H}_{43}\text{N}_8\text{O}_8\text{S}_2$ 779.2640, found 779.2651 (1.5 ppm).

7.7 Synthesis of fluorescent monomers

7.7.1 General procedure VI (monomers)

In a 10 mL flask under nitrogen atmosphere, dry CH_2Cl_2 (0.1 M) and dry NEt_3 (3 equivalents) were added to 1 equivalent of the aromatic amine. The mixture was cooled down to 0 °C (ice bath) and *t*-butyl acetyl chloride (2 equivalents) was added in one portion. The cooling bath was removed and the reaction was allowed to reach 25 °C on its own and stirred for an additional 3 hours. The conversion was followed by TLC analysis. After completion, the reaction was quenched by the addition of water and the mixture was extracted three times with CH_2Cl_2 . The combined organic layers were dried over anhydrous Na_2SO_4 , filtered and concentrated under vacuum. The pure monomeric amide product was obtained after purification by column chromatography.

7.7.2 Synthesis of pyrene-monomer



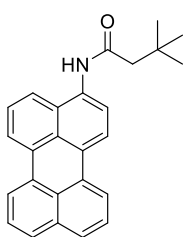
According to the general procedure **VI**, 43 mg (0.2 mmol) of 1-amino-pyrene, 56 μL (54 mg, 0.4 mmol) of *t*-butyl acetyl chloride, 84 μL (61 mg., 0.6 mmol) of dry NEt_3 and 2 mL of dry CH_2Cl_2 yielded 58 mg (0.18 mmol, 315.42 g/mol, 92%) of **pyrene-monomer** as an off-white solid. **Purification:** column (SiO_2)

$\text{CH}_2\text{Cl}_2/\text{MeOH}$ gradient (0.5%, 1% 2%).

R_f = 0.8 (SiO_2 , $\text{CH}_2\text{Cl}_2/\text{MeOH}$ (2%)); **m.p.**: 207 °C - 209 °C; **¹H-NMR** (500 MHz, CDCl_3): δ/ppm = 1.25 (s, 9H, - CH_3), 2.48 (s, 2H, - CH_2 -), 7.71 (s, 1H, NH), 7.99 - 8.19 (m, 8H, aromatics), 8.41 (d, 1H, J = 8.2 Hz, aromatic); **¹³C-NMR** (126 MHz, CDCl_3): δ/ppm = 30.2 (3 - CH_3), 31.6 (1 C), 51.8 (1 - CH_2 -), 120.3 (1 CH aromatic), 122.6 (1 CH aromatic), 123.6 (1 C aromatic), 124.9 (1 C aromatic), 125.2 (1 CH aromatic), 125.3 (1 CH aromatic), 125.3 (1 C aromatic), 125.3 (1 CH aromatic), 125.6 (1 CH aromatic), 127.0 (1 CH aromatic), 127.5 (1 CH aromatic), 128.1 (1 CH aromatic), 129.2 (1 C aromatic), 130.5 (1 C aromatic), 130.9 (1 C aromatic), 131.5 (1 C aromatic), 170.8 (1 C=O); **IR** (neat): $\tilde{\nu}/\text{cm}^{-1}$ 3283, 3034, 2950, 2866, 1650, 1598, 1555, 1521, 1485, 1393, 1364, 1340, 1307,

1271, 1236, 1108, 1040, 961, 913, 841, 822, 794, 755, 709; **HR MS (ESI)** $[M+H]^+$ m/z calculated for $C_{22}H_{22}NO$ 316.1696, observed 316.1697 (0.2 ppm).

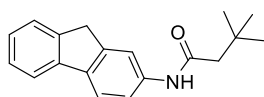
7.7.3 Synthesis of perylene-monomer²⁰⁹



According to the general procedure **VI**, 27 mg (0.1 mmol) of 3-aminoperylene, 28 μ L (27 mg, 0.2 mmol) of *t*-butyl acetyl chloride, 42 μ L (30 mg., 0.3 mmol) of dry NEt_3 and 2 mL of dry CH_2Cl_2 yielded 31 mg (0.085 mmol, 365.48 g/mol, 85%) of **peryene-monomer** as a yellow-orange solid. **Purification:** column (SiO_2) $CH_2Cl_2/MeOH$ (2%).

R_f = 0.4 (SiO_2 , $CH_2Cl_2/MeOH$ (2%)); **m.p.:** 240 °C - 243 °C; **1H -NMR** (400 MHz, $DMSO-d_6$): δ/ppm = 1.11 (s, 9H, $-CH_3$), 2.39 (s, 2H, $-CH_2-$), 7.53-7.57 (m, 2H, aromatics), 7.61 (t, 1H, J = 8.0 Hz, aromatic), 7.76-7.81 (m, 3H, aromatics), 7.95 (d, 1H, J = 8.8 Hz, aromatic), 8.32 (d, 1H, J = 7.4 Hz, aromatic), 8.37 (t, 2H, J = 8.3 Hz, aromatics), 8.41 (d, 1H, J = 7.0 Hz, aromatic), 9.81 (s, 1H, NH); **^{13}C -NMR** (126 MHz, $DMSO-d_6$): δ/ppm = 29.8 (1 $-CH_3$), 31.0 (1 $-CH_2-$), 49.1 (1C), 120.5 (1 C aromatic), 120.7 (1 C aromatic), 120.9 (1 C aromatic), 121.0 (1 C aromatic), 122.5 (1 C aromatic), 122.7 (1 C aromatic), 126.6 (1 C aromatic), 126.9 (1 C aromatic), 127.0 (1 C aromatic), 127.4 (1 C aromatic), 127.5 (1 C aromatic), 127.7 (1 C aromatic), 128.0 (1 C aromatic), 128.5 (1 C aromatic), 128.6 (1 C aromatic), 129.7 (1 C aromatic), 130.5 (1 C aromatic), 130.8 (1 C aromatic), 133.7 (1 C aromatic), 134.3 (1 C aromatic), 170.6 (1 C=O); **IR** (neat): $\tilde{\nu}/cm^{-1}$ 3279, 2957, 2876, 1651, 1535, 1526, 1391, 1366, 1340, 1270, 1260, 1195, 1150, 1051, 989, 834, 814, 767; **HR MS (ESI)** $[M+H]^+$ m/z calculated for $C_{26}H_{24}NO$ 366.1852, observed 366.1848 (-1.1 ppm).

7.7.4 Synthesis of fluorene-monomer



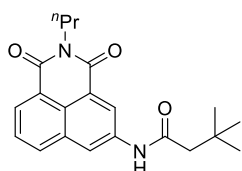
According to the general procedure **VI**, 36 mg (0.2 mmol) of 2-amino-fluorene, 56 μ L (54 mg, 0.4 mmol) of *t*-butyl acetyl chloride, 84 μ L (61 mg., 0.6 mmol) of dry NEt_3 and 2 mL of dry CH_2Cl_2 yielded 56 mg (0.2 mmol, 279.38 g/mol, 99%) of

²⁰⁹ Monomer synthesized by Dr. Francesco Zinna.

fluorene-monomer as an off-white solid. **Purification:** column (SiO₂) CH₂Cl₂/MeOH gradient (1%, 2%).

R_f = 0.8 (SiO₂, CH₂Cl₂/MeOH (2%)); **m.p.:** 176 °C - 177 °C; **¹H-NMR** (500 MHz, CDCl₃): δ/ppm = 1.13 (s, 9H, -CH₃), 2.25 (s, 2H, -CH₂-), 3.89 (s, 2H, -CH₂-), 7.12 (s, 1H, NH), 7.25 - 7.29 (m, 1H, aromatic), 7.32 (dd, 1H, *J* = 8.1 Hz, 2.0 Hz, aromatic), 7.36 (t, 1H, *J* = 7.5 Hz, aromatic), 7.52 (d, 1H, *J* = 7.5 Hz, aromatic), 7.70 (d, 1H, *J* = 8.1 Hz, aromatic), 7.72 (d, 1H, *J* = 7.5 Hz, 2.0 Hz, aromatic), 7.93 (s, 1H, aromatic); **¹³C-NMR** (126 MHz, CDCl₃): δ/ppm = 30.0 (3 -CH₃), 31.5 (1 C), 37.2 (1 -CH₂-), 51.9 (1 -CH₂-), 117.1 (1 CH aromatic), 118.7 (1 CH aromatic), 119.7 (1 CH aromatic), 120.2 (1 CH aromatic), 125.1 (1 CH aromatic), 126.4 (1 CH aromatic), 126.9 (1 CH aromatic), 136.8 (1 C aromatic), 138.2 (1 C aromatic), 141.5 (1 C aromatic), 143.3 (1 C aromatic), 144.5 (1 C aromatic), 170.2 (1 C=O); **IR** (neat): $\tilde{\nu}$ /cm⁻¹ 3283, 2951, 2862, 1650, 1614, 1596, 1532, 1460, 1416, 1364, 1346, 1327, 1307, 1256, 1232, 1201, 1143, 1127, 876, 826, 710; **HR MS (ESI)** [M+H]⁺ *m/z* calculated for C₁₉H₂₂NO 280.1696, observed 280.1686 (-3.7 ppm).

7.7.5 Synthesis of NMI-monomer



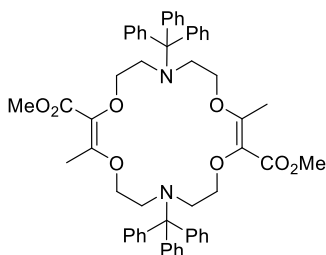
According to the general procedure **VI**, 51 mg (0.2 mmol) of *n*Pr-3-amino-NMI, 56 μ L (54 mg, 0.4 mmol) of *t*-butyl acetyl chloride, 84 μ L (61 mg., 0.6 mmol) of dry NEt₃ and 2 mL of dry CH₂Cl₂ yielded 69 mg (0.2 mmol, 352.43 g/mol, 98%) of **NMI-monomer** as an off-white solid. **Purification:** column (SiO₂): CH₂Cl₂/MeOH (1%).

R_f = 0.7 (SiO₂, CH₂Cl₂/MeOH (2%)); **m.p.:** 226 °C - 227 °C; **¹H-NMR** (500 MHz, CDCl₃): δ/ppm = 1.01 (t, 3H, *J* = 7.4 Hz, -CH₃), 1.16 (s, 9H, -CH₃), 1.72 - 1.79 (m, 2H, -CH₂-), 2.34 (s, 2H, -CH₂-), 4.12 - 4.15 (m, 2H, -CH₂-), 7.42 (s, 1H, NH), 7.72 (dd, 1H, *J* = 8.2 Hz, 7.3 Hz, aromatic), 8.16 (dd, 1H, *J* = 8.2 Hz, 1.1 Hz, aromatic), 8.22 (d, 1H, *J* = 2.2 Hz, aromatic), 8.49 (dd, 1H, *J* = 7.3 Hz, 1.1 Hz, aromatic), 8.99 (d, 1H, *J* = 2.2 Hz, aromatic); **¹³C-NMR** (126 MHz, CDCl₃): δ/ppm = 11.7 (1 -CH₃), 21.5 (1 -CH₂-), 30.0 (3 -CH₃), 31.7 (1 C), 42.2 (1 -CH₂-), 51.9 (1 -CH₂-), 122.4 (1 CH aromatic), 122.6 (1 C aromatic), 123.6 (1 C aromatic), 124.0 (1 CH aromatic), 125.3 (1 C aromatic), 127.7 (1 CH aromatic), 130.1 (1 CH aromatic), 132.8 (1 C aromatic), 133.9 (1 CH aromatic), 136.5 (1 C aromatic), 164.0 (1 C=O), 164.3 (1 C=O), 170.8 (1 C=O); **IR** (neat): $\tilde{\nu}$ /cm⁻¹ 3247, 3072, 2965, 2870,

1699, 1653, 1627, 1596, 1534, 1503, 1463, 1423, 1376, 1338, 1271, 1235, 1124, 1072, 903, 782, 739, 706, 658; **HR MS (ESI)** $[M+H]^+$ m/z calculated for $C_{21}H_{25}N_2O_3$ 353.1860, observed 353.1855 (-1.3 ppm).

7.8 Synthesis of aza-crown ethers

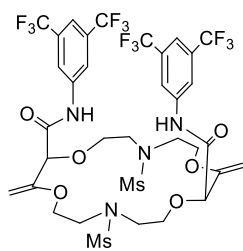
7.8.1 Synthesis of N18C6-Trityl



In a 10 ml vial, 2 mg (0.00141 mmol, 0.1 mol%) of $\text{Rh}_2(\text{S-PTLL})_4(\text{EtOAc})_2$ and 2782 mg (8.46 mmol, 6 equiv.) of *N*-protected morpholine are dissolved in 2.8 ml of CHCl_3 . To this solution, 200 mg (1.41 mmol) of α -diazo- β -ketoester is added in one portion. The vial is sealed and the solution stirred at 25 °C for 20 hours. The

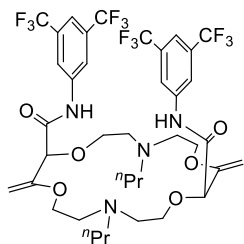
consumption of the diazo reagent is monitored by TLC analysis and infrared spectroscopy (2146 cm^{-1}). After completion of the reaction, the volatiles are evaporated. The mixture is purified by column chromatography (SiO_2 , pentane/ Et_2O 9 :1, 8 :2, 7 :3, 6 :4, 1 :1) and the resulting solid is washed with pentane to yield 286 mg (0.32 mmol, 886.42 g/mol, 46%) of **N18C6-Trityl** as an off-white solid.

R_f = 0.4 (SiO_2 , Et_2O /pentane (1:1)); **m.p.**: 118 °C - 128 °C ; **$^1\text{H-NMR}$** (500 MHz, CDCl_3): δ/ppm = 2.28 (s, 6H, - CH_3), 2.68 - 2.70 (m, 4H, - CH_2 -), 2.77 - 2.80 (m, 4H, - CH_2 -), 3.64 (s, 6H, - CH_3), 3.69 - 3.72 (m, 4H, - CH_2 -), 4.10 - 4.13 (m, 4H, - CH_2 -), 7.12 - 7.15 (m, 6H, aromatics), 7.19 - 7.22 (m, 12H, aromatics), 7.48 - 7.50 (m, 12H, aromatics); **$^{13}\text{C-NMR}$** (126 MHz, CDCl_3): δ/ppm = 16.1 (2 - CH_3), 51.5 (2 - CH_3), 52.2 (2 - CH_2 -), 52.5 (2 - CH_2 -), 68.4 (2 - CH_2 -), 72.6 (2 - CH_2 -), 78.6 (2 C), 126.3 (6 aromatics), 127.8 (12 aromatics), 129.0 (2 C=C), 129.4 (12 aromatics), 143.7 (6 aromatics), 158.7 (2 C=C), 166.7 (2 C=O); **IR** (neat): $\tilde{\nu}/\text{cm}^{-1}$ 2943, 1702, 1619, 1486, 1445, 1377, 1298, 1271, 1187, 1156, 1086, 1010, 934, 900, 760, 742, 708, 632; **HR MS (ESI)** $[\text{M}+\text{H}]^+$ m/z calculated for $\text{C}_{56}\text{H}_{59}\text{N}_2\text{O}_8$ 887.4266, observed 887.4251 (-1.7 ppm).

7.8.2 Synthesis of bisCF₃-N18C6-Ms

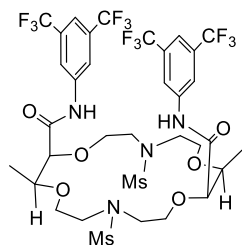
In a 10 mL flask under nitrogen atmosphere, 1 mL of dry THF is added to 56 mg (0.1 mmol) of **N18C6-Ms** and 47 μ L (69 mg, 0.3 mmol, 3 equiv) of 3,5-bis-trifluoromethyl-aniline. The mixture is cooled down to -100 °C (in an EtOH/liquid nitrogen bath). Then 45 mg (0.4 mmol, 4 equiv) of *t*-BuOK is added in one portion. After stirring 1-2 minutes at -100 °C, the cooling bath was removed and the reaction was allowed to reach 25 °C on its own and stirred for an additional 3 hours. The conversion is followed by TLC analysis (SiO₂, CH₂Cl₂/MeOH, 9:1) and LR-ESI-MS (soft positive mode, CH₂Cl₂). At the end, the reaction is quenched with a few drops of MeOH and directly purified by column chromatography (SiO₂, EtOAc/pentane 3:7, 1:1, 7:3, then CH₂Cl₂/MeOH (0%, 5%, 10%)) without further treatment. The resulting oil is purified by selective precipitation (a minimum of CH₂Cl₂ for solubility, followed by a large excess of pentane, 15 hours) affording 73 mg (0.077 mmol, 952.78 g/mol, 77%) of **bisCF₃-N18C6-Ms** as an off-white solid (*dr* 95:5).

R_f = 0.6 (SiO₂, CH₂Cl₂/MeOH (10%)); **m.p.**: 147 °C - 152 °C; **¹H-NMR** (500 MHz, CDCl₃, major diastereoisomer): δ /ppm = 2.92 (s, 6H, -CH₃), 3.34 - 3.38 (m, 2H, -CH₂-), 3.51 - 3.57 (m, 6H, -CH₂-), 3.66 - 3.70 (m, 2H, -CH₂-), 4.01 - 4.06 (m, 6H, -CH₂-), 4.37 (d, 2H, *J* = 3.2 Hz, =CH₂), 4.40 (s, 2H, -CH-), 4.42 (d, 2H, *J* = 3.2 Hz, =CH₂), 7.59 (s, 2H, aromatics), 8.25 (s, 4H, aromatics), 9.59 (s, 2H, NH); **¹³C-NMR** (126 MHz, CDCl₃, major diastereoisomer): δ /ppm = 36.4 (2 -CH₃), 51.0 (2 -CH₂-), 51.1 (2 -CH₂-), 67.7 (2 -CH₂-), 68.6 (2 -CH₂-), 81.7 (2 -CH-), 88.1 (2 =CH₂), 117.6 (2 CH aromatics), 119.8 (4 CH aromatics), 123.1 (q, *J* = 273 Hz, 4 -CF₃), 132.2 (q, *J* = 33 Hz, 4 C aromatics), 139.3 (2 C aromatics), 157.2 (2 C=), 167.7 (2 C=O); **¹⁹F-NMR** (282 MHz, CDCl₃): δ /ppm = -63.0 (4 -CF₃); **IR** (neat): $\tilde{\nu}$ /cm⁻¹ 3301, 2941, 1693, 1633, 1550, 1475, 1442, 1382, 1328, 1282, 1231, 1168, 1126, 1032, 1006, 969, 935, 887, 846, 777, 582; **HR MS (ESI)** [M+H]⁺ *m/z* calculated for C₃₄H₃₆F₁₂N₄O₁₀S₂ 953.1754, observed 953.1739 (-1.5 ppm).

7.8.3 Synthesis of bisCF₃-N18C6-ⁿPr

In a 10 mL flask under nitrogen atmosphere, 1 mL of dry THF is added to 59 mg (0.1 mmol) of **N18C6-COCF₃** and 94 μ L (137 mg, 0.6 mmol, 6 equiv) of 3,5-bis-trifluoromethyl-aniline. The mixture is cooled down to -100 °C (in an EtOH/liquid nitrogen bath). Then 67 mg (0.6 mmol, 6 equiv) of *t*-BuOK is added in one portion. After stirring 1-2 minutes at -100 °C, the cooling bath was removed and the reaction was allowed to reach 25 °C on its own and stirred for an additional 3 hours. The conversion is followed by TLC analysis (SiO₂, CH₂Cl₂/MeOH (10%)) and LR-ESI-MS (soft positive mode, CH₂Cl₂). The reaction is quenched with a few drop of MeOH. Then 58 μ L (46 mg, 0.8 mmol, 8 equiv) of propanal is added and the solution is stirred for 10 min at 25 °C. The formed imine is reduced in situ by adding 212 mg (1.0 mmol, 10 equiv) of NaBH(OAc)₃ (in three portions, 15 min between consecutive additions) and stirred for an additional 1 hour at 25 °C. The conversion is followed by TLC analysis (SiO₂, CH₂Cl₂/MeOH (10%)) and LR-ESI-MS (soft positive mode, CH₂Cl₂). At the end, the reaction is quenched with a few drop of MeOH and directly purified by column chromatography (SiO₂, EtOAc then CH₂Cl₂/MeOH (1%, 5%, 10%)) without further treatment. The resulting oil is purified by selective precipitation (a minimum of CH₂Cl₂ for solubility, followed by a large excess of pentane and evaporation of the solvent under vacuum) affording 64 mg (0.073 mmol, 880.77 g/mol, 73%) of **bisCF₃-N18C6-ⁿPr** as an off-white solid (*dr* 95:5).

R_f = 0.5 (SiO₂, CH₂Cl₂/MeOH (10%)); **m.p.**: 148 °C - 154 °C; **¹H-NMR** (500 MHz, CDCl₃, major diastereoisomer): δ /ppm = 0.61 (t, 6H, *J* = 7.3 Hz, -CH₃), 1.21 - 1.30 (m, 2H, -CH₂-), 2.28 - 2.36 (m, 4H, -CH₂-), 2.65 - 2.76 (m, 6H, -CH₂-), 2.82 - 2.87 (m, 2H, -CH₂-), 3.48 - 3.52 (m, 2H, -CH₂-), 3.79 - 3.91 (m, 6H, -CH₂-), 4.35 (d, 2H, *J* = 2.8 Hz, =CH₂), 4.44 (s, 2H, -CH-), 4.53 (d, 2H, *J* = 2.8 Hz, =CH₂), 7.52 (s, 2H, aromatics), 8.14 (s, 4H, aromatics), 10.23 (s, 2H, NH); **¹³C-NMR** (126 MHz, CDCl₃, major diastereoisomer): δ /ppm = 11.4 (2 -CH₃), 17.2 (2 -CH₂-), 51.8 (2 -CH₂-), 53.8 (2 -CH₃), 55.5 (2 -CH₂-), 65.5 (2 -CH₂-), 67.6 (2 -CH₂-), 83.0 (2 -CH-), 88.1 (2 -CH-), 117.1 (2 CH aromatics), 119.2 (4 CH aromatics), 123.1 (q, *J* = 273 Hz, 4 -CF₃), 132.1 (q, *J* = 34 Hz, 4 C aromatics), 139.7 (2 C aromatics), 156.7 (2 C=), 168.7 (2 C=O); **¹⁹F-NMR** (282 MHz, CDCl₃): δ /ppm = 63.2 (4 -CF₃); **IR** (neat): $\tilde{\nu}$ /cm⁻¹ 3217, 2930, 1688, 1625, 1548, 1471, 1442, 1381, 1276, 1173, 1112, 1065, 1003, 933, 888, 850, 818, 705, 681; **HR MS (ESI)** [M+H]⁺ *m/z* calculated for C₃₈H₄₅F₁₂N₄O₆ 881.3142, observed 881.3109 (-3.7 ppm).

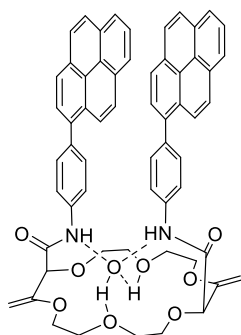
7.8.4 Synthesis of 4[H]-bisCF₃-N18C6-Ms

In a 10 mL flask, 1 mL of dry THF is added to 48 mg (0.05 mmol) of **bisCF₃-N18C6-Ms**. Then 4.8 mg 10% (w/w) of Pd/C (10% Pd, unreduced) is added. The suspension is flushed with H₂ and stirred under H₂ atmosphere (balloon, 1 atm.) for 3 hours. The conversion is followed by LR-ESI-MS (soft positive mode, CH₂Cl₂). The crude mixture is then filtrated and the solvent is

evaporated. The resulting oil is purified by selective precipitation (a minimum of CH₂Cl₂ for solubility, followed by a large excess of pentane, 15 hours) affording 38 mg (0.04 mmol, 956.81 g/mol, 79%) of **4[H]-bisCF₃-N18C6-Ms** as an inseparable diastereomeric mixture (9:1) as an off-white solid.²¹⁰

R_f = 0.6 (SiO₂, CH₂Cl₂/MeOH (10%)); **m.p.**: 194 °C - 197 °C; **¹H-NMR** (500 MHz, CDCl₃, major diastereoisomer): δ/ppm = 1.21 (d, 6H, *J* = 6.4 Hz, -CH₃), 2.94 (s, 6H, -CH₃), 3.34 - 3.48 (m, 4H, -CH₂-), 3.56 - 3.66 (m, 4H, -CH₂-), 3.69 - 3.73 (m, 2H, -CH₂-), 3.76 - 3.80 (m, 2H, -CH₂-), 3.86 - 3.90 (m, 2H, -CH₂-), 4.16 (qd, 2H, *J* = 6.4 Hz, 1.7 Hz, -CH-), 4.25 (d, 2H, *J* = 1.7 Hz, -CH-), 4.29 - 4.33 (m, 2H, -CH₂-), 7.60 (s, 2H, aromatics), 8.27 (s, 4H, aromatics), 9.57 (s, 2H, NH); **¹³C-NMR** (126 MHz, CDCl₃, major diastereoisomer): δ/ppm = 13.5 (2 -CH₃), 37.3 (2 -CH₃), 50.8 (2 -CH₂-), 51.6 (2 -CH₂-), 70.1 (2 -CH₂-), 71.0 (2 -CH₂-), 78.5 (2 -CH-), 83.7 (2 -CH-), 117.7 (2 CH aromatics), 119.9 (4 CH aromatics), 123.3 (q, *J* = 278 Hz, 4 -CF₃), 132.3 (q, *J* = 33 Hz, 4 C aromatics), 139.2 (2 C aromatics), 168.5 (2 C=O); **¹⁹F-NMR** (282 MHz, CDCl₃): δ/ppm = 63.0 (4 -CF₃); **IR** (neat): $\tilde{\nu}$ /cm⁻¹ 3293, 2917, 1686, 1622, 1545, 1474, 1442, 1381, 1325, 1275, 1131, 1100, 1022, 1004, 969, 932, 889, 847, 771, 728, 703, 682, 612, 576; **HR MS (ESI)** [M+H]⁺ *m/z* calculated for C₃₄H₄₁F₁₂N₄O₁₀S₂ 957.2067, observed 957.2061 (-0.6 ppm).

²¹⁰ The configuration of the major diastereoisomer could not be determined unambiguously, but the all-*cis* configuration is thought to be more favored for steric reasons.

7.9 Synthesis of *p*-pyrene-Ph-18C6

In a Schlenk, 1,4-dioxane (4 mL) and distilled water (2 mL) are added to 80 mg (0.1 mmol) of ***p*-I-18C6**, 82 mg (0.25 mmol, 2.5 equiv) of 1-pyrene boronic pinacol ester,²¹¹ 55 mg (0.4 mmol, 4 equiv) of K₂CO₃ and 12 mg (0.1 mmol, 10 mol%) of Pd(PPh₃)₄. The mixture is stirred at 80 °C until completion (followed by TLC analysis (SiO₂, CH₂Cl₂/MeOH, 9:1) and LR-ESI-MS (soft positive mode, CH₂Cl₂)). The solvent is evaporated and the product is purified by column chromatography (SiO₂, EtOAc, then CH₂Cl₂/MeOH gradient (1%, 3%, 5%)) without further treatment. Finally, the solid is purified by selective precipitation (CH₂Cl₂ then pentane and evaporation) affording 81 mg (0.086 mmol, 945.08 g/mol, 86%) of ***p*-pyrene-Ph-18C6** as an off-white solid.

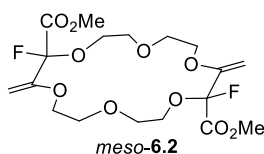
R_f = 0.74 (SiO₂, CH₂Cl₂/MeOH (10%)); **m.p.**: 137 °C - 142 °C; **¹H-NMR** (500 MHz, CDCl₃): δ/ppm = 3.67 - 3.72 (m, 4H, -CH₂-), 3.83 - 3.85 (m, 4H, -CH₂-), 3.86 - 3.94 (m, 4H, -CH₂-), 4.04 - 4.09 (m, 4H, -CH₂-), 4.34 (d, 2H, *J* = 2.7 Hz, =CH₂), 4.43 (s, 2H, -CH-), 4.50 (d, 2H, *J* = 2.7 Hz, =CH₂), 7.45 - 7.47 (m, 4H, aromatics), 7.59 (d, 2H, *J* = 9.2 Hz, aromatics), 7.66 (d, 2H, *J* = 7.8 Hz, aromatics), 7.74 - 7.76 (m, 4H, aromatics), 7.82 - 7.85 (m, 4H, aromatics), 7.93 - 7.96 (m, 6H, aromatics), 8.02 (d, 2H, *J* = 9.2 Hz, aromatics), 8.06 - 8.08 (m, 2H, aromatics), 10.08 (s, 2H, NH); **¹³C-NMR** (126 MHz, CDCl₃): δ/ppm = 66.5 (2 -CH₂-), 68.3 (2 -CH₂-), 69.4 (2 -CH₂-), 70.4 (2 -CH₂-), 84.0 (2 -CH-), 88.6 (2 =CH₂), 120.0 (4 CH aromatics), 124.5 (2 CH aromatics), 124.6 (2 CH aromatics), 124.7 (2 C aromatics), 124.76 (2 C aromatics), 124.81 (2 CH aromatics), 125.0 (2 CH aromatics), 125.7 (2 CH aromatics), 127.1 (2 CH aromatics), 127.19 (2 CH aromatics), 127.24 (2 CH aromatics), 127.4 (2 CH aromatics), 128.3 (2 C aromatics), 130.2 (2 C aromatics), 130.8 (2 C aromatics), 131.0 (4 CH aromatics), 131.3 (2 C aromatics), 136.0 (2 C aromatics), 137.0 (2 C aromatics), 137.4 (2 C aromatics), 156.3 (2 =C), 167.6 (2 C=O); **IR** (neat): $\tilde{\nu}$ /cm⁻¹ 3299, 3040, 2919, 1687, 1595, 1525, 1405, 1288, 1243, 1183, 1096, 1076, 993, 929, 902, 838, 760, 721; **HR MS (ESI)** [M+H]⁺ *m/z* calculated for C₆₀H₅₁N₂O₈ 927.3640, observed 927.3622 (-2.0 ppm).

²¹¹ Beinhoff, M.; Weigel, W.; Jurczok, M.; Rettig, W.; Modrakowski, C.; Brüdgam, I.; Hartl, H.; Schlüter, A. D., *Eur. J. Org. Chem.* **2001**, 2001, 3819-3829.

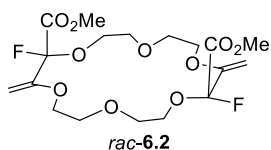
7.10 Synthesis of 6.2

In a 10 mL Schlenk with activated 4Å MS, 80.9 mg (0.20 mmol) of **18C6**, 127.2 mg (1.20 mmol, 6 equiv) of Na₂CO₃ and 155.9 mg (0.44 mmol, 2.2 equiv) of selectfluor® are added. Dry THF (2 mL) is added and the reaction is stirred at 60 °C for 15 hours. The reaction is monitored by TLC analysis (SiO₂, EtOAc). The solvent is evaporated under reduced pressure and EtOAc is added to solubilize the product and precipitate the selectfluor® by-product. The solid by-product is filtrated off and washed with EtOAc. The solvent is evaporated under reduced pressure and the product is filtrated by chromatographic column (Al₂O₃, EtOAc) to yield 57 mg (0.129 mmol, 440.39 g/mol, 65 %) of a white solid of a *meso*/*rac* mixture (1:1).

The *meso*/*rac* mixture (57 mg) is separated by chromatographic column (SiO₂, CH₂Cl₂/EtOAc gradient 1:0, 95:5, 90:10, 70:30, 0:1) to yield 12 mg of *meso* compound (1st eluted) and 23 mg of *rac* (2nd eluted, with some trace of *meso*).



m.p.: 136 °C; **¹H-NMR** (500 MHz, CDCl₃): δ/ppm = 3.71-3.91 (m, 20H, -CH₂-, -CH₃), 3.97 (m, 2H, -CH₂-), 4.40 (t, 2H, *J* = 3 Hz, =CH₂), 4.74 (t, 2H, *J* = 3 Hz, =CH₂); **¹³C-NMR** (126 MHz, CDCl₃): δ/ppm = 53.4 (2 -CH₃), 65.1 (2 -CH₂-), 68.3 (2 -CH₂-), 69.0 (2 -CH₂-), 70.0 (2 -CH₂-), 87.2 (d, *J* = 5.4 Hz, =CH₂), 106.9 (d, *J* = 230.0 Hz, -CF), 154.1 (d, *J* = 37.4 Hz, =C), 165.4 (d, *J* = 32.9 Hz, C=O); **IR** (CDCl₃): $\tilde{\nu}$ /cm⁻¹ 2949, 1759, 1647, 1445, 1309, 1169, 1138, 1079, 847, 768.



m.p.: 121 °C; **¹H-NMR** (500 MHz, CDCl₃): δ/ppm = 3.71-3.96 (m, 22H, -CH₂-, -CH₃), 4.39 (t, 2H, *J* = 3 Hz, =CH₂), 4.71 (t, 2H, *J* = 3 Hz, =CH₂); **¹³C-NMR** (126 MHz, CDCl₃): δ/ppm = 53.4 (2 -CH₃), 64.8 (2 -CH₂-), 68.5 (2 -CH₂-), 69.2 (2 -CH₂-), 69.9 (2 -CH₂-), 87.2 (d, *J* = 5.4 Hz, =CH₂), 106.9 (d, *J* = 230.4 Hz, -CF), 154.3 (d, *J* = 36.5 Hz, =C), 165.6 (d, *J* = 33.7 Hz, C=O); **IR** (CDCl₃): $\tilde{\nu}$ /cm 2947, 1759, 1646, 1448, 1312, 1171, 1136, 1084, 847, 768.

7.11 ^1H NMR Titrations

7.11.1 ^1H NMR titration of Bn-18C6

Procedure: Six NMR tube were prepared with respectively 3 mg, 6 mg, 9 mg, 15 mg, 30 mg and 45 mg of **Bn-18C6** in 700 μL of CDCl_3 of the freshly bottle. The spectra were recorded after 15 min in a 500 MHz spectrometer.

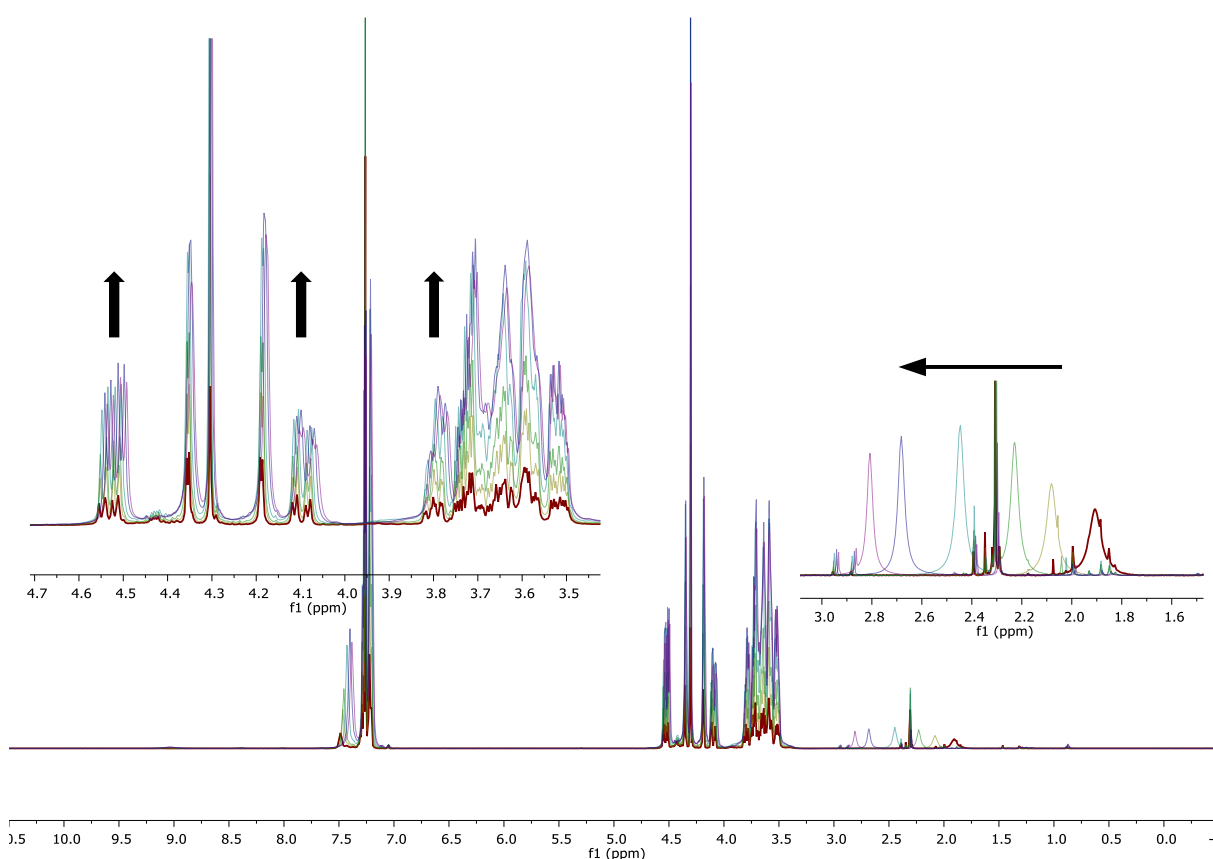


Figure 7.2 Effect of water signal shift as function of the concentration of **Bn-18C6**. ^1H NMR spectra (500 MHz, -0.5-10.5 ppm), CDCl_3 , 298 K.

7.11.2 ^1H NMR titration of cryptands

^1H NMR spectra were recorded in a 4:1 $\text{CDCl}_3/\text{DMSO}-d_6$ solvent mixture. Stock solutions of the cryptand (50 mM), cations tetraphenylborate (250 mM) and anions tetrabutylammonium (125 mM) are prepared. Solutions are prepared directly in the NMR tube by mixing the solution of cryptand, of anion and/or cation and filled to a total volume of 500 μL (final concentration: 2.5 mM of cryptand). The ^1H NMR spectra are recorded on a Bruker III 500 MHz spectrometer, equipped with a 5 mm Cryogenic DCH ($^1\text{H}/^{13}\text{C}$) probe with 16 scans *ca.* 30 minutes after the preparation of the NMR tube at 298 K. The spectra are calibrated on the $\text{DMSO}-d_6$ signal ($\delta = 2.50$ ppm). For more details and information on the titration spectra, see reference 82.

7.11.2.1 Titration of pyr-cryptand with NaNCO , NaSCN , NaNO_3 and KSCN

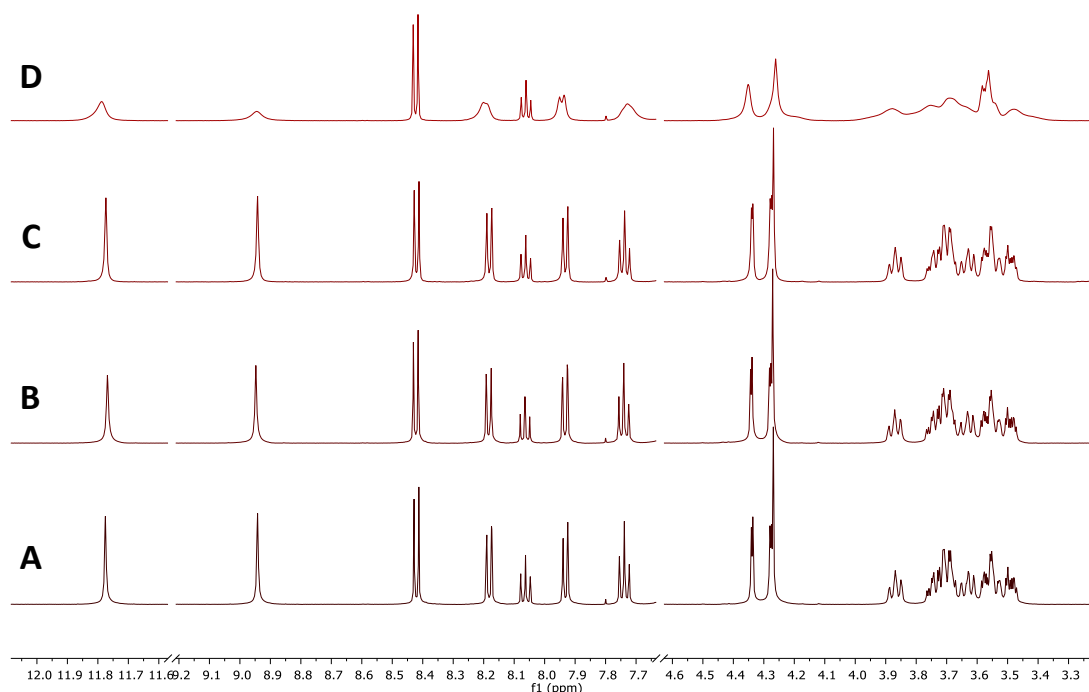


Figure 7.3 ^1H -NMR spectra, selected region (δ 12.1–3.3 ppm), 4:1 $\text{CDCl}_3/\text{DMSO}-d_6$, 298 K: (A) pyr-cryptand; (B) pyr-cryptand + NaBPh_4 (1:1); (C) pyr-cryptand + TBANCO (1:1); (D) pyr-cryptand + NaBPh_4 + TBANCO (1:1:1).

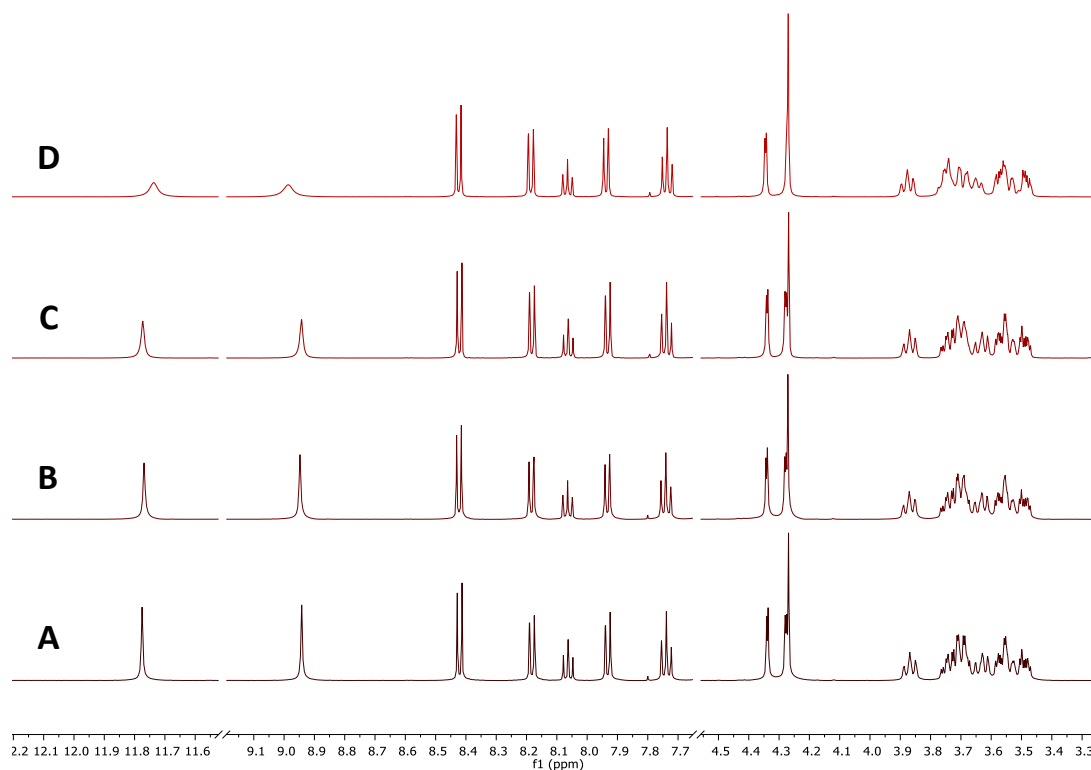


Figure 7.4 ^1H -NMR spectra, selected region (δ 12.2–3.3 ppm), 4:1 $\text{CDCl}_3/\text{DMSO}-d_6$, 298 K: (A) pyr-cryptand; (B) pyr-cryptand + NaBPh₄ (1:1); (C) pyr-cryptand + TBASCN (1:1); (D) pyr-cryptand + NaBPh₄ + TBASCN (1:1:1).

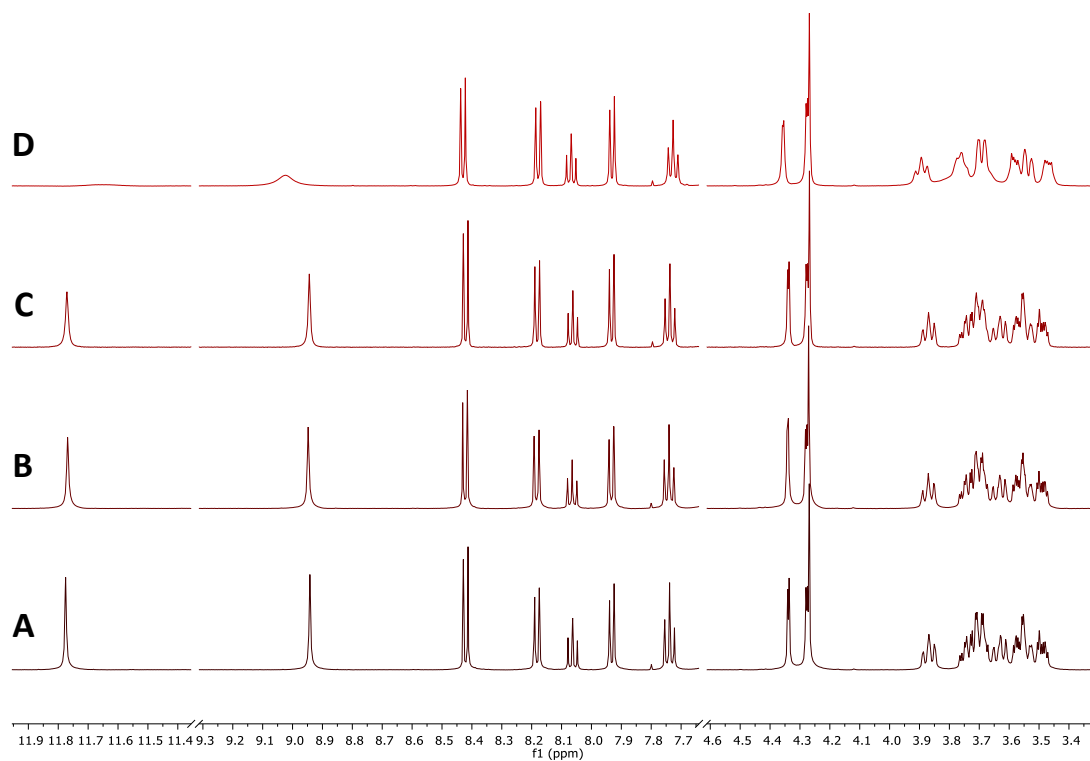


Figure 7.5 ^1H -NMR spectra, selected region (δ 12.0–3.3 ppm), 4:1 $\text{CDCl}_3/\text{DMSO}-d_6$, 298 K: (A) pyr-cryptand; (B) pyr-cryptand + NaBPh₄ (1:1); (C) pyr-cryptand + TBANO₃ (1:1); (D) pyr-cryptand + NaBPh₄ + TBANO₃ (1:1:1).

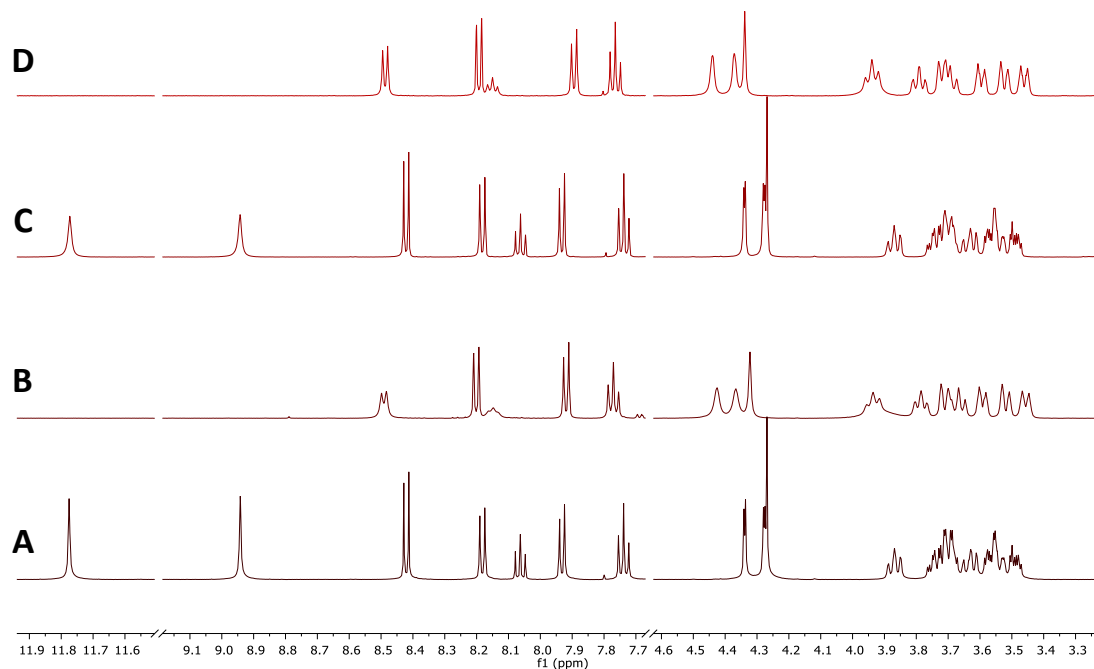


Figure 7.6 ^1H -NMR spectra, selected region (δ 12.0–3.3 ppm), 4:1 $\text{CDCl}_3/\text{DMSO}-d_6$, 298 K: (A) pyr-cryptand; (B) pyr-cryptand + KBPh_4 (1:1); (C) pyr-cryptand + TBASCN (1:1); (D) pyr-cryptand + KBPh_4 + TBASCN (1:1:1).

7.11.2.2 Titration of Cryptands with NaN_3

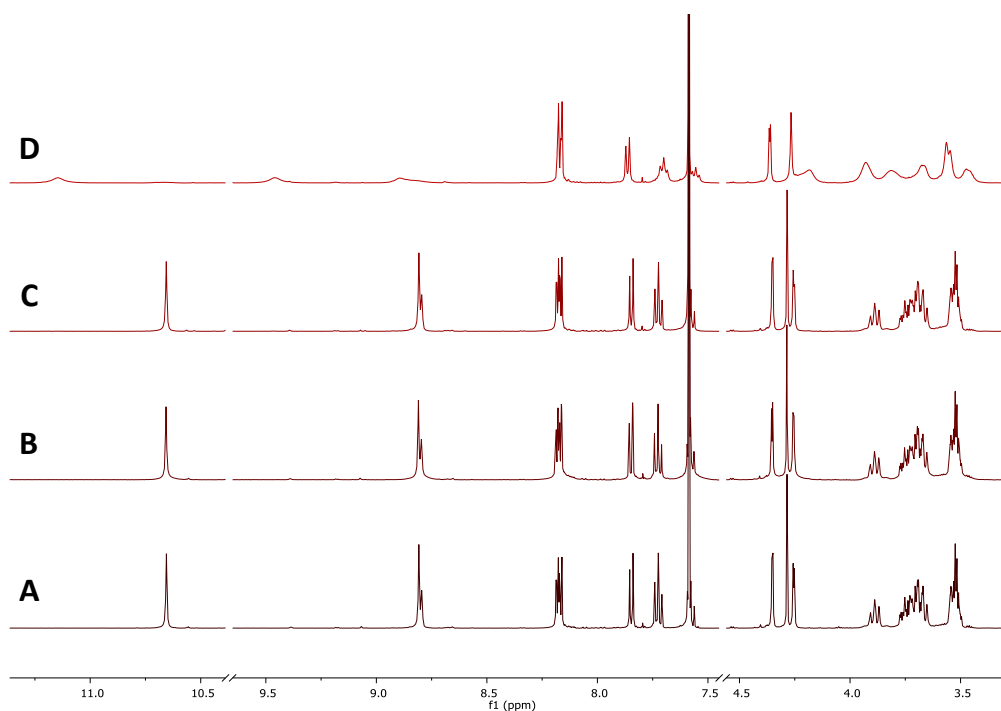


Figure 7.7 ^1H -NMR spectra, selected region (δ 11.5–3.3 ppm), 4:1 $\text{CDCl}_3/\text{DMSO}-d_6$, 298 K: (A) Ph-cryptand; (B) Ph-cryptand + NaBPh_4 (1:1); (C) Ph-cryptand + TBAN_3 (1:1); (D) Ph-cryptand + NaBPh_4 + TBAN_3 (1:1:1).

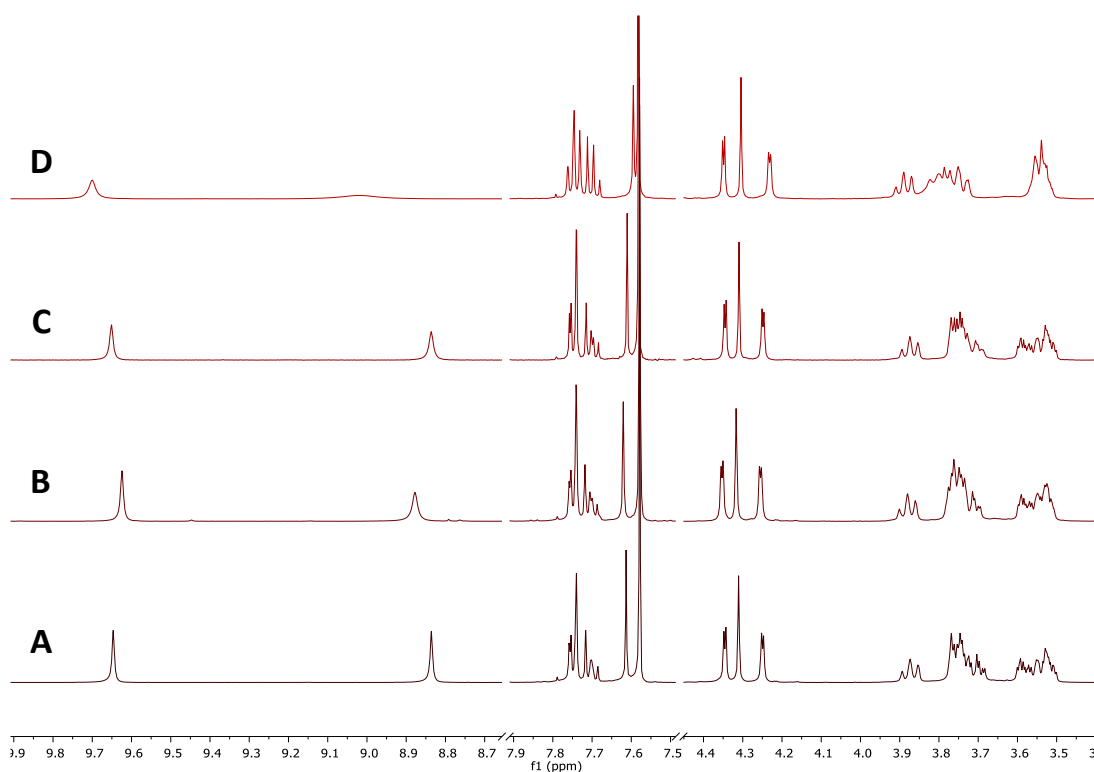


Figure 7.8 ^1H -NMR spectra, selected region (δ 9.9–3.4 ppm), 4:1 $\text{CDCl}_3/\text{DMSO}-d_6$, 298 K: (A) thio-cryptand; (B) thio-cryptand + NaBPh_4 (1:1); (C) thio-cryptand + TBAN_3 (1:1); (D) thio-cryptand + NaBPh_4 + TBAN_3 (1:1:1).

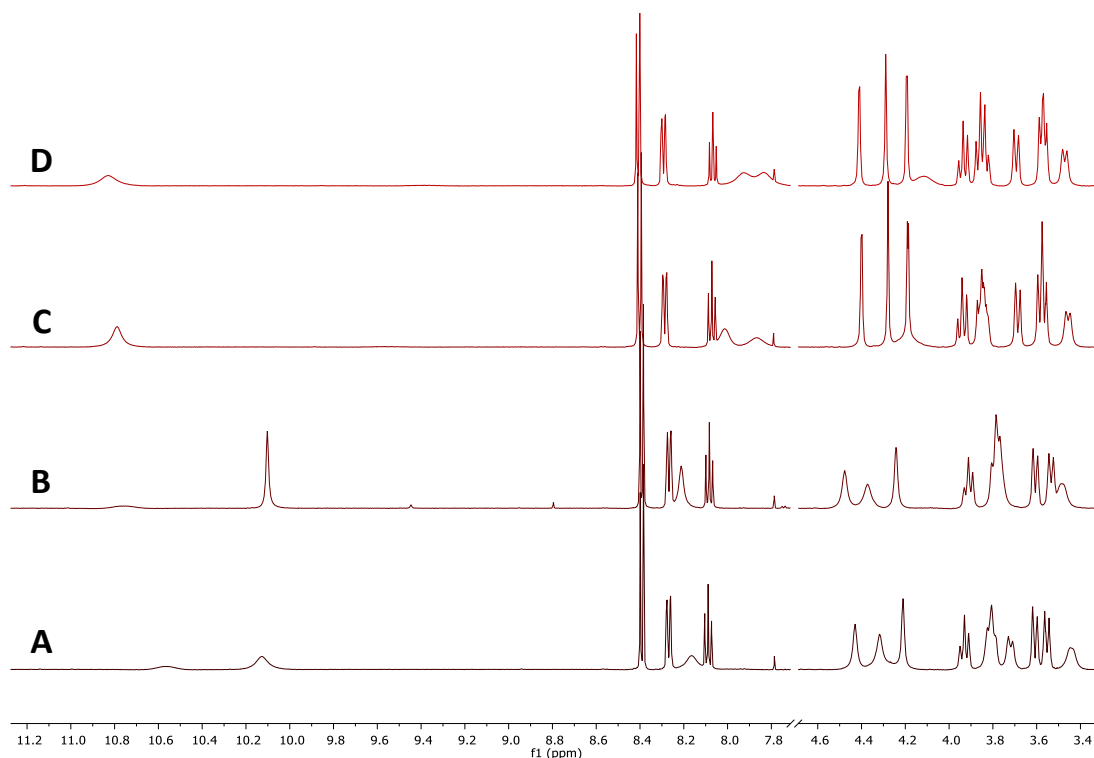


Figure 7.9 ^1H -NMR spectra, selected region (δ 11.2–3.3 ppm), 4:1 $\text{CDCl}_3/\text{DMSO}-d_6$, 298 K: (A) pyr-Ph-cryptand; (B) pyr-Ph-cryptand + NaBPh_4 (1:1); (C) pyr-Ph-cryptand + TBAN_3 (1:1); (D) pyr-Ph-cryptand + NaBPh_4 + TBAN_3 (1:1:1).

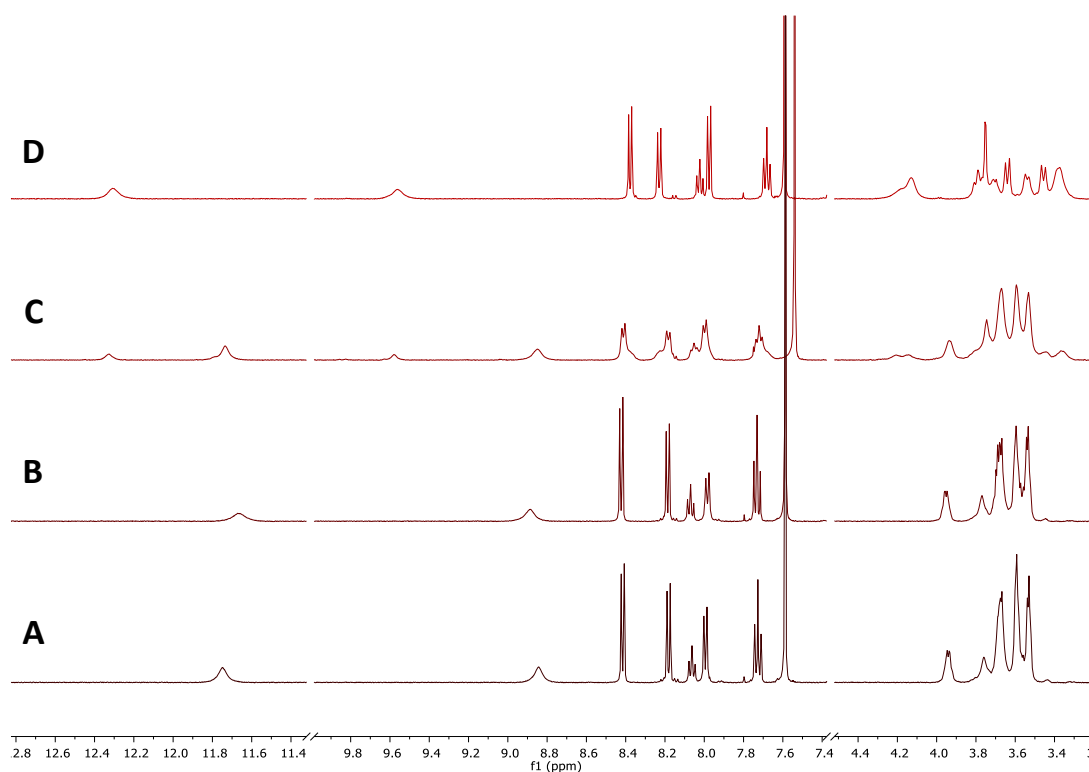


Figure 7.10 ^1H -NMR spectra, selected region (δ 12.8–3.3 ppm), 4:1 $\text{CDCl}_3/\text{DMSO}-d_6$, 298 K: (A) 4[H]-pyr-cryptand; (B) 4[H]-pyr-cryptand + NaBPh_4 (1:1); (C) 4[H]-pyr-cryptand + TBAN_3 (1:1); (D) 4[H]-pyr-cryptand + NaBPh_4 + TBAN_3 (1:1:1).

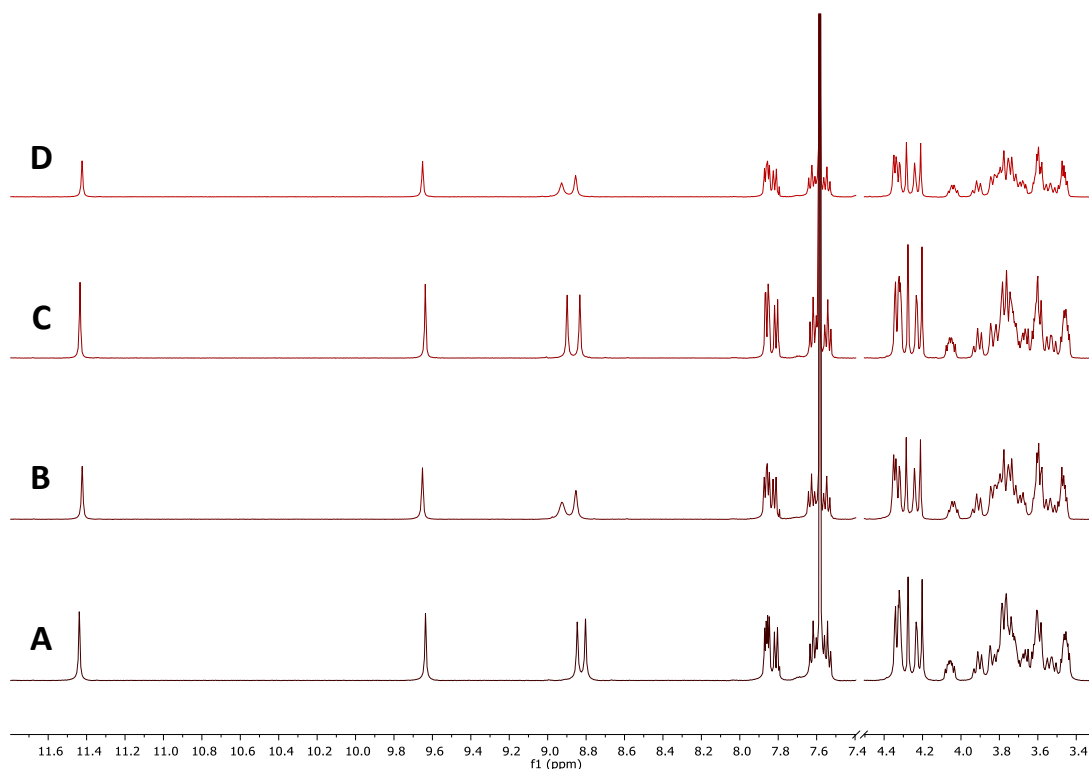


Figure 7.11 ^1H -NMR spectra, selected region (δ 11.8–3.3 ppm), 4:1 $\text{CDCl}_3/\text{DMSO}-d_6$, 298 K: (A) phos-cryptand; (B) phos-cryptand + NaBPh_4 (1:1); (C) phos-cryptand + TBAN_3 (1:1); (D) phos-cryptand + NaBPh_4 + TBAN_3 (1:1:1).

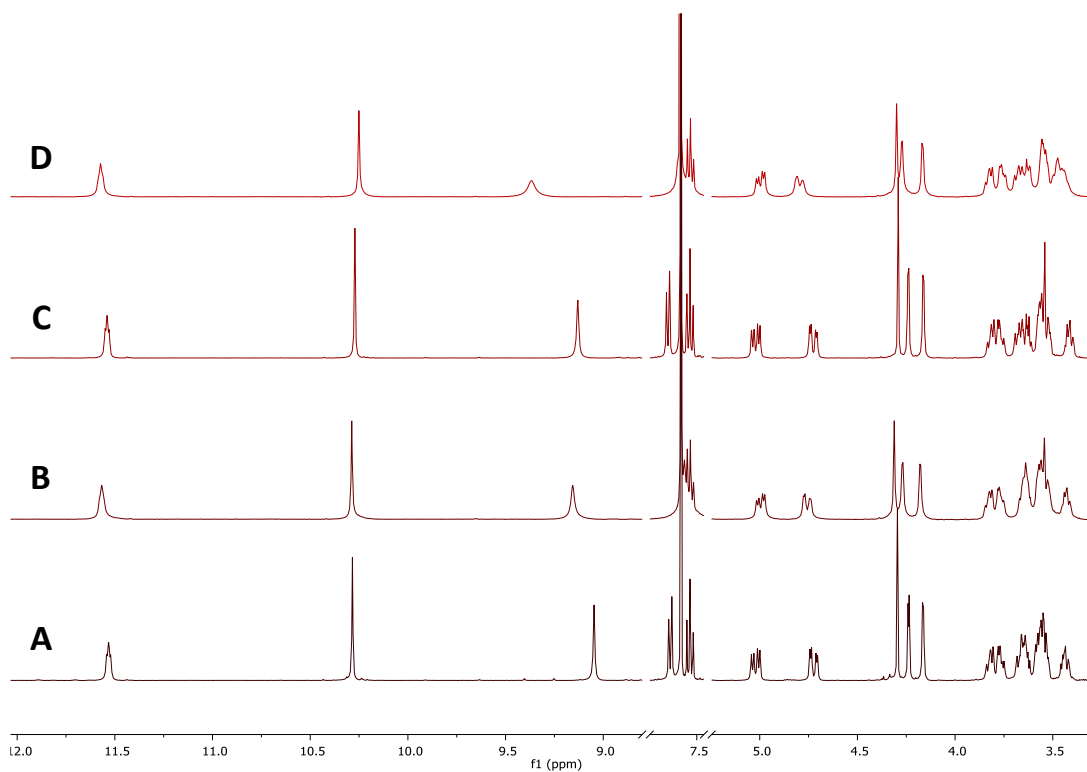


Figure 7.12 ^1H -NMR spectra, selected region (δ 12.0–3.3 ppm), 4:1 $\text{CDCl}_3/\text{DMSO}-d_6$, 298 K: (A) thiourea-cryptand; (B) thiourea-cryptand + NaBPh_4 (1:1); (C) thiourea-cryptand + TBAN_3 (1:1); (D) thiourea-cryptand + NaBPh_4 + TBAN_3 (1:1:1).

7.12 Spectroscopic data

7.12.1 UV-Vis absorption and fluorescence spectroscopies

7.12.1.1 Procedure

In a typical experiment, UV-Vis absorbance and fluorescence spectra of a solution of interest compound (ca. 10^{-5} M) in acetonitrile or CH_2Cl_2 were recorded in a 1 cm cell. For the complexation experiments, an excess of $\text{Ba}(\text{ClO}_4)_2$ or NaBAr_F was added to the solution and the UV-Vis absorbance and fluorescence spectra were recorded again.

7.12.1.2 Summary of optical properties

Table 7.4 Spectroscopic data without and with cation^[a]

Entry	Compound	λ_{max} (nm)			ϕ_f	
		absorption	monomer emission	excimer emission	Without M^{n+}	With M^{n+}
1	pyrene-monomer	341	387	-	24% ^[b]	-
2	pyrene-18C6	345	387	490	24% ^[b]	<1% ^[b]
3	pyrene-18C4	348	387	481	46% ^[b]	<1% ^[b]
4	pyrene-16C4	350	387	491	32% ^[b]	<1% ^[b]
5	perylene-monomer	443	472	-	77% ^[d]	-
6	perylene-18C6	446	470	543	10% ^[d]	62% ^[d]
7	perylene-18C4	446	470	536	19% ^[d]	59% ^[d]
8	perylene-16C4	446	470	tailed	16% ^[d]	50% ^[d]
9	fluorene-monomer	288	335	-	18% ^[c]	-
10	fluorene-18C6	318	-	337	2% ^[c]	-
11	fluorene-18C4	316	-	338	2% ^[c]	-
12	fluorene-16C4	316	-	336	2% ^[c]	-
13	NMI-monomer	338	420	-	17% ^[b]	-
14	NMI-18C6	340	386	485	10% ^[b]	18% ^[b]

[a] $\text{Ba}(\text{ClO}_4)_2/\text{CH}_3\text{CN}$ system used for 18C6 derivatives, $\text{NaBAr}_F/\text{CH}_2\text{Cl}_2$ system used for 18C4 and 16C4 compounds; [b] Relative to anthracene ($\phi = 27\%$ in EtOH); [c] Relative to phenanthrene ($\phi = 12.5\%$ in EtOH); [d] Relative to coumarine 153 ($\phi = 38\%$ in EtOH).

7.12.1.3 UV-Vis and fluorescence spectra

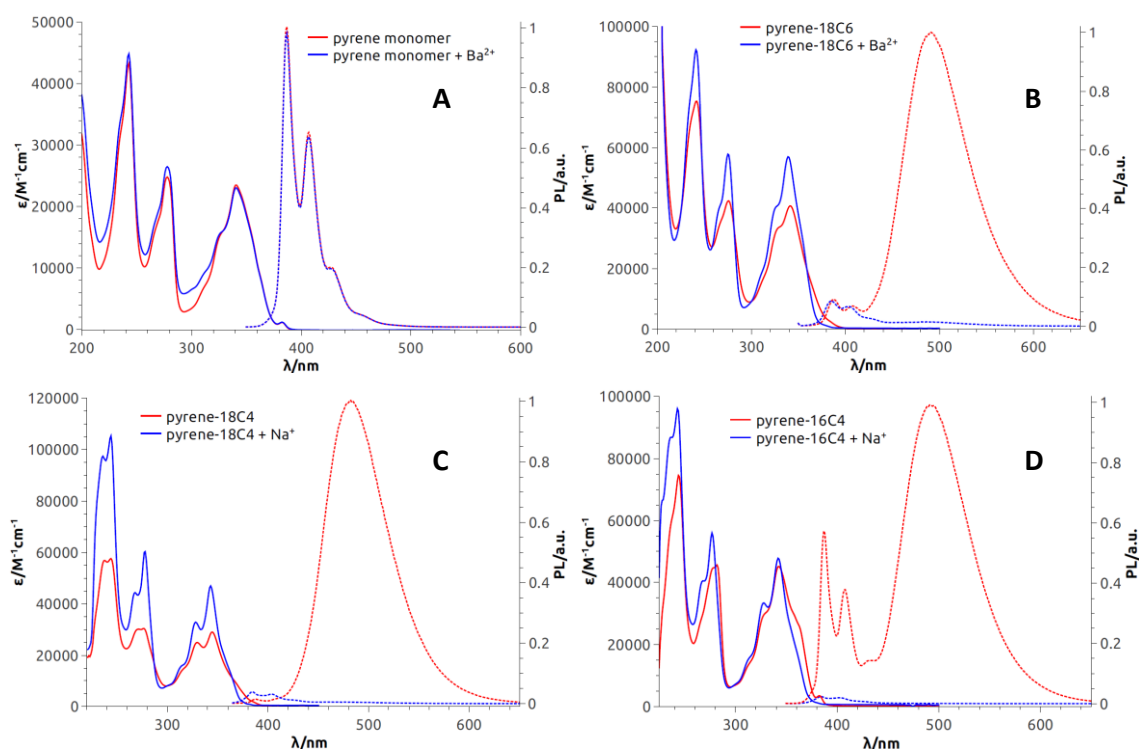


Figure 7.13 Absorption (continuous lines) and fluorescence (dotted lines) spectra of **pyrene-monomer** (A), **pyrene-18C6** (B), **pyrene-18C4** and **pyrene-16C4** (D) in CH₃CN or CH₂Cl₂ without (red) or with (blue) Ba(ClO₄)₂ or NaBAR_F (2 equiv).

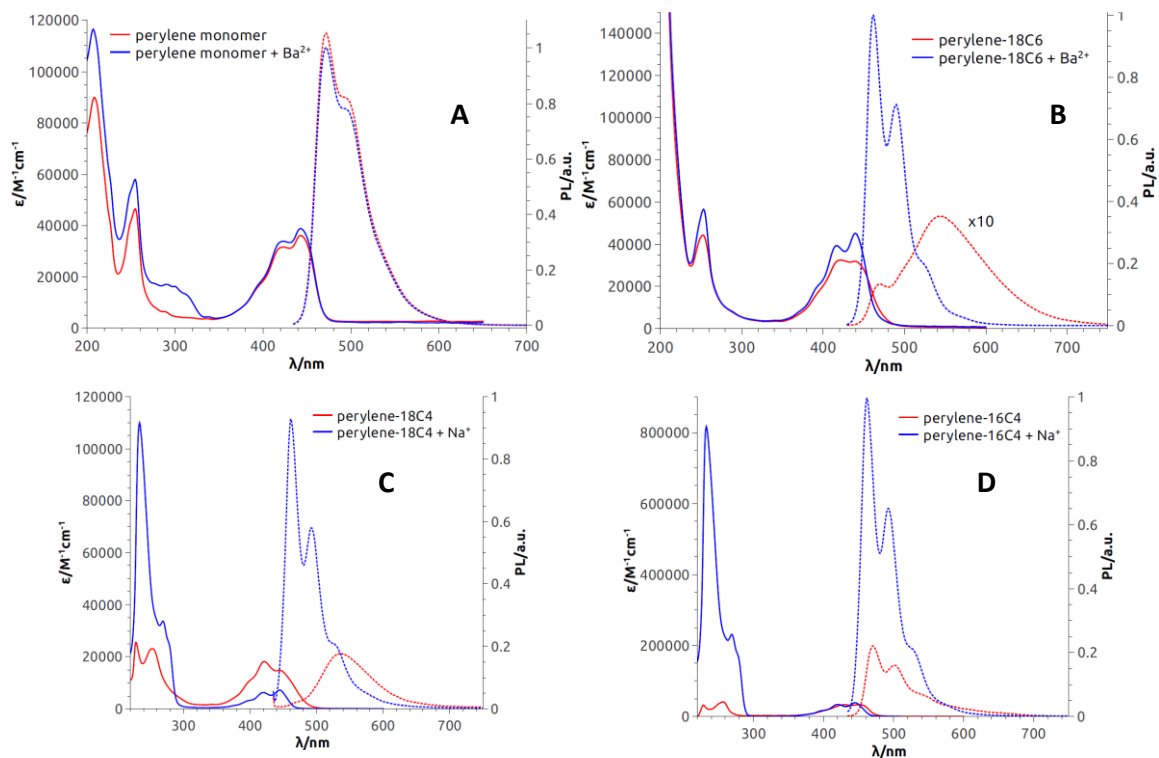


Figure 7.14 Absorption (continuous lines) and fluorescence (dotted lines) spectra of **perylene-monomer** (A), **perylene-18C6** (B), **perylene-18C4** (C) and **perylene-16C4** (D) in CH₃CN or CH₂Cl₂ without (red) or with (blue) Ba(ClO₄)₂ or NaBAR_F (2 equiv).

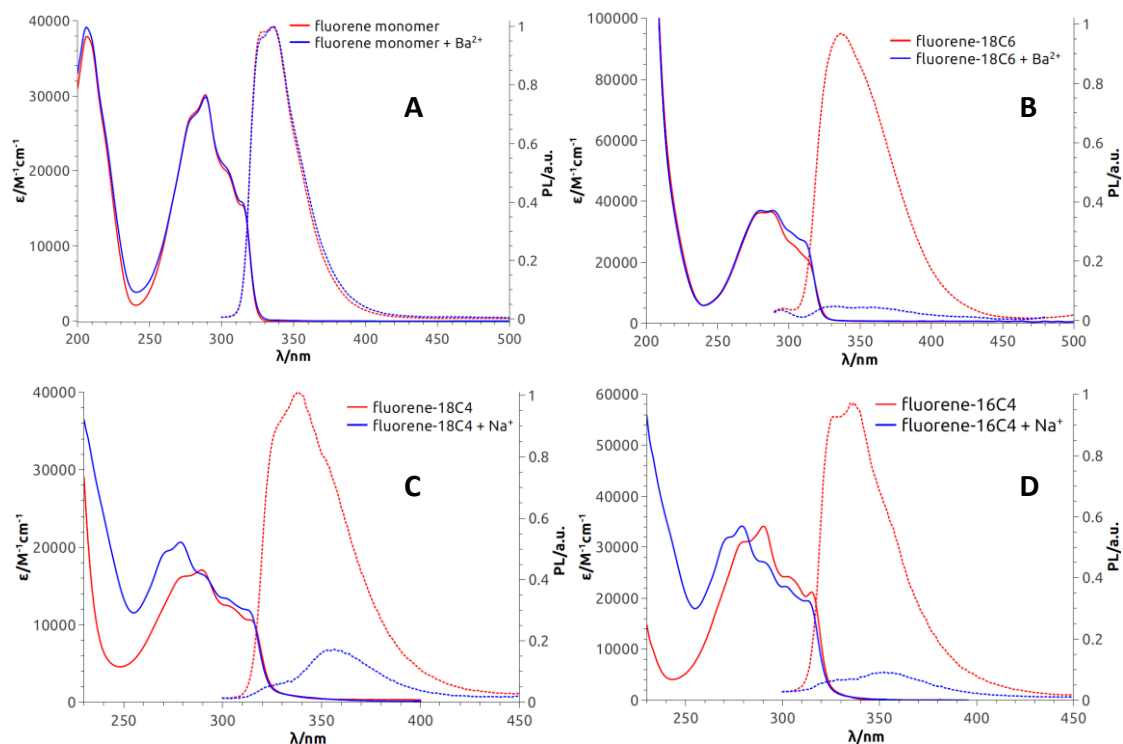


Figure 7.15 Absorption (continuous lines) and fluorescence (dotted lines) spectra of **fluorene-monomer** (A), **fluorene-18C6** (B), **fluorene-18C4** (C) and **fluorene-16C4** (D) in aCH₃CN or CH₂Cl₂ without (red) or with (blue) Ba(ClO₄)₂ or NaBAR_F (2 equiv).

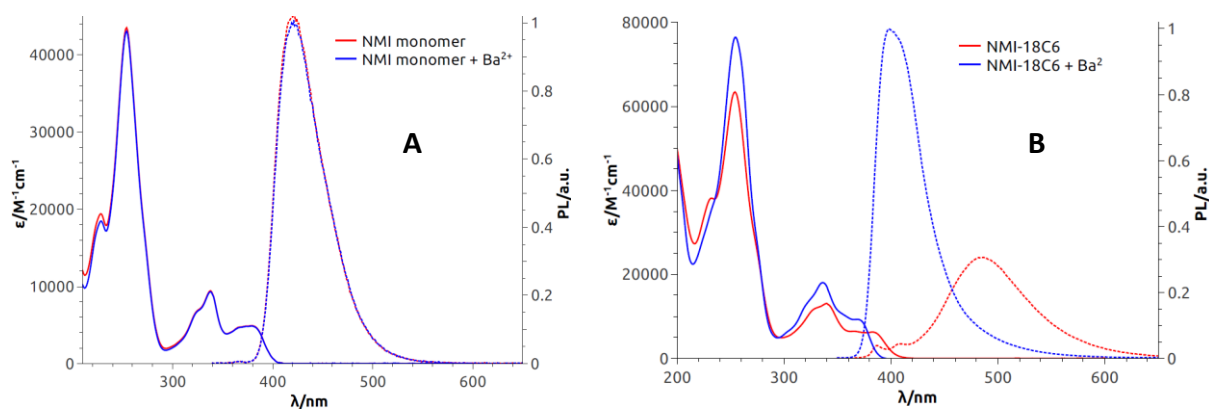


Figure 7.16 Absorption (continuous lines) and fluorescence (dotted lines) spectra of **NMI-monomer** (A) and **NMI-18C6** (B) in CH₃CN or CH₂Cl₂ without (red) or with (blue) Ba(ClO₄)₂ or NaBAR_F (2 equiv).

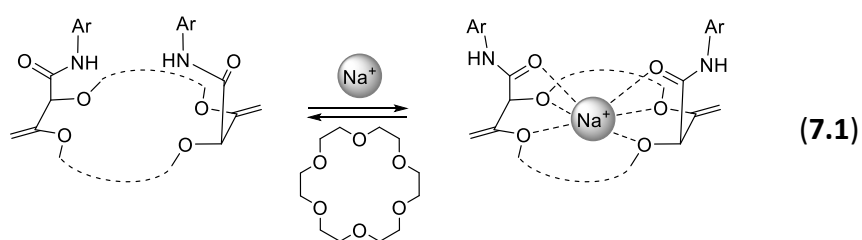
7.12.2 Procedure for ECD and CPL experiments

In a typical experiment, the ECD (or CPL) spectrum of a solution of enantiopure compound (ca. 10^{-5} M) in acetonitrile or CH_2Cl_2 was recorded in a 1 cm cell. For the complexation experiments, 3.0 equivalents (10^{-3} M stock solutions) of NaBAr_F in dichloromethane or $\text{Ba}(\text{ClO}_4)_2$ in acetonitrile were added to the solution and the ECD (or CPL) spectrum was recorded again.

7.12.3 Reversibility experiments

7.12.3.1 Procedure

In a typical experiment, ECD/fluorescence/CPL spectrum of a solution of enantiopure compound (ca. 10^{-5} M) in CH_2Cl_2 was recorded. For the complexation experiments, 2 equiv of NaBAr_F from a 10^{-3} M solution in CH_2Cl_2 were added to the solution and the spectrum was recorded again. To switch back the system, 2 equiv of 18-Crown-6 from a 10^{-3} M solution in CH_2Cl_2 were added to the solution and the spectrum was recorded again.¹⁸⁵ The procedure was repeated over several cycles.



7.12.3.2 ECD reversibility

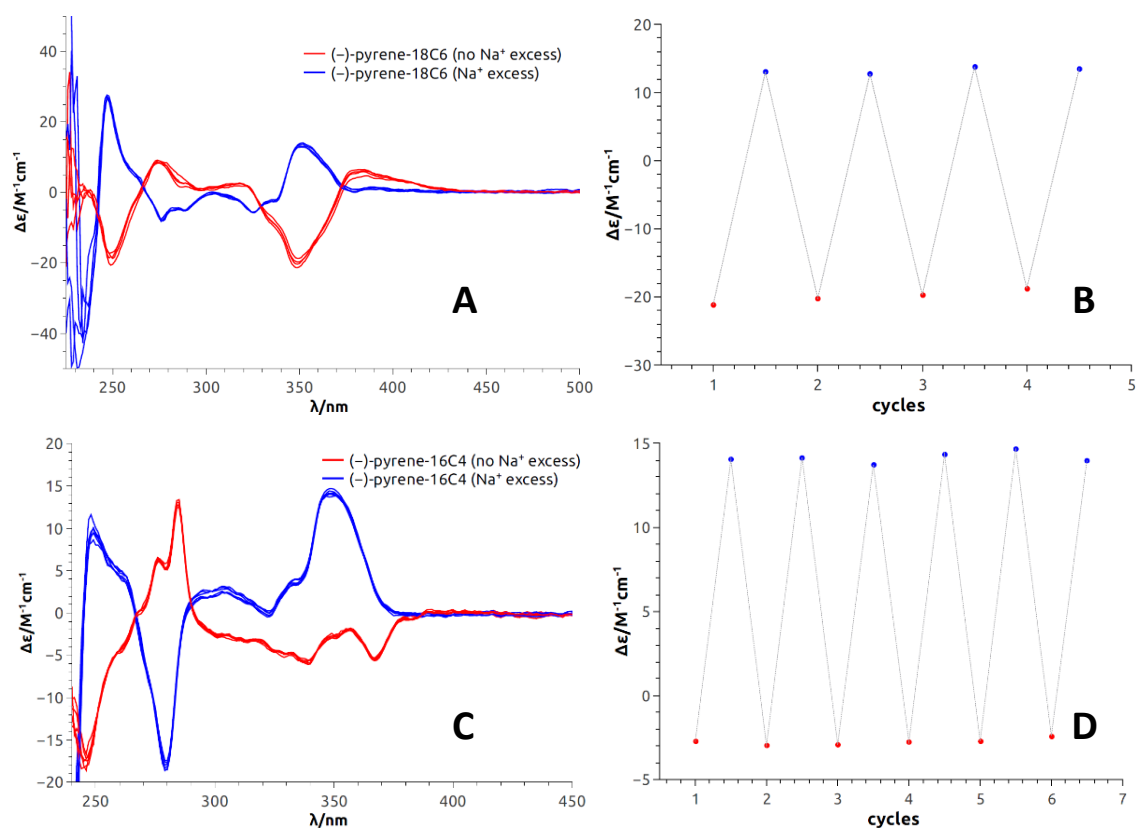


Figure 7.17 Reversible ECD (A) and intensities at 345 nm (B) for the first eluted (–)-enantiomer of **pyrene-18C6** over 4 cycles of NaBAR_F/18-Crown-6 additions (red/blue: without/with NaBAR_F). Reversible ECD (C) and intensities at 342 nm (D) for the first eluted (–)-enantiomer of **pyrene-16C4** over 6 cycles of NaBAR_F/18-Crown-6 additions (red/blue: without/with NaBAR_F).

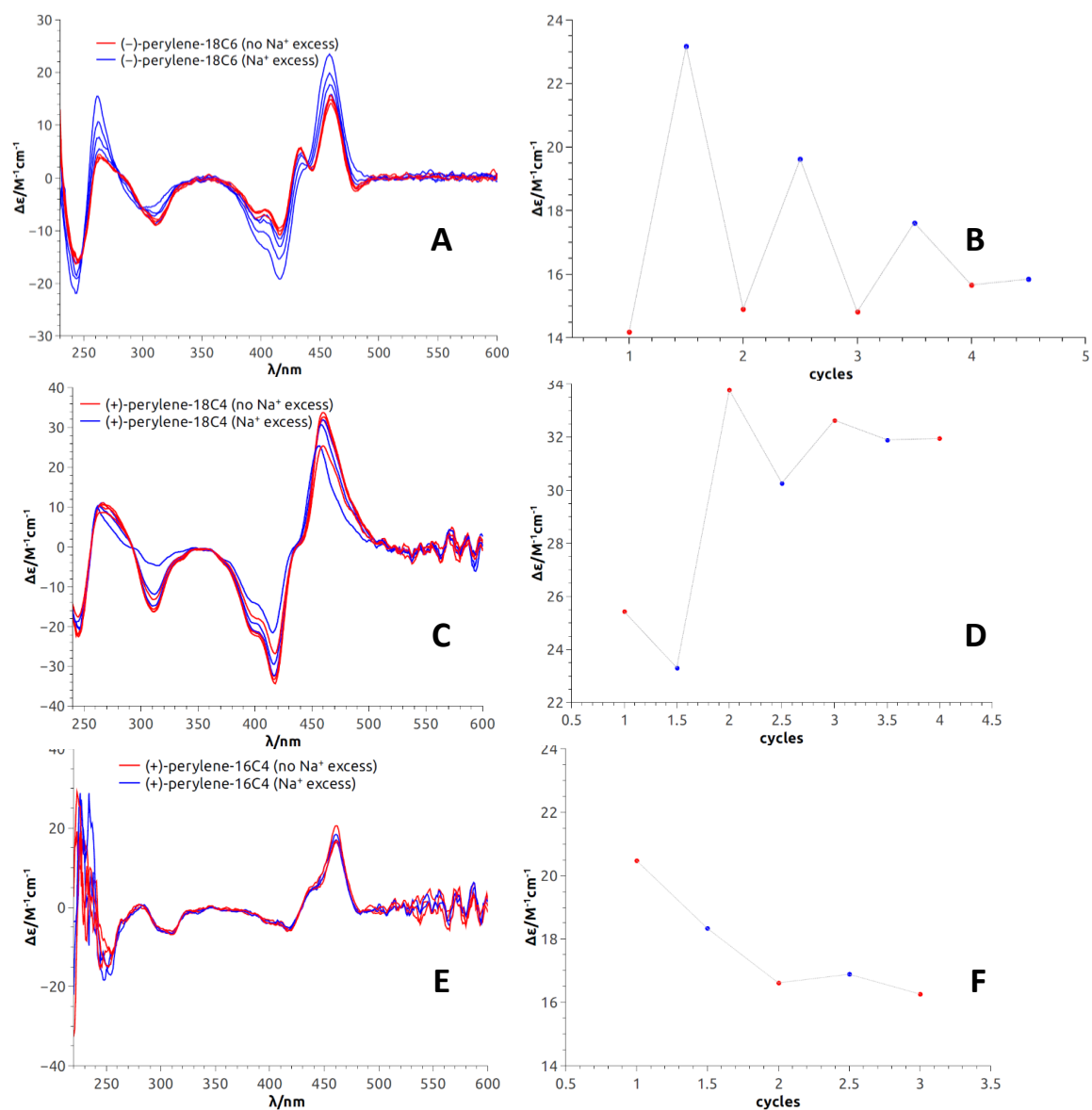


Figure 7.18 Reversible ECD (A) and intensities at 446 nm (B) for the first eluted (-)-enantiomer of **perylen-18C6** over 4 cycles of NaBAR_F/18-Crown-6 additions (red/blue: without/with NaBAR_F). Reversible ECD (C) and intensities at 446 nm (D) for the first eluted (+)-enantiomer of **perylen-18C4** over 4 cycles of NaBAR_F/18-Crown-6 additions (red/blue: without/with NaBAR_F). Reversible ECD (E) and intensities at 446 nm (F) for the first eluted (+)-enantiomer of **perylen-16C4** over 4 cycles of NaBAR_F/18-Crown-6 additions (red/blue: without/with NaBAR_F).

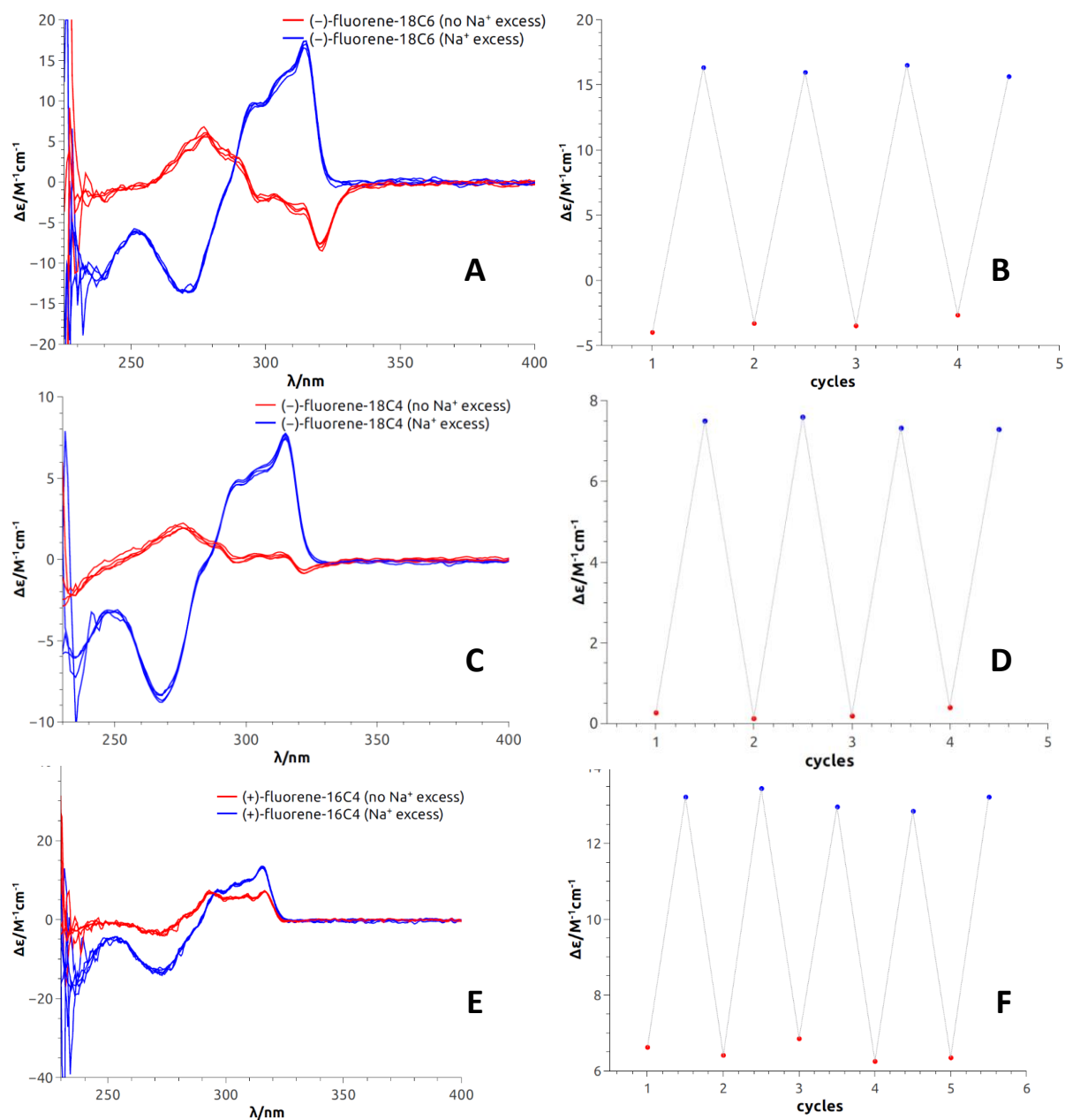


Figure 7.19 Reversible ECD (A) and intensities at 314 nm (B) for the first eluted (–)-enantiomer of **fluorene-18C6** over 4 cycles of NaBAR_F/18-Crown-6 additions (red/blue: without/with NaBAR_F). Reversible ECD (C) and intensities at 314 nm (D) for the first eluted (–)-enantiomer of **fluorene-18C4** over 4 cycles of NaBAR_F/18-Crown-6 additions (red/blue: without/with NaBAR_F). Reversible ECD (E) and intensities at 314 nm (F) for the first eluted (+)-enantiomer of **fluorene-16C4** over 5 cycles of NaBAR_F/18-Crown-6 additions (red/blue: without/with NaBAR_F).

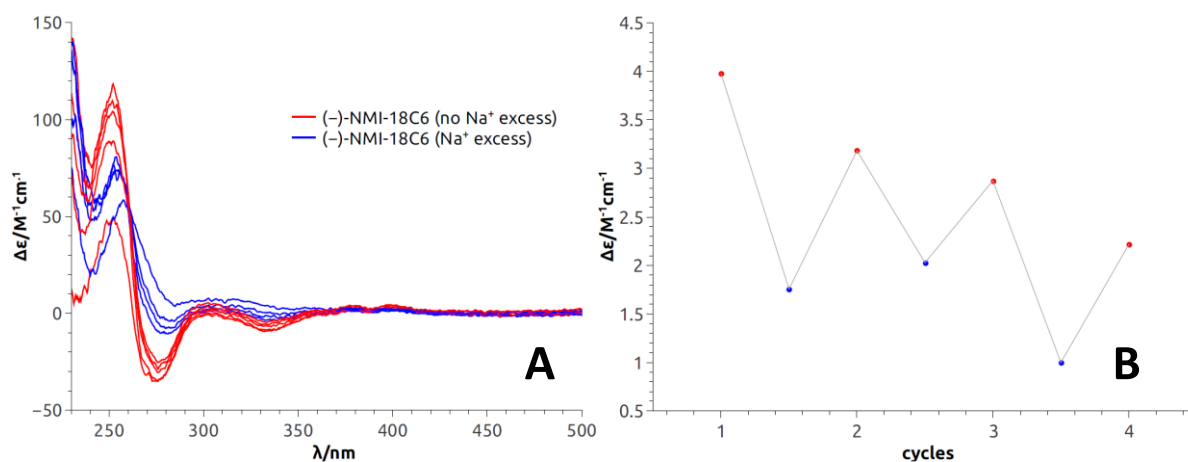


Figure 7.20 Reversible ECD (A) and intensities at 398 nm (B) for the first eluted (–)-enantiomer of **NMI-18C6** over 4 cycles of NaBAr_F/18-Crown-6 additions (red/blue: without/with NaBAr_F).

7.12.3.3 Fluorescence reversibility

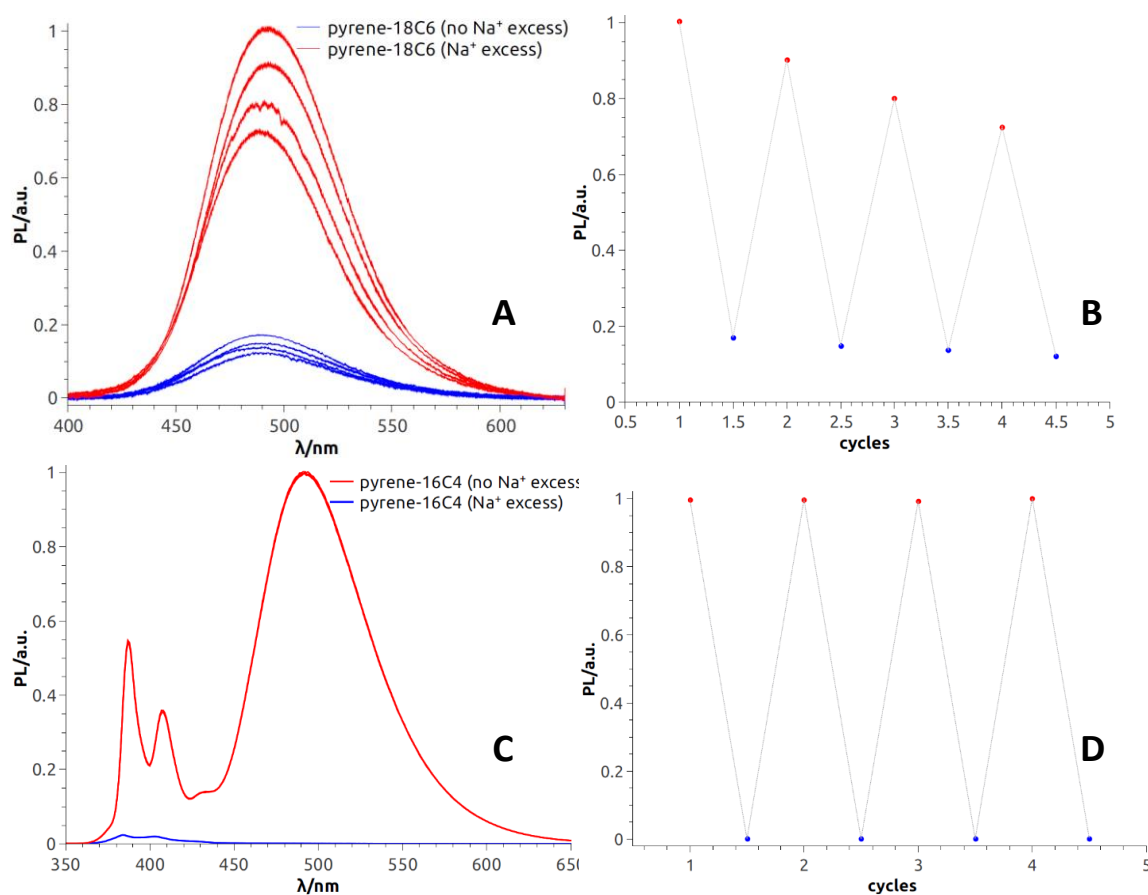


Figure 7.21 Reversible fluorescence (A) and intensities at 490 nm (B) for **pyrene-18C6** over 4 cycles of NaBAr_F/18-Crown-6 additions (red/blue: without/with NaBAr_F). Reversible fluorescence (C) and intensities at 491 nm (D) for **pyrene-16C4** over 4 cycles of NaBAr_F/18-Crown-6 additions (red/blue: without/with NaBAr_F).

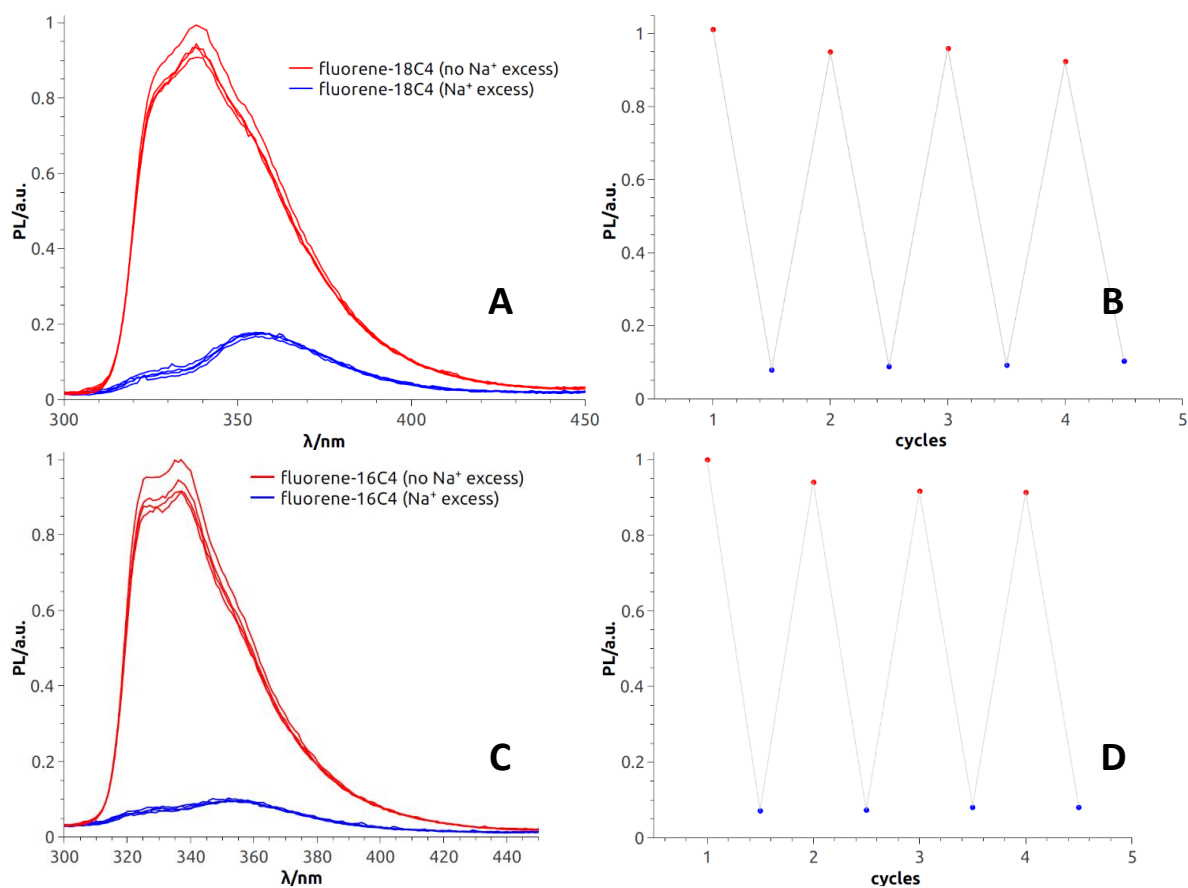


Figure 7.22 Reversible fluorescence (A) and intensities at 338 nm (B) for **fluorene-18C4** over 4 cycles of NaBARF/18-Crown-6 additions (red/blue: without/with NaBARF). Reversible fluorescence (C) and intensities at 336 nm (D) for **fluorene-16C4** over 4 cycles of NaBARF/18-Crown-6 additions (red/blue: without/with NaBARF).

7.13 TDDFT calculations

7.13.1 General remarks

All calculations were run with Gaussian'09 and Gaussian'16 suites of programs using defaults grids and convergence criteria.²¹² The input geometry of all compounds was built starting from the X-ray structure of **pyrene-18C6** with (*S,S*) configuration bound to one water molecule. The conformational space was explored by varying manually the macrocycle–C(=O) and *N*–aryl bonds, and optimizing the resulting structures with DFT at M06-2X-D3/def2-SVP level,¹⁷⁵ including the IEF-PCM implicit solvent model for dichloromethane.²¹³ All converged structures displayed a clear π -stacking interaction between the aromatic rings. TDDFT calculations were run with different combinations of functionals (ω B97X-D, M06-2X, B3LYP, CAM-B3LYP), basis sets (def2-SVP, def2-TZVP) and environment description (in vacuo or with IEF-PCM solvent model for dichloromethane). The number of roots (excited states) varied from 50 to 80 depending on the specific compound. The calculated spectra shown in **Figures 7.23** and **7.24** were obtained with M06-2X and CAM-B3LYP functionals, which yielded the best agreement with the experimental spectra. ECD plots were generated from Gaussian log files using the program SpecDis.²¹⁴ The

²¹² (a) Frisch, M. J.; Trucks, G. W.; Schlegel, H. B.; Scuseria, G. E.; Robb, M. A.; Cheeseman, J. R.; Scalmani, G.; Barone, V.; Petersson, G. A.; Nakatsuji, H.; Li, X.; Caricato, M.; Marenich, A. V.; Bloino, J.; Janesko, B. G.; Gomperts, R.; Mennucci, B.; Hratchian, H. P.; Ortiz, J. V.; Izmaylov, A. F.; Sonnenberg, J. L.; Williams-Young, D.; Ding, F.; Lipparini, F.; Egidi, F.; Goings, J.; Peng, B.; Petrone, A.; Henderson, T.; Ranasinghe, D.; Zakrzewski, V. G.; Gao, J.; Rega, N.; Zheng, G.; Liang, W.; Hada, M.; Ehara, M.; Toyota, K.; Fukuda, R.; Hasegawa, J.; Ishida, M.; Nakajima, T.; Honda, Y.; Kitao, O.; Nakai, H.; Vreven, T.; Throssell, K.; Montgomery, J., J. A.; Peralta, J. E.; Ogliaro, F.; Bearpark, M.; Heyd, J. J.; Brothers, E.; Kudin, K. N.; Staroverov, V. N.; Keith, T. A.; Kobayashi, R.; Normand, J.; Raghavachari, K.; Rendell, A.; Burant, J. C.; Iyengar, S. S.; Tomasi, J.; Cossi, M.; Millam, J. M.; Klene, M.; Adamo, C.; Cammi, R.; Ochterski, J. W.; Martin, R. L.; Morokuma, K.; Farkas, O.; Foresman, J. B.; Fox, D. J. *Gaussian 16, Revision A.03*, Gaussian, Inc.: Wallingford CT, **2016**. (b) Frisch, M. J.; Trucks, G. W.; Schlegel, H. B.; Scuseria, G. E.; Robb, M. A.; Cheeseman, J. R.; Scalmani, G.; Barone, V.; Mennucci, B.; Petersson, G. A.; Nakatsuji, H.; Caricato, M.; Li, X.; Hratchian, H. P.; Izmaylov, A. F.; Bloino, J.; Zheng, G.; Sonnenberg, J. L.; Hada, M.; Ehara, M.; Toyota, K.; Fukuda, R.; Hasegawa, J.; Ishida, M.; Nakajima, T.; Honda, Y.; Kitao, O.; Nakai, H.; Vreven, T.; Montgomery, J., J. A.; Peralta, J. E.; Ogliaro, F.; Bearpark, M.; Heyd, J. J.; Brothers, E.; Kudin, K. N.; Staroverov, V. N.; Kobayashi, R.; Normand, J.; Raghavachari, K.; Rendell, A.; Burant, J. C.; Iyengar, S. S.; Tomasi, J.; Cossi, M.; Rega, N.; Millam, J. M.; Klene, M.; Knox, J. E.; Cross, J. B.; Bakken, V.; Adamo, C.; Jaramillo, J.; Gomperts, R.; Stratmann, R. E.; Yazyev, O.; Austin, A. J.; Cammi, R.; Pomelli, C.; Ochterski, J. W.; Martin, R. L.; Morokuma, K.; Zakrzewski, V. G.; Voth, G. A.; Salvador, P.; Dannenberg, J. J.; Dapprich, S.; Daniels, A. D.; Farkas, O.; Foresman, J. B.; Ortiz, J. V.; Cioslowski, J.; Fox, D. J. *Gaussian 09, Revision D.01*, Gaussian, Inc.: Wallingford CT, **2013**.

²¹³ Mennucci, B.; Cammi, R., *Continuum Solvation Models in Chemical Physics: From Theory to Applications*. Wiley: New York, **2008**.

²¹⁴ Bruhn, T.; Schaumlöffel, A.; Hemberger, Y.; Bringmann, G., *Chirality* **2013**, 25, 243-249.

plotting parameters were chosen on a best-fitting basis, and are listed in the caption of **Figure 7.24**.

7.13.2 Calculation results

Because of the structural complexity and flexibility of the **18C6**-based macrocycles, ECD calculations were mainly intended for investigating the dependence of ECD spectra on the key structural parameters of the macrocycles.

In **Figure 7.23**, four structures of **(S,S)-fluorene-18C6** are reported which were obtained upon rotation around the *N*-aryl and macrocycle–C(=O) bonds. All structures feature a pair of stacked fluorene rings with clear chirality defined by their long axes, *i.e.* the direction along which the main π - π^* transition around 280 nm is polarized. Accordingly, the respective calculated ECD spectra display strong ECD couplets, whose sign depends on the chirality defined by the transition moments. It is apparent that the modification the reciprocal arrangement of the fluorene rings (*i.e.*, exchanging the fluorene in the front with that in the back) causes a sign reversal in the ECD couplet. This rearrangement is caused by concerted rotations around the macrocycle–C(=O) bonds.

While differing in sign and intensity, the four spectra are similar to each other in overall shape and position of bands. The weighted average of the four spectra (obtained using computed internal energies) is shown in **Figure 7.24** (left). It consists in a negative ECD couplet, which is in agreement with experimental spectrum for the 1st eluted enantiomer. The vibrational fine structure in the experimental spectrum cannot be predicted at the current level of calculation, which does not include vibronic effects.

For **pyrene-** and **perylene-18C6** we investigated the impact of switching the ring position on the ECD spectra (Figure S37, two middle columns). For **(S,S)-perylene-18C6** the situation is similar to **fluorene-18C6**: exchanging the ring position from front to back causes a sign reversal in the ECD couplet, which is also accompanied by a strong intensity decrease. The overall ECD profile consists in a negative ECD couplet, as experimentally found for the 2nd eluted enantiomer. The situation for **pyrene-18C6** is more complicated because the two arrangements – obtained after the rings exchange their positions – are associated with very different ECD profiles. The structure

attained from re-optimization of the X-ray geometry is associated with a negative ECD couplet; the second structure with exchanged ring positions is associated instead with a red-shifted positive couplet (**Figure 7.24**). If one assumes that the first conformation is dominant in solution, the combination of the two would yield an overall spectrum similar to that observed for the 2nd eluted enantiomer (**Figure 4.8A**), namely a positive ECD band at 350 nm (mainly due to the major conformer), flanked by a long-wavelength weak negative band (due to the minor conformer).

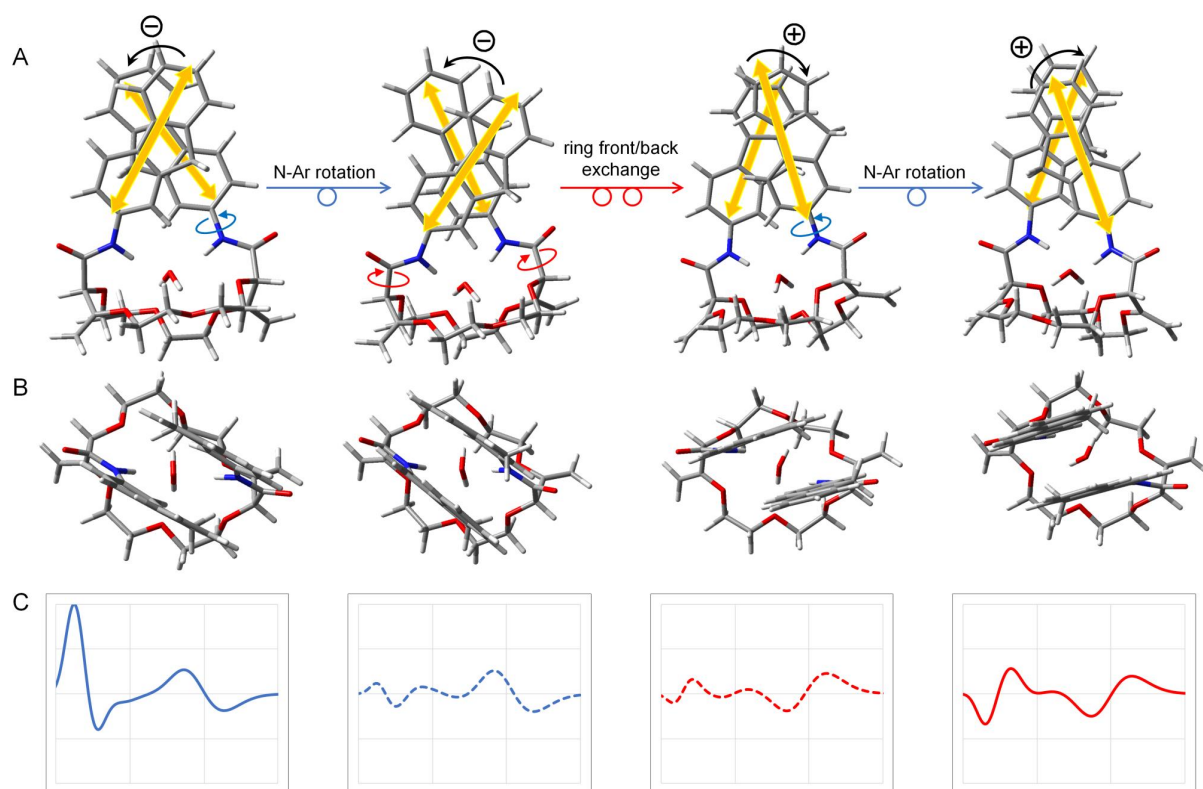


Figure 7.23 (A,B) Structures of (*S,S*)-fluorene-18C6 optimized with DFT at the M06-2X-D3/def2-SVP/PCM level after rotation around the *N*-aryl and macrocycle-C(=O) bonds. **A** and **B** offer two different viewpoints of the same structures. The yellow double arrows depict the direction of the transition moments for the π - π^* transition around 280 nm, and the signed curved arrows the chirality defined by the moments. **(C)** ECD spectra calculated for each structure at CAM-B3LYP/def2-SVP/PCM level. The horizontal and vertical ranges are 190–340 nm and –400/+400, respectively. Plotting parameters: $\sigma = 0.3$ eV, wavelength shift +15 nm.

Finally, for **NMI-18C6** the rotamerism around the *N*-aryl bond has a pronounced impact on the orientation of the transition moments, polarized either along the chromophore long or short axis (see yellow double arrows in **Figure 7.24**). Therefore, we focused our attention on this degree of conformational freedom without switching the reciprocal position of the rings. The two different arrangements (obtained upon 180°-rotation around the *N*-aryl bonds) display ECD

spectra which are almost the mirror image of each other long wavelengths, while having consistent shape and sign at shorter wavelengths (**Figure 7.24**, right). Assuming a coexistence of both structures in solution, this would lead to a signal cancelation at long wavelengths, yielding a positive exciton couplet at short wavelengths. The overall result resembles the ECD measured for the 2nd eluted enantiomer (**Figure 4.11A**).

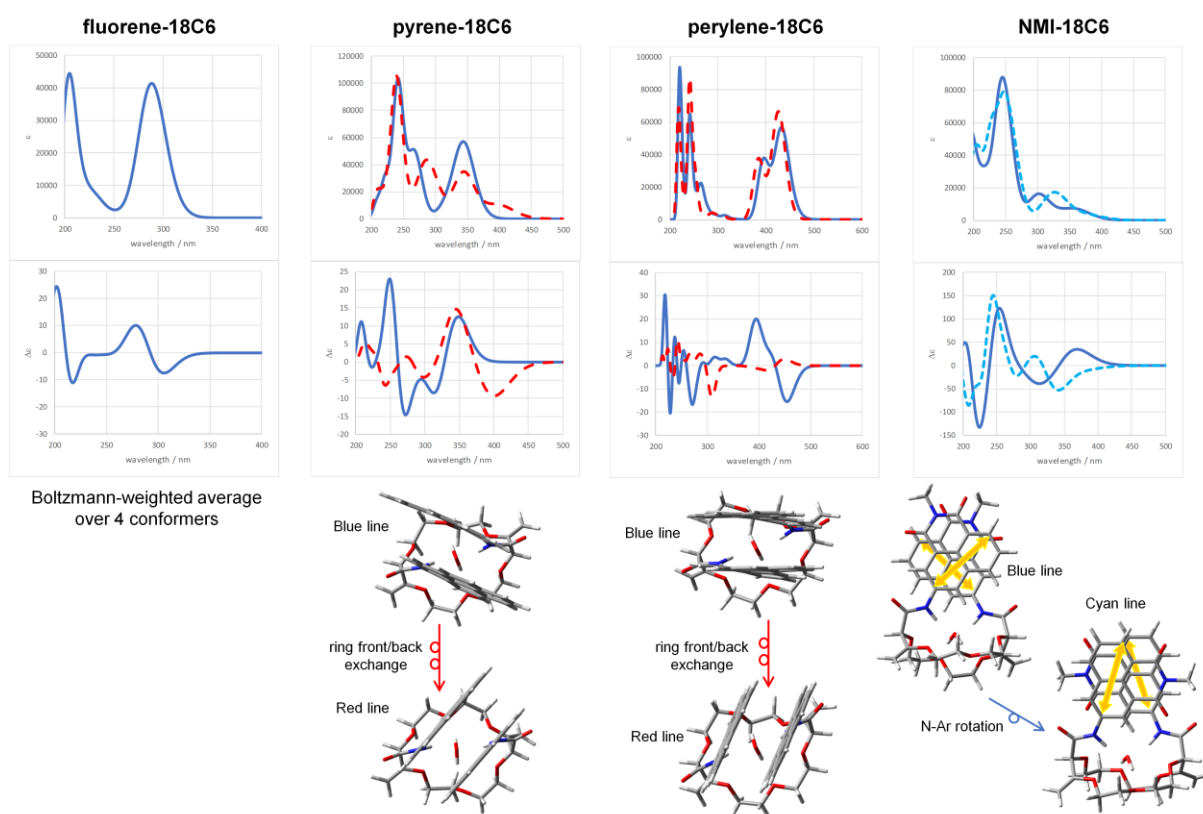


Figure 7.24 Summary of ECD calculation results for the (*S,S*)-18C6 series. Calculation levels and plotting parameters: **fluorene-18C6** (**Figure 7.23**), scaling factor 10; **pyrene-18C6**, M06-2X/def2-TZVP, $\sigma = 0.25$ eV, shift +12 nm, scaling factor 10; **perylene-18C6**, CAM-B3LYP/def2-SVP, $\sigma = 0.15$ eV, shift +20 nm, scaling factor 10; **NMI-18C6**, CAM-B3LYP/def2-TZVP, $\sigma = 0.3$ eV, no shift or scaling. The yellow double arrows depict the direction of the naphthalene long axes of NMI chromophore. See text explanation.

7.14 Crystallographic part

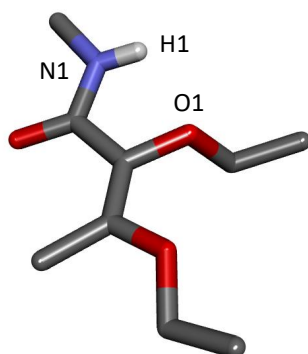
The determination of the solid state structure was performed by Dr. Laure Guénée and Dr. Céline Besnard.

7.14.1 Crystallographic data of 2.1

Empirical formula	$C_{30}H_{38}N_2O_8$	
Formula weight	554.62	
Temperature	180(2) K	
Wavelength	1.54184 Å	
Crystal system	Monoclinic	
Space group	P 1 21/c 1	
Unit cell dimensions	$a = 17.6634(5)$ Å	$\alpha = 90^\circ$.
	$b = 8.6515(2)$ Å	$\beta = 100.296(3)^\circ$.
	$c = 9.4505(3)$ Å	$\gamma = 90^\circ$.
Volume	$1420.93(7)$ Å ³	
Z	2	
Density (calculated)	1.296 Mg/m ³	
Absorption coefficient	0.774 mm ⁻¹	
F(000)	592	
Crystal size	0.2707 x 0.1869 x 0.0762 mm ³	
Theta range for data collection	5.09 to 73.69°.	
Index ranges	-21 ≤ h ≤ 21, -10 ≤ k ≤ 10, -11 ≤ l ≤ 11	
Reflections collected	10598	
Independent reflections	2838 [R(int) = 0.0197]	
Completeness to theta = 67.50°	100.0 %	
Absorption correction	Analytical	
Max. and min. transmission	0.946 and 0.834	
Refinement method	Full-matrix least-squares on F ²	
Data / restraints / parameters	2838 / 0 / 186	
Goodness-of-fit on F ²	1.031	
Final R indices [I > 2σ(I)]	R1 = 0.0334, wR2 = 0.0871	
R indices (all data)	R1 = 0.0367, wR2 = 0.0907	
Largest diff. peak and hole	0.211 and -0.185 e.Å ⁻³	

Comments: the molecule is located around a symmetry center (in the middle of the crown ether) thus leading to only one half of the molecule in the asymmetric unit. There is one intermolecular hydrogen bond (see **Table 7.5**).

Table 7.5. Hydrogen bonds for **2.1** [\AA and $^\circ$].



D-H...A	d(D-H)	d(H...A)	d(D...A)	$\angle(\text{DHA})$
N(1)-H(1)...O(1)#2	0.867(15)	2.180(16)	2.9129(12)	142.0(13)

Symmetry transformations used to generate equivalent atoms: #1 $-x+1, -y+1, -z$ #2 $x, -y+3/2, z-1/2$

7.14.2 Crystallographic data of [Na·Bn-18C6][BAr_F]

Empirical formula	C ₆₂ H ₅₀ BF ₂₄ N ₂ NaO ₈	
Chemical formula moiety	C ₃₀ H ₃₈ N ₂ NaO ₈ , C ₃₂ H ₁₂ BF ₂₄	
Formula weight	1440.84	
Temperature	180(2) K	
Wavelength	1.54184 Å	
Crystal system	Monoclinic	
Space group	P 21/c	
Unit cell dimensions	a = 17.7333(3) Å	α = 90°.
	b = 20.1120(3) Å	β = 93.8737(13)°.
	c = 18.2281(3) Å	γ = 90°.
Volume	6486.24(18) Å ³	
Z	4	
Density (calculated)	1.475 Mg/m ³	
Absorption coefficient	1.327 mm ⁻¹	
F(000)	2928	
Crystal size	0.6999 x 0.4418 x 0.1806 mm ³	
Theta range for data collection	3.33 to 73.65°.	
Index ranges	-17 ≤ h ≤ 21, -22 ≤ k ≤ 24, -22 ≤ l ≤ 18	
Reflections collected	26287	
Independent reflections	12752 [R(int) = 0.0233]	
Completeness to theta = 67.50°	99.9 %	
Absorption correction	Analytical	
Max. and min. transmission	0.801 and 0.545	
Refinement method	Full-matrix least-squares on F ²	
Data / restraints / parameters	12752 / 0 / 911	
Goodness-of-fit on F ²	1.053	
Final R indices [I > 2σ(I)]	R1 = 0.0747, wR2 = 0.2070	
R indices (all data)	R1 = 0.0820, wR2 = 0.2163	
Largest diff. peak and hole	1.390 and -0.973 e.Å ⁻³	

7.14.3 Crystallographic data of [Na·(S)-Me-1-naphth-(S)-18C6][BAr_F]

Empirical formula	C ₇₂ H ₅₈ BF ₂₄ N ₂ NaO ₈	
Formula weight	1569.00	
Temperature	180.15 K	
Wavelength	1.54184 Å	
Crystal system	Orthorhombic	
Space group	P 21 21 21	
Unit cell dimensions	a = 18.8583(7) Å	α = 90°.
	b = 19.3929(5) Å	β = 90°.
	c = 19.5642(7) Å	β = 90°.
Volume	7155.0(4) Å ³	
Z	4	
Density (calculated)	1.457 Mg/m ³	
Absorption coefficient	1.254 mm ⁻¹	
F(000)	3200	
Crystal size	0.358 x 0.128 x 0.085 mm ³	
Theta range for data collection	3.209 to 73.620°.	
Index ranges	-23 ≤ h ≤ 22, -23 ≤ k ≤ 13, -24 ≤ l ≤ 16	
Reflections collected	18332	
Independent reflections	12202 [R(int) = 0.0448]	
Completeness to theta = 67.500°	99.9 %	
Absorption correction	Analytical	
Max. and min. transmission	0.917 and 0.772	
Refinement method	Full-matrix least-squares on F ²	
Data / restraints / parameters	12202 / 0 / 961	
Goodness-of-fit on F ²	1.051	
Final R indices [I > 2σ(I)]	R1 = 0.0823, wR2 = 0.2183	
R indices (all data)	R1 = 0.0993, wR2 = 0.2426	
Absolute structure parameter	-0.19(19)	
Extinction coefficient	n/a	
Largest diff. peak and hole	0.906 and -0.611 e.Å ⁻³	

7.14.4 Crystallographic data of *m*-NH₂-pyr-18C6

CCDC number	1578257
Empirical formula	C _{26.5} H ₄₀ ClN ₆ O ₁₀
Formula weight	638.09
Temperature/K	179.95(10)
Crystal system	monoclinic
Space group	C2/c
a/Å	16.0962(3)
b/Å	20.4161(3)
c/Å	21.2523(3)
α/°	90
β/°	106.8662(18)
γ/°	90
Volume/Å ³	6683.5(2)
Z	8
ρ _{calcd} /mm ³	1.268
m/mm ⁻¹	1.523
F(000)	2704.0
Crystal size/mm ³	0.4998 × 0.2204 × 0.1902
Radiation	CuKα (λ = 1.54184)
2θ range for data collection	7.188 to 148.966°
Index ranges	-16 ≤ h ≤ 19, -20 ≤ k ≤ 25, -26 ≤ l ≤ 21
Reflections collected	15019
Independent reflections	6675 [R _{int} = 0.0183, R _{sigma} = 0.0212]
Data/restraints/parameters	6675/81/460
Goodness-of-fit on F ²	1.050
Final R indexes [I > 2σ (I)]	R ₁ = 0.0811, wR ₂ = 0.2539
Final R indexes [all data]	R ₁ = 0.0887, wR ₂ = 0.2683
Largest diff. peak/hole / e Å ⁻³	0.88/-0.45

Comments: Due to a disordered dichloromethane molecule, the quality of the structure is not optimal. The hydrogen atoms were not clearly visible in the Fourier difference map and the hydrogens positions for the water and the amine were inferred according to possible hydrogen bonds, small density peaks and avoiding short contacts. They are therefore only indicative, especially close to the disordered dichloromethane molecule.

7.14.5 Crystallographic data of pyr-cryptand

CCDC number	1578265
Empirical formula	$C_{69}H_{82}N_{14}O_{23}$
Formula weight	1475.48
Temperature/K	181(5)
Crystal system	triclinic
Space group	P-1
a/Å	12.9098(4)
b/Å	13.9643(4)
c/Å	20.9695(6)
$\alpha/^\circ$	85.801(2)
$\beta/^\circ$	84.021(3)
$\gamma/^\circ$	72.938(3)
Volume/Å ³	3590.63(19)
Z	2
$\rho_{\text{calc}}/\text{cm}^3$	1.365
μ/mm^{-1}	0.873
F(000)	1556.0
Crystal size/mm ³	0.6038 × 0.2878 × 0.1501
Radiation	CuK α (λ = 1.5418)
2 θ range for data collection/ $^\circ$	6.628 to 146.846
Index ranges	-15 ≤ h ≤ 12, -17 ≤ k ≤ 16, -17 ≤ l ≤ 26
Reflections collected	24430
Independent reflections	14026 [R_{int} = 0.0185, R_{sigma} = 0.0242]
Data/restraints/parameters	14026/85/1031
Goodness-of-fit on F^2	1.024
Final R indexes [$I \geq 2\sigma(I)$]	R_1 = 0.0552, wR_2 = 0.1504
Final R indexes [all data]	R_1 = 0.0611, wR_2 = 0.1567
Largest diff. peak/hole / e Å ⁻³	0.76/-0.47

Comments: two macrocycles are present per asymmetric unit. They are superimposable. There is a small disorder on one of the chain of one macrocycle. Distances were restrained to ideal values and rigid-bond restraints were used for anisotropic displacement parameters. Two disordered methanol molecules are also present. Same distances restraints were applied, and restraints and constraints were used on anisotropic displacement parameters.

7.14.6 Crystallographic data of thiophos-cryptand

CCDC number	1034975
Empirical formula	C ₂₈ H ₃₆ N ₆ O ₉ S
Formula weight	632.69
Temperature/K	155.6(10)
Crystal system	monoclinic
Space group	P2 ₁ /c
a/Å	19.1025(6)
b/Å	28.5447(7)
c/Å	15.7139(5)
α/°	90
β/°	111.653(4)
γ/°	90
Volume/Å ³	7963.8(5)
Z	8
ρ _{calc} /cm ³	1.055
μ/mm ⁻¹	1.134
F(000)	2672.0
Crystal size/mm ³	0.697 × 0.1946 × 0.0848
Radiation	CuKα (λ = 1.5418)
2θ range for data collection/°	5.862 to 145.058
Index ranges	-23 ≤ h ≤ 23, -34 ≤ k ≤ 34, -12 ≤ l ≤ 19
Reflections collected	23390
Independent reflections	23390 [R _{int} = ?, R _{sigma} = 0.0158]
Data/restraints/parameters	23390/119/871
Goodness-of-fit on F ²	1.027
Final R indexes [I ≥ 2σ (I)]	R ₁ = 0.0710, wR ₂ = 0.1897
Final R indexes [all data]	R ₁ = 0.0861, wR ₂ = 0.2055
Largest diff. peak/hole / e Å ⁻³	0.54/-0.36

Comments: the crystal is twinned, with two twin domains rotated by 180 degrees along the a axis. Both twin components were integrated and an hklf5 was produced. The structure is disordered. Part of the chain was modelled using two components. Geometrical restraints (SADI) were used, as well as restraints on anisotropic displacement parameters. (SADI) The solvent is also disordered. Methanol molecules were located in the middle of the macrocycle. For the rest of the solvent the squeeze/bypass method was used on the detwinned data (list 8) in platon. R before squeeze procedure: R₁=0.1468 (all data) wR₂=0.3912.

7.14.7 Crystallographic data of thiourea-cryptand

CCDC number	1578261
Empirical formula	$\text{C}_{39}\text{H}_{50}\text{Cl}_6\text{N}_8\text{O}_9\text{S}_2$
Formula weight	1051.69
Temperature/K	180.1(2)
Crystal system	monoclinic
Space group	$P2_1/c$
a/Å	9.85416(16)
b/Å	31.5895(6)
c/Å	16.7321(3)
$\alpha/^\circ$	90
$\beta/^\circ$	106.159(2)
$\gamma/^\circ$	90
Volume/Å ³	5002.72(17)
Z	4
$\rho_{\text{calc}}/\text{cm}^3$	1.396
μ/mm^{-1}	4.401
F(000)	2184.0
Crystal size/mm ³	$0.5763 \times 0.1869 \times 0.0529$
Radiation	$\text{CuK}\alpha$ ($\lambda = 1.54184$)
2 θ range for data collection/ $^\circ$	7.848 to 146.642
Index ranges	$-12 \leq h \leq 7, -37 \leq k \leq 39, -19 \leq l \leq 20$
Reflections collected	32965
Independent reflections	9858 [$R_{\text{int}} = 0.0440, R_{\text{sigma}} = 0.0363$]
Data/restraints/parameters	9858/54/661
Goodness-of-fit on F^2	1.032
Final R indexes [$I \geq 2\sigma(I)$]	$R_1 = 0.0678, wR_2 = 0.1932$
Final R indexes [all data]	$R_1 = 0.0802, wR_2 = 0.2086$
Largest diff. peak/hole / e Å ⁻³	0.61/-1.16

Comments: disordered dichloromethane molecules were refined as rigid-bodies. Restraints and constraints were applied on anisotropic displacement parameters: an antibump restraint was also applied to avoid a low-occupancy dichloromethane molecule to get too close to the macrocycle

7.14.8 Crystallographic data of [pyr-cryptand·NaN₃]

CCDC number	1578264
Empirical formula	C ₃₅ H ₃₉ Cl ₄ N ₁₀ NaO ₁₀
Formula weight	924.55
Temperature/K	180.00(14)
Crystal system	monoclinic
Space group	P2 ₁ /n
a/Å	8.17364(7)
b/Å	26.35975(17)
c/Å	19.91115(14)
α/°	90
β/°	100.5891(8)
γ/°	90
Volume/Å ³	4216.90(6)
Z	4
ρ _{calc} /cm ³	1.456
μ/mm ⁻¹	3.229
F(000)	1912.0
Crystal size/mm ³	0.4352 × 0.2802 × 0.0501
Radiation	CuKα (λ = 1.5418)
2θ range for data collection/°	6.706 to 146.928
Index ranges	-10 ≤ h ≤ 9, -32 ≤ k ≤ 32, -24 ≤ l ≤ 24
Reflections collected	68485
Independent reflections	8400 [R _{int} = 0.0477, R _{sigma} = 0.0198]
Data/restraints/parameters	8400/71/583
Goodness-of-fit on F ²	1.035
Final R indexes [I >= 2σ (I)]	R ₁ = 0.0405, wR ₂ = 0.1053
Final R indexes [all data]	R ₁ = 0.0455, wR ₂ = 0.1100
Largest diff. peak/hole / e Å ⁻³	0.62/-0.63

Comments: one disorder dichloromethane molecule was refined using three components. The major one (75 percent occupancy) was refined using geometrical restraints. The two minor ones (10 and 25 percent occupancy) were refined as rigid bodies. Restraints and constraints were applied on anisotropic displacement parameters.

7.14.9 Crystallographic data of [pyr-cryptand·NaNO₃]

CCDC number	1578259
Empirical formula	C ₃₇ H ₄₃ N ₈ NaO ₁₅
Formula weight	862.78
Temperature/K	179.95(10)
Crystal system	monoclinic
Space group	P2 ₁ /c
a/Å	21.3118(3)
b/Å	9.34735(13)
c/Å	21.5322(3)
α/°	90
β/°	107.8674(16)
γ/°	90
Volume/Å ³	4082.51(11)
Z	4
ρ _{calc} /cm ³	1.404
μ/mm ⁻¹	1.023
F(000)	1808.0
Crystal size/mm ³	0.2259 × 0.0954 × 0.0691
Radiation	CuKα (λ = 1.54184)
2θ range for data collection/°	8.39 to 147.874
Index ranges	-26 ≤ h ≤ 25, -10 ≤ k ≤ 11, -26 ≤ l ≤ 26
Reflections collected	16751
Independent reflections	8070 [R _{int} = 0.0180, R _{sigma} = 0.0244]
Data/restraints/parameters	8070/22/593
Goodness-of-fit on F ²	1.042
Final R indexes [I ≥ 2σ (I)]	R ₁ = 0.0421, wR ₂ = 0.1120
Final R indexes [all data]	R ₁ = 0.0539, wR ₂ = 0.1187
Largest diff. peak/hole / e Å ⁻³	0.31/-0.26

Comments: there is a small disorder on the nitrate ion. The part with the small occupancy was refined as a rigid body. Restraints and constraints were applied on anisotropic displacements parameters.

7.14.10 Crystallographic data of [pyr-cryptand·KNCO]

CCDC number	1578258
Empirical formula	C ₃₆ H ₃₉ Cl ₄ KN ₈ O ₁₁
Formula weight	940.65
Temperature/K	180.00(14)
Crystal system	monoclinic
Space group	P2 ₁ /n
a/Å	8.0322(2)
b/Å	26.1655(7)
c/Å	20.6516(7)
α/°	90
β/°	101.873(3)
γ/°	90
Volume/Å ³	4247.4(2)
Z	4
ρ _{calc} /cm ³	1.471
μ/mm ⁻¹	3.988
F(000)	1944.0
Crystal size/mm ³	0.5022 × 0.3354 × 0.0165
Radiation	CuKα (λ = 1.54184)
2θ range for data collection/°	8.05 to 146.718
Index ranges	-9 ≤ h ≤ 6, -32 ≤ k ≤ 27, -23 ≤ l ≤ 25
Reflections collected	17951
Independent reflections	8299 [R _{int} = 0.0340, R _{sigma} = 0.0407]
Data/restraints/parameters	8299/73/595
Goodness-of-fit on F ²	1.044
Final R indexes [I >= 2σ (I)]	R ₁ = 0.0535, wR ₂ = 0.1400
Final R indexes [all data]	R ₁ = 0.0657, wR ₂ = 0.1504
Largest diff. peak/hole / e Å ⁻³	0.76/-1.08

Comments: one disordered dichloromethane molecule was refined using three rigid bodies. RIGU and SIMU restraints were applied on anisotropic displacement parameters. Hydrogen atoms bound to nitrogen atoms were refined using DFIX restraints.

7.14.11 Crystallographic data of [pyr-cryptand·NaSCN]

CCDC number	1578262
Empirical formula	C ₃₇ H ₄₄ N ₈ NaO ₁₁ S
Formula weight	831.85
Temperature/K	180.00(14)
Crystal system	orthorhombic
Space group	P2 ₁ 2 ₁ 2 ₁
a/Å	12.62984(17)
b/Å	13.9061(2)
c/Å	25.2004(5)
α/°	90
β/°	90
γ/°	90
Volume/Å ³	4425.99(12)
Z	4
ρ _{calc} /cm ³	1.248
μ/mm ⁻¹	1.283
F(000)	1748.0
Crystal size/mm ³	0.6289 × 0.1734 × 0.015
Radiation	CuKα (λ = 1.5418)
2θ range for data collection/°	7.016 to 146.706
Index ranges	-14 ≤ h ≤ 15, -11 ≤ k ≤ 16, -31 ≤ l ≤ 30
Reflections collected	26862
Independent reflections	8677 [R _{int} = 0.0393, R _{sigma} = 0.0339]
Data/restraints/parameters	8677/135/614
Goodness-of-fit on F ²	1.047
Final R indexes [I ≥ 2σ (I)]	R ₁ = 0.0546, wR ₂ = 0.1490
Final R indexes [all data]	R ₁ = 0.0619, wR ₂ = 0.1592
Largest diff. peak/hole / e Å ⁻³	0.88/-0.29
Flack parameter	0.31(3)

Comments: one part of the macrocycle is disordered and was refined using two components. Distances restraints were applied as well as restraints on anisotropic displacement parameters. Partially occupied hexane disordered molecules were refined using geometrical restraints. Constraints were applied on anisotropic displacement parameters. Hydrogen linked to the N atoms were refined using distances restraints.

7.14.12 Crystallographic data of [pyr-cryptand·KSCN]

CCDC number	1578263
Empirical formula	C ₃₄ H _{39.75} KN ₈ O _{12.23} S
Formula weight	827.41
Temperature/K	180.00(14)
Crystal system	triclinic
Space group	P-1
a/Å	10.3284(3)
b/Å	13.5189(5)
c/Å	14.7563(6)
α/°	93.205(3)
β/°	108.501(3)
γ/°	98.464(3)
Volume/Å ³	1921.03(12)
Z	2
ρ _{calc} /cm ³	1.430
μ/mm ⁻¹	2.348
F(000)	865.0
Crystal size/mm ³	0.871 × 0.206 × 0.032
Radiation	CuKα (λ = 1.5418)
2θ range for data collection/°	6.65 to 147.1
Index ranges	-12 ≤ h ≤ 12, -16 ≤ k ≤ 16, -18 ≤ l ≤ 18
Reflections collected	28761
Independent reflections	7603 [R _{int} = 0.0437, R _{sigma} = 0.0288]
Data/restraints/parameters	7603/22/545
Goodness-of-fit on F ²	1.084
Final R indexes [I ≥ 2σ(I)]	R ₁ = 0.0931, wR ₂ = 0.2204
Final R indexes [all data]	R ₁ = 0.1258, wR ₂ = 0.2410
Largest diff. peak/hole / e Å ⁻³	0.62/-0.40

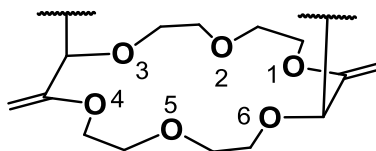
Comments: structure is of low quality as reflected in the large displacement ellipsoids. The diffraction data show that the quality of the crystal was not optimal (slightly split crystal). However, no better crystal was found despite numerous attempt of recrystallization. OW2 and OW1 are refined as rigid bodies. The hydrogen atoms positions for these molecules are visible in difference Fourier map. For OW3, which is a partially occupied water molecule, the hydrogen atoms are just allowed to ride on their parent atom and the hydrogen positions were assigned arbitrarily taking into account possible hydrogen bonds and avoiding possible collisions with neighboring atoms. The thiocyanate was refined as two components, restraining distances to ideal values. Restraints/constraints were also used on anisotropic displacement parameters.

7.14.13 Crystallographic data of [Ph-cryptand·NaN₃]

CCDC number	1578260
Empirical formula	C ₃₆ H ₄₀ Cl ₄ N ₉ NaO ₁₀
Formula weight	923.56
Temperature/K	179.9(3)
Crystal system	monoclinic
Space group	P2 ₁ /n
a/Å	7.9659(3)
b/Å	26.0868(8)
c/Å	20.3623(5)
α/°	90
β/°	96.444(3)
γ/°	90
Volume/Å ³	4204.7(2)
Z	4
ρ _{calc} /cm ³	1.459
μ/mm ⁻¹	3.231
F(000)	1912.0
Crystal size/mm ³	0.2968 × 0.0437 × 0.0199
Radiation	CuKα (λ = 1.54184)
2θ range for data collection/°	8.064 to 147.576
Index ranges	-9 ≤ h ≤ 9, -32 ≤ k ≤ 32, -19 ≤ l ≤ 25
Reflections collected	29642
Independent reflections	8330 [R _{int} = 0.0694, R _{sigma} = 0.0616]
Data/restraints/parameters	8330/52/605
Goodness-of-fit on F ²	1.024
Final R indexes [I ≥ 2σ (I)]	R ₁ = 0.0590, wR ₂ = 0.1432
Final R indexes [all data]	R ₁ = 0.1016, wR ₂ = 0.1720
diff. peak/hole / e Å ⁻³	0.84/-0.32

Comments: H atoms bound to N atoms were refined using distance restraints. Disordered dichloromethane molecules were refined using geometrical restraints. Anisotropic displacement parameters were also restrained and constrained for these molecules.

7.14.14 Summary of the cryptand-salt distances

Table 7.6 Summary of the distances around the alkali cations for **pyr-cryptand** metal complexes

	[pyr-cryptand ·NaNO ₃] ^[a]	[pyr-cryptand ·KNCO]	[pyr-cryptand ·NaN ₃]	[pyr-cryptand ·NaSCN] ^[a]	[pyr-cryptand ·KSCN] ^[a]
O1	2.7758(14)	2.8738(19)	2.794(3)	2.705(3)	3.152(6)
O2	2.7466(16)	2.773(2)	2.656(3)	2.603(3)	2.950(6)
O3	2.6121(14)	2.6516(17)	2.573(2)	2.578(3)	2.788(4)
O4	2.9331(16)	2.8518(18)	2.813(3)	2.996(3) 3.177(4)	2.922(4)
O5	2.6021(14)	2.8093(19)	2.776(3)	2.725(4)	2.885(4)
O6	2.5212(3)	2.6562(17)	2.578(2)	2.538(3)	2.920(5)
Ligand coordinated atom	2.398(8) 2.312(2)	2.698(3)	2.427(3)	2.413(14)	3.299(12) 3.23(1)
O from other macrocycle / water	2.372(2)	2.672(3)	2.400	2.291(14)	2.902(5)
O from C=O					2.862(6)
Least square plane: -average Root Mean Square Deviation (Å)	0.101	0.069	0.251	0.140 0.212	0.573
-(atom with most deviation)	(O2)	(O6)	(O5)	(O6) (O5)	(O2 O3 O4 O6)
-distance M to plane (Å)	0.06	0.03	0.02	0.03 0.08	1.113

[a] For disordered structure, values are given for each of the disordered parts.

8 Appendix

List of publications

1. Poggiali D., Homberg A., Lathion T., Piguet C., Lacour J. "Kinetics of Rh(II)-Catalyzed α -Diazo- β -ketoester Decomposition and Application to the [3+6+3+6] Synthesis of Macrocycles on a Large Scale and at Low Catalyst Loadings." *ACS Catal.* **2016**, 6, 4877-4881.
2. Vishe M., Lathion T., Pascal S., Yushchenko O., Homberg A., Brun E., Vauthey E., Piguet C., Lacour J. "Excimer-Based On-Off Bis(pyreneamide) Macrocyclic Chemosensors." *Helv. Chim. Acta* **2018**, 101, e1700265.
3. Ray S. K.,* Homberg A.,* Vishe M., Besnard C., Lacour J. "Efficient Synthesis of Ditopic Polyamide Receptors for Cooperative Ion Pair Recognition in Solution and Solid States." *Chem. Eur. J.* **2018**, 24, 2944-2951.
4. Brun E., Homberg A., Lacour J., Poggiali D., Zinna F. "Functionalized Polyether Macrocyclic Compounds and Use Thereof as Luminescent Markers" *European Patent Application* **2018**, 51383EP.
5. Homberg A.,* Brun E.,* Zinna F.,* Pascal S., Górecki M., Monnier L., Besnard C., Pescitelli G., Di Bari L., Lacour J., "Combined Reversible Switching of ECD and Quenching of CPL with Chiral Fluorescent Macrocycles" *Chemical Science*, **2018**, 9, 7043-7052.
6. Homberg A.,* Poggiali D.,* Vishe M., Besnard C., Guénée L., Lacour J., "Rh(II)-catalyzed Decomposition of α -Diazo- β -ketoester and Formation of Oxonium Ylide with Morpholines" *manuscript in preparation*.